PolyPublie
Polytechnique Montréal

POLYTECHNIQUE MONTRÉAL
UNIVERSITÉ D'INGÉNIERIE

Titre: Title:	Modeling Viscosity of Molten Slags and Glasses
Auteur: Author:	Wan Yi Kim
Date:	2011
Type:	Mémoire ou thèse / Dissertation or Thesis
Référence: Citation:	Kim, W. Y. (2011). Modeling Viscosity of Molten Slags and Glasses [Ph.D. thesis, École Polytechnique de Montréal]. PolyPublie. https://publications.polymtl.ca/641/

Document en libre accès dans PolyPublie
Open Access document in PolyPublie

URL de PolyPublie: PolyPublie URL:	https://publications.polymtl.ca/641/
Directeurs de recherche: Advisors:	Arthur Pelton, Sergei Decterov, & In-Ho Jung
Programme: Program:	Génie métallurgique

Ce fichier a été téléchargé à partir de PolyPublie, le dépôt institutionnel de Polytechnique Montréal
This file has been downloaded from PolyPublie, the institutional repository of Polytechnique Montréal

https://publications.polymtl.ca

UNIVERSITÉ DE MONTRÉAL

MODELING VISCOSITY OF MOLTEN SLAGS AND GLASSES

WANYI KIM

DÉPARTEMENT DE GÉNIE CHIMIQUE

ÉCOLE POLYTECHNIQUE DE MONTRÉAL

THÈSE PRESENTÉE EN VUE DE L'OBTENTION

DU DIPLÔME DE PHILOSOPHIAE DOCTOR

(GÉNIE MÉTALLURGIQUE)

AOÛT 2011

© WanYi Kim, 2011.

UNIVERSITÉ DE MONTRÉAL

ÉCOLE POLYTECHNIQUE DE MONTRÉAL

Cette thèse intitulée:

MODELING VISCOSITY OF MOLTEN SLAGS AND GLASSES

présentée par: WanYi Kim

en vue de l'obtention du diplôme de : Philosophiae Doctor

a été dûment accepté par le jury d'examen constitué de :

M. CHARTRAND Patrice, Ph.D., président

M. PELTON Arthur, Ph.D., membre et directeur de recherche

M. DECTEROV Sergei, Ph.D., membre et codirecteur de recherche

M. JUNG In-Ho, Ph.D., membre et codirecteur de recherche

M. AJERSCH Frank, Ph.D., membre

Mme. SCHIEFELBEIN Susan L., Ph.D., membre

DEDICATION

I dedicate this work to my parents, So-Yi and my wife Min-Su for all their encouragement, love and support.

ACKNOWLEDGEMENTS

I would like to express my deepest gratitude to my research director; Prof. Arthur Pelton for his support, guidance and continuous encouragement during my research work.

I am also grateful to my co-director, Dr. Sergei Decterov and Dr. In-Ho Jung, for their continual helpful advice and collaboration in my study. I enjoyed all discussions with them during my study. I would like to thank the jury members Prof. Frank Ajersch, Prof. Patrice Chartrand and Dr. Susan Schiefelbein from Corning who have accepted to evaluate this thesis.

I also want to give thank to Guillaume Lambotte, Jean-Philippe Harvey, Adarsh Shukla, Liling Jin and Aimen Gheribi for their support and for the very pleasant time with sports together. A special thank goes to Jacques Melancon for his helpful suggestions to enjoy the life in Montreal. I also would like to express my gratitude to other CRCT members for their assistance and friendship during my study.

I would like to thank to my family and my wife, Min-Su for their unconditional love and encouragement during my study. Their love stands me out on the ground.

At the end, I would like to thank and give the glory to my God. God has been leading my life to what he has promised to me. I praise his faithfulness.

RÉSUMÉ

Récemment, un nouveau modèle de viscosité a été développé dans ce laboratoire pour des laitiers liquides monophasiques relatifs au système CaO-MgO-K_2O-Na_2O-Al_2O_3-SiO_2-B_2O_3[27, 81, 82]. Dans ce modèle, la viscosité est liée à la structure du laitier, caractérisée par les concentrations et la connectivité des espèces Q^i. La structure est calculée à son tour à partir de la description thermodynamique du liquide à l'aide du Modèle Quasichimique Modifié[231, 232] et de la banque de données thermodynamiques de FactSage[14]. Le modèle développé prend en compte, en utilisant la connectivité des espèces Q^i, la formation d'un réseau de silice ou d'oxyde de bore qui a un effet marqué sur la viscosité.

Un modèle de viscosité a été développé pour les systèmes MO_x, MO_x-SiO_2, MO_x-B_2O_3 et B_2O_3-SiO_2 (MO_x = oxyde basique), et quelques paramètres unaires et binaires avec une dépendance en température d'Arrhenius ont été obtenus simultanément à partir des données de viscosité disponibles pour tous les liquides binaires et ternaires. Le modèle comprend deux paramètres ternaires supplémentaires pour chaque système ternaire MO_x–Al_2O_3–SiO_2 à base de Al_2O_3 pour lequel a lieu un Effet de Compensation de Charge (où Al^{3+} occupe une coordination tétraédrique et s'insère dans le réseau de silice avec un cation basique M restant au voisinage de Al^{3+} pour compenser la charge manquante). La viscosité de laitiers multicomposants CaO-MgO-K_2O-Na_2O-Al_2O_3-SiO_2-B_2O_3 [27, 81, 82] a ensuite été prédite par le modèle sans l'ajout de paramètres ajustables supplémentaires, et elle est en bon accord avec les mesures disponibles en deçà des barres d'erreur expérimentales.

Cependant, le modèle ne pouvait pas reproduire le comportement complexe des données de viscosité mesurées dans la région riche en oxyde alcalin des liquides $MO_{0.5}$-SiO_2, ou pour des liquides multicomposants à base d'oxydes alcalins. Dans le présent travail, le modèle est modifié pour reproduire le comportement complexe de la viscosité des systèmes oxyde alcalin-silice du côté riche en oxyde alcalin. Ce comportement est attribué aux agrégats en forme d'anneaux formés par les espèces Q^2 et Q^3. L'ajout d'un paramètre binaire supplémentaire $E^{Ring}_{MO_x\text{-}Si}$ pour chaque système oxyde alcalin-silice permet de prendre en compte la contribution en excès à la viscosité due à la polymérisation des espèces Q^2 et Q^3 sous la forme d'anneaux de grande taille.

Aussi, dans le présent travail, la viscosité de laitiers liquides contenant PbO, ZnO, MnO et TiO_x a été révisée et modélisée à l'aide du modèle modifié. Seulement 6 paramètres du modèle liés à chaque oxyde MO_x (M = Pb, Zn, Mn) sont requis pour reproduire la viscosité de liquides à base de silice. Deux paramètres ($\boldsymbol{A}_{MO_x}$ et $\boldsymbol{E}_{MO_x}$) décrivent la viscosité du liquide pur MO_x; deux paramètres binaires ($\boldsymbol{E}^{1,1}_{MO_x\text{-Si}}$ et $\boldsymbol{E}^{\boldsymbol{R}}_{MO_x\text{-Si}}$) décrivent la viscosité de chaque liquide MO_x - SiO_2; et finalement deux paramètres supplémentaires représentent l'énergie de Gibbs $\Delta\boldsymbol{G}_{MAl_2O_4}$ de formation des "espèces" Al de coordination tétraédrique entrant dans le réseau de silice avec une compensation de charge due au cation M. Ces deux paramètres supplémentaires sont obtenus à partir des viscosités expérimentales des liquides MO_x-Al_2O_3-SiO_2. La viscosité de laitiers multicomposants contenant MO_x est ensuite prédite par le modèle sans l'ajout de paramètres ajustables supplémentaires.

Les liquides à base de silice contenant TiO_x ont requis quatre paramètres ($\boldsymbol{A}_{TiO_2}$, $\boldsymbol{A}_{TiO_{1.5}}$, $\boldsymbol{E}_{TiO_2}$ et $\boldsymbol{E}_{TiO_{1.5}}$) décrivant la viscosité des liquides purs TiO_2 et $TiO_{1.5}$, et quatre paramètres binaires ($\boldsymbol{E}^{1,1}_{TiO_2\text{-Si}}$, $\boldsymbol{E}^{\boldsymbol{R}}_{TiO_2\text{-Si}}$, $\boldsymbol{E}^{1,1}_{TiO_{1.5}\text{-Si}}$ et $\boldsymbol{E}^{\boldsymbol{R}}_{TiO_{1.5}\text{-Si}}$) décrivant la viscosité des liquides TiO_2-SiO_2 et $TiO_{1.5}$-SiO_2. Aucune donnée de viscosité n'était disponible pour rendre compte de l'Effet de Compensation de Charge entre TiO_x, Al_2O_3 et MO_x (TiO_2-Al_2O_3 et Ti_2O_3-MO_x), où MO_x est un oxyde basique, et ainsi aucun paramètre du modèle n'a été ajouté pour cet Effet de Compensation de Charge. La viscosité de laitiers multicomposants contenant TiO_2 et Ti_2O_3 est ensuite prédite par le modèle sans l'ajout de paramètres ajustables supplémentaires.

En guise de test du modèle, les données de viscosité expérimentales disponibles pour tous les sous-systèmes du système SiO_2–Al_2O_3–CaO–MgO–Na_2O–K_2O–PbO–ZnO–MnO–TiO_x ont été rassemblées et utilisées pour calibrer le modèle. L'écart entre les mesures et les viscosités prédites par le modèle n'excède pas la dispersion des points expérimentaux des différents auteurs. En particulier, le modèle prédit la viscosité de laitiers multicomposants à base de silice et de verres commerciaux avec une précision comparable à celle des équations de régression obtenues à partir des données expérimentales sur les gammes de composition restreintes de ces liquides.

Le modèle est aussi étendu dans le présent travail pour décrire et prédire la viscosité de liquides oxy-fluorés contenant MF_x (M = Ca, Mg, Na, K et Al). Une banque de données de

solution simplifiée utilisant un modèle polynômial avec les énergies de Gibbs de chaque liquide pur d'oxyde et de fluorure a été développée, permettant ainsi de calculer approximativement la composition globale "équilibrée" à partir d'une composition initiale donnée des liquides oxy-fluorés. Les rôles structuraux de MF_x (M = Ca, Mg, Na, K et Al) sont examinés, et MF_x est considéré comme un modificateur de réseau dans les liquides à base de silice ou d'oxyde de bore, avec des effets de rupture du réseau de silice ou d'oxyde de bore que nous avons simplement supposés identiques à ceux des oxydes basiques contenant le même cation M.

Un modèle de viscosité a été développé pour les systèmes MF_x, MF_x-SiO_2 et MF_x-B_2O_3 (M = Ca, Mg, Na, K et Al), et quelques paramètres unaires et binaires ont été obtenus simultanément à partir des données de viscosité disponibles pour tous les liquides binaires et ternaires. Aucun effet de compensation de charge n'a été observé entre MF_x et Al_2O_3, et ainsi le modèle reproduit les données expérimentales pour les liquides binaires et ternaires sans appliquer d'effet de compensation de charge entre MF_x et Al_2O_3. En plus des deux paramètres du modèle requis pour chaque liquide MF_x-B_2O_3 (où MF_x est un fluorure basique), les paramètres additionnels $\Delta G_{m(MB_4FO_6)}$, $E_{m(MB_4FO_6)}$ et m sont nécessaires lorsque MF_x est un fluorure alcalin de façon à rendre compte de la formation d'agrégats au voisinage de la composition du tétraborate. Ces paramètres supplémentaires représentent la taille et l'énergie de Gibbs de formation des agrégats ainsi que leur contribution à l'énergie d'activation d'écoulement visqueux. Les données de viscosité disponibles pour tous les sous-systèmes du système MF_x–SiO_2–B_2O_3–Al_2O_3–CaO–MgO–Na_2O–K_2O–PbO–MnO–TiO_y (M = Ca, Mg, Na, K et Al) sont examinées. La viscosité de liquides multicomposants et de liquides ternaires MF_x–NO_y–SiO_2 (où MF_x et NO_y sont des fluorures et des oxydes basiques) est prédite par le modèle uniquement à partir des paramètres unaires, binaires et ternaires. L'écart entre les mesures et les viscosités prédites n'excède pas la dispersion des points expérimentaux et les barres d'erreur expérimentales. La capacité de prédiction du modèle a également été testée sur plusieurs liquides de flux de moule industriels, et nous pensons qu'elle est satisfaisante compte tenu des incertitudes expérimentales des données de viscosité.

Le modèle développé avec une dépendance en température d'Arrhenius pour la viscosité des liquides oxy-fluorés est étendu dans le présent travail pour prendre en compte la dépendance en température non-Arrhenienne des données de viscosité mesurées de la région vitreuse jusqu'à

la région liquide. A l'aide de toutes les données disponibles pour les sous-systèmes du système CaO-MgO-Na_2O-K_2O-ZnO-PbO-Al_2O_3-B_2O_3-SiO_2, les valeurs des paramètres du modèle unaires et binaires $\boldsymbol{A}_{\mathbf{MO_x}}$, $\boldsymbol{E}_{\mathbf{MO_x}}$, $E^{R}_{\mathrm{MO_x-Si}}$ et $E^{i.j}_{\mathrm{MO_x\text{-}Si}}$ ont été réoptimisées simultanément avec l'ajout des paramètres unaires et binaires non-Arrheniens $\boldsymbol{T}_{\mathbf{MO_x}}$, $\boldsymbol{n}_{\mathbf{MO_x}}$, $\boldsymbol{m}_{\mathbf{MO_x\text{-}Si}}$, $\boldsymbol{T}_{\mathbf{MO_x\text{-}Si}}$ et $\boldsymbol{n}_{\mathbf{MO_x\text{-}Si}}$ (M = Ca, Mg, Pb, Zn et Al). De façon à prendre en compte l'Effet de Compensation de Charge pour les verres contenant Al_2O_3, nous avons ajouté deux paramètres supplémentaires dans la fonction $\boldsymbol{\Delta G}_{\mathbf{MAl_xO_y}}$ correspondant à la formation d'une espèce à Charge Compensée telle que $\mathbf{CaAl_2O_4}$ ou $\mathbf{NaAlO_2}$. Cette modification simple du modèle correspond à un bon accord (en deçà des barres d'erreur expérimentales) avec la plupart des données de viscosité pour les systèmes ternaires et d'ordre supérieur contenant Al_2O_3.

A partir des données de viscosité et des études micrographiques disponibles pour les verres binaires MO_x-B_2O_3, il semble que la formation d'agrégats métastables d'apparence solide soit favorable dans ces verres binaires (MO_x = oxyde basique). Pour modéliser la formation de ces agrégats d'apparence solide dans la région vitreuse, nous avons employé des paramètres pour les énergies de Gibbs $\boldsymbol{\Delta G}_{\boldsymbol{m}(\mathbf{MB_xO_y})}$ de formation des agrégats et pour l'effet de taille des agrégats. Au total, cinq paramètres binaires sont utilisés pour reproduire les données de viscosité dans chaque système binaire oxyde basique-oxyde de bore : $A^{*}_{\mathrm{B(MO_x)}}$, $E^{*}_{\mathrm{B(MO_x)}}$, m, $\boldsymbol{\Delta G}_{\boldsymbol{m}(\mathbf{MB_xO_y})}$ et $\boldsymbol{E}_{\boldsymbol{m}(\mathbf{MB_xO_y})}$. La taille moyenne m d'un agrégat a été optimisée différemment suivant le verre binaire MO_x-B_2O_3. Aussi, les agrégats d'apparence solide sont modélisés à partir des données de viscosité pour les verres binaires MO_x-B_2O_3. Seuls les paramètres du modèle $\boldsymbol{A}_{\mathbf{B}}$, $\boldsymbol{E}_{\mathbf{B}}$, $\boldsymbol{T}_{\mathbf{B}}$ et $\boldsymbol{n}_{\mathbf{B}}$ pour B_2O_3 pur, et $\boldsymbol{T}_{\mathbf{AlO_{1.5}\text{-}B}}$ et $\boldsymbol{n}_{\mathbf{AlO_{1.5}\text{-}B}}$ pour le système binaire Al_2O_3-B_2O_3 ont été appliqués au modèle étendu pour reproduire le comportement en viscosité non-Arrhenien des systèmes contenant B_2O_3.

Les données de viscosité disponibles pour les sous-systèmes du système B_2O_3-CaO-MgO-Na_2O-K_2O-ZnO-PbO-Al_2O_3-SiO_2 ont été examinées. Nous démontrons que le modèle étendu reproduit bien le comportement complexe des données expérimentales pour les systèmes binaires et ternaires de la région vitreuse jusqu'à la région liquide, et prédit la viscosité de verres

multicomposants en deçà des barres d'erreur expérimentales. En particulier, le modèle étendu peut être utilisé pour obtenir de bonnes estimations de la viscosité de verres multicomposants, de magmas, de laves et de verres commerciaux. Nous pensons que ce modèle étendu reproduit en deçà des barres d'erreur expérimentales non seulement la dépendance en température mais aussi la dépendance en composition des données de viscosité disponibles, de la région vitreuse jusqu'à la région liquide.

Le modèle étendu s'applique sur la gamme de température complète allant de la région vitreuse jusqu'à la région liquide. Pour la région liquide, le modèle non étendu est légèrement supérieur au modèle étendu. En résumé, le modèle de viscosité reproduit maintenant toutes les données de viscosité disponibles pour les liquides et les verres relatifs au système MF_x–SiO_2–B_2O_3–Al_2O_3–CaO–MgO–Na_2O–K_2O–PbO–ZnO–MnO–TiO_y (M = Ca, Mg, Na, K et Al) en deçà des barres d'erreur expérimentales, à toute composition et sur la gamme de température allant de 300^{o}C à 2000^{o}C.

ABSTRACT

Recently, a new viscosity model was developed in this laboratory to reproduce the viscosity of single-phase oxide melts for the system CaO-MgO-K_2O-Na_2O-Al_2O_3-SiO_2-B_2O_3[27, 81, 82]. In this model, the viscosity is related to the structure of the melt characterized by the amounts and connectivity of Q^i-species. The structure in turn is calculated from the thermodynamic description of the melt using the Modified Quasichemical Model[231, 232] and the FactSage thermodynamic database[14]. Most importantly, the model takes into account the formation of a silicate or borate network which has a profound effect on the viscosity using the connectivity of Q^i-species.

The viscosity model for the systems MO_x, MO_x-SiO_2, MO_x-B_2O_3 and B_2O_3-SiO_2 (M = Basic oxides) was developed, and a few unary and binary parameters with Arrhenian temperature dependence were simultaneously obtained from assessments of the viscosity data of all available binary and ternary melts. For each Al_2O_3-containing ternary system MO_x–Al_2O_3–SiO_2 exhibiting the Charge Compensation Effect (where Al^{3+} assumes a tetrahedral coordination and enters the silica network with a basic cation M staying close to Al^{3+} to compensate the missing charge) the model incorporates two additional ternary parameters. The viscosity of multi-component melts CaO-MgO-K_2O-Na_2O-Al_2O_3-SiO_2-B_2O_3 [27, 81, 82] was then predicted by the model without any additional adjustable model parameters and is in good agreement with available measurements within experimental error limits.

However, the model could not reproduce the complex behavior of the viscosity data measured in the alkali-rich side of $MO_{0.5}$-SiO_2 melts and multi-component melts containing alkali oxides. In the present work, the model is modified to reproduce the complex behavior of the viscosity on the alkali-rich side of the alkali-silica systems. This behavior is attributed to ring clusters formed by Q^2- and Q^3-species. An excess contribution to the viscosity due to polymerization of Q^2- and Q^3-species into large rings is taken into account by the introduction of one additional binary parameter $E^{Ring}_{MO_x\text{-}Si}$ for each alkali-silica system.

Also in the present work, with the modified model, the viscosity of molten slags containing PbO, ZnO, MnO and TiO_x have been reviewed and modeled. In order to reproduce the viscosity of the silicate melts, only 6 model parameters related to each oxide MO_x (M = Pb, Zn,

Mn) are required. Two parameters, $\boldsymbol{A}_{\mathrm{MO}_x}$ and $\boldsymbol{E}_{\mathrm{MO}_x}$, describe the viscosity of pure liquid MO_x; two binary parameters, $\boldsymbol{E}^{1,1}_{\mathrm{MO}_x\text{-Si}}$ and $\boldsymbol{E}^{\boldsymbol{R}}_{\mathrm{MO}_x\text{-Si}}$, describe the viscosity of each MO_x -SiO_2 melt; and, finally, two more parameters represent the Gibbs energy, $\Delta\boldsymbol{G}_{\mathrm{MAl_2O_4}}$, of formation of tetrahedrally-coordinated Al "species" which enter the silica network and are charge-compensated by M. The latter two parameters are obtained from the experimental viscosities of MO_x-Al_2O_3-SiO_2 melts. The viscosity of multicomponent melts containing MO_x is then predicted by the model without any additional adjustable model parameters.

Silicate melts containing TiO_x required four parameters, $\boldsymbol{A}_{\mathrm{TiO_2}}$, $\boldsymbol{A}_{\mathrm{TiO_{1.5}}}$, $\boldsymbol{E}_{\mathrm{TiO_2}}$ and $\boldsymbol{E}_{\mathrm{TiO_{1.5}}}$ which describe the viscosity of pure liquid TiO_2 and $TiO_{1.5}$; and four binary parameters, $\boldsymbol{E}^{1,1}_{\mathrm{TiO_2\text{-}Si}}$, $\boldsymbol{E}^{\boldsymbol{R}}_{\mathrm{TiO_2\text{-}Si}}$, $\boldsymbol{E}^{1,1}_{\mathrm{TiO_{1.5}\text{-}Si}}$ and $\boldsymbol{E}^{\boldsymbol{R}}_{\mathrm{TiO_{1.5}\text{-}Si}}$ which describe the viscosity of TiO_2-SiO_2 and $TiO_{1.5}$-SiO_2 melts. No viscosity data were available to account for the Charge Compensation Effect among TiO_x, Al_2O_3 and MO_x (TiO_2-Al_2O_3 and Ti_2O_3-MO_x), where M is a basic oxide, and thus no model parameters were applied for the Charge Compensation Effect. The viscosity of multicomponent melts containing TiO_2 and Ti_2O_3 is then predicted by the model without any additional adjustable model parameters.

To test the model, available experimental viscosity data of all sub-systems of the SiO_2–Al_2O_3–CaO–MgO–Na_2O–K_2O–PbO–ZnO–MnO–TiO_x system were collected and used to calibrate the model. The deviation of the available experimental data from the viscosities predicted by the model does not exceed the scatter of experimental points among different authors. In particular, the model predicts the viscosity of multicomponent silicate melts and commercial glass melts with an accuracy similar to the accuracy of the regression equations which were fitted to the experimental data over the narrow composition ranges of these melts.

The model is also extended in the present work to describe and predict the viscosities of oxy-fluoride melts containing MF_x (M = Ca, Mg, Na, K and Al). A simple solution database using a polynomial solution model with Gibbs energies of each pure liquid oxide and fluoride was developed to roughly calculate the overall "equilibrated composition" from given initial compositions of oxy-fluoride melts. Structural roles of MF_x (M = Ca, Mg, Na, K and Al) are reviewed and regarded as network modifiers in silicate or borate melts and simply approximated

to have the same breaking effects on silicate or borate networks as basic oxides containing the same cations.

The viscosity model for the system MF_x, MF_x-SiO_2 and MF_x-B_2O_3 (M = Ca, Mg, Na, K and Al) was developed and a few unary and binary parameters were simultaneously obtained from viscosity data of all available binary and ternary melts. No charge compensation effect between MF_x and Al_2O_3 was observed, and thus the model reproduces the experimental data for binary and ternary melts without any applying charge compensation effect between MF_x and Al_2O_3. In addition to the two model parameters that are required for each MF_x-B_2O_3 melt, where MF_x is a basic fluoride, the further parameters $\Delta G_{m(MB_4FO_6)}$, $E_{m(MB_4FO_6)}$ and m are needed when MF_x is an alkali fluoride to account for the formation of clusters near the tetraborate composition. The additional parameters represent the size and Gibbs energy of formation of these clusters and their contribution to the activation energy of the viscous flow. The available viscosity data for all sub-systems of MF_x–SiO_2–B_2O_3–Al_2O_3–CaO–MgO–Na_2O–K_2O–PbO–MnO–TiO_y melts (M = Ca, Mg, Na, K and Al) are reviewed. The viscosity of multicomponent melts and of ternary melts MF_x–NO_y–SiO_2, where MF_x and NO_y are basic fluorides and oxides, is predicted by the model solely from the unary, binary and ternary parameters. The deviation from the available experimental data does not exceed the scatter of the experimental measurements and experimental error limits. The predictive ability of the model has been further tested on several industrial mold flux melts and is believed to be in good agreement with the viscosity data within experimental error limits.

The developed model with Arrhenian temperature dependence for the viscosity of oxy-fluoride melts is further extended in the present work to take into account non-Arrhenian temperature dependence of the viscosity data measured from the glass to the melt regions. Using data for all available sub-systems of the CaO-MgO-Na_2O-K_2O-ZnO-PbO-Al_2O_3-B_2O_3-SiO_2 system, the values of unary and binary model parameters $\boldsymbol{A}_{\mathbf{MO_x}}$, $\boldsymbol{E}_{\mathbf{MO_x}}$, $E^{R}_{\mathrm{MO_x}-\mathrm{Si}}$ and $E^{i.j}_{\mathrm{MO_x}\text{-}\mathrm{Si}}$ were re-optimized simultaneously with the addition of the non-Arrhenian unary and binary parameters $\boldsymbol{T}_{\mathbf{MO_x}}$, $\boldsymbol{n}_{\mathbf{MO_x}}$, $\boldsymbol{m}_{\mathbf{MO_x\text{-}Si}}$, $\boldsymbol{T}_{\mathbf{MO_x\text{-}Si}}$ and $\boldsymbol{n}_{\mathbf{MO_x\text{-}Si}}$ (M = Ca, Mg, Pb, Zn and Al). In order to take into account the Charge Compensation Effect for glasses containing Al_2O_3, two more parameters were added to the function of $\boldsymbol{\Delta G}_{\mathbf{MAl_xO_y}}$ for the formation of Charge Compensated species such as

$\mathbf{CaAl_2O_4}$ or $\mathbf{NaAlO_2}$. This simple modification of the model results in a good agreement with most of the viscosity data of ternary and high-order systems containing Al_2O_3 within experimental error limits.

From available viscosity data and micrographic studies for binary MO_x-B_2O_3 glasses, metastable solid-like clusters seem to form favorably in the binary MO_x-B_2O_3 glasses (M = Basic Oxides). In order to model the formation of these solid-like clusters in the glass region, we employed parameters for the Gibbs energies $\boldsymbol{\Delta G_{m(MB_xO_y)}}$ of formation of clusters and for the size effect of clusters. A total of five binary parameters are used to reproduce the viscosity data in each basic oxide-boron oxide binary system: $A^*_{B(MO_x)}$, $E^*_{B(MO_x)}$, m, $\boldsymbol{\Delta G_{m(MB_xO_y)}}$ and $\boldsymbol{E_{m(MB_xO_y)}}$. The average size of the cluster, m, was optimized differently according to the binary MO_x-B_2O_3 glass. Also, the solid-like clusters are modeled according to the viscosity data of the binary MO_x-B_2O_3 glasses. Only the model parameters $\boldsymbol{A_B}$, $\boldsymbol{E_B}$, $\boldsymbol{T_B}$ and $\boldsymbol{n_B}$ for pure B_2O_3 ,and $\boldsymbol{T_{AlO_{1.5}\text{-}B}}$ and $\boldsymbol{n_{AlO_{1.5}\text{-}B}}$ for the binary Al_2O_3-B_2O_3 system were applied to the extended model to reproduce the non-Arrhenian viscosity behavior of the systems containing B_2O_3.

The available viscosity data for the sub-systems of the B_2O_3-CaO-MgO-Na_2O-K_2O-ZnO-PbO-Al_2O_3-SiO_2 system have been reviewed. It is demonstrated that the extended model reproduces well the complex behavior of the experimental data for the binary and ternary systems from the glass region to the melt region and predicts the viscosities of multi-component glasses within experimental error limits. In particular, the extended model can be used to provide good estimates of the viscosities of multicomponent glasses, magmas, lavas and commercial glasses. Most importantly, the extended model is believed to reproduce not only the temperature dependence but also composition dependence of available viscosity data within experimental error limits from the glass to the melt region.

The extended model applies over the entire temperature range from the glass region to the melt region. For the melt region, the unextended model is slightly superior to the extended model.

In summary, the viscosity model now reproduces all available viscosity data for melts and glasses for the system MF_x–SiO_2–B_2O_3–Al_2O_3–CaO–MgO–Na_2O–K_2O–PbO–ZnO–MnO–TiO_y

(M = Ca, Mg, Na, K and Al) within experimental error limits at all compositions and over the temperature range from 300 to 2000ºC.

CONDENSÉ EN FRANÇAIS

Une compréhension des phénomènes impliqués dans les procédés métallurgiques et une optimisation de ces procédés requiert l'accès à des données précises pour les propriétés physiques des laitiers liquides et des verres impliqués. Parmi ces propriétés physiques telles la viscosité, la tension de surface, la conductivité thermique,…, l'une des propriétés physiques les plus importantes dans le cas de laitiers liquides et de verres est la viscosité. Une connaissance précise de la viscosité d'une grande variété de laitiers liquides est indispensable pour un certain nombre de disciplines scientifiques fondamentales et appliquées. En métallurgie, les liquides à base de silice sont appelés laitiers. La connaissance de la viscosité du laitier est importante pour l'opération des hauts fourneaux et aussi pour le procédé d'affinage de l'acier. Les laitiers sont de plus utilisés comme flux de moule lors du procédé de coulée en continu, où la viscosité des laitiers a une importance considérable. Lors du procédé de coulée en continu propre à la production de l'acier, la viscosité d'un laitier a une influence sur la vitesse d'écoulement du laitier qui contrôle le transfert de masse à l'interface laitier/métal. Cette viscosité devrait être suffisamment faible de façon à assurer une lubrification suffisante (empêchant ainsi le collage), un transfert de chaleur uniforme contrôlé et la prévention de fissures de surface.

La viscosité des liquides à base de silice est aussi un paramètre fondamental pour l'industrie des verres et pour les procédés géologiques impliquant l'écoulement de liquides magmatiques. Il est bien connu qu'il se forme un verre lorsque des liquides à base de silice sont refroidis suffisamment rapidement pour éviter la cristallisation.[6, 7, 47, 49] En métallurgie, les liquides surfondus à base de silice sont appelés verres. En particulier, la viscosité des laitiers liquides est très élevée et la cristallisation de tels liquides (*i.e.* très visqueux) se produit très difficilement. La viscosité d'un verre est importante pour les conditions de fusion et d'affinage dans les fours de verrerie. Dans le procédé de fabrication des verres, il y a plusieurs points critiques largement influencés par la viscosité du verre.

Lors du refroidissement de liquides à base de silice, la viscosité augmente et s'approche de 4 dans l'échelle logarithmique en poise. Ceci s'appelle la température de mise en forme. Une fois que le verre est formé, il devrait être soutenu jusqu'à ce que sa viscosité atteigne une valeur suffisamment élevée (au dessus de 7.6 dans l'échelle logarithmique en poise) pour éviter une

déformation du verre sous son propre poids. Le domaine de température entre ces deux points constitue le domaine de mise en forme. Des domaines de viscosité élevés (entre 12 et 13 dans l'échelle logarithmique en poise) correspondent à des domaines de température importants où le recuit permet de relâcher la contrainte interne du verre.

Ainsi, de nombreux géologues, verriers et métallurgistes ont développé des modèles de viscosité pour tenir compte de la dépendance en composition et en température de la viscosité de laitiers liquides et de verres. [2, 67, 73, 77, 107, 139, 201, 249, 334, 336, 344, 359, 360] La plupart de ces modèles ont été développés comme des modèles empiriques ou numériques ne pouvant pas prendre en compte la structure des liquides à base de silice. La plupart de ces modèles s'appliquent seulement à quelques systèmes binaires, ternaires et multicomposants, et de nombreux paramètres ont été nécessaires pour calculer la viscosité de liquides multicomposants à base de silice malgré une précision du modèle peu satisfaisante. Récemment, de nombreux efforts ont été fournis pour tenter de développer un modèle de viscosité structural basé sur l'information structurale des liquides à base de silice, pouvant être calculée à partir de modèles thermodynamiques tels que le Modèle Quasichimique Modifié de Pelton et Blander[230] et le Modèle des Cellules de Kapoor et Frohberg[115]. Malgré de nombreuses tentatives pour calculer avec précision la viscosité de laitiers liquides et de verres, aucun modèle développé n'a permis de prédire de manière satisfaisante la viscosité de liquides multicomposants à base de silice sur une large gamme de compositions et de températures.

Dans la présente étude, les données de viscosité disponibles sont examinées pour tous les sous-systèmes du système liquide MF_x–SiO_2–B_2O_3–Al_2O_3–CaO–MgO–Na_2O–K_2O–PbO–MnO–TiO_y (M = Ca, Mg, Na, K et Al) et du système de verre SiO_2–B_2O_3–Al_2O_3–CaO–MgO–Na_2O–K_2O–PbO–ZnO. Les données considérées comme les plus fiables sont extraites et comparées aux viscosités calculées à l'aide du modèle. Puisque la viscosité des liquides à base de silice de la région liquide jusqu'à la région vitreuse peut varier sur plus de 15 ordres de grandeur (0 à 10^{15} poise) les techniques expérimentales doivent être différentes suivant la gamme de viscosité, et ainsi d'autres considérations expérimentales telles que la préparation des échantillons, l'analyse chimique et la mesure de température devraient être évaluées avec précaution à partir de la littérature.

Les difficultés associées aux mesures de la viscosité de verres et de liquides sur une large gamme de température proviennent de la présence simultanée des conditions suivantes [212, 339]:

- une très large gamme de viscosités à mesurer;
- les faibles propriétés de conduction thermique du liquide;
- la présence inévitable de petites bulles dans le liquide;
- les inhomogénéités de température dans la zone du viscosimètre réservée à l'échantillon;
- la difficulté pour tremper l'échantillon;
- les phénomènes de cristallisation au cours de l'expérience.

Un viscosimètre rotatif est très adapté aux mesures de la viscosité d'un liquide dans ces conditions. Le domaine optimal pour un viscosimètre rotatif est de -1 à 5 dans l'échelle logarithmique en poise ($\ln(\eta$ / Pa·s) de -4 à 9). Les nombreuses sources d'erreurs systématiques liées à l'utilisation de ce type de viscosimètre et aux mesures de viscosité des liquides d'oxydes en général sont discutées par exemple dans les références [339] et [190]. Lors de mesures de viscosité effectuées par certains des meilleurs laboratoires dans le cadre d'un projet "en rond" [190] en utilisant les mêmes matériaux de référence, la dispersion moyenne des données obtenues par ces différents laboratoires était d'environ 20%. La précision moyenne des données n'est probablement pas meilleure que 50% lorsque les incertitudes relatives à la préparation des échantillons et à leur pureté sont prises en compte.

Dans les liquides oxy-fluorés, les difficultés intrinsèques associées aux mesures de la viscosité de liquides fluorés sur une large gamme de température sont les suivantes:

e.g. $MF_x = CaF_2$

- la perte d'ions fluorure par formation de HF(g) à cause de la présence d'humidité;

$$\mathbf{\underline{CaF_2}(liquid)+H_2O(gas)=\underline{CaO}(liquid)+2HF(gas)}$$

- la perte d'ions fluorure par formation d'une phase gazeuse telle que SiF_4(g) à cause de la volatilité élevée des ions fluorure;

$2\underline{CaF_2}(liquid)+\underline{SiO_2}(liquid)=2\underline{CaO}(liquid)+SiF_4(gas)$

- la forte réactivité du liquide avec les creusets.
- les difficultés d'analyse chimique de chaque constituant des liquides oxy-fluorés.

Ainsi, lorsque l'on considère les difficultés ci-dessus, la précision des mesures de viscosité pour les liquides oxy-fluorés serait très inférieure à la précision des mesures de viscosité pour les liquides d'oxydes.

Pour les mesures de viscosité dans la région vitreuse, la plupart des expériences ont été réalisées à l'aide des méthodes d'élongation de fibre, de pénétration de bille et de micro-pénétration. Les gammes de viscosité applicables pour chacune de ces méthodes sont les suivantes[51, 223, 323]:

- Méthode d'élongation de fibre : viscosité de 7 à 16 dans l'échelle log poise
- Méthode de pénétration de bille : viscosité de 9 à 13 dans l'échelle log poise
- Méthode de micro-pénétration : viscosité de 9 à 13 dans l'échelle log poise
- Méthode de courbure de poutre : viscosité de 6 à 13 dans l'échelle log poise

La mesure de viscosités élevées à des températures plus basses est beaucoup plus difficile que la mesure de faibles viscosités à cause d'une forte tendance à cristalliser au cours de l'expérience. L'aptitude à former un verre peut être prise en compte à l'aide du taux critique de refroidissement du système. Si l'échantillon est trempé plus rapidement que le taux critique de refroidissement, l'échantillon reste à l'état vitreux. Cabral *et al.*[28] ont étudié de façon systématique l'effet de CaO sur le taux critique de refroidissement par ajout de CaO au système Na_2O-SiO_2. Ils ont rapporté que, lors de l'ajout de 33 % mol de CaO, le taux critique de refroidissement du système Na_2O-CaO-SiO_2 était 20 fois plus élevé que celui du système Na_2O-SiO_2[28]. Shelby[285] a également observé dans le cas du système CaO-Al_2O_3-SiO_2 une augmentation de la température de transition vitreuse (T_g) lors d'une augmentation du rapport molaire Al_2O_3/CaO à teneur en SiO_2 constante et lors d'une diminution de la teneur en SiO_2 dans la gamme de composition 5-60 % mol SiO_2 à rapport molaire Al_2O_3/CaO constant. En dessous de la température de transition vitreuse (T_g), le verre (liquide surfondu) se comporte comme un

solide, ce qui causerait une augmentation abrupte de la viscosité. Cela implique qu'un système ayant des teneurs élevées en CaO et en Al_2O_3 aurait de grosses sources d'erreur pour les mesures de viscosité suite à une forte tendance à cristalliser. Si la cristallisation commence durant l'expérience, la viscosité dépendra du temps et donc elle pourrait être significativement différente suivant la durée de l'expérience. De plus, un échantillon de viscosité élevée aurait de faibles propriétés de conduction thermique et cela induirait de grosses sources d'erreur pour la détermination de la viscosité à la température désirée. Pour calibrer et tester le modèle de viscosité proposé, nous avons rassemblé les données expérimentales de viscosité pour le système Al_2O_3–B_2O_3–CaO–MgO–FeO–Fe_2O_3–MnO–NiO–PbO–ZnO–Na_2O–K_2O–TiO_2–Ti_2O_3–SiO_2–F et ses sous-systèmes (liquides), et pour le système Al_2O_3–B_2O_3–CaO–MgO–ZnO–PbO–Na_2O–K_2O–SiO_2 et ses sous-systèmes (verres). A partir de l'analyse critique de toutes les données disponibles issues de la littérature incluant la banque de données Sci-Glass[274], nous pouvons conclure que la plupart des données fiables mesurées par les meilleurs laboratoires présentent pour les mesures de viscosité une incertitude absolue moyenne comprise entre 0.25 et 0.5 (dans une échelle logarithmique en poise) pour les liquides et comprise entre 1 et 2 (dans une échelle logarithmique en poise) pour les verres.

Récemment, un nouveau modèle de viscosité a été développé dans ce laboratoire pour des laitiers liquides relatifs au système CaO-MgO-K_2O-Na_2O-Al_2O_3-SiO_2-B_2O_3[27, 81, 82]. Dans ce modèle, la viscosité est liée à la structure du laitier, caractérisée par les concentrations et la connectivité des espèces Q^i. Les changements structuraux se produisant lors de la formation des réseaux de SiO_2 et B_2O_3 sont mieux caractérisés par le concept des espèces Q^i[199]. Dans la notation Q^i, l'exposant i correspond au nombre de ponts oxygène par atome Si ou par atome B. Dans SiO_2 pur, les quatre oxygènes entourant chaque atome Si sont des oxygènes pontants. Ainsi la fraction des espèces Q^4 est de 1. Un cation silicium dans une chaine est une espèce Q^2 puisque deux de ses quatre oxygènes voisins sont des oxygènes pontants. Lin et Pelton[289] ont montré comment calculer le nombre de monomères, dimères, trimères etc. par mole de solution en utilisant les fractions molaires de O^{2-}, O^- et O^o. Les fractions des espèces Q^i peuvent être calculées de manière similaire. Le Modèle Quasichimique Modifié[231, 232] et la banque de données thermodynamiques optimisée de FactSage[15] peuvent être utilisés pour calculer en fonction de la température et de la composition les nombres de paires seconds-voisins M-M, M-

Si et Si-Si, qui correspondent aux fractions d'oxygènes libres, d'oxygènes non pontants et d'oxygènes pontants, respectivement. Pour chaque système ternaire MO_x–Al_2O_3–SiO_2 à base de Al_2O_3 pour lequel a lieu un Effet de Compensation de Charge (où Al^{3+} occupe une coordination tétraédrique et s'insère dans le réseau de silice avec un cation basique M restant au voisinage de Al^{3+} pour compenser la charge manquante) le modèle comprend deux paramètres ternaires supplémentaires. La viscosité de liquides multicomposants est ensuite prédite par le modèle sans l'ajout de paramètres ajustables supplémentaires. A l'aide de quelques paramètres unaires, binaires et ternaires, le modèle a pu reproduire en deçà des barres d'erreur expérimentales les données de viscosité mesurées dans le liquide pour la plupart des sous-systèmes du système CaO-MgO-K_2O-Na_2O-Al_2O_3-SiO_2-B_2O_3[27, 81, 82] à l'exception des systèmes à base d'oxydes alcalins.

Des difficultés expérimentales intrinsèques sont rencontrées lors des mesures de viscosité pour les laitiers riches en oxydes alcalins à cause de la volatilité des alcalins, de la réactivité du liquide, et surtout de la contamination des échantillons liée à la très forte hygroscopie des liquides et à la forte tendance des liquides produits à partir de carbonates de retenir CO_2. Les données expérimentales dans cette région sont rares et très dispersées. Même des données de différents auteurs apparemment en accord peuvent être sujettes à une erreur systématique substantielle si les échantillons sont contaminés d'une manière similaire. En particulier, pour le système $NaO_{0.5}$–SiO_2, plusieurs auteurs ont rapporté une brusque diminution de viscosité pour une fraction molaire de SiO_2 inférieure à 0.5, bien que d'autres auteurs n'aient pas observé un tel comportement [143]. Si les courbes de viscosité expérimentales sont extrapolées jusqu'à $NaO_{0.5}$ pur, une viscosité exagérément basse est obtenue à moins que les courbes de viscosité ne présentent une seconde inflection conduisant à une courbe en forme de S. Bien que l'on puisse s'attendre à une chute de viscosité similaire dans la région basique du système CaO–SiO_2, un tel phénomène n'a jamais été observé. Pour garder la simplicité du modèle, nous avons initialement ignoré toutes les expériences correspondant à une fraction molaire de silice inférieure à 0.5 et nous n'avons pas tenté de modéliser cette chute de viscosité[82]. Cependant, lors de l'application du modèle initial à de nombreux systèmes multicomposants, nous avons trouvé des données expérimentales supplémentaires suggérant un comportement complexe de la viscosité dans la région riche en oxyde alcalin des systèmes $MO_{0.5}$–SiO_2. Certaines de ces publications

comportaient plus de détails sur les conditions expérimentales, et des résultats similaires étaient rapportés pour des échantillons étudiés dans des atmosphères différentes (où la contamination des échantillons devrait être différente). Etant donnée l'abondance de preuves expérimentales, le modèle proposé précédemment [81, 82] est étendu dans la présente étude pour reproduire le comportement complexe de la viscosité dans la région riche en oxyde alcalin des systèmes $MO_{0.5}$–SiO_2. Ce comportement est attribué aux agrégats en forme d'anneaux formés par les espèces Q^2 et Q^3. L'ajout d'un paramètre binaire supplémentaire $E^{Ring}_{MO_x\text{-Si}}$ pour chaque système oxyde alcalin-silice permet de prendre en compte la contribution en excès à la viscosité due à la polymérisation des espèces Q^2 et Q^3 sous la forme d'anneaux de grande taille. Le modèle comporte des paramètres unaires décrivant la viscosité des oxydes liquides purs et seulement deux paramètres binaires ($E^{R}_{MO_x-Si}$ et $E^{1,1}_{MO_x\text{-Si}}$) pour la plupart des systèmes binaires MO_x–SiO_2 lorsque M n'est pas un alcalin. Pour chaque système oxyde alcalin-silice, un paramètre binaire supplémentaire ($E^{Ring}_{MO_x\text{-Si}}$) est requis. Le modèle comprend deux paramètres ternaires additionnels pour chaque système ternaire MO_x–Al_2O_3–SiO_2 à base de Al_2O_3 pour lequel a lieu un Effet de Compensation de Charge (où Al^{3+} occupe une coordination tétraédrique et s'insère dans le réseau de silice avec un cation basique M restant au voisinage de Al^{3+} pour compenser la charge manquante). La viscosité de laitiers multicomposants est ensuite prédite par le modèle sans l'ajout de paramètres ajustables supplémentaires. Les données de viscosité disponibles pour les sous-systèmes à base d'oxydes alcalins du système Al_2O_3–CaO–MgO–Na_2O–K_2O–SiO_2 ont été examinées. Nous démontrons que le modèle reproduit les données expérimentales pour les liquides binaires et ternaires et prédit les viscosités des liquides multicomposants en deçà des barres d'erreur expérimentales. En particulier, le modèle peut être utilisé pour obtenir de bonnes estimations de la viscosité de verres, de magmas et de laves multicomposants.

Dans la présente étude, la viscosité de laitiers liquides contenant PbO, ZnO, MnO et TiO_x a été révisée à l'aide du modèle modifié. Seulement 6 paramètres du modèle liés à chaque oxyde MO_x (M = Pb, Zn, Mn) sont requis pour reproduire la viscosité de liquides à base de silice. Deux paramètres ($\boldsymbol{A}_{MO_x}$ et $\boldsymbol{E}_{MO_x}$) décrivent la viscosité du liquide pur MO_x; deux paramètres binaires ($\boldsymbol{E}^{1,1}_{MO_x\text{-Si}}$ et $\boldsymbol{E}^{\boldsymbol{R}}_{MO_x\text{-Si}}$) décrivent la viscosité de chaque liquide MO_x - SiO_2; et finalement deux paramètres supplémentaires représentent l'énergie de Gibbs $\Delta\boldsymbol{G}_{MAl_2O_4}$ des "espèces" Al de

coordination tétraédrique entrant dans le réseau de silice avec une compensation de charge due au cation M. Ces deux paramètres supplémentaires sont obtenus à partir des viscosités expérimentales des liquides MO_x-Al_2O_3-SiO_2. La viscosité de laitiers multicomposants contenant MO_x est ensuite prédite par le modèle sans l'ajout de paramètres ajustables supplémentaires.

Les liquides à base de silice contenant TiO_x ont requis quatre paramètres ($\boldsymbol{A}_{TiO_2}$, $\boldsymbol{A}_{TiO_{1.5}}$, $\boldsymbol{E}_{TiO_2}$ et $\boldsymbol{E}_{TiO_{1.5}}$) décrivant la viscosité des liquides purs TiO_2 et $TiO_{1.5}$, et quatre paramètres binaires ($\boldsymbol{E}^{1,1}_{TiO_2\text{-}Si}$, $\boldsymbol{E}^{\boldsymbol{R}}_{TiO_2\text{-}Si}$, $\boldsymbol{E}^{1,1}_{TiO_{1.5}\text{-}Si}$ et $\boldsymbol{E}^{\boldsymbol{R}}_{TiO_{1.5}\text{-}Si}$) décrivant la viscosité des liquides TiO_2-SiO_2 et $TiO_{1.5}$-SiO_2. A partir de la revue critique de toutes les données expérimentales disponibles, nous pensons que l'ajout de TiO_2 ou Ti_2O_3, de même que d'autres oxydes basiques, diminue la viscosité d'un liquide. Aucune donnée de viscosité n'était disponible pour rendre compte de l'Effet de Compensation de Charge entre TiO_x, Al_2O_3 et MO_x (TiO_2-Al_2O_3 et Ti_2O_3-MO_x), où MO_x est un oxyde basique, et ainsi aucun paramètre du modèle n'a été ajouté pour cet Effet de Compensation de Charge. La viscosité de laitiers multicomposants contenant TiO_2 et Ti_2O_3 est ensuite prédite par le modèle sans l'ajout de paramètres ajustables supplémentaires.

En guise de test du modèle, les données de viscosité expérimentales disponibles pour tous les sous-systèmes de SiO_2–Al_2O_3–CaO–MgO–Na_2O–K_2O–PbO–ZnO–MnO–TiO_x ont été rassemblées et utilisées pour calibrer le modèle. L'écart entre les mesures et les viscosités prédites par le modèle n'excède pas la dispersion des points expérimentaux des différents auteurs. En particulier, le modèle prédit la viscosité de laitiers multicomposants à base de silice et de verres commerciaux avec une précision comparable à celle des équations de régression obtenues à partir des données expérimentales sur les gammes de composition restreintes de ces liquides.

Le modèle décrivant la viscosité de systèmes d'oxydes liquides a été étendu dans la présente étude pour décrire et prédire la viscosité de liquides oxy-fluorés contenant MF_x (M = Ca, Mg, Na, K et Al). Les rôles structuraux de MF_x (M = Ca, Mg, Na, K et Al) sont examinés, et MF_x est considéré comme un modificateur de réseau dans les liquides à base de silice ou d'oxyde de bore, avec des effets de rupture du réseau que nous avons simplement supposés identiques à ceux des oxydes basiques contenant le même cation M.

Le modèle étendu pour les liquides oxy-fluorés contenant MF_x (M = Ca, Mg, Na, K et Al) a été développé avec les caractéristiques suivantes :

- MF_x (M = Ca, Mg, Na, K et Al) se comporterait comme un modificateur de réseau dans les liquides à base de silice ou d'oxyde de bore comme cela a été modélisé pour les autres oxydes basiques dans les Chapitres 3 et 4.
- Les "compositions équilibrées" des liquides oxy-fluorés sont calculées à partir des énergies de Gibbs des liquides purs d'oxydes et de fluorures. Ensuite, la fraction molaire X calculée pour chaque liquide d'oxyde et de fluorure est donnée aux équations du modèle développées dans les Chapitres 3 et 4. Il faut noter que la formation de SiF_4 et BF_3 dans les liquides n'est pas considérée. Nous supposons que tous les atomes de Si et B sont liés seulement à des atomes d'oxygène.
- Les constituants MF_x (M = Ca, Mg, Na, K et Al) auraient les mêmes effets de rupture des réseaux de silice ou d'oxyde de bore que les oxydes basiques contenant le même cation. (Note : chaque fluorure et chaque oxyde devraient contenir le même cation). Ainsi, tous les fluorures sont considérés comme des oxydes contenant le même cation seulement pour calculer toutes les paires seconds-voisins possibles du système et la probabilité *p* qu'une paire particulière émane d'un atome Si ou B donné à l'aide de la présente banque de données thermodynamiques[15].

  Les effets de rupture des réseaux de silice assurés par CaO et CaF_2 sont les suivants :

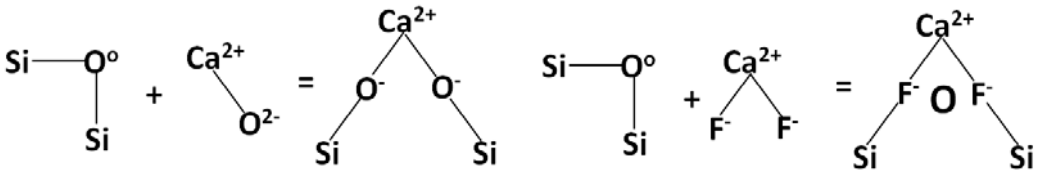

- Les viscosités des systèmes binaires MF_x-SiO_2 et MF_x-B_2O_3 ont été modélisées avec le même type de paramètres unaires et binaires que ceux utilisés dans le modèle des Chapitres 3 et 4.
- Dans le système fluorure alcalin-oxyde de bore NF-B_2O_3 (N = Na et K), la formation d'agrégats d'apparence solide tels que $5(NaB_4FO_6)$ et $5(KB_4FO_6)$ a été modélisée à l'aide des mêmes équations du modèle que celles développées dans le Chapitre 3.

Un modèle de viscosité a été développé pour les systèmes MF_x, MF_x-SiO_2 et MF_x-B_2O_3 (M = Ca, Mg, Na, K et Al), et quelques paramètres unaires et binaires ont été obtenus simultanément à partir des données de viscosité disponibles pour tous les liquides binaires et ternaires. Aucun effet de compensation de charge n'a été observé entre MF_x et Al_2O_3, et ainsi le modèle reproduit les données expérimentales pour les liquides binaires et ternaires sans appliquer d'effet de compensation de charge entre MF_x et Al_2O_3. En plus des deux paramètres du modèle requis pour chaque liquide MF_x-B_2O_3 (où MF_x est un fluorure basique), $\Delta G_{m(MB_4FO_6)}$, $E_{m(MB_4FO_6)}$ et m sont nécessaires lorsque MF_x est un fluorure alcalin de façon à rendre compte de la formation d'agrégats au voisinage de la composition du tétraborate. Ces paramètres supplémentaires représentent la taille et l'énergie de Gibbs de formation des agrégats ainsi que leur contribution à l'énergie d'activation d'écoulement visqueux.

A partir des données de viscosité disponibles impliquant MF_x (M = Ca, Mg, Na, K et Al), tous les paramètres unaires et binaires A_{MF_x}, E_{MF_x}, $\boldsymbol{E}^{1,1}_{MF_x\text{-}Si}$, $\boldsymbol{E}^{\boldsymbol{Ring}}_{MF_x\text{-}Si}$, $\boldsymbol{E}^{\boldsymbol{R}}_{MF_x\text{-}Si}$, $\boldsymbol{A}^{*}_{B(MF_x)}$ et $\boldsymbol{E}^{*}_{B(MF_x)}$ ont été optimisés simultanément de façon à reproduire en deçà des barres d'erreur expérimentales les données de viscosité disponibles à l'aide du modèle de viscosité étendu avec la composition globale d'"équilibre" calculée à partir des énergies de Gibbs des liquides purs d'oxydes et de fluorures. Dans la présente étude, la viscosité de tous les sous-systèmes de MF_x–SiO_2–B_2O_3–Al_2O_3–CaO–MgO–Na_2O–K_2O–MnO–TiO_y (M = Ca, Mg, Na, K et Al) a été analysée de manière critique et prédite par le modèle seulement à partir des paramètres du modèle unaires, binaires et ternaires. L'écart entre les mesures disponibles et les viscosités calculées n'excède pas la dispersion des points expérimentaux et les barres d'erreur expérimentales.

La capacité de prédiction du modèle a également été testée sur plusieurs liquides de flux de moule industriels, et nous pensons qu'elle est satisfaisante compte tenu des incertitudes expérimentales des données de viscosité. En général, le présent modèle prédit très bien la variation en composition de la viscosité.

La très bonne capacité de prédiction du présent modèle rend relativement aisé l'ajout d'un nouveau composant MF_x au système chimique décrit par ce modèle. La viscosité de liquides multicomposants contenant ce nouveau composant peut être évaluée sans avoir besoin de mesurer ni de reproduire la viscosité de liquides multicomposants au voisinage de compositions

spécifiques d'intérêt. Tous les paramètres du modèle nécessaires peuvent être obtenus à partir des données expérimentales pour les liquides MF_x–SiO_2 et MF_x–B_2O_3, de même qu'à partir de la viscosité du liquide pur MF_x si de telles données existent.

Il est bien connu qu'il se forme un verre lorsque des liquides à base de silice sont refroidis suffisamment rapidement pour éviter la cristallisation[6, 7, 47, 49]. En métallurgie, les liquides surfondus à base de silice sont appelés verres. En particulier, la viscosité des laitiers liquides est très élevée et la cristallisation de tels liquides (*i.e.* très visqueux) se produit très difficilement. La viscosité d'un verre est importante pour les conditions de fusion et d'affinage dans les fours de verrerie.

Il est bien connu que la dépendance en température de la viscosité d'un liquide vérifie bien une loi d'Arrhenius ($\ln\eta \propto 1/T$) à toute composition. Cependant, le modèle ne reproduit plus les viscosités élevées mesurées dans la région vitreuse car la dépendance en température des données de viscosité dans la région vitreuse ne suit pas une loi d'Arrhenius. Ainsi, le modèle pour la viscosité de liquides oxy-fluorés est étendu dans la présente étude pour prédire en deçà des barres d'erreur expérimentales la viscosité de verres pour tous les sous-systèmes disponibles du système CaO-MgO-Na_2O-K_2O-ZnO-PbO-Al_2O_3-B_2O_3-SiO_2 de la région vitreuse jusqu'à la région liquide.

A l'aide de toutes les données disponibles pour les sous-systèmes du système CaO-MgO-Na_2O-K_2O-ZnO-PbO-Al_2O_3-B_2O_3-SiO_2, les valeurs des paramètres du modèle unaires et binaires $\boldsymbol{A}_{\mathbf{MO_x}}$, $\boldsymbol{E}_{\mathbf{MO_x}}$, $E^{R}_{\mathrm{MO_x-Si}}$ et $E^{i.j}_{\mathrm{MO_x\text{-}Si}}$ ont été réoptimisées simultanément avec l'ajout des paramètres unaires et binaires non-Arrheniens $\boldsymbol{T}_{\mathbf{MO_x}}$, $\boldsymbol{n}_{\mathbf{MO_x}}$, $\boldsymbol{m}_{\mathbf{MO_x\text{-}Si}}$, $\boldsymbol{T}_{\mathbf{MO_x\text{-}Si}}$ et $\boldsymbol{n}_{\mathbf{MO_x\text{-}Si}}$ (M = Ca, Mg, Pb, Zn et Al). De façon à prendre en compte l'Effet de Compensation de Charge pour les verres contenant Al_2O_3, nous avons ajouté deux paramètres supplémentaires dans la fonction $\boldsymbol{\Delta G}_{\mathbf{MAl_xO_y}}$ correspondant à la formation d'une espèce à Charge Compensée telle que $\mathbf{CaAl_2O_4}$ ou $\mathbf{NaAlO_2}$. Cette modification simple du modèle correspond à un bon accord (en deçà des barres d'erreur expérimentales) avec la plupart des données de viscosité pour les systèmes ternaires et d'ordre supérieur contenant Al_2O_3.

A partir des données de viscosité et des études micrographiques disponibles pour les verres binaires MO_x-B_2O_3, il semble que la formation d'agrégats métastables d'apparence solide soit favorable dans ces verres binaires (MO_x = oxyde basique). Pour modéliser la formation de ces agrégats d'apparence solide dans la région vitreuse, nous avons employé les énergies de Gibbs $\Delta G_{m(MB_xO_y)}$ de formation des agrégats avec l'effet de taille des agrégats. Au total, cinq paramètres binaires sont utilisés pour reproduire les données de viscosité dans chaque système binaire oxyde basique-oxyde de bore: $A^*_{B(MO_x)}$, $E^*_{B(MO_x)}$, m, $\Delta G_{m(MB_xO_y)}$ et $E_{m(MB_xO_y)}$. La taille moyenne m d'un agrégat a été optimisée différemment suivant les verres binaires MO_x-B_2O_3. Aussi, les agrégats d'apparence solide sont modélisés à partir des données de viscosité pour les verres binaires MO_x-B_2O_3. Seuls les paramètres du modèle A_B, E_B, T_B et n_B pour B_2O_3 pur, et $T_{AlO_{1.5}\text{-}B}$ et $n_{AlO_{1.5}\text{-}B}$ pour le système binaire Al_2O_3-B_2O_3 ont été appliqués au modèle étendu pour reproduire le comportement en viscosité non-Arrhenien des systèmes contenant B_2O_3.

Les données de viscosité disponibles pour les sous-systèmes du système CaO-MgO-Na_2O-K_2O-ZnO-PbO-Al_2O_3-B_2O_3-SiO_2 ont été examinées. Nous démontrons que le modèle étendu reproduit les données expérimentales pour les liquides binaires et ternaires et prédit la viscosité de verres multicomposants en deçà des barres d'erreur expérimentales.

Lorsque l'on compare la reproductibilité du modèle précédent développé pour la viscosité des liquides à celle du modèle étendu, le modèle étendu est capable de reproduire les données de viscosité en deçà des barres d'erreur expérimentales non seulement dans la région liquide mais aussi dans la région vitreuse, et la reproductibilité dans la région liquide de ce modèle étendu est comparable à celle du modèle précédent.

En particulier, le modèle étendu peut être utilisé pour obtenir de bonnes estimations de la viscosité de verres multicomposants, de magmas, de laves et de verres commerciaux. Il prédit la viscosité de laitiers multicomposants à base de silice et de verres commerciaux avec une précision comparable à celle des équations de régression obtenues à partir des données expérimentales sur les gammes de composition restreintes de ces liquides. Nous pensons que le modèle étendu reproduit en deçà des barres d'erreur expérimentales non seulement la dépendance en température mais aussi la dépendance en composition des données de viscosité disponibles

pour le système $CaO–MgO–Na_2O–K_2O–ZnO–PbO–Al_2O_3–B_2O_3–SiO_2$, sur la gamme de température allant de 300^{o}C à 2000^{o}C.

Le modèle étendu s'applique sur la gamme de température complète allant de la région vitreuse jusqu'à la région liquide. Pour la région liquide, le modèle non étendu est légèrement supérieur au modèle étendu. En résumé, le modèle de viscosité reproduit maintenant toutes les données de viscosité disponibles pour les liquides et les verres relatifs au système $MF_x–SiO_2–B_2O_3–Al_2O_3–CaO–MgO–Na_2O–K_2O–PbO–ZnO–MnO–TiO_y$ (M = Ca, Mg, Na, K et Al) en deçà des barres d'erreur expérimentales, à toute composition et sur la gamme de température allant de 300^{o}C à 2000^{o}C.

TABLE OF CONTENTS

DEDICATION……III

ACKNOWLEDGEMENTS……IV

RÉSUMÉ ……V

ABSTRACT……X

CONDENSÉ EN FRANÇAIS……XV

TABLE OF CONTENTS…..…..……XXVIII

LIST OF TABLES…….…..……XXXVI

LIST OF FIGURES…..…..…… XXXVIII

LIST OF SYMBOLS…….……LXVII

CHAPTER 1 INTRODUCTION……1

CHAPTER 2 REVIEW OF THE LITERATURE……4

2.1 Viscosity Models for Molten Slags and Glasses……4

2.1.1 The empirical model of Urbain et al. for molten slags...……4

2.1.2 The empirical model of Riboud et al. for molten slags...……5

2.1.3 The Model of Zhang and Jahanshahi for molten slags...……6

2.1.4 The Model of Nakamoto et al. for molten slags…..……6

2.1.5 The Model by Kondratiev and Jak for molten Slags……...……8

2.1.6 Adam-Gibbs model for molten slags and glasses……...……9

2.1.7 Some models based on the Vogel-Fulcher-Tammann Equation……9

2.2 Techniques of Viscosity Measurements……..……11

2.2.1 Rotating Crucible Method…..……11

2.2.2 Oscillating (vibrational) viscometer method...…….……12

2.2.3 Falling body method……13

2.2.4 Fiber elongation method..……..……..……14

2.2.5 Beam-bending method...……..……..……..……15

2.2.6 Parallel plate method...……..……..……16

2.2.7 Micro-penetration method……..……..……..……17

2.2.8 Ball penetration method……..……..……..……18

2.3 The accuracy and reliability of viscosity measurements……..……18

2.3.1 Experimental difficulties of viscosity measurements……..……18

2.3.2 Chemical Analysis of oxy-fluoride melts and vaporization effect of fluorides….21

CHAPTER 3 A MODEL TO CALCULATE THE VISCOSITY OF MOLTEN SLAGS...24

3.1 Structure of Silicate and Borate Melts……..……24

3.2 Calculation of pair fractions using the Modified Quasichemical Model……..……25

3.3 Characterization of the structure of SiO_2 and B_2O_3 networks...……..……27

3.3.1 Combined network formed by SiO_2 and B_2O_3……..……..……30

3.4 A proposed Viscosity Model for Molten Slags……..……..……..……32

3.4.1 Viscosity of the unary systems……..……..……32

3.4.2 Viscosity of the binary systems MO_x-SiO_2 and MO_x-B_2O_3…..……34

3.4.3 Viscosity of the binary systems R_2O-B_2O_3 (R = Na and K)…..……38

3.4.4 Viscosity of multicomponent systems without Al_2O_3……..……41

3.4.5 Taking into account Charge Compensation Effect……..……45

CHAPTER 4 MODIFICATION OF THE MODEL FOR MELTS CONTAINING ALKALI OXIDES……..……49

4.1 Introduction……..……49

4.2 Modification of the model for melts containing alkali oxides……..……49

4.3 Review of the available viscosity data and calibration of the model……..……52

4.3.1 Viscosities of pure alkali oxides and binary $MO_{0.5}$–SiO_2 (M = Li, Na, K) melts……53

4.3.2 Ternary systems without alumina(Al_2O_3)……60

4.3.3 Ternary systems with alumina(Al_2O_3)……70

4.3.4 Multicomponent systems……76

4.3.5 Magmas and lavas……79

4.3.6 Melts used in glass technology……82

4.4 Conclusions……84

CHAPTER 5 MODELING VISCOSITY OF SILICATE MELTS CONTAINING LEAD OXIDE……88

5.1 Introduction……88

5.2 Review of the available viscosity data and calibration of the model……88

5.2.1 Pure PbO……89

5.2.2 Viscosities of Binary PbO–SiO_2 Melts……89

5.2.3 Ternary and Quaternary Melts without Alumina(Al_2O_3)……93

5.2.3.1 PbO-Na_2O-SiO_2 system……94

5.2.3.2 PbO-K_2O-SiO_2 system……97

5.2.3.3 PbO-MgO-SiO_2 system……102

5.2.3.4 PbO-CaO-SiO_2 system……106

5.2.3.5 PbO-K_2O-Na_2O-SiO_2 system……106

5.2.4 Melts with Alumina(Al_2O_3)……107

5.2.5 Melts used in glass technology ……110

5.3 Conclusions……111

CHAPTER 6 MODELING VISCOSITY OF SILICATE MELTS CONTAINING ZINC OXIDE……114

6.1 Introduction……114

6.2 Review of the available viscosity data and calibration of the model……114

6.2.1 Viscosities of binary ZnO-SiO_2 melts ……115

6.2.2 Ternary Melts without Alumina(Al_2O_3)……116

6.2.2.1 ZnO-CaO-SiO_2 system……116

6.2.2.2 ZnO-Na_2O-SiO_2 system……117

6.2.3 Ternary Melts with Alumina(Al_2O_3)……119

6.2.4 Multicomponent systems……122

6.2.4.1 ZnO-CaO-Al_2O_3-SiO_2 system……122

6.2.4.2 ZnO-CaO-MgO-Na_2O-K_2O-SiO_2 system……125

6.2.4.3 ZnO-CaO-MgO-Na_2O-K_2O-Al_2O_3-TiO_2-SiO_2 system……125

6.2.5 Melts used in glass technology……126

6.3 Conclusions……127

CHAPTER 7 MODELING VISCOSITY OF SILICATE MELTS CONTAINING MANGANESE OXIDE……130

7.1 Introduction……130

7.2 Review of the available viscosity data and calibration of the model……130

7.2.1 Viscosities of binary MnO-SiO_2 melts……131

7.2.2 Ternary Melts without Alumina(Al_2O_3)……132

7.2.2.1 MnO-CaO-SiO_2 system……132

7.2.2.2 MnO-Na_2O-SiO_2 system……138

7.2.3 Ternary Melts with Alumina(Al_2O_3)……138

7.2.4 Multicomponent systems……145

7.2.4.1 MnO-CaO-Al_2O_3-SiO_2 system……145

7.2.4.2 $MnO-CaO-MgO-Al_2O_3-SiO_2$ system……147

7.2.4.3 $MnO-K_2O-CaO-Al_2O_3-SiO_2$ system……149

7.2.4.4 $MnO-Na_2O-K_2O-CaO-Al_2O_3-SiO_2$ system……147

7.3 Conclusions……150

CHAPTER 8 MODELING VISCOSITY OF SILICATE MELTS CONTAINING TITANIUM OXIDES……152

8.1 Introduction……152

8.2 Review of the available viscosity data and calibration of the model……152

8.2.1 Viscosities of unary TiO_2 melts……153

8.2.2 Viscosities of binary TiO_2-SiO_2 and TiO_2-MO_y (M = K and Mn) melts…154

8.2.3 Ternary and Higher order Melts……157

8.2.3.1 $TiO_2-CaO-SiO_2$ system……157

8.2.3.2 $TiO_2-Na_2O-SiO_2$ system……162

8.2.3.3 $TiO_2-K_2O-SiO_2$ system……167

8.2.3.4 $TiO_2-MnO-SiO_2$ system……170

8.2.3.5 $TiO_2-K_2O-Na_2O-SiO_2$ and $TiO_2-Al_2O_3-Na_2O-SiO_2$ systems……173

8.2.3.6 $TiO_2-CaO-MgO-Al_2O_3-SiO_2$ system……174

8.2.3.7 TiO_2 and Ti_2O_3 containing system……178

8.3 Conclusions……180

CHAPTER 9 MODIFICATION OF THE MODEL FOR MELTS CONTAINING FLUORIDE AND APPLICATION TO SYSTEMS CONTAINING CaF_2……182

9.1 Introduction……182

9.2 Modification of the model for melts containing CaF_2……183

9.2.1 Structural role of CaF_2 in oxy-fluoride melts……183

9.2.2 Viscosity Model for oxy-fluoride melts……..……..……184

9.3 Review of the available viscosity data and calibration of the model……187

9.3.1 Viscosity of pure CaF_2 melts……..……188

9.3.2 Viscosities of the binary CaF_2–SiO_2 melts……190

9.3.3 Viscosities of the binary CaF_2–Al_2O_3 melts……192

9.3.4 Viscosities of the binary CaF_2–CaO melts……193

9.3.5 Viscosities of the binary CaF_2–MgO melts……194

9.3.6 Viscosities of the binary CaF_2–TiO_2 melts……194

9.3.7 Viscosities of the ternary CaF_2–CaO–SiO_2 melts……195

9.3.8 Viscosities of the ternary CaF_2–Al_2O_3–CaO melts……200

9.3.9 Viscosities of the ternary CaF_2–Al_2O_3–MgO melts……201

9.3.10 Viscosities of the ternary CaF_2–SiO_2–TiO_2 melts……205

9.3.11 Viscosities of the ternary CaF_2–SiO_2–Al_2O_3 melts……206

9.3.12 Viscosities of the ternary CaF_2–MgO–SiO_2 melts……210

9.3.13 Viscosities of the CaF_2-Al_2O_3-CaO-SiO_2 melts……214

9.3.14 Viscosities of the CaF_2-Al_2O_3-MgO-SiO_2 melts……218

9.3.15 Viscosities of the CaF_2-Al_2O_3-B_2O_3-CaO melts……218

9.3.16 Viscosities of the CaF_2-B_2O_3-Na_2O-SiO_2 melts……221

9.3.17 Viscosities of the CaF_2-Al_2O_3-CaO-Na_2O melts……222

9.3.18 Viscosities of CaF_2-Al_2O_3-CaO-MnO and CaF_2-Al_2O_3-CaO-TiO_2 melts…222

9.3.19 Viscosities of CaF_2-CaO-Na_2O-SiO_2 melts……222

9.3.20 Viscosities of CaF_2-Al_2O_3-CaO-MgO-SiO_2 melts……226

9.3.21 Viscosities of Mold Flux melts……228

CHAPTER 10 APPLICATION OF THE MODEL TO MELTS CONTAINING MF_x (M = Mg, Na, K and Al)……230

10.1 Review of the available viscosity data and calibration of the model……230

10.1.1 Viscosities of unary MF_x and binary MF_x-SiO_2 (M = Mg, Na, K and Al) systems....230

10.1.2 Viscosities of the binary KF-B_2O_3 melts…...…….……234

10.1.3 Viscosities of the binary NaF-B_2O_3 melts....…….……235

10.1.4 Viscosities of the ternary NaF-CaO-SiO_2 melts……...…….……236

10.1.5 Viscosities of the ternary MgF-CaO-SiO_2 melts……...…….……236

10.1.6 Viscosities of the ternary NaF-Na_2O-SiO_2 melts……...…….……238

10.1.7 Viscosities of the ternary NaF-Na_2O-B_2O_3 melts……...…….……243

10.1.8 Viscosities of CaO-Al_2O_3-SiO_2-MF_x (M = Al, Na, Mg) melts……...…245

10.1.9 Viscosities of CaF_2-NaF-Na_2O-B_2O_3 melts……...…246

10.2 Conclusions…….……..……..……247

CHAPTER 11 EXTENSION OF THE MODEL TO THE GLASS REGION OF SILICATES ……251

11.1 Introduction…….……..……..……251

11.2 Viscosity Model…..…….……...……252

11.2.1 Structure of Silicate Glasses……..…252

11.2.2 Extended Viscosity Model with Non-Arrhenian Temperature Dependence…253

11.3 Review of the available viscosity data and calibration of the model……256

11.3.1 The Accuracy and Reliability of Viscosity Measurements……...…256

11.3.2 Viscosity of the unary systems……...…257

11.3.3 Viscosity of the binary systems……...…258

11.3.4 Viscosity of the ternary systems without $AlO_{1.5}$……..269

11.3.5 Viscosity of the ternary systems with $AlO_{1.5}$……..287

11.3.6 Magmas, Lavas and Multi-component Glasses……..296

11.3.7 Viscosity of Commercial Glasses……..305

11.4 Conclusions……..……311

CHAPTER 12 EXTENSION OF THE MODEL TO THE GLASS REGION OF BORON–CONTAINING SYSTEMS ……316

12.1 Introduction…….……..……316

12.2 Extended Viscosity Model for Boron-containing Systems…….……317

12.3 Review of the available viscosity data and calibration of the model……319

12.3.1 Viscosity of the unary B_2O_3 system……..…319

12.3.2 Viscosity of the Na_2O-B_2O_3 system……..…322

12.3.3 Viscosity of the K_2O-B_2O_3 system……..…325

12.3.4 Viscosity of the CaO-B_2O_3 system……..…326

12.3.5 Viscosity of the PbO-B_2O_3 system……..…327

12.3.6 Viscosity of the Al_2O_3-B_2O_3 system……..…329

12.3.7 Viscosity of the ZnO-B_2O_3 system……..…332

12.3.8 Viscosity of the MgO-B_2O_3 system……..…332

12.3.9 Viscosity of the Borosilicates (B_2O_3-SiO_2)……..…332

12.3.10 Viscosities of ternary systems……..…333

12.3.11 Viscosity of Multicomponent Glasses……..…344

12.3.12 Viscosity of Commercial Glasses……..…346

12.4 Conclusions…….……..……351

CHAPTER 13 CONCLUSIONS……353

REFERENCES……356

LIST OF TABLES

Table 4.1 Optimized model parameters for the viscosity expressed in Pa·s……..85

Table 4.2: Optimized parameters for ternary systems containing alumina ($J \cdot mol^{-1}$)…….86

Table 4.3 Viscosities of typical soda-lime-silica glass melts and the effect of additions of Al_2O_3, K_2O and MgO. The experimental data of Lakatos et al.[154] are compared with the viscosities calculated by Fluegel's regression equation [67] and predicted by the present model……...86

Table 4.4 Viscosities of glass melts for the production of mineral-wool isolating fiber products. The experimental data of Lakatos et al. [153] are compared with the viscosities predicted by the present model and calculated by Fluegel's regression equation [67]…….87

Table 5.1 Optimized Model parameters for the viscosity expressed in Pa·s……113

Table 5.2 Effect of CaO, MgO and ZnO on the viscosity of a typical lead crystal glass melt. The experimental data of Lakatos et al.[155] are compared with the viscosities calculated by Fluegel's regression equation[67] and predicted by the present model……...113

Table 6.1 Optimized Model parameters for the viscosity expressed in Pa·s……128

Table 6.2 Effect of ZnO on the viscosity of soda-lime-silica and lead crystal glass melts. The experimental data of Lakatos et al. [151, 155] are compared with viscosities calculated by Fluegel's regression equation [67] and predicted by the present model……...129

Table 7.1 Optimized Model parameters for the viscosity expressed in Pa·s……151

Table 8.1 Optimized Model parameters for the viscosity expressed in Pa·s……181

Table 9.1 Optimized Model parameters for the viscosity expressed in Pa·s……229

Table 10.1 Optimized Model parameters for the viscosity expressed in Pa·s……..249

Table 10.2 Optimized parameters for the boron containing systems……...250

Table 11.1 Optimized Model parameters for the viscosity expressed in Pa·s……..313-314

Table 11.2 Optimized non-Arrhenian parameters for the extended viscosity model……314-315

Table 11.3 Optimized parameters for the ternary systems containing alumina ($J\ mol^{-1}$)……315

Table 12.1 Optimized parameters for the boron containing systems……...352

LIST OF FIGURES

Fig. 1.1 Schematic diagrams of Continuous Casting Process and Mold in the steelmaking process……..1

Fig. 1.2 Viscosity of Na_2O-Al_2O_3-SiO_2 as a function of Temperatures and critical viscosity points in glassmaking process…….2

Fig. 2.1 Flow Mechanism in silicate melts by the model of Nakamoto et al. [201] ……...7

Fig. 2.2 Schematic diagram of a rotating crucible method…….....12

Fig. 2.3 Schematic diagram of the fiber elongation method…….....14

Fig. 2.4 Schematic diagram of the beam-bending method…….....15

Fig. 2.5 (a) Schematic diagram of the parallel plate method, (b) Deformation of the sample.....16

Fig. 2.6 Schematic diagram of the micro-penetration method.....17

Fig. 3.1 Structure of (a) orthosilicate and (b) triangular borate.....25

Fig. 3.2 Si-Si, M-Si and M-M pair fractions calculated from the quasichemical thermodynamic model for the systems CaO-SiO_2 and $NaO_{0.5}$-SiO_2.....27

Fig. 3.3 Calculated and experimental [65] fractions of Q^i-species for the PbO–SiO_2 system at 1200 ^oC.....29

Fig. 3.4 Connectivity of silicate network.....30

Fig. 3.5 Viscosity of Pure B_2O_3 [27, 81, 82].....33

Fig. 3.6 Viscosity of Pure SiO_2 [27, 81, 82].....33

Fig. 3.7 Viscosity of binary $AlO_{1.5}$–SiO_2 system [27, 81, 82].....36

Fig. 3.8 Viscosity of binary CaO–SiO_2 system [27, 81, 82].....36

Fig. 3.9 Viscosity of binary PbO–B_2O_3 system [27, 81, 82].....37

Fig. 3.10 Viscosity of Na_2O–B_2O_3 melts: experimental points [112, 158, 162, 203, 281, 362] and calculated lines. Dashed lines are extrapolations below the liquidus.....39

Fig. 3.11 Viscosity of CaO-MgO-SiO_2 melts at weight ratio SiO_2/MgO=3/1 compared with experimental data [27, 81, 82]. 44

Fig. 3.12 Viscosity of Na_2O-Al_2O_3-SiO_2 melts at 67 mol% SiO_2 compared with experimental data [27, 81, 82] 44

Fig. 3.13 Viscosity of CaO-Al_2O_3-SiO_2 melts at 75 mol% SiO_2 compared with experimental data [27, 81, 82] 45

Fig. 3.14 Viscosity of CaO-MgO-Al_2O_3-SiO_2 melts at 5, 10, 15, 20 and 25 wt% MgO and 50 wt% at 1500ºC compared with experimental data [27, 81, 82]. 48

Fig. 3.15 Viscosity along the albite-diopside ($NaAlSi_3O_8$-$CaMgSi_2O_6$) join at 1200ºC, 1300ºC, 1400ºC, 1500ºC and 1600 ºC compared with experimental data [27, 81, 82]. 48

Fig. 4.1 Viscosity of $NaO_{0.5}$–SiO_2 melts. Points are experimental [23, 143, 223, 313, 333] [88, 125, 134, 166, 212, 246, 283, 295, 312, 348]. Figures (a) and (b) compare the modified viscosity model proposed in the present study (solid lines) with the model reported earlier [82] (dash-dot lines). Figure (c) compares the viscosity model proposed in the present study (solid lines) with the model by Jak [107] (dash-dot lines) 55-57

Fig. 4.2 Viscosity of $KO_{0.5}$–SiO_2 melts. Points are experimental [11, 23, 53, 125, 193, 223, 237, 283]. Figure (a) compares the modified viscosity model proposed in the present study (solid lines) with the model reported earlier [82] (dash-dot lines). Figure (b) compares the viscosity model proposed in the present study (solid lines) with the model by Jak [107] (dotted lines) and the model for glass melts by Fluegel [67] (dashed lines corresponding to 1000 ^oC and 1600 ^oC) 58-59

Fig. 4.3 Viscosity of $LiO_{0.5}$–SiO_2 melts: experimental points [23, 223, 283] and calculated lines. The calculated viscosities for $NaO_{0.5}$–SiO_2 and $KO_{0.5}$–SiO_2 melts at 1200 ^oC are also shown for comparison.....60

Fig. 4.4 Viscosity of CaO–Na_2O–SiO_2 melts at 65 mol% SiO_2: experimental points [294, 349] and calculated lines.....61

Fig. 4.5 Viscosity of CaO–Na_2O–SiO_2 melts at 15 mol% Na_2O: experimental points [59, 294, 349, 357] and calculated lines 62

Fig. 4.6 Compositions in the $MgO–Na_2O–SiO_2$ system at which the viscosity was measured [59, 119]. Solid lines show the pseudo-binary sections reported in Figs. 4.7 and 4.8.....63

Fig. 4.7 Viscosity of $MgO–Na_2O–SiO_2$ melts. Experimental points [119] and calculated lines at different molar ratios of Na_2O to SiO_2. Solid lines are calculated using the modified viscosity model proposed in the present study and dash-dot lines correspond to the model reported earlier [81] 63-65

Fig. 4.8 Viscosity of $MgO–Na_2O–SiO_2$ melts. Experimental points [119] and calculated lines at (a) 5, (b) 10, (c) 15 and (d) 20 mol% MgO. Solid lines are calculated using the modified viscosity model proposed in the present study and dash-dot lines correspond to the model reported earlier [81] 66-67

Fig. 4.9 Viscosity of $K_2O–CaO–SiO_2$ melts at a molar ratio of $CaO/SiO_2 = 1.071$: experimental points [357] and calculated lines.....69

Fig. 4.10 Viscosity of $K_2O–Na_2O–SiO_2$ melts at 75 mol% SiO_2: experimental points [125] and calculated lines.....69

Fig. 4.11 Viscosity of $Na_2O–Al_2O_3–SiO_2$ melts at 50 mol% SiO_2: experimental points [200, 252, 324] and calculated lines.....70

Fig. 4.12 Viscosity of $Na_2O–Al_2O_3–SiO_2$ melts at 75 mol% SiO_2: experimental points [20, 36, 146, 252, 269, 307, 324, 335] and calculated lines. Viscosities calculated using Fluegel's model for glass melts [67] are shown by dashed lines within the validity limits of the model and by the dotted lines outside these limits.....71

Fig. 4.13 Compositions in the $K_2O–Al_2O_3–SiO_2$ system at which the viscosity was measured [125, 193, 200, 335]. Lines show the sections of this ternary system reported in Figs. 4.14 to 4.18.....72

Fig. 4.14 Viscosity of $K_2O–Al_2O_3–SiO_2$ melts at 45 mol% SiO_2: experimental points [193] and calculated lines.....73

Fig. 4.15 Viscosity of $K_2O–Al_2O_3–SiO_2$ melts at 50 mol% SiO_2: experimental points [193, 200] and calculated lines.....73

Fig. 4.16 Viscosity of K_2O–Al_2O_3–SiO_2 melts at 55 mol% SiO_2: experimental points [193] and calculated lines.....74

Fig. 4.17 Viscosity of K_2O–Al_2O_3–SiO_2 melts at 75 mol% SiO_2: experimental points [200, 335] and calculated lines.....74

Fig. 4.18 Viscosity of K_2O–Al_2O_3–SiO_2 melts: experimental points [125, 193] and calculated lines using the modified viscosity model proposed in the present study (solid lines) and using the model reported previously [81] (dash-dot lines). (a) 2.5 mol% Al_2O_3, (b) 5 mol% Al_2O_3 and (c) 10 mol% Al_2O_3.....75-76

Fig. 4.19 Viscosity of K_2O–CaO–Al_2O_3–SiO_2 melts for a section between (95 mol% CaO, 5 mol% Al_2O_3) and (73 mol% SiO_2, 7 mol% K_2O , 20 mol% Al_2O_3): experimental points [84, 200, 259] and calculated lines.....77

Fig. 4.20 Changes in the viscosity of CaO–Al_2O_3–SiO_2 melts resulting from additions of Na_2O or K_2O: experimental points [311] and calculated lines.....78

Fig. 4.21 Viscosity of K_2O–Na_2O–Al_2O_3–SiO_2 melts for a section between (18 mol% SiO_2, 0.63 mol% K_2O, 81.7 mol% Na_2O) and (88.2 mol% SiO_2, 3.09 mol% K_2O, 8.7 mol% Al_2O_3): experimental points [91, 200] and calculated lines.....78

Fig. 4.22 Viscosity of albite–anorthite ($NaAlSi_3O_8$–$CaAl_2Si_2O_8$) melts: experimental points [36, 146, 200] and calculated lines.....80

Fig. 4.23 Viscosity of albite–orthoclase ($NaAlSi_3O_8$–$KAlSi_3O_8$) melts: experimental points [200] and calculated lines.....80

Fig. 4.24 Viscosity of anorthite–diopside ($CaAl_2Si_2O_8$–$CaMgSi_2O_6$) melts: experimental points [146, 270] and calculated lines.....81

Fig. 4.25 Viscosity along the section through the albite–anorthite–diopside system at 20 wt% diopside: experimental points [146, 270] and calculated lines.....82

Fig. 5.1 Viscosity of pure liquid PbO: experimental points [219] and calculated line.....89

Fig. 5.2 Viscosity of PbO–SiO_2 melts: (a) experimental points [54, 63, 69, 85, 93, 104, 143, 202, 207, 209, 219, 224, 263, 332, 350] at 800, 900 and 1000°C and calculated lines fitted with parameters $E^{1,1}_{\text{PbO-Si}}$ and $E^{R}_{\text{PbO-Si}}$; (b) experimental points [54, 63, 69, 85, 93, 104, 143, 202, 207, 209, 219, 224, 263, 332, 350] at 800, 900 and 1000°C and calculated lines fitted with parameters $E^{1,1}_{\text{PbO-Si}}$ and $E^{2,5}_{\text{PbO-Si}}$; (c) experimental points [103, 104, 143, 202, 209, 219, 224, 350] for 1100 °C and calculated lines fitted with parameters $E^{1,1}_{\text{PbO-Si}}$ and $E^{2,5}_{\text{PbO-Si}}$ 91-93

Fig. 5.3 Compositions in the PbO–Na_2O–SiO_2 system at which the viscosity was measured [63, 62, 93, 111, 327]. Lines show the sections of this ternary system reported in Figs 5.4 to 5.8.....94

Fig. 5.4 Viscosity of PbO–Na_2O–SiO_2 melts at a molar ratio of SiO_2/PbO = 1: experimental points [93] and calculated lines.....95

Fig. 5.5 Viscosity of PbO–Na_2O–SiO_2 melts at 60 mol% SiO_2: experimental points [63, 327] and calculated lines.....95

Fig. 5.6 Viscosity of PbO–Na_2O–SiO_2 melts at 50 mol% SiO_2: experimental points [62, 93] and calculated lines.....96

Fig. 5.7 Viscosity of PbO–Na_2O–SiO_2 melts at a molar ratio of Na_2O/PbO = 1: experimental points [63, 62, 93, 327] and calculated lines.....96

Fig. 5.8 Viscosity of PbO–Na_2O–SiO_2 melts in the section from (34 mol% Na_2O, 66 mol% SiO_2) to (50 mol% PbO, 50 mol% SiO_2): experimental points [63, 62, 93, 327] and calculated lines.....97

Fig. 5.9 Compositions in the PbO–K_2O–SiO_2 system at which the viscosity was measured. [94, 111, 237, 263, 282] Lines show the sections of this ternary system reported in Figs 5.10 to 5.15.....98

Fig. 5.10 Viscosity of PbO–K_2O–SiO_2 melts in the section from (50 mol% PbO, 50 mol% SiO_2) to (11 mol% K_2O, 89 mol% SiO_2): experimental points [94, 237, 282] and calculated lines.....99

Fig. 5.11 Viscosity of PbO–K_2O–SiO_2 melts at a molar ratio of SiO_2/PbO = 1: experimental points [94] and calculated lines.....99

Fig. 5.12 Viscosity of PbO–K_2O–SiO_2 melts at 10 mol% K_2O: experimental points [94, 263] and calculated lines.....100

Fig. 5.13 Viscosity of PbO–K_2O–SiO_2 melts at 50 mol% SiO_2: experimental points [94, 263] and calculated lines.....100

Fig. 5.14 Viscosity of PbO–K_2O–SiO_2 melts at 60 mol% SiO_2: experimental points [263] and calculated lines.....101

Fig. 5.15 Viscosity of PbO–K_2O–SiO_2 melts at 70 mol% SiO_2: experimental points [263] and calculated lines.....101

Fig. 5.16 Compositions in the PbO–MgO–SiO_2 system at which the viscosity was measured [104, 120, 224]. Lines show the sections of this ternary system reported in Figs 5.17 to 5.19.....102

Fig. 5.17 Viscosity of PbO–MgO–SiO_2 melts at 40 and 60 mol% SiO_2: experimental points [120] and calculated lines.....103

Fig. 5.18 Viscosity of PbO–MgO–SiO_2 melts at 50 mol% SiO_2: experimental points [120, 224] and calculated lines.....103

Fig. 5.19 Viscosity of PbO–MgO–SiO_2 melts in the section from (60 mol% PbO, 40 mol% SiO_2) to (30 mol% MgO, 70 mol% SiO_2): experimental points [104, 120] and calculated lines.....104

Fig. 5.20 Viscosity of PbO–CaO–SiO_2 melts at a molar ratio SiO_2/PbO = 1.66: experimental points [350] and calculated lines.....104

Fig. 5.21 Viscosity of PbO–CaO–SiO_2 melts at a molar ratio SiO_2/PbO = 1.13: experimental points [350] and calculated lines.....105

Fig. 5.22 Viscosity of PbO–CaO–SiO_2 melts at 50 mol% SiO_2: experimental points [224, 350] and calculated lines.....105

Fig. 5.23 Viscosity of PbO–K_2O–Na_2O–SiO_2 melts at 75 mol% SiO_2 and 10 mol% PbO: experimental points [111] and calculated lines.....106

Fig. 5.24 Compositions in the PbO–Al_2O_3–SiO_2 system at which the viscosity was measured. [104, 143] Lines show the pseudo-binary sections of this ternary system reported in Figs 5.25 to 5.28.....108

Fig. 5.25 Viscosity of PbO–Al_2O_3–SiO_2 melts at 5 mol% Al_2O_3: experimental points [104, 143] and calculated lines.....108

Fig. 5.26 Viscosity of PbO–Al_2O_3–SiO_2 melts at 10 mol% Al_2O_3: experimental points [143] and calculated lines.....109

Fig. 5.27 Viscosity of PbO–Al_2O_3–SiO_2 melts at 30 mol% SiO_2: experimental points [143] and calculated lines.....109

Fig. 5.28 Viscosity of PbO–Al_2O_3–SiO_2 melts at 40 mol% SiO_2: experimental points [143] and calculated lines.....110

Fig. 6.1 Calculated viscosity of ZnO-SiO_2 melts compared to experimental points [193] 115

Fig. 6.2 Viscosity of ZnO-CaO-SiO_2 melts at molar ratios CaO/SiO_2 = 0.632, 0.67 and 1.0: experimental points [171, 313] and calculated lines.....116

Fig. 6.3 Compositions in the ZnO-Na_2O-SiO_2 system at which experimental viscosity measurements are available [10, 105, 313]. The lines indicate seven sections of this system selected to show the viscosity as a function of composition in Figs. 6.4 to 6.6.....117

Fig. 6.4 Viscosity of ZnO-Na_2O-SiO_2 melts at molar ratios Na_2O/SiO_2 = 1/4, 3/7, 2/3, 1/1 and 3/2: experimental points [313] and calculated lines.....118

Fig. 6.5 Viscosity of ZnO-Na_2O-SiO_2 melts at 10 mol% ZnO: experimental points [105, 313] and calculated lines.....118

Fig. 6.6 Viscosity of ZnO-Na_2O-SiO_2 melts at 20 mol% ZnO: experimental points [10, 105, 313] and calculated lines.....119

Fig. 6.7 Compositions in the ZnO-Al_2O_3-SiO_2 system at which experimental viscosity measurements are available [193, 287]. The lines indicate four sections of this system selected to show the viscosity as a function of composition in Figs 6.8 to 6.10.....120

Fig. 6.8 Viscosity of ZnO-Al_2O_3-SiO_2 melts at 45, 50, 55 and 60 mol% SiO_2: experimental points [193] and calculated lines.....121

Fig. 6.9 Viscosity of ZnO-Al_2O_3-SiO_2 melts at 40, 45, 50, 55 and 60 mol% SiO_2: experimental points [193] and calculated lines.....121

Fig. 6.10 Viscosity of ZnO-Al_2O_3-SiO_2 melts at 5 mol% Al_2O_3: experimental points [193, 287] and calculated lines.....122

Fig. 6.11 Viscosity of ZnO-CaO-Al_2O_3-SiO_2 melts at 47.1 mol% SiO_2 and 5.5 mol% Al_2O_3: experimental points [287] and calculated lines.....123

Fig. 6.12 Viscosity of ZnO-CaO-Al_2O_3-SiO_2 melts at 40 mol% SiO_2 and 10 mol% Al_2O_3: experimental points [222] and calculated lines.....124

Fig. 6.13 Viscosity of ZnO-CaO-Al_2O_3-SiO_2 melts at molar ratios Al_2O_3/SiO_2 = 0.505 and 0.295 at a constant molar ratio CaO/SiO_2 = 1.071: experimental points [171] and calculated lines.....124

Fig. 6.14 Viscosity of ZnO-CaO-MgO-Na_2O-K_2O-SiO_2 melts at 6 mol% CaO, 5.3 mol% MgO, 13.7 mol% Na_2O and 2.6 mol% K_2O: experimental points [70] and calculated lines.....125

Fig. 6.15 Viscosity of ZnO-CaO-MgO-Na_2O-K_2O-Al_2O_3-TiO_2-SiO_2 melts at 58.7 mol% SiO_2, 2.75 mol% TiO_2, 7.25 mol% Al_2O_3, 0.9 mol% Na_2O and 0.1 mol% K_2O and 4 mol% ZnO: experimental points [121] and calculated lines.....126

Fig. 7.1 Viscosity of $MnO-SiO_2$ system compared to Experimental data at 1400,1500 and 1600°C [187, 248, 275, 335, 353] 132

Fig. 7.2 Compositions in the $MnO-CaO-SiO_2$ system at which experimental viscosity measurements are available [118, 186, 275, 304]. The lines indicate seven sections of this system selected to show the viscosity as a function of composition in Figs 7.3 to 7.9.....133

Fig. 7.3 Viscosity of $MnO-CaO-SiO_2$ melts at 30 mol% MnO compared to experimental data [118, 275] 134

Fig. 7.4 Viscosity of $MnO-CaO-SiO_2$ melts at 40 mol% MnO compared to experimental data [118] 134

Fig. 7.5 Viscosity of $MnO-CaO-SiO_2$ melts at 40 mol% SiO_2 compared to experimental data [118, 186, 275, 304] 135

Fig. 7.6 Viscosity of $MnO-CaO-SiO_2$ melts at 45 mol% SiO_2 compared to experimental data [118, 275] 135

Fig. 7.7 Viscosity of $MnO-CaO-SiO_2$ melts at 50 mol% SiO_2 compared to experimental data [118, 186, 275, 304] 136

Fig. 7.8 Viscosity of $MnO-CaO-SiO_2$ melts for a molar ratio $SiO_2/CaO = 1$ compared to experimental data [118, 275] 136

Fig. 7.9 Viscosity of $MnO-CaO-SiO_2$ melts for a molar ratio $SiO_2/CaO = 1.5$ compared to experimental data [118, 186, 275] 137

Fig. 7.10 Viscosity of $MnO-Na_2O-SiO_2$ melts at 10 mol% MnO compared to experimental data [105] 137

Fig. 7.11 Viscosity of $MnO-Na_2O-SiO_2$ melts at 20 mol% MnO compared to experimental data [10, 105] 138

Fig. 7.12 Compositions in the $MnO-Al_2O_3-SiO_2$ system at which experimental viscosity measurements are available [118, 143, 187, 335]. The lines indicate nine sections of this system selected to show the viscosity as a function of composition in Figs 7.13 to 7.21.....140

Fig. 7.13 Viscosity of MnO-Al_2O_3-SiO_2 melts at 30 mol% SiO_2 compared to experimental data [118, 143, 187] 140

Fig. 7.14 Viscosity of MnO-Al_2O_3-SiO_2 melts at 40 mol% SiO_2 compared to experimental data [118, 143, 187] 141

Fig. 7.15 Viscosity of MnO-Al_2O_3-SiO_2 melts at 50 mol% SiO_2 compared to experimental data [118, 143, 187] 141

Fig. 7.16 Viscosity of MnO-Al_2O_3-SiO_2 melts at 60 mol% SiO_2 compared to experimental data [118, 143, 335] 142

Fig. 7.17 Viscosity of MnO-Al_2O_3-SiO_2 melts at 76 mol% SiO_2 compared to experimental data [335] 142

Fig. 7.18 Viscosity of MnO-Al_2O_3-SiO_2 melts for a molar ratio Al_2O_3/MnO = 1 compared to experimental data [118, 143, 335] 143

Fig. 7.19 Viscosity of MnO-Al_2O_3-SiO_2 melts at 10 mol% Al_2O_3 compared to experimental data [118, 143, 187] 143

Fig. 7.20 Viscosity of MnO-Al_2O_3-SiO_2 melts at 20 mol% Al_2O_3 compared to experimental data [118, 143, 187] 144

Fig. 7.21 Viscosity of MnO-Al_2O_3-SiO_2 melts at 30 mol% Al_2O_3 compared to experimental data [118, 143] 144

Fig. 7.22 Viscosity of MnO-CaO-Al_2O_3-SiO_2 melts at 6 wt% Al_2O_3 and for a molar ratio CaO/SiO_2 = 0.64 compared to experimental data [317] 146

Fig. 7.23 Viscosity of MnO-CaO-Al_2O_3-SiO_2 melts at 10 wt% Al_2O_3 and 40 wt% SiO_2 compared to experimental data [34] 146

Fig. 7.24 Viscosity of MnO-CaO-MgO-Al_2O_3-SiO_2 melts in the section of (21.7 mol% SiO_2, 14.9 mol% Al_2O_3, 19.68 mol% CaO, 43.72 mol% MgO) to (37.08 mol% SiO_2, 24.73 mol% Al_2O_3, 33.63 mol% CaO, 4.54 mol% MnO) with a molar ratio CaO/SiO_2 = 0.907: experimental points [278] 148

Fig. 7.25 Viscosity of MnO-CaO-MgO-Al_2O_3-SiO_2 melts in the section of (34 mol% SiO_2, 10 mol% Al_2O_3, 37.3 mol% CaO, 18 mol% MgO) to (0.8 mol% SiO_2, 0.2 mol% Al_2O_3, 0.9 mol% CaO, 98 mol% MnO) with a molar ratio SiO_2/CaO=0.933: experimental points [346] 148

Fig. 7.26 Viscosity of MnO-K_2O-CaO-Al_2O_3-SiO_2 melts in the section of (2.1 mol% SiO_2, 1 mol% CaO, 0.66 mol% K_2O, 96.23 mol% MnO) to (50.85 mol% SiO_2, 5 mol% Al_2O_3, 25.73 mol% CaO, 18.41 mol% K_2O) with a molar ratio CaO/SiO_2 = 0.506: experimental points [257] 149

Fig. 7.27 Viscosity of MnO-Na_2O-K_2O-CaO-Al_2O_3-SiO_2 melts at 10 wt% Al_2O_3, 12.8 wt% CaO, 17.5 wt% MnO, 2.5 wt% K_2O and 4.2 wt% MgO compared to experimental data [322] 150

Fig. 8.1 Viscosity of pure liquid TiO_2 melts: experimental points [191] and calculated line.....154

Fig. 8.2 Viscosity of TiO_2-SiO_2 melts: experimental points [160] and calculated line.....156

Fig. 8.3 Viscosity of TiO_2-K_2O melts: experimental points [338] and calculated line.....156

Fig. 8.4 Viscosity of TiO_2-MnO melts: experimental points [353] and calculated line.....157

Fig. 8.5 Compositions in the TiO_2-CaO-SiO_2 system at which experimental viscosity measurements are available [42, 202, 272, 357]. The lines indicate four sections of this system selected to show the viscosity as a function of composition in Figs 8.6 to 8.9.....160

Fig. 8.6 Viscosity of TiO_2-CaO-SiO_2 melts for a molar ratio CaO/SiO2 = 0.7179 compared to experimental data [272].....160

Fig. 8.7 Viscosity of TiO_2-CaO-SiO_2 melts for a molar ratio CaO/SiO2 = 1 compared to experimental data [42, 272].....161

Fig. 8.8 Viscosity of TiO_2-CaO-SiO_2 melts for a molar ratio CaO/SiO2 = 1.307 compared to experimental data [272]…….....161

Fig. 8.9 Viscosity of TiO_2-CaO-SiO_2 melts in the section of (76.18 mol% TiO_2, 23.82 mol% CaO) to (80.96 mol% TiO_2, 19.04 mol% CaO) compared to experimental data [272].....162

Fig. 8.10 Compositions in the TiO_2-Na_2O-SiO_2 system at which experimental viscosity measurements are available [3, 42, 64, 167, 202]. The lines indicate five sections of this system selected to show the viscosity as a function of composition in Figs 8.11 to 8.15.....164

Fig. 8.11 Viscosity of TiO_2-Na_2O-SiO_2 melts at 76 mol% SiO_2 compared to experimental data [167].…….....164

Fig. 8.12 Viscosity of TiO_2-Na_2O-SiO_2 melts for a molar ratio Na_2O/TiO_2 = 1 compared to experimental data [3, 202] …….....165

Fig. 8.13 Viscosity of TiO_2-Na_2O-SiO_2 melts for a molar ratio Na_2O/SiO_2 = 1 compared to experimental data [42].…….....165

Fig. 8.14 Viscosity of TiO_2-Na_2O-SiO_2 melts in the section of (74.34 mol% TiO_2, 25.66 mol% Na_2O) to (76 mol% SiO_2, 24 mol% Na_2O) compared to experimental data [3, 42, 167] ……...166

Fig. 8.15 Viscosity of TiO_2-Na_2O-SiO_2 melts at 33.3 mol% Na_2O compared to experimental data [64] …….....166

Fig. 8.16 Compositions in the TiO_2-K_2O-SiO_2 system at which experimental viscosity measurements are available[3, 202, 338]. The lines indicate 5 sections of this system to show the viscosity as a function of composition in Figs. 8.17 to 8.20.……...168

Fig. 8.17 Viscosity of TiO_2-K_2O-SiO_2 melts at 33 mol% K_2O compared to experimental data [338] …….....168

Fig. 8.18 Viscosity of TiO_2-K_2O-SiO_2 melts at 40 mol% K_2O compared to experimental data [338] …….....169

Fig. 8.19 Viscosity of TiO_2-K_2O-SiO_2 melts at 50 mol% K_2O compared to experimental data [338] …….....169

Fig. 8.20 Viscosity of TiO_2-K_2O-SiO_2 melts for a molar ratio K_2O/TiO_2 = 1 compared to experimental data [3, 202, 338] 170

Fig. 8.21 Compositions in the TiO_2-MnO-SiO_2 system at which experimental viscosity measurements are available [353]. The lines indicate four sections of this system selected to show the viscosity as a function of composition in Figs 8.22 to 8.24.....171

Fig. 8.22 Viscosity of TiO_2-MnO-SiO_2 melts at 50 mol% MnO compared to experimental data [353] 171

Fig. 8.23 Viscosity of TiO_2-MnO-SiO_2 melts at 60 mol% MnO compared to experimental data [353].....172

Fig. 8.24 Viscosity of TiO_2-MnO-SiO_2 melts at 70 mol% MnO compared to experimental data [353].....172

Fig. 8.25 Viscosity of TiO_2-K_2O-Na_2O-SiO_2 melts at 50 mol% SiO_2 and 16.7 mol% TiO_2 compared to experimental data [64].....173

Fig. 8.26 Viscosity of TiO_2-Al_2O_3-Na_2O-SiO_2 melts at 33.3 mol% Na_2O and 16.7 mol% TiO_2 compared to experimental data [64]…….....174

Fig. 8.27 Viscosity of TiO_2-CaO-MgO-Al_2O_3-SiO_2 melts at 17 wt% Al_2O_3, 8 wt% MgO and 20 wt% CaO compared to experimental data [277]…….....175

Fig. 8.28 Viscosity of TiO_2-CaO-MgO-Al_2O_3-SiO_2 melts at 17 wt% Al_2O_3, 8 wt% MgO and 25 wt% CaO compared to experimental data [277].....176

Fig. 8.29 Viscosity of TiO_2-CaO-MgO-Al_2O_3-SiO_2 melts for a weight ratio CaO/SiO_2 = 1.2 and Al_2O_3/MgO=2 compared to experimental data [18, 277]…….....176

Fig. 8.30 Viscosity of TiO_2-CaO-MgO-Al_2O_3-SiO_2 melts at 10.1 mol% Al_2O_3, 30.6 mol% CaO and 7.1 mo% MgO compared to experimental data [58]…….....177

Fig. 8.31 Viscosity of TiO_2-CaO-MgO-Al_2O_3-SiO_2 melts at 8.9 mol% Al_2O_3, 20 mol% MgO and 10 mo% TiO_2 compared to experimental data [188, 364]…….....177

Fig. 8.32 Viscosity of CaO-Al_2O_3-MgO-MnO-K_2O-TiO_2-Ti_2O_3-SiO_2 melts in the section of (35.25SiO_2-35.25CaO-25.4MgO-2Al_2O_3-0.3MnO-0.8TiO_2-1K_2O) to (95.9Ti_2O_3-2Al_2O_3-0.3MnO-0.8TiO_2-1K_2O), mol% compared to experimental data [87].....179

Fig. 8.33 Viscosity of CaO-Al_2O_3-MgO-MnO-TiO_2-Ti_2O_3-SiO_2 melts at 11.64 mol% TiO_2, 14.28 mol% SiO_2, 2.3 mol% CaO, 2.1 mol% MgO and 1.2 mol% MnO compared to experimental data [195] 179

Fig. 8.34 Viscosity of Al_2O_3-MgO-MnO-TiO_2-Ti_2O_3-SiO_2 melts at 3.5 mol% Al_2O_3, 4.5 mol% SiO_2, 5.6 mol% MgO and 1.3 mol% MnO compared to experimental data [116].....180

Fig. 9.1 Comparison of Viscosity between CaF_2-SiO_2 and CaO-SiO_2 melts. Experimental points [22, 96, 145, 164, 174, 335] and a calculated line of CaO-SiO_2 melts at 1600°C.....184

Fig. 9.2 Calculated viscosity in CaF_2 system compared to experimental data [12, 38, 78, 97, 102, 149, 174, 216, 273, 309, 341, 347, 354, 356, 366, 365, 368] and to calculated viscosities of the model of Robelin and Chartrand [253].....190

Fig. 9.3 Viscosity of CaF_2-SiO_2 melts: experimental points [102, 174] and calculated lines.....191

Fig. 9.4 Viscosity of CaF_2-Al_2O_3 melts: experimental points [38, 102, 141, 169, 254, 347, 366, 365, 368] and calculated lines.....191

Fig. 9.5 Viscosity of CaF_2-CaO melts: experimental points [38, 79, 255, 341, 354, 366] and calculated lines.....192

Fig. 9.6 Viscosity of CaF_2-MgO melts: experimental points [79, 102, 309] and calculated lines.....193

Fig. 9.7 Viscosity of CaF_2-TiO_2 melts: experimental points [354] and calculated lines.....194

Fig. 9.8 Compositions in the CaF_2-CaO-SiO_2 system at which experimental viscosity measurements are available [90, 114, 196, 280, 292, 357, 368]. The lines indicate seven sections of this system selected to show the viscosity as a function of composition in Figs 9.9 to 9.15.....196

Fig. 9.9 Viscosity of CaF_2-CaO-SiO_2 melts for a molar ratio CaO/SiO_2 = 0.5464 compared to experimental data [292].....197

Fig. 9.10 Viscosity of CaF_2-CaO-SiO_2 melts for a molar ratio CaO/SiO_2 = 0.6857 compared to experimental data [292] 197

Fig. 9.11 Viscosity of CaF_2-CaO-SiO_2 melts in the section of (47.5 mol% CaO, 52.5 mol% SiO_2) to (4.06 mol% CaO, 95.94 mol% CaF_2) compared to experimental data [89, 280, 292, 368] 198

Fig. 9.12 Viscosity of CaF_2-CaO-SiO_2 melts for a molar ratio CaO/SiO_2 = 1 compared to experimental data [89, 368] 198

Fig. 9.13 Viscosity of CaF_2-CaO-SiO_2 melts for a molar ratio CaO/SiO_2 = 1.05851 compared to experimental data [89, 114, 292, 357] 199

Fig. 9.14 Viscosity of CaF_2-CaO-SiO_2 melts in the section of (57.44 mol% CaO, 42.56 mol% SiO_2) to (7.6 mol% CaO, 92.4 mol% CaF_2) compared to experimental data [89, 114, 292].....199

Fig. 9.15 Viscosity of CaF_2-CaO-SiO_2 melts in the section of (56.1 mol% CaO, 43.9 mol% CaF_2) to (17.15 mol% CaO, 82.85 mol% SiO_2) compared to experimental data [89, 196, 280, 292, 368] 200

Fig. 9.16 Compositions in the CaF_2-Al_2O_3-CaO system at which experimental viscosity measurements are available [38, 61, 141, 196, 245, 296, 368]. The lines indicate five sections of this system selected to show the viscosity as a function of composition in Figs 9.17 to 9.21.....202

Fig. 9.17 Viscosity of CaF_2-Al_2O_3-CaO melts for a molar ratio CaO/Al_2O_3 = 1.814 compared to experimental data [38, 61, 141, 245, 296, 368] 202

Fig. 9.18 Viscosity of CaF_2-Al_2O_3-CaO melts for a molar ratio CaO/Al_2O_3 = 2.933 compared to experimental data[38, 245] 203

Fig. 9.19 Viscosity of CaF_2-Al_2O_3-CaO melts for a molar ratio CaO/Al_2O_3 = 1.53 compared to experimental data [38, 245, 368].....203

Fig. 9.20 Viscosity of CaF_2-Al_2O_3-CaO melts in the section of (92.85 mol% CaO, 7.15 mol% CaF_2) to (87.39 mol% Al_2O_3, 12.61 mol% CaF_2) compared to experimental data [245, 296, 368] 204

Fig. 9.21 Viscosity of CaF_2-Al_2O_3-CaO melts at 30mol% Al_2O_3 compared to experimental data [245] 204

Fig. 9.22 Viscosity of CaF_2-Al_2O_3-MgO melts in the section of (65.95 mol% MgO, 34.05 mol% CaF_2) to (43.37 mol% Al_2O_3, 56.63 mol% CaF_2) compared to experimental data [254] 205

Fig. 9.23 Viscosity of CaF_2-SiO_2-TiO_2 melts for a molar ratio SiO_2/CaF_2 = 1.3 compared to experimental data [174] 206

Fig. 9.24 Compositions in the CaF_2-SiO_2-Al_2O_3 system at which experimental viscosity measurements are available [174, 254, 347]. The lines indicate four sections of this system selected to show the viscosity as a function of composition in Figs 9.25 to 9.28.....207

Fig. 9.25 Viscosity of CaF_2-SiO_2-Al_2O_3 melts in the section of (15.87 mol% SiO_2, 84.13 mol% Al_2O_3)-(12.62 mol% SiO_2, 87.38 mol% CaF_2) compared to experimental data [254, 347] 208

Fig. 9.26 Viscosity of CaF_2-SiO_2-Al_2O_3 melts in the section of (29.8 mol% SiO_2, 70.2 mol% Al_2O_3)-(24.52 mol% SiO_2, 75.48 mol% CaF_2) compared to experimental data [254, 347] 208

Fig. 9.27 Viscosity of CaF_2-SiO_2-Al_2O_3 melts in the section of (83.62 mol% CaF_2, 16.38 mol% Al_2O_3)-(8.05 mol% CaF_2, 91.95 mol% SiO_2) compared to experimental data [174, 347] 209

Fig. 9.28 Viscosity of CaF_2-SiO_2-Al_2O_3 melts in the section of (76.11 mol% CaF_2, 23.89 mol% Al_2O_3)-(96.02 mol% SiO_2, 3.98 mol% Al_2O_3) compared to experimental data [174, 347] 209

Fig. 9.29 Compositions in the CaF_2-MgO-SiO_2 system at which experimental viscosity measurements are available [102, 174, 254]. The lines indicate four sections of this system selected to show the viscosity as a function of composition in Figs 9.30 to 9.34.....211

Fig. 9.30 Viscosity of CaF_2-MgO-SiO_2 melts in the section of (5.66 mol% SiO_2, 94.34 mol% MgO)-(84.67 mol% CaF_2, 15.33 mol% SiO_2) compared to experimental data [102, 254] 211

Fig. 9.31 Viscosity of CaF_2-MgO-SiO_2 melts in the section of (73.82 mol% CaF_2, 26.18 mol% MgO)-(68.41 mol% SiO_2, 31.59 mol% MgO) compared to experimental data [102, 174] 212

Fig. 9.32 Viscosity of CaF_2-MgO-SiO_2 melts in the section of (29.7 mol% CaF_2, 70.3 mol% MgO)-(38.64 mol% CaF_2, 61.36 mol% SiO_2) compared to experimental data [174, 254] 212

Fig. 9.33 Viscosity of CaF_2-MgO-SiO_2 melts in the section of (25.6 mol% CaF_2, 74.4 mol% MgO)-(33.91 mol% CaF_2, 66.09 mol% SiO_2) compared to experimental data [174, 254] 213

Fig. 9.34 Viscosity of CaF_2-MgO-SiO_2 melts for a molar ratio SiO_2/CaF_2 = 1.3 compared to experimental data [174] 213

Fig. 9.35 Viscosity of CaF_2-Al_2O_3-CaO-SiO_2 melts in the section of (57.38 mol% SiO_2, 7.39 mol% Al_2O_3, 35.23 mol% CaO)-(32.05 mol% CaF_2, 19.86 mol% Al_2O_3, 48.09 mol% CaO) compared to experimental data [19, 117, 185, 367] 215

Fig. 9.36 Viscosity of CaF_2-Al_2O_3-CaO-SiO_2 melts in the section of (36.03 mol% CaF_2, 13.81 mol% Al_2O_3, 50.16 mol% CaO)-(31.87 mol% CaF_2, 21.37 mol% SiO_2, 45.76 mol% CaO) compared to experimental data [196] 216

Fig. 9.37 Viscosity of CaF_2-Al_2O_3-CaO-SiO_2 melts for molar ratios of Al_2O_3/CaO = 0.4584 and CaO/SiO_2 = 4.286 compared to experimental data [9].....216

Fig. 9.38 Viscosity of CaF_2-Al_2O_3-CaO-SiO_2 melts in the section of (34.23 mol% SiO_2, 2.88 mol% Al_2O_3, 62.88 mol% CaO)-(54.89 mol% CaF_2, 41.61 mol% SiO_2, 3.5 mol% Al_2O_3) compared to experimental data [163].....217

Fig. 9.39 Viscosity of CaF_2-Al_2O_3-CaO-SiO_2 melts in the section of (19.36 mol% SiO_2, 2.85 mol% Al_2O_3, 77.79 mol% CaO)-(71.55 mol% CaF_2, 24.8 mol% SiO_2, 3.65 mol% Al_2O_3) compared to experimental data [163].....217

Fig. 9.40 Viscosity of CaF_2-Al_2O_3-MgO-SiO_2 melts in the section of (49.56 mol% CaF_2, 13.8 mol% SiO_2, 36.64 mol% Al_2O_3)-(31.02 mol% CaF_2, 8.97 mol% SiO_2, 60.02 mol% MgO) compared to experimental data [254] 219

Fig. 9.41 Viscosity of CaF_2-Al_2O_3-MgO-SiO_2 melts in the section of (41.4 mol% CaF_2, 26.9 mol% SiO_2, 31.7 mol% Al_2O_3)-(27.88 mol% CaF_2, 18.12 mol% SiO_2, 54 mol% MgO) compared to experimental data [254] 219

Fig. 9.42 Viscosity of CaF_2-Al_2O_3-B_2O_3-CaO melts in the section of (36.03 mol% CaF_2, 13.81 mol% Al_2O_3, 50.16 mol% CaO)-(33.86 mol% CaF_2, 19 mol% B_2O_3, 47.14 mol% CaO) compared to experimental data [196] 220

Fig. 9.43 Viscosity of CaF_2-Al_2O_3-B_2O_3-CaO melts in the section of [$(CaF_2)_{3.047}$–Al_2O_3]-[CaO–B_2O_3] compared to experimental data [102].....220

Fig. 9.44 Viscosity of CaF_2-B_2O_3-Na_2O-SiO_2 melts in the section of (63.7 mol% SiO_2, 28.45 mol% Na_2O, 9.85 mol% B_2O_3)-(99.42 mol% CaF_2, 0.53 mol% Na_2O, 0.05 mol% B_2O_3) compared to experimental data [215] 221

Fig. 9.45 Viscosity of CaF_2-Al_2O_3-CaO-Na_2O melts in the section of (100 mol% Na_2O)-(65.51 mol% CaO, 21.39 mol% CaF_2, 13.10 mol% Al_2O_3) compared to experimental data [16] 223

Fig. 9.46 Viscosity of CaF_2-Al_2O_3-CaO-Na_2O melts in the section of (63.7 mol% SiO_2, 28.45 mol% Na_2O, 9.85 mol% B_2O_3)-(99.42 mol% CaF_2, 0.53 mol% Na_2O, 0.05 mol% B_2O_3) compared to experimental data [16] 223

Fig. 9.47 Viscosity of CaF_2-Al_2O_3-CaO-MnO melts for molar ratios of Al_2O_3/CaO = 0.385 and CaF_2/Al_2O_3 = 1.488 compared to experimental data [367].....224

Fig. 9.48 Viscosity of CaF_2-Al_2O_3-CaO-TiO_2 melts for molar ratios of Al_2O_3/CaO = 0.385 and CaF_2/Al_2O_3 = 1.492 compared to experimental data [367].....224

Fig. 9.49 Viscosity of CaF_2-CaO-Na_2O-SiO_2 melts for a weight ratio of CaO/SiO_2 = 0.8 and Na_2O = 12wt% compared to experimental data [226].....225

Fig. 9.50 Viscosity of CaF_2-CaO-Na_2O-SiO_2 melts in the section of (64.62 mol% SiO_2, 33.49 mol% Na_2O, 1.89 mol% CaO)-(80 mol% CaF_2, 5.22 mol% SiO_2, 14.78 mol% CaO) compared to experimental data [57]…….....225

Fig. 9.51 Viscosity of CaF_2-CaO-Na_2O-SiO_2 melts in the section of (70.18 mol% SiO_2, 29.05 mol% Na_2O, 0.77 mol% CaO)-(61.2 mol% CaF_2, 24.52 mol% SiO_2, 14.28 mol% CaO) compared to experimental data [57].....226

Fig. 9.52 Viscosity of CaF_2-Al_2O_3-CaO-MgO-SiO_2 melts in the section of (2.03 mol% CaF_2, 4.84 mol% SiO_2, 89.2 mol% CaO, 3.93 mol% MgO)-(17.5 mol% CaF_2, 41.69 mol% SiO_2, 6.91 mol% Al_2O_3, 33.9 mol% MgO) compared to experimental data [198].....227

Fig. 9.53 Viscosity of CaF_2-Al_2O_3-CaO-MgO-SiO_2 melts in the section of (10wt% SiO_2, 30wt% Al_2O_3, 55wt%CaO, 5wt% MgO)-(10 wt% CaF_2, 20 wt% SiO_2, 10 wt% Al_2O_3, 55 wt%CaO, 5 wt% MgO) compared to experimental data [138]…….....227

Fig. 9.54 Viscosity of CaF_2-Al_2O_3-CaO-MgO-SiO_2 melts in the section of (75.3 mol% CaO, 11.46 mol% Al_2O_3, 5.43 mol% MgO, 7.8 mol% CaF_2)-(57.7 mol% SiO_2, 22.98 mol% CaO, 11.5 mol% MgO, 7.8 mol% CaF_2) compared to experimental data [138, 328].....228

Fig. 9.55 Comparison between calculation and experimental data for the viscosity of mold flux melts [31, 156, 182].....229

Fig. 10.1 Calculated viscosity in NaF system compared to Experimental data [1, 25, 29, 40, 56, 217, 240, 342] 231

Fig. 10.2 Calculated viscosity in MgF_2 system compared to Experimental data [97, 149].....232

Fig. 10.3 Calculated viscosity in KF system compared to Experimental data [56]….....232

Fig. 10.4 Calculated viscosity in KF-B_2O_3 system compared to Experimental data [326].....233

Fig. 10.5 Calculated viscosity in NaF-B_2O_3 system compared to Experimental data [221].....234

Fig. 10.6 Viscosity of NaF-CaO-SiO_2 melts for a weight ratio CaO/SiO2 = 1 compared to experimental data [357].....235

Fig. 10.7 Viscosity of MgF_2-CaO-SiO_2 melts for a weight ratio CaO/SiO2 = 0.51 compared to experimental data [292]…….....237

Fig. 10.8 Viscosity of MgF_2-CaO-SiO_2 melts for a weight ratio CaO/SiO2 = 1 compared to experimental data [292].....237

Fig. 10.9 Viscosity of MgF_2-CaO-SiO_2 melts for a weight ratio CaO/SiO2 = 1.28 compared to experimental data[292].....238

Fig. 10.10 Compositions in the NaF-Na_2O-SiO_2 system at which experimental viscosity measurements are available [21, 57]. The lines indicate six sections of this system selected to show the viscosity as a function of composition in Figs 10.11 to 10.16.....239

Fig. 10.11 Viscosity of NaF-Na_2O-SiO_2 melts in the section of (65.91 mol% SiO_2, 34.09 mol% Na_2O) to (94.48 mol% NaF, 5.52 mol% Na_2O) compared to experimental data [57].....240

Fig. 10.12 Viscosity of NaF-Na_2O-SiO_2 melts in the section of (68.21 mol% SiO_2, 31.79 mol% Na_2O) to (96 mol% NaF, 4 mol% Na_2O) compared to experimental data [57]…….....240

Fig. 10.13 Viscosity of NaF-Na_2O-SiO_2 melts at a molar ratio of SiO_2/Na_2O = 1 compared to experimental data [21].....241

Fig. 10.14 Viscosity of NaF-Na_2O-SiO_2 melts at a molar ratio of SiO_2/Na_2O = 0.667 compared to experimental data [21].....241

Fig. 10.15 Viscosity of NaF-Na_2O-SiO_2 melts in the section of (66.18 mol% Na_2O, 33.82 mol% NaF) to (73.45 mol% SiO_2, 26.55 mol% NaF) compared to experimental data [21, 57].....242

Fig. 10.16 Viscosity of NaF-Na_2O-SiO_2 melts in the section of (78.41 mol% Na_2O, 21.59 mol% NaF) to (92.14 mol% SiO_2, 7.86 mol% NaF) compared to experimental data [21, 57].....242

Fig. 10.17 Viscosity of NaF-Na_2O-B_2O_3 melts in the section of (33.33 mol% Na_2O, 66.67 mol% B_2O_3) to (50 mol% NaF, 50 mol% B_2O_3) compared to experimental data [221]…….....243

Fig. 10.18 Viscosity of CaO-Al_2O_3-SiO_2-AlF_3 melts in the section of 3($CaSiO_3$)-Al_2O_3 to AlF_3 compared to experimental data [117].....244

Fig. 10.19 Viscosity of CaO-Al_2O_3-SiO_2-NaF melts in the section of 3($CaSiO_3$)-Al_2O_3 to NaF compared to experimental data [117].....244

Fig. 10.20 Viscosity of CaO-Al_2O_3-SiO_2-MgF_2 melts in the section of 3($CaSiO_3$)-Al_2O_3 to MgF_2 compared to experimental data [117].....245

Fig. 10.21 Viscosity of CaF_2-NaF-Na_2O-B_2O_3 melts in the section of (77.44 mol% CaF_2, 7.56 mol% Na_2O, 15 mol% B_2O_3) to (86.47 mol% NaF, 4.54 mol% Na_2O, 9 mol% B_2O_3) compared to experimental data [308].....246

Fig. 11.1 Calculated and experimental [113] non-bridging oxygens (NBO/Si) of for the MgO-SiO_2 system at 1600°C.....252

Fig. 11.2 Calculated viscosity in PbO system compared to Experimental data [219] as a function of temperature.....258

Fig. 11.3 Calculated viscosity in $NaO_{0.5}$-SiO_2 system compared to Experimental data [23, 51, 88, 134, 166, 167, 208, 212, 223, 238, 246, 267, 283, 290, 294, 298, 299, 312, 333, 349] as a function of composition.....260

Fig. 11.4 Calculated viscosity in $NaO_{0.5}$-SiO_2 system compared to Experimental data [23, 51, 134, 208, 223, 246, 267] as a function of temperature.....261

Fig. 11.5 Calculated viscosity in $KO_{0.5}$-SiO_2 system compared to Experimental data [23, 208, 223, 237, 263, 267, 283] [11, 53, 125, 193, 238] and the model by Fluegel [67] as a function of composition.....263

Fig. 11.6 Calculated viscosity in $KO_{0.5}$-SiO_2 system compared to Experimental data [11, 193, 223, 283] [208, 237, 267] as a function of temperature.....264

Fig. 11.7 (a) Calculated viscosity in PbO-SiO_2 system compared to experimental data [55, 63, 69, 74, 80, 85, 137, 140, 202, 207, 209, 243, 263, 302, 332] (b) Compares experimental data with the extended model and the previous model with an expanded scale.....265-266

Fig. 11.8 Calculated viscosity in CaO-SiO_2 system compared to experimental data [96, 164, 212, 213, 335].....267

Fig. 11.9 Calculated viscosities in binary (a) CaO-SiO_2 and (b) MgO-SiO_2 systems by the model at different temperatures.....268

Fig. 11.10 Compositions in the CaO–Na_2O–SiO_2 system at which the viscosity was measured and experimental data [30, 48, 68, 105, 165, 179, 212, 239, 262, 266, 294, 349]…….....270

Fig. 11.11 Viscosity of CaO–Na_2O–SiO_2 melts at 60 mol% SiO_2: experimental points [30, 105, 212, 294, 349] and calculated lines.....271

Fig. 11.12 Viscosity of CaO–Na_2O–SiO_2 melts at 65 mol% SiO_2: experimental points [30, 239, 279, 294, 349] and calculated lines.....271

Fig. 11.13 Viscosity of CaO–Na_2O–SiO_2 melts at 70 mol% SiO_2: experimental points [105, 165, 179, 239, 262, 279, 294, 349] and calculated lines.....272

Fig. 11.14 Viscosity of CaO–Na_2O–SiO_2 melts at 75 mol% SiO_2: experimental points [30, 48, 279, 294] and calculated lines.....272

Fig. 11.15 Viscosity of CaO–Na_2O–SiO_2 melts at 10 mol% CaO: experimental points [68, 105, 165, 179, 212, 239, 262, 266, 294, 349] and calculated lines.....273

Fig. 11.16 Viscosity of CaO–Na_2O–SiO_2 melts at 15 mol% CaO: experimental points [239, 268, 294] and calculated lines.....273

Fig. 11.17 Compositions in the MgO–Na_2O–SiO_2 system at which the viscosity was measured and experimental data [59, 75, 95, 105, 119, 122, 179, 239, 242, 260].....274

Fig. 11.18 Viscosity of MgO–Na_2O–SiO_2 melts for a pseudo-binary section between the compositions (74.69 mol% SiO_2, 25.31 mol% Na_2O) and (76.21 mol% SiO_2, 23.79 mol% MgO): experimental points [59, 75, 239] and calculated lines.....275

Fig. 11.19 Viscosity of MgO–Na_2O–SiO_2 melts for a pseudo-binary section between the compositions (63.28 mol% SiO_2, 36.72 mol% MgO) and (58.77 mol% SiO_2, 41.23 mol% Na_2O): experimental points [75, 105, 239, 260] and calculated lines.....275

Fig. 11.20 Viscosity of MgO–Na_2O–SiO_2 melts for a pseudo-binary section between the compositions (74.16 mol% SiO_2, 25.84 mol% MgO) and (67.37 mol% SiO_2, 32.63 mol% Na_2O): experimental points [95, 105, 122, 179, 239]and calculated lines.....276

Fig. 11.21 Viscosity of MgO–Na_2O–SiO_2 melts for a pseudo-binary section between the compositions (80.53 mol% SiO_2, 19.47 mol% MgO) and (58.67 mol% SiO_2, 41.33 mol% Na_2O): experimental points [75, 179, 239, 242] and calculated lines.....276

Fig. 11.22 Viscosity of MgO–Na_2O–SiO_2 melts for a pseudo-binary section between the compositions (60 mol% SiO_2, 40 mol% MgO) and (63.6 mol% SiO_2, 36.4 mol% Na_2O): experimental points [75, 239, 242] and calculated lines.....277

Fig. 11.23 Viscosity of $MgO–Na_2O–SiO_2$ melts for a pseudo-binary section between the compositions (87.36 mol% MgO, 12.64 mol% Na_2O) and (82.4 mol% SiO_2, 17.6 mol% Na_2O): experimental points [59, 75, 119] and calculated lines.....277

Fig. 11.24 Viscosity of $MgO–Na_2O–SiO_2$ melts at 10 mol% MgO: experimental points [105, 119, 179, 260] and calculated lines.....278

Fig. 11.25 Viscosity of $MgO–Na_2O–SiO_2$ melts at 77 mol% SiO_2: experimental points [75, 239] and calculated lines.....278

Fig. 11.26 Viscosity of $CaO–MgO–SiO_2$ melts at 50 mol% SiO_2: experimental points [83, 164, 213, 297, 314, 318, 320] and calculated lines.....280

Fig. 11.27 Viscosity of diopside melts as a function of temperature: experimental points [164, 213, 297, 314, 318, 320] and calculated lines.....280

Fig. 11.28 Viscosity of $Na_2O–K_2O–SiO_2$ melts at 87 mol% SiO_2: experimental points [208] and calculated lines.....282

Fig. 11.29 Viscosity of $Na_2O–K_2O–SiO_2$ melts at 95 mol% SiO_2: experimental points [208] and calculated lines.....282

Fig. 11.30 Viscosity of $Na_2O–K_2O–SiO_2$ melts at 34 mol% Na_2O+K_2O total: experimental points [238] and calculated lines.....283

Fig. 11.31 Viscosity of $PbO–K_2O–SiO_2$ melts at 10 mol% K_2O: experimental points [94, 263] and calculated lines.....283

Fig. 11.32 Viscosity of $PbO–K_2O–SiO_2$ melts at 20 mol% K_2O: experimental points [263] and calculated lines.....284

Fig. 11.33 Viscosity of $PbO–K_2O–SiO_2$ melts at 30 mol% K_2O: experimental points [94, 263] and calculated lines.....284

Fig. 11.34 Viscosity of $PbO–Na_2O–SiO_2$ melts for a pseudo-binary section between the compositions (66 mol% SiO_2, 34 mol% Na_2O) and (47.9 mol% SiO_2, 52.1 mol% PbO): experimental points [63, 62, 327] and calculated lines.....285

Fig. 11.35 Viscosity of $ZnO–Na_2O–SiO_2$ melts at 10 mol% ZnO: experimental points [105, 235, 313] and calculated lines.....285

Fig. 11.36 Viscosity of $ZnO–Na_2O–SiO_2$ melts at 20 mol% ZnO: experimental points [105, 313] and calculated lines.....286

Fig. 11.37 Compositions in the $Na_2O–Al_2O_3–SiO_2$ system at which the viscosity was measured and experimental data [98, 125, 214, 252, 269, 297, 307, 321, 324, 335] 288

Fig. 11.38 Viscosity of $Na_2O–Al_2O_3–SiO_2$ melts at 50 mol% SiO_2: experimental points [214, 252, 324] and calculated lines by the extended model and previous model.....289

Fig. 11.39 Viscosity of $Na_2O–Al_2O_3–SiO_2$ melts at 60 mol% SiO_2: experimental points [252, 307, 324] and calculated lines by the extended model and previous model.....289

Fig. 11.40 Viscosity of $Na_2O–Al_2O_3–SiO_2$ melts at 67 mol% SiO_2: experimental points [125, 252, 307, 321, 324] and calculated lines by the extended model and previous model.....290

Fig. 11.41 Viscosity of $Na_2O–Al_2O_3–SiO_2$ melts at 75 mol% SiO_2: experimental points [98, 214, 252, 269, 297, 321, 324, 335] and calculated lines.....290

Fig. 11.42 Viscosity of $Na_2O–Al_2O_3–SiO_2$ melts at 82 mol% SiO_2: experimental points [307, 324] and calculated lines.....291

Fig. 11.43 Compositions in the $CaO–Al_2O_3–SiO_2$ system at which the viscosity was measured and experimental data [58, 83, 98, 109, 145, 172, 256, 270, 297, 303, 318, 320, 323, 330, 335] 292

Fig. 11.44 Viscosity of $CaO–Al_2O_3–SiO_2$ melts at 50 mol% SiO_2: experimental points [83, 98, 145, 172, 270, 297, 303, 318, 320, 323, 335] and calculated lines.....292

Fig. 11.45 Viscosity of $CaO–Al_2O_3–SiO_2$ melts at 67 mol% SiO_2: experimental points [58, 109, 172, 323, 330] and calculated lines.....293

Fig. 11.46 Viscosity of $CaO–Al_2O_3–SiO_2$ melts at 75 mol% SiO_2: experimental points [297, 323] and calculated lines.....293

Fig. 11.47 Viscosity of $CaO–Al_2O_3–SiO_2$ melts at constant molar ratios of $CaO/Al_2O_3 = 1$: experimental points [98, 145, 256, 270, 297, 318, 320, 323, 335] and calculated lines.....294

Fig. 11.48 Viscosity of $MgO–Al_2O_3–SiO_2$ melts at 50 mol% SiO_2: experimental points [168, 251, 323, 335, 363] and calculated lines.....295

Fig. 11.49 Viscosity of $ZnO–Al_2O_3–SiO_2$ melts at 50 mol% SiO_2: experimental points [183, 193] and calculated lines.....295

Fig. 11.50 Viscosity of diopside–anorthite ($CaMgSi_2O_6–CaAl_2Si_2O_8$) melts: experimental points [270, 318, 320]and calculated lines by the extended model and the previous model.....298

Fig. 11.51 Viscosity of nepheline–diopside ($NaAlSiO_4–CaMgSi_2O_6$) melts: experimental points [314] and calculated lines by the extended model and the previous model.....298

Fig. 11.52 Viscosity of anorthite–albite ($CaAl_2Si_2O_8–NaAlSi_3O_8$) melts: experimental points [36, 98, 146, 200]and calculated lines by the extended model and the previous model.....299

Fig. 11.53 Viscosity of CaO-$MgO–Na_2O–SiO_2$ for a pseudo-ternary section between the compositions (74.05 mol% SiO_2, 11.75 mol% CaO, 14.2 mol% Na_2O) and (70.18 mol% SiO_2, 15.6 mol% MgO, 14.2 mol% Na_2O): experimental points [124] and calculated lines.....300

Fig. 11.54 Viscosity of CaO-$MgO–Na_2O–SiO_2$ for a pseudo-ternary section between the compositions (74.11 mol% SiO_2, 10.69 mol% CaO, 15.2 mol% Na_2O) and (70.53 mol% SiO_2, 14.25 mol% MgO, 15.2 mol% Na_2O): experimental points [122] and calculated lines.....301

Fig. 11.55 Viscosity of CaO-$MgO–Na_2O–Al_2O_3–SiO_2$ at 17.3 mol% CaO, 6.41 mol% MgO and 11.43 mol% Al_2O_3: experimental points [218] and calculated lines.....301

Fig. 11.56 Viscosity of CaO-$MgO–Na_2O–Al_2O_3–SiO_2$ at 14.5 mol% Na_2O, 6.44 mol% CaO and 2.95 mol% Al_2O_3: experimental points [124] and calculated lines.....302

Fig. 11.57 Viscosity of CaO-$MgO–Na_2O–Al_2O_3–SiO_2$ for a pseudo-ternary section between the compositions (73.85 mol% SiO_2, 1.77 mol % Al_2O_3, 10.8 mol% CaO, 13.56 mol% Na_2O) and (70.22 mol% SiO_2, 1.77 mol % Al_2O_3, 14.45 mol% MgO, 13.56 mol% Na_2O): experimental points [4] and calculated lines.....302

Fig. 11.58 Viscosity of $CaO–Na_2O–K_2O–Al_2O_3–SiO_2$ at 60 mol% SiO_2, 8 mol% CaO and 16 mol% Al_2O_3: experimental points [305] and calculated lines.....303

Fig. 11.59 Viscosity of CaO-MgO–Na_2O–K_2O–Al_2O_3–SiO_2 at 64.5 mol% SiO_2, 16.8 mol% CaO, 9 mol% Al_2O_3 and 6.2 mol% MgO: experimental points [5] and calculated lines.....303

Fig. 11.60 Viscosity of CaO-MgO–Na_2O–K_2O–Al_2O_3–SiO_2 at 72.3 mol% SiO_2, 8.6 mol% CaO, 1.5 mol% Al_2O_3 and 5.6 mol% MgO: experimental points [5] and calculated lines.....304

Fig. 11.61 Viscosity of ZnO-CaO-MgO-Na_2O-K_2O-SiO_2 at 6 mol% CaO, 5.3 mol% MgO, 13.7 mol% Na_2O and 2.6 mol% K_2O: experimental points [70] and calculated lines.....305

Fig. 11.62 Viscosity of Container and Float Glasses: Experimental points [279] and calculated lines. Figures (a) to (d) compares the viscosity model proposed in the present study (solid lines) with the model by Fluegel [67] (dashed lines).....307-309

Fig. 11.63 Viscosity of CaO-MgO–Na_2O–SiO_2 at 10.27 mol% CaO and 14.79 mol% Na_2O: experimental points [122, 124, 181, 279] and calculated lines (solid lines) compared with the model proposed by Fluegel [67] (dashed lines).....310

Fig. 11.64 Viscosity of CaO-MgO–Na_2O–SiO_2 at 7.42 mol% CaO and 4.23 mol% MgO: experimental points [122, 268, 279] and calculated (solid lines) compared with the model proposed by Fluegel [67] (dashed lines).....311

Fig. 12.1 a) Calculated viscosity in B_2O_3 compared to experimental data [35, 60, 100, 106, 131, 148, 162, 173, 178, 197, 204, 220, 228, 236, 247, 258, 265, 281, 291, 301, 326, 345, 355] b) Comparison of experimental data with the extended model prediction with expanded scale in the melt c) Comparison of experimental data with the extended model with expanded scale in the glass.....321-322

Fig. 12.2 a) Calculated viscosity in Na_2O-B_2O_3 system compared to experimental data [71, 95, 112, 157, 206, 261, 265, 281, 306, 343, 355] with expanded scale b) Compares experimental data with the extended model.....324

Fig. 12.3 a) Calculated viscosity in K_2O-B_2O_3 system compared to experimental data [35, 112, 148, 157, 258, 281, 315, 326, 355] with expanded scale and to the calculated line (dashed line) using the previous model of the Sections 3.3.2 and 3.3.3 at 600ºC b) Comparison of experimental data with the extended model.....325-326

Fig. 12.4 Calculated viscosity in $CaO\text{-}B_2O_3$ system compared to experimental data [101, 133, 205] and to the calculated line (dashed line) using the previous model of the Sections 3.3.2 and 3.3.3 at 700 and 1200ºC.....327

Fig. 12.5 Calculated viscosity in $PbO\text{-}B_2O_3$ system compared to experimental data [39, 55, 74, 86, 131, 210, 241, 300] and to the calculated (dashed line) using the previous model of the Sections 3.3.2 and 3.3.3 at 600ºC.....329

Fig. 12.6 T_g (Glass-transition Temp.) data at 8.5 mol%, 15 mol% and 22 mol% Na_2O in the system $B_2O_3\text{-}Al_2O_3\text{-}Na_2O$ [130, 132] 330

Fig. 12.7 Calculated viscosity in $Al_2O_3\text{-}B_2O_3$ system compared to experimental data [197].....331

Fig. 12.8 Calculated viscosity in $ZnO\text{-}BO_{1.5}$ system compared to experimental data [50, 100, 101, 135, 136, 162, 211, 244, 276].....331

Fig. 12.9 Calculated viscosity in $B_2O_3\text{-}SiO_2$ system compared to experimental data [8, 100, 161, 180, 197, 225, 337].....333

Fig. 12.10 Compositions in the $Na_2O–K_2O–B_2O_3$ system at which the viscosity was measured [95, 150, 178, 261, 343].....335

Fig. 12.11 Viscosity of $Na_2O–K_2O–B_2O_3$ system at constant molar ratios of $Na_2O/K_2O = 1$: experimental points [95, 150, 178, 343] and calculated lines.....335

Fig. 12.12 Viscosity of $Na_2O–K_2O–B_2O_3$ system at 83.33 mol% B_2O_3: experimental points [95] and calculated lines.....336

Fig. 12.13 Viscosity of $Na_2O–K_2O–B_2O_3$ system at 90 mol% B_2O_3: experimental points [261] and calculated lines.....336

Fig. 12.14 Compositions in the $Na_2O–B_2O_3–SiO_2$ system at which the viscosity was measured [51, 203, 229, 290, 316].....338

Fig. 12.15 Viscosity of $Na_2O– B_2O_3–SiO_2$ system at 60 mol% SiO_2: experimental points [51, 203, 229, 290, 316] and calculated lines.....338

Fig. 12.16 Viscosity of $Na_2O– B_2O_3–SiO_2$ system at constant molar ratios of $SiO_2/Na_2O = 1$: experimental points [203, 290] and calculated lines.....339

Fig. 12.17 Compositions in the B_2O_3–PbO–Al_2O_3 system at which the viscosity was measured [194, 210] 340

Fig. 12.18 Viscosity of B_2O_3–PbO–Al_2O_3 system for a pseudo-binary section between the compositions (90.55 mol% B_2O_3, 9.45 mol% PbO) and (87.05 mol% B_2O_3, 12.95 mol% Al_2O_3):: experimental points [210] and calculated lines.....340

Fig. 12.19 Viscosity of B_2O_3–PbO–Al_2O_3 system for a pseudo-binary section between the compositions (83.3 mol% PbO, 16.7 mol% Al_2O_3) and (99.8 mol% B_2O_3, 0.2 mol% PbO): experimental points [194, 210] and calculated lines.....341

Fig. 12.20 Viscosity of B_2O_3–PbO–Al_2O_3 system for a pseudo-binary section between the compositions (67 mol% PbO, 33.3 mol% Al_2O_3) and (99 mol% B_2O_3, 1 mol% PbO): experimental points [194, 210] and calculated lines.....341

Fig. 12.21 Viscosity of B_2O_3–CaO–Al_2O_3 system at 21.5 mol% Al_2O_3: experimental points [142] and calculated lines.....342

Fig. 12.22 Viscosity of B_2O_3–CaO–K_2O system at 3 mol% K_2O: experimental points [35] and calculated lines.....342

Fig. 12.23 Viscosity of ZnO-PbO-B_2O_3 system at 12.5 mol% PbO: experimental points [136] and calculated lines.....343

Fig. 12.24 Viscosity of B_2O_3–CaO–Al_2O_3–K_2O–Na_2O system for a pseudo-binary section between the compositions (64.73 mol% B_2O_3, 15.3 mol% Al_2O_3, 8.41 mol% CaO, 1.56 mol% K_2O) and (61.07 mol% B_2O_3, 14.43 mol% Al_2O_3, 7.94 mol% CaO, 16.56 mol% Na_2O): experimental points [220] and calculated lines.....345

Fig. 12.25 Viscosity of subsystems of B_2O_3–SiO_2–CaO–MgO–Al_2O_3–K_2O–Na_2O system: comparison of experimental points [13, 43, 220, 293, 369] with calculation.....345

Fig. 12.26 Viscosity of E glass-3, Wool glass and Low expansion borosilicate(LEB)-12 glass: Experimental points [279] and calculated lines. Figures (a) to (c) compares the viscosity model proposed in the present study (solid lines) with the model by Fluegel [67] (dashed lines).....347-348

Fig. 12.27 Viscosity of E glass series: Experimental points [279] and calculated lines by the extended model(solid lines) and by Fluegel [67] (dashed lines).....348

Fig. 12.28 Viscosity of wool glass series: Experimental points [279] and calculated lines by the extended model(solid lines) and by Fluegel [67] (dashed lines).....349

Fig. 12.29 Viscosity of low expansion borosilicate(LEB) glass series: Experimental points [279] and calculated lines by the extended model(solid lines) and by Fluegel [67] (dashed lines).....349

LIST OF SYMBOLS

Symbols	Description	Units
A , A^W , A_e	Pre-exponential factor in viscosity	Pa·s
A_τ	Pre-exponential terms for structural relaxation times	Pa·s
B_e	The molar Gibbs free-energy barriers opposing structural rearrangements	J/mol
$\mathbf{C_o}$	The Equipment Constant	Dimensionless
d	The thickness of the cylinder	M
$\mathbf{d_b}$	The diameters of the ball	M
$\mathbf{d_c}$	The diameters of the crucible	M
E , E_η^W , E_V , E_a	The Activation Energy for viscosity	J/mol
ΔE_v	The energy of Vaporization	J/mol
ΔG_i	The Gibbs energy for the formation of *i* species	J/mol
G	The gravitational constant	$N(m/kg)^2$
g	The acceleration of gravity	m/s^2
h	Plank's constant	J·s
h	The height of spindle	m
$\mathbf{h_s}$	The height of sample	m
I	The indent distance	m
κ	The period of oscillation in an empty system	s
k	Boltzmann Constant	J/K
L	The penetration depth	m
M	Torque	N·m
$\mathbf{M_s}$	The applied force	N
m_{SU}	The average mass of a viscous flow structural unit	kg
m_{i-j}	The masses of *i*–*j* second nearest neighbor pair	kg
n_i	Number of moles component *i*	mol
n_{i-j}	Number of moles of *i*–*j* second nearest neighbor pair	mol
n	The revolutions per second	rpm
η	Viscosity	poise, Pa·s
P	The applied Force	$N(m/s^2)$
ρ	Density	kg/m^3
ρ_k	The densities of the ball	kg/m^3

Symbols	Description	Units
ρ_l	The densities of the liquid	kg/m^3
R	Gas Constant	J/mol·K
r	The radius of the cylinder	m
r_i	The radius of spindle	m
r_o	The radius of crucible	m
r_s	The radius of the sphere	m
r_h	The radius of the half-sphere	m
S	Distance between atoms in the liquid	M
S^{conf}	The configuration Entropy	J/K
T	Absolute Temperature	K
T_g	Glass Transition Temperature	K, ºC
t	Time	s
τ	The structural relaxation time	s
θ	The moment of inertia of the oscillation	kg/m^2
λ	The decrement due to the damping effect of the liquid	s^{-1}
v_{SU}	The average volume of a viscous flow structural unit	m^3
v_{i-j}	The volumes of *i–j* second nearest neighbor pair	m^3
v	The velocity of descent or ascent of the sphere	m/s
V	The volume of the sample	m^3
X_i	Mole fraction of component *i*	Dimensionless
X_{i-j}	Mole fractions of *i–j* second nearest neighbor pair	Dimensionless
y	The sagging rate of center part of the sample	m/s

CHAPTER 1 INTRODUCTION

An understanding of the metallurgical process phenomena and an optimization of the processes require access to accurate data of the physical properties of the molten slags and glasses involved. Among those physical properties such as viscosity, surface tension, thermal conductivity etc., one of the most important in the case of molten slags and glasses is the viscosity. An accurate knowledge of the viscosity of a wide variety of molten slags is indispensable for a number of pure and applied scientific disciplines. In metallurgy, silicate melts are known as slags. Knowledge of the viscosity of the slag phase is important for blast furnace operation and also for the steel refining process. Slags are further used as mold fluxes in the continuous casting process where the viscosity of slags is of paramount importance. In the continuous casting process of steelmaking, the viscosity of a slag affects the velocity of circulating slag flow which controls a mass transfer at the slag/metal interface and should be low enough to provide sufficient lubrication to prevent sticking, control uniform heat transfer and prevent surface cracks as shown in Fig. 1.1.

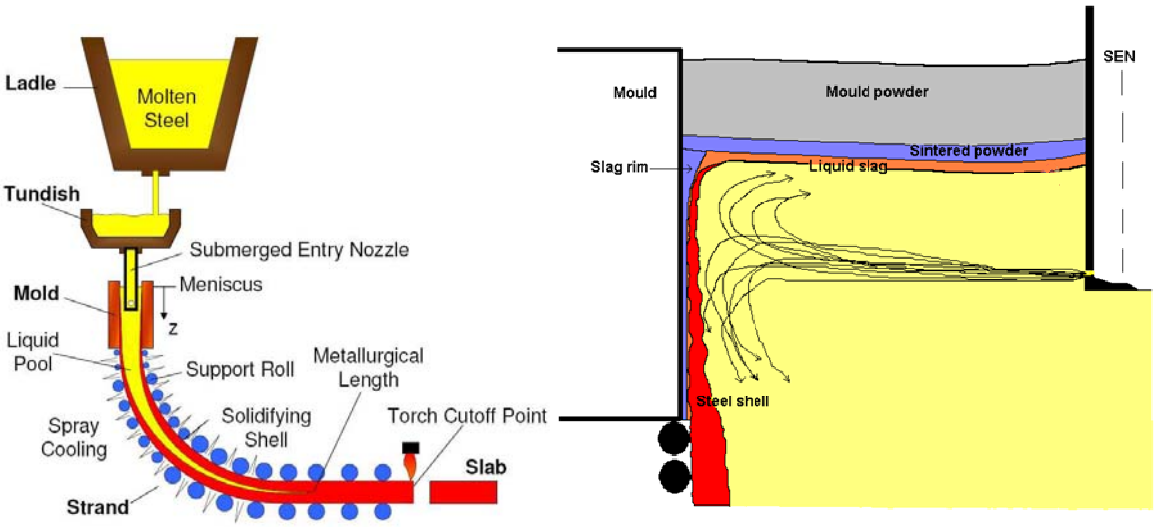

a) Schematic of Continuous Casting Process b) Schematic of Mold

Fig. 1.1 Schematic diagrams of Continuous Casting Process and Mold in the steelmaking process

The viscosity of silicate melts is also a fundamental parameter for the glass industry and for geological processes involving the flow of magmatic melts. It is well known that any liquid forms a glass when melts are supercooled rapidly enough to avoid crystallization. [6, 7, 47, 49] In

metallurgy, the supercooled silicate melts are known as glasses. Especially, the viscosity of liquid glasses is very high and crystallization from such high-viscosity liquid proceeds with great difficulty. The viscosity of the glass is important for the melting and refining conditions in glass furnaces. In the glassmaking process, there are several critical points which are mainly influenced by the viscosity of glass as shown in Fig.1.2.

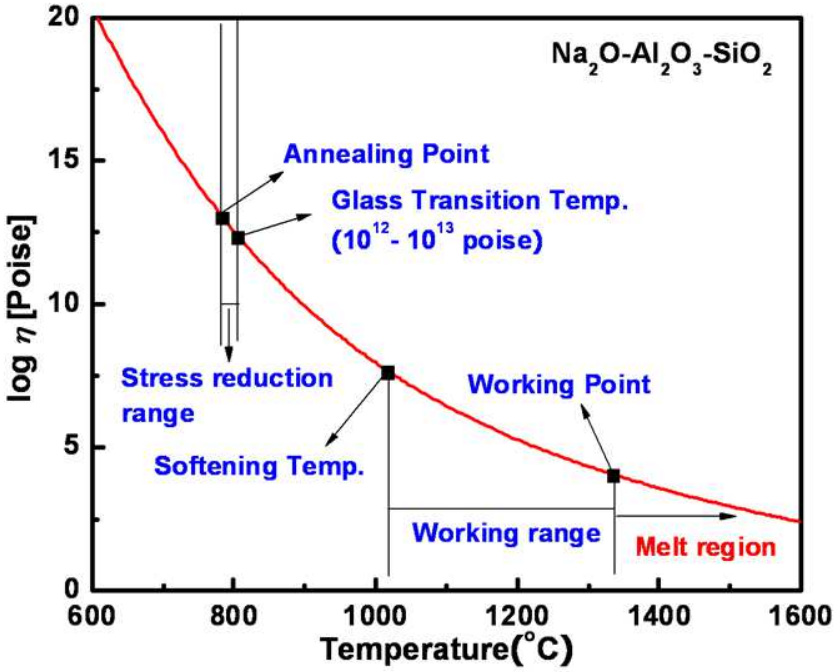

Fig. 1.2 Viscosity of Na_2O-Al_2O_3-SiO_2 as a function of temperatures and critical viscosity points in the glassmaking process

Upon cooling silicate melts, the viscosity increases and approaches 4 in the logarithm poise scale as the glass at the working point is formed. Once glass is formed, the glass should be supported until the viscosity reaches a value sufficiently high to prevent deformation under its own weight which stops at the viscosity 7.6 in the logarithm poise scale. The temperature range between these two points is the working range. High viscosity ranges between 12 and 13 in the logarithm poise scale correspond to important temperature ranges which release the internal stress of the glass by annealing.

Thus, many geological, glass and metallurgical scientists have developed viscosity models to take into account the composition and temperature dependence of viscosity of molten slags and glasses. [2, 67, 73, 77, 107, 139, 201, 249, 334, 336, 344, 359, 360] Most models were developed as empirical or numerical models which do not take into account the structure of silicate melts. Furthermore, no model can satisfactorily predict the viscosity of silicate melts and glasses over a wide composition and temperature range. Most models are only applicable to a few binary, ternary and multi-component systems.

Recently, a new model for the viscosity of silicate melts was developed in this laboratory [81, 82]. In this model, the viscosity is related to the structure of the melt, which in turn is calculated from the thermodynamic description of the melt using the Modified Quasichemical Model [231, 232]. Most importantly, the model takes into account the formation of the silica network which has a profound effect on the viscosity. The model predicts within experimental error limits the viscosity of multicomponent slags from just a few model parameters fitted to the viscosities of the binary and some ternary subsystems. [81, 82] In spite of its good predictability of viscosities in metallurgical molten slags, the model still had some drawbacks for specific systems such as alkali-rich silicate melts and oxy-fluoride melts. In addition, the model was developed only to be applicable to melts and thus was not able to reproduce the viscosity of glasses at temperature below the melt region.

In the present study, the viscosity model is further extended to reproduce the viscosity of all sub-systems of MF_x–SiO_2–B_2O_3–Al_2O_3–CaO–MgO–Na_2O–K_2O–PbO–MnO–TiO_y (M = Ca, Mg, Na, K and Al) melts and SiO_2–B_2O_3–Al_2O_3–CaO–MgO–Na_2O–K_2O–PbO–ZnO glasses. All available experimental data of these sub-systems are critically evaluated and reviewed to develop the viscosity database. Two viscosity databases were developed for preference of industrial workers interested in different viscosity ranges in the process. The reproducibility of the model was also compared with measured viscosities of industrial slags and glasses.

CHAPTER 2 REVIEW OF THE LITERATURE

2.1 Viscosity Models for Molten Slags and Glasses

Many kinds of viscosity models have been developed to predict the viscosity of molten slags and glasses. In most cases, empirical models were developed and numerous parameters were required to calculate the viscosity of multicomponent silicate melts although the accuracy of the models was not satisfactory. Recently several efforts have been made to develop structural viscosity models based on the structural information of silicate melts which can be calculated from thermodynamic models such as Modified Quasichemical Model of Pelton and Blander[230] and the Cell Model of Kapoor and Frohberg [115]. Even though there have been numerous efforts for the accurate calculation of viscosity of molten slags and glasses, no model satisfactorily predicted the viscosity of multicomponent silicates over a wide composition and temperature range. In this section, we will see some representative viscosity models for melts and glasses of silicates.

2.1.1 The empirical model of Urbain et al. for molten slags

Urbain et al. [334, 336] proposed an equation:

$$\eta = AT\exp\left(\frac{10^3 E}{T}\right) \tag{2.1}$$

where T is the temperature in Kelvins, and A and E are two model parameters which can be obtained from the experimental data. In order to describe the slag composition, Urbain et al. [334, 336] classified the oxides into three groups, namely the glass forming oxides: SiO_2, GeO_2, P_2O_5, …; modifier oxides: Na_2O, K_2O, MgO, CaO, FeO, Cr_2O_3, TiO_2,…; and amphoteric oxides: Al_2O_3, Fe_2O_3. Urbain et al. used X_G, X_M and X_A to represent the total mole fractions of the three kinds of oxides. They further introduced the normalized values X_G^*, X_M^* and X_A^* by dividing the mole fractions X_G, X_M and X_A by the term $(1 + X_{CaF_2} + X_{FeO_{1.5}} + X_{TiO_2} + X_{ZrO_2})$. The model's approach has been used to estimate the viscosities of some ionic melts with a certain degree of success. However, the application of the method to some slag systems, for example, CaO-MgO-SiO_2, CaO-MnO-SiO_2 and Fe_nO-MnO-SiO_2, does not appear to be satisfactory. [189]

2.1.2 The empirical model of Riboud et al. for molten slags

This model was developed to estimate the viscosity of liquid mold powders. In this model, the slag constituents are classified into five different categories, and the mole fractions (X) of these categories are given by

$$\begin{aligned} X_{SiO_2} &= X_{SiO_2} + X_{PO_{2.5}} + X_{TiO_2} + X_{ZrO_2} \\ X_{CaO} &= X_{CaO} + X_{MgO} + X_{FeO} + X_{FeO_{1.5}} + X_{MnO} + X_{BO_{1.5}} \\ X_{Al_2O_3} & \\ X_{CaF_2} & \\ X_{Na_2O} &= X_{Na_2O} + X_{K_2O} \end{aligned} \tag{2.2}$$

According to Riboud et al. [249], the viscosity of a mold powder can be expressed empirically by the equation

$$\eta = AT\exp\left(\frac{E}{T}\right) \tag{2.3}$$

where T is the temperature in Kelvins, and A and E are two model parameters which can be calculated from

$$A = \exp\begin{bmatrix} -19.81 + 1.73(X_{CaO} + X_{MnO} + X_{MgO} + X_{FeO}) \\ +5.82X_{CaF_2} + 7.02(X_{Na_2O} + X_{K_2O}) - 35.76X_{Al_2O_3} \end{bmatrix} \tag{2.4}$$

and

$$\begin{aligned} E &= 31140 - 23896(X_{CaO} + X_{MnO} + X_{MgO} + X_{FeO}) \\ &-46356X_{CaF_2} - 39159(X_{Na_2O} + X_{K_2O}) + 68833X_{Al_2O_3} \end{aligned} \tag{2.5}$$

This model has only been useful in the estimation of viscosities of some mold flux compositions over narrow ranges. Furthermore, this empirical model did not properly predict the viscosity of some multicomponent slags of interest containing other fluorides such as NaF or MgF_2.

2.1.3 The Model of Zhang and Jahanshahi for molten slags

Zhang and Jahanshahi [359, 360] adopted an empirical form as follows;

$$\eta = A^W T \exp\left(\frac{E_\eta^W}{RT}\right) \tag{2.6}$$

where

$$E_\eta^W = a + b(N_{O^0})^3 + c(N_{O^-})^2 + d(N_{O^{2-}})^3 \tag{2.7}$$

and

$$\ln(A^W) = a' + b' E_\eta^W \tag{2.8}$$

In the above equations N_{O^0} and $N_{O^{2-}}$ are the fractions of the bridging oxygen and the free oxygen in the melt, respectively. R and T are the gas constant and absolute temperature, respectively. The values of a, b, c, d, a' and b' are model parameters which can be obtained from the experimental data. While N_{O^0} and $N_{O^{2-}}$ are estimated based on a structural model for binary silicate melts, the pre-exponential term A^W, and the activation energy, E_η^W, can be optimized using the experimental data. Zhang and Jahanshahi [359] correlate the viscosity as a function of composition to the concentrations of bridging, non-bridging and free oxygen in the silicate melts calculated by the cell model. The application of this model to a number of binary and ternary silicate systems shows good agreement with experimental data [359]. However, the model calculation did not show a good predictability for the case of quaternary and quinary systems [360].

2.1.4 The Model of Nakamoto et al. for molten slags

Nakamoto et al. [201] have also developed a model that uses the fractions of bridging, non-bridging and free oxygens. Their model is based on the idea which they define as the sum of non-bridging and free oxygen through the network structure. They find that the activation energy for viscous flow is inversely proportional to the distance the “cutting off” points move when shear stress is applied to the liquid as shown in Fig. 2.1.

On the basis of this idea, they have derived a viscosity model with an equation as follows:

$$\eta = AT\exp\left(\frac{E_V}{RT}\right) \tag{2.9}$$

where A is a pre-exponential term, and E_V is the activation energy for viscosity.

Based on the assumption that the activation energy is inversely proportional to the distance S, over which the "cutting-off" point moves when shear stress is applied to the liquid, the following equation is derived.

$$E_V = \frac{E}{1+\alpha(N_{O^-} + N_{O^{2-}})^{1/2}} \tag{2.10}$$

where E is the activation energy of pure SiO_2, N_{O^-} and $N_{O^{2-}}$ are the fractions of non-bridging and free oxygens, respectively, and α is considered as a model parameter relating to the weakness of the bonding between cation and oxygen ion at the "cutting off" point. While this model requires very few optimized model parameters, the reproduction of the experimental data is not very accurate [201].

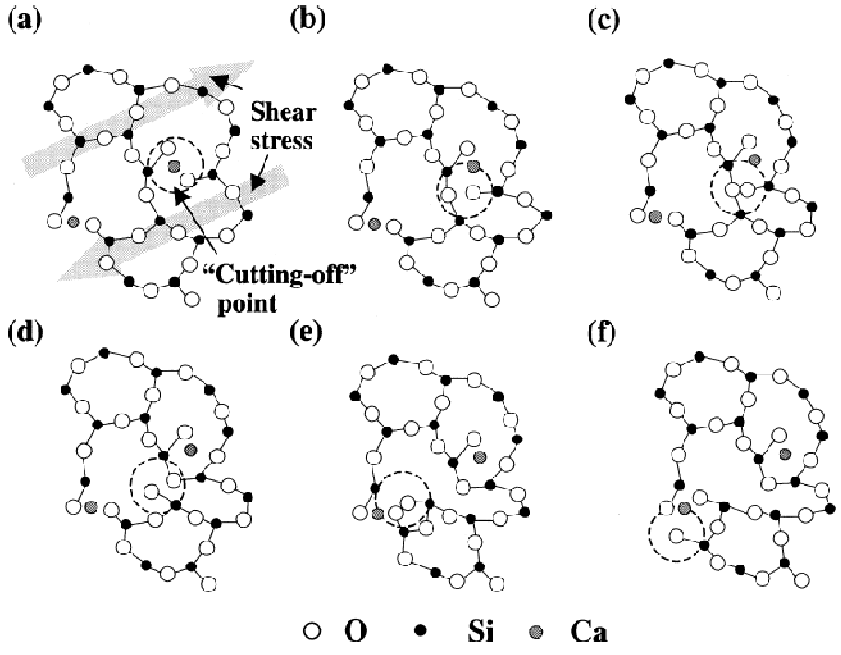

Fig. 2.1 Flow Mechanism in silicate melts by the model of Nakamoto et al. [201]

2.1.5 The Model by Kondratiev and Jak for molten Slags

Kondratiev and Jak[107, 139] developed a viscosity model using the Eyring viscosity equation:

$$h = \frac{2RT}{\Delta E_{\mathrm{v}}} \frac{(2\pi m_{SU} kT)^{1/7}}{v_{SU}^{2/3}} \exp\left(\frac{E_a}{RT}\right) \tag{2.11}$$

where R (J/K/mol) and k (J/K) are the gas constant and the Boltzmann constants, $\pi \approx 3.1416$, T is the absolute temperature(Kelvins), ΔE_v and E_a (J/mol) are the vaporization and activation energies, and m_{SU} (kg) and v_{SU} (m^3) are the average mass and volume of a viscous flow structural unit. The activation energy E_a (J/mol) reflects the interactions between different structural units composing the liquid. The energy of vaporization ΔE_{v} is related to the free volume of the liquid, i.e. to the concentration of the holes in the liquid determined by the energy of the hole formation, and can be approximately related to the latent heat of vaporization.

They also used the mole fractions of bridging, non-bridging and free oxygens indicated as $X_{\text{Si-Si}}$, $X_{\text{Me-Si}}$ and $X_{\text{Me-Me}}$, respectively. These mole fractions were calculated using the Modified Quasichemical Model of Pelton and Blander [230]. The ΔE_{v}, E_a, m_{SU} and v_{SU} values in the model are expressed through the respective mole fractions of the various structural units $X_{\text{Si-Si}}$, $X_{\text{Me-Si}}$ and $X_{\text{Me-Me}}$ present in the melt as shown in following equations;

$$\begin{aligned}
m_{SU} &= m_{\text{Si-Si}} X_{\text{Si-Si}} + m_{\text{Me-Si}} X_{\text{Me-Si}} + m_{\text{Me-Me}} X_{\text{Me-Me}} \\
v_{SU} &= v_{\text{Si-Si}} X_{\text{Si-Si}} + v_{\text{Me-Si}} X_{\text{Me-Si}} + v_{\text{Me-Me}} X_{\text{Me-Me}} \\
E_a &= E_{a,\text{Si-Si}} X_{\text{Si-Si}} + E_{a,\text{Me-Si}} X_{\text{Me-Si}} + E_{a,\text{Me-Me}} X_{\text{Me-Me}} \\
\Delta E_{\mathrm{v}} &= \Delta E_{\mathrm{v,Si-Si}} X_{\text{Si-Si}} + \Delta E_{\mathrm{v,Me-Si}} X_{\text{Me-Si}} + \Delta E_{\mathrm{v,Me-Me}} X_{\text{Me-Me}}
\end{aligned} \tag{2.12}$$

where $m_{\text{Si-Si}}, m_{\text{Me-Si}}, m_{\text{Me-Me}}$ and $v_{\text{Si-Si}}, v_{\text{Me-Si}}, v_{\text{Me-Me}}$ are the masses and the volumes of the respective structural units. This model requires seven binary parameters for each binary system but the reproducibility of the model for the experimental data is not very accurate.

2.1.6 Adam-Gibbs model for molten slags and glasses

The fundamental tenet of the Adam-Gibbs model is that relaxation in viscous liquids becomes increasingly sluggish below the glass transition range as a result of a concomitant dearth of atomic configurations. Specifically, structural relaxation is described in terms of cooperative rearrangements of the melt in mutually independent regions whose minimum size decreases with increasing temperature. Because the structural relaxation times, τ, are inversely proportional to the average probability of these rearrangements, one obtains

$$\tau = A_\tau \exp\left(\frac{B_e}{TS^{conf}}\right) \tag{2.13}$$

and because τ is proportional to viscosity η we can obtain another equation as follows;

$$\eta = A_e \exp\left(\frac{B_e}{TS^{conf}}\right) \tag{2.14}$$

where A_τ and A_e are pre-exponential terms for structural relaxation times and viscosity, respectively. B_e represents the molar Gibbs free-energy barriers opposing structural rearrangements and S^{conf} is the configurational entropy. T is the absolute temperature(Kelvin).

This model has been used frequently to take into account non-Arrhenian temperature dependence of the viscosity of silicate melts with decreasing temperature by correlating the viscosity to the configurational entropy. However, it is very difficult to separate the measured entropy into configurational and vibrational parts. Therefore, practical applications of the Adam-Gibbs entropy model has long been hampered by the difficulties affecting these experimental determinations [250].

2.1.7 Some models based on the Vogel-Fulcher-Tammann Equation

In the glass industry, the most broadly used empirical viscosity model is the Vogel-Fulcher-Tammann equation [73, 344] as shown in Eq.(2.15).

$$\log\ \eta = A + \frac{B}{T - C} \tag{2.15}$$

where T is the absolute temperature(Kelvins). A, B and C are model parameters fitted to the experimental data. A specific feature of this equation is the possibility of describing with reasonable precision, the temperature dependence of viscosity of silicate melts in the viscosity range of 10^2 to 10^{13} poise. However, these parameters A, B and C are independent of the composition of silicate melts. Therefore, this model requires numerous model parameters for calculation of viscosity of multicomponent silicate melts.

Giordano et al. [77] tried to take into account the composition dependence by assuming that the model parameters B and C can be expressed as an linear combinations of oxide components following as;

$$\begin{aligned} B &= \sum_{i=1}^{7}[b_i M_i] + \sum_{j=1}^{3}[b_{1j}(M1_{1j} M2_{1j})] \\ C &= \sum_{i=1}^{6}[c_i N_i] + \sum_{j=1}^{3}[c_{11}(N1_{11} N2_{11})] \end{aligned} \tag{2.16}$$

where M_i and N_i refer to the combinations of mol% oxides. $M1_{1j} M2_{1j}$ and $N1_{11} N2_{11}$ are subordinate numbers of multiplicative oxide cross terms.

Fluegel [67] developed a model for the viscosity of glasses using the Vogel-Fulcher-Tammann equation, based on a global statistical modeling approach. This empirical model is based on multiple regression using polynomial functions. It is most accurate in the vicinity of commercial glass compositions since it is calibrated based on numerous experimental data in these regions which are summarized in the SciGlass database [37]. The model provides a rigorous estimation of errors and validity limits. There are compositional limits of the model.

2.2 Techniques of Viscosity Measurements

Viscosity is the internal friction of a liquid caused by molecular attraction, which makes it resist a tendency to flow. According to Newton's first law of motion, the proportionality of the viscosity is constant between the shear stress and the shear rate. A Newtonian fluid starts to deform or flow when it suffers a strain, thus overcoming the internal friction. Higher viscosity, or internal friction, requires higher stress to make the liquid flow.

Most experiments have been carried out at high temperatures with careful sample treatments. Since the viscosity of silicates in the range from melts to glasses can span more than 15 orders of magnitude (0 to 10^{15} poise) the experimental techniques must be different according to the viscosity range as will be discussed in the next section.

2.2.1 Rotating Crucible Method

A rotating crucible method is the most widely used method for viscosity measurements for molten slags at high temperatures. An inner cylinder, or bob is placed in an outer cylinder, or cup, containing the sample. Either the torque transferred to the inner cylinder is measured while the outer cylinder is rotated at a fixed speed, or the torque required to rotate the inner cylinder at a set speed is measured while the outer cylinder is stationary.

According to the rotating crucible method, the viscosity can be determined from the measurement of the torque generated when the cylinder is rotated at a constant speed. The viscosity (Pa·s) is calculated by the following equation [189];

$$\eta = \frac{\mathbf{M}}{8\pi^2 \mathbf{n h}} \left(\frac{1}{\mathbf{r}_i^2} - \frac{1}{\mathbf{r}_o^2} \right) \tag{2.17}$$

where M is the torque(N·m), n is the revolutions per second, h and r_i are the height and radius(m) of the spindle respectively, and r_o is the radius(m) of the crucible. Eq.(2.17) holds when either the inner or outer cylinder is rotated. For given experimental conditions, r_o, r_i and h are known, so we have

$$\eta = \mathbf{C}_o \frac{\mathbf{M}}{\mathbf{n}} \tag{2.18}$$

where C_o is the equipment constant and can be obtained from calibration using standard viscosity materials because the relationship among the measured torque, rotational speed of the spindle or the crucible and the geometry of the crucible gives a measure of viscous drag exerted by the liquid.

A rotating crucible method has several advantages for molten slags and glasses. Relatively simple geometric shapes of cups and bobs can be made easily with refractory materials. Just a little geometric information of the experimental equipment is required to calculate the viscosity of the sample. This method also has several drawbacks. Temperature measurement should be carried out indirectly during the measurement because only the splindle should be immersed in the sample. Because of high melting temperature of silicates, the contamination of the sample due to the violent reaction of sample with crucibles should be considered.

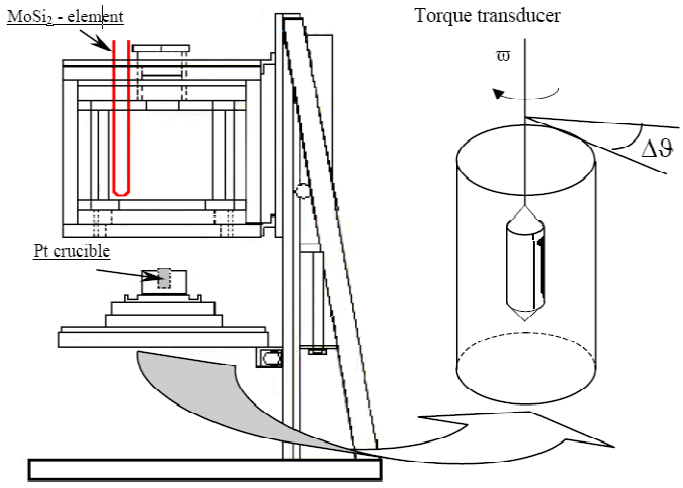

Fig. 2.2 Schematic diagram of a rotating crucible method

2.2.2 Oscillating (vibrational) viscometer method

An oscillating (vibrational) viscometer method consists of a torsional pendulum oscillating in a simple harmonic fashion with an axially symmetrical bob immersed in the fluid. The drag from the fluid causes a damping of the oscillation that can be measured and used to give the viscosity. The viscosity in the oscillating (vibrational) viscometer method can be calculated by Eq.(2.19)

$$\eta = \frac{2}{\pi\rho\kappa}\left(\frac{2\theta\left(\frac{\lambda}{\pi}\right)+\left(\frac{\lambda}{\pi}\right)^2+\ldots}{r^4+r^3 d}\right) \tag{2.19}$$

where ρ is the density of the liquid, κ is the period of oscillation in an empty system, r is the radius of the cylinder, d is the thickness of the cylinder, θ is the moment of inertia of the oscillation, and λ is the decrement due to the damping effect of the liquid. This method is usually used for the measurement of relative viscosity, and the viscometer must be calibrated against standard viscosity materials. Some drawbacks of this method should be considered. Temperature measurement should be carried out indirectly during the measurement because only the bob should be immersed in the sample. Because of high melting temperature of silicates, the contamination of the sample due to the violent reaction of sample with vessels should be considered. In addition, the uncertainties in the damping rates of an oscillating wire during the experiment could give more error sources on the viscosity measurement.

2.2.3 Falling body method

A falling body method is based on the principle that a solid body falling through a fluid reaches a terminal velocity when the viscous forces are balanced by the gravitational force. Measurement of the terminal velocity allows viscosity to be calculated. The viscosity can be expressed mathematically by Stokes' Law:

$$\eta = \frac{2Gr_s^2(\rho_k - \rho_l)}{9v[1+2.1(d_b/d_c)]} \tag{2.20}$$

where G is the gravitational constant, r_s is the radius of the sphere, v is the velocity of descent or ascent of the sphere, ρ_k and ρ_l the densities of the ball and liquid respectively, and d_b and d_c the diameters of the ball and the crucible respectively. This method has been used for the measurements of the viscosities of molten slags. While the technique is convenient for the measurements of high viscosity materials, it does not provide accurate results for relatively low viscosity measurements. A particular concern with this method is that a long fluid column is required for the body to reach terminal velocity and that this column must be within the constant

temperature zone of the furnace. This necessitates the use of a large furnace and a relatively large slag sample.

2.2.4 Fiber elongation method

The fiber elongation method has been widely used for the viscosity measurement of glasses in the range from 7 to 16 on the logarithmic poise scale. The fiber elongation method requires dumbbell-shaped samples. The dumbbell-shaped samples are made by molding the ends of the fiber sample using an oxy-propane torch. [318] A 0.55 to 0.75 mm diameter glass fiber is drawn. One end is fused to make a ball. The glass fiber is cut to 23.5cm length, and then suspended inside a specified furnace, which only covers the top 10 cm [340]. The sagging of the lower end is viewed using a telescope and measured as a function of time. When the glass extends under its own weight, the temperature when the rate of extension of the lower end is 1 mm/min corresponds to the softening point viscosity whose viscosity value is $\log(\eta/\text{poise}) = 7.6$. In this method, the deformation rate of the sample with given applied force should be slow enough to prevent the formation of non-newtonian fluid. The composition of the sample can be changed due to the different temperature distribution between the end part and the center part of the sample when manufacturing the dumbbell-shaped of the sample using an oxy-propane torch. In addition, temperature measurement should be carefully carried out to prevent temperature inhomogeneity between the sample having extremely high viscosity and the furnace.

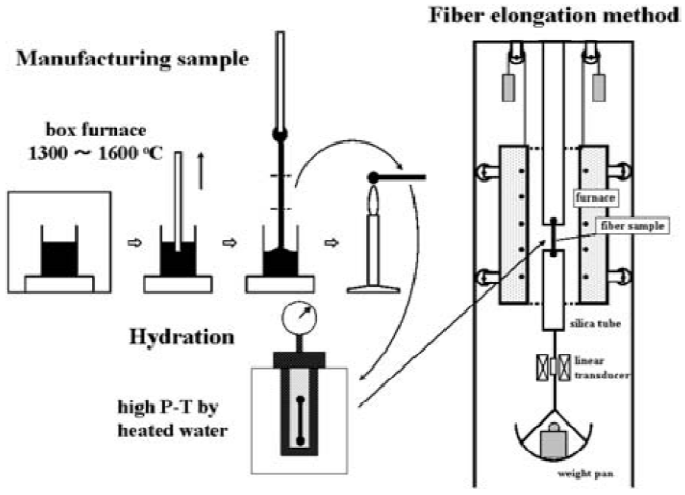

Fig. 2.3 Schematic diagram of the fiber elongation method

2.2.5 Beam-bending method

The beam-bending method has been widely used for measuring high viscosities of glasses at low temperatures in the range from 6 to 13 on the logarithmic poise scale. As shown in Fig.2.4, the furnace is electrically heated by resistance-wire windings of suitable alloys capable of maintaining the appropriate temperatures. Control thermocouples are located as close as possible to the furnace windings for fast response. When a viscous body of a cylindrical form is supported at two ends, the center of the body sags with a constant rate. The shear viscosity of this body is related to sagging rate from the viscosity-elasticity analogy as follows[129];

$$\eta = \frac{5}{288\pi} \frac{\rho g l^4}{(a^2 + b^2) y} \tag{2.21}$$

where a and b are the outer and inner radius of the sample respectively, l is the length between the two supports and ρ is the density of the sample. y and g are the sagging rate of the center part and the acceleration of gravity respectively. Temperature measurement should be carefully carried out to prevent temperature inhomogeneity between the sample having extremely high viscosity and the furnace.

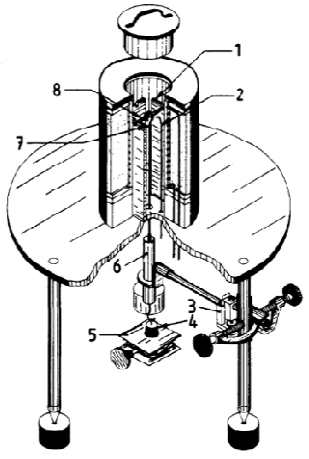

1 Alumina muffle support stand
2 Thermocouple
3 Zero-adjust mechanism for LVDT
4 Weight
5 Laboratory jack
6 LVDT
7 Loading rod
8 Specimen beam

Fig. 2.4 Schematic diagram of the beam-bending method

2.2.6 Parallel plate method

The parallel plate method has been used for measuring high viscosities of glasses in the range from 5 to 11 on the logarithmic poise scale. The principle of a parallel-plate viscometer was described by Dienes and Klemm [41]. Fig.2.5-(a) shows a schematic of the parallel plate viscometer. A disk of glass, roughly 6-12 mm diameter and 4-6 mm high, is sandwiched between two parallel plates inside a well-insulated furnace. The glass sample surfaces should be parallel with an error of +/- 0.01 mm. The upper pedestal (marked “load rod”) is loaded, and the rate of sagging is recorded as a function of time by a linear voltage displacement transducer (LVDT) or similar instrument with a resolution of at least +/- 0.005 mm. The thermal expansion of the alumina plates in Fig.2.5-(a) should be compensated. It is important to pay attention to the geometry of deformation of the sample during the experiments. As shown in Fig.2.5-(b), when no-slip exists, the radial velocity of glass in contact with the plates is zero, and is a maximum at mid- height. When ‘perfect slip’ exists, the radial velocity is a function of radius only. Under these two conditions of slip, the viscosity is determined by

$$\eta(\text{no slip}) = 2\pi M_s g h_s^5 / 3V(dh/dt)(2\pi h^3 + V)$$
$$\eta(\text{perfect slip}) = M_s g h_s^2 / 3V(dh/dt) \qquad (2.22)$$

where **M** and **g** are the applied load and the gravity acceleration respectively. **h** and **V** are the sample height and the sample volume. **dh/dt** is the deformation or sag rate.

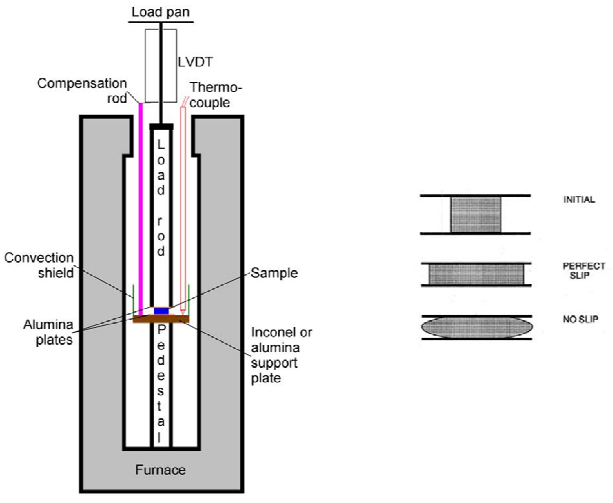

(a) (b)

Fig. 2.5 (a) Schematic diagram of the parallel plate method, (b) Deformation of the sample

2.2.7 Micro-penetration method

The micro-penetration method has also been widely used for measuring high viscosities of glasses in the range from 9 to 13 of the logarithmic poise scale. Fig. 2.6 shows a schematic of the micro-penetration method. This method involves determining the rate at which an Ir-indenter under a fixed load moves into the glass sample surface [46]. The indenter is attached to one end of an alumina rod, which is attached at the other end to a weight pan. The metal connection between the alumina rod and the weight pan acts as the core of a calibrated linear voltage displacement transducer (LVDT). The movement of this metal core as the indenter is pushed into the glass sample yields the displacement. The absolute shear viscosity can be determined from

$$\eta = \frac{0.1875 P t}{r_h^{0.5} I^{1.5}} \tag{2.23}$$

where r_h is the radius of the half-sphere and P is the applied force. I is the indent distance and t is the time.

The advantages of the micro-penetration method are the ability it provides of using relatively small amounts of sample and simple sample geometry constraints compared to other high-viscosity methods such as the parallel plate or fiber elongation methods. Temperature measurement should be carefully carried out to prevent temperature inhomogeneity between the sample having extremely high viscosity and the furnace.

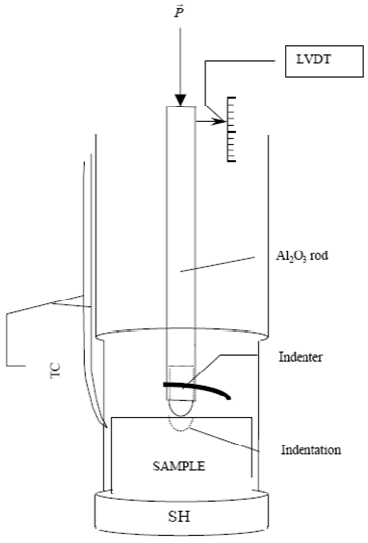

Fig. 2.6 Schematic diagram of the micro-penetration method

2.2.8 Ball penetration method

The ball penetration method is described by Douglas et al. [48] and has been used to determine high viscosities of glasses in the range from 9 to 13 on the logarithmic poise scale. A hard, incompressible, chemically inert sphere about 3 mm diameter is allowed to penetrate a flat specimen of glass. The sag rate is measured with time. The viscosity of the glass can be calculated from the following equation;

$$\eta = \frac{9PG}{32dL/dt(2Lr_s)^{0.5}} \tag{2.24}$$

where P is the applied loading force and G is the gravitational constant. L is the penetration depth and dL/dt is the deformation sag rate. r_s is a radius of the sphere. The advantages of the ball penetration method lie in the simplicity of the method and the ease of the glass sample preparation. However, temperature measurement should be carefully carried out to prevent temperature inhomogeneity between the sample having extremely high viscosity and the furnace.

2.3 The accuracy and reliability of viscosity measurements

In the present study, viscosity data are reviewed for all sub-systems of MF_x–SiO_2–B_2O_3–Al_2O_3–CaO–MgO–Na_2O–K_2O–PbO–MnO–TiO_y (M = Ca, Mg, Na, K and Al) melts and SiO_2–B_2O_3–Al_2O_3–CaO–MgO–Na_2O–K_2O–PbO–ZnO glasses. The data judged to be most reliable are extracted and compared with the viscosities calculated by the model. Since the viscosity of silicates in the range from melts to glasses can span more than 15 orders of magnitude (0 to 10^{15} poise) the experimental techniques must be different according to the viscosity range, and thus other experimental concerns such as sample preparation, chemical analysis and temperature measurement should be carefully evaluated from the literature.

2.3.1 Experimental difficulties of viscosity measurements

The difficulties associated with measurements of the viscosity of glasses and melts over a wide temperature range arise from the simultaneous presence of the following conditions [212, 339]:

- a very wide viscosity range to be measured;
- the poor heat conducting properties of the liquid;
- the invariable presence of small bubbles in the liquid;
- temperature inhomogeneities in the sample area of the viscometer;
- difficulty in quenching of the sample;
- crystallization phenomena during the experiment;
- composition change of the sample due to the violent reaction with crucibles;

The optimum range for a rotational viscometer is from -1 to 5 in the logarithmic poise scale(ln η (Pa·s) from –4 to 9). The numerous sources of systematic error related to the use of this particular type of viscometer and to the viscosity measurements of oxide melts in general are outlined, for example, in Refs. [339] and [190]. When viscosity measurements were carried out by some of the best laboratories in a "round robin" project [190] using the same reference materials, the average spread of data obtained by different laboratories was about 20%. Hence, the average accuracy of viscosity data is probably never better than about 50% when the uncertainties in sample preparation and purity are also taken into account.

In oxy-fluoride melts, e.g. MF_x = CaF_2, the intrinsic difficulties associated with measurements over a wide temperature range are as follows:

- the loss of fluorine ions by formation of HF(g) because of presence of moisture;

$$\mathbf{CaF_2(liquid) + H_2O(gas) = CaO(liquid) + 2HF(gas)} \quad (2.25)$$

- the loss of fluorine ions by formation of a gas phase such as SiF_4(g) because of the high volatility features of fluorine ions

$$\mathbf{2CaF_2(liquid) + SiO_2(liquid) = 2CaO(liquid) + SiF_4(gas)} \quad (2.26)$$

- the violent reactivity of the melt with crucibles.
- difficulties in the chemical analysis of each component of the oxy-fluoride melts

Thus, when considering the above difficulties, the accuracy of viscosity measurement of oxy-fluoride melts would be significantly less than for oxide melts.

For the measurement of viscosity in the glass regions, most experiments were carried out with the fiber-elongation, ball penetration and micro-penetration methods. The applicable viscosity ranges for each method are [51, 223, 323]:

- The fiber-elongation method: viscosity range of 7 to 16 in the log poise scale
- The ball penetration method: viscosity range of 9 to 13 in the log poise scale
- The micro-penetration method: viscosity range of 9 to 13 in the log poise scale
- The beam-bending method: viscosity range of 6 to 13 in the log poise scale

High viscosity measurement at lower temperatures is much more difficult than the low viscosity measurements because of the strong tendency to crystallization during the experiment. The glass-forming ability can be taken into account by the critical cooling rate of the system. If the sample is quenched faster than the critical cooling rate, the sample is retained in a glassy state. Cabral et al. [28] systematically investigated the effect of CaO on the critical cooling rate by addition of CaO to the Na_2O-SiO_2 system. They reported, when adding 33 mol% of CaO, that the critical cooling rate of the Na_2O-CaO-SiO_2 system had changed to become 20 times larger than the critical cooling rate of the Na_2O-SiO_2 system [28]. Shelby [285] also observed in the system of CaO-Al_2O_3-SiO_2 that the glass transition temperature (T_g) increases with increasing molar ratio of Al_2O_3/CaO at constant SiO_2 and with decreasing SiO_2 contents in the composition range from 5 to 60 mol% SiO_2 at constant molar ratio of Al_2O_3/CaO. Below the glass transition temperature (T_g), the glass (supercooled liquid) behaves as a solid which would cause a rapid increase of the viscosity. This implies that a system containing high contents of CaO and Al_2O_3 would have larger errors in viscosity measurements because of the strong tendency to crystallization. If crystallization starts during the experiment, the viscosity is time-dependent and then the viscosity could be significantly different depending on the elapsed time. In addition, there would be a large error in the temperature measurement due to the difficulty of achieving temperature homogeneity between the sample and the furnace, due to poor heat conduction and the extremely high viscosity of the sample.

For calibration and testing of the proposed viscosity model, experimental viscosity data were collected for the Al_2O_3–B_2O_3–CaO–MgO–FeO–Fe_2O_3–MnO–NiO–PbO–ZnO–Na_2O–K_2O–TiO_2–Ti_2O_3–SiO_2–F system and its subsystems for the melts and the Al_2O_3–B_2O_3–CaO–MgO–

$ZnO–PbO–Na_2O–K_2O–SiO_2$ system and its subsystems for the glasses. Based on the critical evaluation and analysis of all available data collected from all literature data including the Sci-Glass database [274], it can be concluded that most reliable data measured by different best laboratories show average absolute uncertainty of viscosity measurements within 0.25 to 0.5 for oxide melts, and within 1 to 2 for glasses in the logarithm poise scale. However, viscosity measurement for the oxy-fluoride melts would have larger errors than that of oxide melts due to the difficulties of the chemical analysis of the system caused from the effect of volatilization of the fluorides and the presence of the moisture in the sample. The average absolute uncertainty of viscosity measurements of oxy-fluoride melts was shown within 0.65 to 0.9 in log poise scale from the

2.3.2 Chemical Analysis of oxy-fluoride melts and vaporization effect of fluorides

The chemical analysis of silicate melts without any fluorides can be accurately carried out by many analytical methods such as ICP-AES, SEM-EDS and EPMA. However, in the case of oxy-fluoride melts, chemical analysis of the components is still uncertain. Chemical analysis of the components in the oxy-fluoride melts is crucial to analyze the effects of each component on the viscosity of the melts. The vaporization effect of fluorides during the experiments would also effect considerable changes of composition of the system. In 1934, Herty et al. [89] stressed that the actual change in composition in certain cases may be considerably greater than the published results indicate because of the high volatile properties of CaF_2 and the analytical difficulties in fluorine determination. Furthermore, the composition change of the sample would be time-dependent with the evaporation of the fluoride gases. Thus, it would be inaccurate to say that the viscosities measured in the middle stage of the experiments are directly related to the analyzed composition of the sample.

Recently, Persson et al. [234] studied the kinetics of fluoride evaporation from the subsystems of CaF_2-Al_2O_3-CaO-MgO-SiO_2 using thermogravimetric analysis (TGA) and found that the evaporation of fluorine as HF(g) or SiF_4(g) was minimal in the absence of moisture. Suk and Park [310] also studied the vaporization behavior of CaF_2 in the system CaF_2-CaO-MgO-SiO_2 using thermogravimetric analysis (TGA). Suk and Park [310], however, reported that there

were significant weight changes of the sample and that they would be caused by the formation of CaF_2(g) and SiF_4(g).

On the other hand, some authors [226, 233, 280] who measured the viscosity of CaF_2–containing systems analyzed the initial and final compositions of the samples using XRF [226, 233, 280] and electrode spectrometry [233, 280] after dissolving the samples in NaOH solution for analyzing fluorine ions. All their results were in agreement that there was no significant change from the initial compositions of the sample. In all their experiments they thoroughly removed moisture from the injected gas and the sample.

However, the quantitative analysis of fluoride and oxide in the sample using XRF or electrode spectrometry still has a limitation because XRF or electrode spectrometry analyzes the concentrations of cations or anions, and then converts them to those of compounds which are assumed to be the most likely to exist in a sample [110]. Therefore, in order to quantify a fluorine compound and other constituents in a sample, the existing form of fluorine should be identified in advance. These methods would be more unreliable for the case of multicomponent systems containing fluorides. For example, Park et al. [226] measured viscosities of CaF_2-CaO-Na_2O-SiO_2 and analyzed the cations (Ca, Na and Si) using XRF (X-ray fluorescence spectrometry) because direct analysis for fluorine ions is not possible. They identified no difference in the amount of cations in the sample after the experiments and concluded that the overall compositions were the same as the initial compositions. During the experiments, however, the equilibrated composition would be newly established according to the stability of each phase. It is well-known that NaF is the most favorable phase to be formed. Thus, we could expect to have some amount of NaF in the sample but the present XRF cannot analyze accurately how many Na cations are bonded with fluorine and oxygen ions respectively. Because of the lack of a thermodynamic database and the limitation of chemical analysis equipment, more thermodynamic studies and the development of more advanced chemical analysis methods are required.

From the critical review of all available experimental data, we found that most studies were carried out with thorough removal of moisture from the gas injected and the sample to prevent the formation of HF(g) from the sample. However, most authors who measured the

viscosities of oxy-fluoride melts could not accurately analyze the final compositions because of the limitations of chemical analysis equipment.

In the present study, the initial compositions of the published literature were used for model modification and optimization. We simply extracted all available experimental data with the following assumptions;

- During the experiment, there was no significant change from initial composition because of absence of moisture in the sample.
- Vaporization effects by HF(g), SiF_4(g) and MF_x(g) (M = Ca, Mg, Na, K and Al) would be negligible.

  (e.g. $\mathbf{MF_x(l) = MF_x(g)}$, $\mathbf{P_{(CaF_2)} = 8.55 \bullet 10^{-4} atm}$ **and** $\mathbf{P_{(MgF_2)} = 8.04 \bullet 10^{-3} atm}$ **at** $\mathbf{1600^oC}$)

CHAPTER 3 A MODEL TO CALCULATE THE VISCOSITY OF MOLTEN SLAGS

In this Chapter, the previous work [27, 81, 82] will be discussed.

Recently a new viscosity model was developed in this laboratory to reproduce the viscosity of molten slags for the system CaO-MgO-K_2O-Na_2O-Al_2O_3-SiO_2-B_2O_3 [27, 81, 82]. In this model, the viscosity is related to the structure of the melt, which in turn is calculated from the thermodynamic description of the melt using the Modified Quasichemical Model [231, 232].

3.1 Structure of Silicate and Borate Melts

The Si atoms in silicate melts are always tetrahedrally bonded to four oxygens as shown in Fig.3.1-(a). Virtually every SiO_2 that is added to a very basic $MO_{0.5}$ or MO melt (where M = basic cations) enters the solution as an SiO_4^{4-} orthosilicate ion. On increasing the silica content above the orthosilicate composition, the silicate tetrahedral unit start to polymerize, first forming dimers, then trimers, then even longer chains and rings. At even higher SiO_2 contents, the rings and chains coalesce forming a three-dimensional network.

On the other hand, the structure of MO_x-B_2O_3 binary systems (where MO_x is a basic oxide) is very complicated. In solid compounds, boron is known to assume both triangular and tetrahedral coordination with oxygen but it is believed that mostly triangular coordination is present in pure B_2O_3 melts as shown in Fig.3.1-(b). The tetrahedral coordination is charge-compensated by alkali or alkaline earth cation which are located in the vicinity of the BO_4 group. Boron atoms in tetrahedral and triangular coordination can co-polymerize to form various clusters.

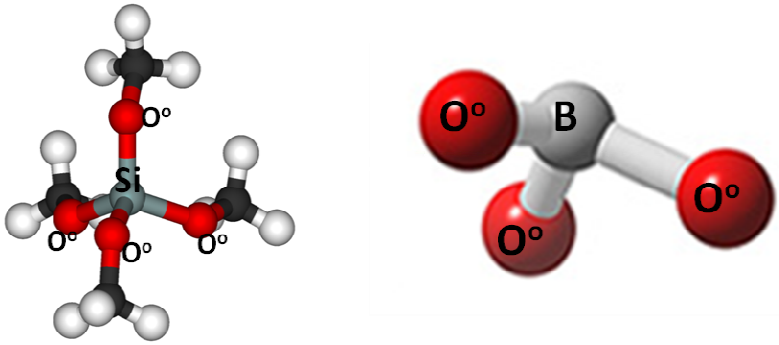

(a) (b)

Fig. 3.1 Structure of (a) orthosilicate and (b) triangular borate

3.2 Calculation of pair fractions using the Modified Quasichemical Model

The goal of a CALPHAD-like optimization is to obtain parameters of model equations for the Gibbs energies of all phases in a system as a function of composition and temperature that simultaneously satisfy all experimental thermodynamic and phase diagram data. Numerous models have been proposed to model the Gibbs energy of liquid oxides. Over twenty years ago the modified quasichemical model [230] was developed by one of the authors to model the Gibbs energy of the liquid phase. This model has been particularly successful in modeling liquids that display strong short-range-ordering. The model has continually been refined and extended [232] and large databases have been developed for multicomponent systems along with a software package that allows the calculation of phase diagrams and thermodynamic properties of multicomponent systems [15]. The following is a short synopsis of the quasichemical model and its application to silicate liquids.

The quasichemical model treats a binary MO_x-SiO_2 system by assuming that M and Si mix substitutionally on one quasi-lattice and oxygen completely occupies a second quasi-lattice. Every Si or M has oxygen as first nearest neighbors and there are three types of second-nearest-neighbor pairs, namely M-M pairs, M-Si pairs and Si-Si pairs. The model considers the formation of two M-Si pairs from a M-M and a Si-Si pair according to the quasichemical reaction:

$$(\mathbf{M\text{-}M}) + (\mathbf{Si\text{-}Si}) = 2(\mathbf{M\text{-}Si}) \tag{3.1}$$

The Gibbs energy change of this reaction is expanded as a polynomial in either the component mole fractions or the pair fractions. It is the coefficients of this expansion which are the parameters of the model. These parameters are optimized in order to simultaneously reproduce all carefully evaluated experimental thermodynamic and phase diagram data. In this way, optimized parameters are obtained for binary and many ternary systems. Through the model the thermodynamic properties of multicomponent systems can be calculated from the binary and ternary parameters. A large database for multicomponent molten oxides has been developed by this means over the past 30 years. Using this database, and the quasichemical model, it is possible to calculate the concentrations of M-M, M-Si and Si-Si pairs in multicomponent slags as a function of temperature and composition. This provides a powerful tool to model physical properties such as viscosity. The Si-Si, M-Si and M-M next-nearest-neighbor pairs as calculated by the quasichemical model are conceptually and numerically equivalent [230] to the fractions of bridging O^0, non-bridging O^- and free O^{2-} oxygen introduced by Fincham and Richardson [66], the concentrations of which can also be calculated by other models such as the cell model of Kapoor and Frohberg [115].

Fig. 3.2 shows the pair fractions for the systems $NaO_{0.5}$-SiO_2 and CaO-SiO_2 that are calculated from the thermodynamic optimization of these systems using the quasichemical model [9,10]. Both CaO and $NaO_{0.5}$ are strongly basic oxides. The Gibbs energy of mixing of the liquid is V-shaped with a sharp minimum at the orthosilicate composition (Na_4SiO_4 and Ca_2SiO_4 respectively). The energy change of the quasichemical reaction (Eq. 3.1) is consequently very negative and the reaction is displaced strongly to the right. The liquid therefore shows virtually perfect second-nearest-neighbor ordering leading to the fraction of Na-Si and Ca-Si next-nearest-neighbor pairs being very close to unity at the composition of maximum ordering. At higher SiO_2 contents the fraction of Na-Na or Ca-Ca pairs is almost zero. The systems $KO_{0.5}$-SiO_2 [351] and MgO-SiO_2 [352] are very similar to the systems $NaO_{0.5}$-SiO_2 and CaO-SiO_2.

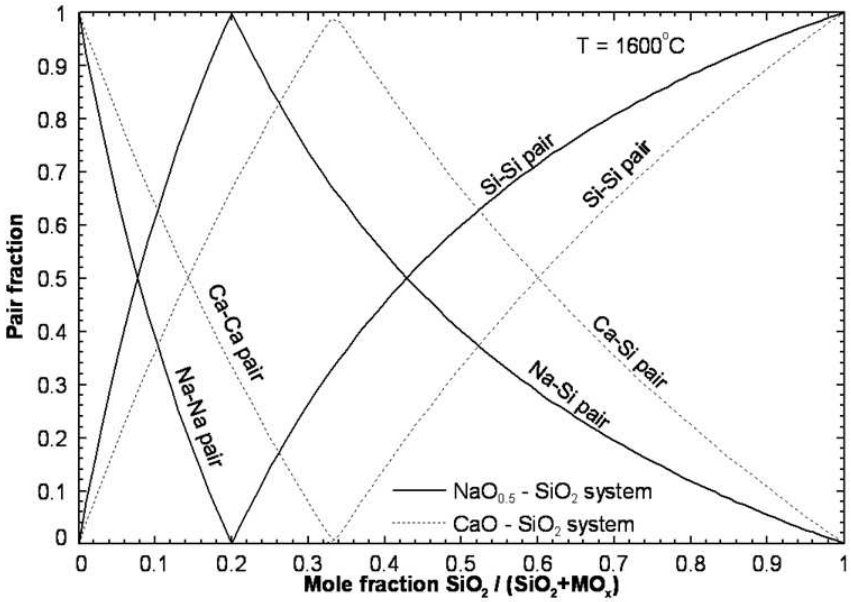

Fig. 3.2 Si-Si, M-Si and M-M pair fractions calculated from the quasichemical thermodynamic model for the systems CaO-SiO_2 and $NaO_{0.5}$-SiO_2.

3.3 Characterization of the structure of SiO_2 and B_2O_3 networks

The structural changes taking place upon formation of SiO_2 and B_2O_3 networks are best characterized by the concept of Q^i-species [199]. In the Q^i-notation the superscript *i* denotes the number of bridging oxygens per Si atom or B atom. In pure SiO_2, all four oxygens surrounding each Si are bridging oxygens. Thus the fraction of Q^4-species is 1. A silicon cation in a chain is a Q^2-species if two of its four surrounding oxygens are bridging oxygens.

Lin and Pelton [289] showed how to calculate the number of monomers, dimers, trimers etc. per mole of solution using the mole fractions of O^{2-}, O^- and O^o. The fractions of Q^i-species can be calculated in a similar manner. The Modified Quasichemical Model [231, 232] and the optimized FactSage thermodynamic database [15] can be used to calculate the numbers of M-M, M-Si and Si-Si second-nearest-neighbor pairs, which correspond to the fractions of free oxygens, non-bridging and bridging oxygens respectively, as functions of temperature and composition.

Let us define p as the probability that a particular pair emanating from a given Si atom is a Si–Si pair. Then, as a first approximation, p can be calculated by dividing the number of Si–Si pairs emanating from all Si atoms by the number of all Si–Si and Si–M pairs:

$$p = \frac{2n_{\text{Si-Si}}}{2n_{\text{Si-Si}} + \sum_{\text{M}} n_{\text{Si-M}}} \tag{3.2}$$

where $n_{i–j}$ is the number of i–j pairs. Note that every Si–Si pair is counted twice as emanating from one and from the other Si atom in the pair.

As mentioned in section 3.1, every silicon is tetrahedrally coordinated by four oxygens. If every one of the four oxygens has an equal probability p of being a bridging oxygen then the fractions of Q^i-species per mole of silicon (i.e. the probability that a given silicon is a Q^i-species) can be calculated from a binomial distribution as:

$$\begin{aligned} Y(Q^4) &= p^4 \\ Y(Q^3) &= 4 \cdot p^3 \cdot (1-p) \\ Y(Q^2) &= 6 \cdot p^2 \cdot (1-p)^2 \\ Y(Q^1) &= 4 \cdot p \cdot (1-p)^3 \\ Y(Q^0) &= (1-p)^4 \end{aligned} \tag{3.3}$$

Note that $\sum Y(Q^i) = 1$. As can be seen from Eq. (3.3), the probability that a given Si atom is a Q^4-species is p^4 because four Si–Si pairs emanate from this Si atom. Similarly, we can calculate the probabilities that a given Si atom is a Q^i-species as well as the fractions of all five Q^i-species in a melt.

The fractions of Q^i-species in a melt (in situ measurements) or in a quenched glass can be determined using Raman spectroscopy or nuclear magnetic resonance (NMR) measurements as these spectra reveal the bonding characteristics of Si. Fig.3.3 compares the fractions of Q^i-species in the PbO–SiO_2 system calculated by FactSage [15] from the Modified Quasichemical Model with the fractions determined by NMR spectroscopy [65]. It can be seen that there is good agreement between the calculated and experimentally determined curves. A possible source of error in the calculations is the assumption of randomly distributed bonds. For example, the probability that a particular pair emanating from a given Si atom is a Si–Si pair may depend on how many other Si–Si pairs emanate from this Si atom. On the other hand, the experimental

fractions of the Q^i-species are derived under certain assumptions from the relative intensities of spectral lines and can have substantial uncertainties.

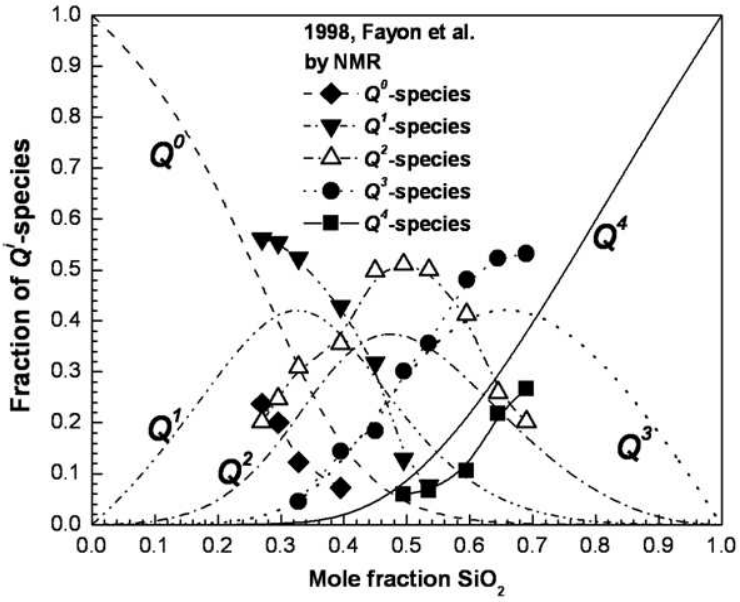

Fig. 3.3 Calculated and experimental [65] fractions of Q^i-species for the PbO–SiO_2 system at 1200 ^oC

Fig. 3.4 shows a schematic of the connectivity of the silicate network. Basic oxides such as M^{2+} and Al^{3+} break the silicate network and are bonded with non-bridging oxygens. The silicon atoms (shown in green and red) are Q^4-species. The silicon atom (shown in red) is bonded to four other Q^4-species to form a cluster of five interconnected Q^4-species with at least 16 connected oxygen bridges or Si-Si pairs.

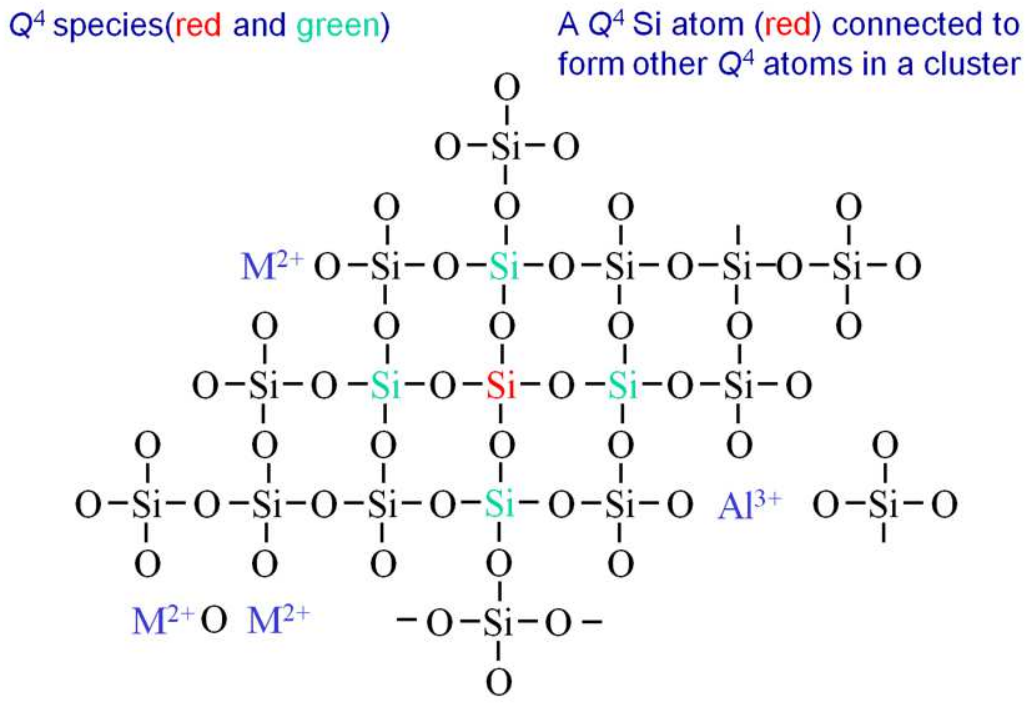

Fig. 3.4 Connectivity of silicate network

The probability that a given Si atom is part of a cluster of at least *n* interconnected Si–Si pairs is proportional to p^n. This is only an approximate relation. Clearly there are restrictions on the arrangement of bonds because of the local structure of the melts, which is similar to the diamond lattice structure of cristobalite. The approximation becomes better for larger values of *n*. In any case, the function p^n is clearly a measure of the connectivity of the network.

It is postulated in the viscosity model [27, 81, 82] that a certain critical cluster size can be defined that mimics the formation of a percolating SiO_2 network. When this cluster size is reached the viscosity will increase dramatically. Analysis of the viscosity data indicates that a group of 40 interconnected Si–Si pairs is a good choice for the critical cluster size.

3.3.1 Combined network formed by SiO_2 and B_2O_3

Si and B are both network formers. Although reality is undoubtedly more complex, the model [27, 81, 82] assumes that the B- and Si-based networks join in a single complex network by forming B–O^o–Si oxygen bridges in addition to the Si–O^o–Si and B–O^o–B bridges. However, some boron cations can act instead as breakers of the silica network. In this case, for each B^{3+} cation, three broken bridges Si–O^- are formed, coordinated with the one B^{3+} cation. The Modified

Quasichemical Model [231, 232] and thermodynamic database [15] can be used to calculate the numbers of B–B, B–Si and Si–Si second-nearest-neighbor pairs, but cannot predict whether a B–Si pair is an oxygen bridge or a broken bridge.

Let us define $p_{\mathrm{Si}}^{\mathrm{B,Si}}$ as the probability that a particular pair emanating from a given Si atom is a Si–Si or Si–B network pair [27, 81, 82]. Then, as a first approximation, $p_{\mathrm{Si}}^{\mathrm{B,Si}}$ can be calculated by dividing the number of Si–Si and Si–B network pairs emanating from all Si atoms by the number of all Si–Si and Si–B pairs:

$$p_{\mathrm{Si}}^{\mathrm{B,Si}} = \frac{2n_{\mathrm{Si\text{-}Si}} + cn_{\mathrm{B\text{-}Si}}}{2n_{\mathrm{Si\text{-}Si}} + n_{\mathrm{B\text{-}Si}}} \tag{3.4}$$

where $n_{i\text{-}j}$ is the number of *i–j* pairs. Note that every Si–Si pair is counted twice, as emanating from one and from the other Si atom in the pair. In Eq.(3.4), *c* is a "coupling factor" representing the fraction of the B–Si pairs which are oxygen bridges. It is reasonable to assume, as we do, that *c* is not a function of composition. This is an adjustable model parameter which is obtained by fitting the viscosity of the B_2O_3–SiO_2 system.

Similarly, the probability that a particular pair emanating from a given B atom is a B–B or B–Si network pair is:

$$p_{\mathrm{B}}^{\mathrm{B,Si}} = \frac{2n_{\mathrm{B\text{-}B}} + cn_{\mathrm{B\text{-}Si}}}{2n_{\mathrm{B\text{-}B}} + n_{\mathrm{B\text{-}Si}}} \tag{3.5}$$

Furthermore, the probability that a particular pair emanating from a given B or Si atom is a B–B, Si–Si or B–Si network pair is:

$$p_{\mathrm{B,Si}}^{\mathrm{B,Si}} = \frac{2(n_{\mathrm{B\text{-}B}} + n_{\mathrm{Si\text{-}Si}} + cn_{\mathrm{B\text{-}Si}})}{2(n_{\mathrm{B\text{-}B}} + n_{\mathrm{Si\text{-}Si}} + n_{\mathrm{B\text{-}Si}})} \tag{3.6}$$

The probabilities $p_{\mathrm{Si}}^{\mathrm{B,Si}}$, $p_{\mathrm{B}}^{\mathrm{B,Si}}$ and $p_{\mathrm{B,Si}}^{\mathrm{B,Si}}$ for multicomponent melts are given by the following equations [27, 81, 82]:

$$p_{\mathrm{Si}}^{\mathrm{B,Si}} = \frac{2n_{\mathrm{Si\text{-}Si}} + c\left(X_{\mathrm{B}} + X_{\mathrm{Si}}\right)n_{\mathrm{B\text{-}Si}}}{2n_{\mathrm{Si\text{-}Si}} + n_{\mathrm{B\text{-}Si}} + \sum_{\mathrm{M}} n_{\mathrm{M\text{-}Si}}} \tag{3.7}$$

$$p_{\mathrm{B}}^{\mathrm{B,Si}} = \frac{2n_{\mathrm{B\text{-}B}} + c\left(X_{\mathrm{B}} + X_{\mathrm{Si}}\right) n_{\mathrm{B\text{-}Si}}}{2n_{\mathrm{B\text{-}B}} + n_{\mathrm{B\text{-}Si}} + \sum_{\mathrm{M}} n_{\mathrm{M\text{-}B}}} \tag{3.8}$$

$$p_{\mathrm{B,Si}}^{\mathrm{B,Si}} = \frac{2\left[n_{\mathrm{B\text{-}B}} + n_{\mathrm{Si\text{-}Si}} + c\left(X_{\mathrm{B}} + X_{\mathrm{Si}}\right) n_{\mathrm{B\text{-}Si}}\right]}{2\left(n_{\mathrm{B\text{-}B}} + n_{\mathrm{Si\text{-}Si}} + n_{\mathrm{B\text{-}Si}}\right) + \sum_{\mathrm{M}} n_{\mathrm{M\text{-}Si}} + \sum_{\mathrm{M}} n_{\mathrm{M\text{-}B}}} \tag{3.9}$$

3.4 A proposed Viscosity Model for Molten Slags

3.4.1 Viscosity of the unary systems

The development in this section is taken from the previous papers [27, 81, 82].

The viscosity η of unary systems as a function of temperature is given by an Arrhenius like equation

$$\ln(\eta) = A + \frac{E}{RT} \tag{3.10}$$

$$\ln \eta_{\mathrm{MO}_x} = A_{\mathrm{MO}_x} + \frac{E_{\mathrm{MO}_x}}{RT} \tag{3.11}$$

where η is the viscosity in Pa·s, R is the gas constant and T is temperature in Kelvins.

If experimental viscosity data for pure basic oxides(MO_x) are available for a unary system, the pre-exponential term A_{MO_x} and the activation energy for viscous flow E_{MO_x} are fitted to the experimental data and these parameters are used when optimizing the viscosity parameters of multicomponent system. If no experimental data are available, the viscosity of the unary system is obtained by extrapolation from binary viscosity data.

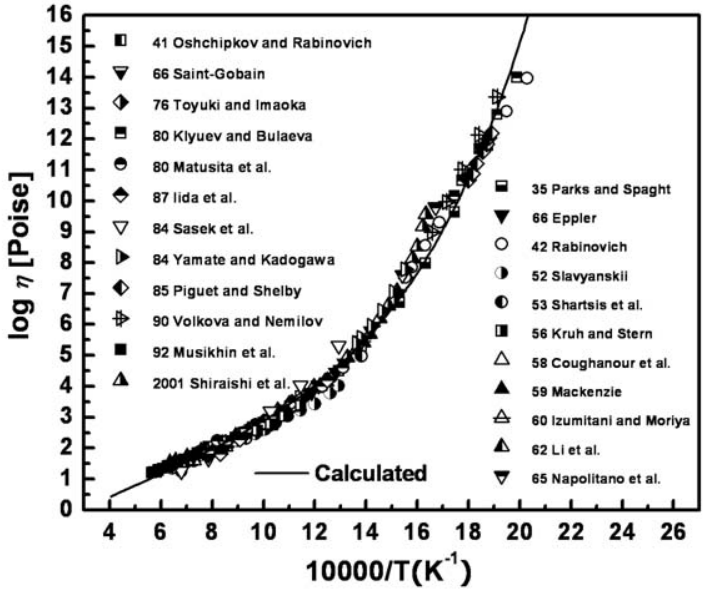

Fig. 3.5 Viscosity of Pure B_2O_3 [27, 81, 82]

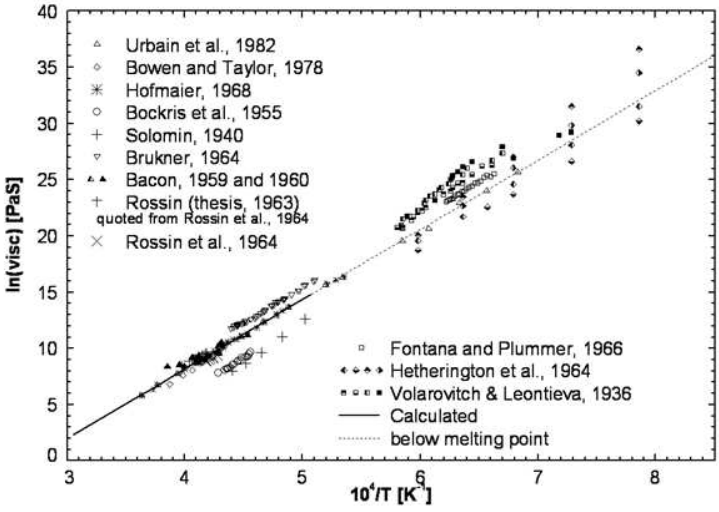

Fig. 3.6 Viscosity of Pure SiO_2 [27, 81, 82]

It is well known that the viscosity as a function of temperature deviates for the glass phase at low temperatures. In the case of viscosities of pure B_2O_3, the viscosity data show obvious non-

Arrhenian behaviour unlike other pure liquid oxides including SiO_2 as shown in Figs 3.5 and 3.6. Thus in the case of B_2O_3, a non-Arrhenian term in Eq.(3.12) was applied [27, 81, 82] as follows:

$$\ln(\eta_B) = A_B + \frac{E_B}{RT}\cdot\left[1+\left(\frac{T_B}{T}\right)^{n_B}\right] \tag{3.12}$$

This equation contains four adjustable parameters A_B, E_B, T_B and n_B optimized from data for pure B_2O_3.

$\ln\eta^*_{Si} = A^*_{Si} + \frac{E^*_{Si}}{RT}$ represents the hypothetical viscosity of SiO_2 if it behaved like a basic oxide and did not form a network. An excess contribution per Si atom of large clusters of Q^4-species, which contain at least 40 interconnected Si–Si pairs, is proportional to p^{40}. This contribution is represented by the parameters E^E_{Si} and A^E_{Si}. This is the contribution of the silica network which is assumed to be independent of other cations M. Therefore, the viscosity of pure SiO_2 is:

$$\ln\eta_{Si} = (A^*_{Si} + A^E_{Si}) + \frac{(E^*_{Si} + E^E_{Si})}{RT} \tag{3.13}$$

3.4.2 Viscosity of the binary systems MO_x-SiO_2 and MO_x-B_2O_3

Consider a liquid oxide melt with composition given by the metal mole fractions X_M. For example, for a binary system $AlO_{1.5}$–SiO_2, the mole fractions of Al and Si are

$$X_{AlO_{1.5}} = \frac{n_{AlO_{1.5}}}{n_{AlO_{1.5}} + n_{SiO_2}}; \quad X_{Si} = \frac{n_{SiO_2}}{n_{AlO_{1.5}} + n_{SiO_2}} \tag{3.14}$$

where n_i are the mole fractions of the components.

The following equations were proposed [27, 81, 82] for the viscosity of liquid melts.

$$\ln(\eta) = A + \frac{E}{RT} \tag{3.15}$$

$$E = X_{MO_x}E_{MO_x} + X_{Si}\left\{E^*_{Si} + E^E_{Si}p^{40} + (p^4 - p^{40})\left(X_{MO_x}E^R_{MO_x-Si}\right)\right\} + X_{MO_x}X_{Si}E^{i,j}_{MO_x\text{-}Si} \tag{3.16}$$

$$A = X_{MO_x}A_{MO_x} + X_{Si}\left\{A^*_{Si} + A^E_{Si}p^{40} + (p^4 - p^{40})\left(X_{MO_x}A^R_{MO_x-Si}\right)\right\} + X_{MO_x}X_{Si}A^{i,j}_{MO_x\text{-}Si} \tag{3.17}$$

where η is the viscosity in Pa·s, R is the gas constant and T is temperature in Kelvins.

An excess contribution per Si atom for the rest of the Q^4-species, that is of smaller clusters which contain less than 40 interconnected Si–Si pairs, is proportional to $(p^4 - p^{40})$. This contribution is represented by binary parameters $E^R_{MO_x\text{-}Si}$ and $A^R_{MO_x\text{-}Si}$. Since these clusters are smaller, the M cations are located closer to a given Si atom so that the contribution of this Si atom depends on M.

Figs 3.7 and 3.8 show the lines calculated by the model using Eqs. (3.15)-(3.17) compared with the experimental data of $AlO_{1.5}$-SiO_2 and CaO-SiO_2 systems [27, 81, 82]. The model [27, 81, 82] reproduces well the viscosity behaviour of binary $AlO_{1.5}$-SiO_2 and CaO-SiO_2 systems at all temperatures.

Eqs. (3.16) and (3.17) contain the additional polynomial binary parameters $E^{i,j}_{MO_x\text{-}Si}$ and $A^{i,j}_{MO_x\text{-}Si}$. In most binary systems, it was assumed that only one such parameter, $E^{1,1}_{MO_x\text{-}Si}$, was needed to account for small nonlinearities of the viscosity, if any, as a function of composition in the basic regions of the binary systems MO_x–SiO_2. Here these terms are generalized to allow more flexibility in fitting experimental viscosity data in a binary system. In particular, it will be shown that one additional polynomial term is required to accurately reproduce the viscosity of binary PbO–SiO_2 melts in Ch. 6.

It should be noted that parameters $A^R_{MO_x\text{-}Si}$ and $A^{i,j}_{MO_x\text{-}Si}$ are almost never needed and can almost always be set equal to zero. So far the model has been applied to multicomponent oxide liquids containing Si, B, Al, Ca, Mg, Li, Na, K, Mn, Ni, Fe^{2+}, Fe^{3+}, Pb, Zn, Ti. Only one non-zero parameter, $A^R_{AlO_{1.5}\text{-}Si}$, was introduced and even in this case the description was already very good without it.

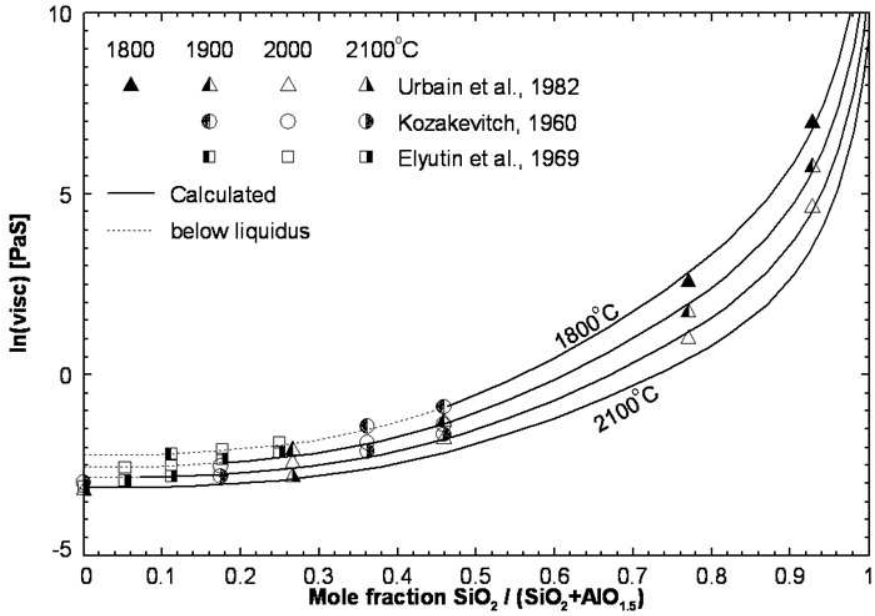

Fig. 3.7 Viscosity of binary $AlO_{1.5}$–SiO_2 system [27, 81, 82]

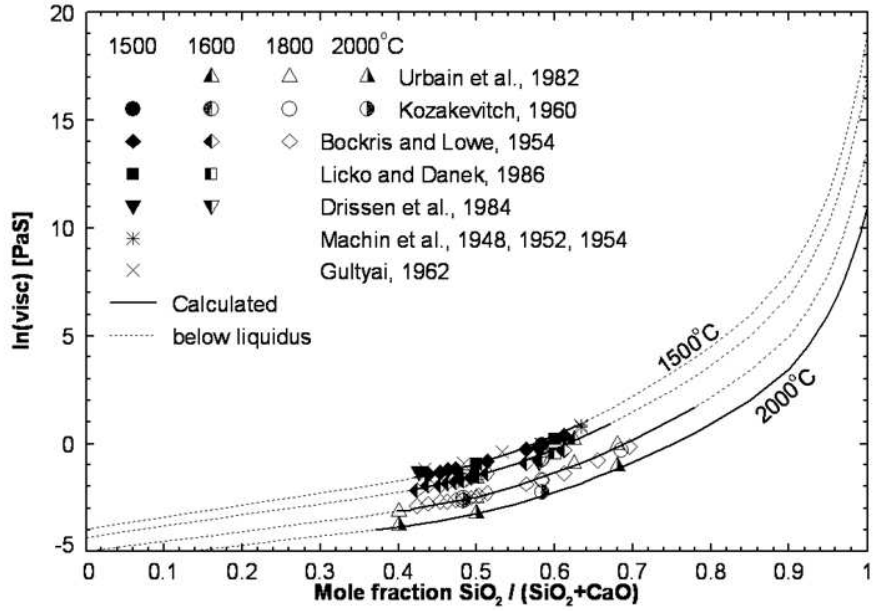

Fig. 3.8 Viscosity of binary CaO–SiO_2 system [27, 81, 82]

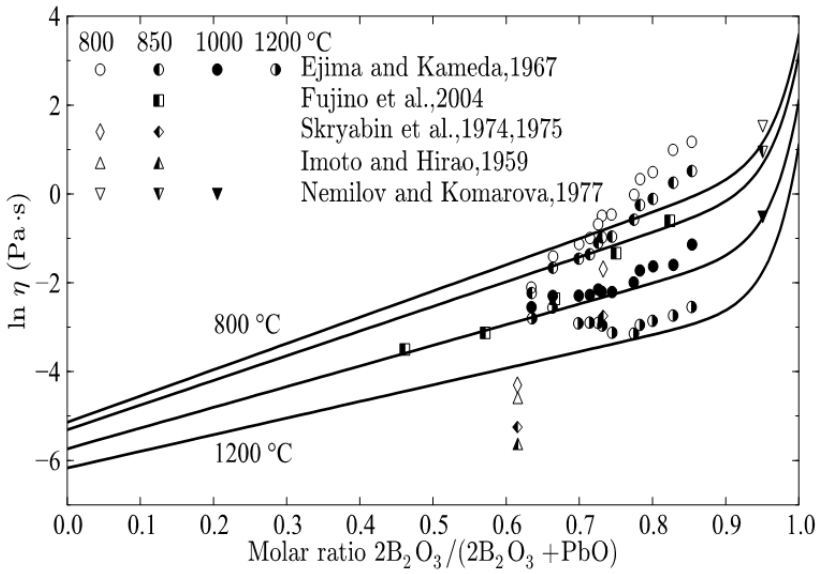

Fig. 3.9 Viscosity of binary PbO–B_2O_3 system [27, 81, 82]

The viscosity of MO_x-B_2O_3 melts , where M is a basic oxide, can be expressed by analogy with Eqs. (3.15)-(3.17) of viscosity for MO_x-SiO_2 melts, taking into account Eq.(3.12) for pure B_2O_3:

$$\ln(\eta) = A + \frac{E}{RT} \tag{3.18}$$

$$E = X_{\mathrm{MO_x}} E_{\mathrm{MO_x}} + X_B \left\{ E^*_{\mathrm{B(MO_x)}} + \left(p_{\mathrm{B}}^{\mathrm{B}} \right)^{40} \left(E_{\mathrm{B}} \left[1 + \left(\frac{T_{\mathrm{B}}}{T} \right)^{n_{\mathrm{B}}} \right] - E^*_{\mathrm{B(MO_x)}} \right) \right\} \tag{3.19}$$

$$A = X_{\mathrm{MO_x}} A_{\mathrm{MO_x}} + X_{\mathrm{B}} \left\{ A^*_{\mathrm{B(MO_x)}} + \left(p_{\mathrm{B}}^{\mathrm{B}} \right)^{40} \left(A_{\mathrm{B}} - A^*_{\mathrm{B(MO_x)}} \right) \right\} \tag{3.20}$$

where $X_{\mathrm{MO_x}}$ and X_B are the cation fractions of M and B. The equation

$$\ln \eta^*_{\mathrm{B(MO_x)}} = A^*_{\mathrm{B(MO_x)}} + \frac{E^*_{\mathrm{B(MO_x)}}}{RT} \tag{3.21}$$

represents the viscosity of hypothetical non-polymerized B_2O_3 surrounded by MO_x, as if B_2O_3 were acting like a basic oxide and not forming a network. (It should be noted that the similar values for silica, η^*_{Si}, A^*_{Si}, and E^*_{Si}, were considered to be independent of the other cations

that are present in the system. That is, as a first approximation, it was assumed that $\eta^*_{\mathrm{Si(MO_x)}} = \eta^*_{\mathrm{Si}}$, $E^*_{\mathrm{Si(MO_x)}} = E^*_{\mathrm{Si}}$ and $A^*_{\mathrm{Si(MO_x)}} = A^*_{\mathrm{Si}}$.)

As mentioned in section 3.3, the probability that a given B atom is part of a cluster of at least *n* interconnected B-B pairs is proportional to p^n. Even though this is only approximate relation, the function of p^n is clearly a measure of the connectivity of the network. The term $\left(p_{\mathrm{B}}^{\mathrm{B}}\right)^{40}\left(A_{\mathrm{B}} - A^*_{\mathrm{B(MO_x)}}\right)$ in Eq.(3.20) and the corresponding term in Eq.(3.19) essentially represent an excess contribution per B atom of large clusters containing at least 40 interconnected B–B pairs. This is the contribution of the B_2O_3 network. Analysis of the viscosity data of the binary MO_x-B_2O_3 systems (M=basic oxides) indicates that a group of 40 interconnected B-B pairs is a good choice for the B_2O_3 network.

The parameters $A^*_{\mathrm{B(MO_x)}}$ and $E^*_{\mathrm{B(MO_x)}}$ were optimized to reproduce the viscosity in each MO_x-B_2O_3 binary system. No other binary parameters were needed. That is, parameters $E^R_{\mathrm{MO_x-B}}$, $A^R_{\mathrm{MO_x-B}}$, $E^{i,j}_{\mathrm{MO_x-B}}$ and $A^{i,j}_{\mathrm{MO_x-B}}$, analogous to the parameters $E^R_{\mathrm{MO_x-Si}}$, $A^R_{\mathrm{MO_x-Si}}$, $E^{i,j}_{\mathrm{MO_x-Si}}$ and $A^{i,j}_{\mathrm{MO_x-Si}}$ which were required for the MO_x–SiO_2 systems as discussed previously, were not required for the MO_x-B_2O_3 systems [27].

Fig. 3.9 shows the lines calculated by the model using Eqs. (3.18)-(3.21) compared with the experimental data of PbO-B_2O_3 system [27, 81, 82]. The model [27, 81, 82] reproduces well the viscosity behaviour of binary PbO-B_2O_3 system at all temperatures within experimental error limits.

3.4.3 Viscosity of the binary systems R_2O-B_2O_3 (R = Na and K)

The addition of basic oxides including Alkali metals to B_2O_3 has a complicating effect on viscosity, known as the "*Boron-Alkali Anomaly*" or "*Borate Anomaly*" [284]. As temperature decreases, adding small quantities of alkali oxide to B_2O_3 melts causes the viscosity to rise to the maximum value at around 20 mol% of R_2O as shown in Fig. 3.10 (where R is an alkali metal such as Na and K). Beyond this maximum, the viscosity decreases monotonically with increasing alkali concentration. In the binary R_2O-B_2O_3 system, the clusters at the tetraborate composition, Na:B = 1:4, and diborate composition, Na:B = 1:2, have been proposed based on studies by

Raman and Infrared spectroscopy, ^{11}B NMR, and X-ray and neutron diffraction [44]. It should be noted that NaB_4 and NaB_2 are simply the overall compositions where stable clusters seem to form. The average size of these clusters is not known. With decreasing temperatures, these stable clusters seem to be formed and have similar physical properties to those of solid compounds formed at tetraborate or diborate compositions. Thus, the formation of these solid-like clusters would give significant increasing effect on viscosity with decreasing temperatures.

The effect of these solid-like cluters on viscosity is different from the effect of phase separation of the liquid and the crystallization phenomena of the sample. For the phase separation of liquids, the viscosity can be affected from the composition of separated phases and this can be estimated from the summation of contribution of each phase on the viscosity of the liquid (It should be noted that the present model is intended for single phase melts). When crystallization is occurred during the measurement, the composition of the sample would change and this can contribute to the change of viscosity. On the other hand, the volume fraction of solid phase in the sample would increase with the process of crystallization. This can contribute to the increasing effect on viscosity of the sample.

In order to take into account the "*Borate anomaly*" of the viscosity in the binary R_2O-B_2O_3 melts, the formation of solid-like clusters at the composition of alkali tetraborates $RB_4O_{6.5}$ (M = Na, K) [26] was applied to reproduce the viscosity data measured in the melt region.

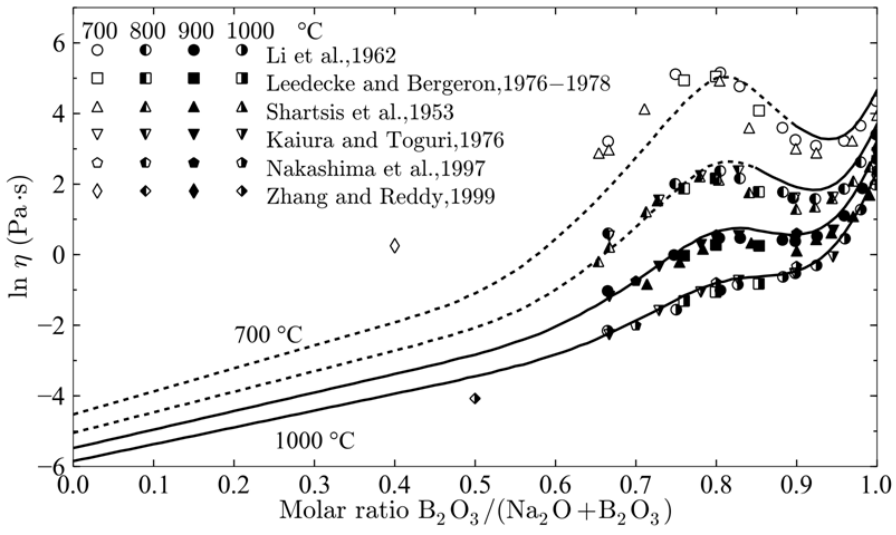

Fig. 3.10 Viscosity of Na_2O–B_2O_3 melts: experimental points [112, 158, 162, 203, 281, 362] and calculated lines. Dashed lines are extrapolations below the liquidus

The modeling for the depolymerization of borate melts by addition of basic oxides (MO_x) was discussed in the preceding section 3.4.2. Depolymerization caused by an alkali oxide is qualitatively identical to that caused by any basic oxide. This is described by two adjustable model parameters, $A^*_{B(MO_x)}$ and $E^*_{B(MO_x)}$ which represent the hypothetical viscosity of non-polymerized B_2O_3 surrounded by M_2O as shown in Eq.(3.21).

The second effect is modeled as follows. Let us assume that clusters $m(RB_4O_{6.5})$ with the tetraborate composition are formed according to the reaction:

$$m \cdot RO_{0.5} + 4m \cdot BO_{1.5} \rightleftarrows m(RB_4O_{6.5}) \tag{3.22}$$

The model parameter in the viscosity model is simply the Gibbs energy of this reaction which, as a first approximation, is assumed to be independent of temperature. The second model parameter is *m*, the average size of these clusters. We can write an equilibrium constant:

$$K_{m(RB_4O_{6.5})} = -\exp\left[\frac{\Delta G_{m(RB_4O_{6.5})}}{RT}\right] = \frac{X'_{m(RB_4O_{6.5})}}{\left(X'_{RO_{0.5}}\right)^m \left(X'_{BO_{1.5}}\right)^{4m}} \tag{3.23}$$

Using mole fractions instead of activities in Eq.(3.23) is, of course, a simplification, but is acceptable because $\Delta G_{m(RB_4O_{6.5})}$ will be calibrated based on the experimental viscosity data and Eq.(3.23) gives a qualitatively correct compositional dependence of the viscosity which reflects the formation of clusters at the tetraborate composition.

At each given overall composition $X_{RO_{0.5}}$ and $X_B (= X_{BO_{1.5}})$, where $X_{RO_{0.5}}$ and X_B are the mole fractions of cations of each oxide and $X_{RO_{0.5}} + X_B = 1$, Eq.(3.23) can be solved, taking into account the mass balance constraints, to obtain the number of moles of each species: $n'_{RO_{0.5}}$, n'_B and $n'_{m(RB_4O_{6.5})}$.

The viscosity of R_2O–B_2O_3 melts is assumed to be the sum of two contributions: the contribution of the clusters, $\ln \eta_{m(RB_4O_{6.5})}$, and the contribution of the rest of the melt, $\ln \eta^*$. The simplest assumption is to postulate that each contribution is linearly proportional to the fraction of cations forming the associates and the rest of the melt as shown in Eq.(3.24), and the

assumption leads to a very good representation of the experimental data of binary R_2O–B_2O_3 melts:

$$\ln\eta = \frac{n'_{RO_{0.5}} + n'_B}{n_{total}} \ln\eta^*\left(X^*_{RO_{0.5}}, X^*_B\right) + \frac{5mn'_{m(RB_4O_{6.5})}}{n_{total}} \ln\eta_{m(RB_4O_{6.5})} \tag{3.24}$$

where η is the viscosity in Pa·s,

$$n_{total} = X_{RO_{0.5}} + X_B = n'_{RO_{0.5}} + n'_B + 5mn'_{m(RB_4O_{6.5})} \tag{3.25}$$

$$X^*_{RO_{0.5}} = \frac{X'_{RO_{0.5}}}{X'_{RO_{0.5}} + X'_B} \tag{3.26}$$

$$X^*_B = \frac{X'_B}{X'_{RO_{0.5}} + X'_B} \tag{3.27}$$

η^* is calculated by substituting $X^*_{RO_{0.5}}$ and X^*_B instead of X_{MO_x} and X_B into Eqs. (3.18)-(3.20). $\eta_{m(RB_4O_{6.5})}$ is expressed in Pa·s and represents the contribution of the associates to the viscosity of the melt per mole of cations in the associates:

$$\ln\eta_{m(RB_4O_{6.5})} = A_{m(RB_4O_{6.5})} + \frac{E_{m(RB_4O_{6.5})}}{RT} \tag{3.28}$$

where

$$A_{m(RB_4O_{6.5})} = \frac{1}{5}A_{RO_{0.5}} + \frac{4}{5}A_{B(RO_{0.5})} \tag{3.29}$$

and $E_{m(RB_4O_{6.5})}$ is an adjustable model parameter which is fitted to the viscosity data in the R_2O–B_2O_3 system.

Therefore, a total of five binary parameters are used to reproduce the viscosity data in each alkali oxide – boron oxide binary system: $A^*_{B(RO_{0.5})}$, $E^*_{B(RO_{0.5})}$, m, $\Delta G_{m(RB_4O_{6.5})}$ and $E_{m(RB_4O_{6.5})}$. It should be noted that the same optimized average cluster size, m = 5, is used for all these systems.

3.4.4 Viscosity of multicomponent systems without Al_2O_3

The overall viscosity of multicomponent systems, η, is assumed to be the sum of two contributions: from the alkali-boron associates, $\eta_{5(RB_4O_{6.5})}$, and from the rest of the melt, $\eta^*(X_i^*)$. These contributions are weighted by the cation fractions:

$$\ln\eta = \frac{n^*_{total}}{n_{total}} \ln\eta^*\left(X^*_{Si}, X^*_B, X^*_{MO_x}\right) + \sum_{M=Alkali}\left[\frac{25n_{5(RB_4O_{6.5})}}{n_{total}} \ln\eta_{5(RB_4O_{6.5})}\right] \tag{3.30}$$

where $\eta_{5(RB_4O_{6.5})}$ is the contribution of the $5(RB_4O_{6.5})$ associates per mole of cations in the associates. Since

$$\begin{aligned} \ln\eta &= A + \frac{E}{RT} \\ \ln\eta^* &= A^* + \frac{E^*}{RT} \\ \ln\eta_{5(RB_4O_{6.5})} &= A_{5(RB_4O_{6.5})} + \frac{E_{5(RB_4O_{6.5})}}{RT} \end{aligned} \tag{3.31}$$

equations similar to (3.30) apply also to *A* and *E*. In particular the activation energy is:

$$E = \frac{n^*_{total}}{n_{total}} E^*\left(X^*_{Si}, X^*_B, X^*_{MO_x}\right) + \sum_{M=Alkali}\left[\frac{25n_{5(RB_4O_{6.5})}}{n_{total}} E_{5(RB_4O_{6.5})}\right] \tag{3.32}$$

where the total adjusted number of cations in the melt without counting the boron-alkali associates is

$$n^*_{total} = n^*_{Si} + n_B + \sum_M n_{MO_x} \tag{3.33}$$

and the total adjusted number of cations in the melt is

$$n_{total} = n^*_{total} + 25n_{5(NaB_4)} + 25n_{5(KB_4)} + \ \ldots \tag{3.34}$$

Thus, the contribution of the rest of the melt in multicomponent systems is calculated from the following equations

Consider a melt with the overall composition

$$X^*_{Si},\ X^*_B,\ X^*_{MO_x},\ \ldots \tag{3.35}$$

$$\ln(\eta^*) = A^* + \frac{E^*}{RT} \tag{3.36}$$

$$\begin{aligned} E^* &= \sum_{\mathrm{M}} (X^*_{\mathrm{MO_x}} E_{\mathrm{MO_x}}) + \sum_{\mathrm{M}} \left(X^*_{\mathrm{MO_x}} X^*_{\mathrm{Si}} E^{i,j}_{\mathrm{MO_x\text{-}Si}} \right) \\ &+ X^*_{\mathrm{Si}} \left\{ E^*_{\mathrm{Si}} + \left(p^{\mathrm{B,Si}}_{\mathrm{Si}} \right)^4 \left(p^{\mathrm{B,Si}}_{\mathrm{B,Si}} \right)^{36} E^E_{\mathrm{Si}} + \left(p^{\mathrm{B,Si}}_{\mathrm{Si}} \right)^4 \left[1 - \left(p^{\mathrm{B,Si}}_{\mathrm{B,Si}} \right)^{36} \right] \left[\frac{\sum_{\mathrm{M}} (X^*_{\mathrm{MO_x}} E^R_{\mathrm{MO_x\text{-}Si}})}{\sum_{\mathrm{M}} X^*_{\mathrm{MO_x}}} \right] \right\} \\ &+ X^*_{\mathrm{B}} \left\{ E^*_{\mathrm{B}} + \left(p^{\mathrm{B,Si}}_{\mathrm{B}} \right)^3 \left(p^{\mathrm{B,Si}}_{\mathrm{B,Si}} \right)^{37} \left(E_{\mathrm{B}} \left[1 + \left(\frac{T_B}{T} \right)^{n_B} \right] - E^*_{\mathrm{B}} \right) \right\} \end{aligned} \tag{3.37}$$

$$\begin{aligned} A^* &= \sum_{\mathrm{M}} (X^*_{\mathrm{MO_x}} A_{\mathrm{MO_x}}) + \sum_{\mathrm{M}} \left(X^*_{\mathrm{MO_x}} X^*_{\mathrm{Si}} A^{i,j}_{\mathrm{MO_x\text{-}Si}} \right) \\ &+ X^*_{\mathrm{Si}} \left\{ A^*_{\mathrm{Si}} + \left(p^{\mathrm{B,Si}}_{\mathrm{Si}} \right)^4 \left(p^{\mathrm{B,Si}}_{\mathrm{B,Si}} \right)^{36} A^E_{\mathrm{Si}} + \left(p^{\mathrm{B,Si}}_{\mathrm{Si}} \right)^4 \left[1 - \left(p^{\mathrm{B,Si}}_{\mathrm{B,Si}} \right)^{36} \right] \left[\frac{\sum_{\mathrm{M}} (X^*_{\mathrm{MO_x}} A^R_{\mathrm{MO_x\text{-}Si}})}{\sum_{\mathrm{M}} X^*_{\mathrm{MO_x}}} \right] \right\} \\ &+ X^*_{\mathrm{B}} \left\{ A^*_{\mathrm{B}} + \left(p^{\mathrm{B,Si}}_{\mathrm{B}} \right)^3 \left(p^{\mathrm{B,Si}}_{\mathrm{B,Si}} \right)^{37} \left(A_{\mathrm{B}} - A^*_{\mathrm{B}} \right) \right\} \end{aligned} \tag{3.38}$$

where

$$E^*_{\mathrm{B}} = \frac{X^*_{\mathrm{Si}} E^*_{\mathrm{B(Si)}} + \sum_{\mathrm{M}} \left(X^*_{\mathrm{MO_x}} E^*_{\mathrm{B(MO_x)}} \right)}{X^*_{\mathrm{Si}} + \sum_{\mathrm{M}} X^*_{\mathrm{MO_x}}}, A^*_{\mathrm{B}} = \frac{X^*_{\mathrm{Si}} A^*_{\mathrm{B(Si)}} + \sum_{\mathrm{M}} \left(X^*_{\mathrm{MO_x}} A^*_{\mathrm{B(MO_x)}} \right)}{X^*_{\mathrm{Si}} + \sum_{\mathrm{M}} X^*_{\mathrm{MO_x}}} \tag{3.39}$$

The viscosities of ternary and higher-order melts without Al_2O_3 can be predicted by the model based on the unary and binary viscosity parameters without any additional adjustable parameters. For example, as shown in Fig. 3.11, the viscosity data of CaO-MgO-SiO_2 system are in good agreement with the predicted lines of the model using only a few unary and binary parameters [27, 81, 82].

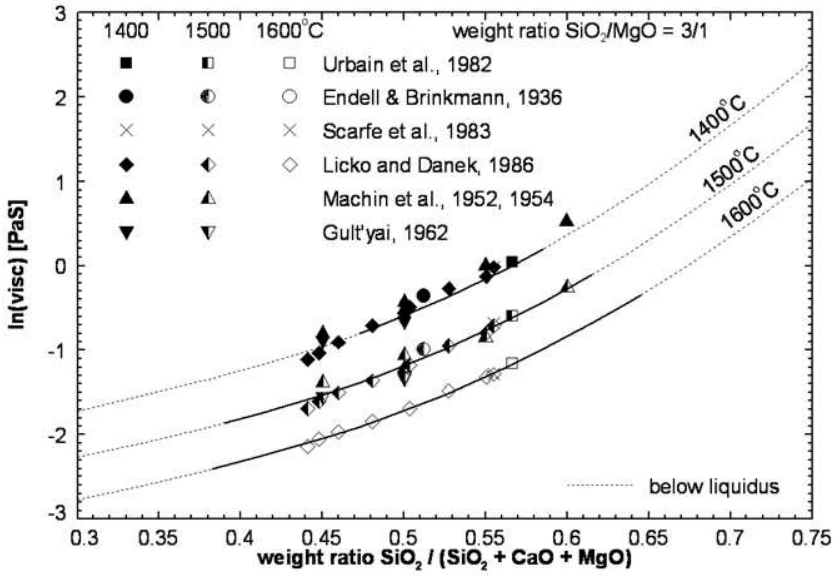

Fig. 3.11 Viscosity of CaO-MgO-SiO_2 melts at weight ratio SiO_2/MgO=3/1 compared with experimental data [27, 81, 82]

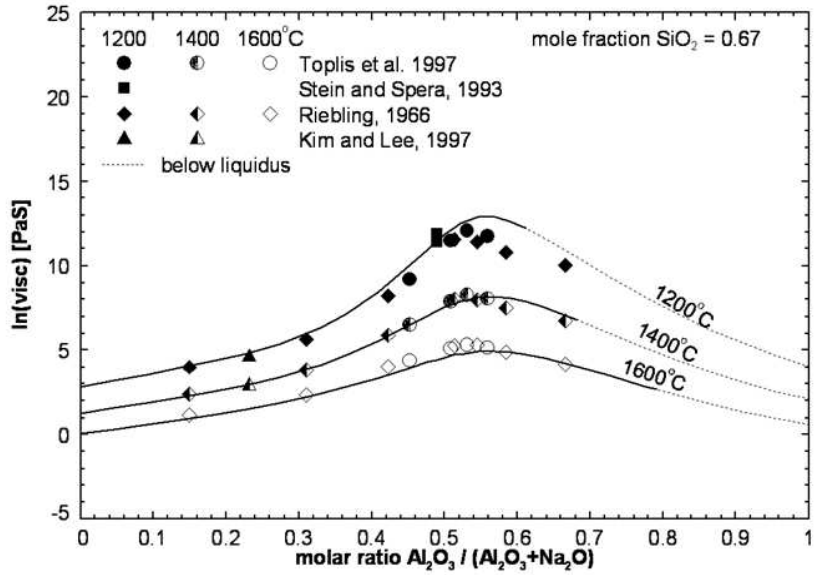

Fig. 3.12 Viscosity of Na_2O-Al_2O_3-SiO_2 melts at 67 mol% SiO_2 compared with experimental data [27, 81, 82]

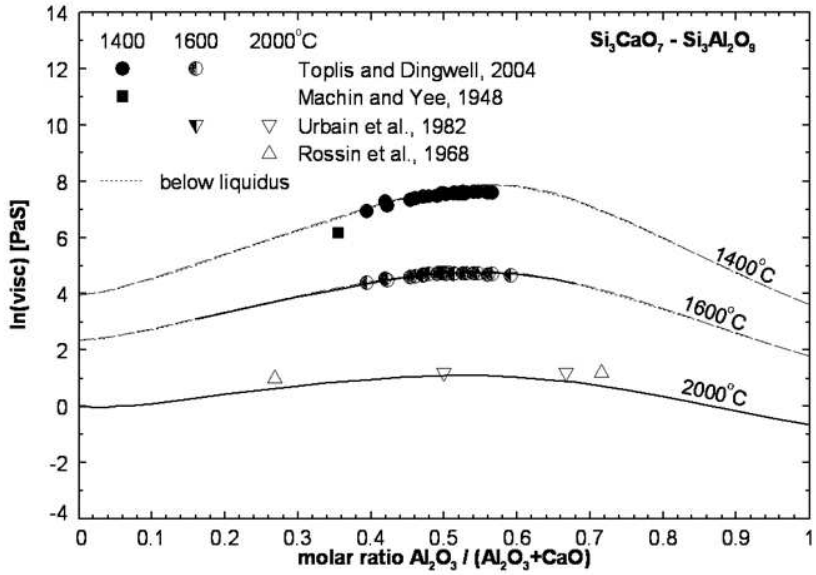

Fig. 3.13 Viscosity of CaO-Al_2O_3-SiO_2 melts at 75 mol% SiO_2 compared with experimental data [27, 81, 82]

3.4.5 Taking into account Charge Compensation Effect

The most prominent feature in MO_x-$AlO_{1.5}$-SiO_2 ternary systems is a viscosity maximum with a ridge running along the metaluminous composition as shown in Figs 3.12 and 3.13 [27, 81, 82]. The maximum is particularly prominent in the $NaO_{0.5}$-$AlO_{1.5}$-SiO_2 system.

Certain amphoteric oxides such as Al_2O_3 can behave in profoundly different ways in a silicate melt depending on the overall composition. When added to a pure silica melt, Al_2O_3 acts as a network-modifier, breaking the oxygen bridges of the pure silica network, thereby substantially decreasing the viscosity. However, in a melt containing both $AlO_{1.5}$ and MO_x the Al^{3+} can partially substitute for Si^{4+} in the silica network, thereby acting as a network forming Al^{3+} remains associated with the M^{1+} or M^{2+} ions that compensate for the missing charge. This concept has become generally accepted and is termed the “Charge Compensation Effect”. Due to this “Charge Compensation Effect” [199], there is a maximum in the viscosity when the molar ratio of Al_2O_3 to MO or M_2O is unity as shown in Figs 3.12 and 3.13.

The thermodynamic database of Modified Quasichemical Model parameters, upon which the viscosity model is based, does not explicitly consider the different structural roles of Al. Hence, in order to model the viscosity maximum, the amount of network-forming Al must be evaluated *a posteriori*. This is done as follows.

Consider, for example, the Al_2O_3–CaO–Na_2O–SiO_2 system. We can write two reactions to form tetrahedrally-coordinated Al that enters the silica network and is charge-compensated by either Na or Ca:

$$AlO_{1.5} + NaO_{0.5} \rightleftarrows NaAlO_2 \tag{3.40}$$

$$2AlO_{1.5} + CaO \rightleftarrows CaAl_2O_4 \tag{3.41}$$

It is assumed that the $NaAlO_2$ and $CaAl_2O_4$ "species" have the same effect on the viscosity as one or two SiO_2 species respectively. The model parameters are simply the Gibbs energies of reactions (3.40) and (3.41). These Gibbs energies are not dependent on temperature, but are found to vary linearly as a function of SiO_2 content, becoming more negative at higher SiO_2 concentrations. Hence, only two parameters are required to model the Charge Compensation Effect in each ternary system MO_x–Al_2O_3–SiO_2 (including the limiting MO_x–Al_2O_3 binary systems).

The equilibrium constants for reactions (3.40) and (3.41) can be written as

$$K_{NaAlO_2} = \exp\left(\frac{-\Delta G_{NaAlO_2}}{RT}\right) = \frac{X'_{NaAlO_2}}{X'_{NaO_{0.5}} X'_{AlO_{1.5}}} \tag{3.42}$$

$$K_{CaAl_2O_4} = \exp\left(\frac{-\Delta G_{CaAl_2O_4}}{RT}\right) = \frac{X'_{CaAl_2O_4}}{X'_{CaO} (X'_{AlO_{1.5}})^2} \tag{3.43}$$

At each given overall composition $\boldsymbol{X}_{\mathbf{NaO_{0.5}}}$, $\boldsymbol{X}_{\mathbf{CaO}}$, $\boldsymbol{X}_{\mathbf{AlO_{1.5}}}$ and $\boldsymbol{X}_{\mathbf{Si}}$, Eqs. (3.42) and (3.43) can be solved, taking into account the mass balance constraints, to calculate

$$\boldsymbol{X'_{NaO_{0.5}}, X'_{CaO}, X'_{AlO_{1.5}}, X'_{Si}, X'_{NaAlO_2}, \text{ and } X'_{CaAl_2O_4}}$$

Here $(X'_{NaAlO_2} + 2X'_{CaAl_2O_4})$ gives the amount of network-forming Al, while $X'_{AlO_{1.5}}$ gives the amount of network-modifying Al.

Since we assume that $NaAlO_2$ and $CaAl_2O_4$ species have exactly the same effect on the viscosity as one or two SiO_2 species respectively, the viscosity can be calculated by substituting the following adjusted mole fractions into Eqs. (3.37) and (3.38):

$$
\begin{aligned}
&X^*_{\mathrm{Si}} = \left(X'_{\mathrm{Si}} + X'_{\mathrm{NaAlO_2}} + 2X'_{\mathrm{CaAl_2O_4}} \right) / N^*_{tot} \\
&X^*_{\mathrm{AlO_{1.5}}} = X'_{\mathrm{AlO_{1.5}}} / N^*_{tot} \\
&X^*_{\mathrm{CaO}} = X'_{\mathrm{CaO}} / N^*_{tot} \\
&X^*_{\mathrm{NaO_{0.5}}} = X'_{\mathrm{NaO_{0.5}}} / N^*_{tot} \\
&\text{where } N^*_{tot} = X'_{\mathrm{NaO_{0.5}}} + X'_{\mathrm{CaO}} + X'_{\mathrm{AlO_{1.5}}} + X'_{\mathrm{Si}} + X'_{\mathrm{NaAlO_2}} + 2X'_{\mathrm{CaAl_2O_4}}
\end{aligned}
\tag{3.44}
$$

Obviously, this proposed treatment of the Charge Compensation Effect is a simplification. Strictly speaking, the charge-compensated $AlO_{1.5}$ that enters the silica network does not form chemically distinct species such as $NaAlO_2$ and $CaAl_2O_4$; the contribution of network-forming $AlO_{1.5}$ to the viscosity may be different from that of Si and, finally, mole fractions are used in Eqs. (3.42)–(3.43) instead of activities. However, the proposed treatment gives a qualitatively correct functional dependence of the viscosity on temperature and composition, and the description is made quantitative by fitting the Gibbs energies of reactions (3.40) and (3.41) to experimental viscosity data in the ternary MO_x–Al_2O_3–SiO_2 systems.

The viscosities of ternary and higher-order melts can be predicted by the model based on the unary, binary and ternary viscosity parameters without any additional adjustable parameters as shown in Figs 3.14 and 3.15. Viscosity data of many ternary and higher-order systems for CaO-MgO-K_2O-Na_2O-Al_2O_3-SiO_2-B_2O_3 systems show a good agreement with the predicted lines by the model within experimental error limits except for alkali-rich silicate melts [27, 26, 81, 82].

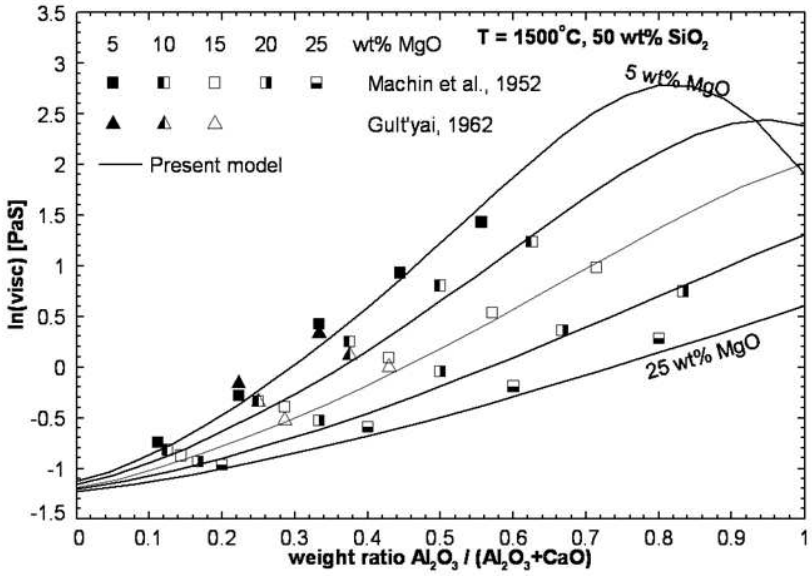

Fig. 3.14 Viscosity of CaO-MgO-Al_2O_3-SiO_2 melts at 5, 10, 15, 20 and 25 wt% MgO and 50 wt% at 1500ºC compared with experimental data [27, 81, 82]

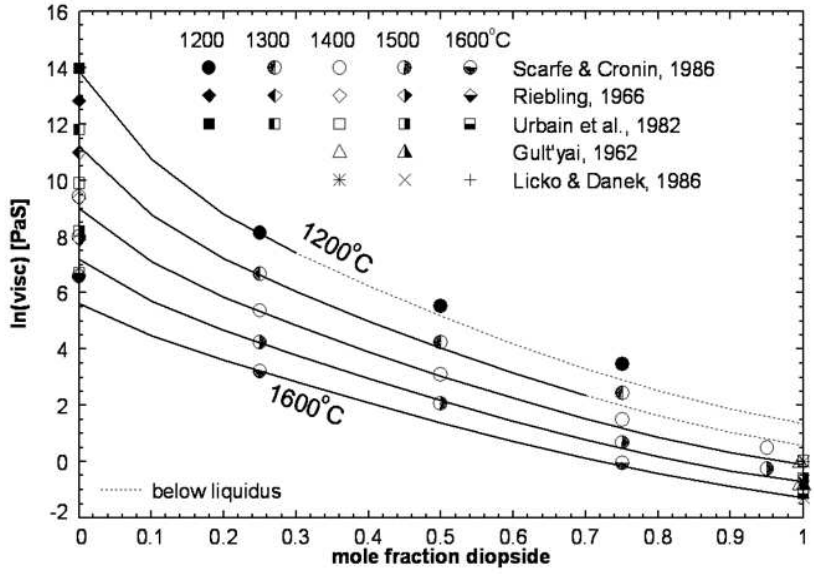

Fig. 3.15 Viscosity along the albite-diopside ($NaAlSi_3O_8$-$CaMgSi_2O_6$) join at 1200ºC, 1300ºC, 1400ºC, 1500ºC and 1600 ºC compared with experimental data [27, 81, 82]

CHAPTER 4 MODIFICATION OF THE MODEL FOR MELTS CONTAINING ALKALI OXIDES

From this chapter on, the results of the present work will be discussed.

4.1 Introduction

Intrinsic experimental difficulties are encountered in measurements of the viscosity of alkali-rich slags due to the volatility of alkalis, the reactivity of the liquid and, most importantly, contamination of samples due to extremely high hygroscopicity and a strong tendency of melts produced from carbonates to retain CO_2. Experimental data in this region are scarce and widely scattered. Even seemingly consistent data from different authors can still be subject to a substantial systematic error if samples are contaminated in a similar manner. In particular, for the $NaO_{0.5}$–SiO_2 system, several authors reported a sharp decrease of the viscosity below a mole fraction of SiO_2 equal to 0.5, although others did not observe such behaviour [143]. If the experimental viscosity curves are smoothly extrapolated to pure $NaO_{0.5}$, an unreasonably low viscosity is obtained unless the viscosity curves show a second inflection leading to an S-shaped curve. Although one might expect a similar drop of the viscosity in the basic region of the CaO–SiO_2 system, this has never been observed. To keep the model simple, we initially ignored all experiments below a silica mole fraction of 0.5 and did not attempt to model the dip in the viscosity [82]. However in applying the model to many multi-component systems, we came across additional experimental data which support the complex behaviour of the viscosity on the alkali-rich side of the $MO_{0.5}$–SiO_2 systems. Some of these publications contained more details about experimental conditions, and similar results were reported for samples studied in different atmospheres where the contamination of the samples should be different. In view of this preponderance of experimental evidence, the model proposed earlier [81, 82] is further developed in the present study to reproduce the complex behaviour of the viscosity on the alkali-rich side of the $MO_{0.5}$–SiO_2 systems.

4.2 Modification of the model for melts containing alkali oxides

As can be seen from the previous chapter 3, only Q^4-species were assumed to provide a substantial excess contribution to the viscosity. The excess contribution from Q^2- and Q^3-species

was considered to be negligibly small in comparison. Comparing Figs 4.1-4.3 with Figs 3.7-3.8 the experimental data of the $MO_{0.5}$-SiO_2 (M=Na, K and Li) system show very different behavior of the viscosity compared with the $AlO_{1.5}$-SiO_2 and CaO-SiO_2 systems on the MO_x-rich side. As can be seen from Figs. 4.1-4.3 in section 4.3, there is experimental evidence for complex behaviour of the viscosity on the alkali-rich side of the $MO_{0.5}$–SiO_2 systems where M is an alkali. In this composition region mostly Q^2- and Q^3-species are present. If these species can join together to form large clusters, their contribution can be substantial.

In particular, rings formed by Q^2- and Q^3-species have been reported to form in binary alkali oxide – silica systems based on evidence from NMR and Raman spectroscopy [175, 177]. Formation of these rings is facilitated by monovalent alkali cations which are very strong network breakers. On the other hand, when a divalent cation, such as Ca^{2+}, breaks the silica network, the two Si–O^- groups that are formed must be arranged in such a way that two negatively charged oxygen atoms are located close to one Ca^{2+} cation in order to maintain local electroneutrality. This would be expected to create a strain in the structure and make the formation of similar rings in the MO–SiO_2 systems less favourable. Therefore, for alkali oxide – silica systems, an additional excess contribution of Q^2- and Q^3-species polymerized into large rings has been added to the viscosity formulae (3.14)-(3.16) as follows.

The probability that a given Si atom is a Q^2-species (*i.e.* is linked to two other Si atoms through oxygen bridges and to two broken bridges) is proportional to $p^2(1-p)^2$. The probability that a given Si atom is a Q^2-species linked to at least one Q^3-species forming a cluster:

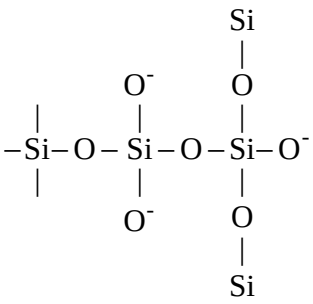

is proportional to $p^2(1-p)^2\ p^2(1-p) = p^4(1-p)^3$. In general, the probability that a given Si atom is part of a cluster formed by a number of Q^1-, Q^2- and Q^3-species linked together is approximately proportional to $p^n(1-p)^m$. Since it is not known how many Q-species form these clusters, and since clusters of different size are likely to form, we simply postulate as a first

approximation that an excess contribution of such clusters per Si atom is proportional to $p^n(1-p)^m$ where n and m are parameters of the model. The values $n = 7$ and $m = 3$ were selected based on an analysis of all viscosity data for alkali oxide – SiO_2 binary systems and are the same for all these systems.

Therefore, an additional term is added to Eqs. (3.36) and (3.37) which becomes;

$$\ln(\eta^*) = A^* + \frac{E^*}{RT} \tag{4.1}$$

$$\begin{aligned} E^* = & \sum_{\mathrm{M}} (X^*_{\mathrm{MO_x}} E_{\mathrm{MO_x}}) + \sum_{\mathrm{M}} \left(X^*_{\mathrm{MO_x}} X^*_{\mathrm{Si}} E^{i,j}_{\mathrm{MO_x\text{-}Si}} \right) \\ & + X^*_{\mathrm{Si}} \left\{ \begin{array}{l} E^*_{\mathrm{Si}} + \left(p^{\mathrm{B,Si}}_{\mathrm{Si}}\right)^4 \left(p^{\mathrm{B,Si}}_{\mathrm{B,Si}}\right)^{36} E^E_{\mathrm{Si}} + \left(p^{\mathrm{B,Si}}_{\mathrm{Si}}\right)^4 \left[1-\left(p^{\mathrm{B,Si}}_{\mathrm{B,Si}}\right)^{36}\right] \left[\dfrac{\sum_{\mathrm{M}} (X^*_{\mathrm{MO_x}} E^R_{\mathrm{MO_x\text{-}Si}})}{\sum_{\mathrm{M}} X^*_{\mathrm{MO_x}}} \right] \\ + \left(p^{\mathrm{Si}}_{\mathrm{Si}}\right)^7 \left(1-p^{\mathrm{Si}}_{\mathrm{Si}}\right)^3 \left[\dfrac{\sum_{\mathrm{M=Alkali}} (X^*_{\mathrm{MO_x}} E^{Ring}_{\mathrm{MO_x\text{-}Si}})}{\sum_{\mathrm{M}} X^*_{\mathrm{MO}_x}} \right] \end{array} \right\} \\ & + X^*_{\mathrm{B}} \left\{ E^*_{\mathrm{B}} + \left(p^{\mathrm{B,Si}}_{\mathrm{B}}\right)^3 \left(p^{\mathrm{B,Si}}_{\mathrm{B,Si}}\right)^{37} \left(E_{\mathrm{B}} \left[1 + \left(\frac{T_B}{T} \right)^{n_B} \right] - E^*_{\mathrm{B}} \right) \right\} \end{aligned} \tag{4.2}$$

$$\begin{aligned} A^* = & \sum_{\mathrm{M}} (X^*_{\mathrm{MO_x}} A_{\mathrm{MO_x}}) + \sum_{\mathrm{M}} \left(X^*_{\mathrm{MO_x}} X^*_{\mathrm{Si}} A^{i,j}_{\mathrm{MO_x\text{-}Si}} \right) \\ & + X^*_{\mathrm{Si}} \left\{ \begin{array}{l} A^*_{\mathrm{Si}} + \left(p^{\mathrm{B,Si}}_{\mathrm{Si}}\right)^4 \left(p^{\mathrm{B,Si}}_{\mathrm{B,Si}}\right)^{36} A^E_{\mathrm{Si}} + \left(p^{\mathrm{B,Si}}_{\mathrm{Si}}\right)^4 \left[1-\left(p^{\mathrm{B,Si}}_{\mathrm{B,Si}}\right)^{36}\right] \left[\dfrac{\sum_{\mathrm{M}} (X^*_{\mathrm{MO_x}} A^R_{\mathrm{MO_x\text{-}Si}})}{\sum_{\mathrm{M}} X^*_{\mathrm{MO_x}}} \right] \\ + \left(p^{\mathrm{Si}}_{\mathrm{Si}}\right)^7 \left(1-p^{\mathrm{Si}}_{\mathrm{Si}}\right)^3 \left[\dfrac{\sum_{\mathrm{M=Alkali}} (X^*_{\mathrm{MO_x}} A^{Ring}_{\mathrm{MO_x\text{-}Si}})}{\sum_{\mathrm{M}} X^*_{\mathrm{MO}_x}} \right] \end{array} \right\} \\ & + X^*_{\mathrm{B}} \left\{ A^*_{\mathrm{B}} + \left(p^{\mathrm{B,Si}}_{\mathrm{B}}\right)^3 \left(p^{\mathrm{B,Si}}_{\mathrm{B,Si}}\right)^{37} \left(A_{\mathrm{B}} - A^*_{\mathrm{B}} \right) \right\} \end{aligned} \tag{4.3}$$

where

$$E^*_{\mathrm{B}} = \frac{X^*_{\mathrm{Si}} E^*_{\mathrm{B(Si)}} + \sum_{\mathrm{M}} \left(X^*_{\mathrm{MO_x}} E^*_{\mathrm{B(MO_x)}} \right)}{X^*_{\mathrm{Si}} + \sum_{\mathrm{M}} X^*_{\mathrm{MO_x}}}, A^*_{\mathrm{B}} = \frac{X^*_{\mathrm{Si}} A^*_{\mathrm{B(Si)}} + \sum_{\mathrm{M}} \left(X^*_{\mathrm{MO_x}} A^*_{\mathrm{B(MO_x)}} \right)}{X^*_{\mathrm{Si}} + \sum_{\mathrm{M}} X^*_{\mathrm{MO_x}}} \tag{4.4}$$

where $\boldsymbol{E}^{\boldsymbol{Ring}}_{\mathbf{MO_x\text{-}Si}}$ is a binary parameter which is non-zero only for alkali oxide – silica systems. It should be noted that a similar additional term was never needed in Eq.(4.3) for *A*. That is, all parameters $\boldsymbol{A}^{\boldsymbol{Ring}}_{\mathbf{MO_x\text{-}Si}} = \mathbf{0}$.

In summary, for most binary systems MO_x–SiO_2 only two binary parameters, $\boldsymbol{E}^{\mathbf{1,1}}_{\mathbf{MO_x\text{-}Si}}$ and $\boldsymbol{E}^{\boldsymbol{R}}_{\mathbf{MO_x\text{-}Si}}$, were required to fit the experimental viscosity data, while for each alkali oxide – SiO_2 system one additional binary parameter, $\boldsymbol{E}^{\boldsymbol{Ring}}_{\mathbf{MO_x\text{-}Si}}$, was needed.

4.3 Review of the available viscosity data and calibration of the model

In the present study, viscosity data were collected for all sub-systems of the Al_2O_3–CaO–MgO–Na_2O–K_2O–SiO_2 system. The most reliable data for alkali-containing systems are shown in the figures below. Experimental data and calculated curves for alkali-free subsystems were presented previously [81, 82]. To improve the legibility of the figures, the results of a few studies which substantially deviate from those of other authors are not shown. For multicomponent subsystems, preference was given to extensive systematic studies. If the viscosity was reported for just a few compositions in a multicomponent system and the description of the experiments was insufficient, it is very difficult to evaluate the real accuracy of the data unless similar compositions were also studied by other authors.

The proposed model is intended for liquid melts. The extension of the model to describe the viscosity of glasses will be reported in Chapters 11 and 12. Therefore, the viscosity data were collected mostly for temperatures above the liquidus. Phase equilibrium calculations were carried out using the FactSage thermochemical software and databases [14] to check that the viscosity was indeed measured in a single liquid region. If an abnormally high viscosity value was reported for a temperature below the liquidus, this is most likely the result of crystallization. In most obvious cases such data points were discarded, but sometimes these points are still shown in the figures if it is deemed possible that they correspond to a supercooled liquid which does not contain precipitated solids.

4.3.1 Viscosities of pure alkali oxides and binary $MO_{0.5}$–SiO_2 (M = Li, Na, K) melts

The system $NaO_{0.5}$–SiO_2 is of primary importance to the glass industry and has been studied by many authors. Most measurements were conducted using a rotating crucible or rotating cylinder viscometer employing Pt/Rh or Pt/Ir crucibles [119, 125, 134, 143, 166, 167, 212, 246, 312, 313, 333, 348, 362] or molybdenum crucibles [23]. Some investigators [223, 283, 295] measured the viscosity using the counterbalanced sphere method with platinum spheres and crucibles. Heidtkamp and Endell [88] used the counterbalanced sphere method for viscosities above 0.8 Pa·s and an oscillating ball method for viscosities below 0.8 Pa·s.

Alkali oxides are extremely corrosive, hygroscopic and difficult to work with at high temperature. Therefore, no viscosity measurements exist for pure Na_2O, K_2O and Li_2O. Accordingly, the parameters A_{MO_x} and E_{MO_x} representing the viscosity of the pure liquid alkali oxides must be obtained from extrapolation of the experimental viscosity data for the corresponding binary systems M_2O–SiO_2. However, as can be seen from Figs. 4.1 to 4.3, a smooth extrapolation of the viscosity in the alkali-rich regions to pure M_2O results in unreasonably low viscosities of the pure alkali oxides unless the viscosity curve shows a second inflection point. Since molten alkali oxides are ionic liquids, the viscosities of molten salts can provide an insight into the viscosity of M_2O liquids. For example, it can be assumed as a first approximation that the viscosities of NaCl and Na_2O at their boiling points should be similar. The boiling point of NaCl [14] is 1486 °C. Extrapolation of the viscosity of NaCl to this temperature gives $\ln[\eta\ (\text{Pa·s})] = -7.93$ [192]. The viscosity of Na_2O, as optimized in the present study, has the following value at its boiling point (1840°C): $\ln[\eta\ (\text{Pa·s})] = -7.56$. As can be seen from Fig. 4.1, this results in two inflection points on the isothermal viscosity curve in the Na_2O-rich region of the Na_2O–SiO_2 system. Similarly, the optimized viscosity of liquid K_2O has the value $\ln[\eta\ (\text{Pa·s})] = -7.79$ at its boiling point (1573 °C) which is close to $\ln[\eta\ (\text{Pa·s})] = -8.04$ for KCl at its boiling point of 1434 °C. See Fig. 4.2.

The viscosity parameters A^{*}_{Si}, A^{E}_{Si}, E^{*}_{Si} and E^{E}_{Si} for pure SiO_2 are taken from the previous publication [82]. Three parameters for each $MO_{0.5}$–SiO_2 binary system, $E^{1,1}_{\mathrm{MO}_x\text{-Si}}$, $E^{R}_{\mathrm{MO}_x\text{-Si}}$ and $E^{Ring}_{\mathrm{MO}_x\text{-Si}}$, were fitted to the experimental data shown in Figs. 4.1 to 4.3. The parameters $A^{1,1}_{\mathrm{MO}_x\text{-Si}}$, $A^{R}_{\mathrm{MO}_x\text{-Si}}$ and $A^{Ring}_{\mathrm{MO}_x\text{-Si}}$ were not required and were set equal to zero. The optimized model parameters are listed in Table 4.1.

The modified model proposed in the present study and the one reported earlier in Chapter 3 [82] give almost identical descriptions in the high-silica regions. However in the alkali-rich regions, the modified model is in good agreement with the majority of experimental data whereas the previous model as shown in Chapter 3 is in agreement only with the results of Kou et al. [143] which do not show the drop in the viscosity. As can be seen from Fig. 4.1-(b), the scatter of experimental data can be as high as 1.0 in the ln scale and the modified model describes the measurements within experimental error limits.

As can be seen from Fig. 4.2, the modified model describes very well all experimental data for $KO_{0.5}$–SiO_2 melts except for two points by Bockris et al. [23] at high temperature and close to pure SiO_2. It should be noted that the viscosity of pure SiO_2 reported in the same paper [23] is substantially lower than that reported by other authors as shown in Fig. 6 of the first paper [82]. The reason for this disagreement is not clear. One possible cause may be a reaction of the melt with the molybdenum crucible and cylinder at high temperature since Bockris et al. [23] reported that molybdenum reacted violently with silica at 1900 °C. Difficulties of removing bubbles originating from the decomposition of K_2CO_3 and the high volatility of potassium at high temperature may have also contributed to the experimental error.

An alternative viscosity model which uses the thermodynamic database of FactSage [15] was developed by Jak [107]. It is based on the Eyring equation for the viscosity with cation pair fractions calculated by FactSage employed as concentration variables. This model requires 7 binary parameters for each of the binary systems $NaO_{0.5}$–SiO_2 and $KO_{0.5}$–SiO_2. As can be seen from Figs. 4.1 and 4.2, the model developed in the present study provides a much better fit of the experimental data even though it requires only 3 binary parameters for each of these systems.

An accurate description of the viscosities of glass melts was proposed by Fluegel [67]. This model is based on multiple regression using polynomial functions. It is most accurate in the

vicinity of the commercial glass compositions since it is calibrated based on numerous experimental data for these regions. The viscosity of $KO_{0.5}$–SiO_2 melts calculated using the Fluegel's model is shown in Fig. 4.2-(b) over the concentration range which is within the validity limits of the model. Outside these limits the model is not applicable and it diverges rapidly from the experimental data. The comparison with Fluegel's model estimates for multicomponent glass melts will be discussed below in Section 4.3.6. For the $KO_{0.5}$–SiO_2 system, the present model is more accurate with the Fluegel's model being lower than the experimental data at low temperatures and higher at high temperatures.

Although a thermodynamic description of the $LiO_{0.5}$–SiO_2 system is not available in the FactSage thermodynamic database, the cation pair fractions for $LiO_{0.5}$–SiO_2 and $NaO_{0.5}$–SiO_2 melts at the same composition should be fairly close. This assumption was used to model the viscosity of $LiO_{0.5}$–SiO_2 melts. As can be seen from Fig. 4.3, the drop in the viscosity in the alkali-rich region becomes more pronounced in the sequence Li < Na < K.

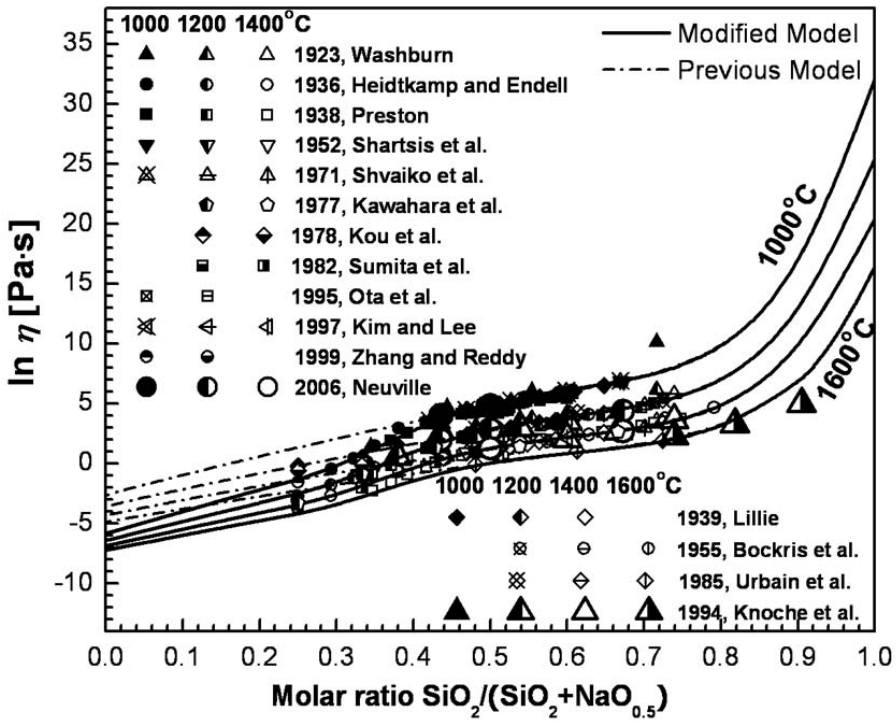

(a)

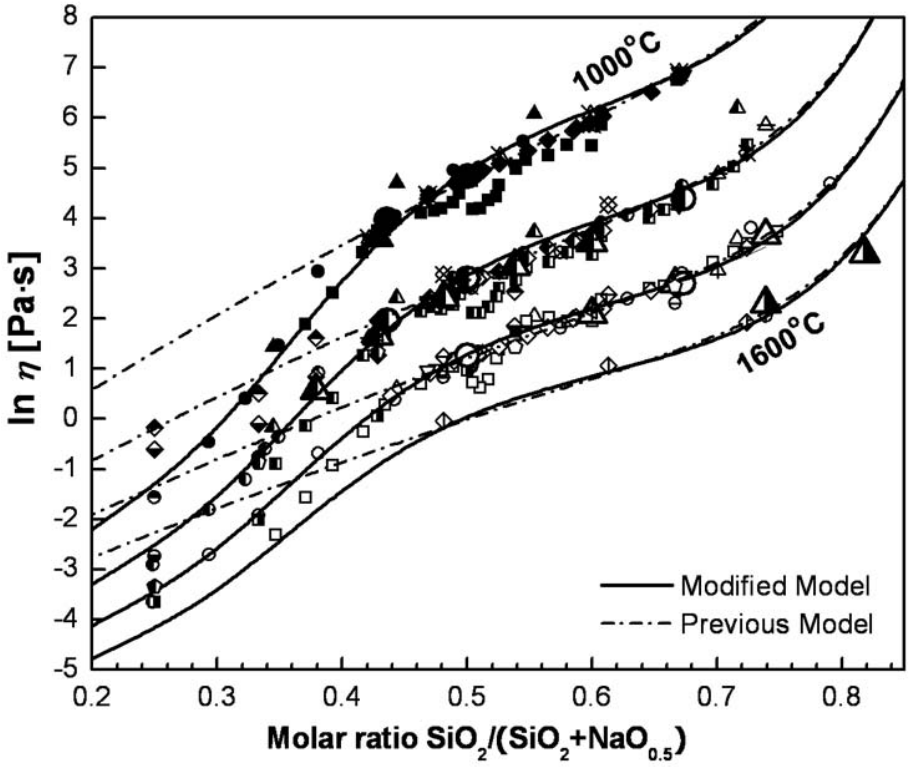
ln η [Pa·s]
Molar ratio SiO2/(SiO2+NaO0.5)
1000°C
1600°C
Modified Model
Previous Model

(b)

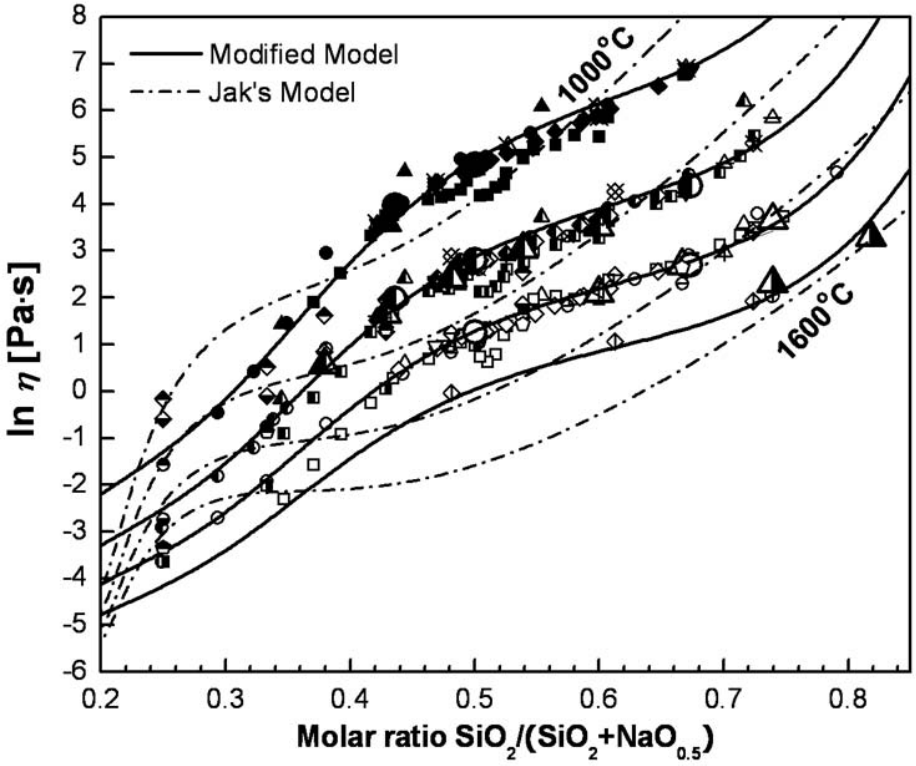

(c)

Fig. 4.1 Viscosity of $NaO_{0.5}$–SiO_2 melts. Points are experimental [23, 143, 223, 313, 333]. Figures (a) and (b) compare the modified viscosity model proposed in the present study (solid lines) with the model reported earlier [82] (dash-dot lines). Figure (c) compares the viscosity model proposed in the present study (solid lines) with the model by Jak [107] (dash-dot lines)

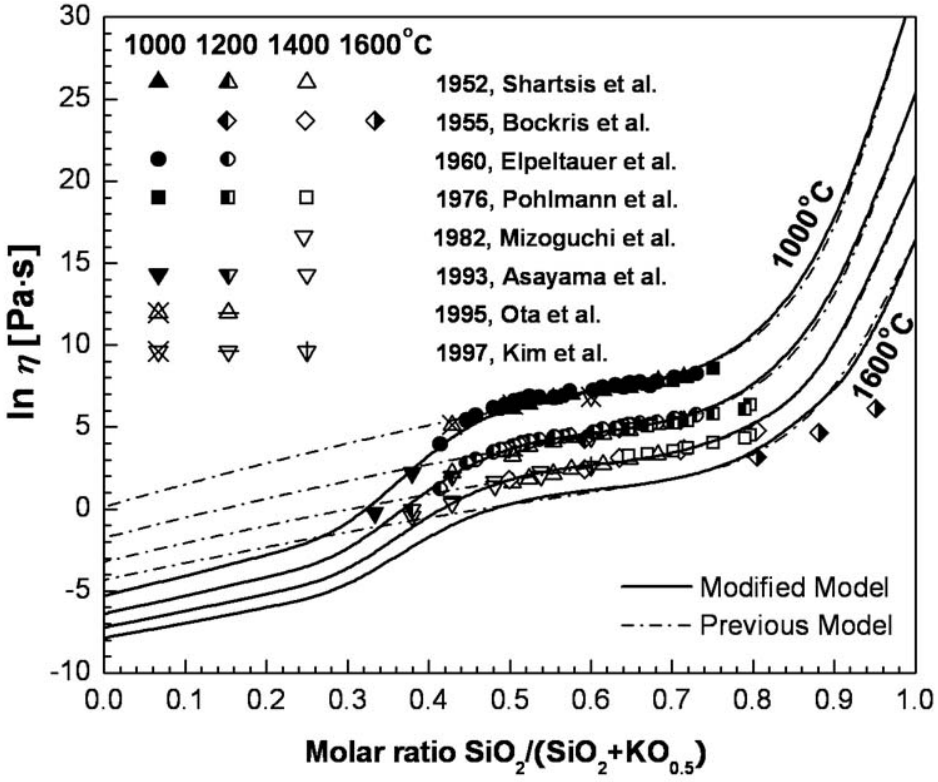
1000 1200 1400 1600°C
1952, Shartsis et al.
1955, Bockris et al.
1960, Elpeltauer et al.
1976, Pohlmann et al.
1982, Mizoguchi et al.
1993, Asayama et al.
1995, Ota et al.
1997, Kim et al.
1000°C
1600°C
Modified Model
Previous Model
ln η [Pa·s]
Molar ratio SiO2/(SiO2+KO0.5)

(a)

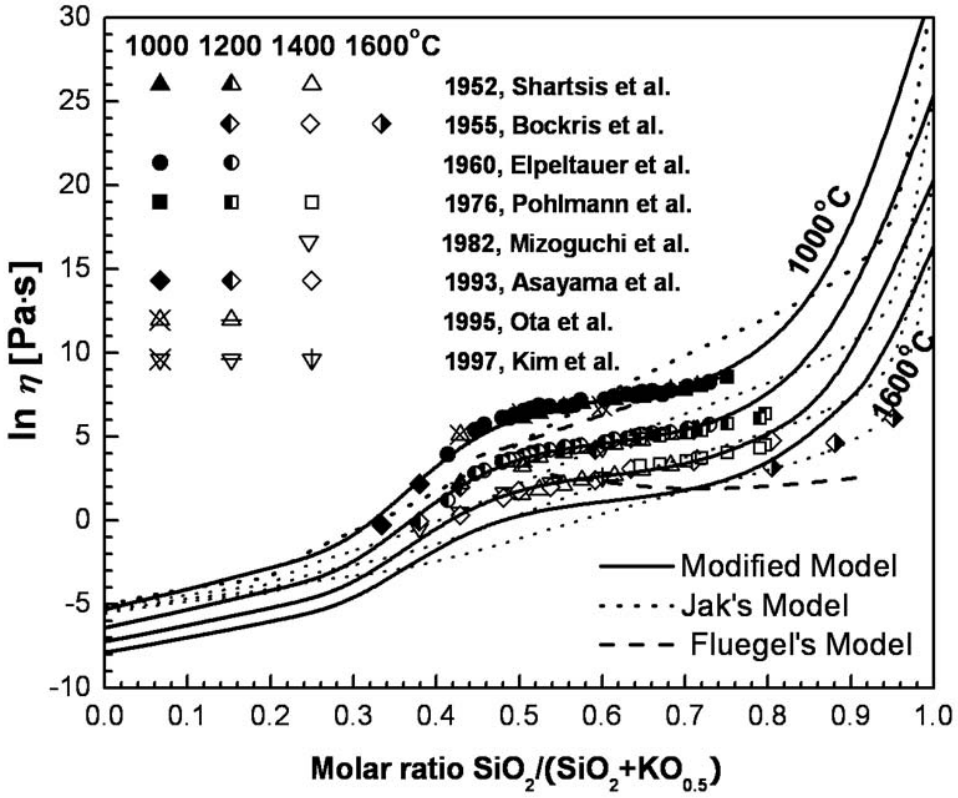

(b)

Fig. 4.2 Viscosity of $KO_{0.5}$–SiO_2 melts. Points are experimental [11, 23, 53, 125, 193, 223, 237, 283]. Figure (a) compares the modified viscosity model proposed in the present study (solid lines) with the model reported earlier [82] (dash-dot lines). Figure (b) compares the viscosity model proposed in the present study (solid lines) with the model by Jak [107] (dotted lines) and the model for glass melts by Fluegel [67] (dashed lines corresponding to 1000 ^{o}C and 1600 ^{o}C)

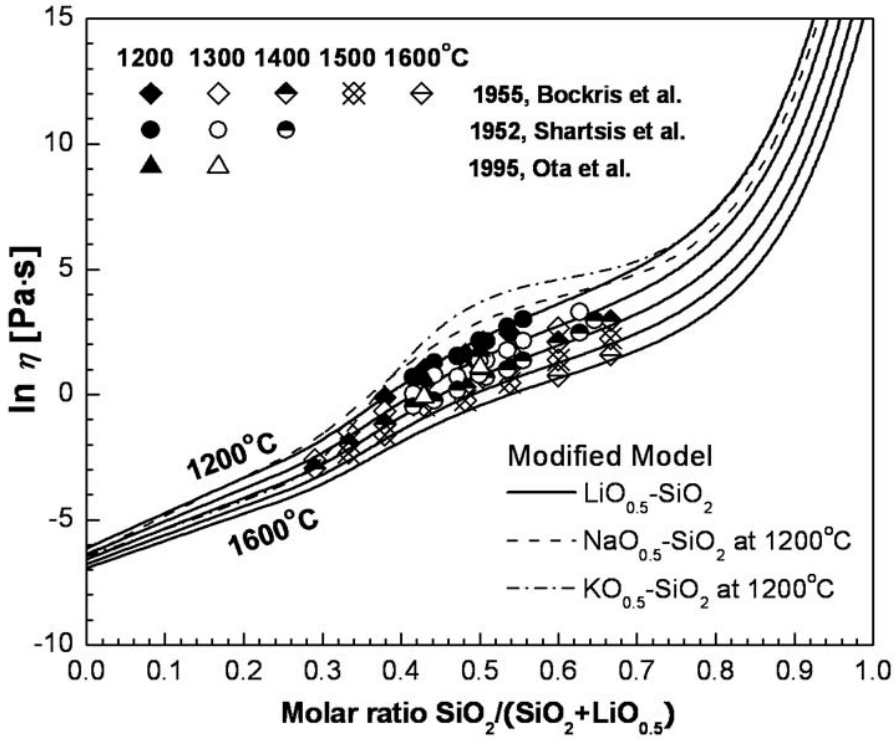

Fig. 4.3 Viscosity of $LiO_{0.5}$–SiO_2 melts: experimental points [23, 223, 283] and calculated lines. The calculated viscosities for $NaO_{0.5}$–SiO_2 and $KO_{0.5}$–SiO_2 melts at 1200 ^{o}C are also shown for comparison

4.3.2 Ternary systems without alumina(Al_2O_3)

The viscosities of ternary melts without alumina are predicted by the model using only the model parameters describing the viscosity of pure oxides and the binary parameters for MO_x–SiO_2 melts. No additional ternary parameters are used. Hence, the agreement of experimental data points and calculated lines shown in the figures in this section is not the result of fitting, but rather an indication of how well the model can predict the viscosity of ternary melts.

As can be seen from Figs. 4.4 and 4.5, the model describes ternary CaO–Na_2O–SiO_2 melts within the experimental scatter. Since the data are limited to the region which is not rich in Na_2O, the model reported earlier [82] reproduces the data equally well. The effect of the modification of

the model proposed in the present study is more visible for $MgO–Na_2O–SiO_2$ melts shown in Figs. 4.6 to 4.8. Clearly, the modified model is in excellent agreement with the experimental data [119], while the earlier model gives systematically higher viscosities in the Na_2O-rich region.

Figs 4.7 and 4.8 show only the experimental points of Kawahara et al. [119] who used the rotating crucible method with Pt-Rh crucibles. Their data for the $Na_2O–SiO_2$ system are in good agreement with the other measurements as can be seen from Fig. 4.1. An early experimental study of $MgO–Na_2O–SiO_2$ melts was reported by English [59]. Most likely it is subject to a large systematic error because his results are not consistent with the majority of the data on the $Na_2O–SiO_2$ system.

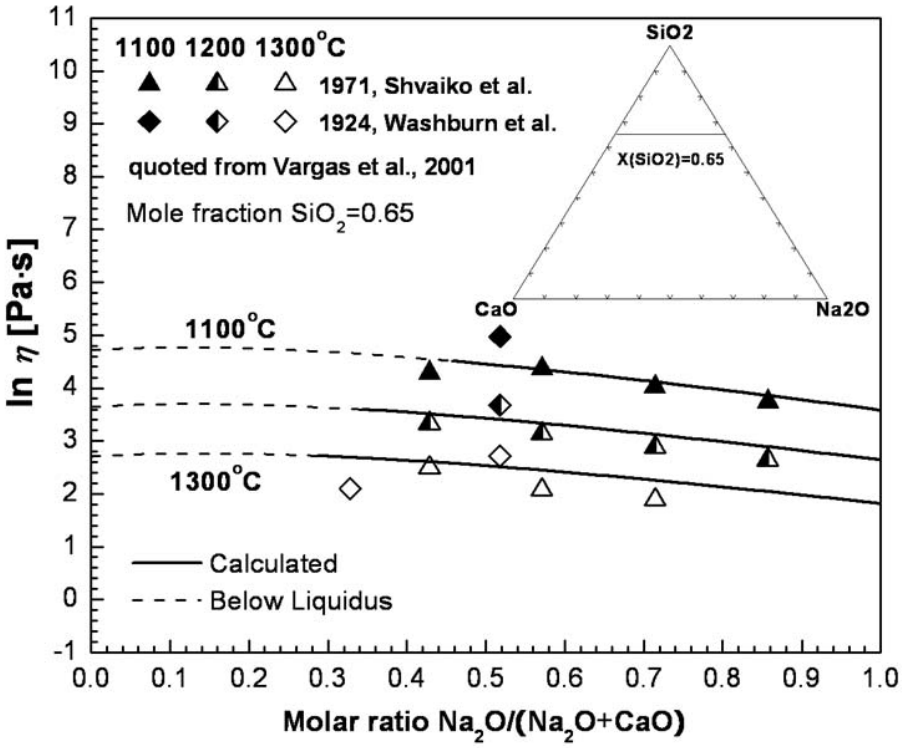

Fig. 4.4 Viscosity of $CaO–Na_2O–SiO_2$ melts at 65 mol% SiO_2: experimental points [294, 349] and calculated lines

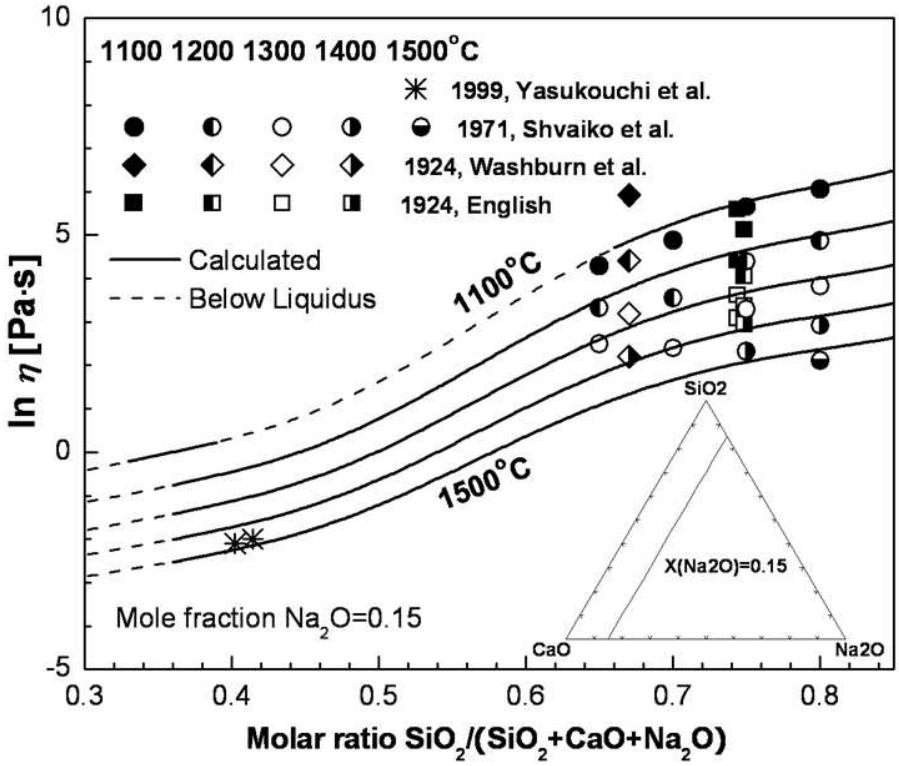

Fig. 4.5 Viscosity of $CaO–Na_2O–SiO_2$ melts at 15 mol% Na_2O: experimental points [59, 294, 349, 357] and calculated lines

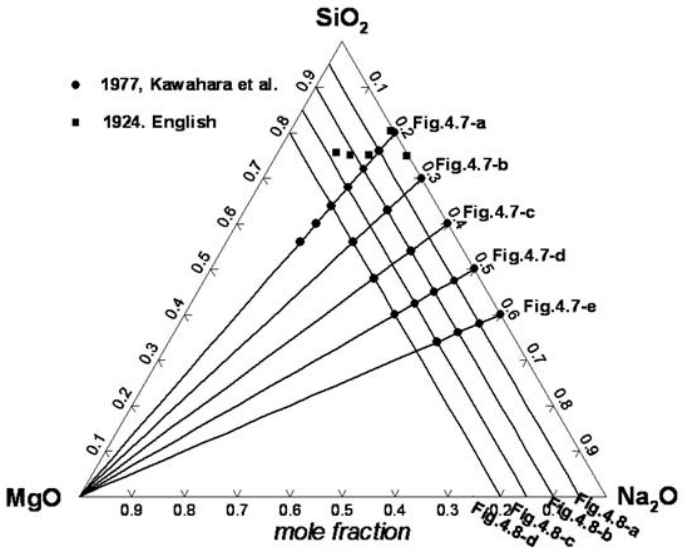

Fig. 4.6 Compositions in the $MgO–Na_2O–SiO_2$ system at which the viscosity was measured [59, 119]. Solid lines show the pseudo-binary sections reported in Figs. 4.7 and 4.8

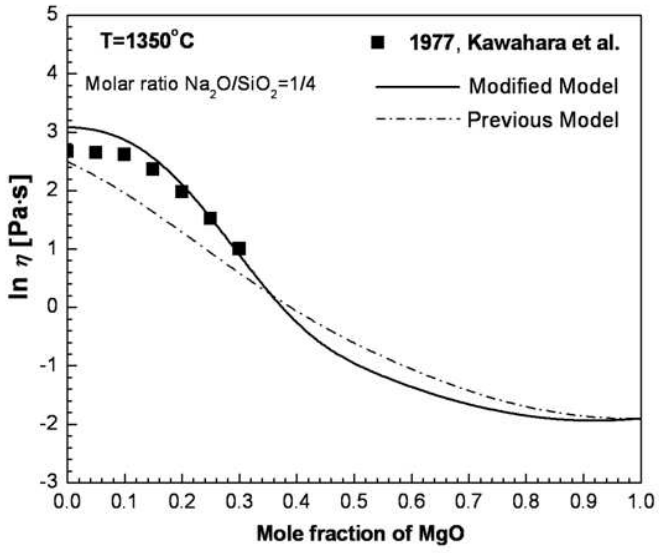

(a)

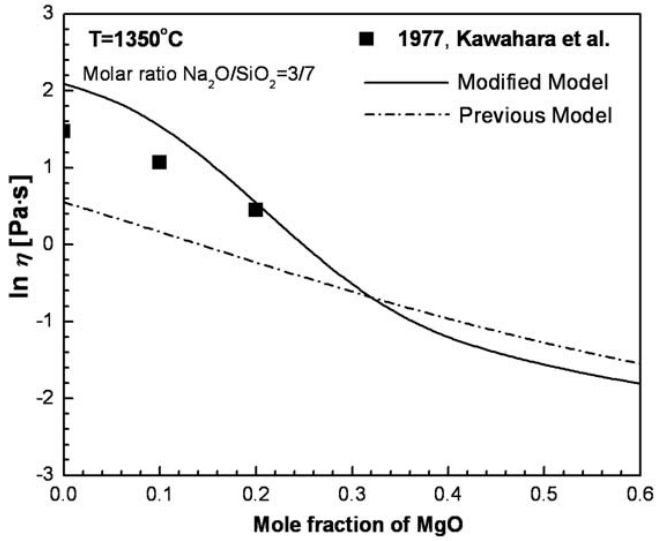
T=1350°C
Molar ratio Na2O/SiO2=3/7
1977, Kawahara et al.
Modified Model
Previous Model
ln η [Pa·s]
Mole fraction of MgO

(b)

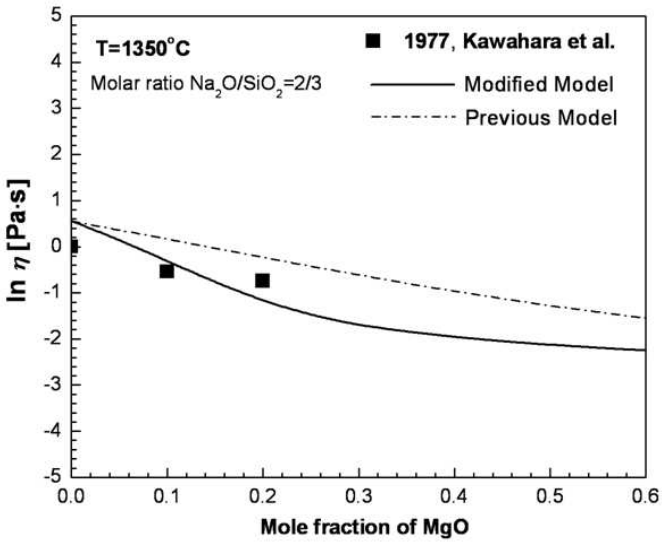
T=1350°C
Molar ratio Na2O/SiO2=2/3
1977, Kawahara et al.
Modified Model
Previous Model
ln η [Pa·s]
Mole fraction of MgO

(c)

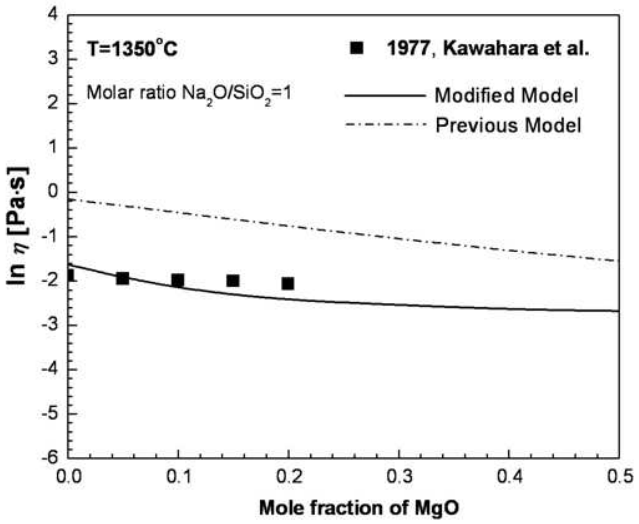

(d)

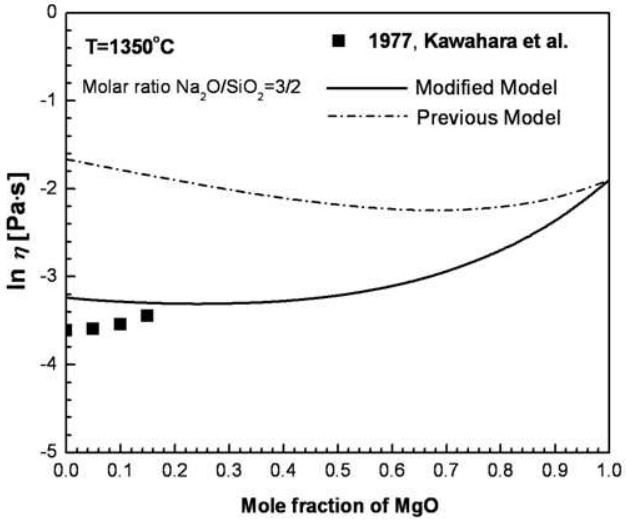

(e)

Fig. 4.7 Viscosity of $MgO–Na_2O–SiO_2$ melts. Experimental points [119] and calculated lines at different molar ratios of Na_2O to SiO_2. Solid lines are calculated using the modified viscosity model proposed in the present study and dash-dot lines correspond to the model reported earlier [81]

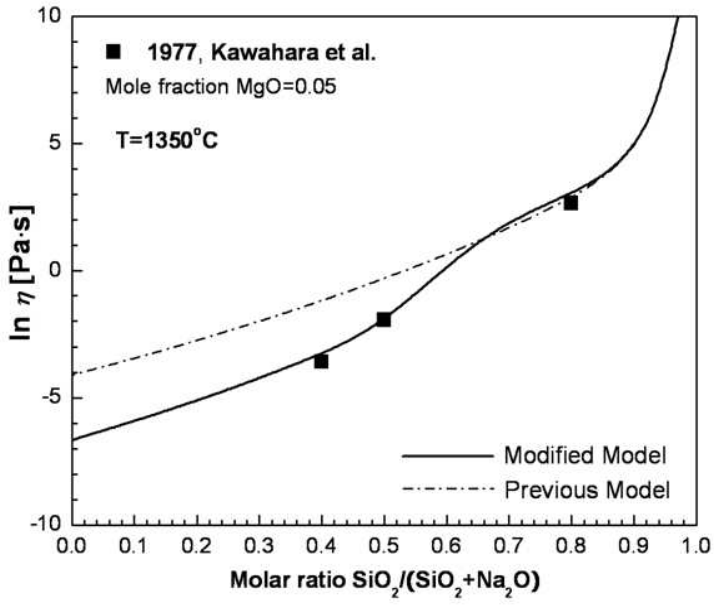
1977, Kawahara et al.
Mole fraction MgO=0.05
T=1350°C
Modified Model
Previous Model
ln η [Pa·s]
Molar ratio SiO2/(SiO2+Na2O)

(a)

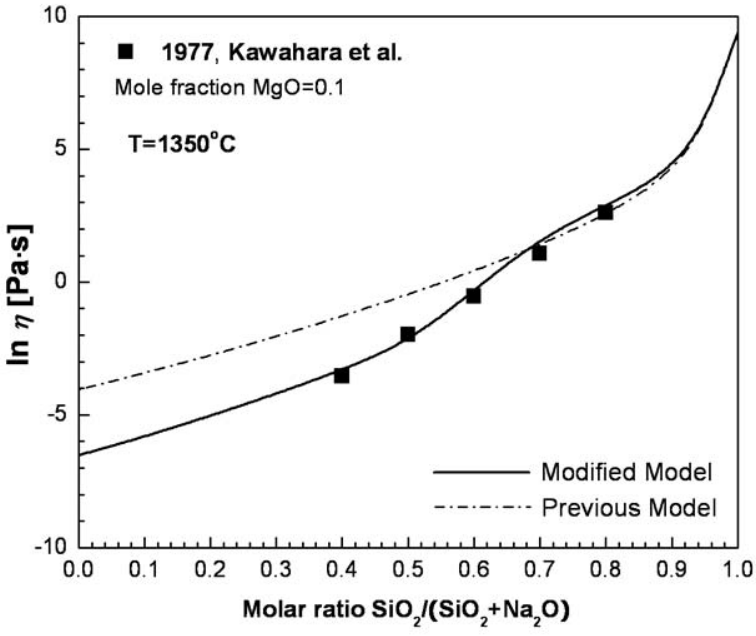
1977, Kawahara et al.
Mole fraction MgO=0.1
T=1350°C
Modified Model
Previous Model
ln η [Pa·s]
Molar ratio SiO2/(SiO2+Na2O)

(b)

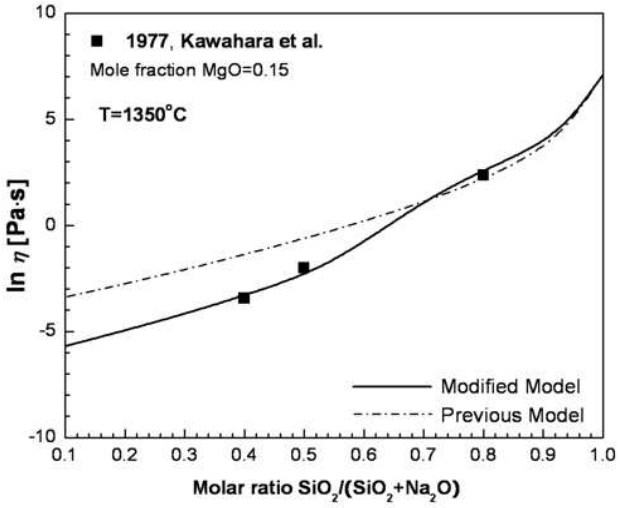

(c)

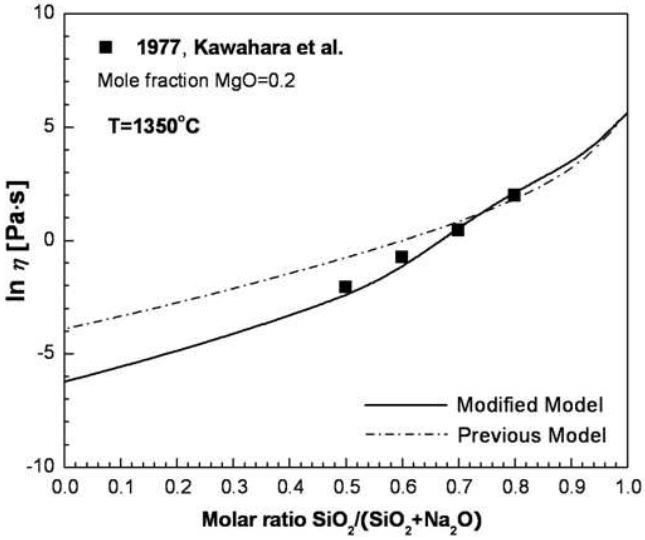

(d)

Fig. 4.8 Viscosity of $MgO–Na_2O–SiO_2$ melts. Experimental points [119] and calculated lines at (a) 5, (b) 10, (c) 15 and (d) 20 mol% MgO. Solid lines are calculated using the modified viscosity model proposed in the present study and dash-dot lines correspond to the model reported earlier [81]

Experimental information for ternary melts containing K_2O is limited. The available data are compared with predictions of the model in Figs. 4.9 and 4.10. Yasukouchi et al. [357] measured the viscosities of K_2O–CaO–SiO_2 melts at constant molar ratio $CaO/SiO_2 = 1.071$ using a rotating crucible viscometer with Pt-Rh crucibles. Although the difference between these data and the viscosity predicted by the model seems to be systematic, the maximum absolute deviation is not large and is comparable with average experimental errors of viscosity measurements. Unfortunately, the measurements were not made for higher K_2O concentrations; this would have permitted a more thorough comparison with the new model. The viscosity of K_2O–CaO–SiO_2 melts was also reported by Shilo et al. [288] who used an electro-viscometer. However their data for CaO-SiO_2 and Al_2O_3-CaO-SiO_2 melts are substantially higher than the data of other authors. Therefore these results were not considered in the present study.

Kim and Lee [125] measured the viscosities of K_2O–Na_2O–SiO_2 melts at 75 mol % SiO_2 in the temperature range from 1000 ° to 1400 °C using the rotating cylinder method with Pt-30% Rh crucibles. The calculated viscosities are compared with these data in Fig. 4.10. Obviously, the agreement is good, although the model predicts an almost linear interpolation between the K_2O–SiO_2 and Na_2O–SiO_2 binaries whereas the experimental data suggest a slight curvature which becomes more pronounced at lower temperatures. It should be noted that this effect can be very well reproduced by the model by incorporation of an additional binary term $X_{NaO_{0.5}} X_{KO_{0.5}} E_{NaO_{0.5}\text{-}KO_{0.5}}$. However, this was not deemed to be justified considering the average accuracy of the viscosity measurements.

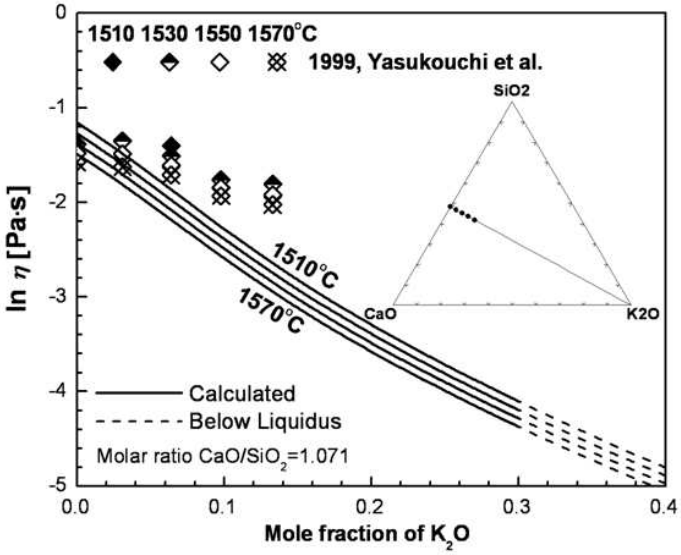

Fig. 4.9 Viscosity of K_2O–CaO–SiO_2 melts at a molar ratio of CaO/SiO_2 = 1.071: experimental points [357] and calculated lines

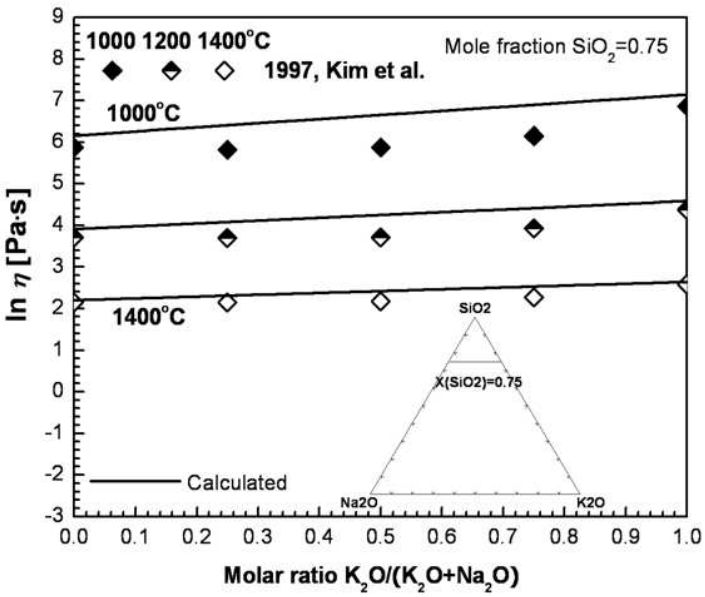

Fig. 4.10 Viscosity of K_2O–Na_2O–SiO_2 melts at 75 mol% SiO_2: experimental points [125] and calculated lines

4.3.3 Ternary systems with alumina(Al_2O_3)

As discussed earlier in the section 3.4.5, Al cations can assume tetrahedral coordination and replace Si in the liquid network when the missing charge is compensated by a basic cation M. This results in a maximum in the viscosity when the molar ratio of Al_2O_3 to MO or M_2O is unity. This effect is modeled by two parameters for each ternary system MO_x–Al_2O_3–SiO_2 which describe the Gibbs energy of reaction (3.40) or (3.41) as a function of composition. These model parameters for the Al_2O_3–CaO–MgO–Na_2O–K_2O–SiO_2 system are summarized in Table 4.2. Only parameters for $\Delta G_{\mathrm{KAlO_2}}$ were optimized in the present study. The other values in Table 4.2 were taken from the previous publication [81] and used with the modified viscosity model proposed here. This resulted in a good description of the experimental data for Na_2O–Al_2O_3–SiO_2 melts as shown by Figs. 4.11 and 4.12. Not only the magnitude, but also the shape of the viscosity maxima is well reproduced.

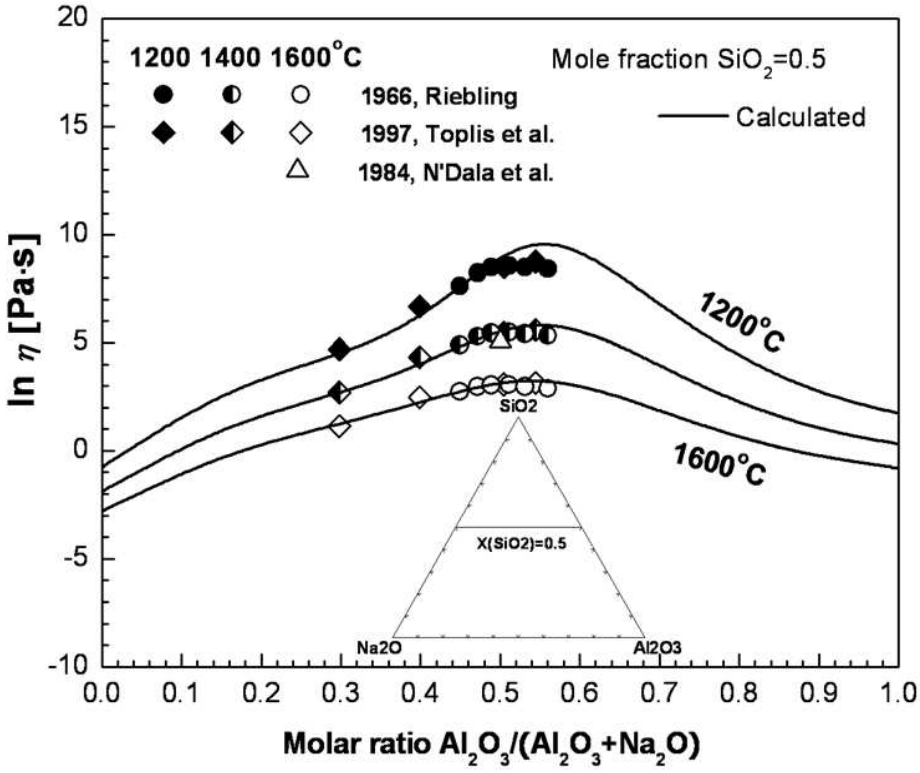

Fig. 4.11 Viscosity of Na_2O–Al_2O_3–SiO_2 melts at 50 mol% SiO_2: experimental points [200, 252, 324] and calculated lines

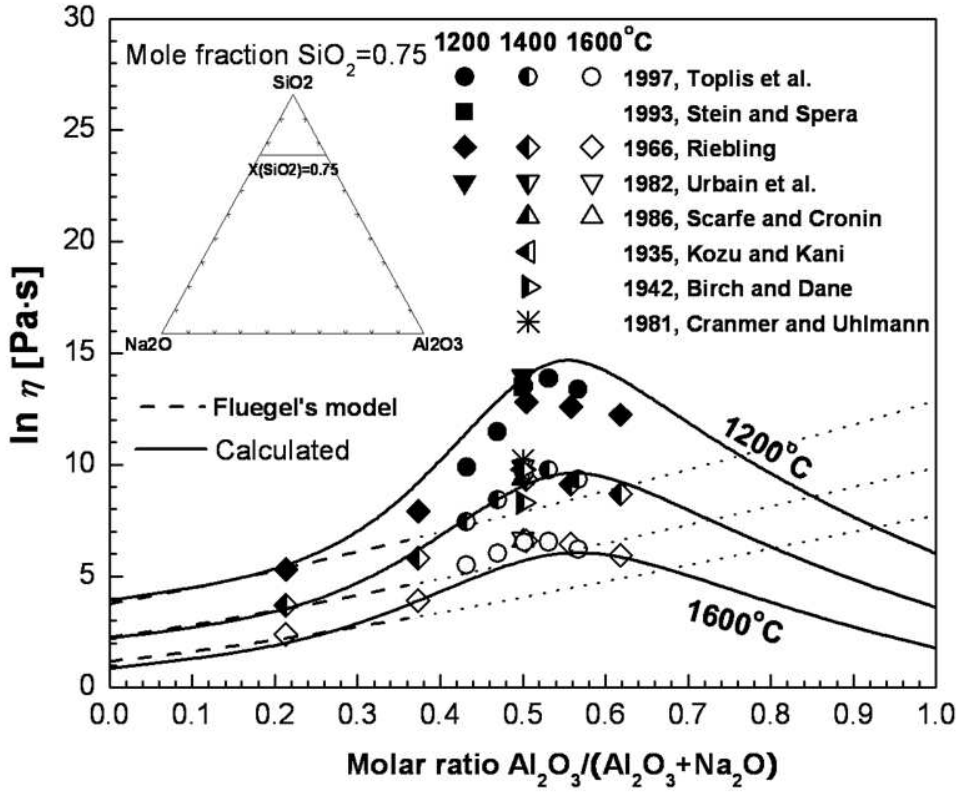

Fig. 4.12 Viscosity of Na_2O–Al_2O_3–SiO_2 melts at 75 mol% SiO_2: experimental points [20, 36, 146, 252, 269, 307, 324, 335] and calculated lines. Viscosities calculated using Fluegel's model for glass melts [67] are shown by dashed lines within the validity limits of the model and by the dotted lines outside these limits

As can be seen from Fig. 4.12, the regression equation for glass melts reported by Fluegel [67] does not reproduce the viscosity maximum: the calculated lines start to deviate from the experimental points at the onset of the maximum, leaving most of it outside the validity range of the model.

The viscosity of K_2O–Al_2O_3–SiO_2 melts was studied by Urbain et al. [335], N'Dala et al. [200], Kim and Lee [125] and Mizoguchi et al. [193] using rotating crucible or rotating cylinder viscometers with Pt [193], Pt/Rh [125, 335], or molybdenum [200] crucibles. The phase diagram of the K_2O–Al_2O_3–SiO_2 system was reported by several authors [24, 147, 271, 325]. Based on these studies, only viscosity measurements above the liquidus were used for optimization of two model parameters corresponding to ΔG_{KAlO_2} in Table 4. 2.

The experimental data points are compared with the calculated lines in Figs. 4.13 to 4.20. The agreement is believed to be within experimental error limits. The points of N'Dala et al. [200] in Fig. 4.15 lie slightly higher than the calculated lines, although some crystallization may have occurred in the experiments because the liquidus temperature at this composition should be above 1800 °C [24, 147, 271, 325]. It should be noted that the point of N'Dala et al. [200] in Fig. 4.11 for a similar composition in the Na_2O–Al_2O_3–SiO_2 system is also higher than the results of other authors. Similarly, the data points of Kim and Lee [125] in Figs. 4.18-(b) and (c) are probably below the liquidus at 1000 °C and 1200 °C.

Fig. 4.17 shows that the data of Urbain et al. [335] and N'Dala et al. [200] are in good agreement for the orthoclase composition, $KAlSi_3O_8$. The temperature dependence of these data is well reproduced by the present model, even though the model does not contain any temperature-dependent parameters. Birch and Dane [20] also measured the viscosity at the orthoclase composition, but their data are higher than the results of the other authors by about 3.0 in the natural logarithm scale.

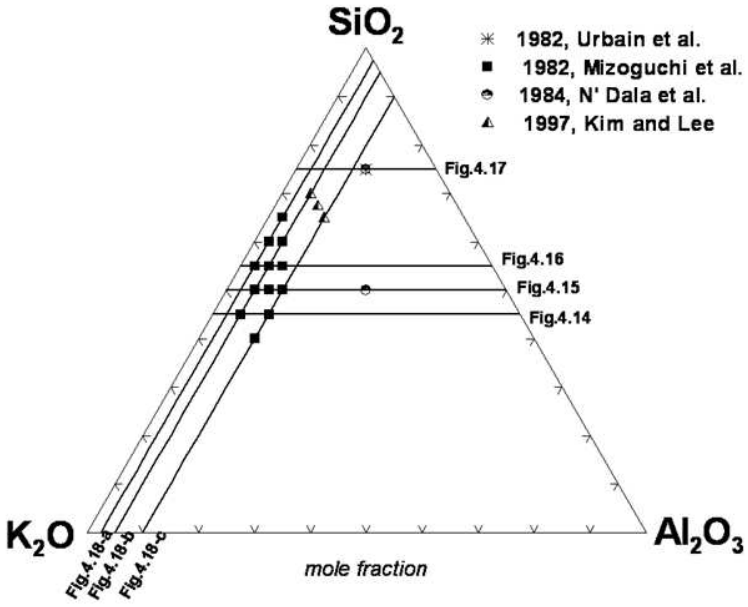

Fig. 4.13 Compositions in the K_2O–Al_2O_3–SiO_2 system at which the viscosity was measured [125, 193, 200, 335]. Lines show the sections of this ternary system reported in Figs. 4.14 to 4.18

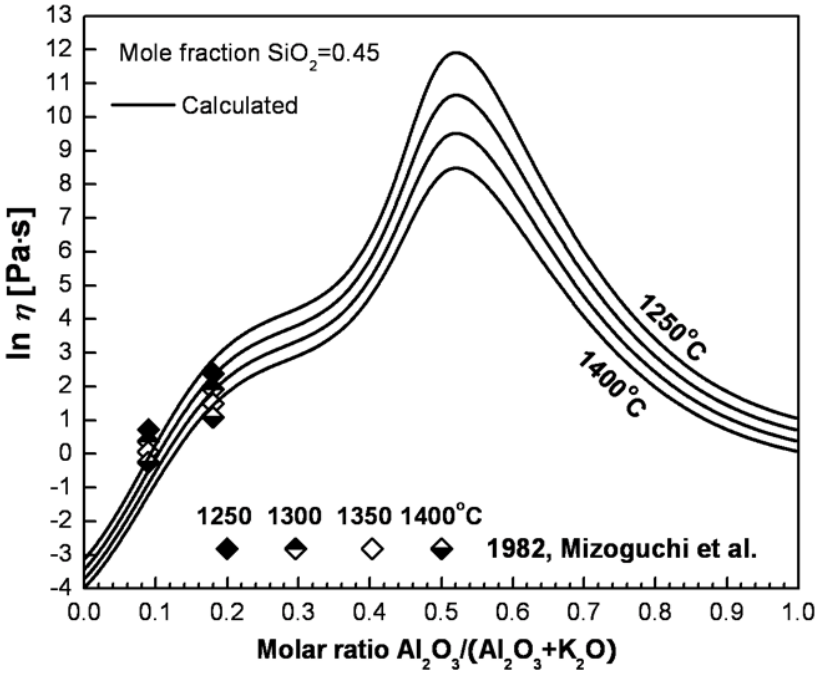

Fig. 4.14 Viscosity of K_2O–Al_2O_3–SiO_2 melts at 45 mol% SiO_2: experimental points [193] and calculated lines

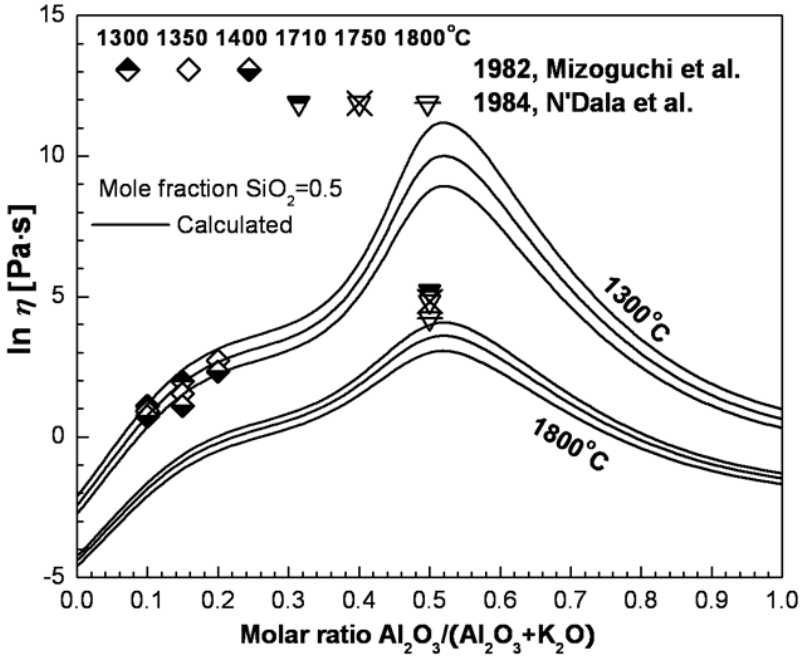

Fig. 4.15 Viscosity of K_2O–Al_2O_3–SiO_2 melts at 50 mol% SiO_2: experimental points [193, 200] and calculated lines

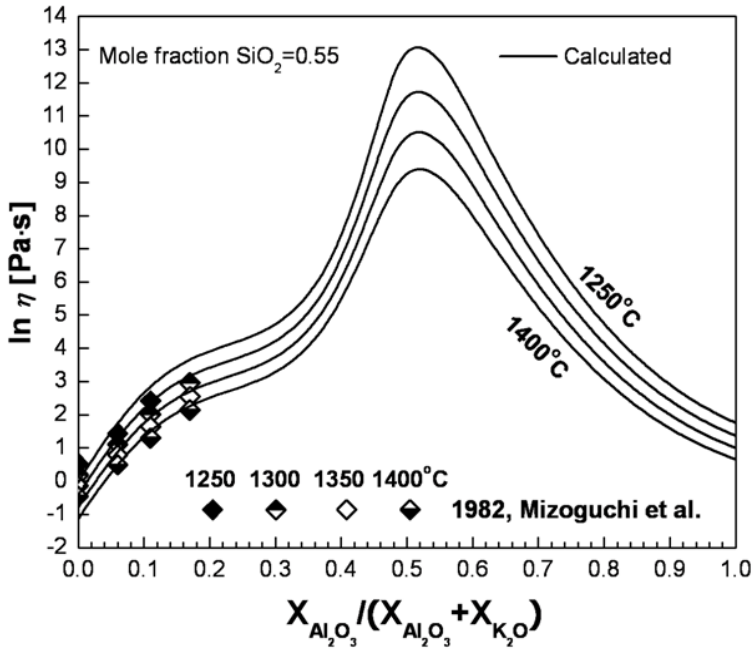

Fig. 4.16 Viscosity of K_2O–Al_2O_3–SiO_2 melts at 55 mol% SiO_2: experimental points [193] and calculated lines

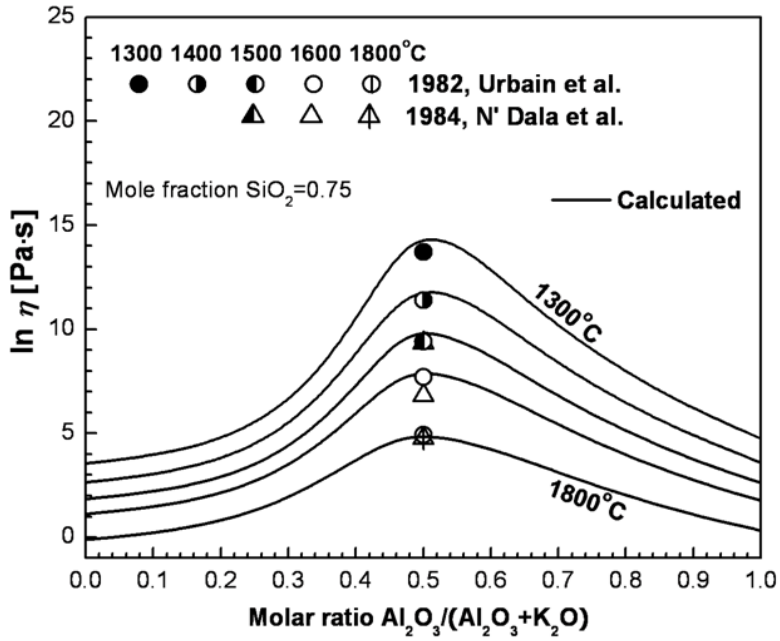

Fig. 4.17 Viscosity of K_2O–Al_2O_3–SiO_2 melts at 75 mol% SiO_2: experimental points [200, 335] and calculated lines

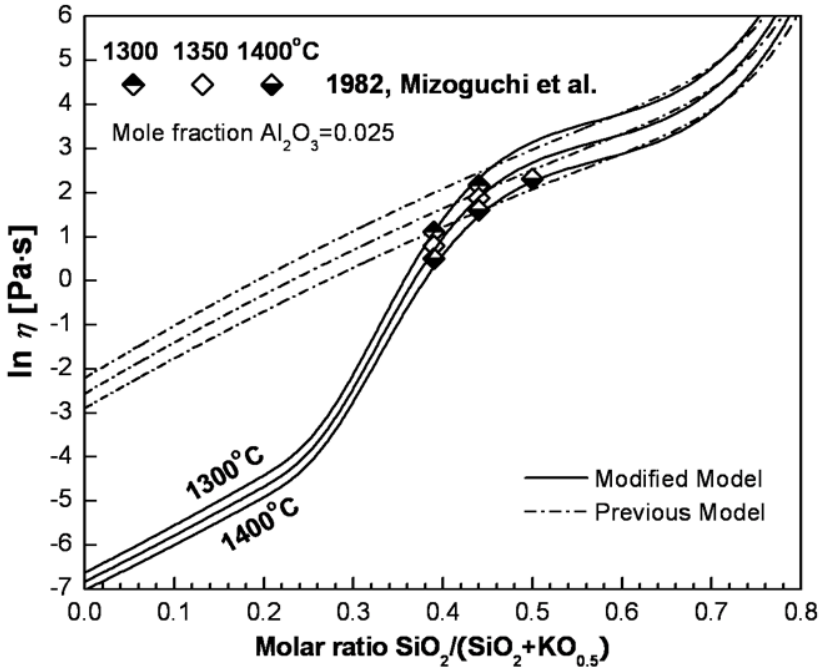
1300 1350 1400°C
1982, Mizoguchi et al.
Mole fraction Al2O3=0.025
ln η [Pa·s]
1300°C
1400°C
Modified Model
Previous Model
Molar ratio SiO2/(SiO2+KO0.5)

(a)

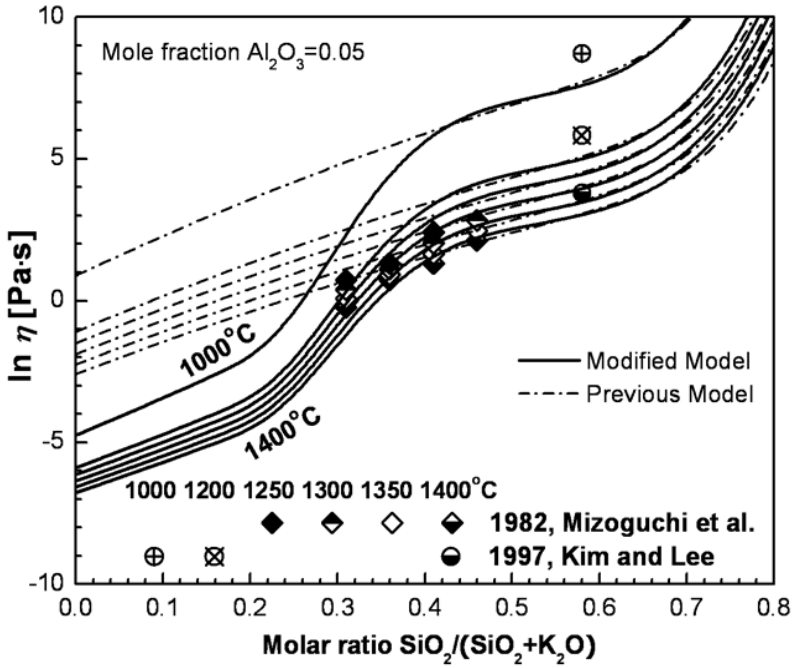
Mole fraction Al2O3=0.05
ln η [Pa·s]
1000°C
1400°C
Modified Model
Previous Model
1000 1200 1250 1300 1350 1400°C
1982, Mizoguchi et al.
1997, Kim and Lee
Molar ratio SiO2/(SiO2+K2O)

(b)

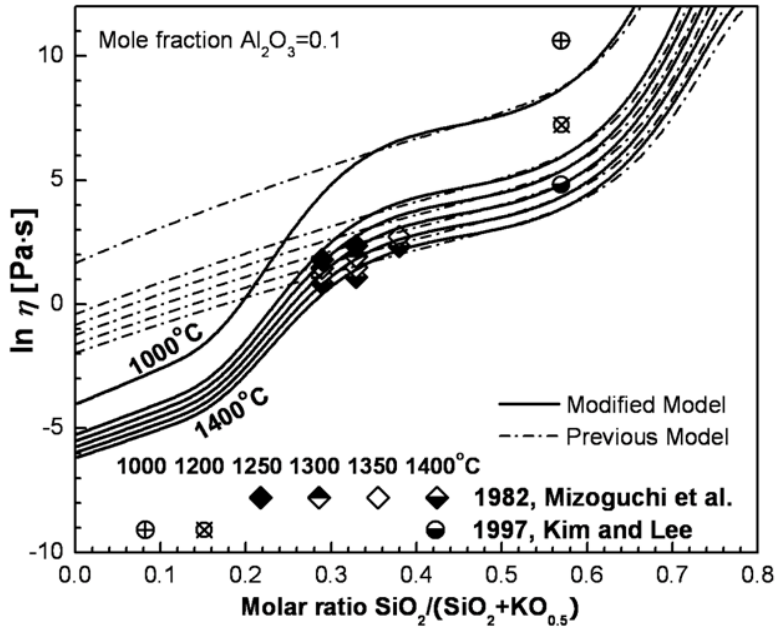

(c)

Fig. 4.18 Viscosity of K_2O–Al_2O_3–SiO_2 melts: experimental points [125, 193] and calculated lines using the modified viscosity model proposed in the present study (solid lines) and using the model reported previously [81] (dash-dot lines). (a) 2.5 mol% Al_2O_3, (b) 5 mol% Al_2O_3 and (c) 10 mol% Al_2O_3

4.3.4 Multicomponent systems

The viscosity of multicomponent systems is predicted by the model from the unary, binary and ternary parameters given in Tables 4.1 and 4.2 with no additional parameters.

The viscosities along pseudo-binary sections through several quaternary systems are shown in Figs. 4.19 to 4.21. As can be seen from the figures, the predicted viscosities of Na_2O–CaO–Al_2O_3–SiO_2, K_2O–CaO–Al_2O_3–SiO_2 and K_2O–Na_2O–Al_2O_3–SiO_2 melts are in good agreement with the experimental data.

The experimental measurements of Sukenaga et al. [311] shown in Fig. 4.20 indicate that the viscosity decreases with Na_2O additions to the CaO–Al_2O_3–SiO_2 melts, but initially increases with additions of K_2O. The model predicts this general trend although the predicted increase with K_2O is somewhat less than the experimental. However, the deviations are small and within the

scatter limits of the data from the various researchers. The explanation for the different trends in the viscosity with Na_2O and K_2O additions is related to the Charge Compensation Effect which is more pronounced with K_2O than with Na_2O as can be seen from the higher and sharper maxima for the viscosity in Figs. 4.14-4.17 as compared to Figs. 4.11-4.12.

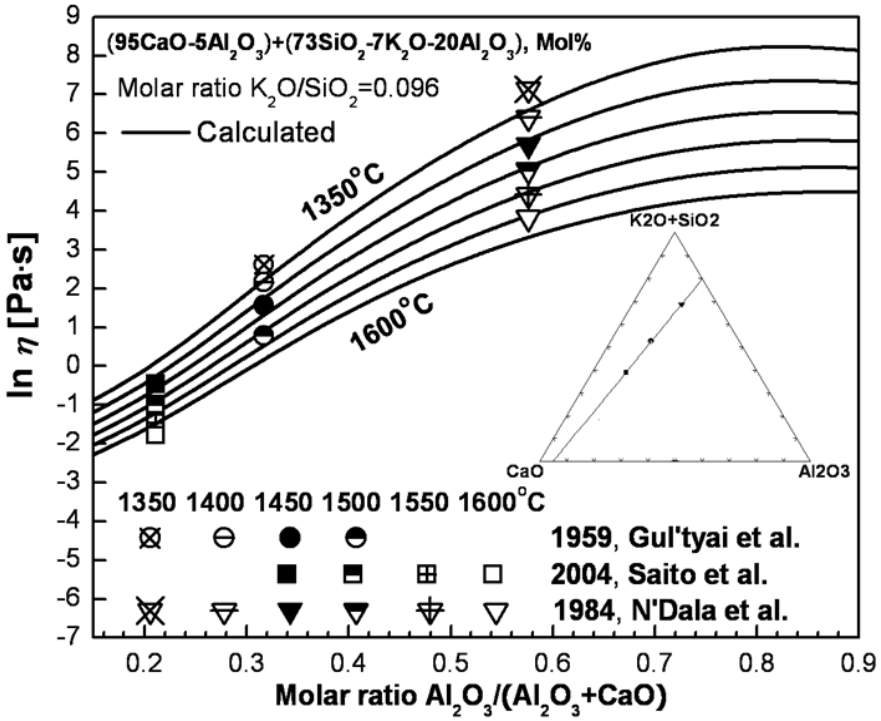

Fig. 4.19 Viscosity of K_2O–CaO–Al_2O_3–SiO_2 melts for a section between (95 mol% CaO, 5 mol% Al_2O_3) and (73 mol% SiO_2, 7 mol% K_2O , 20 mol% Al_2O_3): experimental points [84, 200, 259] and calculated lines

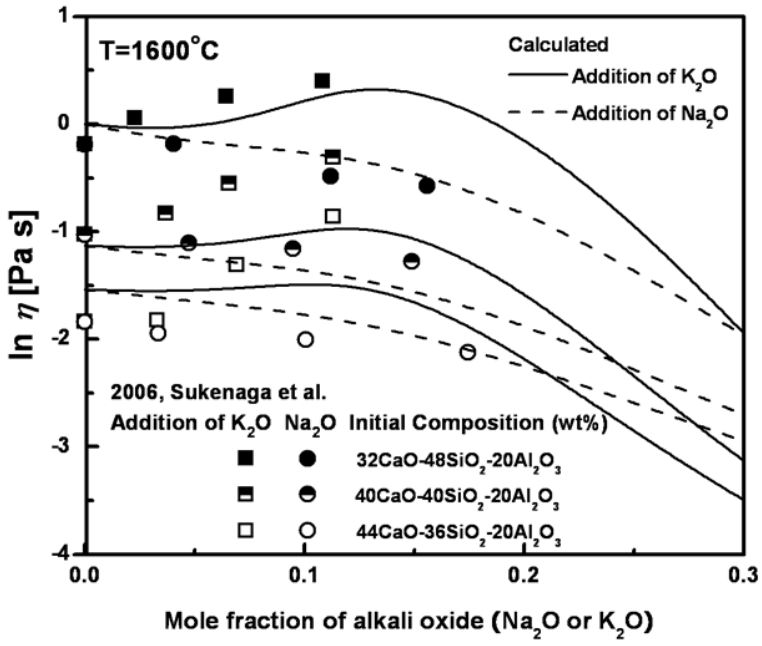

Fig. 4.20 Changes in the viscosity of $CaO–Al_2O_3–SiO_2$ melts resulting from additions of Na_2O or K_2O: experimental points [311] and calculated lines

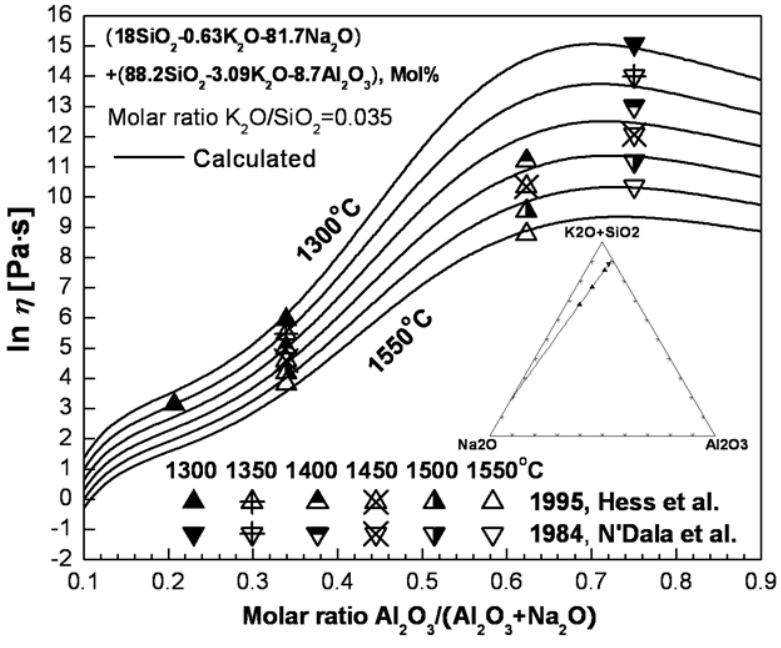

Fig. 4.21 Viscosity of $K_2O–Na_2O–Al_2O_3–SiO_2$ melts for a section between (18 mol% SiO_2, 0.63 mol% K_2O, 81.7 mol% Na_2O) and (88.2 mol% SiO_2, 3.09 mol% K_2O, 8.7 mol% Al_2O_3): experimental points [91, 200] and calculated lines

4.3.5 Magmas and lavas

The Al_2O_3–CaO–MgO–Na_2O–K_2O–SiO_2 system contains subsystems of importance for petrology. In particular, a knowledge of the viscosity of silicate melts formed by albite–orthoclase–anorthite feldspars, diopside and nepheline is important to the understanding of the generation, transport and emplacement of igneous rocks. The viscosity of these melts was studied by Kozu and Kani [146], Birch and Dane [20], N'Dala et al. [200], Scarfe et al. [269, 270] and Sykes et al. [314].

The viscosities along the albite–anorthite, albite–orthoclase and anorthite–diopside sections predicted by the model are compared with the experimental data in Figs. 4.22 to 4.24. The section albite-diopside was reported earlier [81]. The calculated lines in Fig. 4.22 are in good agreement with the experimental points. Even though Kozu and Kani [146] reported somewhat higher viscosities of pure albite, this is within the experimental error limits as can be seen from the measurements by different authors in Fig. 4.12.

For the albite–orthoclase section shown in Fig. 4.23, the model predicts a smooth variation of the viscosity when Na_2O is replaced by K_2O whereas the measurements [200] appear to indicate an abrupt change of the slope in the middle of the plot. Since there is no obvious physical reason for such behaviour, it is most likely an artifact caused by the scatter of the experimental data which is slightly more than 1.0 in the natural logarithm scale in this case. This section was also measured by Birch and Dane [20], but their points are widely scattered and are higher by 3.0 in the natural logarithm scale than the results of N'Dala et al. [200] and Urbain et al. [335] for pure $KAlSi_3O_8$. Therefore, these points are not shown in Fig. 4.23.

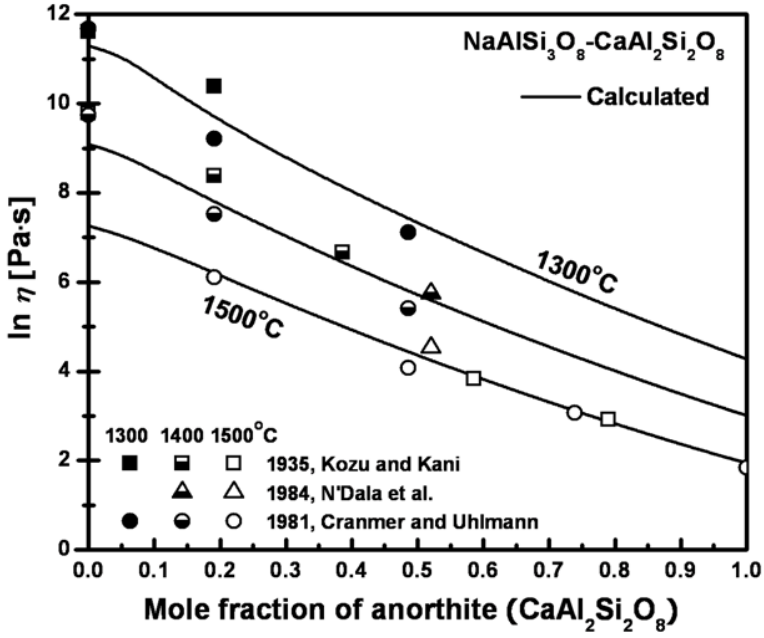

Fig. 4.22 Viscosity of albite–anorthite ($NaAlSi_3O_8$–$CaAl_2Si_2O_8$) melts: experimental points [36, 146, 200] and calculated lines

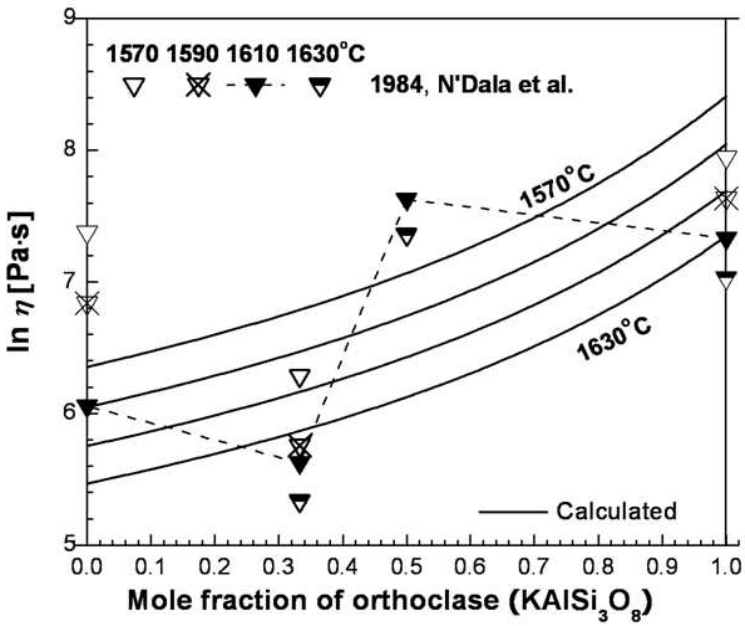

Fig. 4.23 Viscosity of albite–orthoclase ($NaAlSi_3O_8$–$KAlSi_3O_8$) melts: experimental points [200] and calculated lines.

As can be seen from Fig. 4.24, the calculated viscosities along the anorthite–diopside section are in excellent agreement with the measurements of Scarfe et al. [270]. The results of Kozu and Kani [146] progressively deviate from those of Scarfe et al. as the amount of diopside increases. The reason for this disagreement is not clear, but it should be noted that the data of Scarfe et al. for pure diopside are consistent with the measurements of other authors shown in Fig. 3 of the previous study [81]. This trend persists for the ternary albite–anorthite–diopside melts studied by Kozu and Kani [146]. Hence, their data seem to be more reliable only for relatively small contents of diopside. In particular, their results are in good agreement with the calculated lines for the pseudo-binary section through the albite–anorthite–diopside system at 20 wt% of diopside shown in Fig. 4.25.

The viscosities calculated by the model for the nepheline–diopside section are in similarly good agreement with the experimental measurements by Sykes et al. [314]. Therefore, it can be concluded that for these systems of petrological interest, the model predicts the viscosities within experimental error limits.

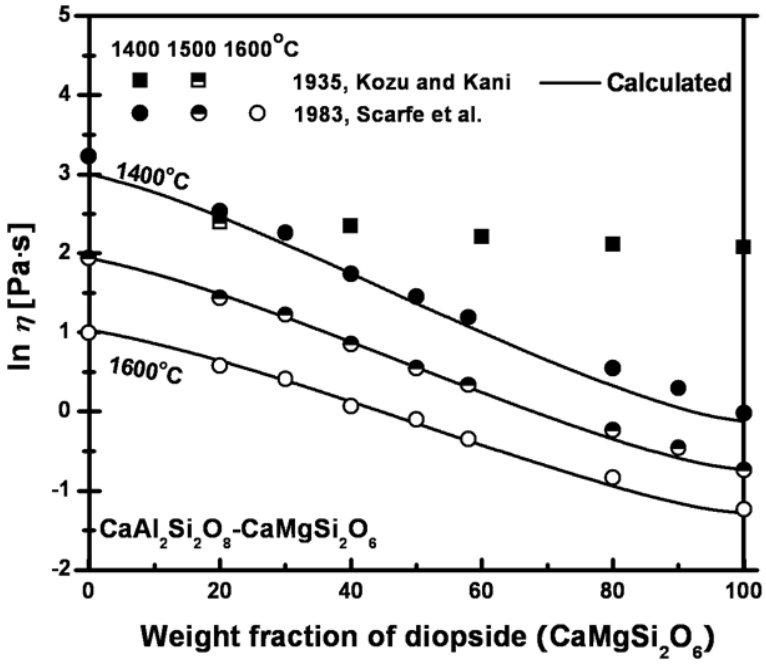

Fig. 4.24 Viscosity of anorthite–diopside ($CaAl_2Si_2O_8$–$CaMgSi_2O_6$) melts: experimental points [146, 270] and calculated lines.

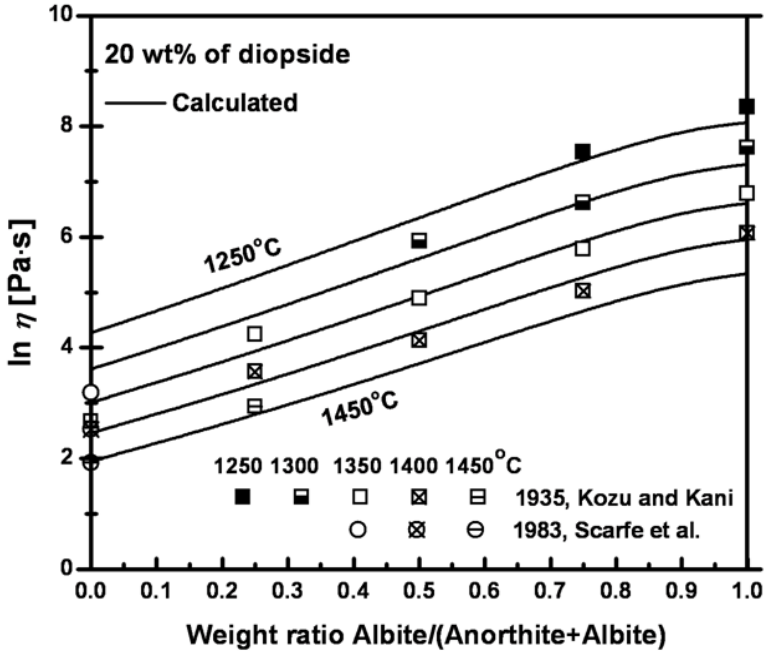

Fig. 4.25 Viscosity along the section through the albite–anorthite–diopside system at 20 wt% diopside: experimental points [146, 270] and calculated lines.

4.3.6 Melts used in glass technology

A large number of viscosity measurements are available for glass-forming melts in the Al_2O_3–CaO–MgO–Na_2O–K_2O–SiO_2 system around some technologically significant compositions. In particular, the compositions of typical soda-lime-silica melts for the production of container glasses and float glasses are within this six-component system. The concentrations of additional minor components such as Fe_tO, CrO_x, $LiO_{0.5}$ or PbO are normally less than 1.0 wt %. The calculation of viscosity of commercial glasses was carried out by the extended model with ignorance of the amount of these minor components.

In some cases, extensive experiments were carried out in a very well controlled manner by the same authors using the same equipment and well-characterized samples in a narrow composition range corresponding to a particular type of glass. Melts used in glass technology may also be easier to work with since they are specifically designed to avoid crystallization. This minimized the scatter of the experimental data and allowed the authors to fit the experimental points very accurately using fairly simple regression equations. The equations so obtained can be

used for reliable interpolations within the limited composition range covered by the grid of experimental points, but extrapolations outside this range are not possible.

A few regression equations for melts used in glass technology were obtained based on the viscosity measurements by several investigators. In particular, the recent statistical model of Fluegel [67] fits a very large amount of experimental information on melts used in glass technology which is summarized in the SciGlass database [37]. The model provides a rigorous estimation of errors and validity limits. This model [67] is based on multiple regression using polynomial functions. Fluegel claims that his analysis of systematic differences between laboratories improves the overall accuracy of interpolation [67]. Fluegel's model is most accurate in the vicinity of the commercial glass compositions since it is calibrated based on numerous experimental data for these regions.

The model developed in the present study, on the other hand, is designed particularly for wide-range extrapolations in composition. No experimental data for multicomponent melts used in glass technology have been used for the calibration of our model which is based solely upon parameters obtained by fitting data for binary and Al_2O_3-containing ternary systems. It is applicable at any composition, contrary to the regression equations mentioned above which cannot be extrapolated outside their validity limits. It is interesting to examine how the present model compares with existing regression equations within their own ranges of validity.

Table 4.3 shows the viscosities of typical soda-lime-silica melts and the effect of additions of Al_2O_3, K_2O and MgO. The experimental data of Lakatos et al. [154] are compared with the viscosities calculated by Fluegel's regression equation [67] and with those predicted by the present model. The agreement is very good and the accuracy of the present model seems to be comparable to Fluegel's regression equation.

Table 4.4 shows the viscosities of less typical melts used in glass technology which are used for the production of mineral-wool isolating fiber products. These compositions are outside the validity range of Fluegel's regression equation [67] and were not used for its calibration. As one would expect, the regression equation cannot reliably predict the viscosities of these melts, whereas the predictions of the present model are in good agreement with the experiment.

4.4 Conclusions

In the previous model for the viscosity of slags as shown in Chapter 3, the viscosity is related to the structure of the melt characterized by the amounts and connectivity of Q^i-species. The structure in turn is calculated from the thermodynamic description of the melt using the Modified Quasichemical Model [231, 232] and the FactSage optimized thermodynamic database [14].

The model is extended in the present study to reproduce the complex behaviour of the viscosity on the alkali-rich side of the alkali oxide – silica systems. This behaviour is attributed to ring clusters formed by Q^2- and Q^3-species. An excess contribution to the viscosity due to polymerization of Q^2- and Q^3-species into large rings is taken into account by the introduction of one additional binary parameter for each alkali oxide – silica system. The extended model is almost equivalent to the earlier model in Chapter 3 if the total mole fraction of alkali oxides, $MO_{0.5}$, is less than 0.5. However, in the alkali-rich region, the difference between the models can be substantial as can be seen, for example, from Figs. 4.1, 4.2 and 4.8.

In summary, the model contains unary parameters describing the viscosity of pure liquid oxides and only two binary parameters, $E^{R}_{MO_x-Si}$ and $E^{1,1}_{MO_x\text{-}Si}$, for most binary systems MO_x–SiO_2 when M is not an alkali. For each alkali oxide – SiO_2 system one additional binary parameter, $E^{Ring}_{MO_x\text{-}Si}$, is needed. For each Al_2O_3-containing ternary system MO_x–Al_2O_3–SiO_2 exhibiting the Charge Compensation Effect (where Al^{3+} assumes a tetrahedral coordination and enters the silica network with a basic cation M staying close to Al^{3+} to compensate the missing charge) the model incorporates two additional ternary parameters. The viscosity of multicomponent melts is then predicted by the model without any additional adjustable model parameters.

The available viscosity data for the alkali-containing subsystems of the Al_2O_3–CaO–MgO–Na_2O–K_2O–SiO_2 system have been reviewed. It is demonstrated that the model reproduces the experimental data for the binary and ternary melts and predicts the viscosities of multicomponent melts within experimental error limits. In particular, the model can be used to provide good estimates of the viscosities of multicomponent melts used in glass technology, magmas and lavas.

Table 4.1 Optimized model parameters for the viscosity expressed in Pa·s.

System	Parameters $\boldsymbol{A}$	Parameters $\boldsymbol{E}$ (J·mol^{-1})
SiO_2	$\boldsymbol{A}^{*}_{Si} = -10.56$ $\boldsymbol{A}^{\boldsymbol{E}}_{Si} = -6.13$	$\boldsymbol{E}^{*}_{Si} = 217200$ $\boldsymbol{E}^{\boldsymbol{E}}_{Si} = 298520$
$AlO_{1.5}$	$\boldsymbol{A}_{AlO_{1.5}} = -9.22$	$\boldsymbol{E}_{AlO_{1.5}} = 120400$
CaO	$\boldsymbol{A}_{CaO} = -12.27$	$\boldsymbol{E}_{CaO} = 137650$
MgO	$\boldsymbol{A}_{MgO} = -10.58$	$\boldsymbol{E}_{MgO} = 117160$
$NaO_{0.5}$	$\boldsymbol{A}_{NaO_{0.5}} = -10.15$	$\boldsymbol{E}_{NaO_{0.5}} = 45500$
$KO_{0.5}$	$\boldsymbol{A}_{KO_{0.5}} = -13.35$	$\boldsymbol{E}_{KO_{0.5}} = 84500$
$LiO_{0.5}$	$\boldsymbol{A}_{LiO_{0.5}} = -9.85$	$\boldsymbol{E}_{LiO_{0.5}} = 45500$
$AlO_{1.5}$–SiO_2	$\boldsymbol{A}^{\boldsymbol{R}}_{AlO_{1.5}\text{-}Si} = -12.30$	$\boldsymbol{E}^{1,1}_{AlO_{1.5}\text{-}Si} = -75000$ $\boldsymbol{E}^{\boldsymbol{R}}_{AlO_{1.5}\text{-}Si} = 303500$
CaO–SiO_2		$\boldsymbol{E}^{1,1}_{CaO\text{-}Si} = -101750$ $\boldsymbol{E}^{\boldsymbol{R}}_{CaO\text{-}Si} = 81400$
MgO–SiO_2		$\boldsymbol{E}^{\boldsymbol{1,1}}_{\boldsymbol{MgO\text{-}Si}} = \boldsymbol{-86250}$ $\boldsymbol{E}^{\boldsymbol{R}}_{\boldsymbol{MgO\text{-}Si}} = \boldsymbol{72600}$
$NaO_{0.5}$–SiO_2		$\boldsymbol{E}^{1,1}_{NaO_{0.5}\text{-}Si} = 32500$ $\boldsymbol{E}^{\boldsymbol{R}}_{NaO_{0.5}\text{-}Si} = 10200$ $\boldsymbol{E}^{\boldsymbol{Ring}}_{NaO_{0.5}\text{-}Si} = 20444358$
$KO_{0.5}$–SiO_2		$\boldsymbol{E}^{1,1}_{KO_{0.5}\text{-}Si} = -38200$ $\boldsymbol{E}^{\boldsymbol{R}}_{KO_{0.5}\text{-}Si} = 39000$ $\boldsymbol{E}^{\boldsymbol{Ring}}_{KO_{0.5}\text{-}Si} = 42390018$
$LiO_{0.5}$–SiO_2		$\boldsymbol{E}^{1,1}_{LiO_{0.5}\text{-}Si} = 10752$ $\boldsymbol{E}^{\boldsymbol{R}}_{LiO_{0.5}\text{-}Si} = 32000$ $\boldsymbol{E}^{\boldsymbol{Ring}}_{LiO_{0.5}\text{-}Si} = 12441119$

Table 4.2 Optimized parameters for ternary systems containing alumina ($J \cdot mol^{-1}$)

System	
$KO_{0.5}$–$AlO_{1.5}$–SiO_2	$\Delta G_{KAlO_2} = -57000 - 35000 X_{SiO_2}$
$NaO_{0.5}$–$AlO_{1.5}$–SiO_2	$\Delta G_{NaAlO_2} = -26000 - 57000 X_{SiO_2}$
CaO–$AlO_{1.5}$–SiO_2	$\Delta G_{CaAl_2O_4} = 5000 - 100000 X_{SiO_2}$
MgO–$AlO_{1.5}$–SiO_2	$\Delta G_{MgAl_2O_4} = 13000 - 105000 X_{SiO_2}$

Table 4.3 Viscosities of typical soda-lime-silica glass melts and the effect of additions of Al_2O_3, K_2O and MgO. The experimental data of Lakatos et al. [154] are compared with the viscosities calculated by Fluegel's regression equation [67] and predicted by the present model.

SiO_2	Al_2O_3	CaO	Na_2O	K_2O	MgO	Temperature	Viscosity, ln(Pa•s)		
mass %	mass %	mass %	mass %	mass %	mass %	°C	Lakatos et al. [154]	Fluegel, [67]	Present model
72.41	1.23	12.17	14.19			1007.4	6.91	7.11	7.04
72.41	1.23	12.17	14.19			1012.1	6.91	7.03	6.97
72.69	1.23	12.21	13.87			1016.8	6.91	7.03	6.97
73.66	1.25	10.66	14.44			1021.8	6.91	6.98	6.96
73.23	1.24	12.30	13.22			1026.2	6.91	7.03	6.96
73.91	1.25	10.35	14.49			1023.8	6.91	6.97	6.96
74.07	1.26	12.44	12.23			1040.1	6.91	7.04	6.96
74.95	1.27	9.09	14.69			1031.9	6.91	6.94	6.93
76.55	1.30	7.14	15.00			1044.4	6.91	6.90	6.87
77.66	1.32	5.80	15.22			1053.0	6.91	6.88	6.82
70.68	3.60	11.87	13.85			1030.3	6.91	6.96	7.07
69.43	5.30	11.66	13.61			1043.5	6.91	6.92	7.17
69.27	1.18	11.64	13.58	4.34		984.0	6.91	6.92	7.10
66.38	1.13	11.15	13.01	8.33		956.0	6.91	6.98	7.26
71.37	1.21	11.99	13.99		1.44	1013.2	6.91	6.91	6.80
70.86	1.20	11.90	13.89		2.14	1013.5	6.91	6.86	6.71

Table 4.4 Viscosities of melts for the production of mineral-wool isolating fiber products. The experimental data of Lakatos et al. [153] are compared with the viscosities predicted by the present model and calculated by Fluegel's regression equation [67].

SiO_2	Al_2O_3	CaO	MgO	Na_2O	K_2O	Temperature	Viscosity, ln(Pa•s)		
mass %	mass %	mass %	mass %	mass %	mass %	°C	Lakatos et al. [153]	Present model	Fluegel, [67] **
60	10	11	16	2.00	1.00	1506	1.15	1.01	2.30
58	13	19	8	1.33	0.67	1518	1.15	1.22	0.96
53	16	15	12	2.67	1.33	1469	1.15	1.14	1.26
49	19	23	4	3.33	1.67	1488	1.15	1.13	-1.42
54	10	24	8	2.67	1.33	1408	1.15	1.13	0.57
50	13	16	16	3.33	1.67	1379	1.15	0.92	1.19
49	16	28	4	2.00	1.00	1413	1.15	1.10	-2.33
47	19	20	12	1.33	0.67	1404	1.15	0.84	-1.53
48	10	25	12	3.33	1.67	1325	1.15	0.80	-0.24
46	13	33	4	2.67	1.33	1345	1.15	0.82	-3.28
45	16	21	16	1.33	0.67	1352	1.15*	0.52	-2.46
41	19	29	8	2.00	1.00	1339	1.15*	0.63	-14.51
46	10	38	4	1.33	0.67	1307	1.15*	0.63	-2.71
42	13	30	12	2.00	1.00	1280	1.15*	0.56	-6.16
37	16	34	8	3.33	1.67	1277	1.15*	0.44	-21.40
35	19	26	16	2.67	1.33	1276	1.15*	0.32	-28.32

* These experimental viscosities may be overestimated due to the onset of crystallization since the reported temperatures are slightly below the liquidus calculated by FactSage [14] and the silica contents are not high enough to prevent crystallization of supercooled melts.

** All compositions are outside the validity range of Fluegel's model [67]. This column is shown only to illustrate the spread of values that a regression equation can produce outside its validity range.

CHAPTER 5 MODELING VISCOSITY OF SILICATE MELTS CONTAINING LEAD OXIDE

5.1 Introduction

Silicate slags containing lead oxide are formed during pyrometallurgical production of lead either from metal scrap or from ores. Of particular importance is the slag viscosity which quantifies the flow properties of the slag and affects the degree of refractory attack, the amount of entrained metal in the slag, mass transfer at the slag/metal interface and heat transfer through the slag [17]. The viscosity of PbO-containing oxide melts is also of primary importance to the glass industry.

In the present study, viscosity data are reviewed for melts formed by PbO with SiO_2, Al_2O_3, CaO, MgO, Na_2O and K_2O. A few model parameters are optimized to reproduce the viscosities of PbO, PbO-SiO_2 and PbO-Al_2O_3-SiO_2 melts. Then the available experimental viscosity data for other ternary and higher-order PbO-containing systems are compared to the viscosities calculated by the model without using any additional adjustable model parameters.

5.2 Review of the available viscosity data and calibration of the model

In the present study, viscosity data are reviewed for all PbO-containing subsystems of the PbO–SiO_2–Al_2O_3–CaO–MgO–Na_2O–K_2O system and using the model introduced in Chapter 4.(See Eqs. (4.1)-(4.4)) The data judged to be most reliable are shown in the figures below.

The proposed model is intended for melts. The extension of the model to describe the viscosity of glasses will be reported in Chapters 11 and 12. Therefore, the viscosity data were collected mainly for melts above the liquidus or for slightly supercooled melts where crystallization did not occur. These measurements were mostly made with rotational or vibrational viscometers. Phase equilibrium calculations were carried out using the FactSage thermochemical software and databases [14] to check that the viscosity was indeed measured in a single-phase liquid region. If an abnormally high viscosity value was reported for a temperature below the liquidus, this was most likely the result of crystallization. Parameters of the model for

PbO-containing melts that were fitted to the experimental viscosity data are listed in Table 5.1. The model parameters for melts without PbO were shown in Tables 4.1 and 4.2.

5.2.1 Pure PbO

The viscosity of PbO was measured by Oliver [219] using a rotating crucible viscometer with platinum crucibles under Ar gas atmosphere in the temperature range of 900 to 1150ºC. The formation of PbO_2 from pure liquid PbO is negligible under the given condition. As shown in Fig. 5.1, these experimental data are well reproduced by a linear Arrhenian function. The model parameters A_{PbO} and E_{PbO} are given in Table 5.1.

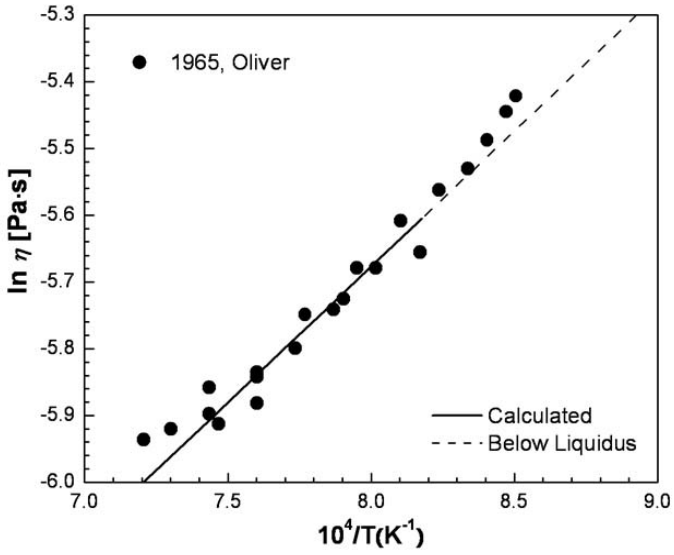

Fig. 5.1 Viscosity of pure liquid PbO: experimental points [219] and calculated line.

5.2.2 Viscosities of Binary PbO–SiO_2 Melts

The viscosity of PbO–SiO_2 melts has been studied repeatedly due to the relatively low liquidus temperatures and the importance of this system to the lead smelting process. Urbain [361], Gupta [85], Wright et al. [350], Kou et al. [143] and Nakamura et al. [202] measured the viscosity by the rotating crucible method with Pt–Rh crucibles and spindles to reduce

experimental errors caused from the chemical attack by the melts. Frohberg and Rohde [69] and Nemilov and Ignat'ev [207, 209] used the rotating cylinder method with alumina crucibles.

Hino et al. [93], Ejima et al. [54], Ouchi and Kato [224], Evstrop'ev [63] and Saringyulyan and Kostanyan [263] measured the viscosity using the counter-balanced sphere method with Pt−Rh crucibles. The former two studies came from the same group and reported substantially higher viscosities than the other authors, most likely indicating the presence of systematic errors.

Ito et al. used Pt−Rh crucibles to measure the viscosity by the oscillation method and by the rotating crucible method [103]. As can be seen from Fig. 5.2-(c), the latter method produced results that are in good agreement with the other authors although the viscosities obtained by the oscillation method are substantially lower. The authors attributed the difference to a systematic error caused by the uncertainties in the damping rates of an oscillating wire.

Initially, two model parameters, $E^{1,1}_{\text{PbO-Si}}$ and $E^{R}_{\text{PbO-Si}}$, were optimized to fit the viscosities of $PbO–SiO_2$ melts. As can be seen from Fig. 5.2-(a), the model reproduces well the experimental data, but the calculated curves are higher than the two points by Saringyulan and Kostanyan [263] at a mole fraction of SiO_2 equal to 0.7. To the best of our knowledge no other authors have measured the viscosities of $PbO–SiO_2$ melts at these high silica concentrations which are below the liquidus. To fit these two points, the slope of the viscosity curves must decrease and then increase again when approaching pure silica. The physical reason for such behavior is unclear. However, if this disagreement is attributed to the experimental uncertainties and ignored, the predicted viscosities of lead crystal glass melts are systematically slightly higher than the experimental data of Lakatos et al. [152, 154, 155]. The compositions of lead crystal glasses are close to the $K_2O–PbO–SiO_2$ system as shown below in Fig. 5.9. Since the mole fraction of SiO_2 in these glasses varies from about 75 to 80 mol %, the viscosities of lead crystal glass melts calculated by the model are defined by the viscosities of $PbO–SiO_2$ melts at these high silica concentrations which are substantially below the liquidus and cannot be measured experimentally. On the other hand, in the $K_2O–PbO–SiO_2$ system, viscosity measurements can be made at such high silica contents as can be seen for example from Fig. 5-12. These data substantiate the existence of the second inflection point on the viscosity curves in the $PbO–SiO_2$ system.

Therefore, the viscosities of $PbO–SiO_2$ melts were finally fitted with two polynomial parameters, $E^{1,1}_{PbO\text{-}Si}$ and $E^{2,5}_{PbO\text{-}Si}$, which are given in Table 5.1. As can be seen from Figs 5.2-(b) and 5.2-(c), these parameters give a slightly better description of the experimental data at high silica contents than the fit shown in Fig. 5.2-(a). However, the viscosity values extrapolated to $X(SiO_2)$ = 0.8 are substantially different for these two variants.

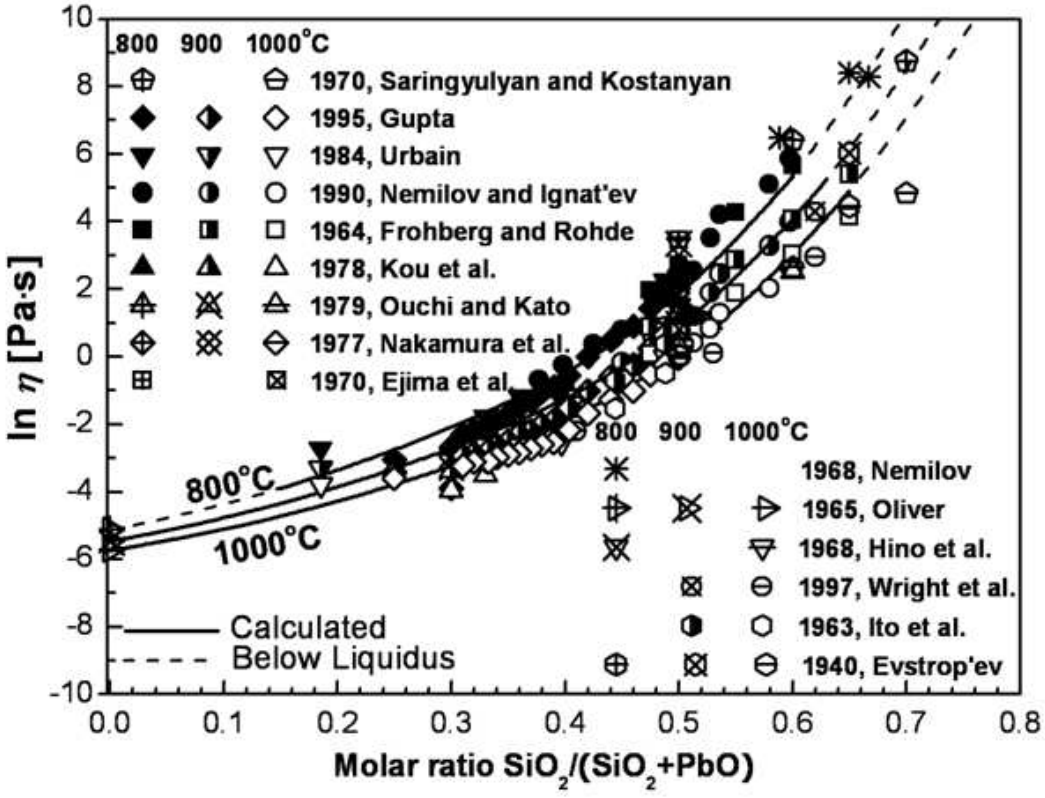

(a)

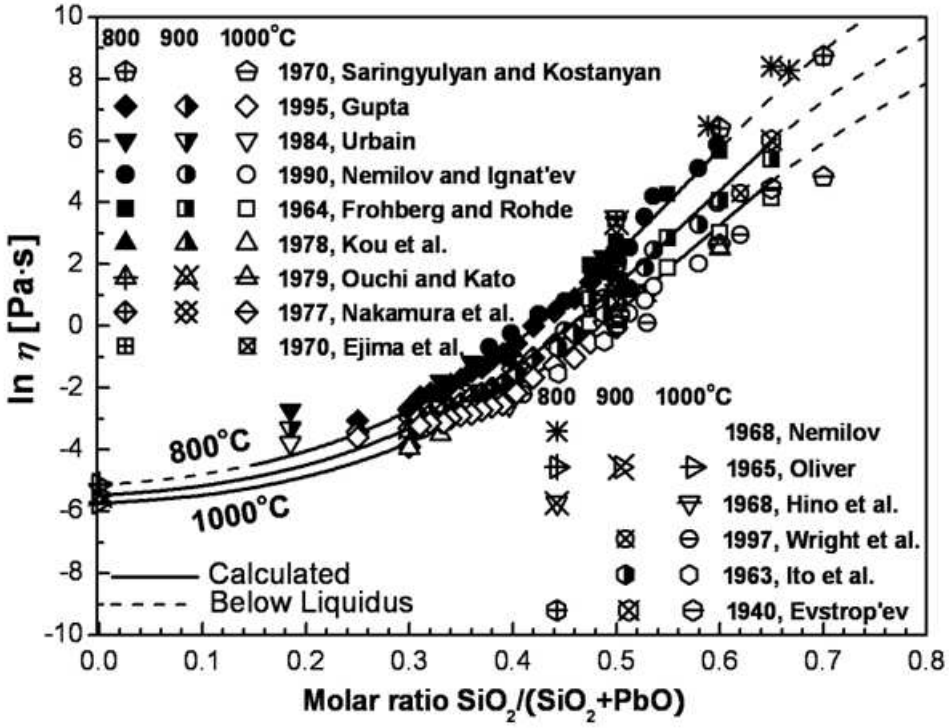
800 900 1000°C
1970, Saringyulyan and Kostanyan
1995, Gupta
1984, Urbain
1990, Nemilov and Ignat'ev
1964, Frohberg and Rohde
1978, Kou et al.
1979, Ouchi and Kato
1977, Nakamura et al.
1970, Ejima et al.
800 900 1000°C
1968, Nemilov
1965, Oliver
1968, Hino et al.
1997, Wright et al.
1963, Ito et al.
1940, Evstrop'ev
800°C
1000°C
Calculated
Below Liquidus
ln η [Pa·s]
Molar ratio SiO2/(SiO2+PbO)

(b)

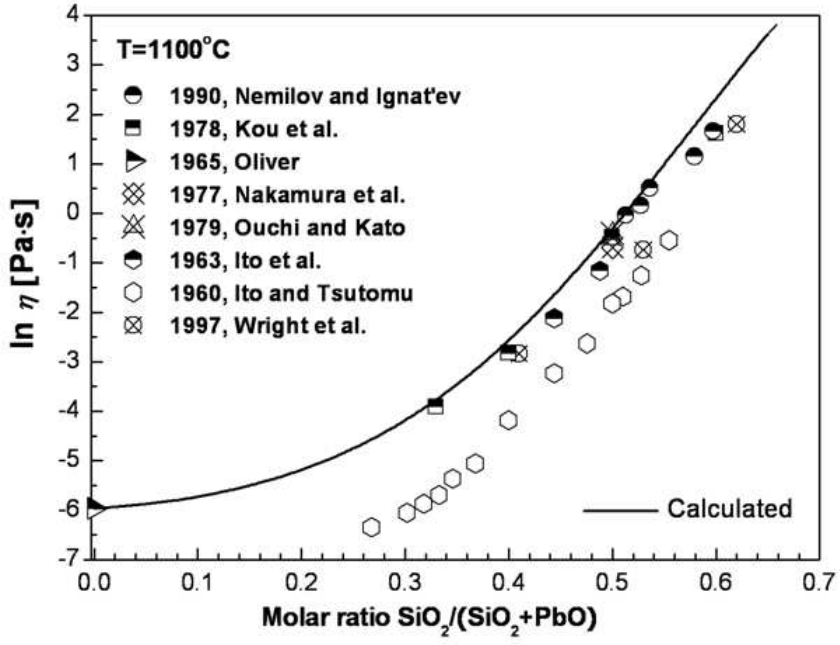

(c)

Fig. 5.2 Viscosity of PbO–SiO_2 melts: (a) experimental points [54, 63, 69, 85, 93, 104, 143, 202, 207, 209, 219, 224, 263, 332, 350] at 800, 900 and 1000°C and calculated lines fitted with parameters $E^{1,1}_{\text{PbO-Si}}$ and $E^{R}_{\text{PbO-Si}}$; (b) experimental points [54, 63, 69, 85, 93, 104, 143, 202, 207, 209, 219, 224, 263, 332, 350] at 800, 900 and 1000°C and calculated lines fitted with parameters $E^{1,1}_{\text{PbO-Si}}$ and $E^{2,5}_{\text{PbO-Si}}$; (c) experimental points [103, 104, 143, 202, 209, 219, 224, 350] for 1100 °C and calculated lines fitted with parameters $E^{1,1}_{\text{PbO-Si}}$ and $E^{2,5}_{\text{PbO-Si}}$.

5.2.3 Ternary and Quaternary Melts without Alumina(Al_2O_3)

The viscosities of ternary and higher-order melts without Al_2O_3 were predicted by the model based on the unary and binary viscosity parameters without any additional adjustable parameters.

5.2.3.1 PbO-Na_2O-SiO_2 system

The viscosities of PbO–Na_2O–SiO_2 melts were measured by the platinum ball pulling-up method [111] and by the counter-balanced sphere method [63, 62, 93, 327] at compositions shown in Fig. 5.3. Experimental points and calculated curves are shown in Figs 5.4 to 5.8. As can be seen from Fig. 5.5, the data of Tret'yakova and Mazurin [327] are systematically lower than the viscosity predicted by the model although the difference is fairly small. It should be noted that extrapolation of these data to the Na_2O–SiO_2 system would result in lower viscosities than reported by many other authors as shown in Chapter 4, indicating that the data of Tret'yakova and Mazurin [327] have a small systematic error. The data of Evstrop'ev [63] are in good agreement, with the calculated lines being slightly lower (see Figs 5.5, 5.7 and 5.8), while his earlier results are higher (see Figs 5.6 and 5.7). Overall, the viscosities predicted by the model are in agreement with the experimental data within the experimental scatter in the PbO–Na_2O–SiO_2 ternary and the limiting binary systems.

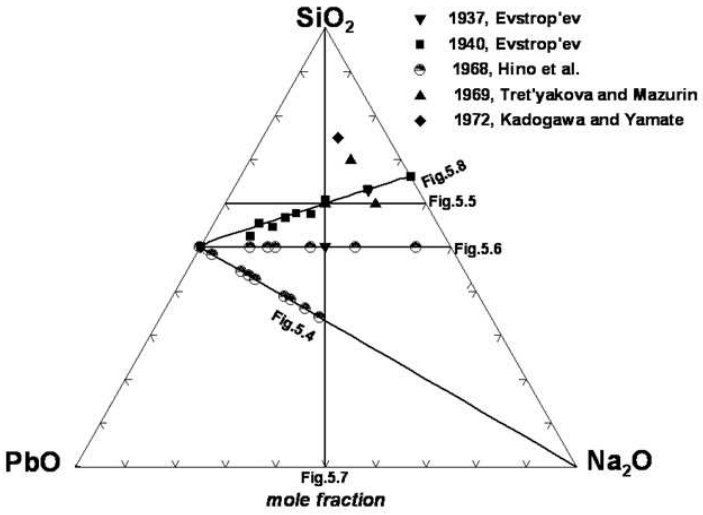

Fig. 5.3 Compositions in the PbO–Na_2O–SiO_2 system at which the viscosity was measured [63, 62, 93, 111, 327]. Lines show the sections of this ternary system reported in Figs 5.4 to 5.8

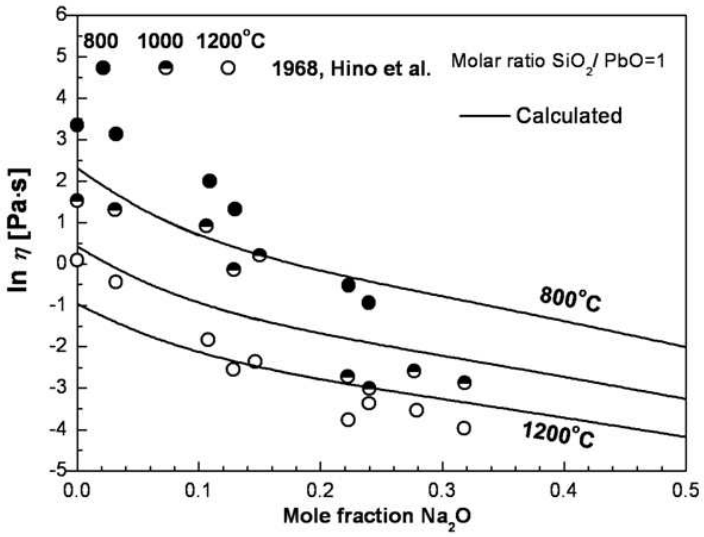

Fig. 5.4 Viscosity of $PbO–Na_2O–SiO_2$ melts at a molar ratio of $SiO_2/PbO = 1$: experimental points [93] and calculated lines

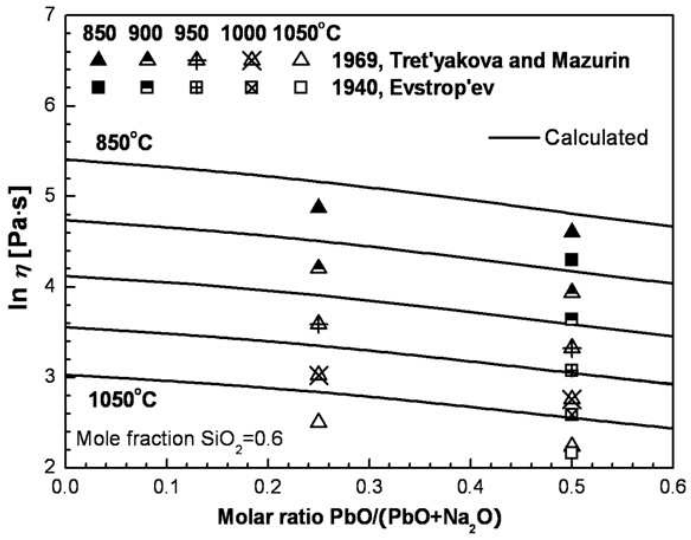

Fig. 5.5 Viscosity of $PbO–Na_2O–SiO_2$ melts at 60 mol% SiO_2: experimental points [63, 327] and calculated lines

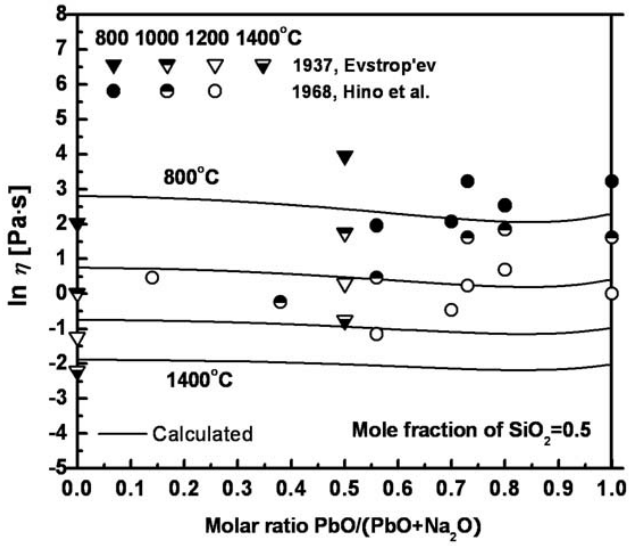

Fig. 5.6 Viscosity of $PbO–Na_2O–SiO_2$ melts at 50 mol% SiO_2: experimental points [62, 93] and calculated lines

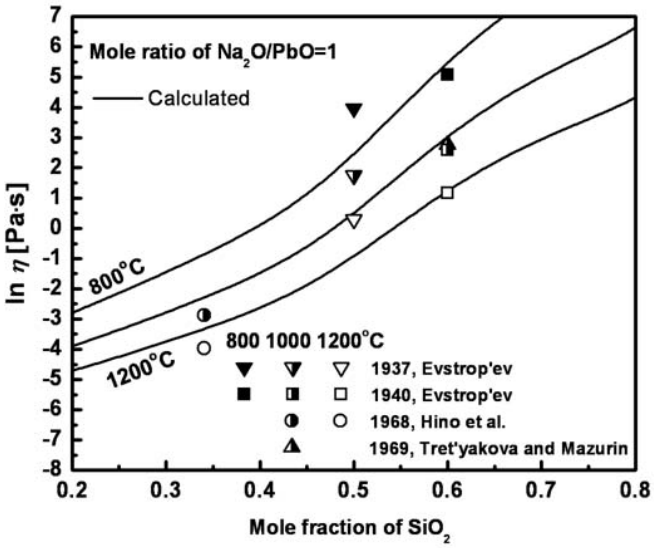

Fig. 5.7 Viscosity of $PbO–Na_2O–SiO_2$ melts at a molar ratio of $Na_2O/PbO = 1$: experimental points [63, 62, 93, 327] and calculated lines

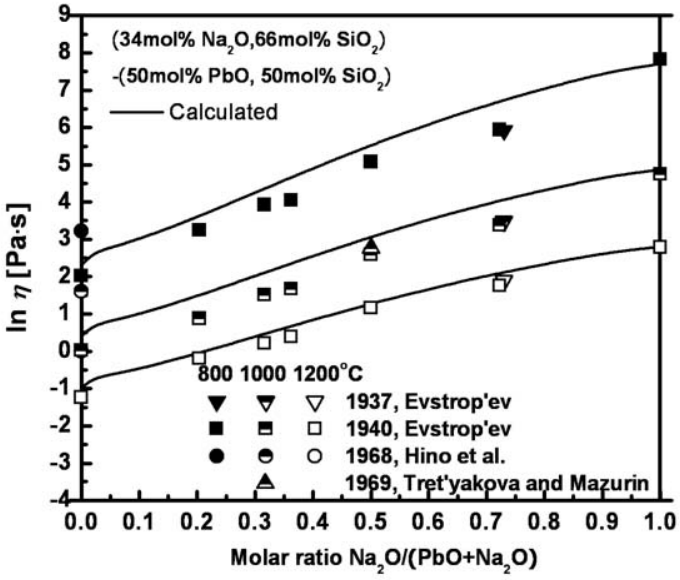

Fig. 5.8 Viscosity of PbO–Na_2O–SiO_2 melts in the section from (34 mol% Na_2O, 66 mol% SiO_2) to (50 mol% PbO, 50 mol% SiO_2): experimental points[63, 62, 93, 327] and calculated lines

5.2.3.2 PbO-K_2O-SiO_2 system

Hino et al. [94], Shartsis and Spinner [282] and Saringyulyan and Kostanyan [263] measured the viscosities of PbO–K_2O–SiO_2 melts by the counter-balanced sphere method with Pt–Rh and Pt crucibles, respectively. Pohlmann [237] used a rotating viscometer with alumina crucibles and Kadogawa and Yamate [111] applied the platinum ball pulling-up method to measure the viscosity at a single composition. The studied compositions are shown in Fig. 5.9.

Experimental error can be inferred for example from the comparison of the calculated lines with the experimental points at the right and left boundaries in Fig. 5.10 which correspond to binary melts. In particular, the left boundary represents one composition in the PbO–SiO_2 system, so the calculated lines at this point reproduce experimental data of the many authors shown in Fig.5.2, indicating that the measurements of Hino et al.[94] are systematically higher.

The six sections through the $PbO–K_2O–SiO_2$ system presented in Figs 5.10 to 5.15 show good agreement between the experimental data and the viscosities predicted by the model. The trends of the experimental points correspond very well with the slopes of the calculated lines. In particular, the measurements of Saringyulyan and Kostanyan [263] depicted in Fig. 5.12 extend to very high-silica contents and cover viscosity values varying over several orders of magnitude. The calculated lines are in good agreement with the experiments and show two inflection points originating from the description of $PbO–SiO_2$ melts with two polynomial terms. Overall, the accuracy of the model predictions for $PbO–K_2O–SiO_2$ melts is no worse than the experimental scatter in the $PbO–SiO_2$ binary system.

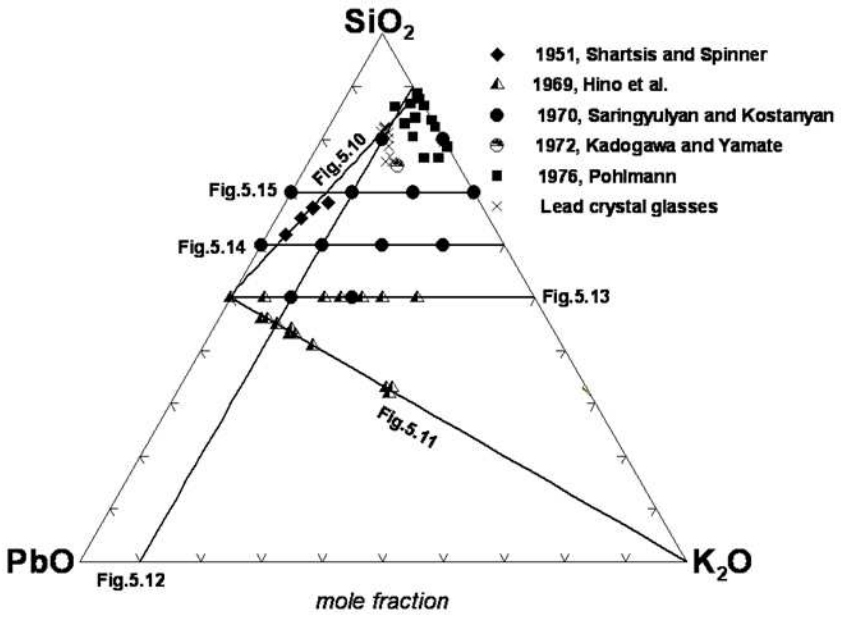

Fig. 5.9 Compositions in the $PbO–K_2O–SiO_2$ system at which the viscosity was measured. [94, 111, 237, 263, 282] Lines show the sections of this ternary system reported in Figs 5.10 to 5.15

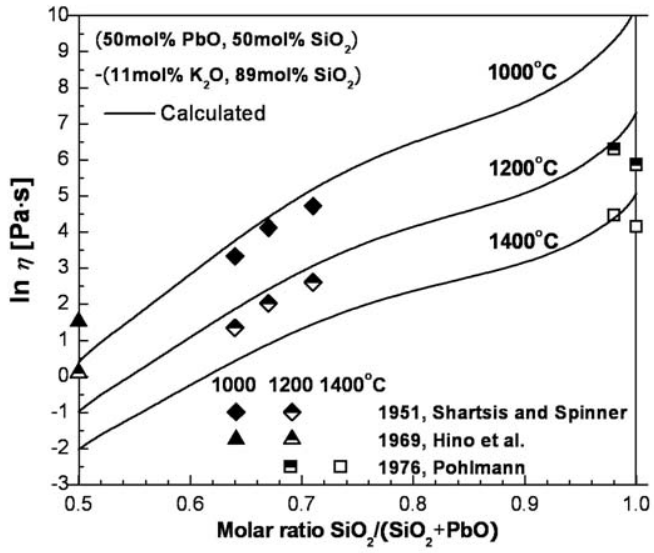

Fig. 5.10 Viscosity of $PbO–K_2O–SiO_2$ melts in the section from (50 mol% PbO, 50 mol% SiO_2) to (11 mol% K_2O, 89 mol% SiO_2): experimental points [94, 237, 282] and calculated lines

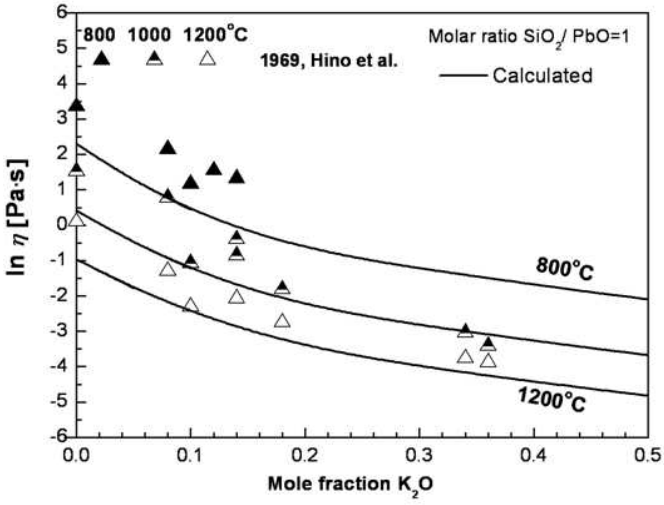

Fig. 5.11 Viscosity of $PbO–K_2O–SiO_2$ melts at a molar ratio of $SiO_2/PbO = 1$: experimental points [94] and calculated lines

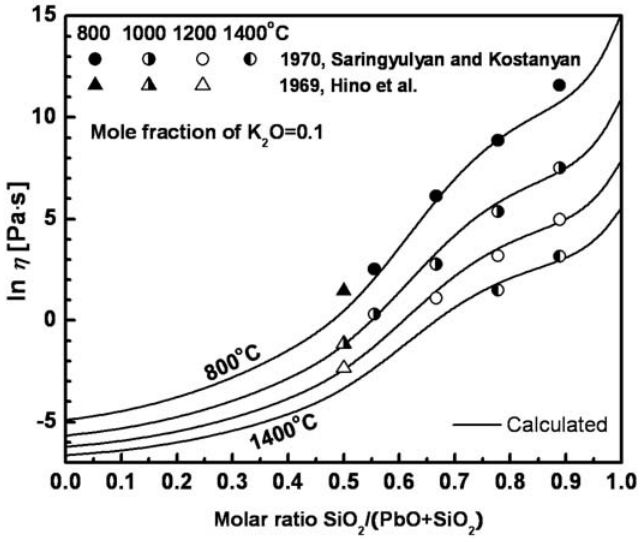

Fig. 5.12 Viscosity of $PbO–K_2O–SiO_2$ melts at 10 mol% K_2O: experimental points [94, 263] and calculated lines

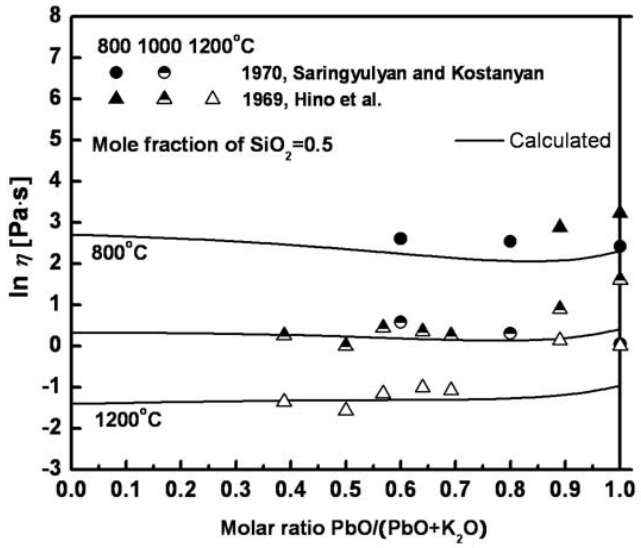

Fig. 5.13 Viscosity of $PbO–K_2O–SiO_2$ melts at 50 mol% SiO_2: experimental points [94, 263] and calculated lines

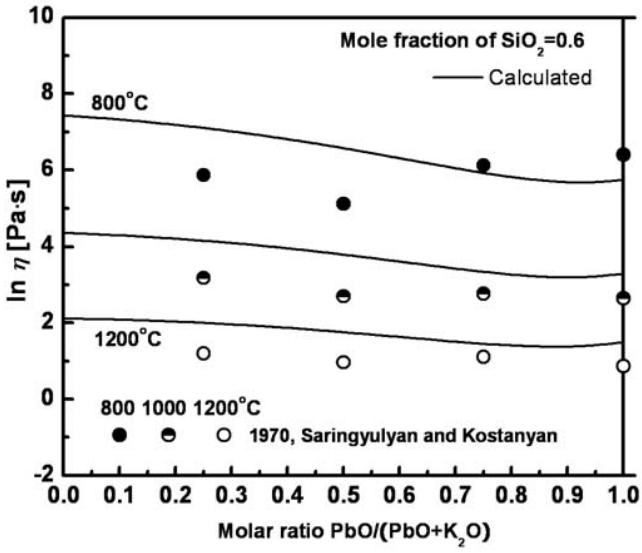

Fig. 5.14 Viscosity of $PbO–K_2O–SiO_2$ melts at 60 mol% SiO_2: experimental points [263] and calculated lines

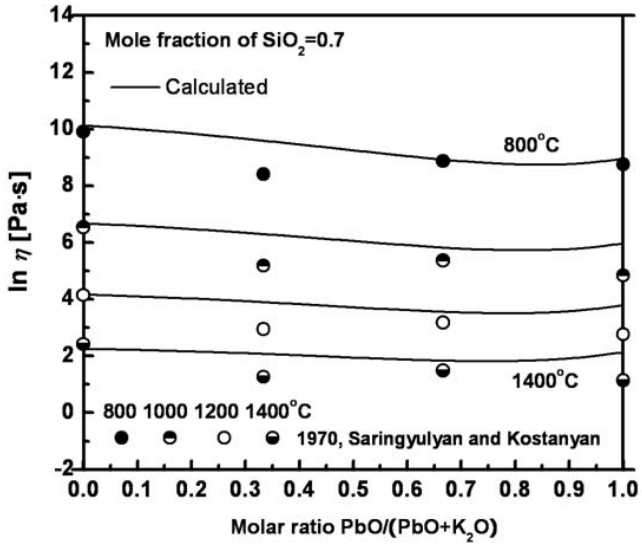

Fig. 5.15 Viscosity of $PbO–K_2O–SiO_2$ melts at 70 mol% SiO_2: experimental points [263] and calculated lines

5.2.3.3 PbO-MgO-SiO_2 system

Kawahara et al. [120] and Ouchi and Kato [224] measured the viscosities of PbO–MgO–SiO_2 melts by the counter-balanced sphere method while Ito et al. [104] used the rotating crucible method. The studied compositions are shown in Fig. 5.16. As can be seen from the sections shown in Figs 5.17 to 5.19, Kawahara et al. [120] reported an increase in the viscosity as PbO is substituted by MgO at constant mole fraction of silica. The calculated lines are in perfect agreement with the experiments at $X(SiO_2)$ = 0.4 and show the same trend at $X(SiO_2)$ = 0.5. However, the model predicts that this effect flattens out at $X(SiO_2)$ = 0.6. If the experimental points [120] at $X(SiO_2)$ = 0.6 and 0.5 are extrapolated to the MgO–SiO_2 binary system, this would result in viscosity values which seem too high compared to the experimental data available for the MgO–SiO_2 and MgO–CaO–SiO_2 systems [81]. The maximum difference between the calculated lines and the data of Kawahara et al. [120] is about 1.0 in the natural logarithm scale which is similar to the normal scatter observed between the results of different authors for these systems. Unfortunately, to the best of our knowledge, no other authors have measured the viscosities of MgO–CaO–SiO_2 melts at relatively high MgO contents. The data of Ouchi and Kato [224] are in very good agreement with the predictions of the present model.

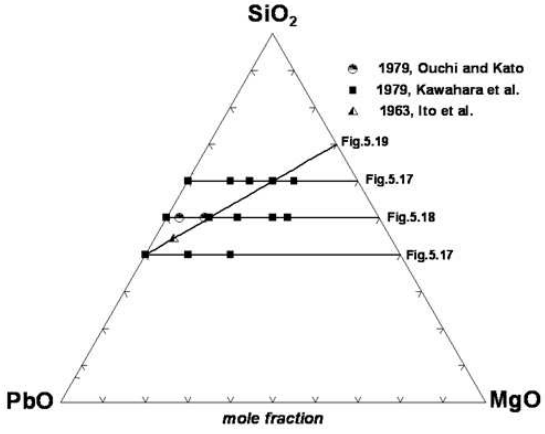

Fig. 5.16 Compositions in the PbO–MgO–SiO_2 system at which the viscosity was measured [104, 120, 224]. Lines show the sections of this ternary system reported in Figs 5.17 to 5.19

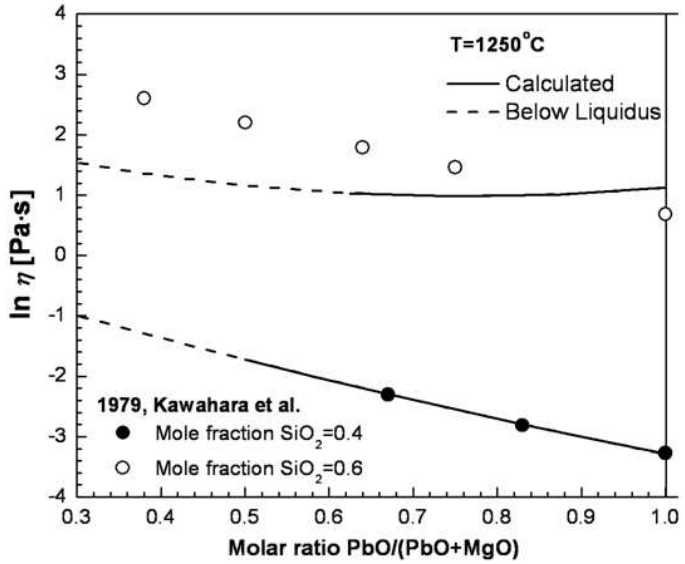

Fig. 5.17 Viscosity of PbO–MgO–SiO_2 melts at 40 and 60 mol% SiO_2: experimental points [120] and calculated lines

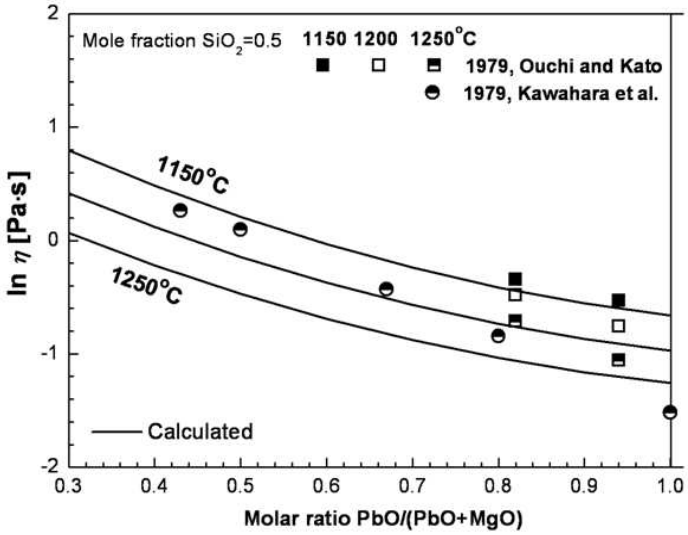

Fig. 5.18 Viscosity of PbO–MgO–SiO_2 melts at 50 mol% SiO_2: experimental points [120, 224] and calculated lines

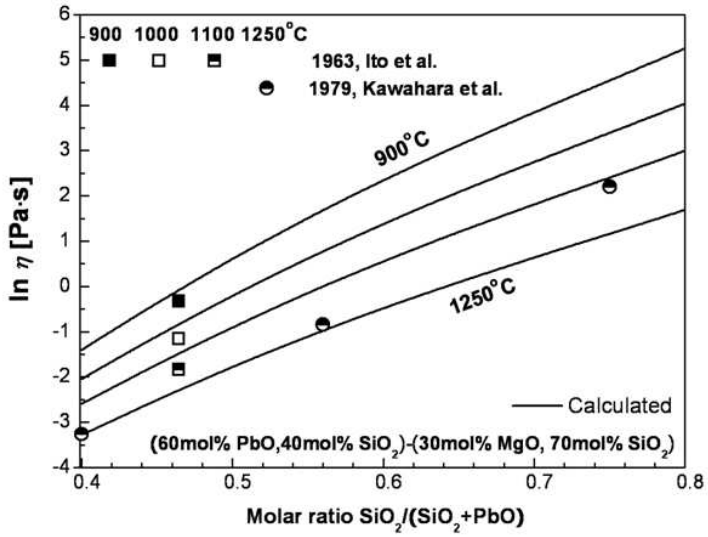

Fig. 5.19 Viscosity of PbO–MgO–SiO_2 melts in the section from (60 mol% PbO, 40 mol% SiO_2) to (30 mol% MgO, 70 mol% SiO_2): experimental points [104, 120] and calculated lines

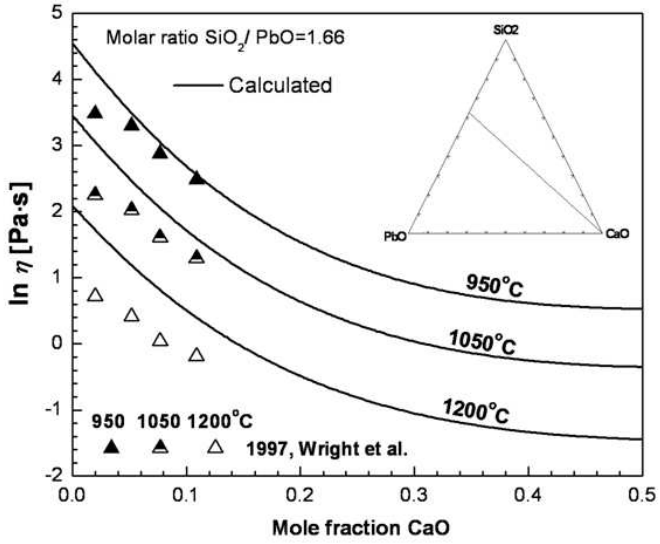

Fig. 5.20 Viscosity of PbO–CaO–SiO_2 melts at a molar ratio SiO_2/PbO = 1.66: experimental points [350] and calculated lines

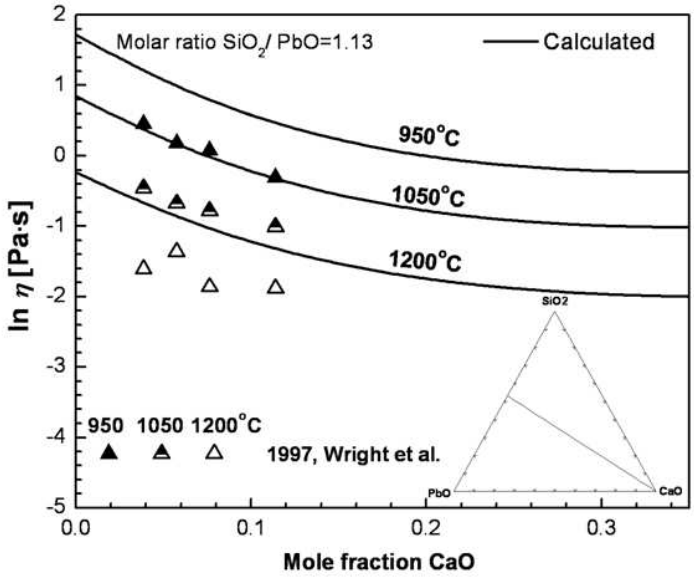

Fig. 5.21 Viscosity of PbO–CaO–SiO_2 melts at a molar ratio SiO_2/PbO = 1.13: experimental points [350] and calculated lines

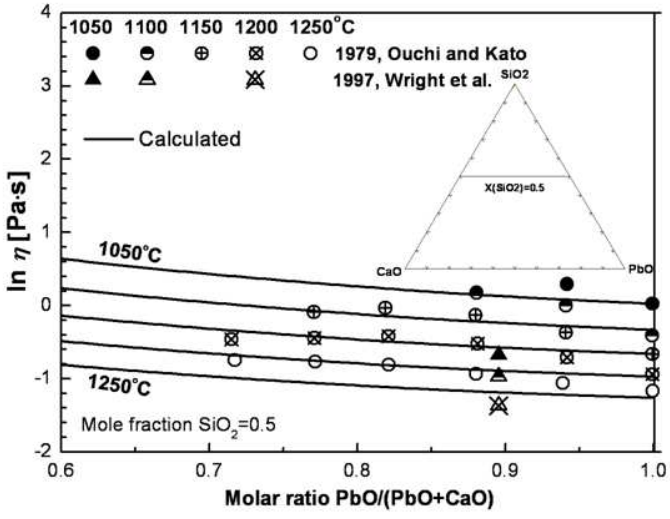

Fig. 5.22 Viscosity of PbO–CaO–SiO_2 melts at 50 mol% SiO_2: experimental points [224, 350] and calculated lines

5.2.3.4 PbO-CaO-SiO_2 system

The viscosities of PbO−CaO−SiO_2 melts were measured by the rotating crucible method [350] and the counter-balanced sphere method [224]. As can be seen from Fig. 5.2, the data of Wright et al. [350] are somewhat lower while the data of Ouchi and Kato [224] are slightly higher than the best fit of all experimental data for the PbO–SiO_2 system. As can be seen from the three sections in Figs 5.20 to 5.22, this systematic error persists in the ternary system, indicating that the agreement with the viscosities predicted by the model is within the experimental scatter.

5.2.3.5 PbO-K_2O-Na_2O-SiO_2 system

As can be seen from Fig. 5.23, the viscosities of PbO−K_2O−Na_2O−SiO_2 melts predicted by the model are in good agreement with the measurements of Kadogawa and Yamate [111] who used the platinum ball pulling-up method. The viscosity varies nearly linearly as Na_2O is substituted by K_2O at constant mole fractions of SiO_2 and PbO, while the maximum difference between the experimental points and the calculated lines does not exceed 0.5 in the natural logarithm scale.

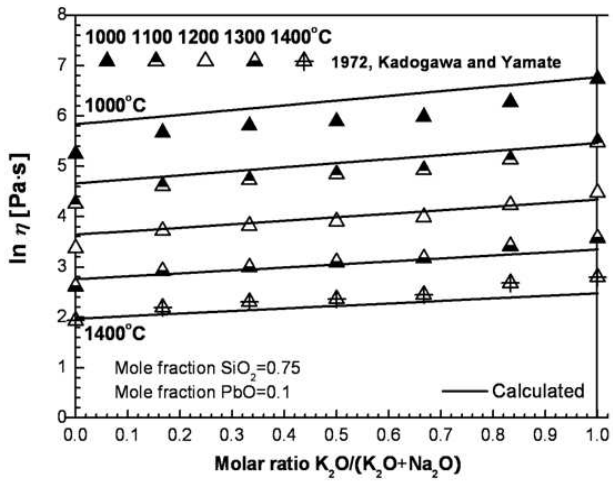

Fig. 5.23 Viscosity of PbO−K_2O−Na_2O−SiO_2 melts at 75 mol% SiO_2 and 10 mol% PbO: experimental points [111] and calculated lines

5.2.4 Melts with Alumina(Al_2O_3)

The viscosities of $PbO–Al_2O_3–SiO_2$ melts were measured [104, 143] at compositions indicated in Fig. 5.24 by the rotating crucible method with Pt–Rh crucibles. These measurements are in good agreement with each other, whereas the results of Sheludyakov et al. [167] are substantially higher and are not used in the present study.

This system exhibits the Charge Compensation Effect which the viscosity model takes into account by assuming that tetrahedrally-coordinated Al which enters the silica network and is charge-compensated by the reaction:

$$2AlO_{1.5} + PbO \rightleftarrows PbAl_2O_4 \tag{5.1}$$

It is further assumed that the $PbAl_2$ "species" have the same effect on the viscosity as two Si atoms. The Gibbs energy of reaction (5.1) was optimized based on the experimental data [104, 143] to be:

$$\Delta \boldsymbol{G}_{PbAl_2O_4} = -14226 - 48953 \boldsymbol{X}_{SiO_2} \ \text{J·mol}^{-1} \tag{5.2}$$

As can be seen from Figs 5.25 to 5.28, the model reproduces very well both the temperature and the composition dependence of the viscosity even though $\Delta G_{PbAl_2O_4}$ is temperature independent. The maxima in the calculated curves near the equimolar PbO/Al_2O_3 ratio are characteristic of the Charge Compensation Effect. Such maxima are observed in all $MO_x–Al_2O_3–SiO_2$ systems studied where M is an alkali or alkali-earth metal.

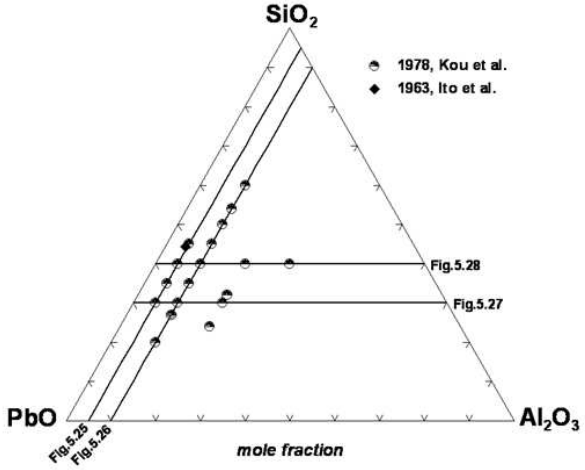

Fig. 5.24 Compositions in the $PbO–Al_2O_3–SiO_2$ system at which the viscosity was measured. [104, 143] Lines show the pseudo-binary sections of this ternary system reported in Figs 5.25 to 5.28

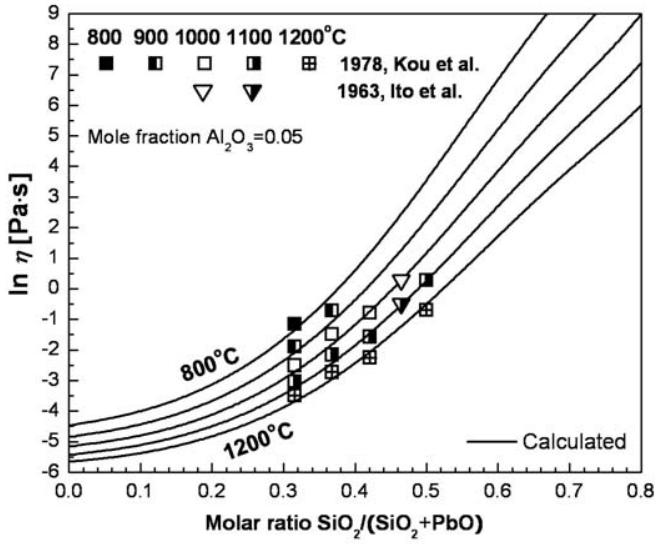

Fig. 5.25 Viscosity of $PbO–Al_2O_3–SiO_2$ melts at 5 mol% Al_2O_3: experimental points [104, 143] and calculated lines

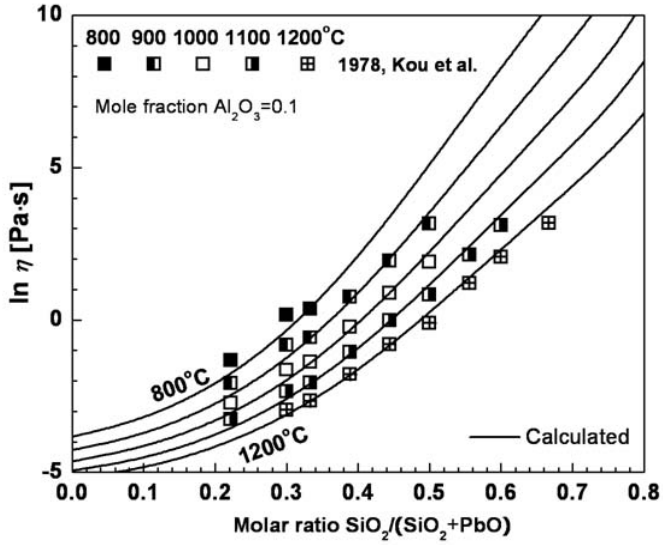

Fig. 5.26 Viscosity of PbO–Al_2O_3–SiO_2 melts at 10 mol% Al_2O_3: experimental points [143] and calculated lines

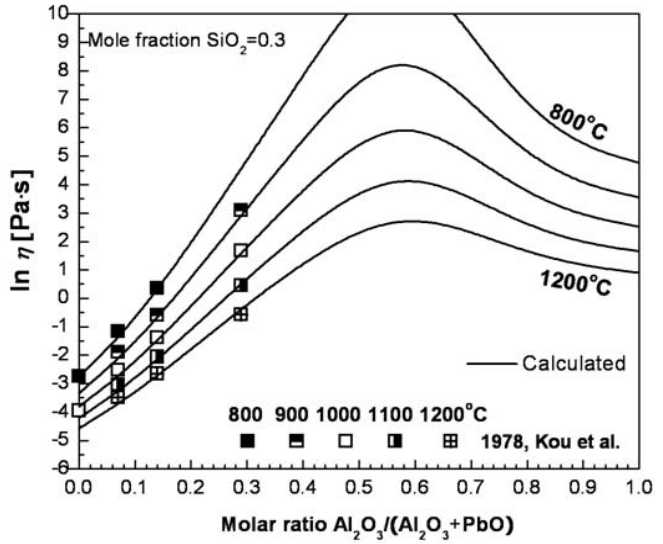

Fig. 5.27 Viscosity of PbO–Al_2O_3–SiO_2 melts at 30 mol% SiO_2: experimental points [143] and calculated lines

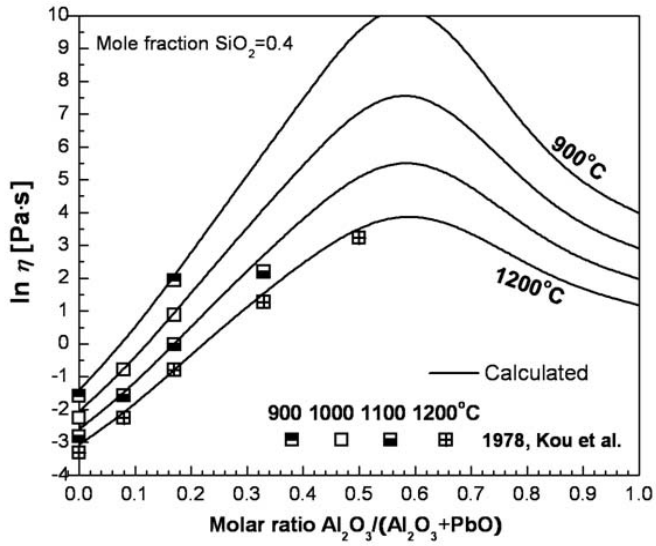

Fig. 5.28 Viscosity of $PbO–Al_2O_3–SiO_2$ melts at 40 mol% SiO_2: experimental points [143] and calculated lines

5.2.5 Melts used in glass technology

A great many viscosity measurements are available for melts of lead crystal glasses. The base composition of lead crystal glasses is close to the relatively small region in the $PbO–K_2O–SiO_2$ system shown in Fig. 5.9. However, additional minor components, such as Na_2O, CaO, MgO and ZnO, are often used to modify the properties of lead crystal glasses, for example to increase chemical resistance or to decrease the melting temperature.

Several regression equations have been proposed specifically to describe the viscosity of melts used in glass technology. In particular, the recent statistical model of Fluegel [67] fits a very large amount of experimental information on melts used in glass technology which is summarized in the SciGlass database [274]. The model is based on multiple regression using polynomial functions and provides a rigorous estimation of errors and validity limits. Fluegel claims that his analysis of systematic differences between laboratories improves the overall accuracy of interpolation [67]. Fluegel's model is most accurate within the limited composition ranges covered by the grid of the experimental points in the vicinity of the commercial glass

compositions since it is calibrated based on numerous experimental data for these regions. However, extrapolations outside these ranges are not possible.

The model developed in the present study, on the other hand, is designed particularly for wide-range extrapolations in composition. No experimental data for multicomponent melts used in glass technology have been used for the calibration of our model which is based solely upon parameters obtained by fitting data for binary and Al_2O_3-containing ternary systems. It is applicable at any composition contrary to the regression equations mentioned above which cannot be extrapolated outside their validity limits. It is interesting to examine how the present model compares with existing regression equations for glasses in their own ranges of validity. Table 5.2 shows the viscosities of typical lead crystal glass melts and the effect of additions of CaO, MgO and ZnO. The experimental data of Lakatos et al. [155] are compared with the viscosities calculated by Fluegel's regression equation [67] and predicted by the present model. The agreement is very good and the accuracy of the present model appears comparable to Fluegel's regression equation.

Lakatos et al. [154] studied the effect of additions of up to 12 wt % PbO on the viscosity of soda-lime-silica melts. These data are also very well reproduced by the present model.

5.3 Conclusions

To calculate the viscosity of PbO-containing silicate melts, only six model parameters related to PbO are required. Two parameters, $\boldsymbol{A}_{\mathrm{PbO}}$ and $\boldsymbol{E}_{\mathrm{PbO}}$, reproduce the viscosity of pure liquid PbO; the other two parameters are fitted to the viscosity of binary PbO–SiO_2 melts; and, finally, two more parameters represent the Gibbs energy, $\Delta \boldsymbol{G}_{\mathrm{PbAl_2O_4}}$, of tetrahedrally-coordinated Al “species” which enter the silica network and are charge-compensated by Pb. The latter two parameters are obtained from the experimental viscosities of PbO–Al_2O_3–SiO_2 melts. The viscosity of other ternary and multicomponent melts containing PbO is then predicted by the model with no additional adjustable model parameters.

To test the model, all experimental viscosity data were collected for melts formed by PbO with SiO_2, Al_2O_3, CaO, MgO, Na_2O and K_2O. To the best of our knowledge, no data are available for subsystems without silica. Although there are some viscosity data for all five ternary sub-systems formed by PbO and SiO_2 with the other oxides, no systematic studies have been

made for higher-order PbO-containing subsystems except for $PbO–Na_2O–K_2O–SiO_2$. The deviation of the available experimental data from the viscosities predicted by the model does not exceed the scatter of experimental points from different authors in the binary systems that were used to calibrate the model. The model predicts the viscosity for melts of lead crystal glasses with the accuracy similar to the accuracy of the regression equations of Fluegel [67] which were fitted to the experimental data over the narrow composition range of these melts.

Table 5.1 Optimized Model parameters for the viscosity expressed in Pa·s

System	Model parameter	Model parameters ($J \cdot mol^{-1}$)
PbO	$A_{Pb} = -8.93$	$E_{PbO} = 33814$
$PbO–SiO_2$		$E^{1,1}_{PbO\text{-}Si} = -155000$ $E^{2,5}_{PbO\text{-}Si} = 2650000$
$PbO–Al_2O_3–SiO_2$		$\Delta G_{PbAl_2O_4} = -14226 - 48953 X_{SiO_2}$

The model parameters for subsystems without PbO that are used for the viscosity calculations in the present study were optimized and reported elsewhere (see Tables 4.1 and 4.2).

Table 5.2 Effect of CaO, MgO and ZnO on the viscosity of a typical lead crystal glass melt. The experimental data of Lakatos et al. [155] are compared with the viscosities calculated by Fluegel's regression equation [67] and predicted by the present model.

SiO_2	PbO	Na_2O	K_2O	CaO	MgO	ZnO	Total	Temperature	Viscosity, ln(Pa•s)		
mass %	mass %	mass %	mass %	mass %	mass %	mass %	mass %	°C	Lakatos et al. [155]	Fluegel [67]	Present model
55.2	28.0	1.9	14.4				99.50	1242.4	3.45	3.39	3.77
52.8	26.6	1.7	13.4			5.2	99.70	1268.2	3.45	3.19 *	3.49
53.9	27.2	1.7	13.8		3.2		99.80	1283.0	3.45	3.47 *	3.27
52.2	25.9	1.5	11.8	8.58			99.98	1190.0	3.45	3.30 *	3.88
55.2	28.0	1.9	14.4				99.50	1024.3	5.76	5.62	6.26
52.8	26.6	1.7	13.4			5.2	99.70	1060.5	5.76	5.28 *	5.74
53.9	27.2	1.7	13.8		3.2		99.80	1075.8	5.76	5.63 *	5.46
52.2	25.9	1.5	11.8	8.58			99.98	1015.1	5.76	5.69 *	5.91
55.2	28.0	1.9	14.4				99.50	876.0	8.06	7.91	8.49
52.8	26.6	1.7	13.4			5.2	99.70	916.9	8.06	7.39 *	7.77
53.9	27.2	1.7	13.8		3.2		99.80	930.7	8.06	7.85 *	7.45
52.2	25.9	1.5	11.8	8.58			99.98	897.8	8.06	8.13 *	7.61

* Compositions slightly outside the validity range of Fluegel's model. [67]

CHAPTER 6 MODELING VISCOSITY OF SILICATE MELTS CONTAINING ZINC OXIDE

6.1 Introduction

Silicate slags containing zinc oxide are formed during pyrometallurgical production. The fuming of zinc from slags is the basis of a number of pyrometallurgical processes used industrially to recover zinc from zinc blast furnace slags and from residues and wastes of other metallurgical operations [108]. Of particular importance is the slag viscosity which quantifies the flow properties of the slag and affects the degree of refractory attack, the amount of entrained metal in the slag, mass transfer at the slag/metal interface and heat transfer through the slag [17]. The viscosity of ZnO-containing oxide melts is also of importance to the glass industry.

In the present study, viscosity data are reviewed for melts formed by ZnO with SiO_2, Al_2O_3, PbO, CaO, MgO, Na_2O and K_2O. A few model parameters are optimized to reproduce the viscosities of ZnO, ZnO-SiO_2 and ZnO-Al_2O_3-SiO_2 melts. Then the available experimental viscosity data for other ternary and higher-order ZnO-containing systems are compared to the viscosities calculated by the model without any additional adjustable model parameters.

6.2 Review of the available viscosity data and calibration of the model

In the present study, viscosity data are reviewed for all ZnO-containing subsystems of the ZnO–SiO_2–Al_2O_3–CaO–MgO–Na_2O–K_2O–PbO system and using the model introduced in Chapter 4 (see Eqs. (4.1)-(4.4)). The data judged to be most reliable are shown in the figures below.

The proposed model is intended for melts. The extension of the model to describe the viscosity of glasses will be reported in Chapters 11 and 12. Therefore, the viscosity data were collected mainly for melts above the liquidus or for slightly supercooled melts where crystallization did not occur. These measurements were mostly made with rotational or vibrational viscometers. Phase equilibrium calculations were carried out using the FactSage thermochemical software and databases [14] to check that the viscosity was indeed measured in a

single-phase liquid region. If an abnormally high viscosity value was reported for a temperature below the liquidus, this was most likely the result of crystallization. Parameters of the model for ZnO-containing melts that were fitted to the experimental viscosity data are listed in Table 6.1. The model parameters for melts without ZnO were shown in Tables 4.1, 4.2 and 5.1.

6.2.1 Viscosities of binary ZnO-SiO_2 melts

Due to the extremely high melting temperature and volatility of ZnO, there are no viscosity data for pure liquid ZnO. The viscosity of ZnO-SiO_2 melts was studied only by Mizoguchi et al. [193] who used a rotational viscometer with Pt crucibles. They only measured two points which are not sufficient to permit us to optimize the viscosity of pure liquid ZnO and to obtain the binary ZnO-SiO_2 parameters.

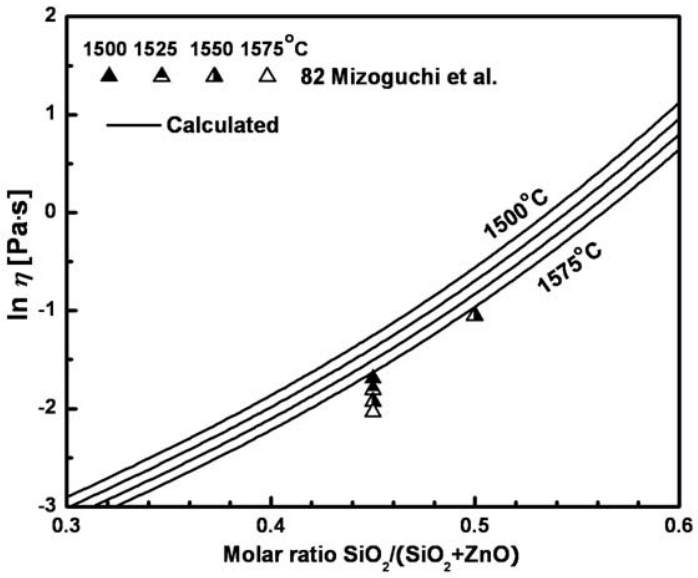

Fig. 6.1 Calculated viscosity of ZnO-SiO_2 melts compared to experimental points [193]

In order to optimize the four model parameters, A_{ZnO}, E_{ZnO}, $E^{1,1}_{ZnO\text{-}Si}$ and $E^{R}_{ZnO\text{-}Si}$, the experimental data for the ZnO-B_2O_3 binary system [27] and for the ZnO-CaO-SiO_2 and ZnO-Na_2O-SiO_2 ternary systems were used simultaneously with the data for the ZnO-SiO_2 binary melts. The optimized model parameters are given in Table 6.1. As can be seen from Fig. 6.1, the

data of Mizoguchi et al. [193] are systematically lower than the viscosity predicted by the model although the difference is relatively small. The agreement is well within experimental error limits.

6.2.2 Ternary Melts without Alumina(Al_2O_3)

The viscosities of the ZnO-CaO-SiO_2 and ZnO-Na_2O-SiO_2 ternary systems were calculated based on the unary and binary viscosity parameters without any additional adjustable parameters.

6.2.2.1 ZnO-CaO-SiO_2 system

The viscosities of ZnO-CaO-SiO_2 melts were measured by a rotational [313] and vibrational [171] viscometer method at molar ratios CaO/SiO_2 = 0.632, 0.67 and 1.0. The data of Sumita et al. [313] are slightly lower than the model calculations because their data for binary CaO-SiO_2 melts are also systematically lower than the best fit of all available data provided by the model. However, the observed decreasing trend of the viscosity with increasing ZnO content is well reproduced.

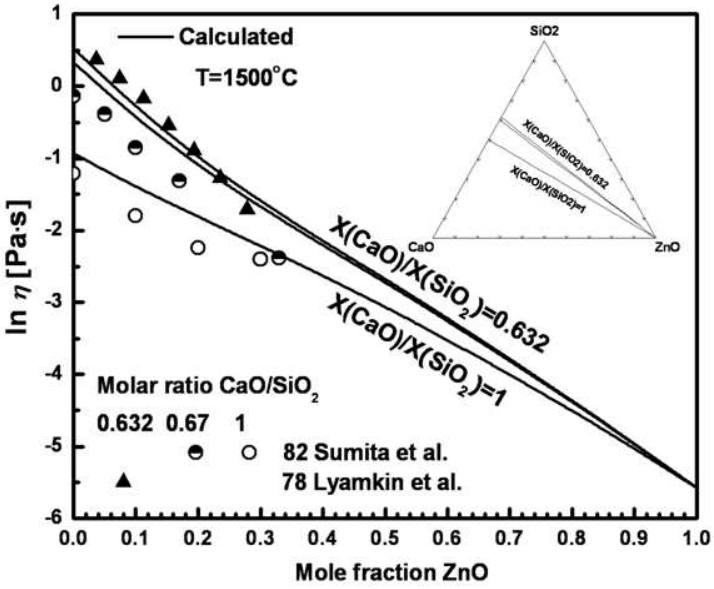

Fig. 6.2 Viscosity of ZnO-CaO-SiO_2 melts at molar ratios CaO/SiO_2 = 0.632, 0.67 and 1.0: experimental points [171, 313] and calculated lines

6.2.2.2 ZnO-Na_2O-SiO_2 system

The viscosities of ZnO-Na_2O-SiO_2 melts were measured with a rotational viscometer [10, 105, 313]. The experimental and calculated viscosities are compared in Figs. 6.4 to 6.6 along the sections shown in Fig. 6.3. As can be seen from these figures, the viscosities of ternary melts are very well described by the model using only the unary and binary parameters. The agreement is well within experimental error limits.

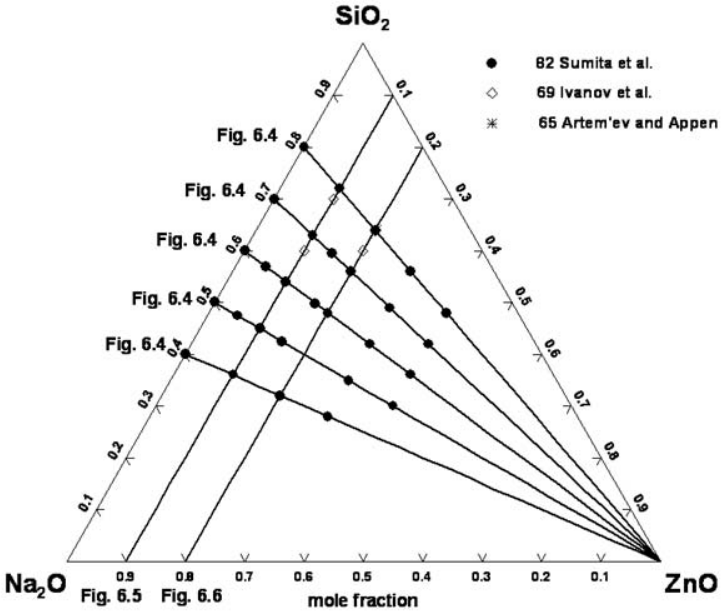

Fig. 6.3 Compositions in the ZnO-Na_2O-SiO_2 system at which experimental viscosity measurements are available [10, 105, 313]. The lines indicate seven sections of this system selected to show the viscosity as a function of composition in Figs. 6.4 to 6.6

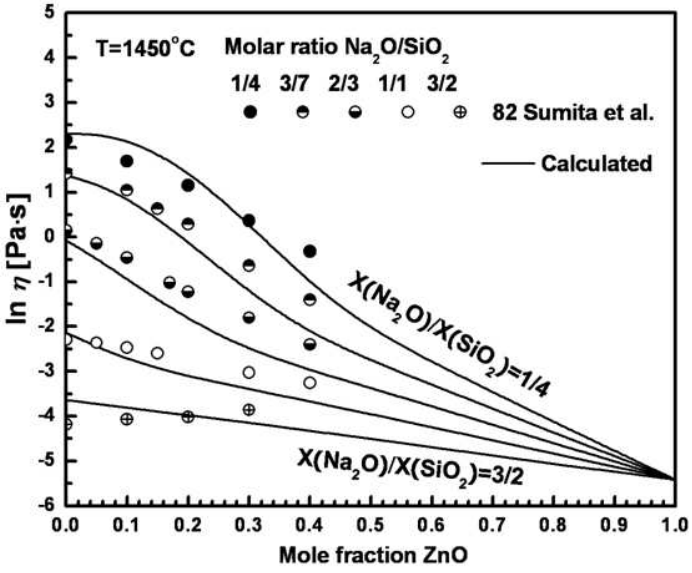

Fig. 6.4 Viscosity of ZnO-Na_2O-SiO_2 melts at molar ratios Na_2O/SiO_2 = 1/4, 3/7, 2/3, 1/1 and 3/2: experimental points [313] and calculated lines

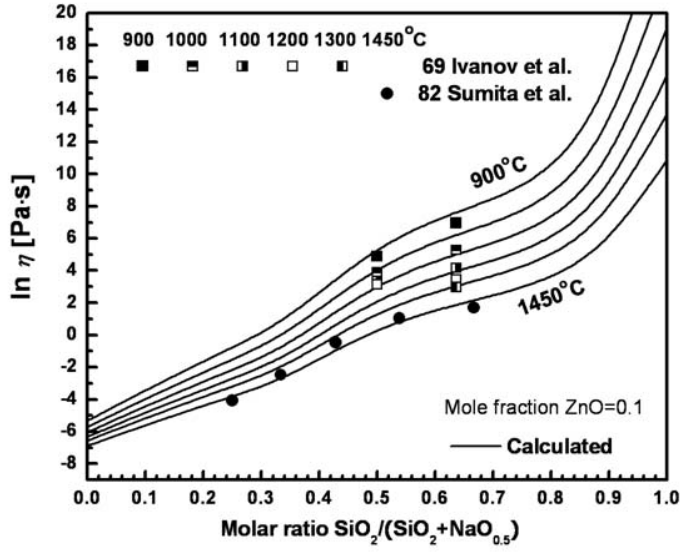

Fig. 6.5 Viscosity of ZnO-Na_2O-SiO_2 melts at 10 mol% ZnO: experimental points [105, 313] and calculated lines

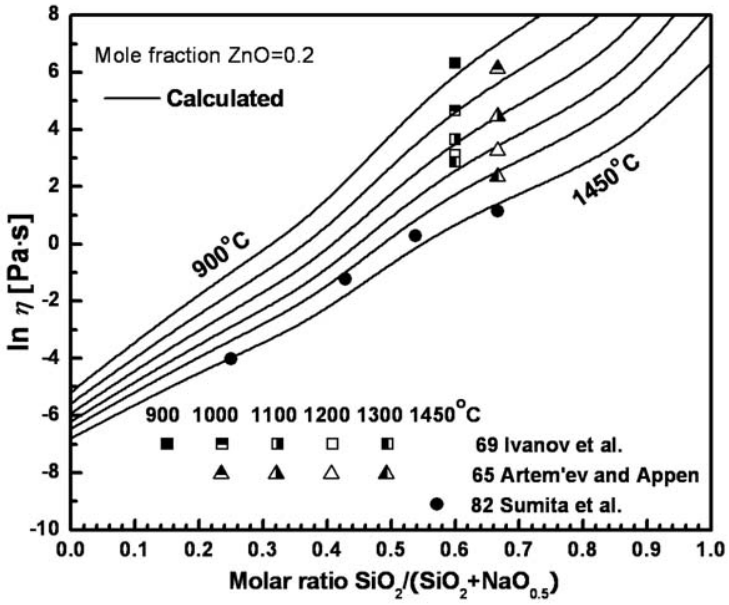

Fig. 6.6 Viscosity of ZnO-Na_2O-SiO_2 melts at 20 mol% ZnO: experimental points [10, 105, 313] and calculated lines

6.2.3 Ternary Melts with Alumina(Al_2O_3)

Viscosities of ZnO-Al_2O_3-SiO_2 melts have been measured at the compositions indicated in Fig. 6.7 by rotational viscometer [193] and vibrational viscometer [287] methods.

This system exhibits the Charge Compensation Effect which the viscosity model takes into account by assuming that tetrahedrally-coordinated Al which enters the silica network and is charge-compensated by Zn is formed by the reaction:

$$2AlO_{1.5} + ZnO \rightleftarrows ZnAl_2O_4 \tag{6.1}$$

It is further assumed that the $ZnAl_2$ "species" have the same effect on the viscosity as two Si atoms. The Gibbs energy of reaction (6.1) was optimized based on the experimental data [193, 287] to be:

$$\Delta G_{ZnAl_2O_4} = 25.5 - 94.5\,X_{SiO_2}\ \text{kJ}\cdot\text{mol}^{-1} \tag{6.2}$$

As can be seen from Figs 6.8 to 6.10, the model reproduces well both the temperature and the composition dependence of the viscosity within experimental error limits even though $\Delta G_{ZnAl_2O_4}$ is temperature independent. The maxima in the calculated curves near the equimolar ZnO/Al_2O_3 ratio are characteristic of the Charge Compensation Effect. Such maxima are observed in all MO_x-Al_2O_3-SiO_2 systems studied where M is an alkali or alkali-earth metal.

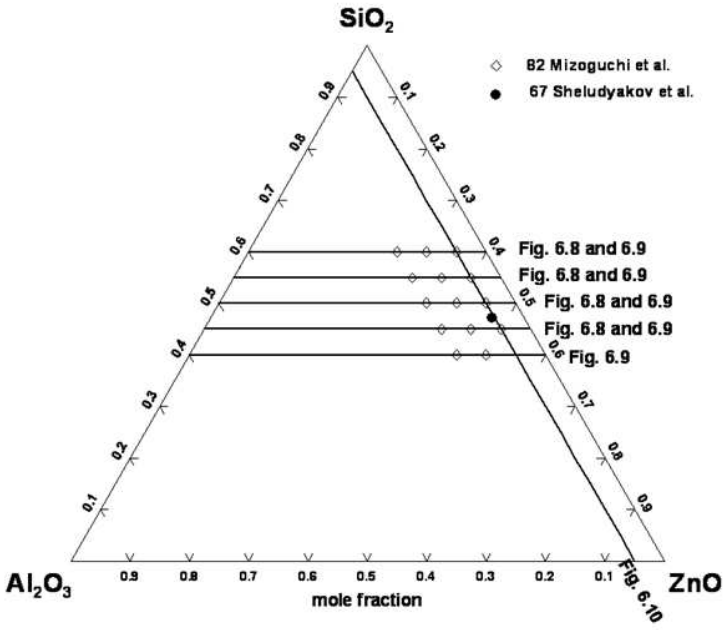

Fig. 6.7 Compositions in the ZnO-Al_2O_3-SiO_2 system at which experimental viscosity measurements are available [193, 287] . The lines indicate four sections of this system selected to show the viscosity as a function of composition in Figs 6.8 to 6.10

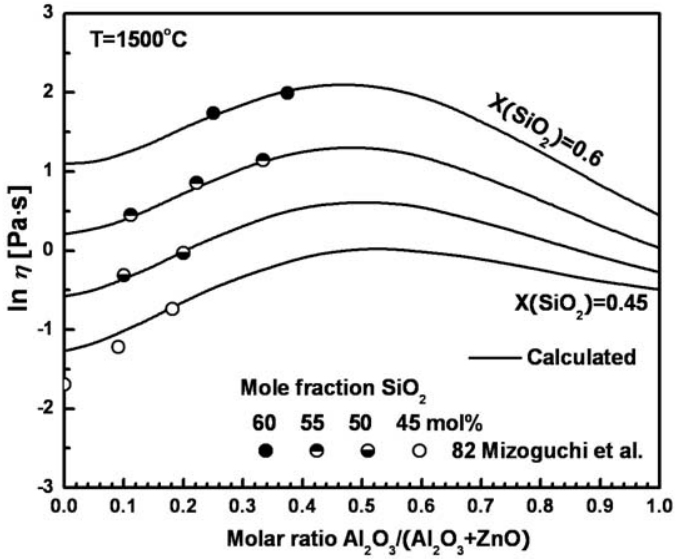

Fig. 6.8 Viscosity of ZnO-Al_2O_3-SiO_2 melts at 45, 50, 55 and 60 mol% SiO_2: experimental points [193] and calculated lines

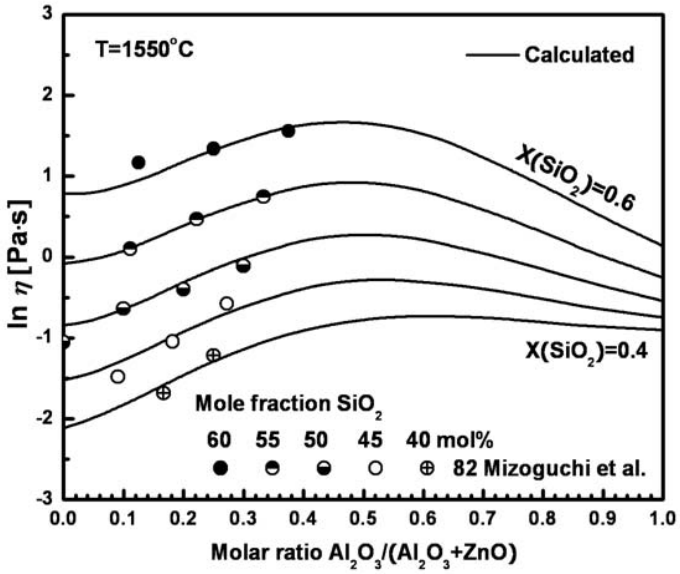

Fig. 6.9 Viscosity of ZnO-Al_2O_3-SiO_2 melts at 40, 45, 50, 55 and 60 mol% SiO_2: experimental points [193] and calculated lines

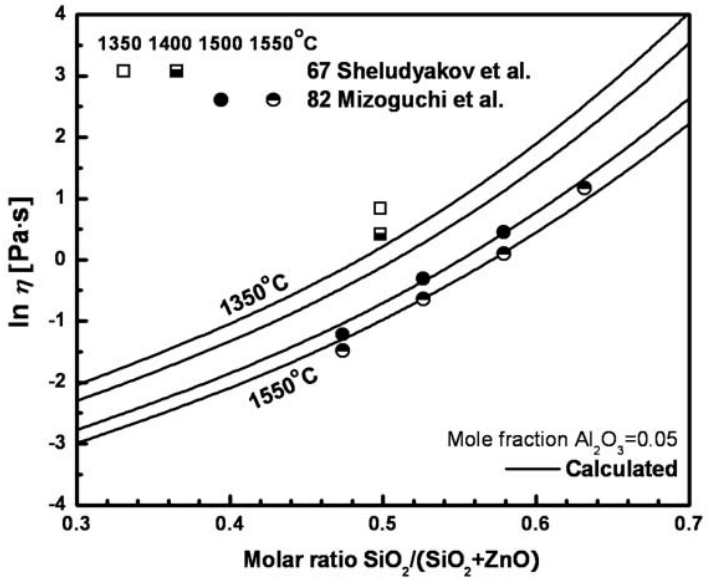

Fig. 6.10 Viscosity of ZnO-Al_2O_3-SiO_2 melts at 5 mol% Al_2O_3: experimental points [193, 287] and calculated lines

6.2.4 Multicomponent systems

6.2.4.1 ZnO-CaO-Al_2O_3-SiO_2 system

Figs 6.11 to 6.13 compare the viscosities of ZnO-CaO-Al_2O_3-SiO_2 melts predicted by the model with all available experimental data [167, 171, 222]. Fig 6.11 shows the predicted viscosities at constant 47.1 mol% SiO_2 and 5.5 mol% Al_2O_3 along with the experimental data of Sheludyakov et al. [167] who used a vibrational viscometer method. Their data for the ternary ZnO-Al_2O_3-SiO_2 system are slightly higher than the calculated lines as was shown in Fig. 6.10 and thus their reported viscosities of ZnO-CaO-Al_2O_3-SiO_2 quaternary melts are also slightly higher although the difference is relatively small.

Ota et al. [222] measured viscosities with additions of ZnO to the CaO-Al_2O_3-SiO_2 system using the counter-balanced sphere method. As can be seen from Fig. 6.12, the experimental data show systematically higher values. However, their data for the ternary CaO-Al_2O_3-SiO_2 system (left-hand edge of Fig. 6.12) also show higher values than the calculated lines,

whereas our previous study [81] showed that our calculations for the $CaO-Al_2O_3-SiO_2$ system are in good agreement with the data of many other authors.

Lyamkin et al. [171], who also reported viscosities in the $ZnO-CaO-SiO_2$ ternary system (Fig. 6.2), measured viscosities using a vibrational viscometer method at constant molar ratio Al_2O_3/SiO_2 = 0.505 and 0.295. As can be seen from Fig. 6.13, the experimental data are systematically higher than the calculated lines although the difference is relatively small. Again, these data are also higher for the $CaO-Al_2O_3-SiO_2$ system, indicating a probable small systematic error. The observed trend of decreasing viscosity with increasing ZnO content is well predicted by the calculations. Overall, the viscosities predicted by the model for $ZnO-CaO-Al_2O_3-SiO_2$ melts are believed to be in agreement with the measurements within experimental error limits.

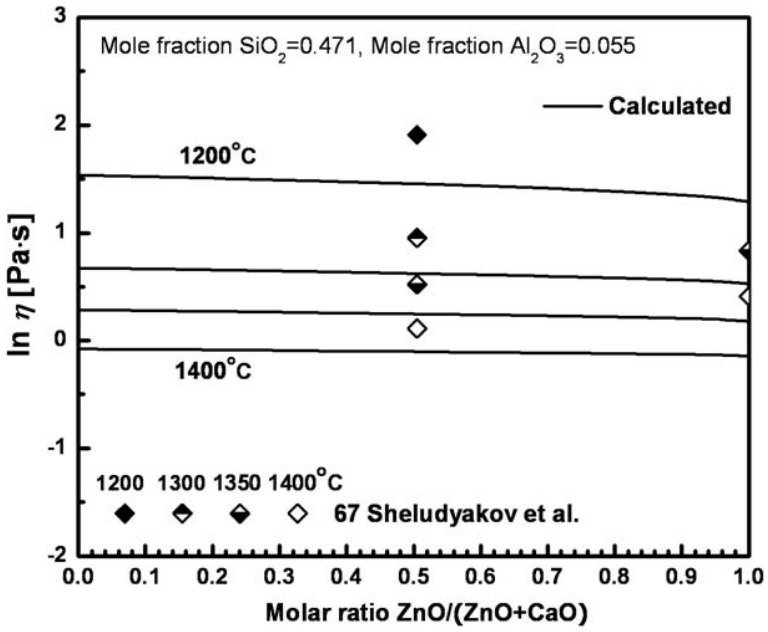

Fig. 6.11 Viscosity of $ZnO-CaO-Al_2O_3-SiO_2$ melts at 47.1 mol% SiO_2 and 5.5 mol% Al_2O_3: experimental points [287] and calculated lines

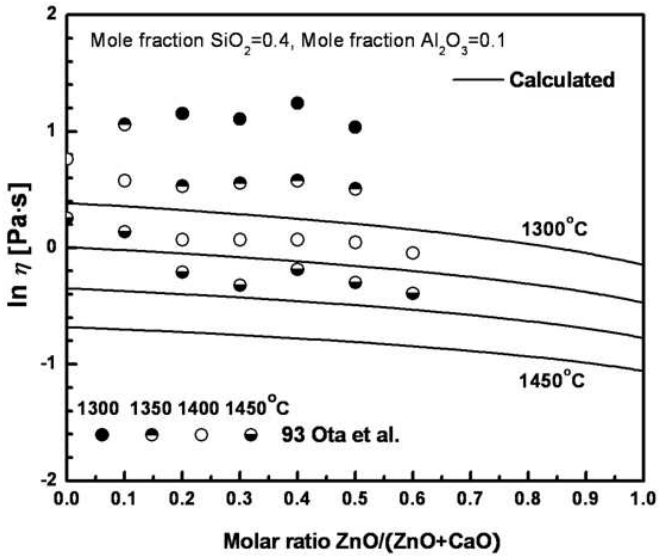

Fig. 6.12 Viscosity of ZnO-CaO-Al_2O_3-SiO_2 melts at 40 mol% SiO_2 and 10 mol% Al_2O_3: experimental points [222] and calculated lines

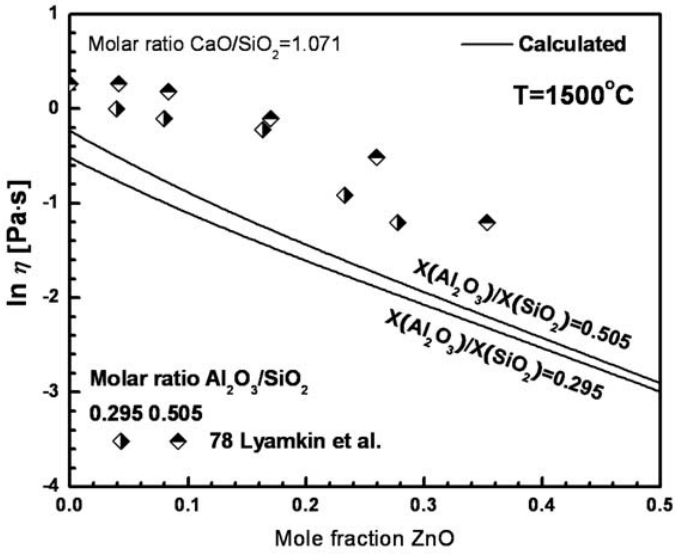

Fig. 6.13 Viscosity of ZnO-CaO-Al_2O_3-SiO_2 melts at molar ratios Al_2O_3/SiO_2 = 0.505 and 0.295 at a constant molar ratio CaO/SiO_2 = 1.071: experimental points [171] and calculated lines.

6.2.4.2 ZnO-CaO-MgO-Na_2O-K_2O-SiO_2 system

Fig. 6.14 compares the viscosities of ZnO-CaO-MgO-Na_2O-K_2O-SiO_2 melts predicted by the model with the measurements of Fromberg et al. [70] who used a rotational viscometer for melts and the fiber-elongation method for glasses. In the present study, only the viscosities measured for the melts are considered. As can be seen from Fig. 6.14, the viscosities of the melts are very well predicted by the model from only the unary and binary parameters. In particular, the composition dependence predicted by the model is in good agreement with the experiments

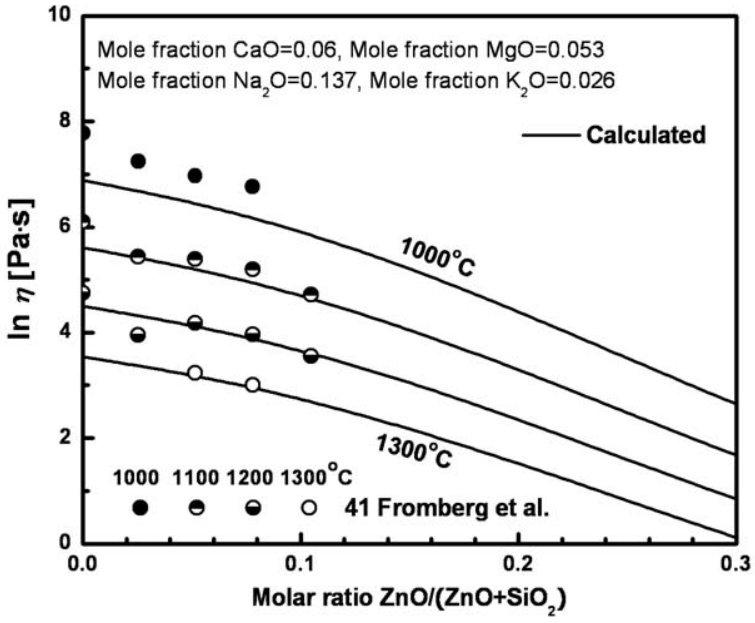

Fig. 6.14 Viscosity of ZnO-CaO-MgO-Na_2O-K_2O-SiO_2 melts at 6 mol% CaO, 5.3 mol% MgO, 13.7 mol% Na_2O and 2.6 mol% K_2O: experimental points [70] and calculated lines

6.2.4.3 ZnO-CaO-MgO-Na_2O-K_2O-Al_2O_3-TiO_2-SiO_2 system

Kawamoto [121] measured the viscosity of ZnO-CaO-MgO-Na_2O-K_2O-Al_2O_3-TiO_2-SiO_2 melts using a rotational viscometer method. As can be seen from Fig. 6.15, the viscosities of the melts are very well predicted by the model from the unary and binary parameters. The maximum difference of 0.4 in the natural logarithm scale is certainly within experimental error limits.

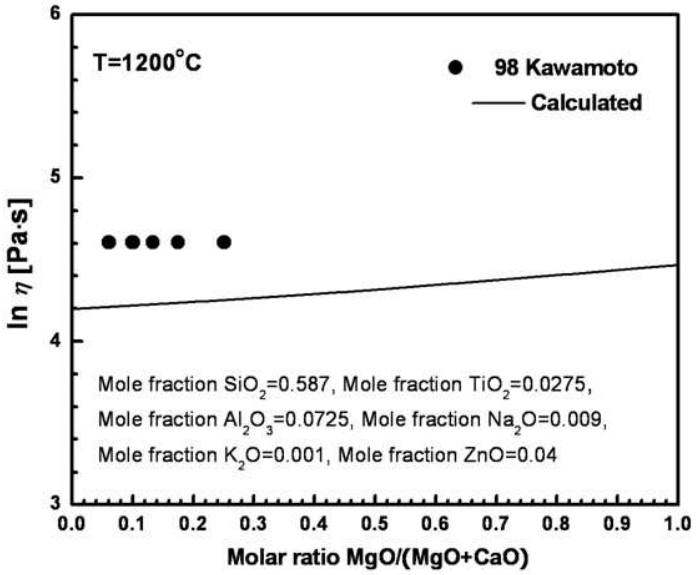

Fig. 6.15 Viscosity of ZnO-CaO-MgO-Na_2O-K_2O-Al_2O_3-TiO_2-SiO_2 melts at 58.7 mol% SiO_2, 2.75 mol% TiO_2, 7.25 mol% Al_2O_3, 0.9 mol% Na_2O and 0.1 mol% K_2O and 4 mol% ZnO: experimental points [121] and calculated lines

6.2.5 Melts used in glass technology

Lakatos et al. studied the effect of ZnO on the viscosity for melts of soda-lime-silica [151] and lead crystal [155] glasses. These data are compared with the viscosities predicted by the present model in Table 6.2.

Several regression equations have been proposed that fit numerous experimental data on the viscosity of melts used in glass technology. In particular, the recent statistical model of Fluegel [67] fits a very large amount of experimental information on melts used in glass technology which is summarized in the SciGlass database [274]. The model provides a rigorous estimation of errors and validity limits. It is obtained by multiple regression analysis using polynomial functions and is most accurate in the vicinity of the commercial glass compositions since it is calibrated based on numerous experimental data for these regions. The viscosities calculated by this model are also given in Table 6.2.

The model developed in the present study, on the other hand, is designed particularly for wide-range extrapolations in composition. No experimental data for multicomponent glass melts have been used for the calibration of our model which is based solely upon parameters obtained by fitting data for binary and ternary systems. The experimental data for multicomponent melts used in glass technology have not been used for the calibration of our model. It is applicable at any composition contrary to the regression equations mentioned above which normally cannot be extrapolated outside their validity limits. As can be seen from Table 6.2, the present model provides a very good prediction of the variation of the viscosity with addition of ZnO to soda-lime-silica and lead crystal melts. This prediction is no worse than calculations using the regression equation [67] which was calibrated based on the experimental viscosity data for melts used in glass technology.

6.3 Conclusions

To calculate the viscosity of ZnO-containing silicate melts, only 6 model parameters related to ZnO are required. Two parameters, A_{ZnO} and E_{ZnO}, describe the viscosity of pure liquid ZnO; two binary parameters, $E^{1,1}_{\mathrm{ZnO\text{-}Si}}$ and $E^{R}_{\mathrm{ZnO\text{-}Si}}$, describe the viscosity of ZnO-SiO_2 melts; and, finally, two more parameters represent the Gibbs energy, $\Delta G_{\mathrm{ZnAl_2O_4}}$, of tetrahedrally-coordinated Al "species" which enter the silica network and are charge-compensated by Zn. The latter two parameters are obtained from the experimental viscosities of ZnO-Al_2O_3-SiO_2 melts. The viscosity of multicomponent melts containing ZnO is then predicted by the model without any additional adjustable model parameters.

To test the model, all experimental viscosity data were collected for melts formed by ZnO with SiO_2, Al_2O_3, CaO, MgO, Na_2O, K_2O and PbO. The deviation of the available experimental data from the viscosities predicted by the model does not exceed the scatter of experimental points among different authors in all binary and ternary sub-systems of ZnO–SiO_2–Al_2O_3–CaO–MgO–Na_2O–K_2O–PbO that were used to calibrate the model. In particular, the model predicts the viscosity of multicomponent ZnO-containing soda-lime-silica and lead crystal melts with the accuracy similar to the accuracy of the regression equations which were fitted to the experimental data over the narrow composition ranges of these melts.

Table 6.1 Optimized Model parameters for the viscosity expressed in Pa·s

System	Model parameter	Model parameters ($J \cdot mol^{-1}$)
ZnO	$A_{ZnO} = -11$	$E_{ZnO} = 80000$
$ZnO\text{-}SiO_2$		$E^{1,1}_{ZnO\text{-}Si} = -18677$ $E^{R}_{ZnO\text{-}Si} = 95000$
$ZnO\text{-}Al_2O_3\text{-}SiO_2$		$\Delta G_{ZnAl_2O_4} = 25500 - 94500 X_{SiO_2}$

The model parameters for subsystems without ZnO that are used for the viscosity calculations in the present study were optimized and reported elsewhere (see Tables 4.1, 4.2 and 5.1).

Table 6.2 Effect of ZnO on the viscosity of soda-lime-silica and lead crystal glass melts. The experimental data of Lakatos et al. [151, 155] are compared with viscosities calculated by Fluegel's regression equation [67] and predicted by the present model.

Temp.	SiO_2	Al_2O_3	CaO	Na_2O	K_2O	PbO	ZnO	Viscosity, ln(Pa·s)		
°C	mass %	mass %	mass %	mass %	mass %	mass %	mass %	Lakatos [151, 155]	Fluegel [67]	Present model
soda-lime-silica glass melts										
1416.1	72.41	1.23	12.17	14.19			0	2.30	2.42	2.75
1007.4	72.41	1.23	12.17	14.19			0	6.91	7.11	7.04
1417.8	70.39	1.19	9.85	13.8			4.77	2.30	2.48*	2.70
1006.7	70.39	1.19	9.85	13.8			4.77	6.91	7.25*	7.00
1437.3	69.36	1.18	6.47	13.59			9.39	2.30	2.53*	2.60
1017.2	69.36	1.18	6.47	13.59			9.39	6.91	7.31*	6.90
lead crystal glass melts										
1321.0	62.1			2.9	10.8	23.5	0	3.45	3.49	3.44
1079.7	62.1			2.9	10.8	23.5	0	5.76	5.91	5.99
916.8	62.1			2.9	10.8	23.5	0	8.06	8.39	8.31
1333.7	61.2			2.7	10.7	23.1	1.8	3.45	3.39	3.37
1099.0	61.2			2.7	10.7	23.1	1.8	5.76	5.71	5.81
938.5	61.2			2.7	10.7	23.1	1.8	8.06	8.07	8.02
1268.0	54.3			1.9	13.4	27.1	2.6	3.45	3.24	3.56
1050.3	54.3			1.9	13.4	27.1	2.6	5.76	5.43	5.96
904.7	54.3			1.9	13.4	27.1	2.6	8.06	7.59	8.06
1268.2	52.8			1.7	13.4	26.6	5.2	3.45	3.19*	3.49
1060.5	52.8			1.7	13.4	26.6	5.2	5.76	5.28*	5.74
916.9	52.8			1.7	13.4	26.6	5.2	8.06	7.39*	7.77

* Compositions slightly outside the validity range of Fluegel's model [67].

CHAPTER 7 MODELING VISCOSITY OF SILICATE MELTS CONTAINING MANGANESE OXIDE

7.1 Introduction

Viscosity is one of the key properties of slags which influence the performance of pyrometallurgical processes in many ways. Manganese is added to all commercial steels to deoxidize it and to combine with sulfur to form globular MnS. In the blast furnace process of ironmaking and steelmaking, the control of the viscosity of slags containing MnO is very important for stable mass transfer at the slag/metal interface and heat transfer through the slag. Because of these important reasons, the viscosity of slags containing MnO has been investigated by many groups.

In the present study, viscosity data are reviewed for melts formed by MnO with SiO_2, Al_2O_3, CaO, MgO, Na_2O and K_2O. A few model parameters are optimized to reproduce the viscosities of MnO, MnO-SiO_2 and MnO-Al_2O_3-SiO_2 melts. Then the available experimental viscosity data for other ternary and higher-order MnO-containing systems are compared to the viscosities calculated by the model without using any additional adjustable model parameters.

7.2 Review of the available viscosity data and calibration of the model

In the present study, viscosity data are reviewed for all MnO-containing subsystems of the MnO–SiO_2–Al_2O_3–CaO–MgO–Na_2O–K_2O system and using the model introduced in Chapter 4 (see Eqs. (4.1)-(4.4)). The data judged to be most reliable are shown in the figures below.

The proposed model is intended for melts. The extension of the model to describe the viscosity of glasses will be reported in Chapters 11 and 12. Therefore, the viscosity data were collected mainly for melts above the liquidus or for slightly supercooled melts where crystallization did not occur. These measurements were mostly made with rotational or vibrational viscometers. Phase equilibrium calculations were carried out using the FactSage thermochemical software and databases [14] to check that the viscosity was indeed measured in a single-phase liquid region. If an abnormally high viscosity value was reported for a temperature

below the liquidus, this was most likely the result of crystallization. Parameters of the model for MnO-containing melts that were fitted to the experimental viscosity data are listed in Table 7.1. The model parameters for melts without MnO were shown in Tables 4.1, 4.2, 5.1 and 6.1.

7.2.1 Viscosities of binary $MnO\text{-}SiO_2$ melts

Due to the extremely high melting temperature of MnO, no viscosity measurements exist. The system $MnO\text{-}SiO_2$ has been investigated by several groups as shown in Fig. 7.1. The viscosity of the $MnO\text{-}SiO_2$ system were measured using the rotating crucible method with Pt-Rh crucibles [275, 335, 353] and Mo crucibles [187] under Ar gas atmosphere to keep the reduced atmosphere. Rait et al. [248] measured the viscosity of the $MnO\text{-}SiO_2$ system using the logarithmic decrement method with Mo crucibles and spindles under reducing atmosphere. As shown in Fig. 7.1, most data points show a good agreement with the calculated lines except for the data of Rait et al. [248]. The data of Rait et al. show higher values than other data at all temperatures. The data were measured by the logarithmic decrement method which requires information of the density data of the liquid sample for viscosity measurements. This can contribute to a large error sources for the viscosity measurements. Except for the data points of Rait et al. [248], all available viscosity data of $MnO\text{-}SiO_2$ system were used to obtain the unary and binary parameters A_{MnO}, E_{MnO}, $E^{1,1}_{\mathrm{MnO\text{-}Si}}$ and $E^{R}_{\mathrm{MnO\text{-}Si}}$. The parameter $E^{Ring}_{\mathrm{MnO\text{-}Si}}$ was not necessary for the $MnO\text{-}SiO_2$ system and was set equal to 0.

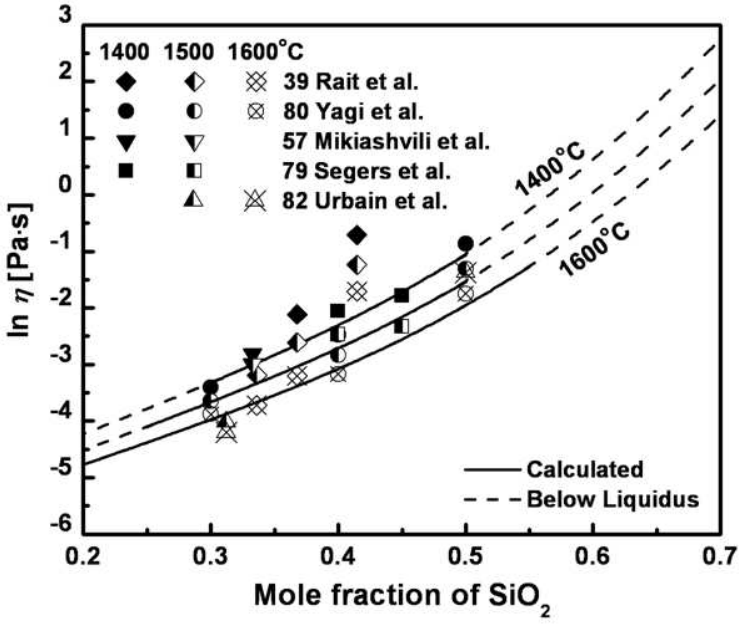

Fig. 7.1 Viscosity of MnO-SiO_2 system compared to experimental data at 1400,1500 and 1600°C [187, 248, 275, 335, 353]

7.2.2 Ternary Melts without Alumina(Al_2O_3)

The viscosities of ternary melts without Al_2O_3 were predicted by the model based on the unary and binary viscosity parameters without any additional adjustable parameters.

7.2.2.1 MnO-CaO-SiO_2 system

Viscosities of MnO-CaO-SiO_2 melts have been measured at the compositions indicated in Fig. 7.2. Figs 7.3-7.9 show the calculated viscosity of the MnO-CaO-SiO_2 system compared to experimental data measured by Segers et al. [275], Mikiashvili et al. [186], Sridhar et al. [304] and Kawahara et al. [118] using the rotating crucible method. In Figs 7.3-7.4, the viscosities are predicted at 30 and 40 mol% MnO. The data of Segers et al. [275] and Kawahara et al. [118] show slightly lower values than the predicted lines. However, the temperature dependence and the curvature trend of the data points with increasing SiO_2 contents show a good agreement with the predicted lines at all temperatures. It seems that the viscosity model shows a good relation with the all experimental data within the experimental error limits.

In Figs 7.5-7.7, the viscosities are predicted at 40, 45 and 50 mol% SiO_2. Most data points except the data of Mikiashvili et al. [186] show good agreement with the predicted lines at all temperatures within the experimental error limits. The data of Mikiashvili et al. [186] were most likely measured below the liquidus. The authors reported that they observed a solid crystalline phase during the experiment. This could contribute to the higher viscosities during the viscosity measurements as shown in Figs 7.5-7.7. As shown in Figs 7.5-7.7, the data points show a good linearity as a function of molar basic oxides. The assumption that $\ln(\eta)$ of the ternary system can be simply calculated from a linear combination of parameters A and E of the binary systems as seen in Eqs. (4.2)-(4.3) leads to a very good representation of the experimental data.

In Figs 7.8-7.9, the viscosities are predicted for molar ratios SiO_2/CaO = 1 and 1.5. As shown Figs 7.8-7.9, the data points of Kawahara et al. [118] show slightly lower values. However, the decreasing curvature trend of the data points with increasing MnO contents shows a quite good relation with the predicted lines at all temperatures. Mikiashvili et al. [186] also show higher values than other authors. The crystallization of the sample was reported during viscosity measurement [186] and it would lead to higher apparent viscosities.

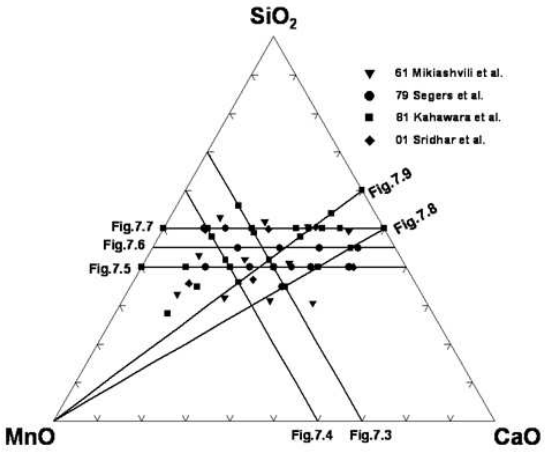

Fig. 7.2 Compositions in the MnO-CaO-SiO_2 system at which experimental viscosity measurements are available [118, 186, 275, 304]. The lines indicate seven sections of this system selected to show the viscosity as a function of composition in Figs 7.3 to 7.9

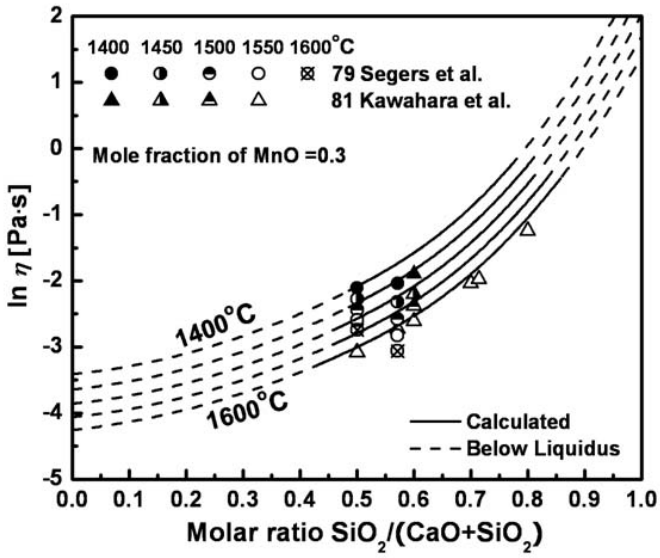

Fig. 7.3 Viscosity of MnO-CaO-SiO_2 melts at 30 mol% MnO compared to experimental data [118, 275]

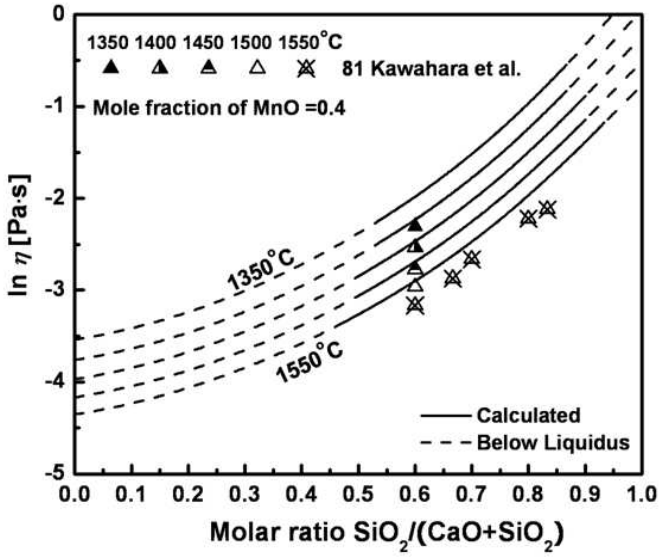

Fig. 7.4 Viscosity of MnO-CaO-SiO_2 melts at 40 mol% MnO compared to experimental data [118]

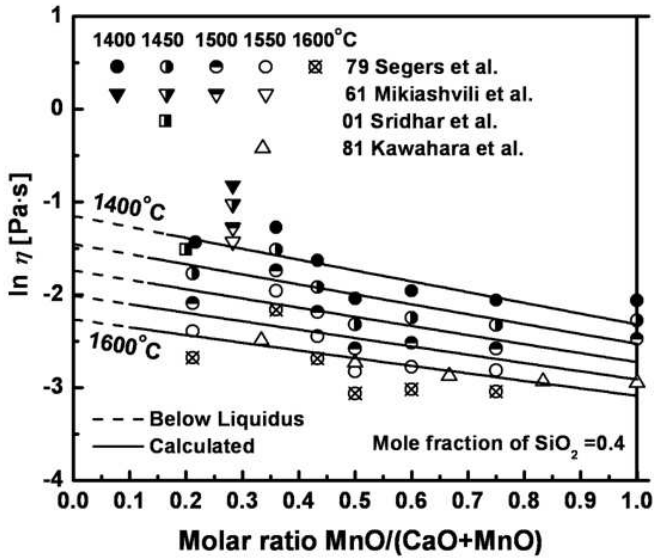

Fig. 7.5 Viscosity of MnO-CaO-SiO_2 melts at 40 mol% SiO_2 compared to experimental data [118, 186, 275, 304]

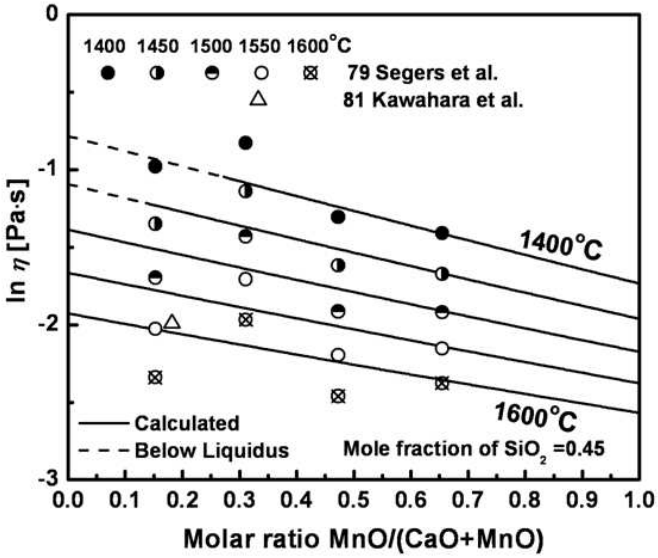

Fig. 7.6 Viscosity of MnO-CaO-SiO_2 melts at 45 mol% SiO_2 compared to experimental data [118, 275]

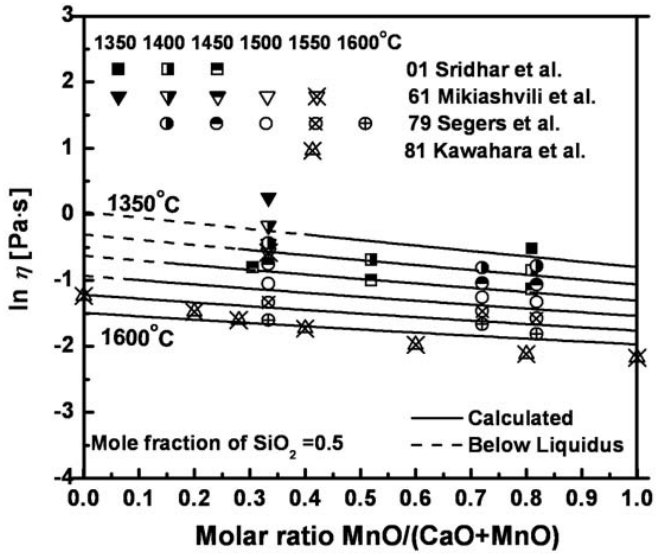

Fig. 7.7 Viscosity of MnO-CaO-SiO_2 melts at 50 mol% SiO_2 compared to experimental data [118, 186, 275, 304]

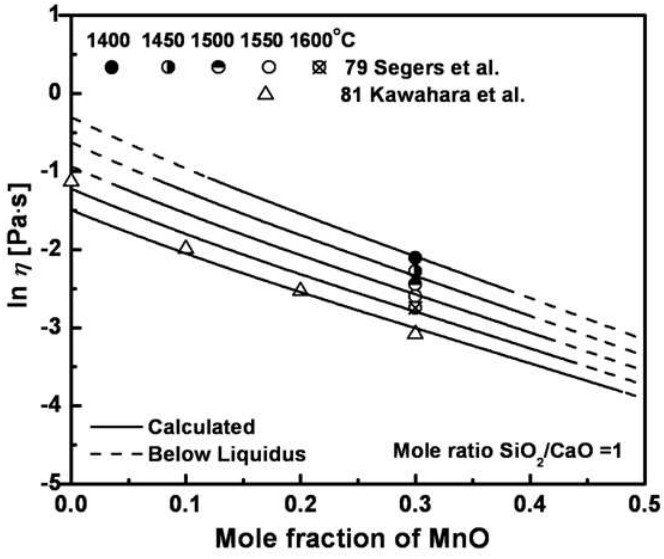

Fig. 7.8 Viscosity of MnO-CaO-SiO_2 melts for a molar ratio SiO_2/CaO = 1 compared to experimental data [118, 275]

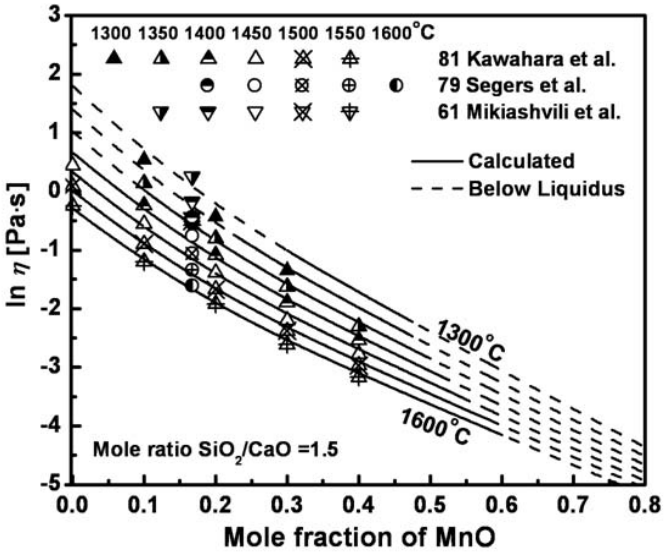

Fig. 7.9 Viscosity of MnO-CaO-SiO_2 melts for a molar ratio SiO_2/CaO = 1.5 compared to experimental data [118, 186, 275]

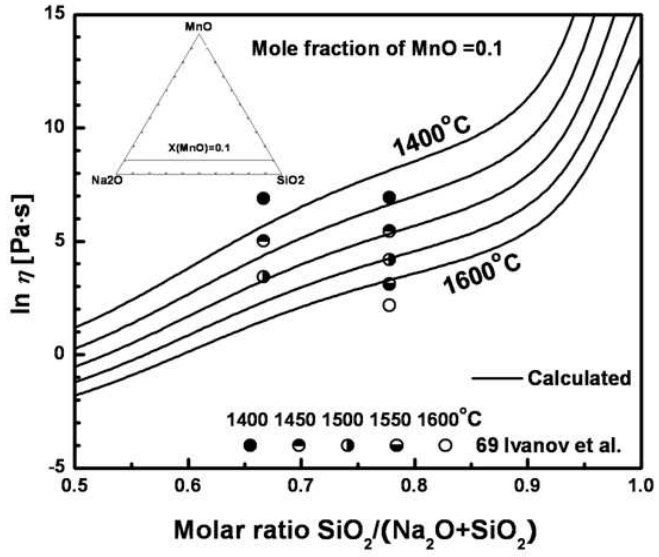

Fig. 7.10 Viscosity of MnO-Na_2O-SiO_2 melts at 10 mol% MnO compared to experimental data [105]

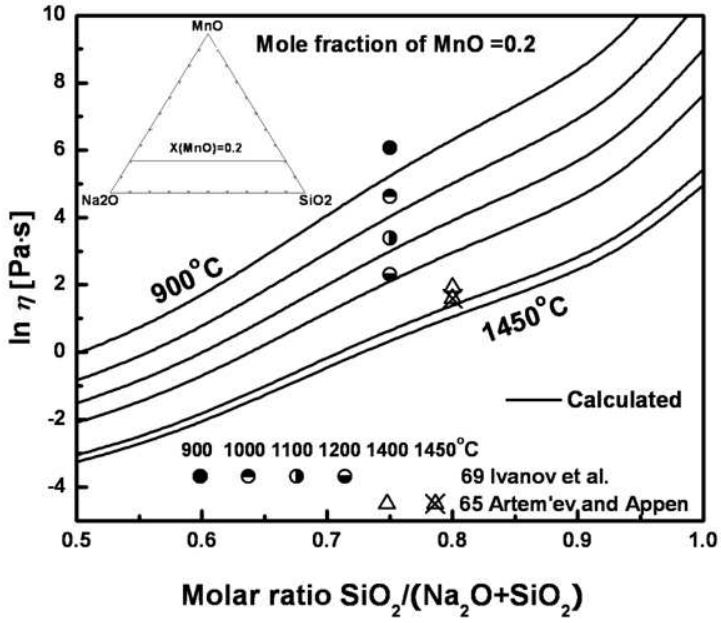

Fig. 7.11 Viscosity of MnO-Na_2O-SiO_2 melts at 20 mol% MnO compared to experimental data [10, 105]

7.2.2.2 MnO-Na_2O-SiO_2 system

Figs 7.10 and 7.11 show the calculated viscosity of the MnO-Na_2O-SiO_2 system compared to experimental data measured by Ivanov et al. [105] and Artem'ev and Appen [10] using the rotating crucible method with Pt crucibles. All data points show a reasonable relation at all temperatures within the experimental error limits.

7.2.3 Ternary Melts with Alumina(Al_2O_3)

The only adjustable parameters required to model the viscosity of the ternary systems containing $AlO_{1.5}$ are the values of ΔG^o as shown in Eqs. (3.40)-(3.43). Only the values of $\Delta G^o_{MnAl_2O_4}$ for the reaction of Eq.(7.1) were optimized in this study as shown in Table 7.1. The other values were taken from Tables 4.1, 4.2, 5.1 and 6.1, and used to predict the viscosity of multi-component systems containing alumina.

$$2AlO_{1.5} + MnO \rightleftarrows MnAl_2O_4 \quad (7.1)$$

Figs 7.13-7.21 show the calculated viscosity of the MnO-Al_2O_3-SiO_2 system compared to experimental data [118, 143, 187, 335]. Mikiashvili et al. [187], Urbain et al. [335] and Kawahara et al. [118], who also measured the system MnO-SiO_2, measured the viscosity using the rotating crucible method with Mo [187] and Pt-Rh crucibles [118, 335]. Kou et al. [143] measured viscosities of the MnO-Al_2O_3-SiO_2 system using the rotating crucible method with Pt-Rh crucibles. The calculated viscosity is compared to the experimental data as shown in Figs 7.13-7.21. Several data points can be identified that were measured below the liquidus temperature and consequently show abnormally high viscosities. Except for those data points, the calculated lines show an excellent relation with most of the data points at all temperatures even though the optimized parameters of $\Delta G^o_{MnAl_2O_4}$ have no temperature dependence.

In Figs 7.13-7.17, the viscosities are predicted at 30, 40, 50, 60 and 76 mol% SiO_2. Most data points except for the data of Mikiashvili et al. [187] show a good agreement with the predicted lines at all temperatures within the experimental error limits. As shown in Figs 7.13-7.15, the data points of Mikiashvili et al. [187] in the MnO-Al_2O_3-SiO_2 system show a narrower temperature dependence than other data. Their data, as shown in Fig. 7.1, also show narrower temperature dependence in the MnO-SiO_2 system, indicating a systematic experimental error.

In Fig.7.18, the viscosity is predicted at the molar ratio of $Al_2O_3/MnO = 1$. All data points show a good agreement with the predicted lines at all temperatures. In Figs 7.19-7.21, the viscosity is predicted at 10, 20 and 30 mol% Al_2O_3. Again, the data points of Mikiashvili et al.[187] show a narrower temperature dependence than other data. Some of the data points of Mikiashvili et al. [187] show abnormally higher viscosities which could be due to partial crystallization of the samples.

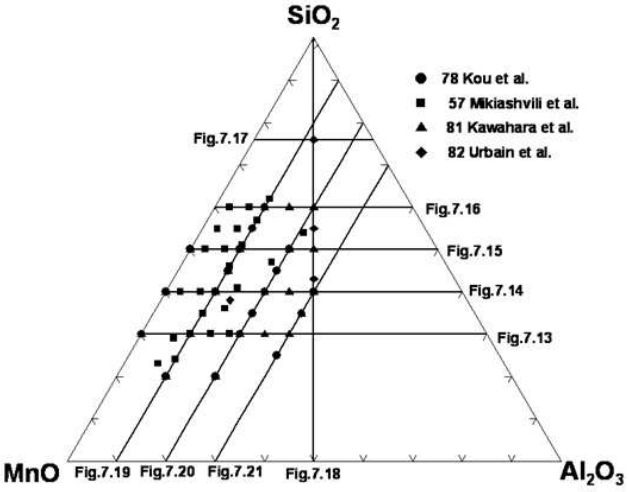

Fig. 7.12 Compositions in the $MnO\text{-}Al_2O_3\text{-}SiO_2$ system at which experimental viscosity measurements are available [118, 143, 187, 335]. The lines indicate nine sections of this system selected to show the viscosity as a function of composition in Figs 7.13 to 7.21

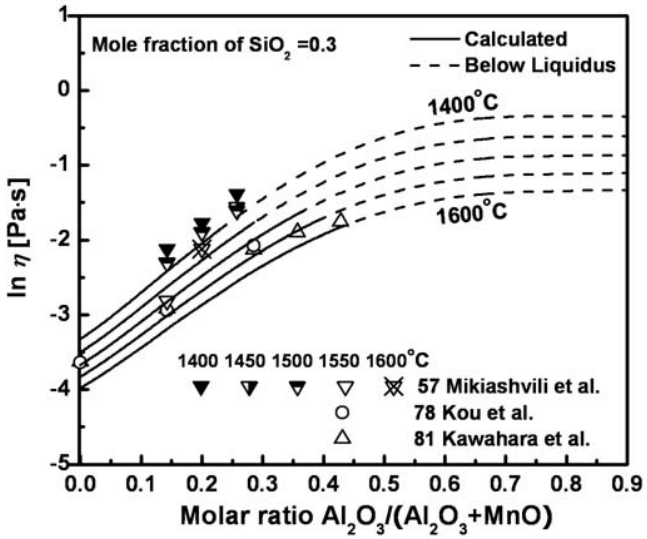

Fig. 7.13 Viscosity of $MnO\text{-}Al_2O_3\text{-}SiO_2$ melts at 30 mol% SiO_2 compared to experimental data [118, 143, 187]

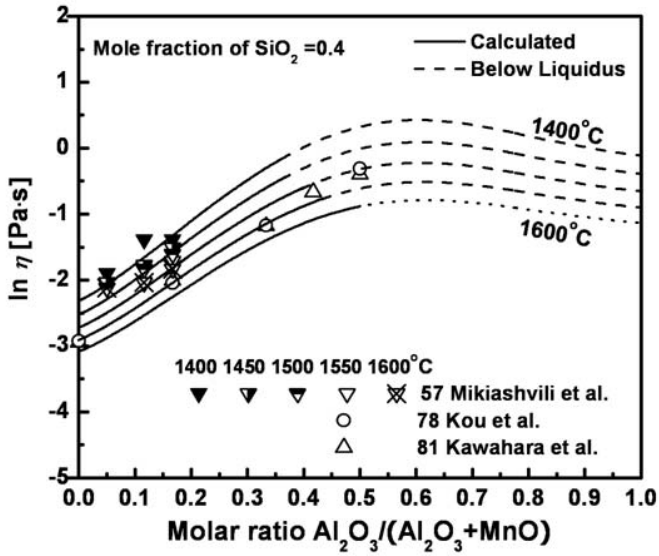

Fig. 7.14 Viscosity of MnO-Al_2O_3-SiO_2 melts at 40 mol% SiO_2 compared to experimental data [118, 143, 187]

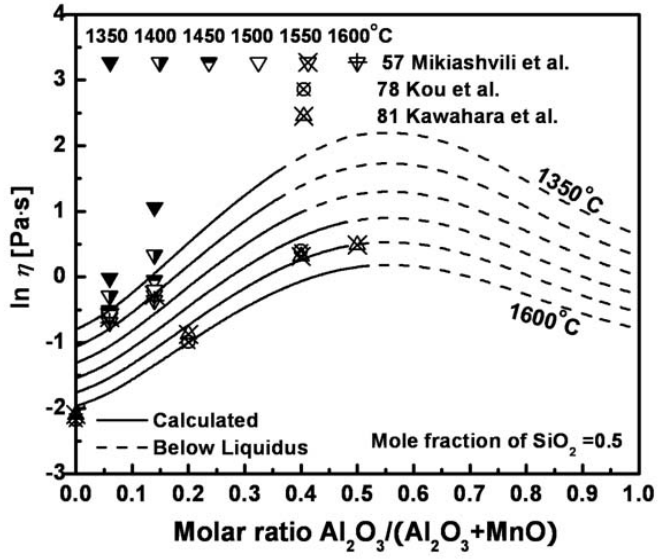

Fig. 7.15 Viscosity of MnO-Al_2O_3-SiO_2 melts at 50 mol% SiO_2 compared to experimental data [118, 143, 187]

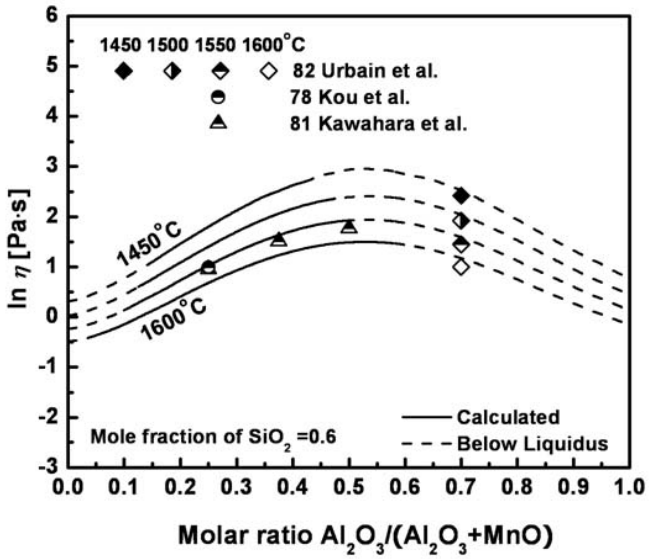

Fig. 7.16 Viscosity of MnO-Al_2O_3-SiO_2 melts at 60 mol% SiO_2 compared to experimental data [118, 143, 335]

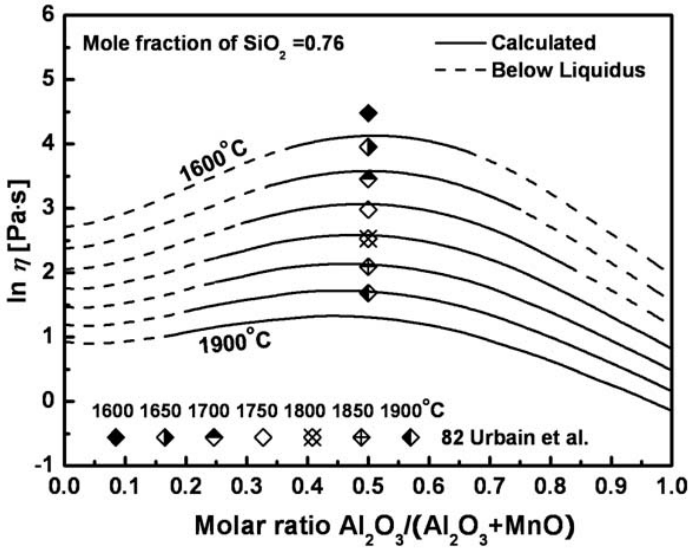

Fig. 7.17 Viscosity of MnO-Al_2O_3-SiO_2 melts at 76 mol% SiO_2 compared to experimental data [335]

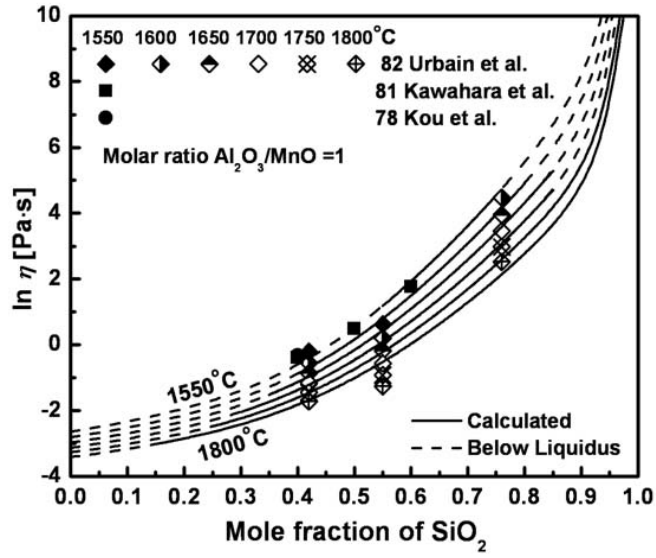

Fig. 7.18 Viscosity of MnO-Al_2O_3-SiO_2 melts for a molar ratio Al_2O_3/MnO = 1 compared to experimental data [118, 143, 335]

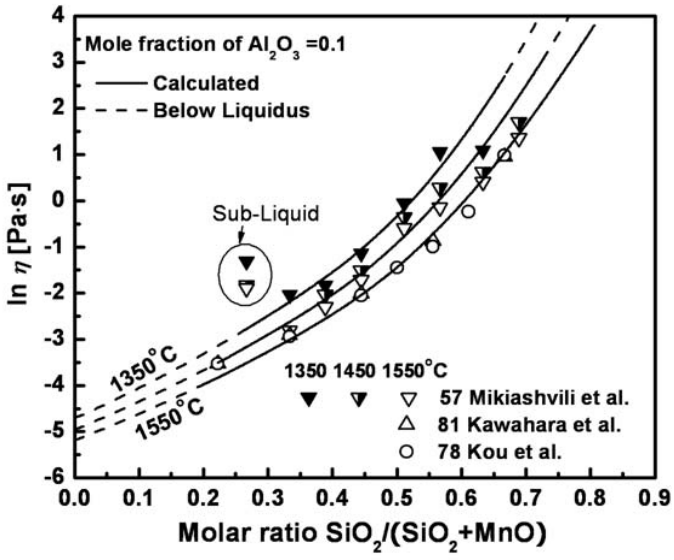

Fig. 7.19 Viscosity of MnO-Al_2O_3-SiO_2 melts at 10 mol% Al_2O_3 compared to experimental data [118, 143, 187]

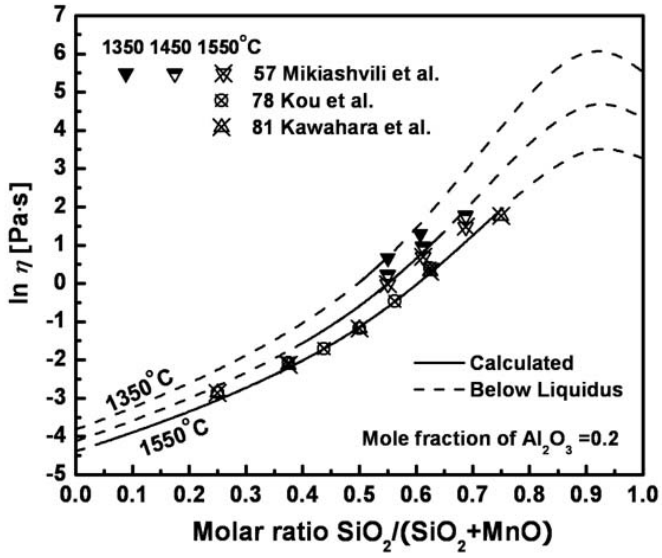

Fig. 7.20 Viscosity of MnO-Al_2O_3-SiO_2 melts at 20 mol% Al_2O_3 compared to experimental data [118, 143, 187]

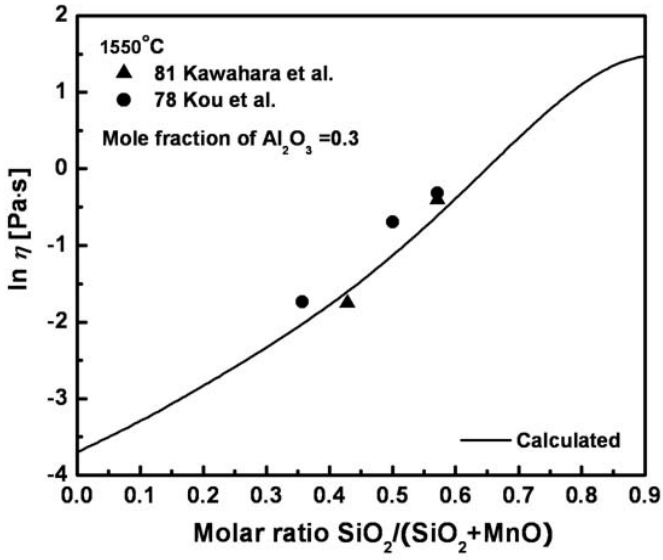

Fig. 7.21 Viscosity of MnO-Al_2O_3-SiO_2 melts at 30 mol% Al_2O_3 compared to experimental data [118, 143]

7.2.4 Multicomponent systems

The viscosity of multicomponent systems is predicted by the model from the unary, binary and ternary parameters given from Tables 4.1, 4.2, 5.1, 6.1 and 7.1 with no additional parameters. Several data points can be identified that were measured below the liquidus temperature and consequently show abnormally high viscosities.

7.2.4.1 $MnO-CaO-Al_2O_3-SiO_2$ system

Figs 7.22 and 7.23 compare the viscosities of $MnO-CaO-Al_2O_3-SiO_2$ melts predicted by the model with all available experimental data [34, 317]. Fig. 7.22 shows the predicted viscosities at 6 wt% Al_2O_3 with the molar ratio $CaO/SiO_2 = 0.64$ along with the experimental data of Tanabe et al. [317] who used a rotational viscometer. Most of the data show a good agreement with the lines calculated by the model. It seems that the observed trend of decreasing viscosity with increasing MnO content is well predicted by the model within the experimental error limits. Chubinidze and Kekelidze [34] measured the viscosities of $MnO-CaO-Al_2O_3-SiO_2$ melts at 40wt% SiO_2 and 10wt% Al_2O_3 using a vibration viscometer with Mo crucibles. The measured data points show a good agreement with the calculated lines in the temperature range of 1500 to 1700ºC while the data points measured below 1400ºC are slightly higher, although the difference is fairly small. The data points show a somewhat different temperature dependence from that of the model. It seems that viscosity data from 1400°C deviate from Arrhenian temperature dependence of Eq.(4.1) and indicate non-Arrhenian temperature dependence with decreasing temperatures. It should be noted that the present model is developed using an Arrhenian relation in Eq.(4.1) and the extension of the model for the viscosity of glasses showing non-Arrhenian temperature dependence will be discussed in Chapters 11 and 12.

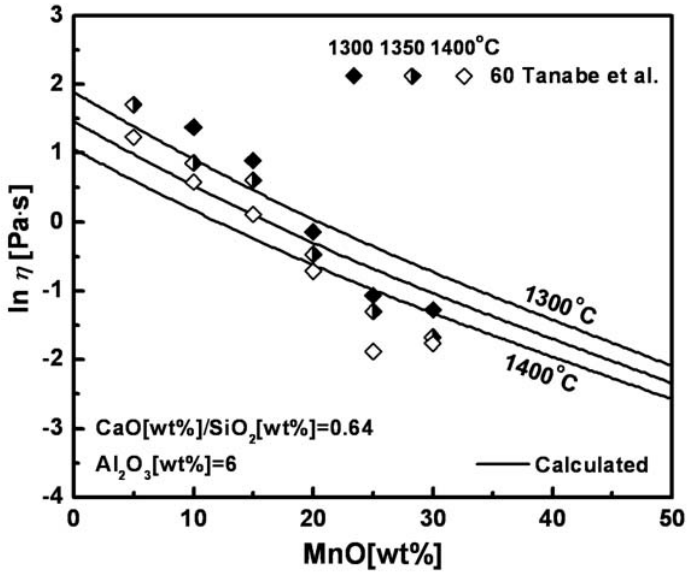

Fig. 7.22 Viscosity of MnO-CaO-Al_2O_3-SiO_2 melts at 6 wt% Al_2O_3 and for a molar ratio CaO/SiO_2 = 0.64 compared to experimental data [317]

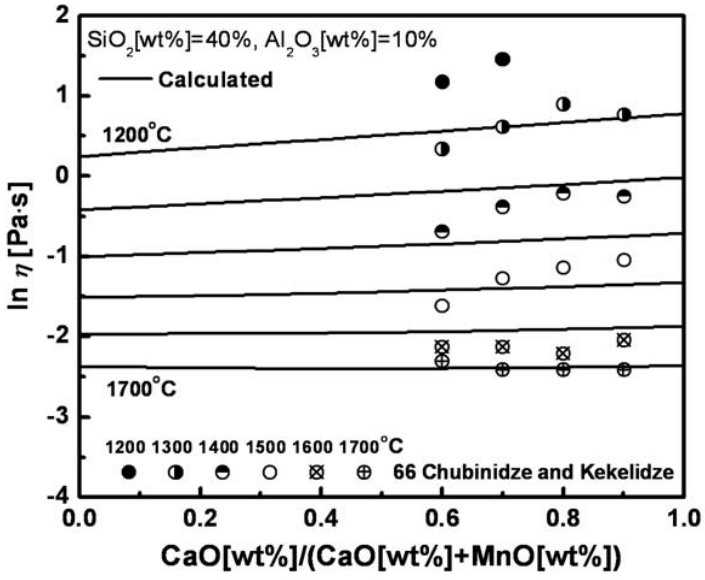

Fig. 7.23 Viscosity of MnO-CaO-Al_2O_3-SiO_2 melts at 10 wt% Al_2O_3 and 40 wt% SiO_2 compared to experimental data [34]

7.2.4.2 MnO-CaO-MgO-Al_2O_3-SiO_2 system

Figs 7.24 and 7.25 compare the viscosities of MnO-CaO-MgO-Al_2O_3-SiO_2 melts predicted by the model with available experimental data [278, 346]. Fig. 7.24 shows the predicted viscosities compared with the experimental data of Semik [278] who used a rotational viscometer. The measured data points show a good agreement with the calculated lines in the temperature range of 1500 to 1600ºC while the data points measured below 1400ºC are slightly higher, although the difference is fairly small. Again, the data points show somewhat different temperature dependence from that of the model. It seems that viscosity data from 1400°C deviate from an Arrhenian temperature dependence of Eq.(4.1) and indicate non-Arrhenian temperature dependence with decreasing temperatures. It should be noted that the present model is developed using an Arrhenian relation in Eq.(4.1) and the extension of the model for viscosity of glasses showing non-Arrhenian temperature dependence will be reported in Chapters 11 and 12.

Vulchev and Tororov, who also measured the viscosities in the CaO-MgO-Al_2O_3-SiO_2 melts, measured viscosities using a rotational viscometer with the addition of MnO. As can be seen in Fig. 7.25, the experimental data in the temperature range of 1350 to 1550ºC are systematically higher than the calculated lines in the MnO-CaO-MgO-Al_2O_3-SiO_2 melts although the difference is fairly small. Their data points measured in the CaO-MgO-Al_2O_3-SiO_2 melts also show systematically higher viscosities than the calculated lines by the model, indicating a most probably systematic experimental error. However, the observed trend of decreasing viscosity with the addition of MnO is well predicted by the calculations. Overall, the viscosities predicted by the model for MnO-CaO-MgO-Al_2O_3-SiO_2 melts are believed to be in agreement with the measurements within experimental error limits.

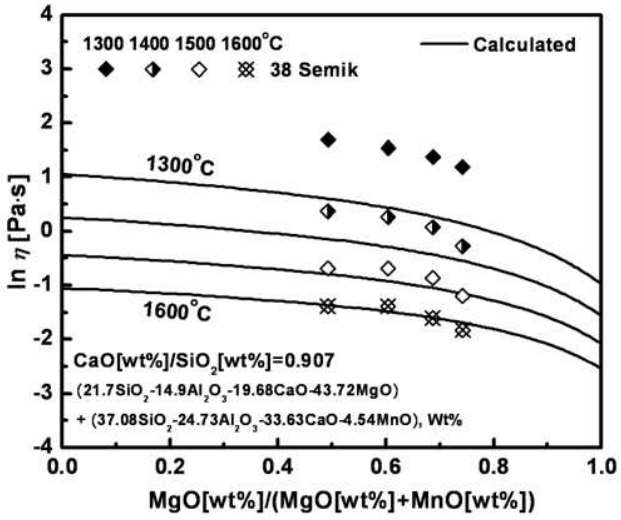

Fig. 7.24 Viscosity of MnO-CaO-MgO-Al_2O_3-SiO_2 melts in the section of (21.7 mol% SiO_2, 14.9 mol% Al_2O_3, 19.68 mol% CaO, 43.72 mol% MgO) to (37.08 mol% SiO_2, 24.73 mol% Al_2O_3, 33.63 mol% CaO, 4.54 mol% MnO) with a molar ratio CaO/SiO_2 = 0.907: experimental points [278]

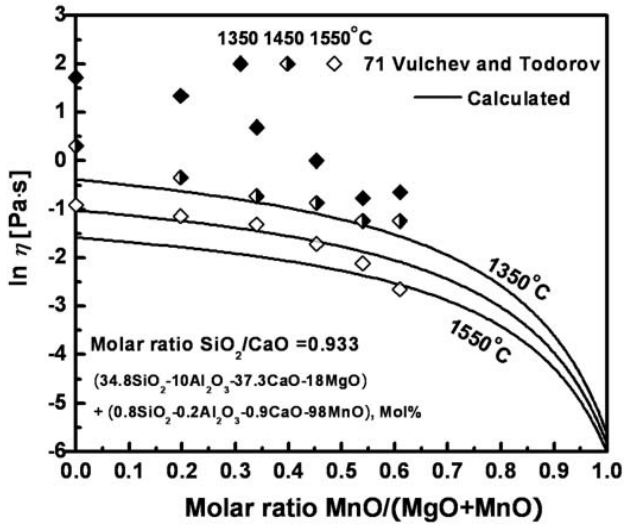

Fig. 7.25 Viscosity of MnO-CaO-MgO-Al_2O_3-SiO_2 melts in the section of (34 mol% SiO_2, 10 mol% Al_2O_3, 37.3 mol% CaO, 18 mol% MgO) to (0.8 mol% SiO_2, 0.2 mol% Al_2O_3, 0.9 mol% CaO, 98 mol% MnO) with a molar ratio SiO_2/CaO = 0.933: experimental points [346]

7.2.4.3 $MnO-K_2O-CaO-Al_2O_3-SiO_2$ system

The viscosities of $MnO-K_2O-CaO-Al_2O_3-SiO_2$ melts were measured only by Rudneva et al. [257] who used an electrical viscometer. As can be seen in Fig. 7.26, the observed trend in viscosity of the data points is quite well predicted by the model, although some of the data points show an abnormal increasing trend with decreasing SiO_2 contents. Since there is no obvious physical reason for such behavior, it is most likely caused from partial crystallization of the sample during the experiments. As mentioned in the section 2.3.1, the sample containing low SiO_2 contents is hard to keep the glassy state [285] due to the strong crystallization trend of the sample.

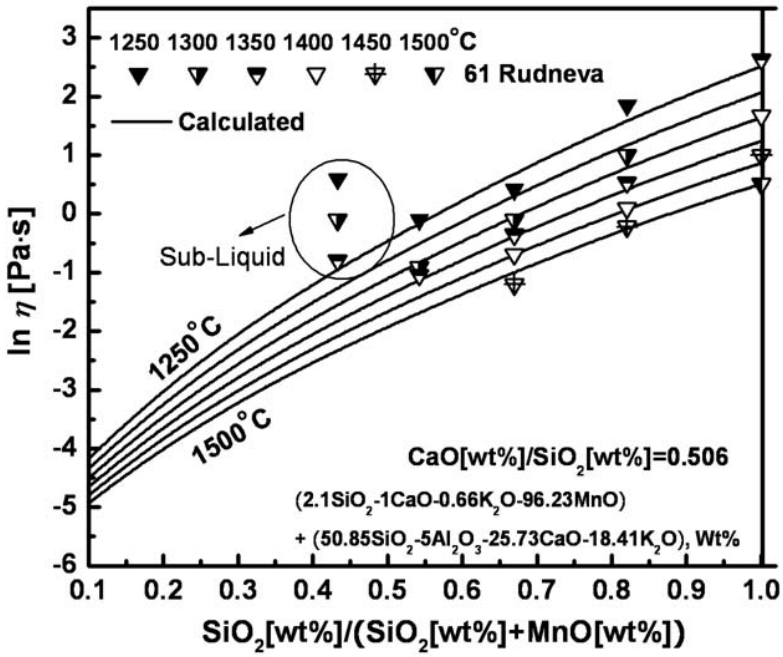

Fig. 7.26 Viscosity of $MnO-K_2O-CaO-Al_2O_3-SiO_2$ melts in the section of (2.1 mol% SiO_2, 1 mol% CaO, 0.66 mol% K_2O, 96.23 mol% MnO) to (50.85 mol% SiO_2, 5 mol% Al_2O_3, 25.73 mol% CaO, 18.41 mol% K_2O) with a molar ratio $CaO/SiO_2 = 0.506$: experimental points [257]

7.2.4.4 MnO-Na_2O-K_2O-CaO-Al_2O_3-SiO_2 system

Fig. 7.27 compares the viscosities of MnO-Na_2O-K_2O-CaO-Al_2O_3-SiO_2 melts predicted by the model with the measurements of Tkach et al. [322]. Considering the expanded scale of the y-axis, it seems that the data points of Tkach et al. [322] at all temperatures show an excellent agreement with the lines predicted by the model using only a few unary, binary and ternary parameters.

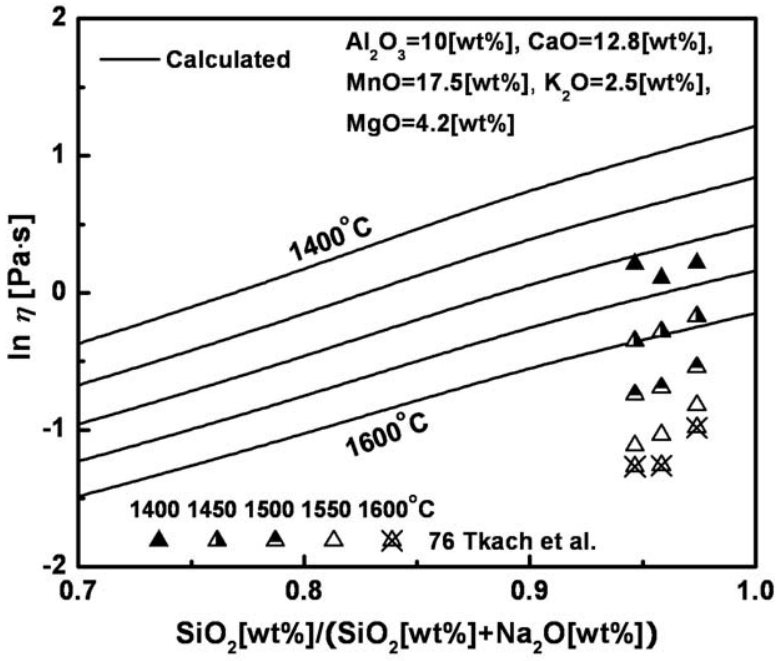

Fig. 7.27 Viscosity of MnO-Na_2O-K_2O-CaO-Al_2O_3-SiO_2 melts at 10 wt% Al_2O_3, 12.8 wt% CaO, 17.5 wt% MnO, 2.5 wt% K_2O and 4.2 wt% MgO compared to experimental data [322]

7.3 Conclusions

To calculate the viscosity of MnO-containing silicate melts, only 6 model parameters related to MnO are required. Two parameters, A_{MnO} and E_{MnO}, describe the viscosity of pure liquid MnO; two binary parameters, $E^{1,1}_{MnO\text{-}Si}$ and $E^{R}_{MnO\text{-}Si}$, describe the viscosity of MnO-SiO_2 melts; and, finally, two more parameters represent the Gibbs energy, $\Delta G_{MnAl_2O_4}$, of tetrahedrally-

coordinated Al “species” which enter the silica network and are charge-compensated by Mn. The latter two parameters are obtained from the experimental viscosities of MnO-Al_2O_3-SiO_2 melts. The viscosity of multicomponent melts containing MnO is then predicted by the model without any additional adjustable model parameters.

To test the model, all experimental viscosity data were collected for melts formed by MnO with SiO_2, Al_2O_3, CaO, MgO, Na_2O and K_2O. The deviation of the available experimental data from the viscosities predicted by the model does not exceed the scatter of experimental points among different authors in all binary and ternary sub-systems of MnO–SiO_2–Al_2O_3–CaO–MgO–Na_2O–K_2O that were used to calibrate the model. Overall, model parameters have been obtained which permit MnO to be added to the database and which permit the accurate prediction of the viscosity of multicomponent MnO-containing melts.

Table 7.1 Optimized Model parameters for the viscosity expressed in Pa·s

System	Model parameter	Model parameters ($J \cdot mol^{-1}$)
MnO	$A_{MnO} = -9$	$E_{MnO} = 44040$
MnO-SiO_2		$E^{1,1}_{MnO\text{-}Si} = -50000$ $E^{R}_{MnO\text{-}Si} = 81000$
MnO-Al_2O_3-SiO_2		$\Delta G_{MnAl_2O_4} = 14500 - 94500\, X_{SiO_2}$

The model parameters for subsystems without MnO that are used for the viscosity calculations in the present study were optimized and reported elsewhere (see Tables 4.1, 4.2 ,5.1 and 6.1).

CHAPTER 8 MODELING VISCOSITY OF SILICATE MELTS CONTAINING TITANIUM OXIDES

8.1 Introduction

In the blast furnace processing of titaniferrous iron ore, the control of the viscosity of slags containing TiO_x is very important to avoid a lack of fluidity which causes shutdown of an arc furnace. Titanium is also added to many grade steels as an alloying element to improve mechanical properties via grain refinement [72]. However, titanium is very reactive with oxygen and the formed TiO_x causes nozzle clogging [123]. Thus, control of the viscosity of slags containing TiO_x is a key factor for stable mass transfer at the slag/metal interface to prevent nozzle clogging; and also to improve heat transfer through the slag and the lifetime of refractory materials. Because of these important reasons, the viscosity of slags containing TiO_x has been investigated by many groups.

In the present study, viscosity data are reviewed for melts formed by TiO_2 and Ti_2O_3 with SiO_2, Al_2O_3, CaO, MgO, Na_2O, K_2O and MnO. A few model parameters are optimized to reproduce the viscosities of pure TiO_2, Ti_2O_3, TiO_2–SiO_2 and Ti_2O_3–SiO_2 melts. Then the available experimental viscosity data for other ternary and higher-order TiO_x-containing systems are compared to the viscosities calculated by the model without using any additional adjustable model parameters.

8.2 Review of the available viscosity data and calibration of the model

In the present study, viscosity data are reviewed for all TiO_x-containing subsystems of the TiO_x–MnO–SiO_2–Al_2O_3–CaO–MgO–Na_2O–K_2O–PbO system and using the model introduced in Chapter 4. (See Eqs. (4.1)-(4.4)) The data judged to be most reliable are shown in the figures below.

The proposed model is intended for melts. The extension of the model to describe the viscosity of glasses will be reported in Chapters 11 and 12. Therefore, the viscosity data were collected mainly for melts above the liquidus or for slightly supercooled melts where

crystallization did not occur. These measurements were mostly made with rotational or vibrational viscometers. Phase equilibrium calculations were carried out using the FactSage thermochemical software and databases [14] to check that the viscosity was indeed measured in a single-phase liquid region. If an abnormally high viscosity value was reported for a temperature below the liquidus, this was most likely the result of crystallization. Parameters of the model for TiO_x-containing melts that were fitted to the experimental viscosity data are listed in Table 8.1. The model parameters for melts without TiO_x were shown in Tables 4.1, 4.2, 5.1, 6.1 and 7.1.

8.2.1 Viscosities of unary TiO_2 melts

All optimized model parameters are listed in Table 8.1.

No viscosity data for pure Ti_2O_3 were available. The viscosity of pure TiO_2 was measured by Mitin and Nagibin [191] in the temperature range 1850 to 2350°C using a damped torsional vibration method with Mo crucibles under Ar gas atmosphere. As shown in Fig. 8.1, the calculated line shows a slightly different slope from that of the experimental data. The melting point of TiO_2 is very high (approximately 1857°C) [14]. Under Ar gas atmosphere at such a high temperature, pure TiO_2 might be expected to dissociate to Ti_2O_3. There is no information about the impurity of purified Ar gas used in the experiment. It is known that the purified Ar gas used in the experiment approximately contains 10^{-4} vol% of the O_2 gas as the impurity. [319] We tried to calculate how much Ti_2O_3 can be formed from pure TiO_2 under $P_{O_2(g)} = 10^{-4}$ atm using the FactSage thermochemical software and database [14]. At 1850°C, the amount of Ti_2O_3 formed is approximately 0.013 mol%. On the other hand, at 2350°C, the amount of Ti_2O_3 formed is approximately 21.39 mol%. Thus, the dissociation of pure TiO_2 to Ti_2O_3 could be considerably occurred at higher temperatures. Thus, this dissociation of TiO_2 could give some effects on the change of viscosity. Because of lack of information for the impurity of Ar gas used by Mitin and Nagibin [191], these data were not considered for the optimization of unary Ti_2O_3 system. Because of the high temperatures, the authors used an optical pyrometer to measure the temperature. There is an inherent weakness of non-contact temperature measurement such as the optical pyrometer because of gas or fume formed from the sample during the experiment which prevents reading the accurate emissivity of the surface of the sample from the optical pyrometer. Furthermore, the prediction of binary and ternary systems containing TiO_2 measured at low temperatures would be very sensitive to the extrapolation of the data points for unary TiO_2 to low

temperatures. Thus, as shown in Section 8.2.2, the unary parameters of TiO_2 were carefully optimized by considering the data of unary TiO_2 and binary TiO_2-K_2O and TiO_2-MnO systems. As shown in Figs 8.1, 8.3 and 8.4, the lines calculated by the model seems to be in good agreement with all data points within experimental error limits.

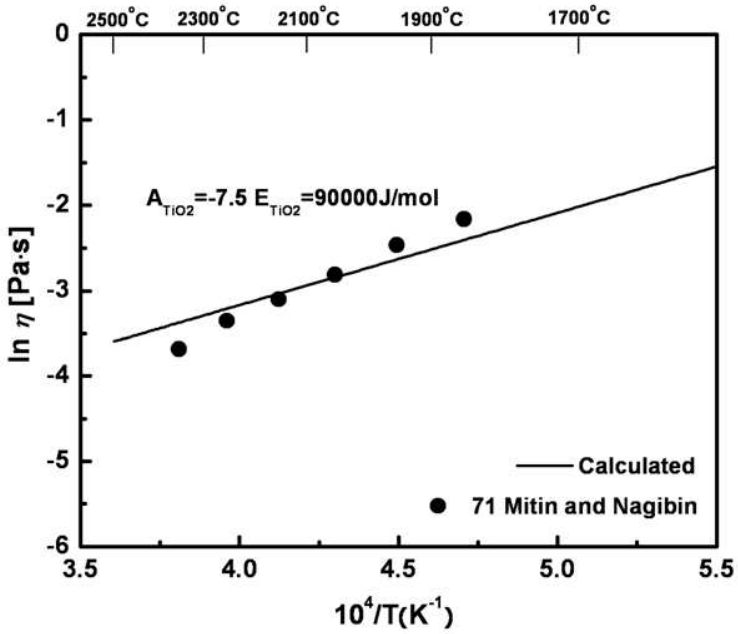

Fig. 8.1 Viscosity of pure liquid TiO_2 melts: experimental points [191] and calculated line

8.2.2 Viscosities of binary TiO_2-SiO_2 and TiO_2-MO_y (M = K and Mn) melts

Figs 8.2-8.4 show the calculated viscosities of binary systems of TiO_2-SiO_2 and TiO_2-MO_y (M = K and Mn) along with the experimental data of Leko et al. [160], Van Bemst and Delaunois [338] and Yagi et al. [353]. No data for binary systems containing Ti_2O_3 were available.

As shown in Fig. 8.2, the only available viscosity data for the binary TiO_2-SiO_2 system were measured by Leko et al. [160]using the beam-bending method at compositions rich in SiO_2. However, their data show abnormally higher viscosities than the viscosities calculated by the model and even higher than those of unary SiO_2 at all temperatures. The model showed an

excellent agreement with the experimental data of unary SiO_2 as shown in Fig. 3.6 [82]. Thus, the data points of Leko et al. [160] were not considered for the optimization of binary parameters. In the present study, all available ternary systems containing TiO_2 were considered for the optimization of binary parameters of the system TiO_2-SiO_2. In the case of the Ti_2O_3-SiO_2 binary system, there are no available data. The binary Ti_2O_3-SiO_2 system was optimized from the higher order systems as shown later.

In Fig. 8.3, the viscosity is predicted by the model from the linear combination of the model parameters for each unary basic oxide TiO_2 and $KO_{0.5}$ comparing the data points measured by Van Bemst and Delaunois [338] using the rotating crucible method with iron [338] under Ar gas atmosphere. As can be seen in Fig. 8.3, the model shows an excellent agreement with most data except for two data points showing abnormally high viscosities which could have been measured in the sub-liquidus region with partial crystallization of the sample during the experiment.

In Fig. 8.4, the viscosity is predicted by the model from the linear combination of the unary model parameters for TiO_2 and MnO comparing the data points measured by Yagi et al.[353] using the rotating crucible method with Pt-Rh crucibles under air atmosphere [353]. As can be seen in Fig. 8.4, the model is in good agreement with all data points at all temperatures. Again, as shown in Figs 8.3-8.4, it seems that the assumption that the viscosity of binary basic oxides MO_x–NO_y where MO_x and NO_y are basic oxides can be predicted from a linear combination of parameters A and E of the unary basic oxides as seen in Eqs. (4.2)-(4.3) leads to a very good representation of the experimental data.

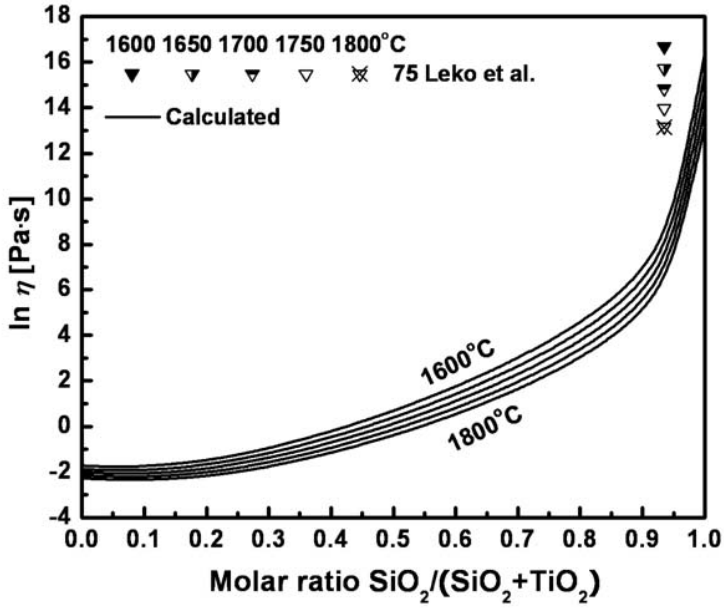

Fig. 8.2 Viscosity of TiO_2-SiO_2 melts: experimental points [160] and calculated line

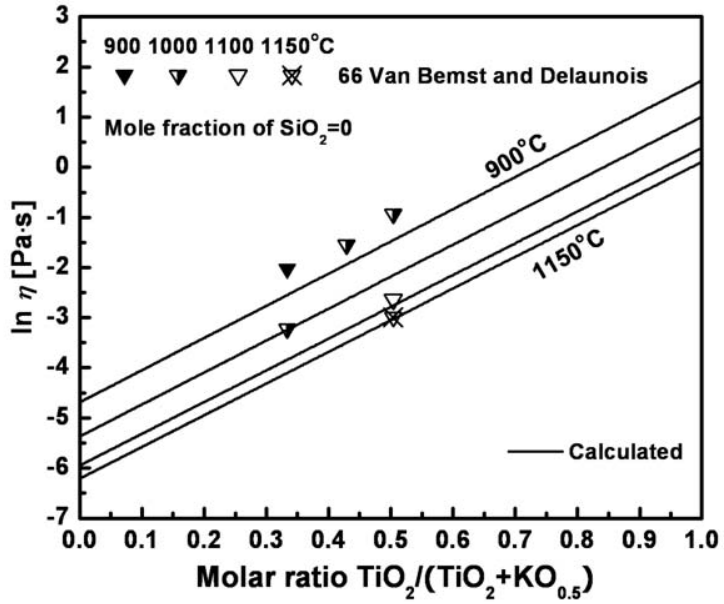

Fig. 8.3 Viscosity of TiO_2-K_2O melts: experimental points [338] and calculated line

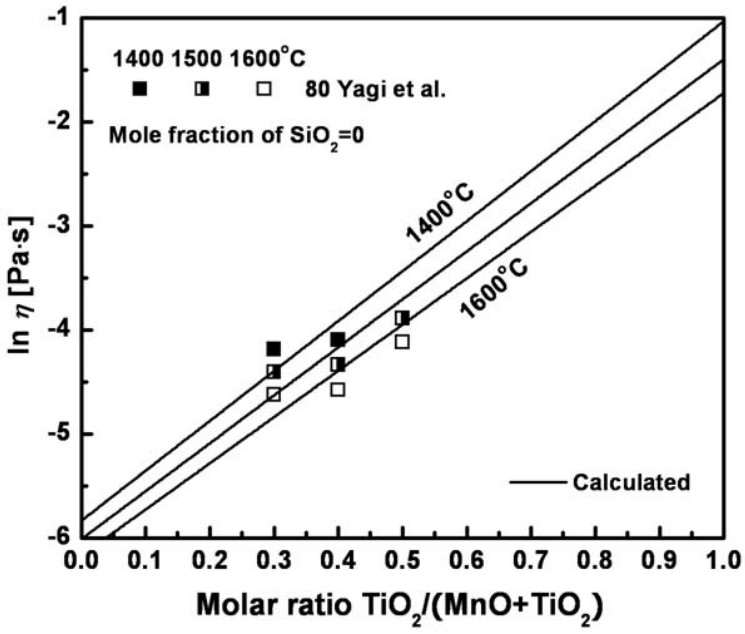

Fig. 8.4 Viscosity of TiO_2-MnO melts: experimental points [353] and calculated line

8.2.3 Ternary and Higher order Melts

There are no available viscosity data between Ti_2O_3 and MO_x (M = Basic oxides except for Al). Furthermore, the viscosity data in ternary and higher-order silicates containing TiO_2 and Al_2O_3 can be reproduced by the model without introducing the Charge Compenstaion Effect. Therefore, it seems that the Al^{3+} cation cannot be compensated by Ti^{4+} cations, most likely because the Ti ion has a higher charge than other cations such as M^+ or M^{2+}. Thus, in the present study, only the Charge Compensation Effect between Al_2O_3 and MO_x was considered. The viscosities of ternary and higher-order melts containing TiO_2 or Ti_2O_3 were predicted by the model based on the unary and binary viscosity parameters given from Tables 4.1, 5.1, 5.2, 6.1, 7.1 and 8.1 without any additional adjustable parameters.

8.2.3.1 TiO_2-CaO-SiO_2 system

The viscosities of the ternary systems without $AlO_{1.5}$ were calculated by linear combination of the binary viscosity parameters according to Eqs. (4.2)-(4.3) with no additional

parameters. Therefore, the binary viscosity parameters of the system TiO_x-SiO_2 were optimized from these ternary systems.

Figs 8.6-8.9 show the calculated viscosities of the TiO_2-CaO-SiO_2 system compared to experimental data measured by Schenck and Frohberg [272], Dingwell [42], Yasukouchi et al. [357] and Nakamura and Morinaga [202] using the rotating crucible method with Pt-Rh [202, 286, 357] and carbon crucibles [272] under air [202, 286, 357] and CO gas atmosphere [272]. Under the experimental conditions of Schenck and Frohberg [272], the dissociation of TiO_2 to Ti_2O_3 in liquid slag can be expected as shown in the reaction (8.1):

$$2TiO_2(l)_{\text{in Slag}} + C(s) \rightleftarrows Ti_2O_3(l)_{\text{in Slag}} + CO(g) \tag{8.1}$$

$$K_{(8.1)} = \exp\left(\frac{-\Delta G_{(8.1)}}{RT}\right) = \frac{a_{Ti_2O_3(l)} P_{CO(g)}}{a^2_{TiO_2(l)} a_{C(s)}} \tag{8.2}$$

where $a_{TiO_2(l)}$, $a_{Ti_2O_3(l)}$ and $a_{C(s)}$ are activities of TiO_2, Ti_2O_3 in liquid slag and solid carbon respectively. $P_{CO(g)}$ is the partial pressure of CO gas in the experiment.

Using the FactSage thermochemical software and database [14], we are able to calculate the thermodynamic properties for a system under given experimental conditions. However, the present thermodynamic database [14] has not been fully optimized for the system CaO-SiO_2-TiO_2, and thus is not able to calculate accurately the thermodynamic properties of the CaO-SiO_2-TiO_2 system.

As shown in Eq.(8.2), the dissociation of TiO_2 to Ti_2O_3 in liquid slag with carbon crucibles, $a_{C(s)} = 1$, is mainly dependent on the partial pressure of CO gas $P_{CO(g)}$. The activity of Ti_2O_3 increases with decreasing $P_{CO(g)}$. However, under the given experimental conditions, $P_{CO(g)}$ is 1 atm, and this would minimize the increase of $a_{Ti_2O_3(l)}$ at a given composition during the experiment. However, we still have a possibility of dissociation of TiO_2 to Ti_2O_3 in liquid slag and the reaction (8.1) to form CO gas in the sample with dissociation of TiO_2 liquid. Thus, Schenck and Frohberg [272] carefully carried out experiments to look for the existence of gas formation from the sample during the experiment. They pointed out that there was no observation

of gas formation during the experiments except for two points indicated as ‘CO gas formed’ as shown in Fig. 8.9.

In Figs 8.7 and 8.8, the data points measured in the TiO_2-CaO-SiO_2 system by Schenck and Frohberg [272] who also measured the CaO-SiO_2 binary system are systematically higher than the calculated lines at all temperatures, although the differences are fairly small. It was shown that the calculated lines for the CaO-SiO_2 system were in a good agreement with many other authors as shown in Fig. 3.8 [82]. Some data showing abnormal high viscosities appear to have been measured at low temperatures under partial crystallization of the sample during the experiment. However, the observed trend of decreasing viscosity with increasing TiO_2 content is in a good agreement with the calculations. The data points of Dingwell [42] show more sharply decreasing trends with the addition of TiO_2 than the data reported by Schenck and Frohberg [272] as shown in Fig. 8.7. This discrepancy between two authors [42, 272] is not clear. When comparing the data of unary TiO_2 measured by Mitin and Nagibin [191], however, the extrapolated viscosities of Dingwell [42] at 1600°C up to unary TiO_2 are almost same as that of the data of Mitin and Nagibin [191] at 2300°C. Thus, the extrapolated viscosity from the data of Dingwell [42] show much lower values than the viscosity data of Mitin and Nagibin [191]. See Figs 8.1 and 8.7. It should be noted that the unary parameters of TiO_2 were carefully optimized with consideration of the data of unary TiO_2 and binary TiO_2-K_2O and TiO_2-MnO systems as shown in Figs 8.1, 8.3 and 8.4.

In Fig. 8.9, the observed trends of the viscosity data of Schenck and Frohberg[272] show good agreement with the lines calculated by the model except for two points indicated as ‘CO gas formed’. Schenck and Frohberg [272]reported that they observed the formation of CO gas in the melt during the viscosity measurement at these points. Thus, as shown in the reaction (8.1), the dissociation of TiO_2 to Ti_2O_3 with CO gas formation in the sample would cause viscosity to decrease.

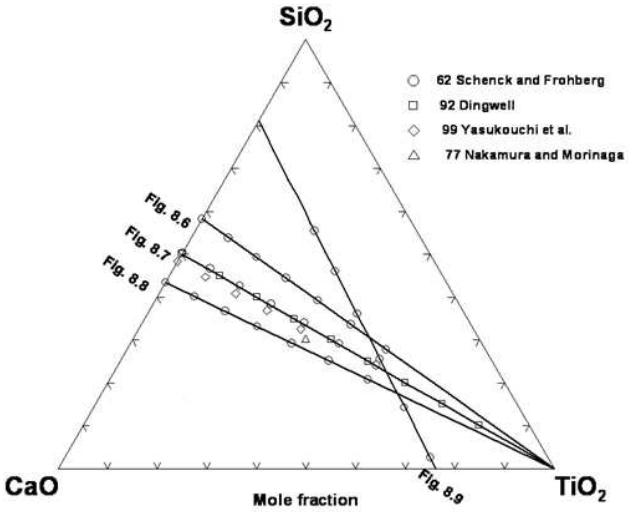

Fig. 8.5 Compositions in the TiO_2-CaO-SiO_2 system at which experimental viscosity measurements are available [42, 202, 272, 357]. The lines indicate four sections of this system selected to show the viscosity as a function of composition in Figs 8.6 to 8.9

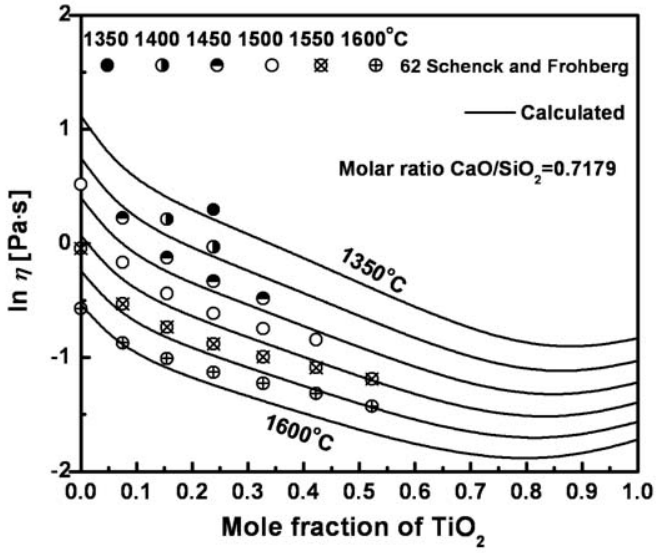

Fig. 8.6 Viscosity of TiO_2-CaO-SiO_2 melts for a molar ratio CaO/SiO_2 = 0.7179 compared to experimental data [272]

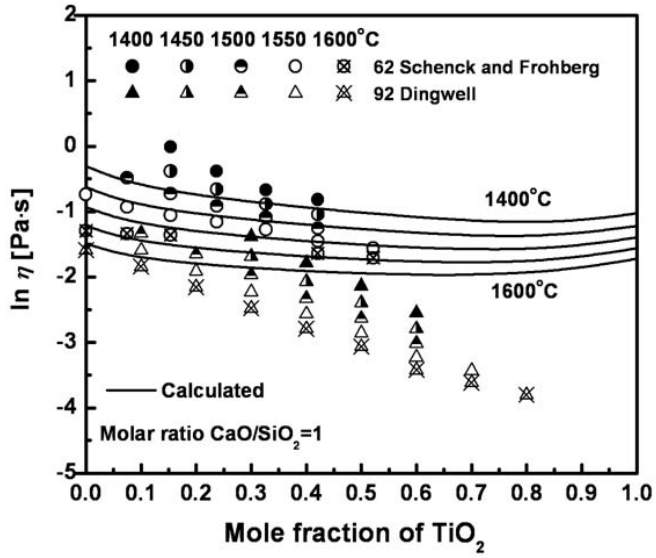

Fig. 8.7 Viscosity of TiO_2-CaO-SiO_2 melts for a molar ratio CaO/SiO_2 = 1 compared to experimental data [42, 272]

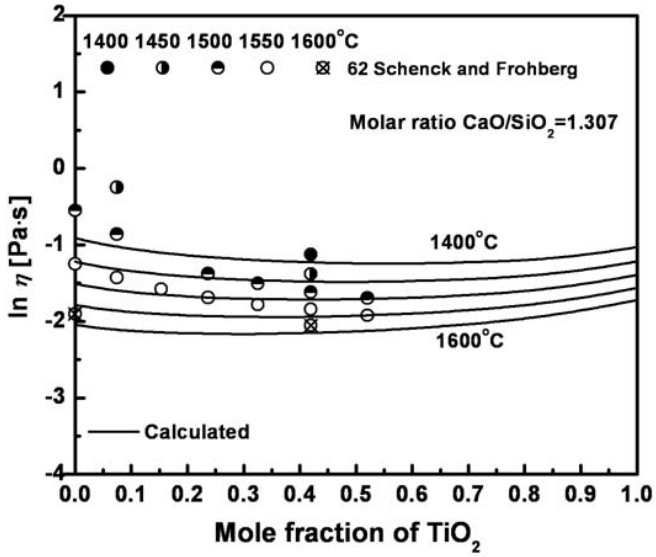

Fig. 8.8 Viscosity of TiO_2-CaO-SiO_2 melts for a molar ratio CaO/SiO_2 = 1.307 compared to experimental data [272]

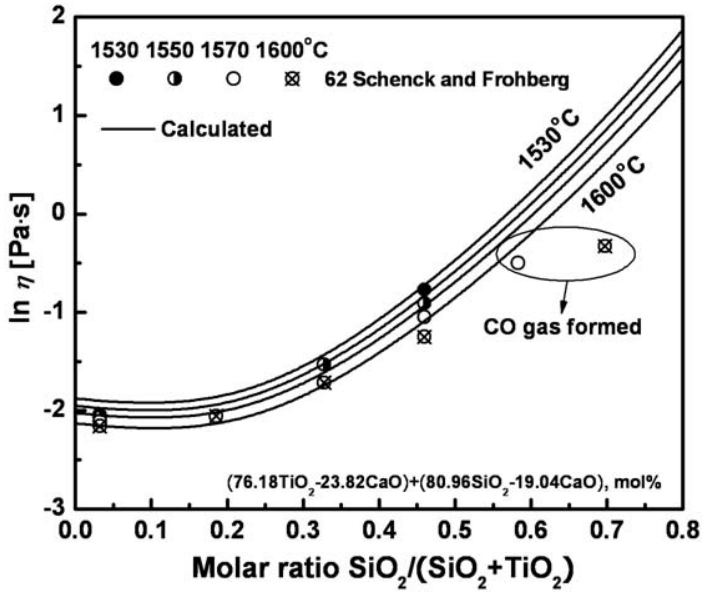

Fig. 8.9 Viscosity of TiO_2-CaO-SiO_2 melts in the section of (76.18 mol% TiO_2, 23.82 mol% CaO) to (80.96 mol% TiO_2, 19.04 mol% CaO) compared to experimental data [272]

8.2.3.2 TiO_2-Na_2O-SiO_2 system

Figs 8.11-8.15 show the calculated viscosity of the TiO_2-Na_2O-SiO_2 system compared to experimental data reported by Dingwell[42], Bouhifd et al. [3], Nakamura and Morinaga [202], Evstrop'ev et al. [64] and Liska et al. [167] using the rotating crucible method with Pt-Rh or Pt crucibles under air atmosphere. In Fig. 8.11, some of the data points of Liska et al. [167] show higher viscosities which were most likely would be measured with partial crystallization during the experiment. However, most of data points show an excellent relation with the lines calculated by the model at all temperatures. The data points on the section with molar ratio $Na_2O/TiO_2 = 1$ in Fig. 8.12 show slightly lower viscosities than the calculated lines although the difference is fairly small.

In Fig. 8.13, the data points measured by Dingwell [42]who also measured the system of TiO_2-CaO-SiO_2, show a sharp decreasing trend compared to the lines calculated by the model. Again, as also shown in Fig. 8.7, the extrapolated viscosity from the data of Dingwell [42] up to pure TiO_2 show much lower viscosities than the viscosity data of Mitin and Nagibin [191] at the

same temperatures. Figure 8.14 compares the calculated lines with the experimental data measured by three different authors who used the same experimental method [3, 42, 167]. The decreasing trend of the data points with increasing TiO_2 is sharper than the lines calculated by the model. This difference is mainly a result of the model parameters of pure TiO_2. The viscosity of binary basic oxides MO_x–NO_y where MO_x and NO_y are basic oxides, is predicted by the model from a linear combination of the model parameters of each basic oxide as shown in Eqs. (4.2) and (4.3) and this approach gave quite good results as shown in Figs 8.3 and 8.4. Again, the trend of the data points in Fig. 8.14 would result in much lower viscosities in the binary TiO_2-Na_2O system and this would result in inconsistent viscosities for pure TiO_2 as compared to other authors [191, 338, 353] as discussed in Figs 8.1, 8.3 and 8.4. Figure 8.15 shows the predicted viscosities at constant 33.3 mol% Na_2O along with the experimental data of Evstrop'ev et al. [64] who also measured the binary Na_2O-SiO_2 system. As can be seen in Fig. 8.15, the experimental data are systematically lower than the calculated lines. Their data in the binary Na_2O-SiO_2 system are also lower by about 2 in the natural logarithm scale at all temperatures, whereas our previous study as shown in Fig. 4.1 showed that our calculated lines for the system Na_2O-SiO_2 are in good agreement with the data of many other authors. The observed trend of decreasing viscosity with increasing of TiO_2 content, however, is well predicted by the calculations.

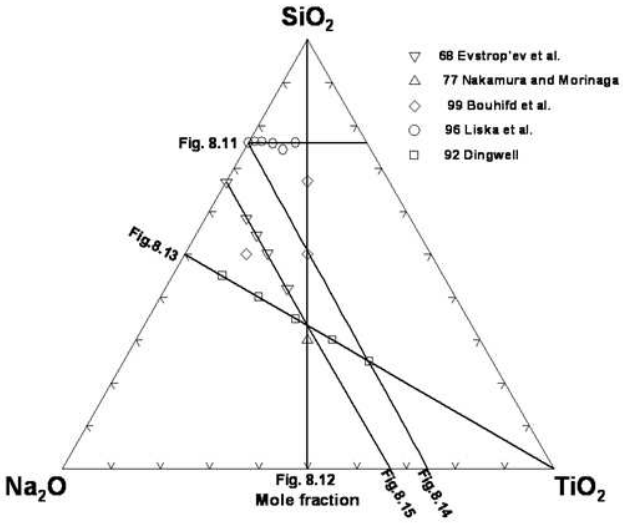

Fig. 8.10 Compositions in the TiO_2-Na_2O-SiO_2 system at which experimental viscosity measurements are available [3, 42, 64, 167, 202]. The lines indicate five sections of this system selected to show the viscosity as a function of composition in Figs 8.11 to 8.15

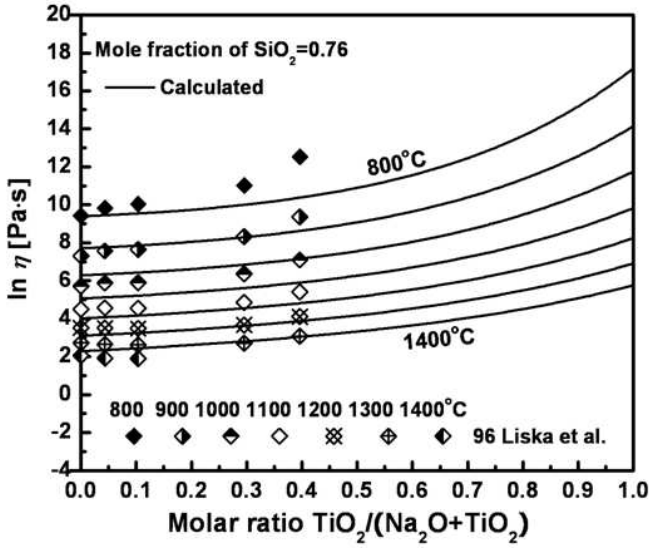

Fig. 8.11 Viscosity of TiO_2-Na_2O-SiO_2 melts at 76 mol% SiO_2 compared to experimental data [167]

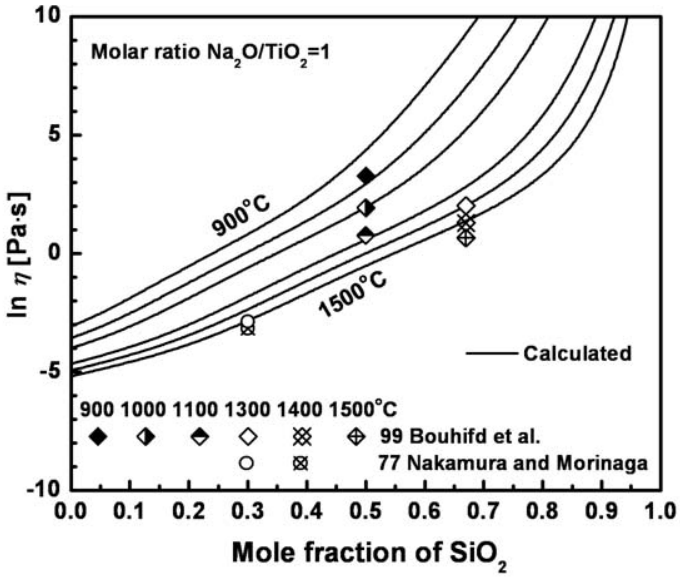

Fig. 8.12 Viscosity of TiO_2-Na_2O-SiO_2 melts for a molar ratio Na_2O/TiO_2 = 1 compared to experimental data [3, 202]

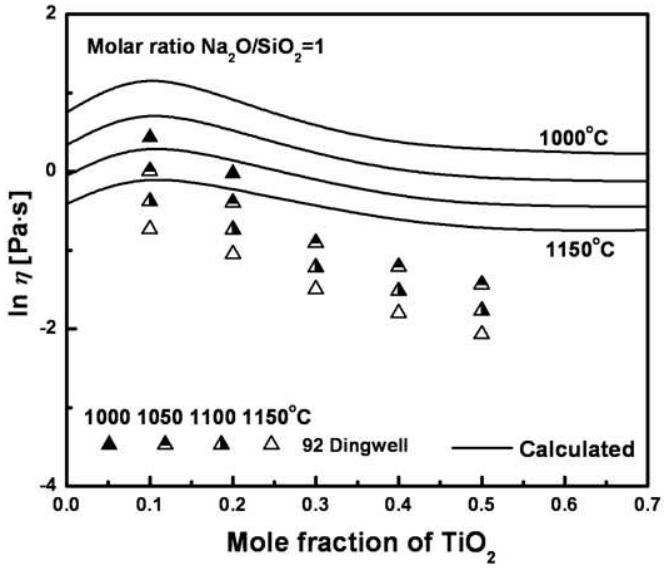

Fig. 8.13 Viscosity of TiO_2-Na_2O-SiO_2 melts for a molar ratio Na_2O/SiO_2 = 1 compared to experimental data [42]

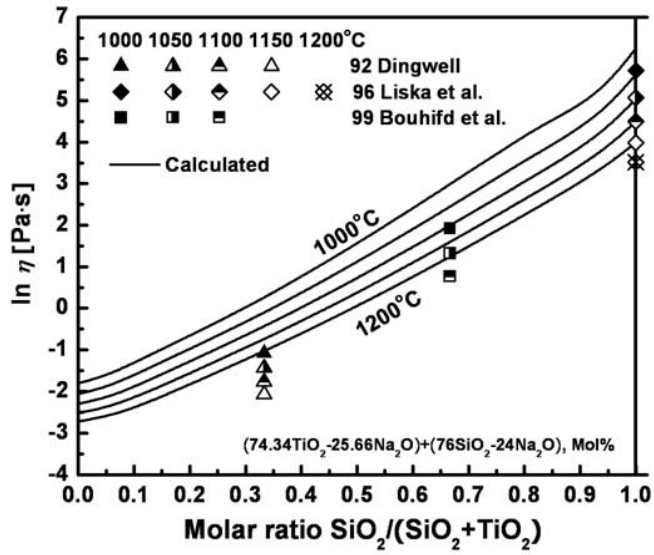

Fig. 8.14 Viscosity of TiO_2-Na_2O-SiO_2 melts in the section of (74.34 mol% TiO_2, 25.66 mol% Na_2O) to (76 mol% SiO_2, 24 mol% Na_2O) compared to experimental data [3, 42, 167]

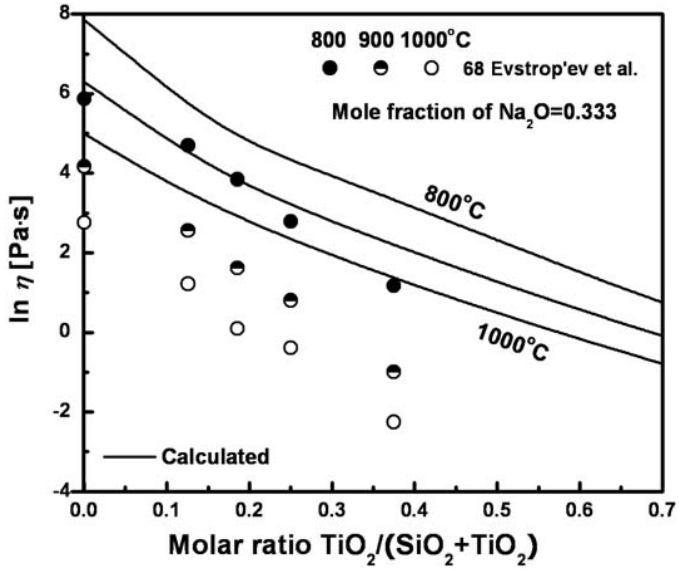

Fig. 8.15 Viscosity of TiO_2-Na_2O-SiO_2 melts at 33.3 mol% Na_2O compared to experimental data [64]

8.2.3.3 TiO_2-K_2O-SiO_2 system

Figs 8.17-8.21 show the calculated viscosity of the TiO_2-K_2O-SiO_2 system compared to the experimental data reported by Nakamura and Morinaga [202], Bouhifd et al. [3] and Van Bemst and Delaunois [338] using the rotating crucible method with iron [338] or Pt-Rh crucibles [3, 202] under air [3, 202] or Ar [338] atmosphere.

In Figs 8.17-8.19, the viscosities are predicted at 33, 40 and 50 mol% K_2O. Most data points measured by Van Bemst and Delaunois [338] (except several points indicated as 'sub-liquid') show good agreement with the lines calculated by the model. These exceptional data points could have been measured in the sub-liquidus regions with partial crystallization of the sample during the experiments. In Fig. 8.19, the data points of Van Bemst and Delaunois [338], who also measured the binary K_2O-SiO_2 system, show systematically higher viscosities than the lines calculated by the model at the K_2O-rich side. Their data are also higher for the K_2O-SiO_2 system, indicating most probably a systematic experimental error, whereas our previous study as shown in Fig. 4.2 showed that our calculated lines for the system K_2O-SiO_2 are in good agreement with the data of many other authors. As shown in Fig. 8.20, all data points of authors [3, 202, 338] at all temperatures show an excellent agreement with the lines calculated by the model. Overall, the viscosities predicted by the model for TiO_2-K_2O-SiO_2 melts are believed to be in agreement with measurements.

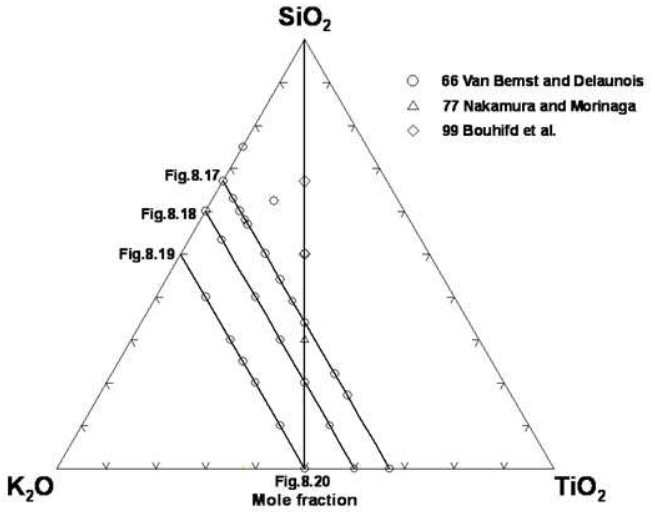

Fig. 8.16 Compositions in the TiO_2-K_2O-SiO_2 system at which experimental viscosity measurements are available [3, 202, 338]. The lines indicate five sections of this system to show the viscosity as a function of composition in Figs. 8.17 to 8.20

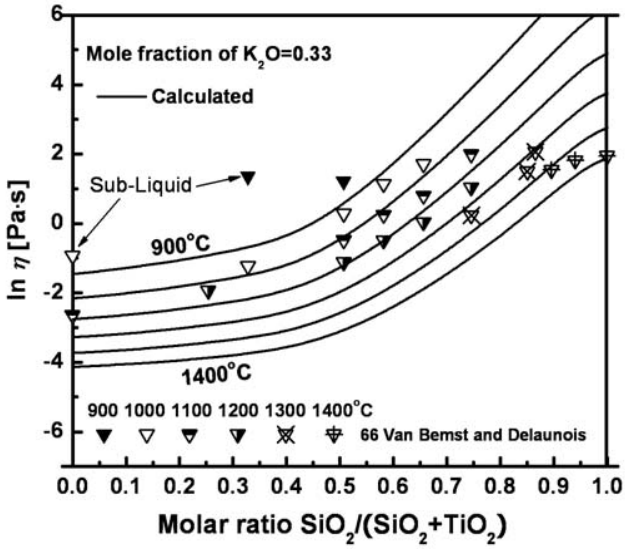

Fig. 8.17 Viscosity of TiO_2-K_2O-SiO_2 melts at 33 mol% K_2O compared to experimental data [338]

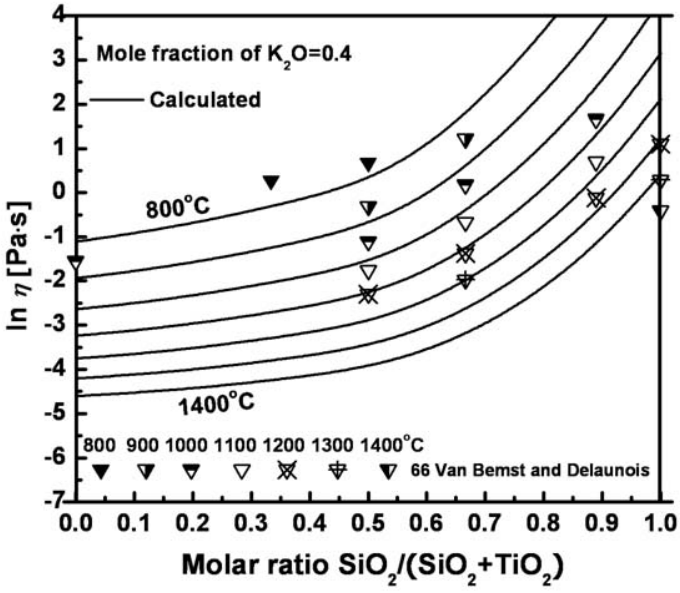

Fig. 8.18 Viscosity of TiO_2-K_2O-SiO_2 melts at 40 mol% K_2O compared to experimental data [338]

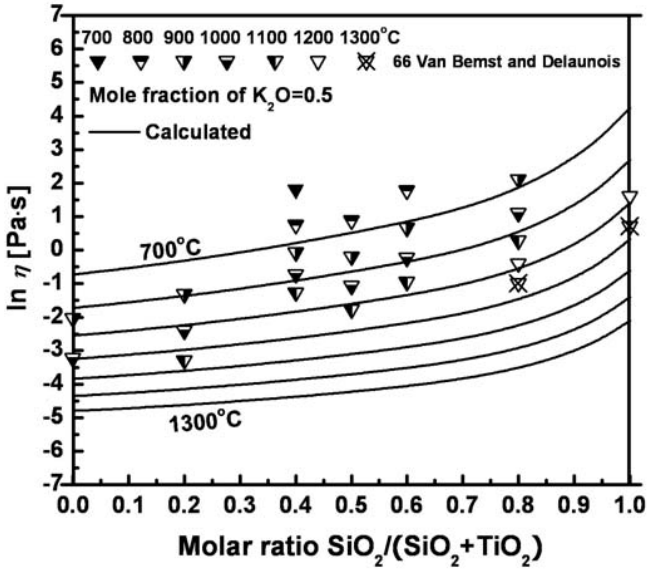

Fig. 8.19 Viscosity of TiO_2-K_2O-SiO_2 melts at 50 mol% K_2O compared to experimental data [338]

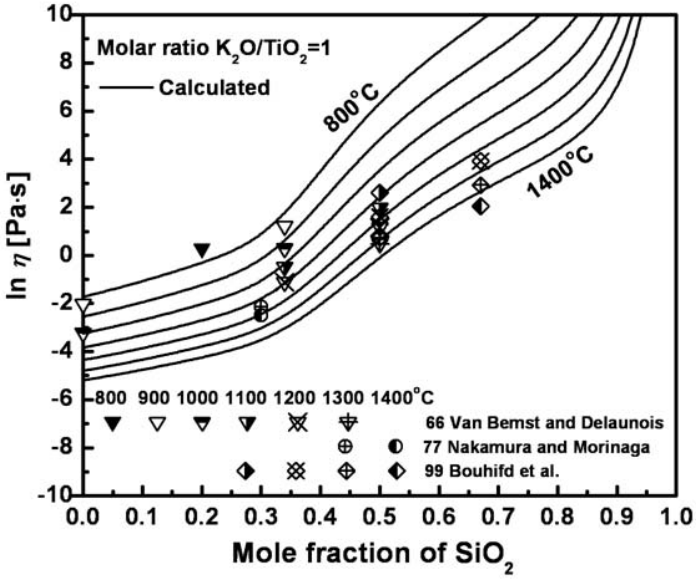

Fig. 8.20 Viscosity of TiO_2-K_2O-SiO_2 melts for a molar ratio K_2O/TiO_2 = 1 compared to experimental data [3, 202, 338]

8.2.3.4 TiO_2-MnO-SiO_2 system

Figs 8.22-8.24 show the calculated viscosity of TiO_2-MnO-SiO_2 system compared to the experimental data measured by Yagi et al. [353] using the rotating crucible method with Pt-Rh crucibles under air atmospheres [353]. As can be seen from Figs 8.22-8.24, the viscosities are predicted at 50, 60 and 70 mol% MnO. Considering the expanded scale of the y-axis, most data points show a good agreement within experimental error limits with the lines calculated by the model using only a few unary and binary parameters.

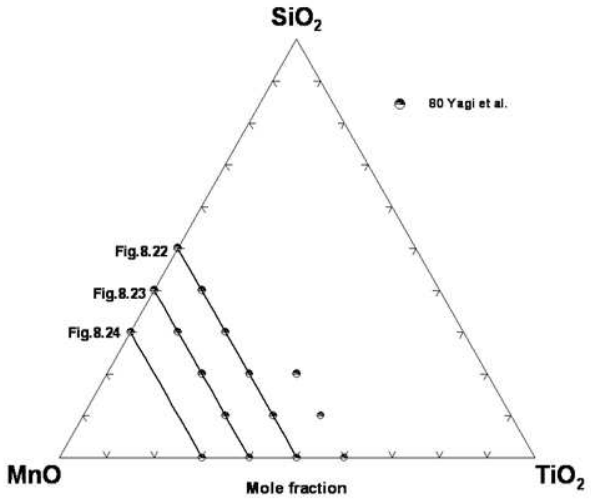

Fig. 8.21 Compositions in the TiO_2-MnO-SiO_2 system at which experimental viscosity measurements are available [353]. The lines indicate four sections of this system selected to show the viscosity as a function of composition in Figs 8.22 to 8.24

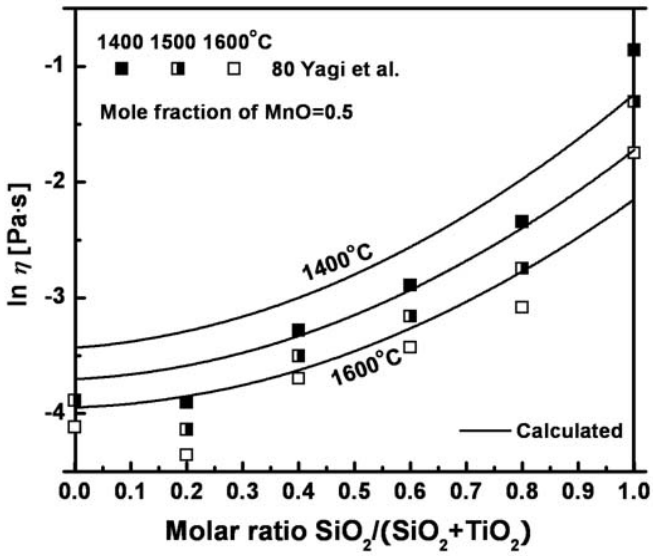

Fig. 8.22 Viscosity of TiO_2-MnO-SiO_2 melts at 50 mol% MnO compared to experimental data [353]

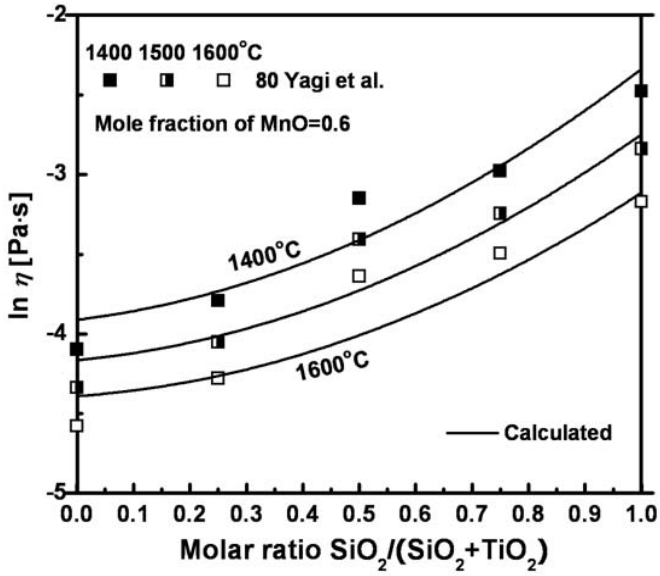

Fig. 8.23 Viscosity of TiO_2-MnO-SiO_2 melts at 60 mol% MnO compared to experimental data [353]

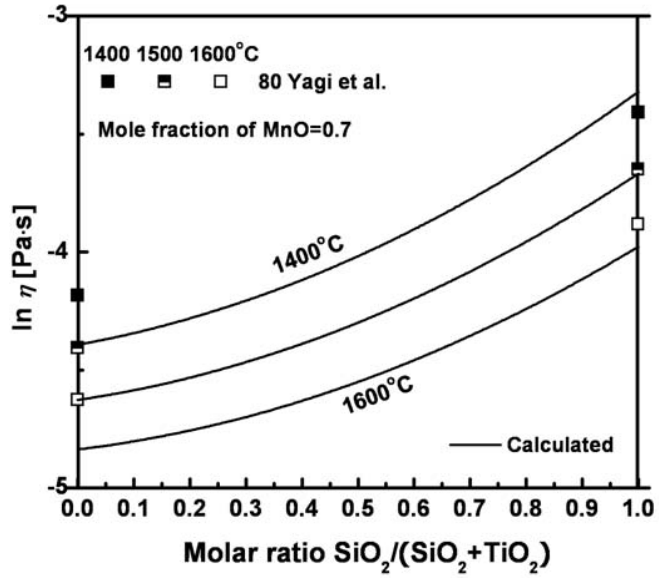

Fig. 8.24 Viscosity of TiO_2-MnO-SiO_2 melts at 70 mol% MnO compared to experimental data [353]

8.2.3.5 TiO_2-K_2O-Na_2O-SiO_2 and TiO_2-Al_2O_3-Na_2O-SiO_2 systems

Figs 8.25 and 8.26 show the calculated viscosities compared to the data points measured in the TiO_2-K_2O-Na_2O-SiO_2 and TiO_2-Al_2O_3-Na_2O-SiO_2 melts by Evstrop'ev et al. [64], who also measured the TiO_2-Na_2O-SiO_2 system, indicating systematically lower viscosities than the lines predicted by the model. Their data points, as shown in Fig. 8.15, are also systematically lower for the Na_2O-SiO_2 and TiO_2-Na_2O-SiO_2 systems, indicating most probably a systematic experimental error. However, the observed trend of the viscosity data shown in Figs 8.25 and 8.26 is well predicted by the calculations.

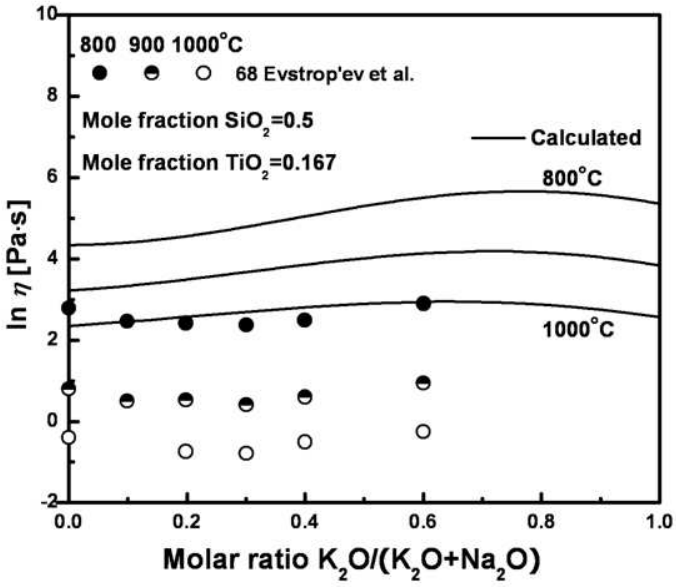

Fig. 8.25 Viscosity of TiO_2-K_2O-Na_2O-SiO_2 melts at 50 mol% SiO_2 and 16.7 mol% TiO_2 compared to experimental data [64]

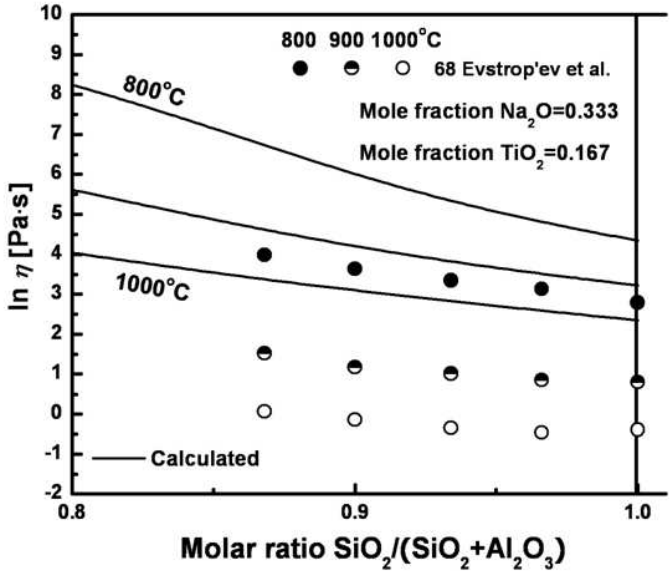

Fig. 8.26 Viscosity of TiO_2-Al_2O_3-Na_2O-SiO_2 melts at 33.3 mol% Na_2O and 16.7 mol% TiO_2 compared to experimental data [64]

8.2.3.6 TiO_2-CaO-MgO-Al_2O_3 -SiO_2 system

Blast furnace final slag is made from the meltdown of sinter, lump, coke and flux at high temperature, and can be considered approximately as a mixture of the five oxides, TiO_2, CaO, MgO, Al_2O_3 and SiO_2. The effect of TiO_2 on blast furnace slags has been studied by many authors [18, 58, 188, 277, 364].

Semik[277] measured viscosities of TiO_2-CaO-MgO-Al_2O_3-SiO_2 melts at constant Al_2O_3, MgO and CaO contents using the rotating crucible method with carbon crucibles under CO+N_2 gas atmosphere as shown in Figs 8.27 and 8.28. Some points indicated as 'Sub-Liquid' show abnormally high viscosities which most likely were measured in the sub-liquidus region with partial crystallization of the sample during the experiments, whereas most points show an excellent agreement with the lines calculated by the model. The observed trend of increasing viscosity with increasing SiO_2 contents is well predicted by the calculations. In Fig. 8.29, the viscosities predicted by the model compare well with the data points measured by Semik [277]

and Benesch et al. [18] who used the rotating crucible method with graphite crucibles. The agreement is well within experimental error limits.

Endell and Brinkmann [58] measured viscosities with additions of TiO_2 to CaO-MgO-Al_2O_3-SiO_2 melts using the counter-balanced method with Pt crucibles. As can be seen from Fig. 8.30, the experimental data show systematically higher viscosities although the difference is fairly small. These data are also higher for the CaO-MgO-Al_2O_3-SiO_2 system, indicating a small systematic error. However, the observed trend of decreasing viscosity with increasing TiO_2 content is quite well predicted by the model.

In Fig. 8.31, the viscosities are calculated at 8.9 mol% Al_2O_3, 20 mol% MgO and 10 mol% TiO_2 along with the experimental data of Zhilo et al. [364] and Miller and Babushkin [188] who measured viscosities using the rotating crucible method with Mo crucibles[364] and carbon crucibles [188]. As can be seen from Fig. 8.31, the data of Miller and Babushkin [188] show higher viscosities than the calculated lines although the difference is within experimental error limits. The scatter of experimental data measured by Zhilo et al. [364] seems to be as high as 1.0 in the natural logarithm scale. Overall, the viscosities predicted by the model for TiO_2-CaO-MgO-Al_2O_3-SiO_2 melts are believed to be in agreement with the measurements within experimental error limits.

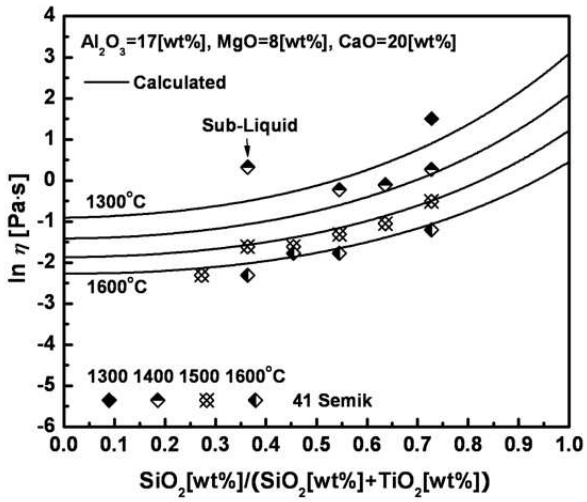

Fig. 8.27 Viscosity of TiO_2-CaO-MgO-Al_2O_3-SiO_2 melts at 17 wt% Al_2O_3, 8 wt% MgO and 20 wt% CaO compared to experimental data [277]

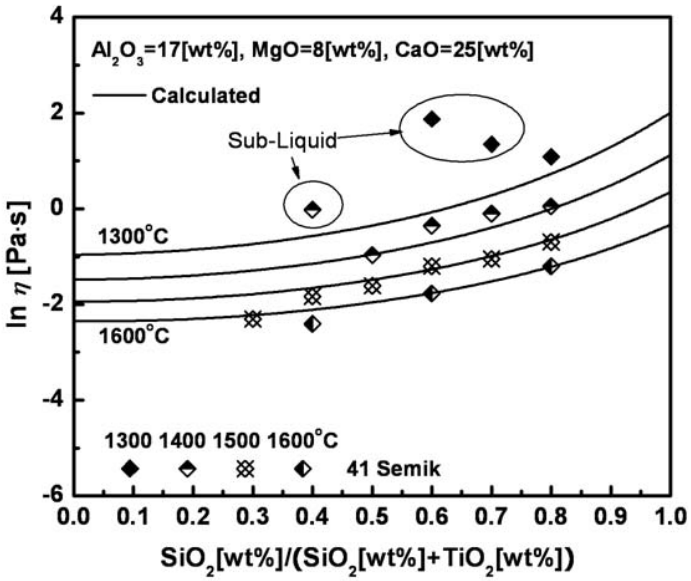

Fig. 8.28 Viscosity of TiO_2-CaO-MgO-Al_2O_3-SiO_2 melts at 17 wt% Al_2O_3, 8 wt% MgO and 25 wt% CaO compared to experimental data [277]

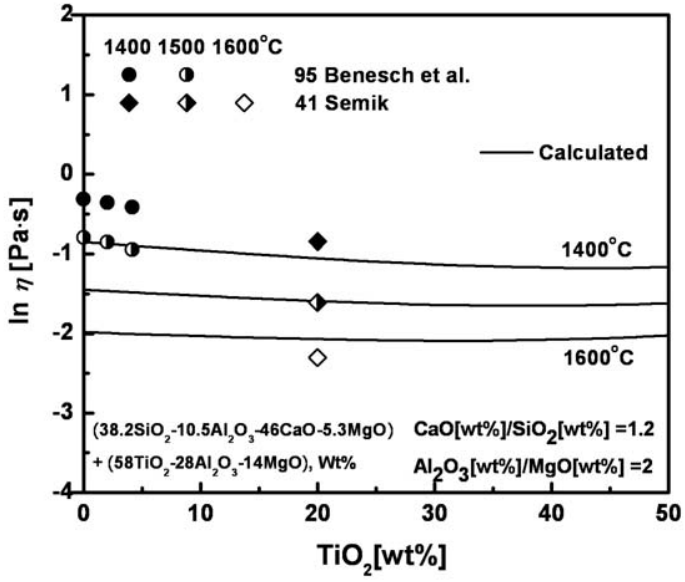

Fig. 8.29 Viscosity of TiO_2-CaO-MgO-Al_2O_3-SiO_2 melts for a weight ratio CaO/SiO_2 = 1.2 and Al_2O_3/MgO = 2 compared to experimental data [18, 277]

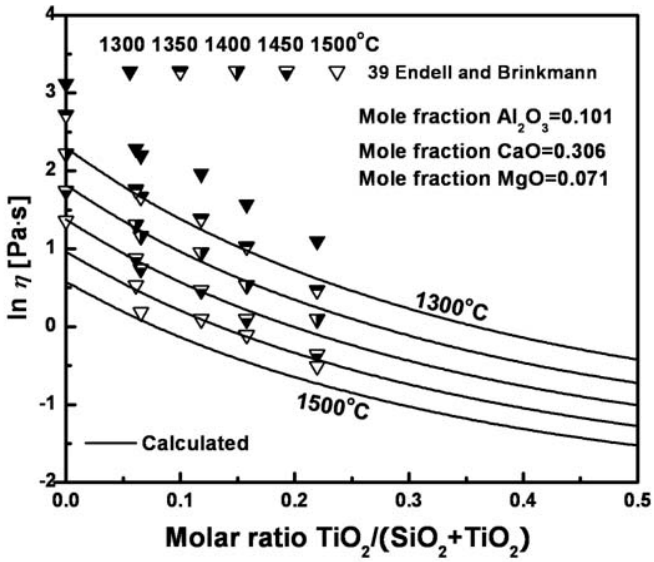

Fig. 8.30 Viscosity of TiO_2-CaO-MgO-Al_2O_3-SiO_2 melts at 10.1 mol% Al_2O_3, 30.6 mol% CaO and 7.1 mo% MgO compared to experimental data [58]

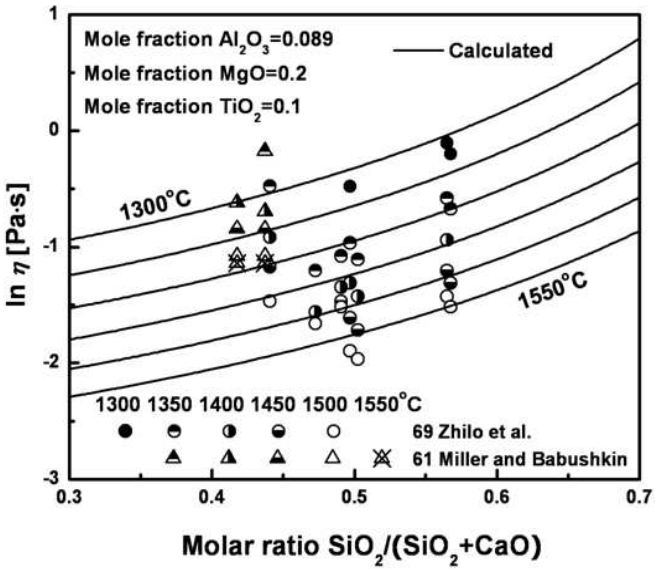

Fig. 8.31 Viscosity of TiO_2-CaO-MgO-Al_2O_3-SiO_2 melts at 8.9 mol% Al_2O_3, 20 mol% MgO and 10 mo% TiO_2 compared to experimental data [188, 364]

8.2.3.7 TiO_2 and Ti_2O_3 containing system

The model parameters of unary $TiO_{1.5}$ and binary $TiO_{1.5}$-SiO_2 system were optimized using data from mulcomponent systems containing both TiO_2 and Ti_2O_3 with the assumption that the model parameters of unary $TiO_{1.5}$ and the binary $TiO_{1.5}$-SiO_2 system would be similar to those of TiO_2 and the TiO_2-SiO_2 system, since no available data exist for binary and ternary systems. The model parameters are listed in Table 8.1.

Figs 8.32-8.34 compares the viscosities of the systems containing both TiO_2 and Ti_2O_3 with the experimental data of Handfield et al. [87], Morozov et al. [195] and Karyazin et al. [116]. Handfield et al. [87] measured viscosities with additions of Ti_2O_3 to the CaO-Al_2O_3-MgO-MnO-K_2O-TiO_2-SiO_2 system using the rotating crucible method with Mo crucibles under Ar gas atmosphere as shown in Fig. 8.32. The observed trend of data points is well predicted by the model at all temperatures.

Morozov et al. [195] measured viscosities for CaO-Al_2O_3-MgO-MnO-TiO_2-Ti_2O_3-SiO_2 melts at 1500 and 1550ºC using the rotating crucible method. As shown in Fig. 8.33, the observed trend of the data shows a fairly good agreement with the calculated lines although the data points measured at 1500ºC show somewhat higher viscosities. This difference is believed to be within experimental error limits.

Karyazin et al. [116]measured viscosities for the system of Al_2O_3-MgO-MnO- -TiO_2-Ti_2O_3-SiO_2 melts in the temperature range of 1550 to 1650ºC using the rotating crucible method. As can be seen from Fig. 8.34, the model shows a fairly good agreement with the data points measured at 1650ºC although the scatter of the data points seems to be slightly more than 1.0 in the natural logarithm scale. On the other hand, several data points measured at 1600ºC show abnormally high viscosities compared with the calculated lines. In this case, the sample containing very low SiO_2 contents (4.5 mol%) would strongly promote partial crystallization of the sample during the experiment with decreasing temperatures. Overall, the optimized unary and binary parameters for unary $TiO_{1.5}$ and binary $TiO_{1.5}$-SiO_2 system result in good reproducibility within experimental error limits for the viscosities of multicomponent systems containing both TiO_2 and Ti_2O_3.

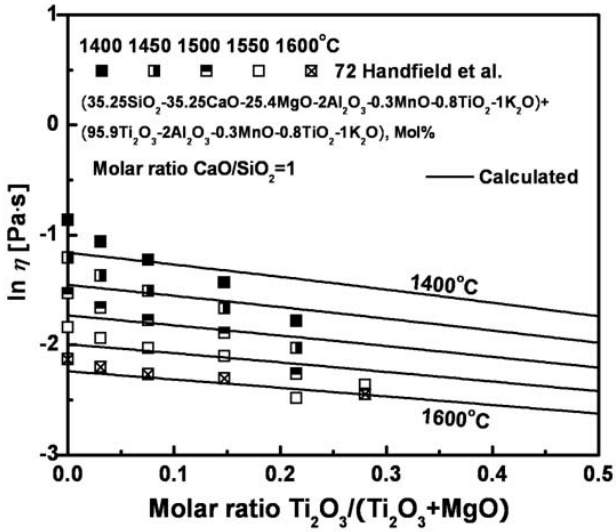

Fig. 8.32 Viscosity of $CaO\text{-}Al_2O_3\text{-}MgO\text{-}MnO\text{-}K_2O\text{-}TiO_2\text{-}Ti_2O_3\text{-}SiO_2$ melts in the section of ($35.25SiO_2$-35.25CaO-25.4MgO-$2Al_2O_3$-0.3MnO-$0.8TiO_2$-$1K_2O$) to ($95.9Ti_2O_3$-$2Al_2O_3$-0.3MnO-$0.8TiO_2$-$1K_2O$), mol% compared to experimental data [87]

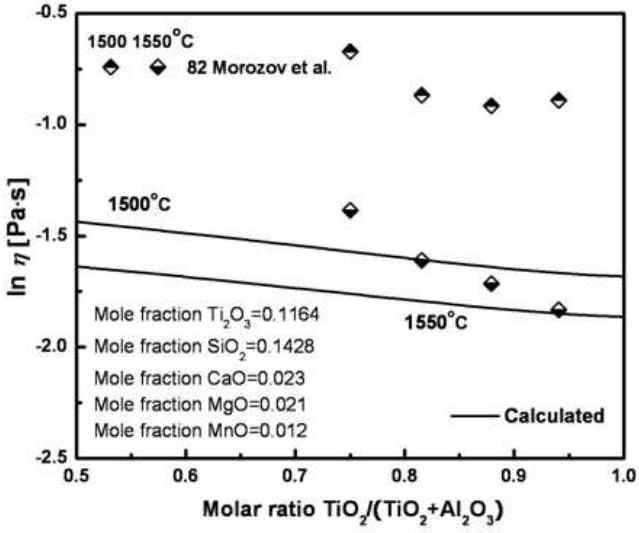

Fig. 8.33 Viscosity of $CaO\text{-}Al_2O_3\text{-}MgO\text{-}MnO\text{-}TiO_2\text{-}Ti_2O_3\text{-}SiO_2$ melts at 11.64 mol% TiO_2, 14.28 mol% SiO_2, 2.3 mol% CaO, 2.1 mol% MgO and 1.2 mol% MnO compared to experimental data [195]

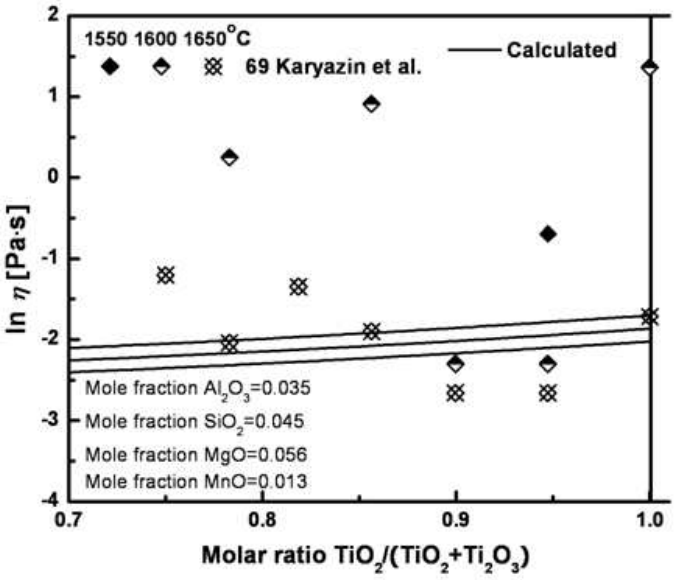

Fig. 8.34 Viscosity of Al_2O_3-MgO-MnO-TiO_2-Ti_2O_3-SiO_2 melts at 3.5 mol% Al_2O_3, 4.5 mol% SiO_2, 5.6 mol% MgO and 1.3 mol% MnO compared to experimental data [116]

8.3 Conclusions

To calculate the viscosity of TiO_x-containing silicate melts, only eight model parameters related to TiO_x are required. Four parameters, A_{TiO_2}, $A_{TiO_{1.5}}$, E_{TiO_2} and $E_{TiO_{1.5}}$ describe the viscosity of pure liquid TiO_2 and $TiO_{1.5}$; four binary parameters, $E^{1,1}_{TiO_2\text{-Si}}$, $E^{R}_{TiO_2\text{-Si}}$, $E^{1,1}_{TiO_{1.5}\text{-Si}}$ and $E^{R}_{TiO_{1.5}\text{-Si}}$ describe the viscosity of TiO_2-SiO_2 and $TiO_{1.5}$-SiO_2 melts. No viscosity data were available to account for the Charge Compensation Effect among TiO_x, Al_2O_3 and MO_x (TiO_2-Al_2O_3 and Ti_2O_3-MO_x), where M is a basic oxide, and thus no model parameters were applied for the Charge Compensation Effect. The viscosity of multicomponent melts containing TiO_2 and Ti_2O_3 is then predicted by the model without any additional adjustable model parameters.

To optimize the model parameters using the model, all experimental viscosity data were collected for melts formed by TiO_2 and Ti_2O_3 with SiO_2, Al_2O_3, CaO, MgO, Na_2O, K_2O and MnO. From a critical review of all available experimental data, the addition of TiO_2 or Ti_2O_3 is believed, as is the case for other basic oxides, to give negative effects on viscosity in the melt.

The deviation of the available experimental data from the viscosities predicted by the model does not exceed the scatter of experimental points among different authors and the experimental error limits in all sub-systems of SiO_2–Al_2O_3–CaO–MgO–Na_2O–K_2O–TiO_x-MnO that were used to calibrate the model. Overall, model parameters have been obtained which permit TiO_2 and Ti_2O_3 to be added to the database and which permit the accurate prediction of the viscosity of multicomponent TiO_x-containing melts.

Table 8.1 Optimized Model parameters for the viscosity expressed in Pa·s

System	Model parameter	Model parameters ($J \cdot mol^{-1}$)
TiO_2	$A_{TiO_2} = -7.5$	$E_{TiO_2} = 90000$
$TiO_{1.5}$	$A_{TiO_{1.5}} = -7.5$	$E_{TiO_{1.5}} = 73500$
TiO_2–SiO_2		$E^{1,1}_{TiO_2\text{-}Si} = -99250$ $E^{R}_{TiO_2\text{-}Si} = 95000$
$TiO_{1.5}$–SiO_2		$E^{1,1}_{TiO_{1.5}\text{-}Si} = -99250$ $E^{R}_{TiO_{1.5}\text{-}Si} = 95000$

The model parameters for subsystems without TiO_x that are used for the viscosity calculations in the present study were optimized and reported elsewhere (see Tables 4.1, 4.2, 5.1, 6.1 and 7.1).

CHAPTER 9 MODIFICATION OF THE MODEL FOR MELTS CONTAINING FLUORIDE AND APPLICATION TO SYSTEMS CONTAINING CaF_2

9.1 Introduction

Slags based on CaF_2 are widely used in the continuous casting process of steelmaking, welding and electroslag remelting. In the continuous casting process of steelmaking, the viscosity of a slag affects the velocity of circulating slag flow which controls mass transfer at the slag/metal interface and should be low enough to provide sufficient lubrication to prevent sticking, control uniform heat transfer and prevent surface cracks. It is well-known that the addition of CaF_2 significantly decreases the viscosity of slags, and thus some amounts of CaF_2 have been added in the mold flux of continuous casting process. On the other hand, the addition of fluorides poses severe problems for environmental pollution. Thus, the design for the proper composition of mold flux or other slags is required in the steelmaking process. However, there is no clear model which can predict the viscosity of multicomponent systems containing CaF_2 within experimental error limits. In addition, intrinsic experimental difficulties are encountered in measurements of the viscosity of CaF_2–containing slags due to the volatility of CaF_2 and the violent reactivity of the liquid with crucibles.

Unfortunately, our present oxide database [15] is not able to calculate the thermodynamic information of oxy-fluoride melts. Therefore, simple assumptions were needed to take into account the structure of oxy-fluoride melts as will be shown in next section. In the present study, the model is further developed to reproduce the viscosity of multicomponent systems containing fluorides such as CaF_2, NaF, KF, MgF_2 and AlF_3. In the present chapter, available viscosity data of melts containing CaF_2 will be treated. In Chapter 10, available viscosity data of melts containing other fluorides MF_x (M = Na, K, Mg, Al) will be introduced.

9.2 Modification of the model for melts containing CaF_2

9.2.1 Structural role of CaF_2 in oxy-fluoride melts

The structural role of CaF_2 in oxy-fluoride melts was investigated by many authors [99, 170, 227, 264, 329]. Tsunawaki et al. [329] studied the structural role of CaF_2 using Raman spectra in the system CaO-SiO_2-CaF_2. They concluded that CaF_2 contributed to the breakage of some Si-O bonds when the CaF_2 concentration was less than 20 mol% and the CaO/SiO_2 ratio was smaller than unity. Iguchi et al. [99] also concluded that CaF_2 in the basic CaO-SiO_2 system behaved as a diluent, while the addition of CaF_2 to the acid CaO-SiO_2 system caused an increase in the intensity of the designated Raman band. This was attributed to a higher number of non-bringing oxygens in the CaO-SiO_2-CaF_2 system. In other words, the structural role of CaF_2 in acid CaO-SiO_2 melts is a network modifier which breaks the silicate network. Park et al. [227] also studied the structural role of CaF_2 in the system of CaO-SiO_2-CaF_2 using FT-IR spectroscopy. They also concluded that the effect of CaF_2 on the viscous flow of molten slags can be understood by a decrease in the degree of polymerization of silicate melts by F^- as well as by O^{2-} ions. [227]

On the other hand, Luth [170] studied fluorine ions in the CaF_2-CaO-SiO_2 system using Raman spectroscopy and observed an increase in Q^3-species with a decrease of Q^0-species when adding CaF_2. Because of the highly ionic bonds of Ca-F, Luth could not observe Ca-F complexes using Raman spectroscopy [170]. Thus, he suggested that the substitution of CaF_2 for CaO at a fixed SiO_2 content would cause an increase in bulk polymerization of silicate melts by the formation of Ca-F complexes. Sasaki et al. [264] studied the effect of Ca and Na cations on the polymerization of silicate melts containing F ions in the system CaF_2-CaO-SiO_2 and CaF_2-NaF-CaO-SiO_2 using a molecular dynamic simulation. They also concluded that the substitution of F^- for O^{2-} enhances the polymerization of the melt due to the formation of loosely bonded Ca-2F complexes.

Therefore, the structural role of CaF_2 in silicate melts is still uncertain. However, from a critical review of available viscosity data of CaF_2-containing systems, we can see that the addition of CaF_2 decreases the viscosity of silicate melts and this implies that the addition of CaF_2 decreases the degree of polymerization of silicate melts. Thus, we conclude that CaF_2

behaves as a network modifier in silicate melts as we modeled for basic oxides in Chapters 3 and 4.

Fig. 9.1 shows the calculated viscosity of the $CaO\text{-}SiO_2$ system at 1600°C compared to the experimental data for the $CaF_2\text{-}SiO_2$ and $CaO\text{-}SiO_2$ systems. As shown in Fig. 9.1, the viscosity of the $CaF_2\text{-}SiO_2$ system shows very similar behavior to the $CaO\text{-}SiO_2$ system and this suggests that the effect of CaF_2 on the viscosity is very similar to that of CaO.

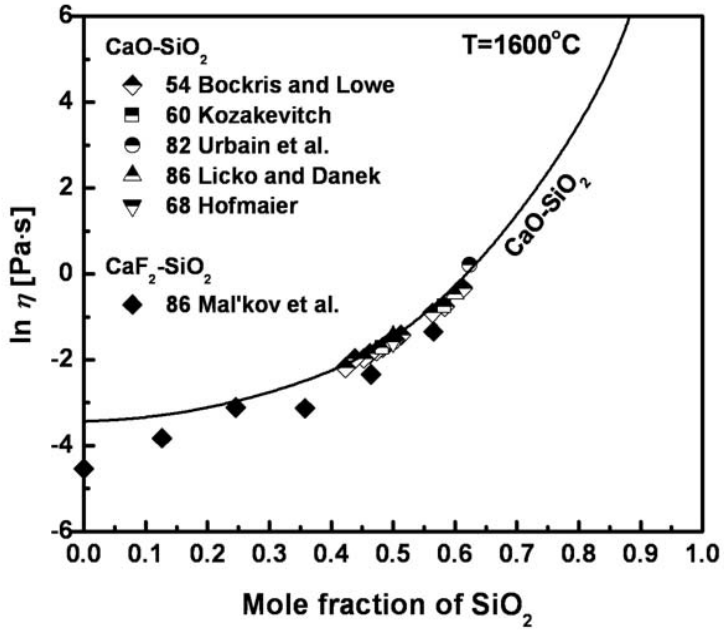

Fig. 9.1 Comparison of Viscosity between $CaF_2\text{-}SiO_2$ and $CaO\text{-}SiO_2$ melts. Experimental points [22, 96, 145, 164, 174, 335] and a calculated line of $CaO\text{-}SiO_2$ melts at 1600°C

9.2.2 Viscosity Model for oxy-fluoride melts

The structure of oxy-fluoride liquids is very complex. Unfortunately, the Modified Quasichemical Model [231, 232] and thermodynamic database[14] were not developed for all oxy-fluoride melts. Therefore, *p* in Eqs (3.4)-(3.9) cannot be calculated from the present thermodynamic data [14]. We should note that the viscosity of the $CaF_2\text{-}SiO_2$ system is very similar to the $CaO\text{-}SiO_2$ system as shown in Fig. 9.1.

Thus, we propose two simple assumptions as follows:

- All fluorides will behave as network modifiers in silicate or borate melts
- All fluorides will have same breaking effects on silicate or borate networks as all basic oxides containing the same cation.

The breaking effect of CaO and CaF_2 in silicates networks are shown schematically as follows:

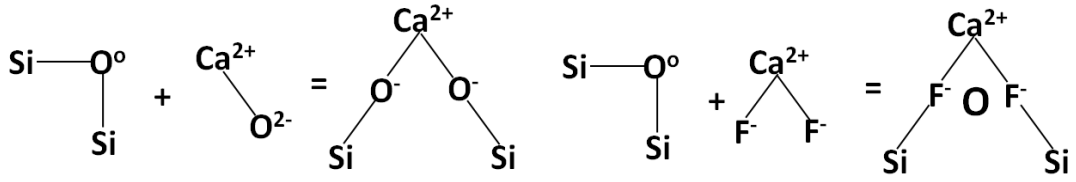

Therefore, we postulate that for all systems, MF_{2x} and MO_x have the same bridge-breaking behavior for the same metal M.

Thus, for the binary CaF_2-SiO_2 system, we calculate p by using the thermodynamic database with CaF_2 replaced by CaO. Then we use the previous viscosity model equations from Chapters 3 and 4 with optimized viscosity parameters for CaF_2 which will be similar to, but a bit different from, that for CaO (e.g. $E^{R}_{CaF_2\text{-Si}} = 67750$ and $E^{R}_{CaO\text{-Si}} = 81400$). For all fluorides, we apply similar unary and binary viscosity parameters as for other basic oxides as in Chapters 3 and 4.

For a multi-component system, such as, CaO-CaF_2-Al_2O_3-AlF_3-SiO_2, we therefore first calculate p by replacing (CaO+CaF_2) and ($AlO_{1.5}$+AlF_3) by CaO and $AlO_{1.5}$ respectively. Then we use the previous viscosity equations using optimized unary and binary viscosity parameters for the systems CaO-SiO_2, CaF_2-SiO_2, $AlO_{1.5}$-SiO_2 and AlF_3-SiO_2.

A problem arises because this is a reciprocal system (one containing 2 or more cations and 2 or more anions) with a charge neutrality condition: ($2n_{Ca} + 3n_{Al} + 4n_{Si} = n_F + 2n_O$). Hence, it is a 4-component system (not 5-component) in the sense of the Phase Rule and requires only 3 independent composition variables. That is, the composition can be expressed in several ways in terms of the mole fractions of CaO, CaF_2, Al_2O_3, AlF_3 and SiO_2. For instance, a solution described as containing 0.5 moles SiO_2, 0.2 moles CaO, 0.1 moles $AlO_{1.5}$ and 0.1 moles AlF_3 is

identical to one containing 0.5 moles SiO_2, 0.15 moles CaF_2, 0.2 moles $AlO_{1.5}$ and 0.05 moles CaO as shown in the reaction 9.1.

Which mole fractions should be added in the model equations from Chapters 3 and 4 for the viscosity calculation? An approximate solution to this question is as follows:

$$1.5CaO(l) + AlF_{1.5}(l) \rightleftarrows 1.5CaF_2(l)+AlO_{1.5}(l)\ ;\ \Delta G^{o}_{(9.1)} \tag{9.1}$$

$$K_{(9.1)} = \exp\left(\frac{-\Delta G^{o}_{(9.1)}}{RT}\right) = \frac{a^{1.5}_{CaF_2} a_{AlO_{1.5}}}{a^{1.5}_{CaO} a_{AlF_3}} \approx \frac{X^{1.5}_{CaF_2} X_{AlO_{1.5}}}{X^{1.5}_{CaO} X_{AlF_3}} \tag{9.2}$$

where $\Delta G^{o}_{(9.1)}$ is Gibbs energy change for the reaction (9.1) and $K_{(9.1)}$ is the equilibrium constant of reaction (9.1). R and T are the gas constant (J/mol) and absolute temperature (Kelvins) respectively. a_{CaF_2}, a_{CaO}, a_{AlF_3} and $a_{AlO_{1.5}}$ are the acitivities of CaF_2, CaO, AlF_3 and $AlO_{1.5}$ in the solution respectively and X_{CaF_2}, X_{CaO}, X_{AlF_3} and $X_{AlO_{1.5}}$ are the mole fractionos of CaF_2, CaO, AlF_3 and $AlO_{1.5}$ in the solution respectively.

First, we input the overall composition in terms of any convenient set of components. Secondly, $\Delta G^{o}_{(9.1)}$ is calculated from the Gibbs free energies of the pure liquid oxides and fluorides. Then, the X_i calculated from Eq. (9.2) for each liquid oxide and fluoride will give the "equilibrated composition" or "formal composition" which is then used in the model equations from Chapters 3 and 4. In the present example, if $\Delta G_{(9.1)} << 0$ (and $K_{(9.1)} >> 1$), CaF_2 and $AlO_{1.5}$ would predominate over CaO and AlF_3.

Physically, this means that in the liquid solution, there is a strong tendency for Ca and F to form clusters and for Al and O to form clusters; that is, Ca-F and Al-O are preferential first-nearest-neighbor pairs. Hence, the viscosity of the multicomponent solution will be calculated mainly from the binary parameters for the CaF_2-SiO_2 and $AlO_{1.5}$-SiO_2 systems, and will depend upon the binary CaO-SiO_2 or AlF_3-SiO_2 parameters only insofar as there is an excess of CaO or AlF_3. In other words, the system will be treated, depending upon the overall mass balance, either as the CaF_2-Al_2O_3-CaO-SiO_2 (with $X_{AlF_3} \approx 0$) or the CaF_2-Al_2O_3-AlF_3-SiO_2 system (with $X_{CaO} \approx 0$).

This proposed treatment is a simplication. Strictly speaking, a real solution of oxy-fluoride melts would be different from a solution of each pure liquid oxides and fluorides. However, the proposed treatment gives a qualitatively correct functional dependence of the viscosity on temperature and composition, and the description is made quantitiatively by fitting the viscosity data using unary and binary model parameters of MF_x-SiO_2 or MF_x-$BO_{1.5}$ systems (M=basic cations).

Thus, for all cations M, equilibrium contants as shown in Eq. (9.2) are calculated using the Gibbs free energies of the pure liquid oxides and fluorides. Note that we do not consider SiF_4 and BF_3 formation. We assume all Si and B atoms are bonded only to oxygens because the formation of $SiF_4(l)$ and $BF_3(l)$ in liquid solution is very unstable [15].

The same approach for MF_x-B_2O_3 systems (M = basic cation) was applied for the modification of the model with Eqs (3.18)-(3.21). Especially, in alkali borate NF-B_2O_3 melts (N=Na and K), the observed trends of viscosities are quite similar to those of the $NO_{0.5}$-B_2O_3 systems. From the review of experimental data of the system NF-B_2O_3 melts (N = Na and K), it appears that the clusters at the tetraborate composition K:B = 1:4 or Na:B = 1:4 are the most likely clusters to be formed strongly in the systems NF-B_2O_3(N = Na and K) as will be shown in Figs 10.4-10.5.

In order to take into account the "*Borate anomaly*" in the melts, in Chapter 3 we employed the formation of solid-like clusters at the composition of alkali tetraborates NB_4 (N = Na, K) [26]. In the present study, we extended the model further to reproduce the abnormal behavior of viscosity for each NF_x-B_2O_3(N = Na and K) melt by employing the formation of solid-like clusters at the composition of alkali tetraborates NB_4FO_6(N = Na and K) via reaction (9.3) using Eqs (3.23) to (3.29).

$$m \cdot \mathrm{NF} + 4m \cdot \mathrm{BO}_{1.5} \rightleftarrows m(\mathrm{NB_4FO_6})(\mathrm{N = Na\ and\ K}) \tag{9.3}$$

9.3 Review of the available viscosity data and calibration of the model

In the present study, viscosity data are reviewed for available MF_x-containing subsystems (M = Ca, Mg, Na, K and Al) of the MF_x–SiO_2–B_2O_3–Al_2O_3–CaO–MgO–Na_2O–K_2O–MnO–TiO_y

system. The data judged to be most reliable are shown in the figures below. In this chapter, only CaF_2-containing systems are introduced and systems with other fluorides (MgF_2, NaF, KF and AlF_3) will be introduced in Chapter 10.

The proposed model is intended for oxy-fluoride melts in a single-phase region. The extension of the model to describe the viscosity of glasses will be reported in Chapters 11 and 12. Therefore, the viscosity data were collected mainly for melts above the liquidus or for slightly supercooled melts where crystallization did not occur. These measurements were mostly made with rotational or vibrational viscometers. If an abnormally high viscosity value was reported for a temperature below the liquidus, this is most likely the result of crystallization. In obvious cases such data points were discarded, but sometimes these points are still shown in the figures if it is deemed possible that they correspond to a supercooled liquid which does not contain precipitated solids. Viscosities of glasses, measured for example by a fiber elongation or beam-bending method, were not considered in the present study.

As mentioned in the section 2.3.1, viscosity measurement for the oxy-fluoride melts would have larger errors than that of oxide melts due to the difficulties of the chemical analysis of the system caused from the effect of volatilization of the fluorides and the presence of the moisture in the sample. The average absolute uncertainty of viscosity measurements of oxy-fluoride melts was shown within 1.5 to 2 in ln [Pa·s] scale from available viscosity data of the subsystems of MF_x–SiO_2–B_2O_3–Al_2O_3–CaO–MgO–Na_2O–K_2O–MnO–TiO_y (M = Ca, Mg, Na, K and Al).

9.3.1 Viscosity of pure CaF_2 melts

All optimized unary parameters of CaF_2 and binary parameters of CaF_2-SiO_2 are listed in Table 9.1. In oxy-fluoride melts, as shown in section 9.2.2, we would expect the formation of other fluorides such as NaF and MgF_2 from the initial composition of the melt. Thus, we have to consider the effect of other fluorides on viscosity in oxy-fluoride melts when considering the overall “equilibrated composition” calculated from the given initial composition of the melts by the thermodynamic database [14]. Thus, all unary and binary parameters A_{MF_x}, E_{MF_x}, $E^{1,1}_{MF_x\text{-}Si}$, $E^{Ring}_{MF_x\text{-}Si}$, $E^{R}_{MF_x\text{-}Si}$, $A^{*}_{B(MF_x)}$ and $E^{*}_{B(MF_x)}$ were optimized simultaneously using the developed

viscosity model to fit available viscosity data within experimental error limits. The unary and binary parameters of other fluorides (MgF_2, NaF, KF and AlF_3) will be shown in Chapter 10.

In order to evaluate the viscosities of silicate melts containing CaF_2 the evaluation of the viscosity of pure CaF_2 is indispensable. However, as shown in Fig. 9.2, the assessment of these data is extremely difficult because the reported viscosities differ by two orders of magnitude. The most probable source of error lies in the use of techniques which are unsuitable for the required viscosity range. Other error sources are sample impurities or violent reaction with crucibles. Viscosities of pure CaF_2 were measured by many investigators using the rotating crucible method [38, 216, 273, 356, 366, 365] and the vibrational viscometer method [12, 78, 97, 102, 149, 174, 309, 341, 347, 354, 368]. Even measurements with the same method show a wide scatter, although the viscosity data measured by the rotating crucible method show somewhat consistent results. The electro-vibrational method and the oscillation method can contribute to large systematic errors in viscosity measurements by the uncertainties in the damping rates of an oscillating wire [104]. On the other hand, the rotating crucible method requires only information for the radius and the height of a bob which is rotated in the sample liquid. As shown in Fig. 9.2, the data reported by Hoshino et al. [97], Kulifeev et al. [149] and Gladkii et al. [78] show too low values and are inconsistent with other data. In order to obtain the unary and binary parameters for CaF_2 and CaF_2-SiO_2, all available unary, binary and ternary systems containing CaF_2 were considered and all parameters were optimized simultaneously. The data of Zhmoidin [366, 365], Vyatkin et al. [347], Zhukova and Sheludyakov [368],Stepanov et al. [309], Istomin et al. [102] and Mal'kov [174] were considered for the optimization and the parameters A_{CaF_2} and E_{CaF_2} were obtained. The calculated viscosities the model are also compared with the calculated viscosities of another group in this laboratories [253]. Robelin and Chartrand [253] developed the viscosity model to reproduce the viscosity data of the NaF-AlF_3-CaF_2-Al_2O_3 system. The viscosity of unary CaF_2 in their model has been calibrated by considering the viscosity data of both unary CaF_2 and other sub-systems of the NaF-AlF_3-CaF_2-Al_2O_3 system [253]. The result shows slightly different temperature dependence from that of the model in the present study. However, the reproducibility of the model of Robelin and Chartrand [253] are very similar to that of the model in the present study.

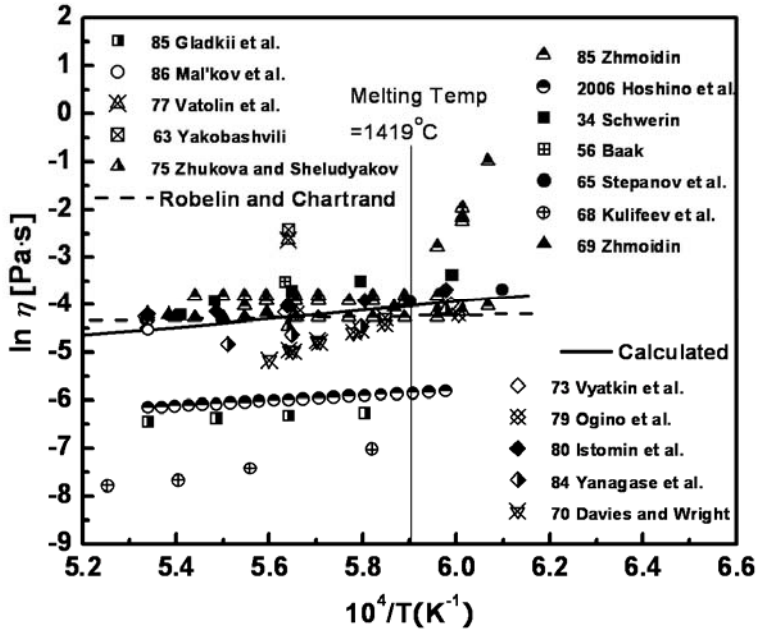

Fig. 9.2 Calculated viscosity in CaF_2 system compared to experimental data [12, 38, 78, 97, 102, 149, 174, 216, 273, 309, 341, 347, 354, 356, 366, 365, 368] and to calculated viscosities of the model of Robelin and Chartrand [253]

9.3.2 Viscosities of the binary CaF_2–SiO_2 melts

Viscosities of the CaF_2-SiO_2 melts were measured by Istomin et al. [102] and Mal'kov [174] using the vibration viscometer method. The viscosity measurement in the binary CaF_2-SiO_2 system could include many error sources by HF(g) formed by the reaction with moisture and SiF_4(g) formed by SiO_2 liquid with CaF_2 liquid as shown in Eqs. (2.24)-(2.25). As mentioned in section 2.3.2, however, the effect of vaporization by HF(g), SiF_4(g) and CaF_2(g) would be negligible because most studies were carried out with thorough removal of moisture of the injected gas and the sample. The unary and binary parameters A_{CaF_2}, E_{CaF_2}, $E^{1,1}_{CaF_2\text{-}Si}$ and $E^{R}_{CaF_2\text{-}Si}$ were carefully and simultaneously optimized using the unary CaF_2 and all available binary and some ternary systems. As shown in Fig. 9.3, the experimental data are in good agreement with the lines calculated by the model at all temperatures.

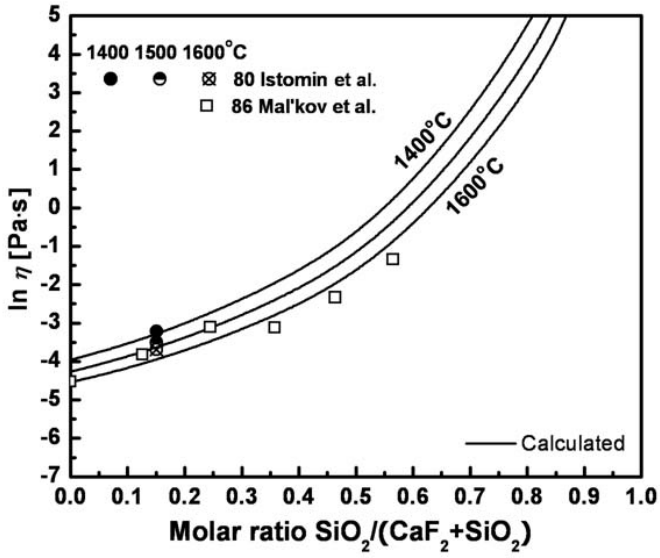

Fig. 9.3 Viscosity of CaF_2-SiO_2 melts: experimental points [102, 174] and calculated lines

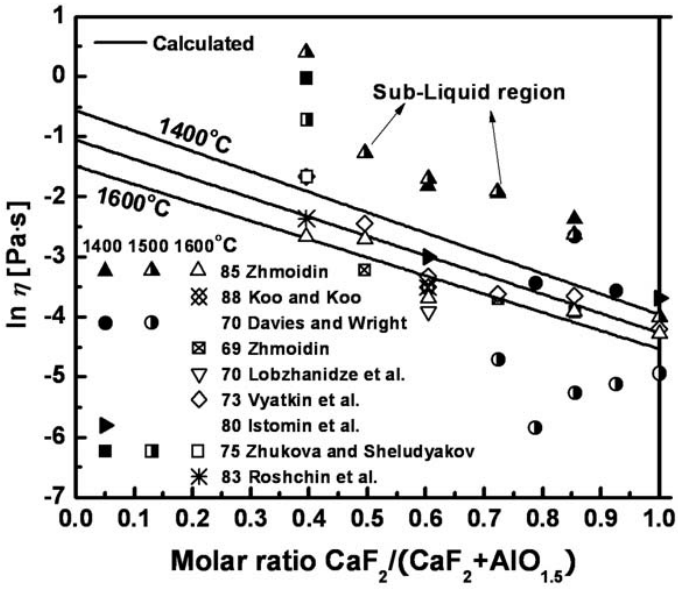

Fig. 9.4 Viscosity of CaF_2-Al_2O_3 melts: experimental points [38, 102, 141, 169, 254, 347, 366, 365, 368] and calculated lines

9.3.3 Viscosities of the binary CaF_2–Al_2O_3 melts

The viscosity of the CaF_2-Al_2O_3 melts was measured by several investigators using the rotating crucible method [38, 141, 366, 365] and the vibration viscometer method [102, 254, 347, 368]. As shown in Fig. 9.4, these calculated lines were reproduced linearly by the unary parameters of CaF_2 and $AlO_{1.5}$ according to Eqs (3.37)-(3.38). Most data except for the data of Istomin et al. [102] show higher viscosities than the calculated lines at 1400°C and 1500°C. Those data would have been measured in the sub-liquidus region and they show abnormally high viscosities because of partial crystallization of the sample. However, the observed trend of decreasing viscosity with increasing CaF_2 content is well predicted by the model. At 1600°C, most data show a good agreement with the calculated line within experimental error limits. The data of Davies and Wright [38] show systematically lower viscosities than the other data of all systems containing CaF_2. Again, we assumed that there is no charge compensation effect in the system containing CaF_2 and Al_2O_3. Without involving charge-compensated species such as $CaAl_2FO_3$, the calculated lines reproduce well the viscosity data within experimental error limits.

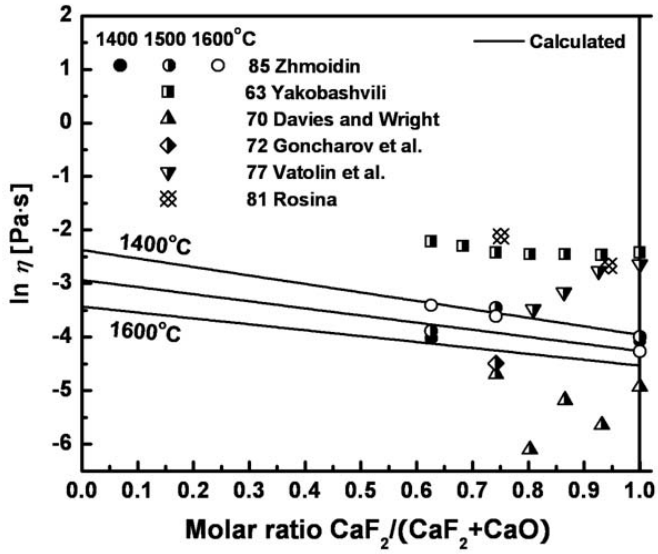

Fig. 9.5 Viscosity of CaF_2-CaO melts: experimental points [38, 79, 255, 341, 354, 366] and calculated lines

9.3.4 Viscosities of the binary CaF_2–CaO melts

The viscosity of the CaF_2-CaO melts were measured by several investigators using the rotating crucible method [38, 366] and the vibration viscometer method [79, 255, 341, 354]. All calculated lines were reproduced linearly by the unary parameters of CaF_2 and CaO according to Eqs (3.37)-(3.38). In the CaF_2-CaO system, there would be replacement only between fluorine and oxygen ions. Thus, the viscosity of this system would be expressed linearly as a function of the molar ratio $CaF_2/(CaF_2+CaO)$. In Fig. 9.5, the data measured at 1500ºC by different authors show a big scatter of viscosities which is more than 2 in the natural logarithm scale. The data of Yakobashvili [354] show systematically higher viscosities than the calculated lines because his unary CaF_2 data were higher than other data as shown in Fig. 9.2. On the other hand, the data of Davies and Wright [38] show systematically lower viscosities than other data for all systems containing CaF_2. However, it can be seen that the observed linear trend of viscosity data is fairly well predicted by the model.

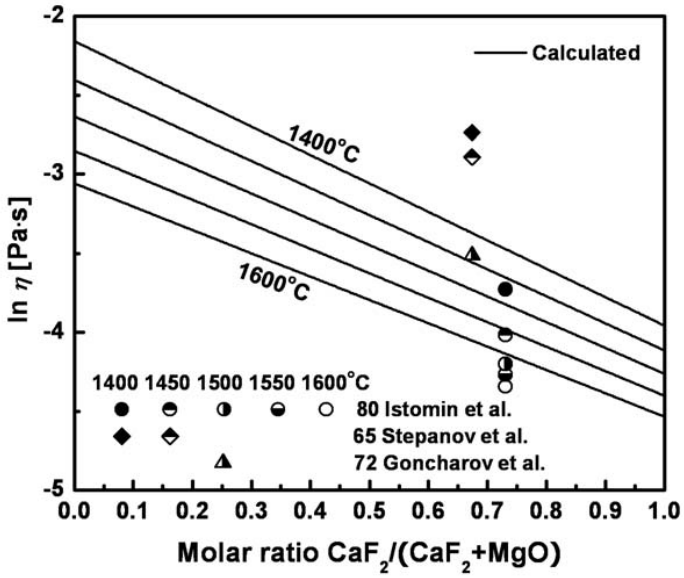

Fig. 9.6 Viscosity of CaF_2-MgO melts: experimental points [79, 102, 309] and calculated lines

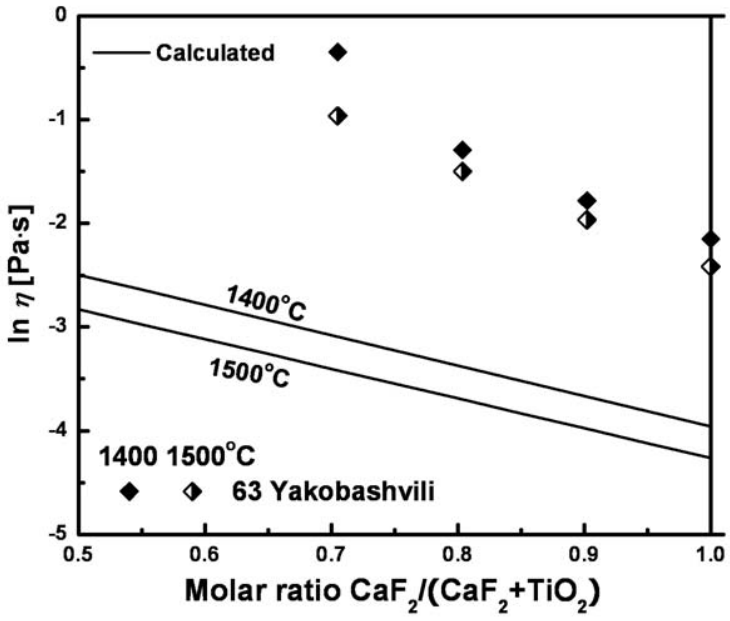

Fig. 9.7 Viscosity of CaF_2-TiO_2 melts: experimental points [354] and calculated lines

9.3.5 Viscosities of the binary CaF_2–MgO melts

The viscosity of the CaF_2-MgO melts was measured by several investigators using the vibration viscometer method [79, 102, 309]. In Fig. 9.6, all calculated lines were reproduced linearly by the unary parameters of CaF_2 and MgO according to Eqs (3.37)-(3.38) and are in a good agreement with all viscosity data within experimental error limits.

9.3.6 Viscosities of the binary CaF_2–TiO_2 melts

The viscosity of the CaF_2-TiO_2 melts was only measured by Yakobashvili [354] using the vibration viscometer method. As can be seen in Fig. 9.7, all data points show systematically higher viscosities than the lines calculated by the model because their unary CaF_2 data are systematically higher than the other data as shown in Fig. 9.2. All calculated lines were reproduced linearly by the unary parameters of CaF_2 and TiO_2 according to Eqs (3.37)-(3.38) and the observed trend of viscosity data is well predicted by the model.

9.3.7 Viscosities of the ternary CaF_2–CaO–SiO_2 melts

The viscosities of ternary and higher-order melts containing CaF_2 were predicted by the model based on the unary and binary viscosity parameters given from Tables 4.1, 5.1, 5.2, 6.1, 7.1, 8.1, 9.1, 10.1 and 10.2 without any additional adjustable parameters.

The viscosity of the CaF_2-CaO-SiO_2 melts has been well-investigated by many researchers to carry out systematic studies of viscosities of the mold flux in the continuous casting process of steelmaking. Figs 9.9-9.15 show the calculated viscosities of the CaF_2-CaO-SiO_2 system compared to experimental data [90, 114, 196, 280, 292, 357, 368] measured by the rotating crucible method [90, 280, 292, 357], the vibrational viscometer method [196, 368] and the oscillation viscometer method [114]. As shown in Figs. 9.9 to 9.14, the data points of the CaO-SiO_2 system reported by Shiraishi and Saito [292] lie slightly higher than the calculated lines at all temperatures although the difference is fairly small. It was shown that the calculated lines for the CaO-SiO_2 system were in a good agreement with many other authors as shown in Fig. 3.8 [82].

In Figs. 9.9 to 9.10, viscosities were calculated at constant molar ratio of CaO/SiO_2 with the addition of CaF_2 and most data show good agreement with the calculated lines at all temperatures within experimental error limits. It is seen that the observed trend of decreasing viscosity with the addition of CaF_2 is well predicted by the calculations obtained from only unary and binary parameters of the model. As can be seen in Figs. 9.11 to 9.15, most data except for the data of Shahbazian et al. [280] show a fairly good agreement with the lines calculated by the model within experimental error limits. As can be seen from Fig. 9.12, the model is well able to reproduce the decreasing trend of the viscosities of the CaF_2-CaO-SiO_2 with addition of CaF_2 from 0 to 53 mol%. However, as shown in Fig. 9.13, the decreasing trend of the viscosity data of Yasukouchi et al. [357] and Shiraishi and Saito [292] is somewhat different from those of calculated lines of the model. However, the extrapolation of those viscosity data of two authors [292] [357] would lead to systematically lower viscosities of unary CaF_2 than the calculated viscosities. It should be noted that the viscosity of CaF_2 were carefully evaluated and most of data show good agreement with the calculated line as shown in Fig. 9.2.The data of Shahbazian et al. [280], who used the rotating crucible method with iron crucible and spindles, show systematically lower viscosities than the other data as shown in Fig. 9.11 and 9.15, although the

difference is fairly small. This difference might be caused from contamination of the sample by the iron crucibles and spindles.

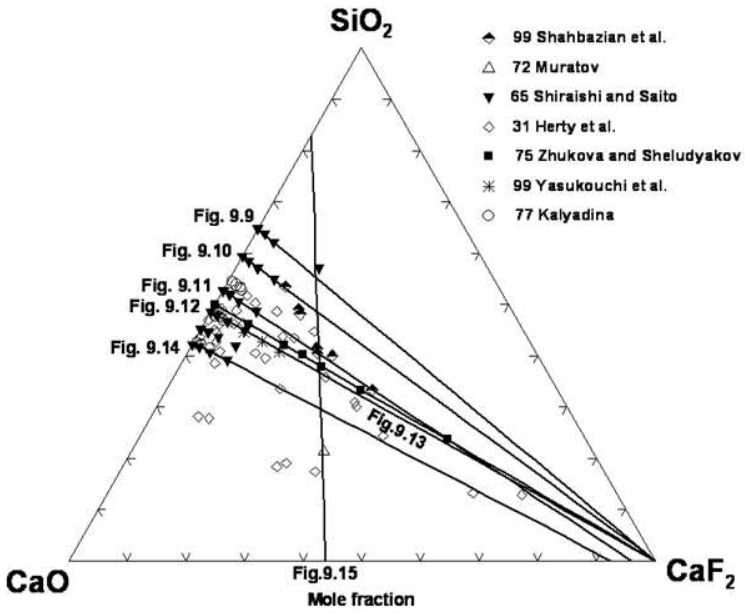

Fig. 9.8 Compositions in the CaF_2-CaO-SiO_2 system at which experimental viscosity measurements are available [90, 114, 196, 280, 292, 357, 368]. The lines indicate seven sections of this system selected to show the viscosity as a function of composition in Figs 9.9 to 9.15.

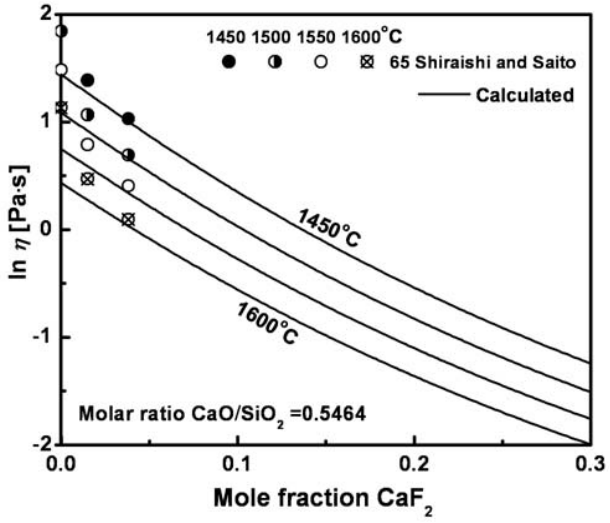

Fig. 9.9 Viscosity of CaF_2-CaO-SiO_2 melts for a molar ratio CaO/SiO_2 = 0.5464 compared to experimental data [292]

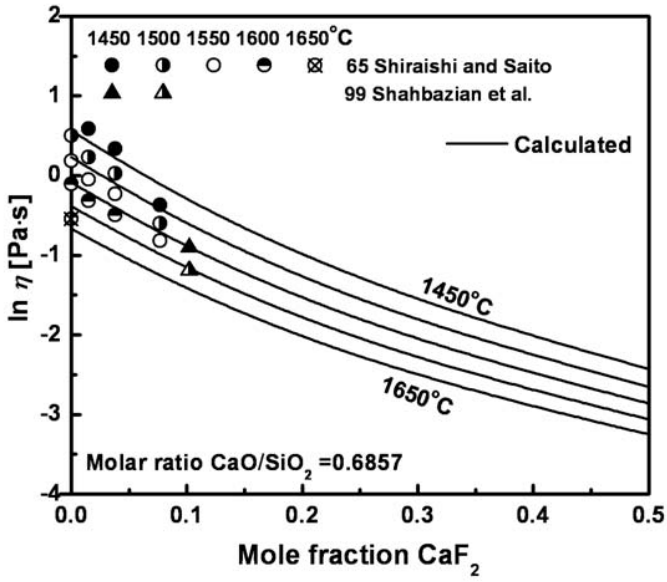

Fig. 9.10 Viscosity of CaF_2-CaO-SiO_2 melts for a molar ratio CaO/SiO_2 = 0.6857 compared to experimental data [292]

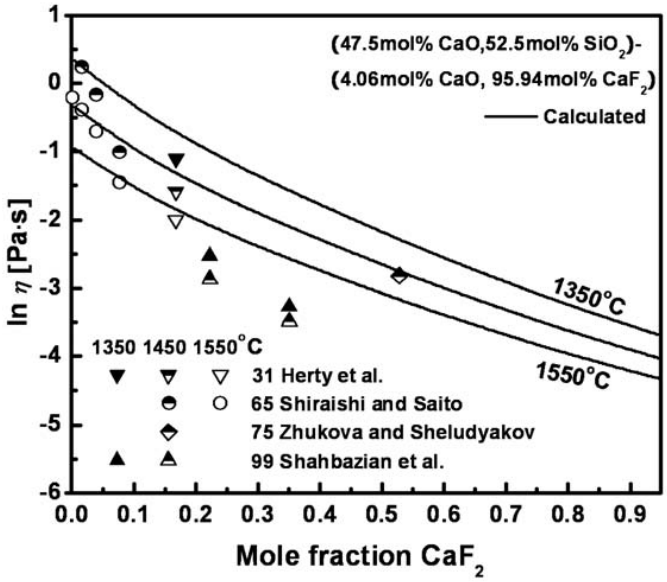

Fig. 9.11 Viscosity of CaF_2-CaO-SiO_2 melts in the section of (47.5 mol% CaO, 52.5 mol% SiO_2) to (4.06 mol% CaO, 95.94 mol% CaF_2) compared to experimental data [89, 280, 292, 368]

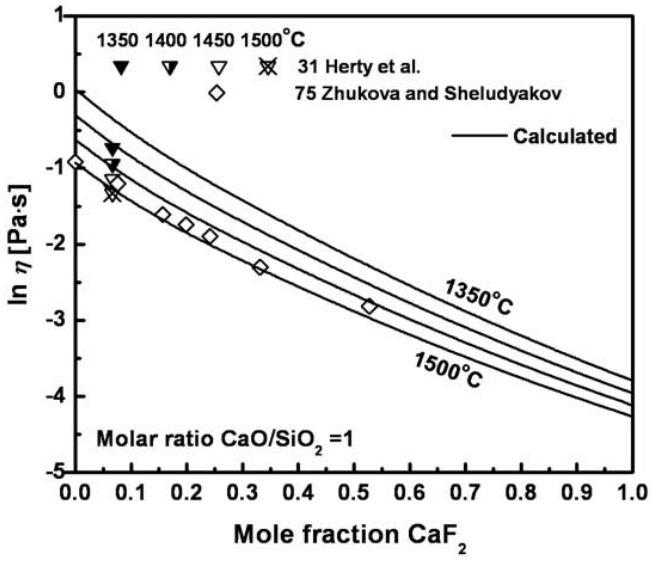

Fig. 9.12 Viscosity of CaF_2-CaO-SiO_2 melts for a molar ratio CaO/SiO_2 = 1 compared to experimental data [89, 368]

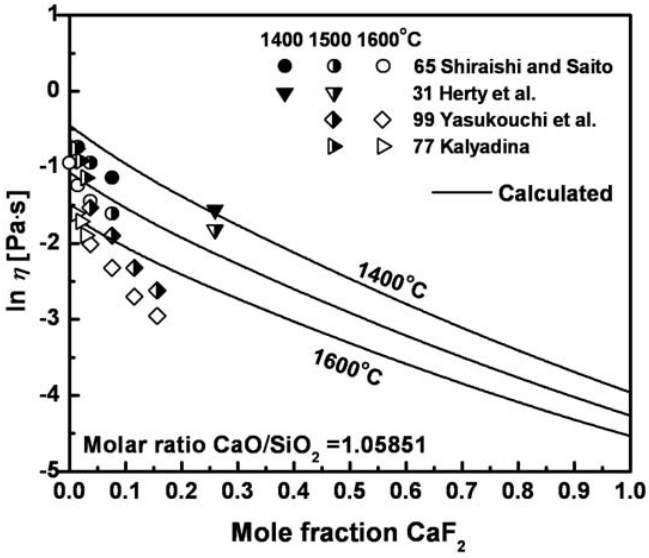

Fig. 9.13 Viscosity of CaF_2-CaO-SiO_2 melts for a molar ratio CaO/SiO_2 = 1.05851 compared to experimental data [89, 114, 292, 357]

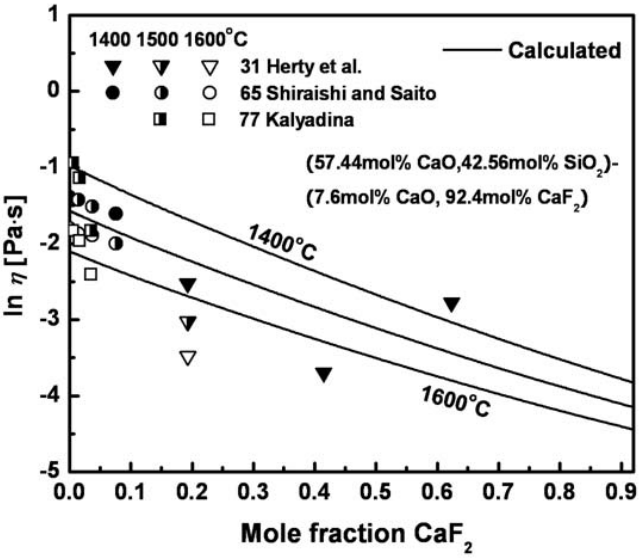

Fig. 9.14 Viscosity of CaF_2-CaO-SiO_2 melts in the section of (57.44 mol% CaO, 42.56 mol% SiO_2) to (7.6 mol% CaO, 92.4 mol% CaF_2) compared to experimental data [89, 114, 292]

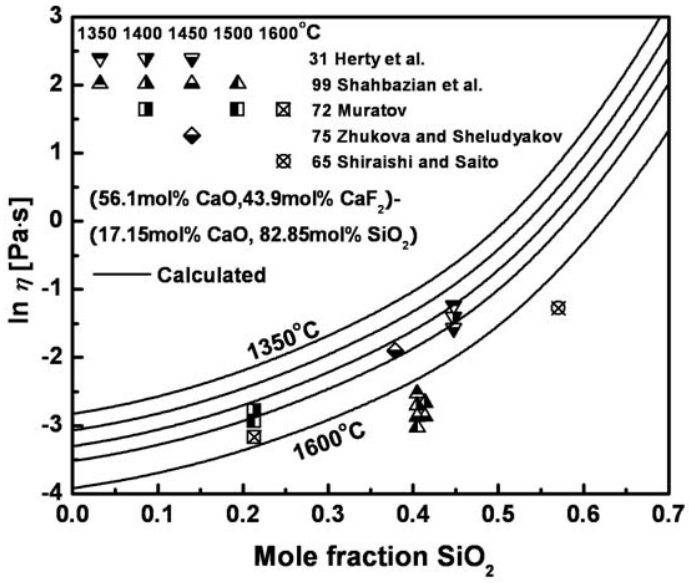

Fig. 9.15 Viscosity of CaF_2-CaO-SiO_2 melts in the section of (56.1 mol% CaO, 43.9 mol% CaF_2) to (17.15 mol% CaO, 82.85 mol% SiO_2) compared to experimental data [89, 196, 280, 292, 368]

9.3.8 Viscosities of the ternary CaF_2–Al_2O_3–CaO melts

The viscosity of the CaF-Al_2O_3-CaO melts has also been well-investigated by many researchers to carry out systematic studies of viscosities of slags used in the refining process of steelmaking. Figs 9.17-9.21 show the calculated viscosities of CaF-Al_2O_3-CaO melts compared to the experimental data [38, 61, 141, 196, 245, 296, 368] measured using the rotating crucible method [38, 141] and the vibrational viscometer method [61, 196, 245, 296, 368].

Figs 9.17-9.19 show the calculated viscosities of the CaF-Al_2O_3-CaO melts at constant molar ratio of CaO/Al_2O_3 = 1.814, 2.933 and 1.53, respectively. It can be seen that most of data except for the data of Davies and Wright [38] are in good agreement with the calculated lines within experimental error limits. It is seen that the observed trends of decreasing viscosity with the addition of CaF_2 are well predicted by the model using only unary and binary parameters. Again, the data points of Davies and Wright [38] show systematically lower viscosities in all CaF_2 containing oxy-fluoride melts.

In Fig. 9.20, the viscosities are calculated in the section of 92.85 mol% CaO-7.15 mol% CaF_2 to 87.39 mol% Al_2O_3-12.61 mol% CaF_2 along with the experimental data of Povolotskii et al. [245], Sikora and Zielinski [296] and Zhukova and Sheludyakov [368]. The scatter of experimental data measured by Povolotskii et al. [245] is slightly more than 1 in the natural logarithm scale. As can be seen from Fig. 9.20, the viscosities predicted by the model are believed to be in agreement with the measurements within experimental error limits at all temperatures.

In Fig. 9.21, viscosities were calculated at 30 mol% Al_2O_3 as a function of molar ratio of CaF_2 and CaO along with the data points of Povolotskii et al. [245]. As can be seen from Fig. 9.21, the data points of of Povolotskii et al. [245] at the binary CaO-Al_2O_3 system show systematically higher viscosities than the calculated lines. In addition, the data points show an abrupt decrease, and then show linearly decreasing trends with increasing CaF_2. Since there is no physical reason for such an abrupt decreasing trend, it is most likely just an artifact caused from the crystallization of the sample during the experiment. It should be noted that the viscosity of CaO-Al_2O_3 reported in the previous paper [81] are fairly in good agreement with other authors' data within experimental error limits. Overall, it seems that the observed trends of the viscosity data are well predicted by the model within experimental error limits.

9.3.9 Viscosities of the ternary CaF_2–Al_2O_3–MgO melts

In Fig. 9.22, the viscosities of the CaF_2-Al_2O_3-MgO melts are calculated in the section of (65.95 mol% MgO - 34.05 mol% CaF_2) to (43.37 mol% Al_2O_3 - 56.63 mol% CaF_2) along with the experimental data measured by Roshchin et al. [254] using the vibrational viscometer method at 1600°C. As can be seen from Fig. 9.22, the data points of Roshchin et al. [254] indicate an abrupt change of the slope in the middle of the plot where the model predicts a smooth variation of the viscosity when MgO is replaced by Al_2O_3. Since there is no obvious physical reason for such behavior, it is most likely an artifact caused by the scatter of the experimental data which is within experimental error limits.

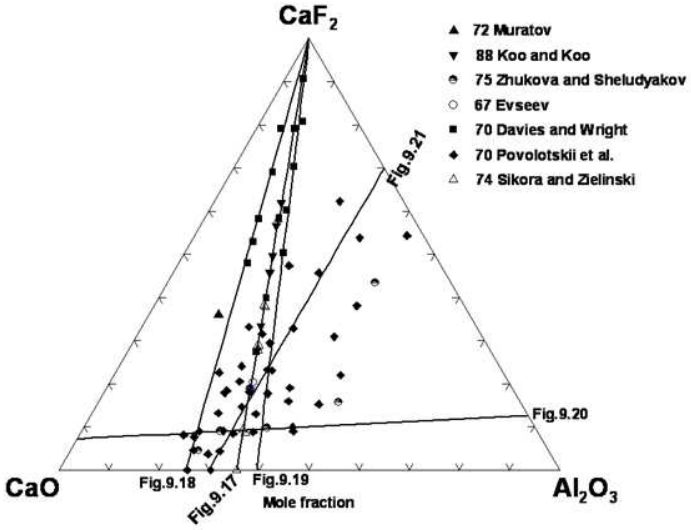

Fig. 9.16 Compositions in the CaF_2-Al_2O_3-CaO system at which experimental viscosity measurements are available [38, 61, 141, 196, 245, 296, 368]. The lines indicate five sections of this system selected to show the viscosity as a function of composition in Figs 9.17 to 9.21.

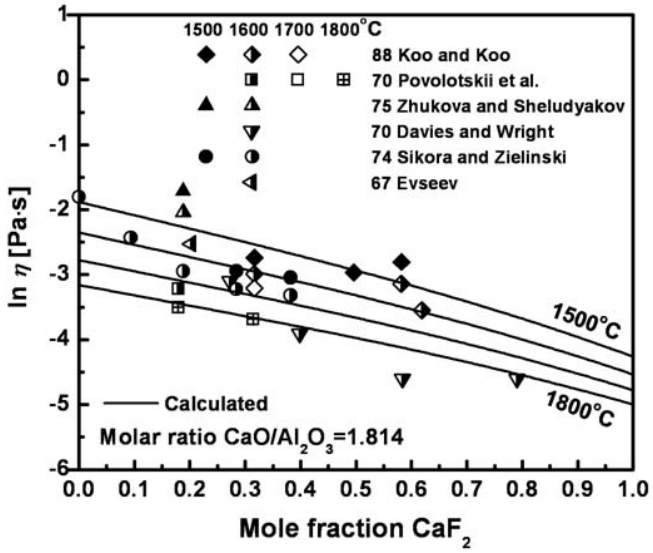

Fig. 9.17 Viscosity of CaF_2-Al_2O_3-CaO melts for a molar ratio CaO/Al_2O_3 = 1.814 compared to experimental data [38, 61, 141, 245, 296, 368]

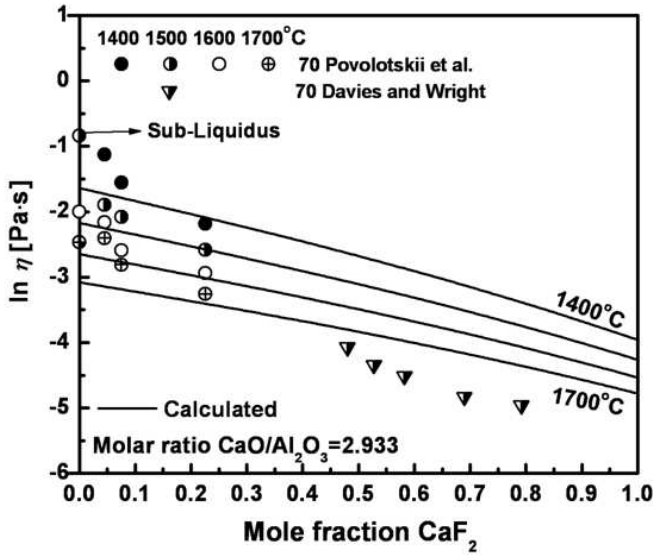

Fig. 9.18 Viscosity of CaF_2-Al_2O_3-CaO melts for a molar ratio CaO/Al_2O_3 = 2.933 compared to experimental data [38, 245]

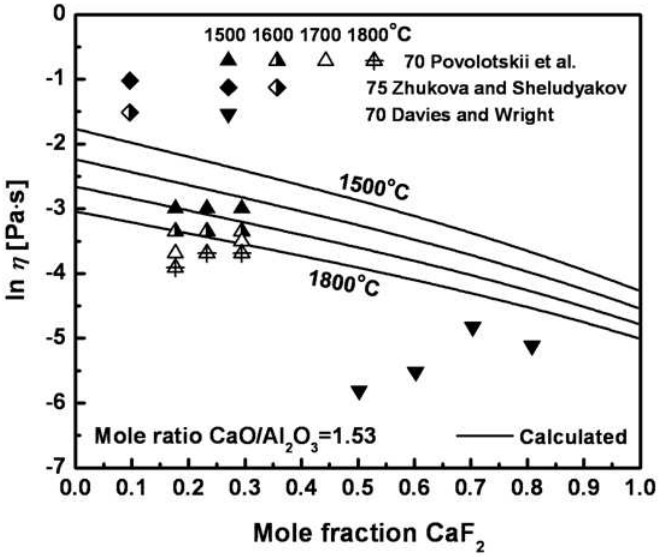

Fig. 9.19 Viscosity of CaF_2-Al_2O_3-CaO melts for a molar ratio CaO/Al_2O_3 = 1.53 compared to experimental data [38, 245, 368]

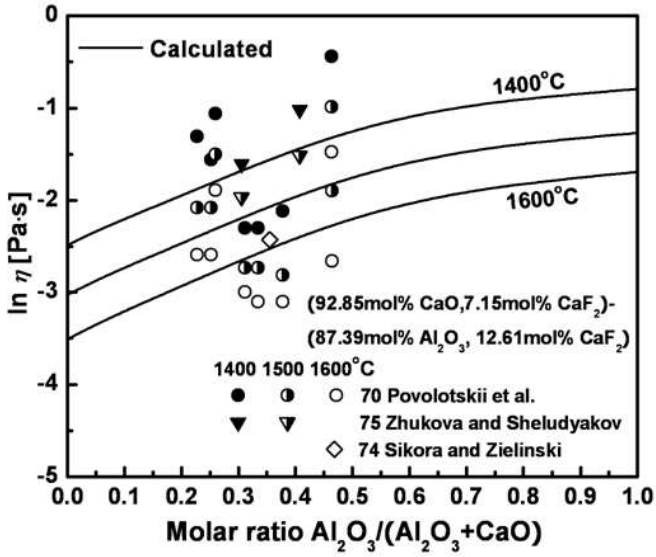

Fig. 9.20 Viscosity of CaF_2-Al_2O_3-CaO melts in the section of (92.85 mol% CaO, 7.15 mol% CaF_2) to (87.39 mol% Al_2O_3, 12.61 mol% CaF_2) compared to experimental data [245, 296, 368]

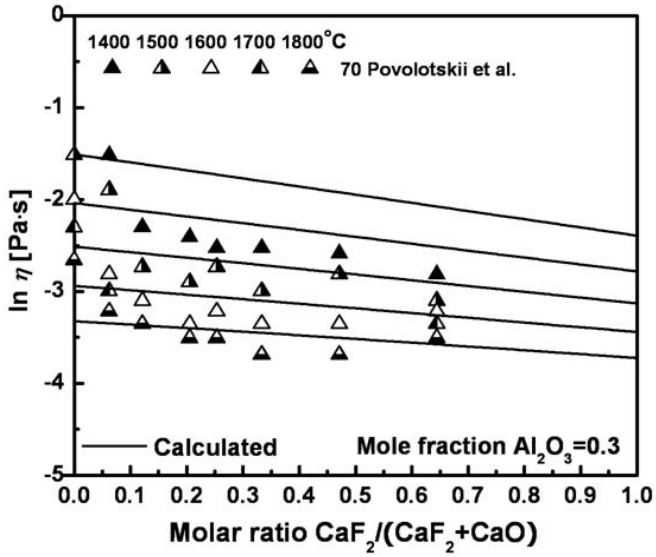

Fig. 9.21 Viscosity of CaF_2-Al_2O_3-CaO melts at 30 mol% Al_2O_3 compared to experimental data [245]

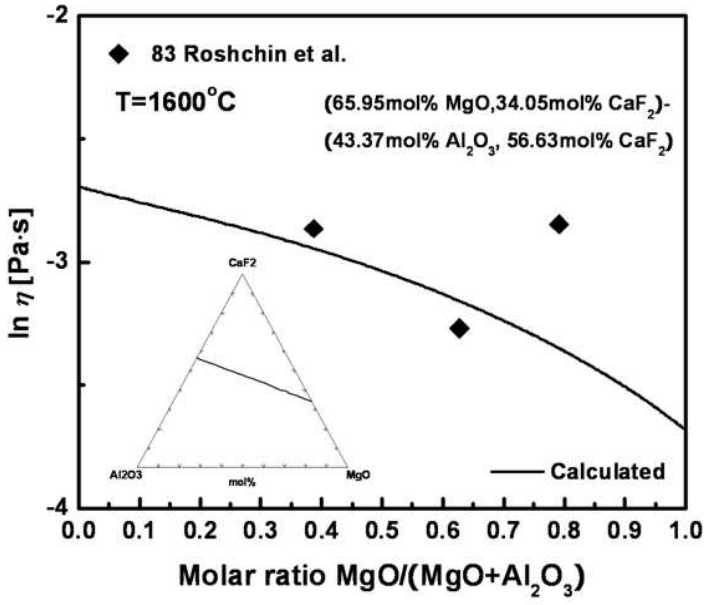

Fig. 9.22 Viscosity of CaF_2-Al_2O_3-MgO melts in the section of (65.95 mol% MgO, 34.05 mol% CaF_2) to (43.37 mol% Al_2O_3, 56.63 mol% CaF_2) compared to experimental data [254]

9.3.10 Viscosities of the ternary CaF_2–SiO_2–TiO_2 melts

In Fig. 9.23, the viscosities of the CaF-SiO_2-TiO_2 melts are calculated at constant molar ratio of SiO_2/CaF_2 = 1.3 along with the experimental data measured by Mal´kov et al. [174], who also measured the viscosities of CaF_2-SiO_2 melts using the vibrational viscometer method. As can be seen from Fig. 9.23, the experimental data show a good agreement with the calculated lines within experimental error limits.

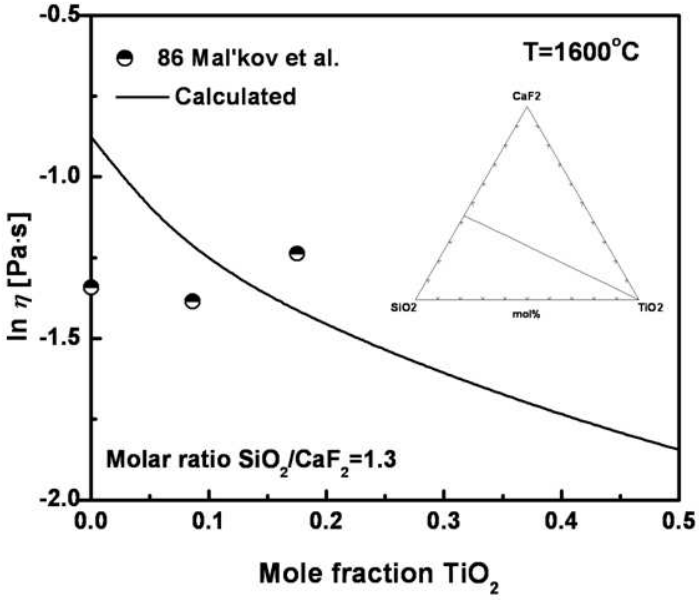

Fig. 9.23 Viscosity of CaF_2-SiO_2-TiO_2 melts for a molar ratio SiO_2/CaF_2 = 1.3 compared to experimental data [174]

9.3.11 Viscosities of the ternary CaF_2–SiO_2–Al_2O_3 melts

Figs 9.25-9.28 show the calculated viscosities of the CaF_2-SiO_2-Al_2O_3 melts compared to the experimental data measured by Vyatkin et al. [347], Mal´kov et al. [174] and Roshchin et al. [254] using the vibrational viscometer method.

In Figs 9.25-9.26, the viscosities are predicted by the model along the two pseudo-binary sections, (15.85 mol% SiO_2, 84.13 mol% Al_2O_3)-(12.62 mol% SiO_2, 87.38 mol% CaF_2) and (29.8 mol% SiO_2, 70.2 mol% Al_2O_3)-(24.52 mol% SiO_2, 75.48 mol% CaF_2) comparing the data measured by Vyatkin et al. [347] and Roshchin et al. [254], respectively. As can be seen from Fig. 9.25-9.26, the model is in good agreement with all data points at all temperatures. Especially, the observed trends of decreasing viscosities with the addition of CaF_2 are well predicted by the model within experimental error limits. Again, no Charge Compensation Effect was applied to the model and it gave a good result.

In Fig. 9.27-9.28, the viscosities are predicted by the model along the two pseudo-binary sections, (83.62 mol% SiO_2, 16.38 mol% Al_2O_3)-(8.05 mol% CaF_2, 91.95 mol% SiO_2) and (76.11

mol% CaF_2, 23.89 mol% Al_2O_3)-(96.02 mol% SiO_2, 3.98 mol% Al_2O_3) comparing the data measured by Vyatkin et al. [347] and Mal'kov et al. [174]. As can be seen from Figs 9.27-9.28, the model reproduces well the viscosities of CaF-SiO_2-Al_2O_3 melts at all temperatures within experimental error limits.

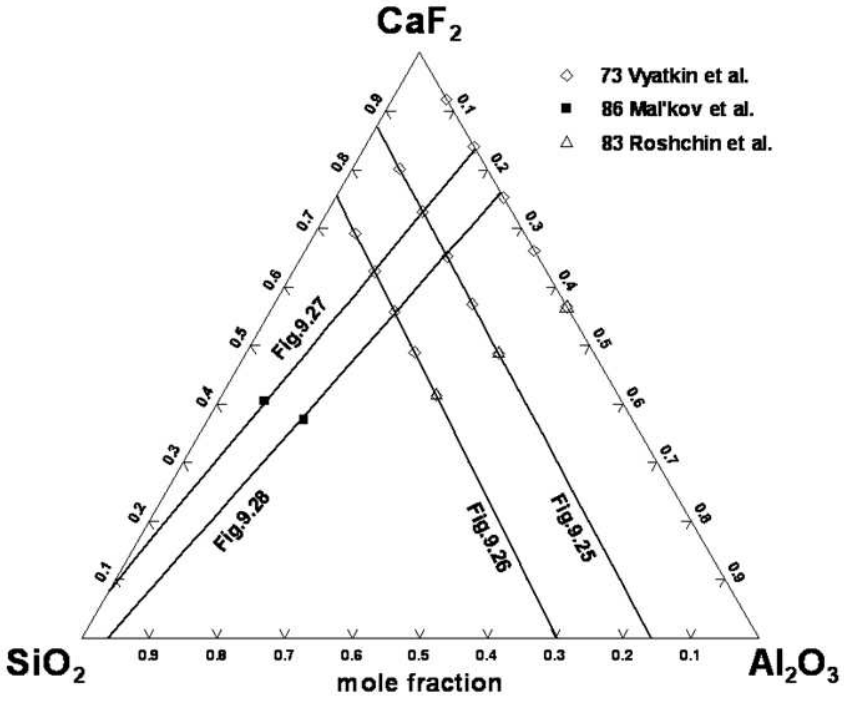

Fig. 9.24 Compositions in the CaF_2-SiO_2-Al_2O_3 system at which experimental viscosity measurements are available [174, 254, 347]. The lines indicate four sections of this system selected to show the viscosity as a function of composition in Figs 9.25 to 9.28.

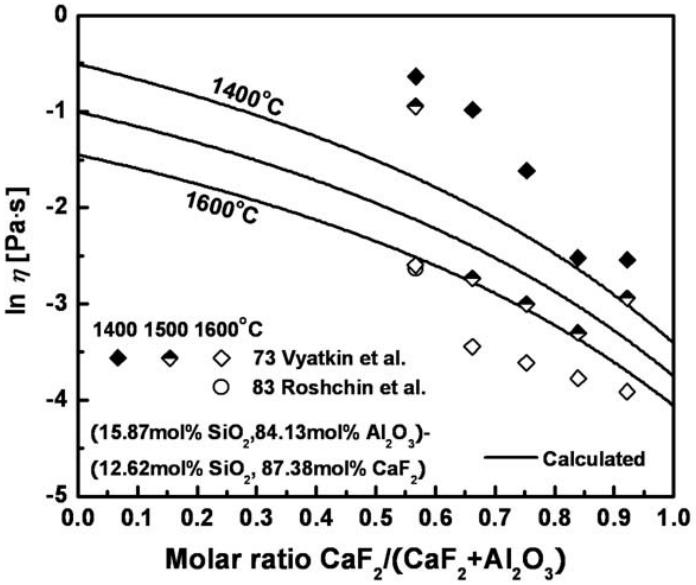

Fig. 9.25 Viscosity of CaF_2-SiO_2-Al_2O_3 melts in the section of (15.87 mol% SiO_2, 84.13 mol% Al_2O_3)-(12.62 mol% SiO_2, 87.38 mol% CaF_2) compared to experimental data [254, 347]

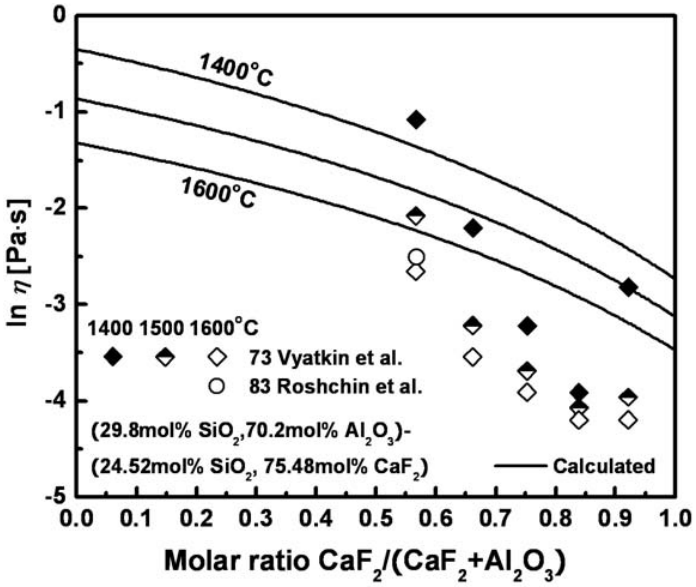

Fig. 9.26 Viscosity of CaF_2-SiO_2-Al_2O_3 melts in the section of (29.8 mol% SiO_2, 70.2 mol% Al_2O_3)-(24.52 mol% SiO_2, 75.48 mol% CaF_2) compared to experimental data [254, 347]

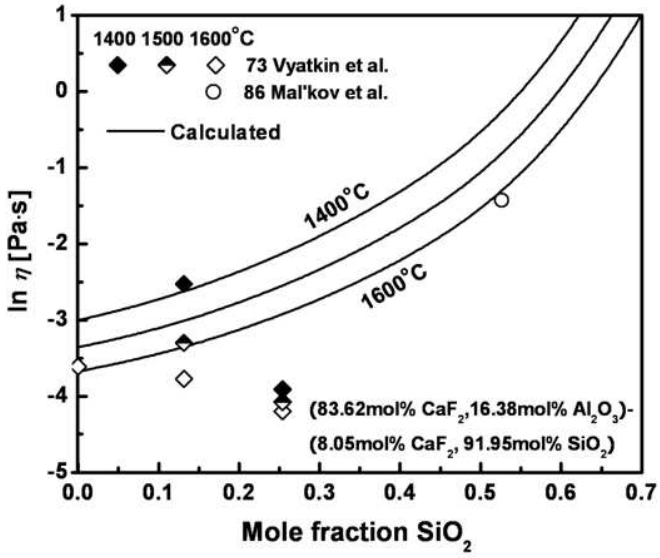

Fig. 9.27 Viscosity of CaF_2-SiO_2-Al_2O_3 melts in the section of (83.62 mol% CaF_2, 16.38 mol% Al_2O_3)-(8.05 mol% CaF_2, 91.95 mol% SiO_2) compared to experimental data [174, 347]

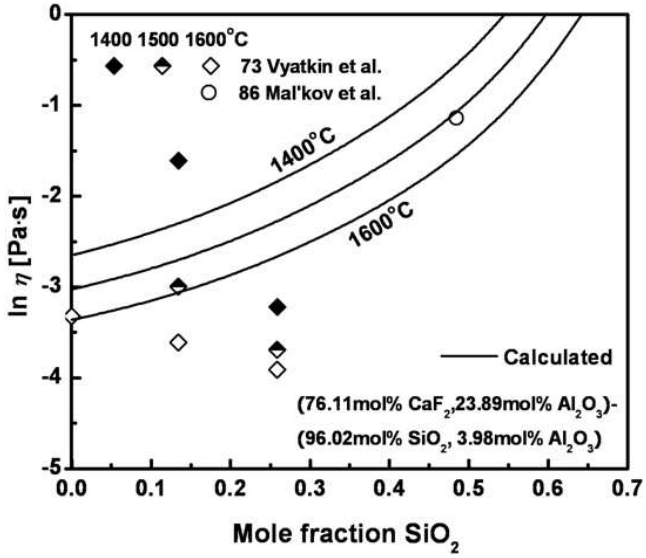

Fig. 9.28 Viscosity of CaF_2-SiO_2-Al_2O_3 melts in the section of (76.11 mol% CaF_2, 23.89 mol% Al_2O_3)-(96.02 mol% SiO_2, 3.98 mol% Al_2O_3) compared to experimental data [174, 347]

9.3.12 Viscosities of the ternary CaF_2–MgO–SiO_2 melts

Figs 9.29-9.33 show the calculated viscosities of the CaF_2-MgO-SiO_2 melts compared to the data measured by Istomin et al. [102], Mal'kov et al. [174] and Roshchin et al. [254] using the vibrational viscometer method.

Fig. 9.30 shows the calculated viscosities by the model along the pseudo-binary section (5.66 mol% SiO_2, 94.34 mol% MgO)-(84.67 mol% CaF_2, 15.33 mol% SiO_2) comparing the data of Istomin et al. [102] and Roshchin et al. [254]. As can be seen from Fig. 9.30, the data of Roshchin et al. [254] show a slightly higher viscosity than the calculated line although the difference is fairly small. The calculations by the model are in good agreement with the data points within experimental error limits at all temperatures.

Fig. 9.31 shows the calculated viscosities by the model along the pseudo-binary section (73.82 mol% CaF_2, 26.18 mol% MgO)-(68.41 mol% SiO_2, 31.59 mol% MgO) comparing the data of Istomin et al. [102] and Mal'kov et al. [174]. As can be seen from Fig. 9.31, all data points show an excellent relation with the calculated lines by the model. The observed trends of increasing viscosity with increasing SiO_2 are well predicted by the model within experimental error limits.

In Figs. 9.32-9.33, the viscosities are calculated along the two pseudo-binary sections, (29.7 mol% CaF_2, 70.3 mol% MgO)-(38.64 mol% CaF_2, 61.36 mol% SiO_2) and (25.6 mol% CaF_2, 74.4 mol% MgO)-(33.91 mol% CaF_2, 66.09 mol% SiO_2) comparing the data points measured by Mal'kov et al. [174] and Roshchin et al. [254] at 1600ºC. In Fig. 9.32 and 9.33, the data points of Roshchin et al. [254] show slightly higher and lower viscosities than the calculated lines, respectively. It is most likely the scatter of the experimental data which is within experimental error limits. All data points are in a good agreement with the model.

Fig. 9.34 compares the calculated viscosities of CaF_2-MgO-SiO_2 melts at constant molar ratio of SiO_2/CaF_2 = 1.3 along with the data points measured by Mal'kov et al. [174]. The observed trends of decreasing viscosity with the addition of MgO are well predicted by the model using only a few unary and binary parameters.

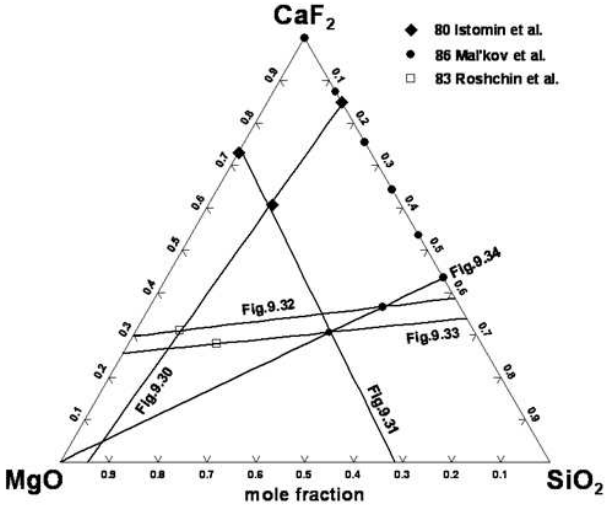

Fig. 9.29 Compositions in the CaF_2-MgO-SiO_2 system at which experimental viscosity measurements are available [102, 174, 254]. The lines indicate four sections of this system selected to show the viscosity as a function of composition in Figs 9.30 to 9.34.

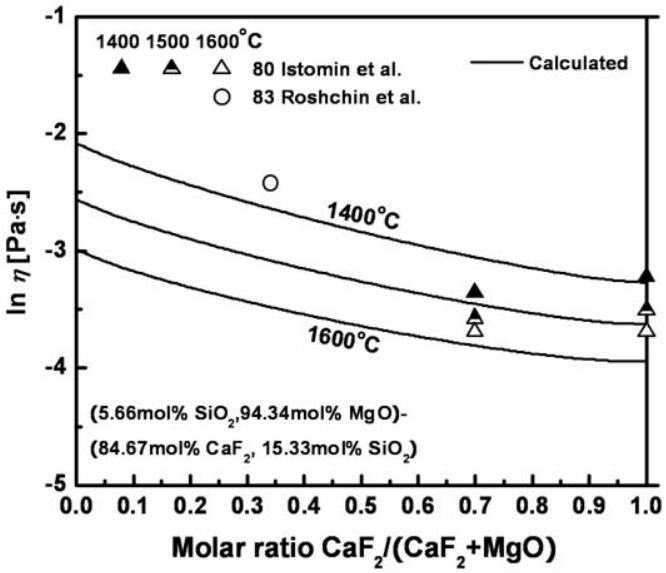

Fig. 9.30 Viscosity of CaF_2-MgO-SiO_2 melts in the section of (5.66 mol% SiO_2, 94.34 mol% MgO)-(84.67 mol% CaF_2, 15.33 mol% SiO_2) compared to experimental data [102, 254]

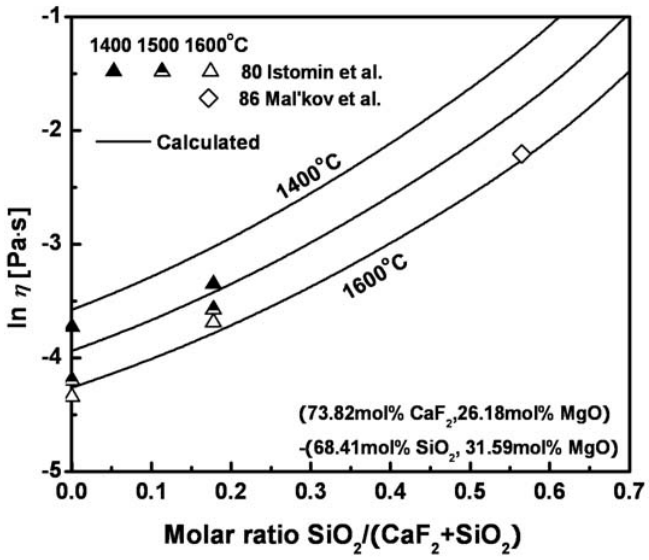

Fig. 9.31 Viscosity of CaF_2-MgO-SiO_2 melts in the section of (73.82 mol% CaF_2, 26.18 mol% MgO)-(68.41 mol% SiO_2, 31.59 mol% MgO) compared to experimental data [102, 174]

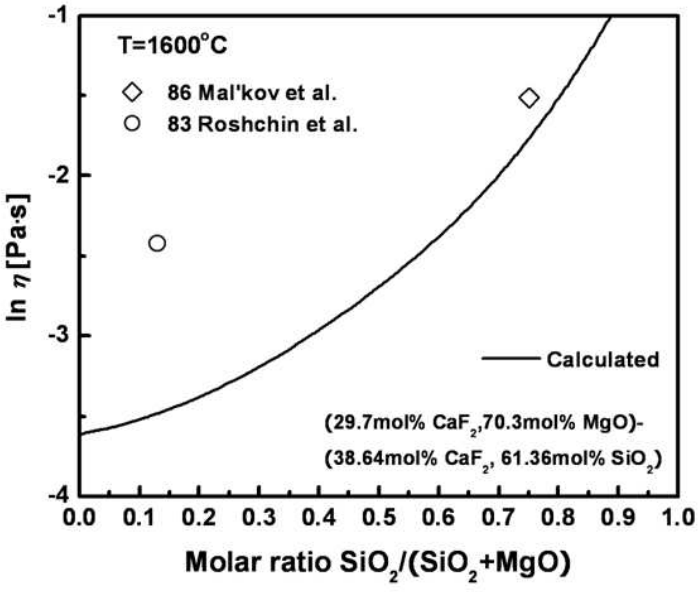

Fig. 9.32 Viscosity of CaF_2-MgO-SiO_2 melts in the section of (29.7 mol% CaF_2, 70.3 mol% MgO)-(38.64 mol% CaF_2, 61.36 mol% SiO_2) compared to experimental data [174, 254]

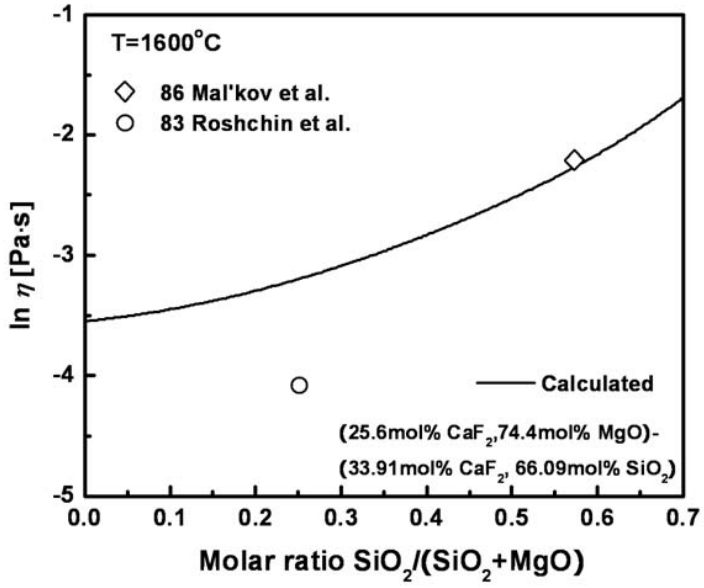

Fig. 9.33 Viscosity of CaF_2-MgO-SiO_2 melts in the section of (25.6 mol% CaF_2, 74.4 mol% MgO)-(33.91 mol% CaF_2, 66.09 mol% SiO_2) compared to experimental data [174, 254]

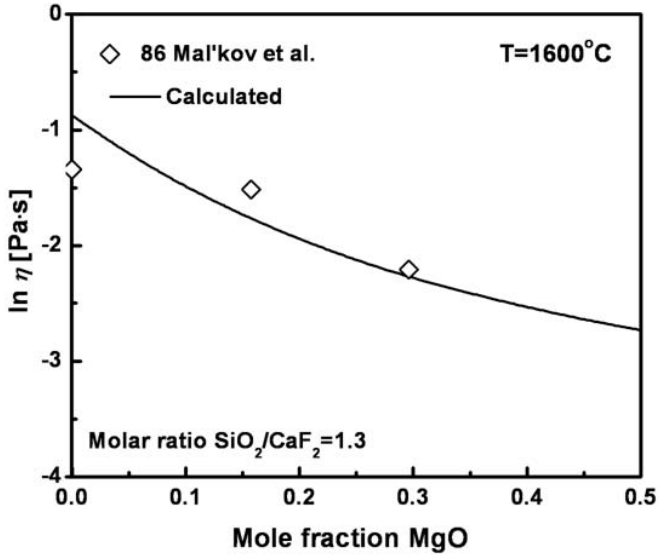

Fig. 9.34 Viscosity of CaF_2-MgO-SiO_2 melts for a molar ratio SiO_2/CaF_2 = 1.3 compared to experimental data [174]

9.3.13 Viscosities of the CaF_2-Al_2O_3-CaO-SiO_2 melts

In the continuous casting process of steelmaking, the system CaF_2-Al_2O_3-CaO-SiO_2 is a key system. Therefore many authors [9, 19, 117, 163, 185, 196, 367] measured the viscosities in this system as shown in Figs 9.35-9.39.

Fig. 9.35 compares the calculated viscosities with the experimental data measured by Zhmoidin and Moldavskii [367], Bills [19], Kato and Minowa [117], and Michel and Mitchell [185] using the rotating crucible [185, 367] and the counter-balanced sphere viscometer methods [19, 117]. Most of the data except for those of Kato and Minowa [117] show good agreement with the calculated lines within experimental error limits. Kato and Minowa [117] systematically measured viscosities of CaO-Al_2O_3-SiO_2-MF_x (M = Ca, Mg, Na, Al) using the counter-balanced sphere viscometer method. All data in these quaternary systems show systematically lower viscosities than the lines predicted by the model as will be shown in Chapter 10. This difference could be caused by the counter-balanced sphere viscometer method contributing to large systematic errors by the uncertainties in the damping rates of an oscillating wire [104]. The observed trends of decreasing viscosity with the addition of CaF_2 are well predicted by the model within experimental error limits.

In Figs 9.36-9.37, the calculated lines are compared with the experimental data measured by Muratov [196] and Artamonov et al. [9] using the vibrational viscometer method. As can be seen from Fig 9.36, the predicted lines by the model show an excellent reproducibility with all data points of Muratov [196]. The data points of Artamonov et al. [9] in Fig. 9.37 show slightly lower viscosities at all temperatures although the difference is within experimental error limits. However, the observed trends of decreasing viscosity with the addition of CaF_2 are fairly well predicted by the model.

Li Tao-Chao and Tsylev [163] measured the viscosities of CaF_2-Al_2O_3-CaO-SiO_2 melts using the rotating crucible method with carbon crucibles and the data points were compared with the calculated lines by the model as shown in Figs 9.38-9.39. The data points at all temperatures show systematically lower viscosities than the calculated lines although the difference is fairly small. On the other hand, as shown in Fig. 9.39, the data points at 1200ºC show experimental scatter which is more than 2 in the natural logarithm scale. This could be caused from partial crystallization of the melt preventing accurate viscosity measurements from the rotating spindle.

However, it seems that the observed trends of the viscosity data are well predicted by the model within experimental error limits at all temperatures.

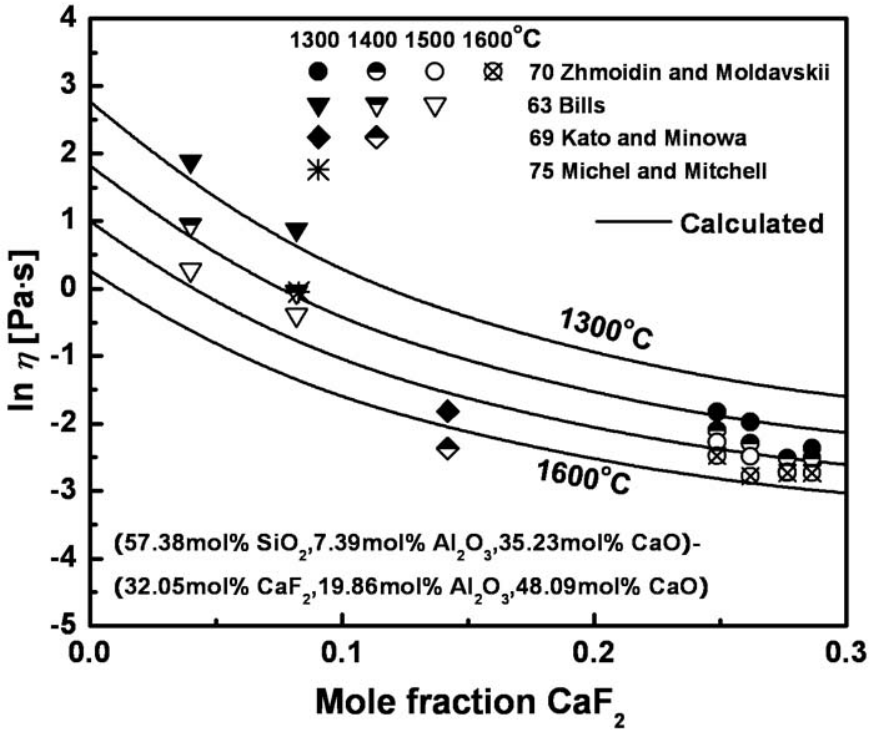

Fig. 9.35 Viscosity of CaF_2-Al_2O_3-CaO-SiO_2 melts in the section of (57.38 mol% SiO_2, 7.39 mol% Al_2O_3, 35.23 mol% CaO)-(32.05 mol% CaF_2, 19.86 mol% Al_2O_3, 48.09 mol% CaO) compared to experimental data [19, 117, 185, 367]

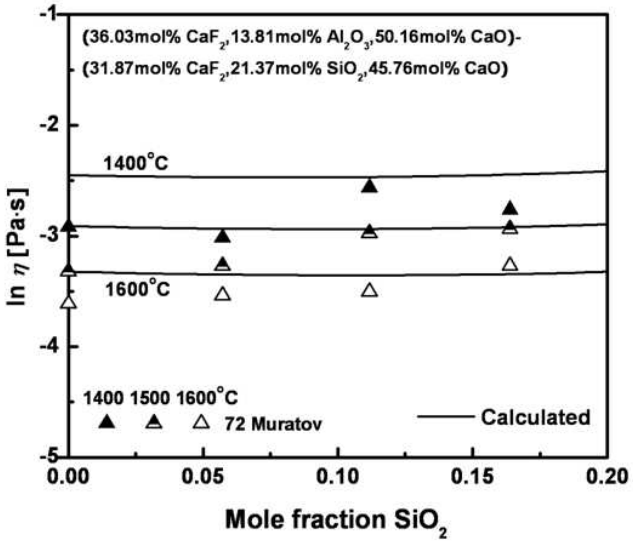

Fig. 9.36 Viscosity of CaF_2-Al_2O_3-CaO-SiO_2 melts in the section of (36.03 mol% CaF_2, 13.81 mol% Al_2O_3, 50.16 mol% CaO)-(31.87 mol% CaF_2, 21.37 mol% SiO_2, 45.76 mol% CaO) compared to experimental data [196]

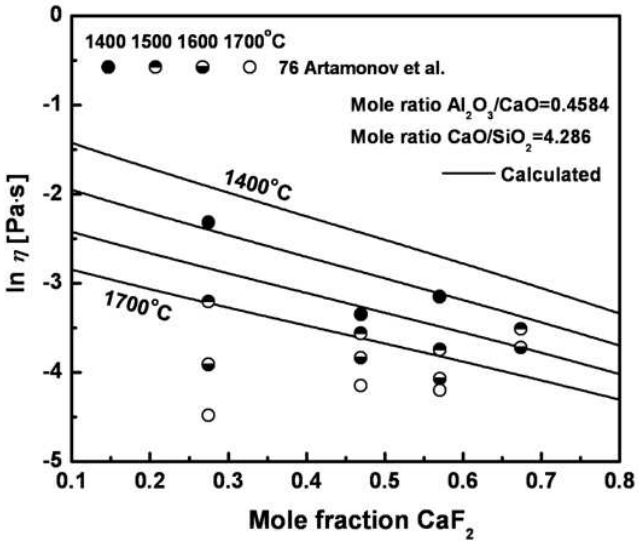

Fig. 9.37 Viscosity of CaF_2-Al_2O_3-CaO-SiO_2 melts for molar ratios of Al_2O_3/CaO = 0.4584 and CaO/SiO_2 = 4.286 compared to experimental data [9]

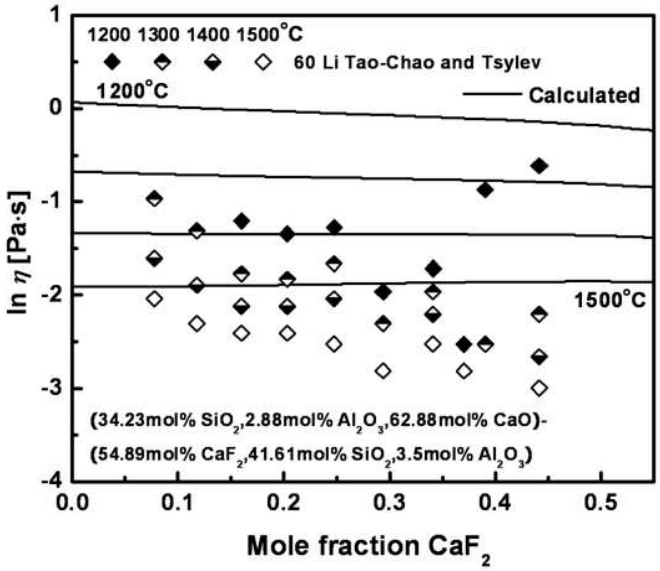

Fig. 9.38 Viscosity of CaF_2-Al_2O_3-CaO-SiO_2 melts in the section of (34.23 mol% SiO_2, 2.88 mol% Al_2O_3, 62.88 mol% CaO)-(54.89 mol% CaF_2, 41.61 mol% SiO_2, 3.5 mol% Al_2O_3) compared to experimental data [163]

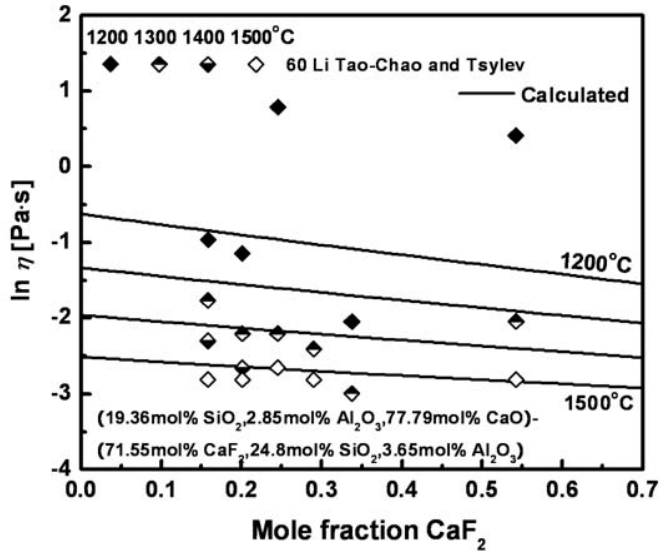

Fig. 9.39 Viscosity of CaF_2-Al_2O_3-CaO-SiO_2 melts in the section of (19.36 mol% SiO_2, 2.85 mol% Al_2O_3, 77.79 mol% CaO)-(71.55 mol% CaF_2, 24.8 mol% SiO_2, 3.65 mol% Al_2O_3) compared to experimental data [163]

9.3.14 Viscosities of the CaF_2-Al_2O_3-MgO-SiO_2 melts

Roshchin et al. [254] measured the viscosities of CaF_2-Al_2O_3-SiO_2 and CaF_2-Al_2O_3-MgO-SiO_2 melts using the vibrational viscometer method at 1600ºC as shown in Figs 9.40 and 9.41. All data are well reproduced by the model and the observed trends of decreasing viscosity with the addition of MgO are well predicted by the model within experimental error limits.

9.3.15 Viscosities of the CaF_2-Al_2O_3-B_2O_3-CaO melts

Fig. 9.42 compares the calculated viscosities comparing to the data points measured in CaF_2-Al_2O_3-B_2O_3-CaO melts by Muratov [196] who also measured the system CaF_2-Al_2O_3-CaO using the vibrational viscometer method. The data points show systematically lower viscosities than the calculated lines although the difference is fairly small. All data points seem to be in good agreement with the predicted lines by the model within experimental error limits.

Fig. 9.43 compares the viscosities of CaF_2-Al_2O_3-B_2O_3-CaO melts measured by Istomin et al. [102] (who also measured CaF_2-Al_2O_3 melts) using the vibrational viscometer method, with the lines calculated by the model. All data show systematically lower viscosities than the predicted lines although the difference is fairly small. The observed trends of viscosity data are somewhat different from that of the model. Considering the experimental difficulties with viscosity measurements, however, we can conclude that the data points are in good agreement with the model within experimental error limits.

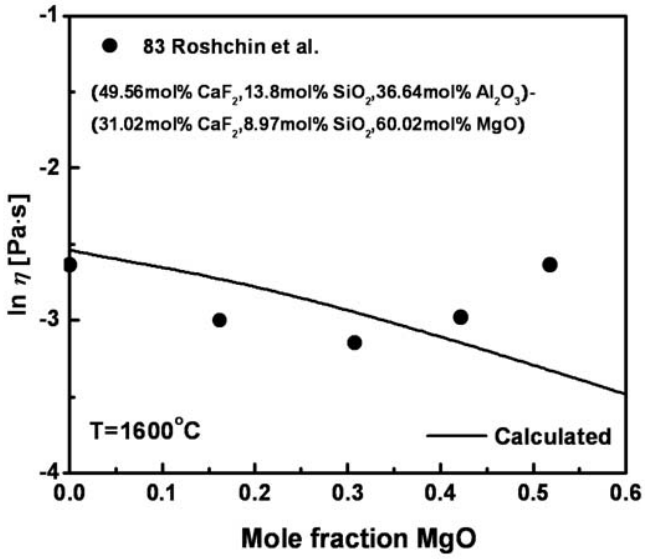

Fig. 9.40 Viscosity of CaF_2-Al_2O_3-MgO-SiO_2 melts in the section of (49.56 mol% CaF_2, 13.8 mol% SiO_2, 36.64 mol% Al_2O_3)-(31.02 mol% CaF_2, 8.97 mol% SiO_2, 60.02 mol% MgO) compared to experimental data [254]

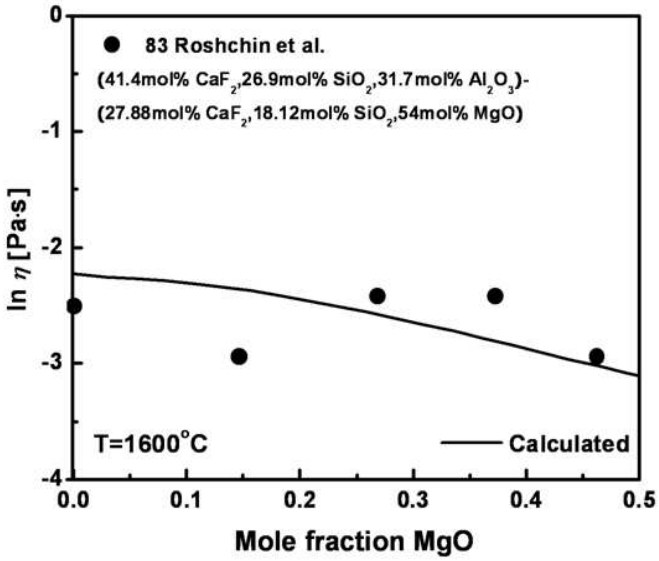

Fig. 9.41 Viscosity of CaF_2-Al_2O_3-MgO-SiO_2 melts in the section of (41.4 mol% CaF_2, 26.9 mol% SiO_2, 31.7 mol% Al_2O_3)-(27.88 mol% CaF_2, 18.12 mol% SiO_2, 54 mol% MgO) compared to experimental data [254]

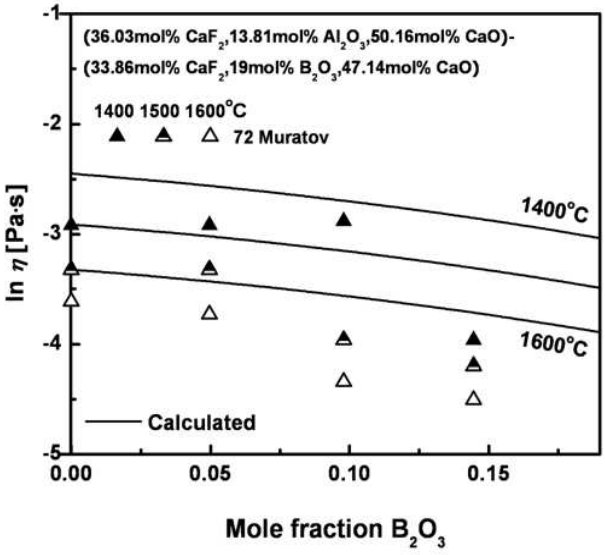

Fig. 9.42 Viscosity of CaF_2-Al_2O_3-B_2O_3-CaO melts in the section of (36.03 mol% CaF_2, 13.81 mol% Al_2O_3, 50.16 mol% CaO)-(33.86 mol% CaF_2, 19 mol% B_2O_3, 47.14 mol% CaO) compared to experimental data [196]

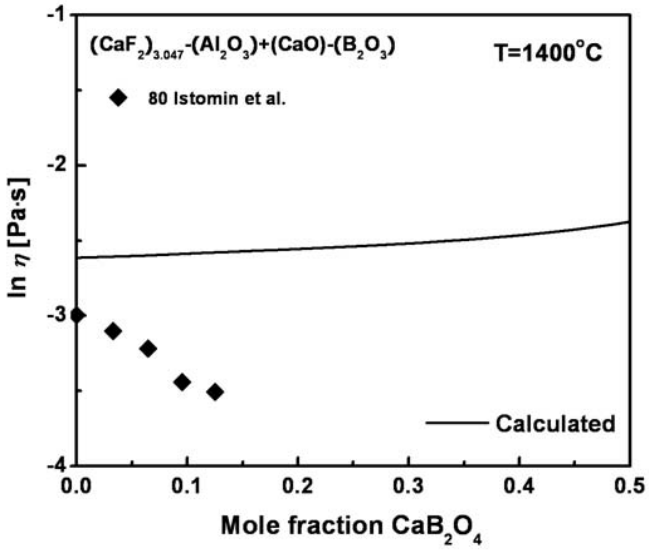

Fig. 9.43 Viscosity of CaF_2-Al_2O_3-B_2O_3-CaO melts in the section of [$(CaF_2)_{3.047}$–Al_2O_3]-[CaO–B_2O_3] compared to experimental data [102]

9.3.16 Viscosities of the CaF_2-B_2O_3-Na_2O-SiO_2 melts

Fig. 9.44 shows the viscosities of the CaF_2-B_2O_3-Na_2O-SiO_2 melts measured by Nikitin et al. [215] who also measured the viscosities of B_2O_3-Na_2O-SiO_2 melts using the rotating crucible method with alumina crucibles. As can be seen from Fig. 9.44, the data for CaF_2-B_2O_3-Na_2O-SiO_2 melts show systematically lower viscosities than the lines calculated by the model although the difference is fairly small. The contamination of the sample due to the reaction with alumina crucibles could bring a large change of the composition of the sample and give error sources on viscosity measurement. Their data for B_2O_3-Na_2O-SiO_2 melts are also systematically lower by about 2 in the natural logarithm scale at all temperatures, whereas our previous work [26] showed that our calculated lines for the system B_2O_3-Na_2O-SiO_2 are in good agreement with the data of many other authors [26].

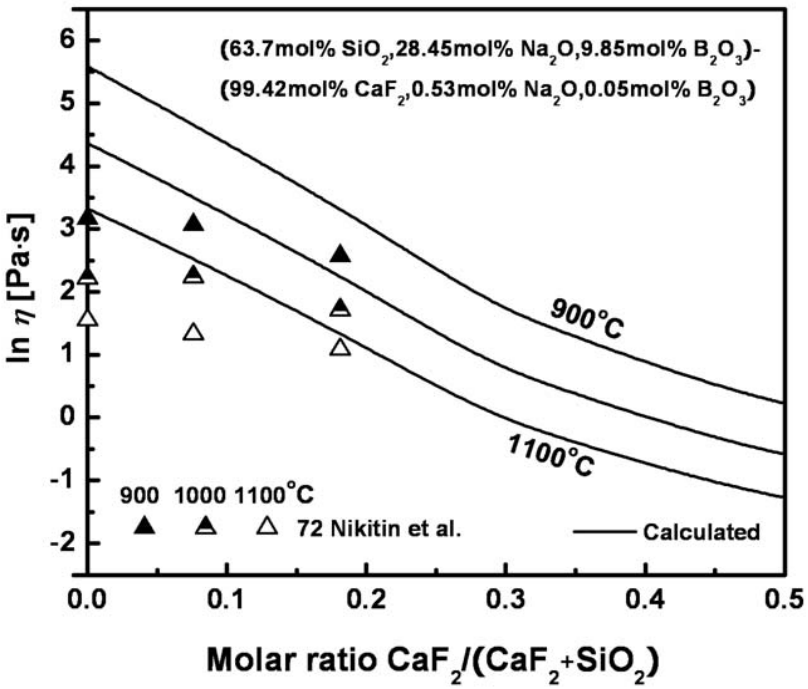

Fig. 9.44 Viscosity of CaF_2-B_2O_3-Na_2O-SiO_2 melts in the section of (63.7 mol% SiO_2, 28.45 mol% Na_2O, 9.85 mol% B_2O_3)-(99.42 mol% CaF_2, 0.53 mol% Na_2O, 0.05 mol% B_2O_3) compared to experimental data [215]

9.3.17 Viscosities of the CaF_2-Al_2O_3-CaO-Na_2O melts

In Figs 9.45-9.46, the calculated lines of the model are compared with the data measured by Basov et al. [16] using the rotating crucible method with Mo crucibles. As can be seen from Figs 9.45 and 9.46, all data points are systematically higher than the predicted lines although the difference is fairly small. On the other hand, the observed trends of viscosity data are well predicted by the model within experimental error limits.

9.3.18 Viscosities of CaF_2-Al_2O_3-CaO-MnO and CaF_2-Al_2O_3-CaO-TiO_2 melts

Figs 9.47 and 9.48 show the calculated viscosities compared to the data measured in CaF_2-Al_2O_3-CaO-MnO and CaF_2-Al_2O_3-CaO-TiO_2 melts by Zhmoidin and Moldavskii [367] who also measured the viscosities of CaF_2-Al_2O_3-CaO melts using the rotating crucible method with Mo crucibles. As can be seen from Figs 9.47 and 9.48, all data are systematically lower than the calculated lines by the model although the difference is within experimental error limits. The observed trends of viscosity data with the addition of MnO or TiO_2 are well predicted by the model, and thus the predicted viscosities of CaF_2-Al_2O_3-CaO-MnO and CaF_2-Al_2O_3-CaO-TiO_2 melts are believed to be in agreement with the measurements within experimental error limits considering the intrinsic experimental difficulties on viscosity measurements of CaF_2 bearing systems.

9.3.19 Viscosities of CaF_2-CaO-Na_2O-SiO_2 melts

Figs 9.49-9.51 compare the predicted viscosities of CaF_2-CaO-Na_2O-SiO_2 melts with the experimental data measured by Park et al. [226] and Endell and Strasmann [57] using the rotating crucible method with Pt crucibles. In Fig. 9.49, the data points of Park et al. [226] at the CaO-Na_2O-SiO_2 system indicate systematically higher viscosities than the calculated lines even though the difference is small and within experimental error limits. As can be seen from Figs 9.49-9.51, all data points are in good agreement with the lines calculated by the model at all temperatures. In particular, the decreasing trends of the viscosity observed in Figs 9.49-9.51 with the addition of CaF_2 are well predicted within experimental error limits.

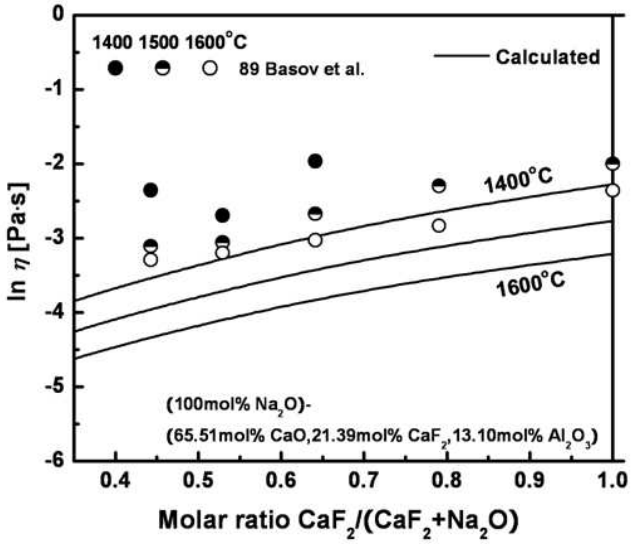

Fig. 9.45 Viscosity of CaF_2-Al_2O_3-CaO-Na_2O melts in the section of (100mol% Na_2O)-(65.51mol% CaO, 21.39mol% CaF_2, 13.10mol% Al_2O_3) compared to experimental data [16]

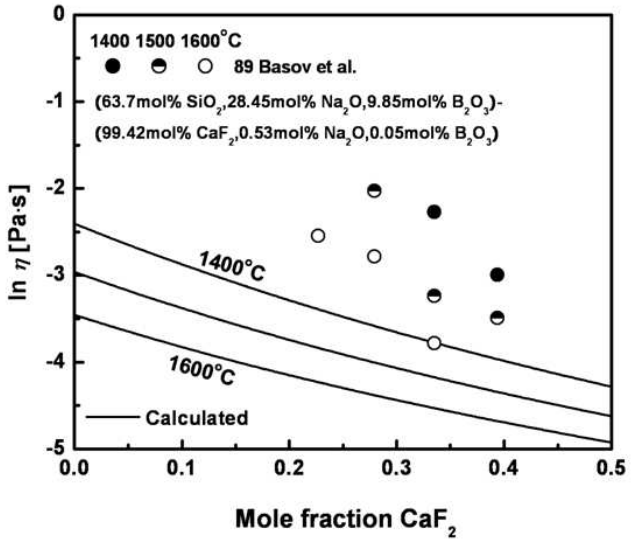

Fig. 9.46 Viscosity of CaF_2-Al_2O_3-CaO-Na_2O melts in the section of (63.7mol% SiO_2, 28.45mol% Na_2O, 9.85mol% B_2O_3)-(99.42mol% CaF_2, 0.53mol% Na_2O, 0.05mol% B_2O_3) compared to experimental data [16]

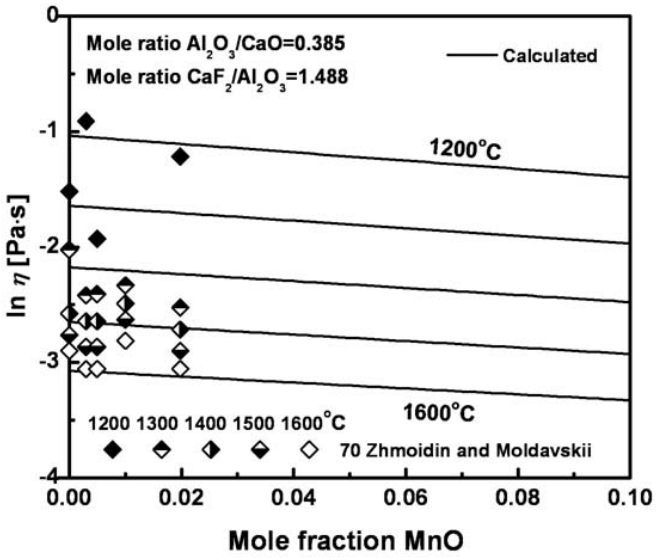

Fig. 9.47 Viscosity of CaF_2-Al_2O_3-CaO-MnO melts for molar ratios of Al_2O_3/CaO = 0.385 and CaF_2/Al_2O_3 = 1.488 compared to experimental data [367]

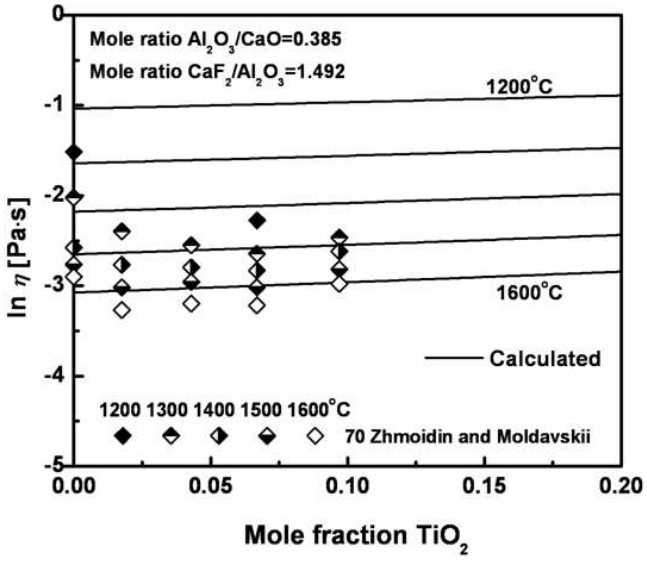

Fig. 9.48 Viscosity of CaF_2-Al_2O_3-CaO-TiO_2 melts for molar ratios of Al_2O_3/CaO = 0.385 and CaF_2/Al_2O_3 = 1.492 compared to experimental data [367]

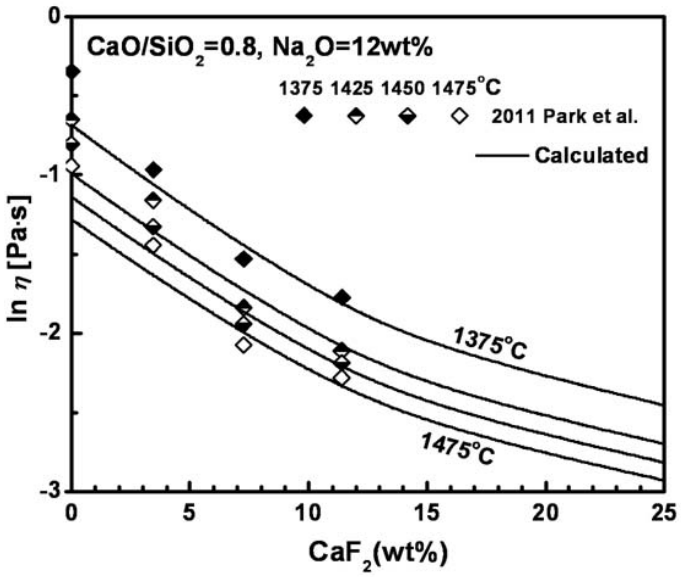

Fig. 9.49 Viscosity of CaF_2-CaO-Na_2O-SiO_2 melts for a weight ratio of CaO/SiO_2 = 0.8 and Na_2O = 12wt% compared to experimental data [226]

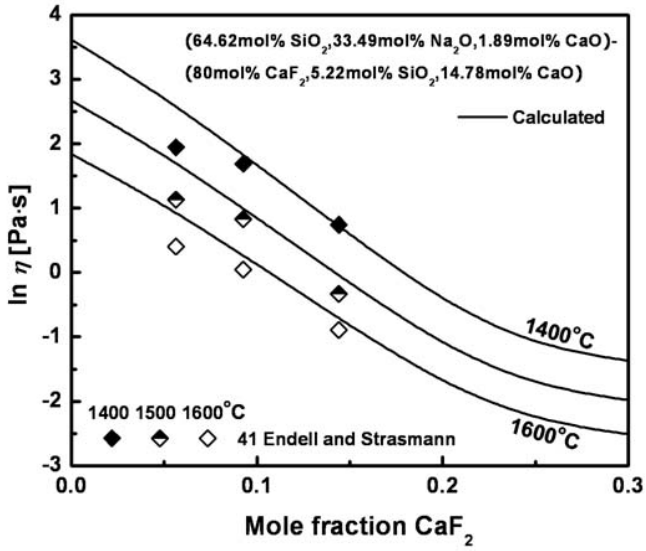

Fig. 9.50 Viscosity of CaF_2-CaO-Na_2O-SiO_2 melts in the section of (64.62mol% SiO_2, 33.49mol% Na_2O, 1.89mol% CaO)-(80mol% CaF_2, 5.22mol% SiO_2, 14.78mol% CaO) compared to experimental data [57]

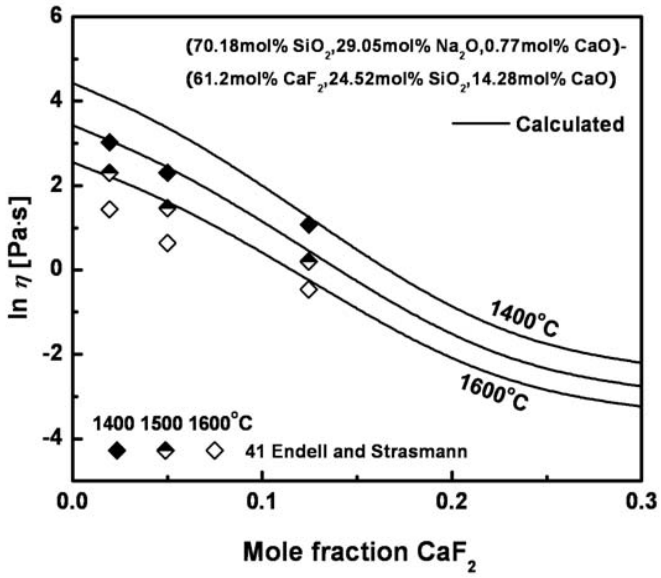

Fig. 9.51 Viscosity of CaF_2-CaO-Na_2O-SiO_2 melts in the section of (70.18mol% SiO_2, 29.05mol% Na_2O, 0.77mol% CaO)-(61.2mol% CaF_2, 24.52mol% SiO_2, 14.28mol% CaO) compared to experimental data [57]

9.3.20 Viscosities of CaF_2-Al_2O_3-CaO-MgO-SiO_2 melts

Figs 9.52-9.54 compare the calculated viscosities of CaF_2-Al_2O_3-CaO-MgO-SiO_2 melts with the experimental data measured by Musorin [198], Komel'kov et al. [138] and Tribe et al. [328] using the rotating crucible method. Most data except for some showing abnormally high viscosities in Fig. 9.59 which would most likely have been measured under partial crystallization of the melt show an excellent agreement with the calculated lines. From the results in Figs 9.52-9.54, the predicted viscosities of CaF_2-Al_2O_3-CaO-MgO-SiO_2 melts are believed to be in good agreement with measurements within experimental error limits.

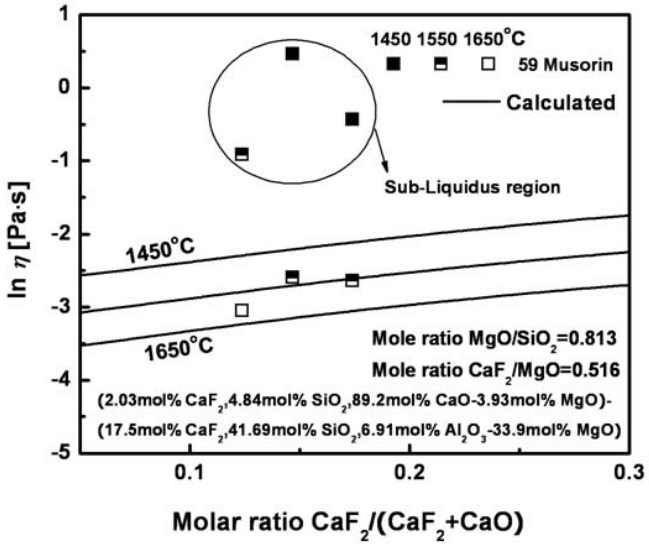

Fig. 9.52 Viscosity of CaF_2-Al_2O_3-CaO-MgO-SiO_2 melts in the section of (2.03mol% CaF_2, 4.84mol% SiO_2, 89.2mol% CaO, 3.93mol% MgO)-(17.5mol% CaF_2, 41.69mol% SiO_2, 6.91mol% Al_2O_3, 33.9mol% MgO) compared to experimental data [198]

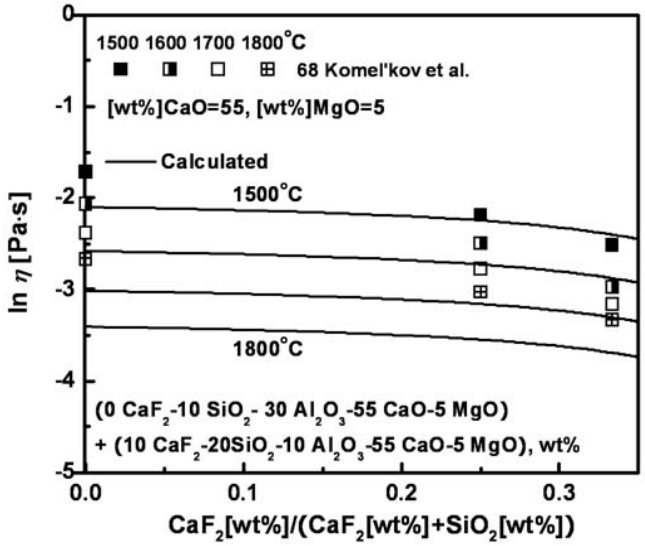

Fig. 9.53 Viscosity of CaF_2-Al_2O_3-CaO-MgO-SiO_2 melts in the section of (10 wt% SiO_2, 30 wt% Al_2O_3, 55 wt%CaO, 5 wt% MgO)-(10wt% CaF_2, 20wt% SiO_2, 10 wt% Al_2O_3, 55 wt%CaO, 5 wt% MgO) compared to experimental data [138]

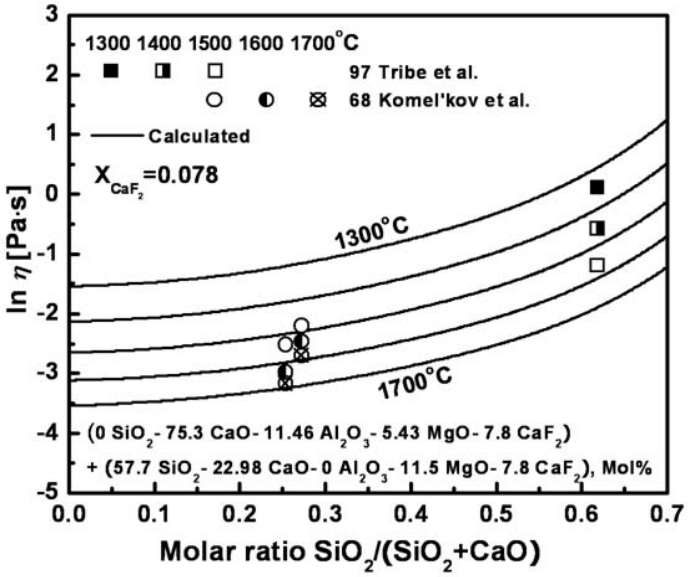

Fig. 9.54 Viscosity of CaF_2-Al_2O_3-CaO-MgO-SiO_2 melts in the section of (75.3mol% CaO, 11.46mol% Al_2O_3, 5.43mol% MgO, 7.8mol% CaF_2)-(57.7mol% SiO_2, 22.98mol% CaO, 11.5mol% MgO, 7.8mol% CaF_2) compared to experimental data [138, 328]

9.3.21 Viscosities of Mold Flux melts

The viscosity of mold flux melts is a key parameter determining the optimum casting conditions in the continuous casting process of steelmaking. Several experimental studies [31, 156, 182] have been carried out using the rotating crucible method for industrial slags as well as synthetic slags with compositions close to industrial mold fluxes which are the subsystems of the CaF_2-CaO-Al_2O_3-MgO-MnO-FeO-Na_2O-K_2O-B_2O_3-TiO_2-Fe_2O_3-SiO_2 system.

In Fig. 9.55, the calculated viscosities and experimental data [31, 156, 182] containing up to 31.23 wt% CaF_2 are compared in the natural logarithm scale. All data show an excellent relation with the predicted viscosities by the model using only a few unary, binary and ternary parameters within experimental error limits. Overall, the developed model can reliably reproduce the viscosities of industrial mold fluxes within experimental error limits.

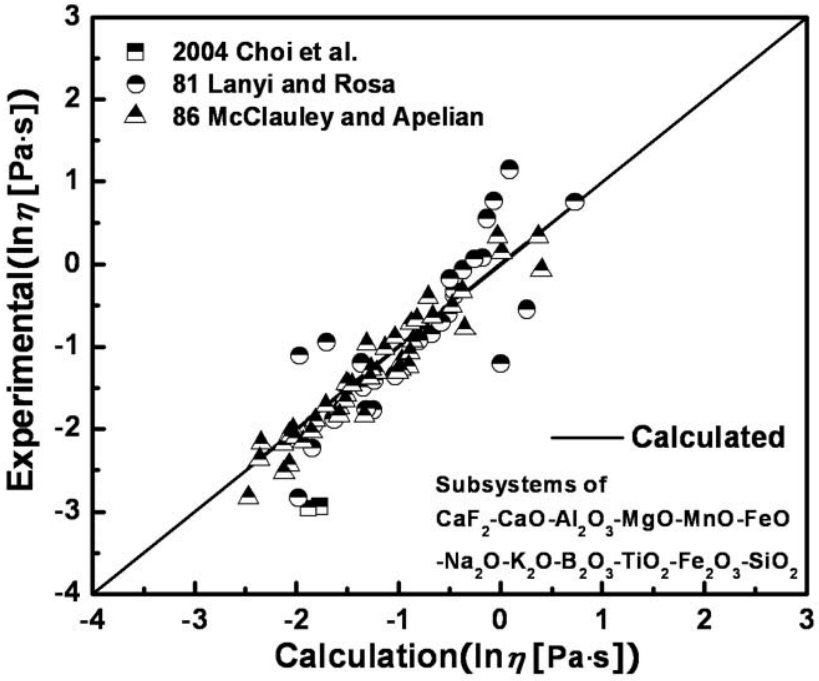

Fig. 9.55 Comparison between calculations and experimental data for the viscosity of mold flux melts [31, 156, 182]

Table 9.1 Optimized Model parameters for the viscosity expressed in Pa·s

System	Model parameter	Model parameters ($J \cdot mol^{-1}$)
CaF_2	$A_{CaF_2} = -9.35$	$E_{CaF_2} = 75000$
CaF_2–SiO_2		$E_{CaF_2\text{-}Si} = -74250$ $E^{R}_{CaF_2\text{-}Si} = 67750$ $E^{Ring}_{CaF_2\text{-}Si} = 0$
CaF_2–B_2O_3	$A^{*}_{B(CaF_2)} = -9.35$	$E^{*}_{B(CaF_2)} = 75000$

The model parameters for subsystems without CaF_2 that are used for the viscosity calculations in the present study were optimized and reported elsewhere (see Tables 4.1, 4.2, 5.1, 6.1, 7.1 and 8.1).

CHAPTER 10 APPLICATION OF THE MODEL TO MELTS CONTAINING MF_x (M = Mg, Na, K and Al)

10.1 Review of the available viscosity data and calibration of the model

In the present study, viscosity data are reviewed for available MF_x-containing subsystems (M = Ca, Mg, Na, K and Al) of the MF_x–SiO_2–Al_2O_3–CaO–MgO–Na_2O–K_2O–MnO–TiO_y system. The data judged to be most reliable are shown in the figures below.

The proposed model is intended for oxide melts in a single-phase region. The extension of the model to describe the viscosity of glasses will be reported in Chapters 11 and 12. Therefore, the viscosity data were collected mainly for melts above the liquidus or for slightly supercooled melts where crystallization did not occur. These measurements were mostly made with rotational or vibrational viscometers. If an abnormally high viscosity value was reported for a temperature below the liquidus, this is most likely the result of crystallization. In obvious cases such data points were discarded, but sometimes these points are still shown in the figures if it is deemed possible that they correspond to a supercooled liquid which does not contain precipitated solids. For example, viscosities of glasses measured by a fiber elongation or beam-bending method, were not considered in the present study.

10.1.1 Viscosities of unary MF_x and binary MF_x-SiO_2 (M = Mg, Na, K and Al) systems

All optimized unary parameters of MF_x and binary parameters of MF_x-SiO_2 (M = Mg, Na, K and Al) are listed in Table 10.1. The unary CaF_2 and binary CaF_2-SiO_2 parameters were listed in Table 9.1. No viscosity data of the binary NaF-SiO_2, KF-SiO_2, MgF_2-SiO_2 and AlF_3-SiO_2 systems were available. However, we had to consider the effect of other fluorides on the viscosity when considering the overall “equilibrated composition” or “formal composition” (see section 9.2.2) of the oxy-fluoride melts. Thus, all unary and binary parameters A_{MF_x}, E_{MF_x}, $E^{1,1}_{MF_x\text{-}Si}$, $E^{Ring}_{MF_x\text{-}Si}$, $E^{R}_{MF_x\text{-}Si}$, $A^{*}_{B(MF_x)}$ and $E^{*}_{B(MF_x)}$ (M = Ca, Mg, Na, K and Al) were optimized simultaneously using the developed viscosity model.

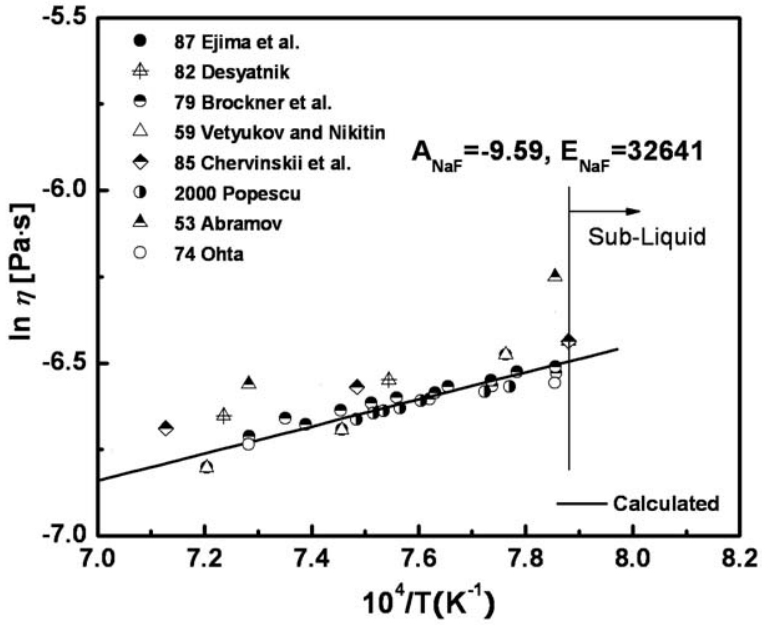

Fig. 10.1 Calculated viscosity in NaF system compared to Experimental data [1, 25, 29, 40, 56, 217, 240, 342]

The viscosity of pure NaF were measured by many authors using the oscillation method [29, 40, 56, 217, 240, 342] and the torsional balance method [342]. As can be seen from Fig. 10.1, most of the data show consistently linear trends as a function of temperature except for the data of Abramov [1] which shows systematically higher viscosities than the other data. The data of Popescu [240], Brockner et al. [25] and Vetyukov and NiKitin [342] were considered for the optimization of the unary parameters A_{NaF} and E_{NaF} as shown in Fig. 10.1.

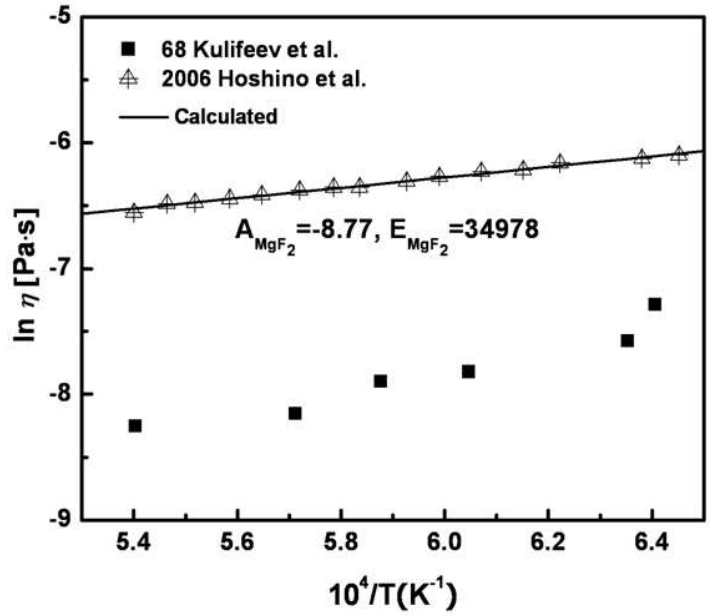

Fig. 10.2 Calculated viscosity in MgF_2 system compared to experimental data [97, 149]

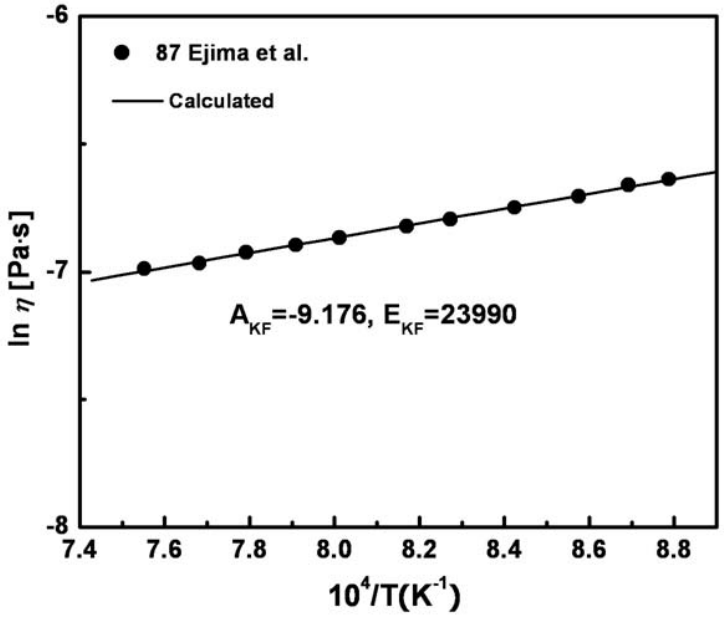

Fig. 10.3 Calculated viscosity in KF system compared to experimental data [56]

The viscosity of pure MgF_2 was measured by Kulifeev et al. [149] and Hoshino et al. [97] using the oscillation method. As can be seen from Fig. 10.2, the data of two authors[97, 149] show a large difference of about 1.5 in the natural logarithm scale at all temperatures. The data of Hoshino et al. were selected for the optimization of the unary parameters A_{MgF_2} and E_{MgF_2} since the data of Kulifeev et al. [149] show too low viscosities, almost equal to the viscosity of water at room temperatures.

The viscosities of pure KF were measured only by Ejima et al.[56] using the oscillation method. The data were used for the optimization of the unary parameters A_{KF} and E_{KF}. As can be seen from the unary data of CaF_2 as shown in Fig. 9.2 and other MF_x (M = Mg, Na, K) viscosity data as shown in Figs 10.1-10.3, these fluorides have viscosities in the range of -4.5 to -7 on the natural logarithm scale. In the case of AlF_3, there are no available data. Thus, the unary parameters of AlF_3 were estimated by considering the viscosities of other pure fluorides and the viscosities of the system $3(CaSiO_3):Al_2O_3–AlF_3$ measured by Kato and Minowa [117] as shown in Fig. 10.18.

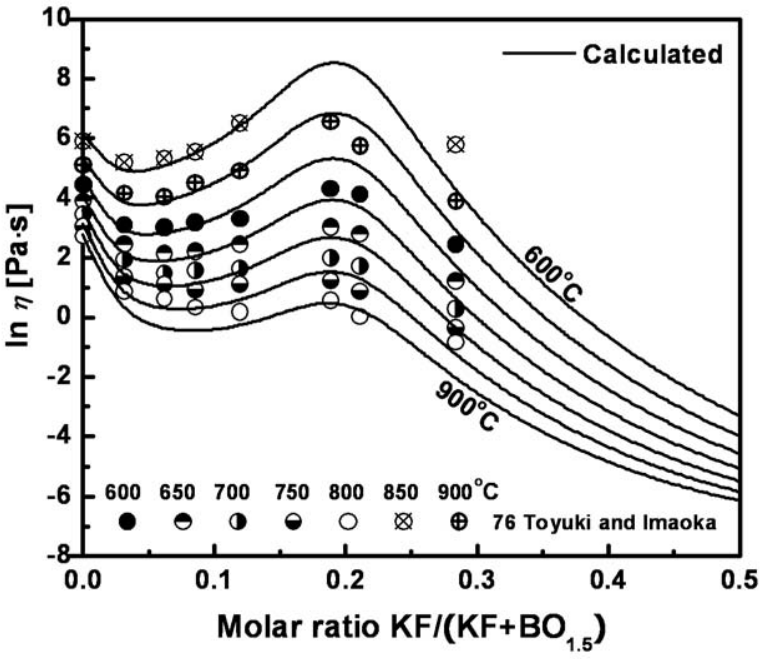

Fig. 10.4 Calculated viscosity in $KF-B_2O_3$ system compared to experimental data [326]

10.1.2 Viscosities of the binary KF-B_2O_3 melts

The viscosities of KF-B_2O_3 melts were reported only by Toyuki and Imaoka [326] using the counter-balanced sphere viscometer method with platinum spheres. As can be seen from Fig. 10.4, the data are in good agreement at all temperatures. The height of the maximum rapidly declines with increasing temperature, most likely indicating that the solid-like clusters tend to decompose at high temperatures, as is to be expected.

All five model parameters given in Tables 10.1 and 10.2 were optimized to fit the experimental data. The parameters $A^*_{B(NF)}$ and $E^*_{B(NF)}$ (N = Na and K) were optimized to reproduce the sharp decrease in the viscosity that is observed when less than 10 mol% KF is added to B_2O_3. The parameters $\Delta G_{m(NB_4FO_6)}$ and $E_{m(NB_4FO_6)}$ in Eqs (3.23) and (3.28) were obtained from the temperature dependence of the viscosity maximum while the cluster size, *m*, controls the width of the viscosity maximum.

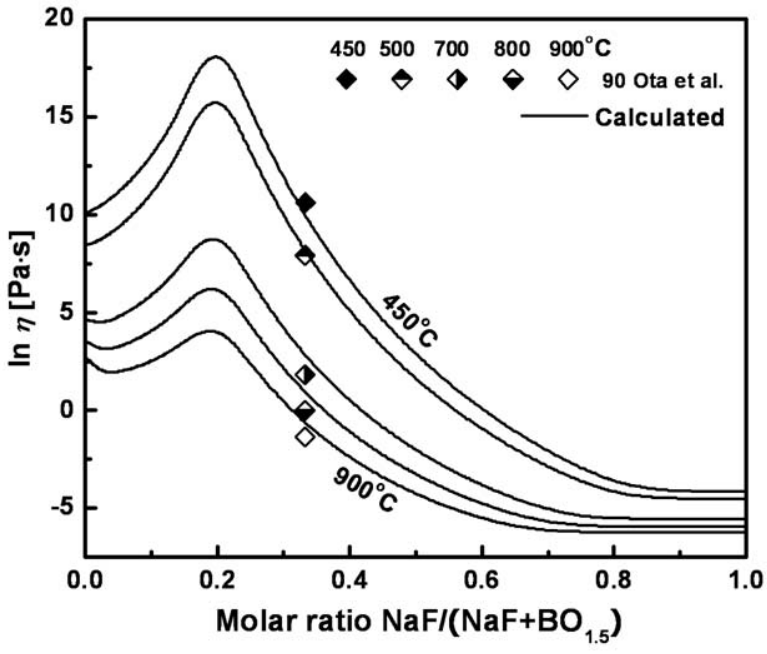

Fig. 10.5 Calculated viscosity in NaF-B_2O_3 system compared to experimental data [221]

10.1.3 Viscosities of the binary NaF-B_2O_3 melts

The viscosities of NaF-B_2O_3 melts were measured only by Ota et al. [221] using the rotating crucible method with platinum crucibles. Ota et al. [221] measured viscosities only at one composition at different temperatures. Thus the maximum trend of the viscosity as shown in KF-B_2O_3 system was not observed. However, without applying the parameters $A^*_{B(NF)}$, $E^*_{B(NF)}$, m, $\Delta G_{m(NB_4FO_6)}$ and $E_{m(NB_4FO_6)}$ (N = Na and K) the experimental data could not be reproduced. The optimized parameters are given in Tables 10.1 and 10.2. As can be seen from Fig. 10.5, the model fits the experimental data well within experimental error limits. No available viscosity data for binary systems AlF_3-B_2O_3 and MgF-B_2O_3 exist. Only the binary parameters $A^*_{B(AlF_3)}$, $A^*_{B(MgF_2)}$, $E^*_{B(AlF_3)}$ and $E^*_{B(MgF_2)}$ for AlF_3-B_2O_3 and MgF-B_2O_3 systems were used in the model and set to the same values as the unary parameters A_{AlF_3}, A_{MgF_2}, E_{AlF_3} and E_{MgF_2} for the unary AlF_3 and MgF_2 systems. They are summarized in Table 10.1.

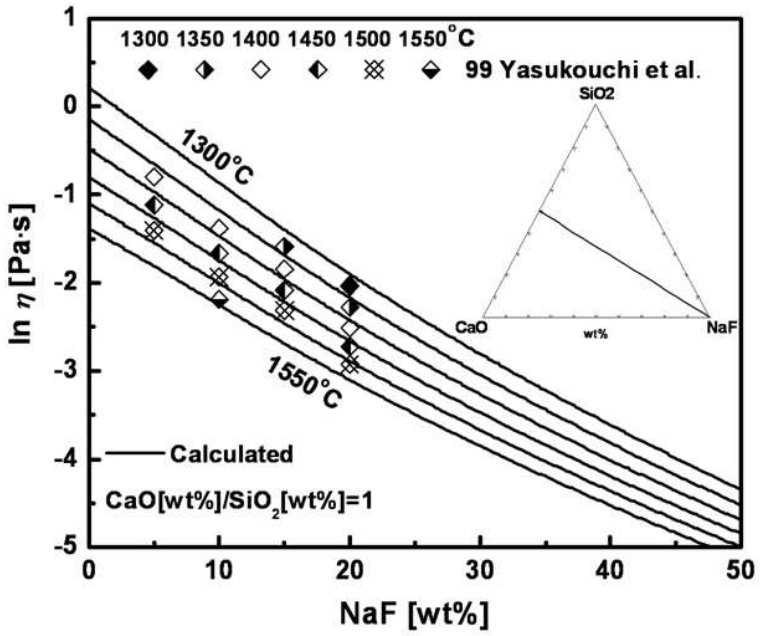

Fig. 10.6 Viscosity of NaF-CaO-SiO_2 melts for a weight ratio CaO/SiO_2 = 1 compared to experimental data [357]

10.1.4 Viscosities of the ternary NaF-CaO-SiO_2 melts

The viscosities of ternary and higher-order melts containing MF_x (M = Mg, Na, K and Al) were predicted by the model based on the unary and binary viscosity parameters given from Tables 4.1, 4.2, 5.1, 6.1, 7.1, 8.1, 9.1 and Tables 10.1-10.2 without any additional adjustable parameters.

Fig. 10.6 shows the calculated viscosities of the system NaF-CaO-SiO_2 at constant weight ratio of CaO/SiO_2 = 1 along with the data points measured by Yasukouchi et al. [357] using the rotating crucible method. As can be seen from Fig. 10.6, all data show an excellent agreement with the lines calculated by the model. In particular, the observed trends of decreasing viscosity with the addition of NaF are well predicted by the calculations obtained from only unary and binary parameters of the model.

10.1.5 Viscosities of the ternary MgF_2-CaO-SiO_2 melts

Figs 10.7-10.9 show the calculated viscosities of the system MgF_2-CaO-SiO_2 at constant weight ratio of CaO/SiO_2 = 0.51, 1 and 1.28 along with the experimental data measured by Shiraishi and Saito [292] who also measured the binary CaO-SiO_2 system using the rotating crucible method with graphite crucibles. The data measured for the CaO-SiO_2 system are systematically higher than the calculated lines at all temperatures, though the differences are fairly small. It was shown that our calculated lines for the CaO-SiO_2 system as shown in Fig. 3.8 were in good agreement with many other authors [82]. As can be seen from the Figs 10.7-10.9, all data points show a good agreement with the calculated lines within experimental error limits. The observed trends of decreasing viscosity with addition of MgF_2 are well predicted by the model.

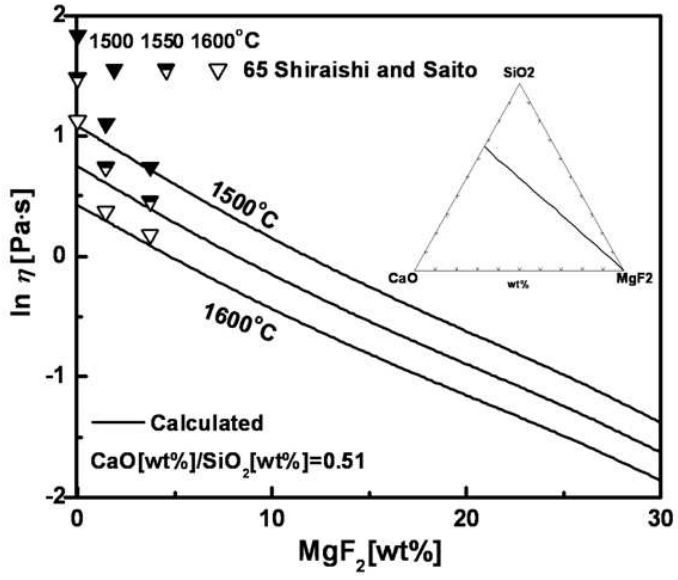

Fig. 10.7 Viscosity of MgF_2-CaO-SiO_2 melts for a weight ratio CaO/SiO_2 = 0.51 compared to experimental data [292]

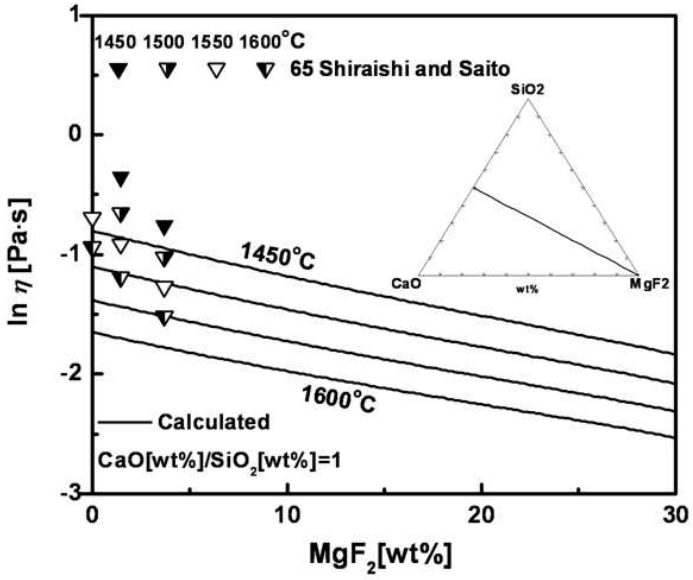

Fig. 10.8 Viscosity of MgF_2-CaO-SiO_2 melts for a weight ratio CaO/SiO_2 = 1 compared to experimental data [292]

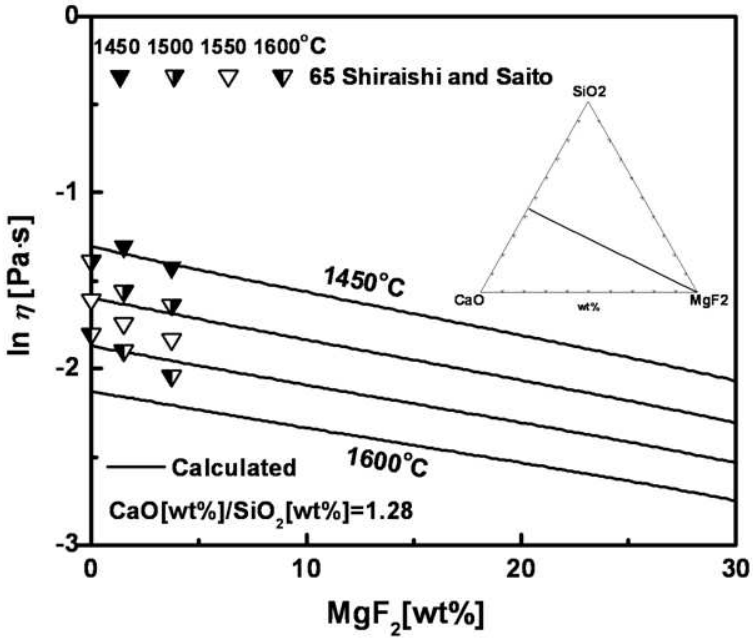

Fig. 10.9 Viscosity of MgF_2-CaO-SiO_2 melts for a weight ratio CaO/SiO_2 = 1.28 compared to experimental data [292]

10.1.6 Viscosities of the ternary NaF-Na_2O-SiO_2 melts

The viscosity of the NaF-Na_2O-SiO_2 system was investigated by Bobylev et al. [21] using the oscillation method and Endell and Strasmann [57] using the rotating crucible method with platinum crucibles. Figs 10.11-10.16 show the calculated viscosities of NaF-Na_2O-SiO_2 melts obtained from only unary and binary parameters of the model compared to experimental data of Bobylev et al. [21] and Endell and Strasmann [57].

In Figs 10.11-10.12, viscosities were calculated in two pseudo-binary sections of NaF-Na_2O and Na_2O-SiO_2. All data points of Endell and Strasmann [57] show a good agreement with the calculated lines at all temperatures within experimental error limits. In particular, the observed trends of decreasing viscosity with the addition of NaF are excellently predicted by the calculations obtained from only unary and binary parameters of the model.

Figs 10.13-10.14 show the calculated viscosities at constant molar ratio of SiO_2/Na_2O = 1 and 0.667 along with the experimental data measure by Bobylev et al. [21]. The observed trends

of decreasing viscosity of the data points with addition of NaF are sharper than the lines predicted by the model. When this decreasing trend of the data points of Bobylev et al. [21] was extrapolated to pure NaF, the viscosities obtained for pure NaF were much lower than the experimental data for pure NaF measured by several authors [1, 25, 29, 40, 56, 217, 240, 342] in Fig. 10.1. Bobylev et al. [21] measured the viscosities of NaF-Na_2O-SiO_2 melts using the oscillation method which can contribute to large systematic errors in the viscosity measurements through the uncertainties in the damping rates of an oscillating wire [104]. On the other hand, the rotating crucible method used by Endell and Strasmann [57] requires only information on the radius and the height of the bob which is rotated in the sample liquid.

As shown in Figs 10.15 and 10.16, the data of Endell and Strasmann [57] are in good agreement with the calculated lines at all temperatures within experimental error limits while the data of Bobylev et al. [21] show systematically lower viscosities than the lines calculated by the model although the difference is fairly small.

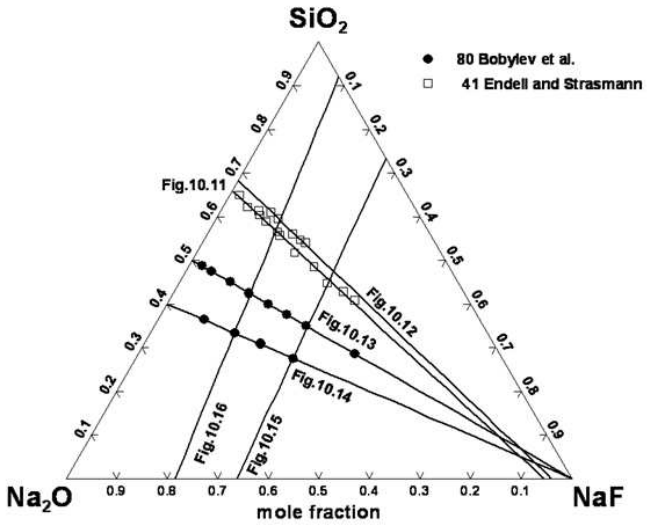

Fig. 10.10 Compositions in the NaF-Na_2O-SiO_2 system at which experimental viscosity measurements are available [21, 57]. The lines indicate six sections of this system selected to show the viscosity as a function of composition in Figs 10.11 to 10.16.

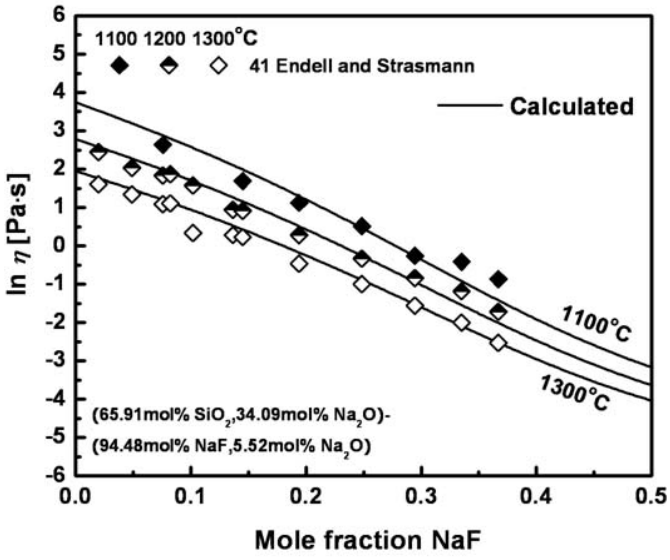

Fig. 10.11 Viscosity of NaF-Na_2O-SiO_2 melts in the section of (65.91 mol% SiO_2, 34.09 mol% Na_2O) to (94.48 mol% NaF, 5.52 mol% Na_2O) compared to experimental data [57]

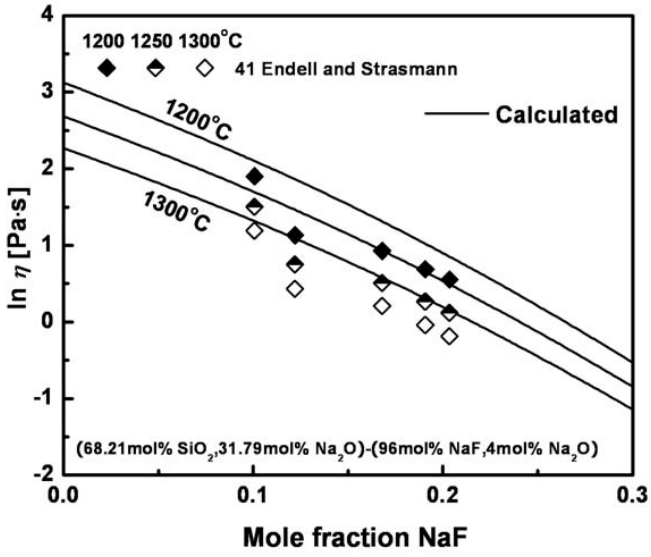

Fig. 10.12 Viscosity of NaF-Na_2O-SiO_2 melts in the section of (68.21 mol% SiO_2, 31.79 mol% Na_2O) to (96 mol% NaF, 4 mol% Na_2O) compared to experimental data [57]

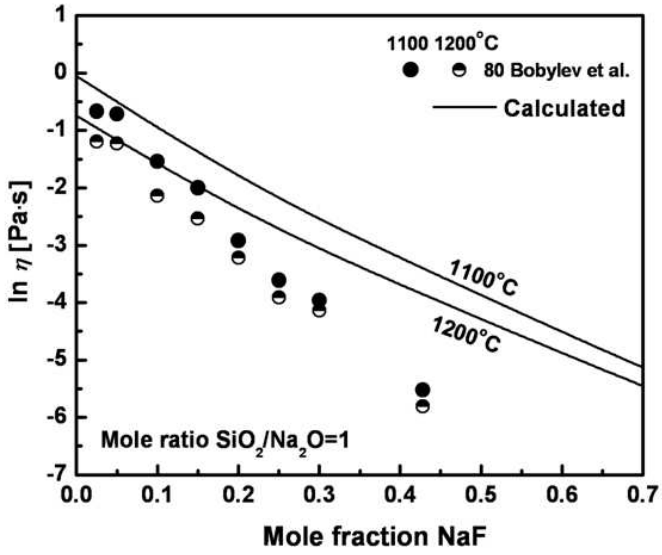

Fig. 10.13 Viscosity of NaF-Na_2O-SiO_2 melts at a molar ratio of SiO_2/Na_2O = 1 compared to experimental data [21]

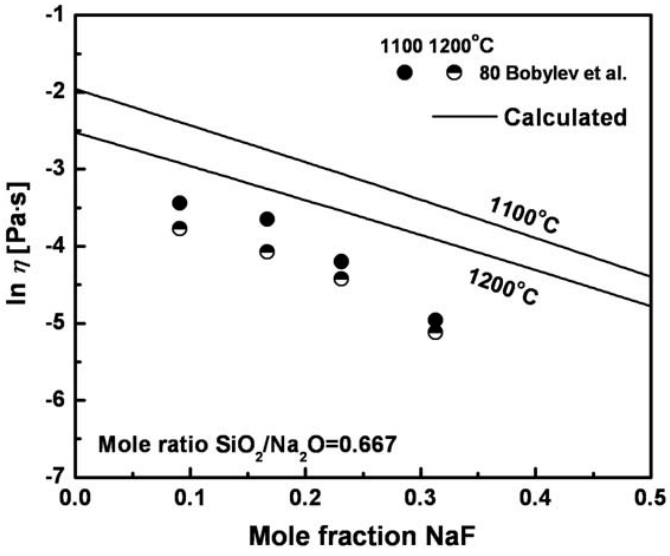

Fig. 10.14 Viscosity of NaF-Na_2O-SiO_2 melts at a molar ratio of SiO_2/Na_2O = 0.667 compared to experimental data [21]

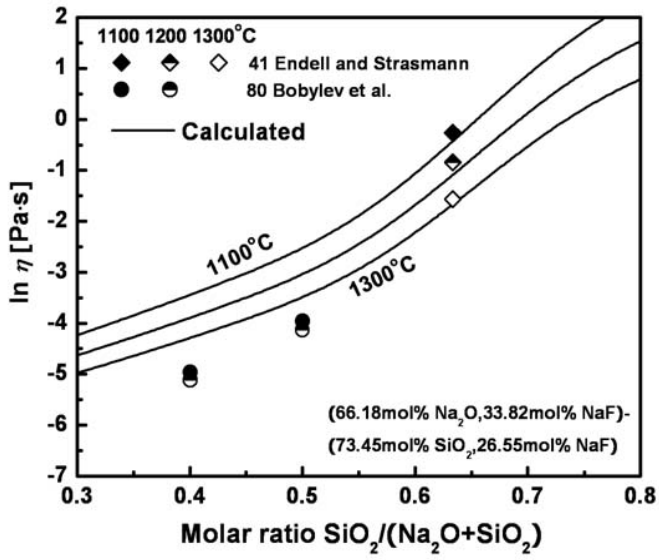

Fig. 10.15 Viscosity of NaF-Na_2O-SiO_2 melts in the section of (66.18 mol% Na_2O, 33.82 mol% NaF) to (73.45 mol% SiO_2, 26.55 mol% NaF) compared to experimental data [21, 57]

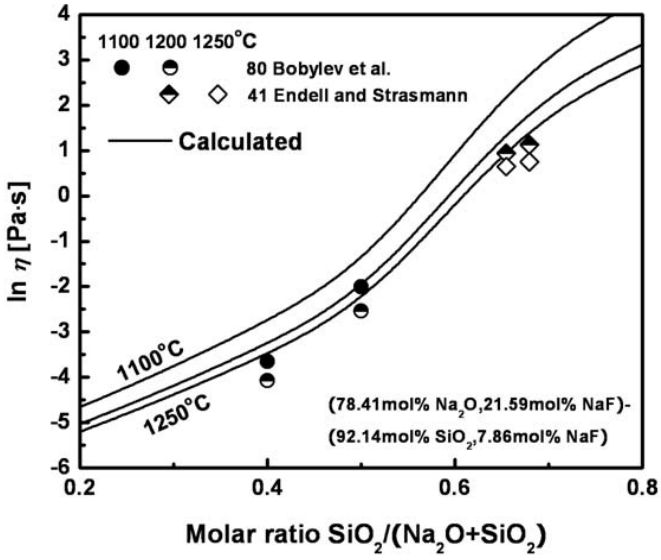

Fig. 10.16 Viscosity of NaF-Na_2O-SiO_2 melts in the section of (78.41 mol% Na_2O, 21.59 mol% NaF) to (92.14 mol% SiO_2, 7.86 mol% NaF) compared to experimental data [21, 57]

10.1.7 Viscosities of the ternary NaF-Na_2O-B_2O_3 melts

Fig. 10.17 shows the calculated viscosities of the system NaF-Na_2O-B_2O_3 in the section from 33.33 mol% Na_2O-66.67 mol% B_2O_3 to 50 mol% NaF-50 mol% B_2O_3 along with the experimental data measured by Ota et al. [221], who also measured the viscosity of the binary Na_2O-B_2O_3 and NaF-B_2O_3 systems, using the rotating crucible method with platinum crucibles. As can be seen from Fig. 10.17, the lines predicted by the model are believed to be in agreement with the measurements within experimental error limits.

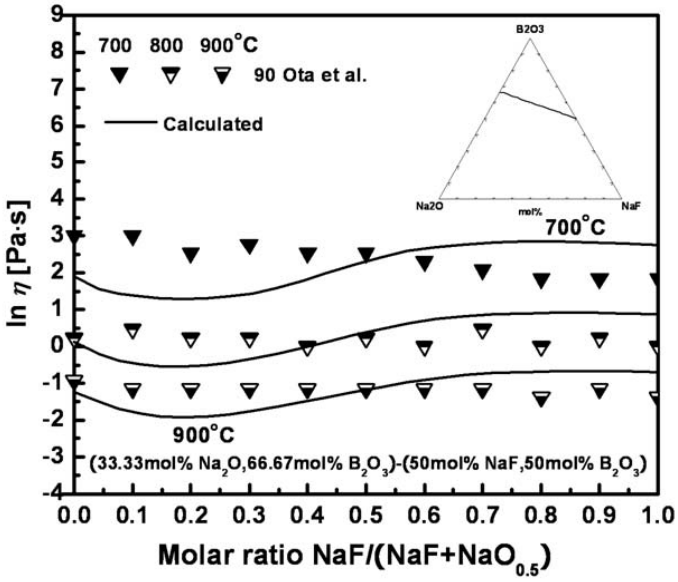

Fig. 10.17 Viscosity of NaF-Na_2O-B_2O_3 melts in the section of (33.33 mol% Na_2O, 66.67 mol% B_2O_3) to (50 mol% NaF, 50 mol% B_2O_3) compared to experimental data [221]

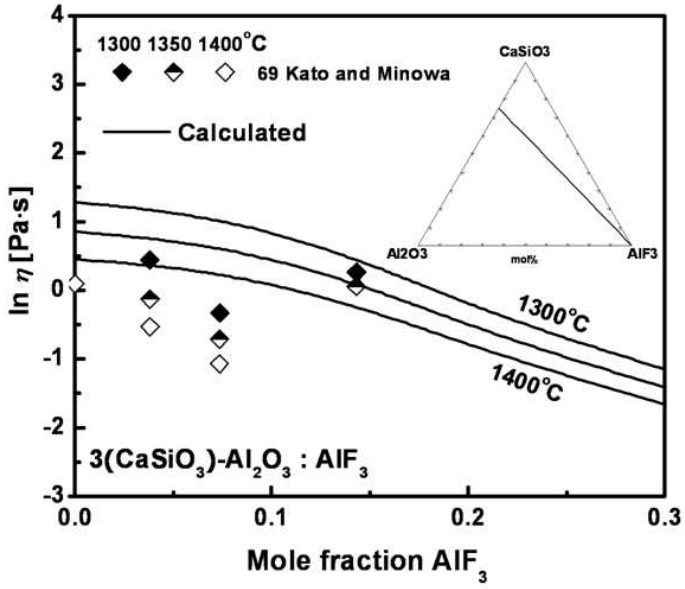

Fig. 10.18 Viscosity of CaO-Al_2O_3-SiO_2-AlF_3 melts in the section of $3(CaSiO_3)$-Al_2O_3 to AlF_3 compared to experimental data [117]

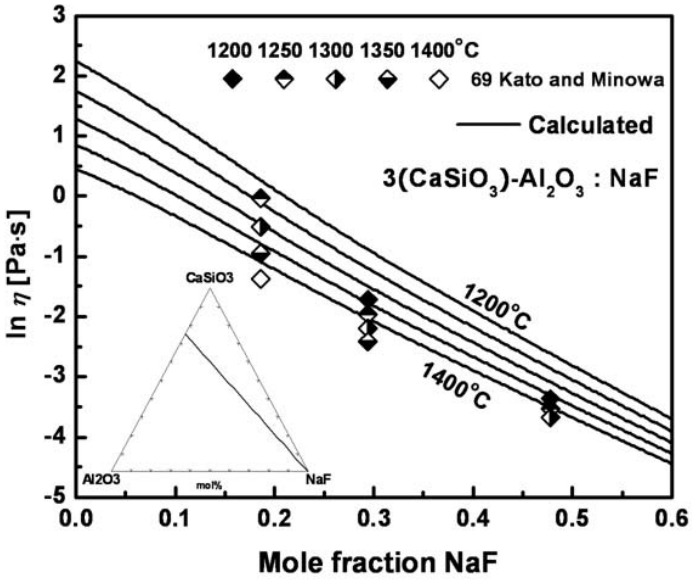

Fig. 10.19 Viscosity of CaO-Al_2O_3-SiO_2-NaF melts in the section of $3(CaSiO_3)$-Al_2O_3 to NaF compared to experimental data [117]

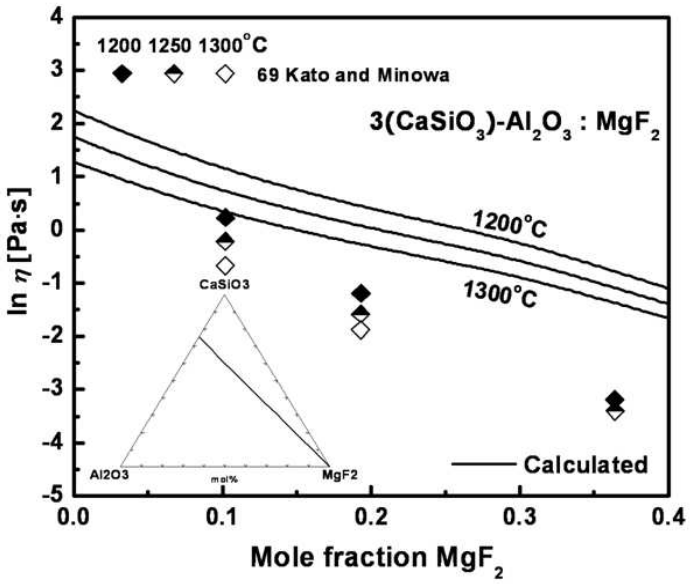

Fig. 10.20 Viscosity of CaO-Al_2O_3-SiO_2-MgF_2 melts in the section of $3(CaSiO_3)$-Al_2O_3 to MgF_2 compared to experimental data [117]

10.1.8 Viscosities of CaO-Al_2O_3-SiO_2-MF_x (M = Al, Na, Mg) melts

Figs 10.18-10.20 show the calculated viscosities of the system CaO-Al_2O_3-SiO_2-MF_x (M = Al, Na, Mg) in the section from $3(CaSiO_3)$-Al_2O_3 to MF_x (M = Al, Na, Mg) along with the experimental data measured by Kato and Minowa [117], who also measured the viscosity of the CaO-SiO_2 system, using the counter-balanced sphere viscometer method.

As can be seen from Figs. 10.18 and 10.19, most of data show systematically lower viscosities than the lines calculated by the model although the difference is fairly small. The observed trends of decreasing viscosity with addition of AlF_3 or NaF are fairly well predicted by the model within experimental error limits.

On the other hand, as shown in Fig. 10.20, the data of CaO-Al_2O_3-SiO_2-MgF_2 show more rapidly decreasing trends with addition of MgF_2 than the predicted lines. This trend can be fit by re-optimizing the unary parameters A_{MF_x} and E_{MF_x}. If this trend is smoothly extrapolated to pure MgF_2, however, the viscosities of pure MgF_2 obtained by the model are much too low, lower even than the data of Kulifeev et al. [149] in Fig. 10.2 which show physically unreasonable low

viscosities. Therefore, the data of Kato and Minowa [117] in the system $CaO-Al_2O_3-SiO_2-MgF_2$ would have most probably systematic experimental errors caused from the intrinsic experimental difficulties for viscosity measurement of oxy-fluoride melts.

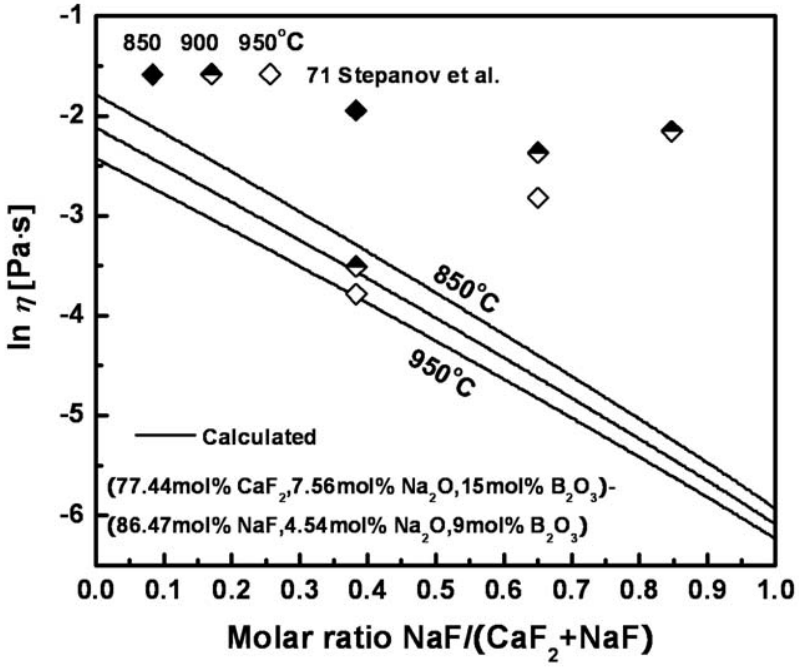

Fig. 10.21 Viscosity of CaF_2-NaF-Na_2O-B_2O_3 melts in the section from (77.44 mol% CaF_2, 7.56 mol% Na_2O, 15 mol% B_2O_3) to (86.47 mol% NaF, 4.54 mol% Na_2O, 9 mol% B_2O_3) compared to experimental data [308]

10.1.9 Viscosities of CaF_2-NaF-Na_2O-B_2O_3 melts

In Fig. 10.21, the calculated viscosities of the system CaF_2-NaF-Na_2O-B_2O_3 are compared to the experimental data measured by Stepanov et al. [308] using the vibrational viscometer method with Mo crucibles. As can be seen from Fig. 10.21, the reproducibility of the model is not in good agreement with most of data points. Some of data show abnormally high viscosities, perhaps measured in the sub-liquidus region.

No available viscosity data measured in systems of order higher than quaternary systems exist. However, the calibrated viscosity model as shown in Figs 10.1-10.21 shows that the viscosities of oxy-fluoride melts can be reproduced by the developed viscosity model using only

a few unary, binary and ternary model parameters within experimental error limits. This viscosity calculation is automatically performed using the FactSage thermodynamic software and database [14].

10.2 Conclusions

Our recently developed model for the viscosity of oxide melts as introduced in Chapters 3 and 4 has been extended to oxy-fluoride melts containing MF_x (M = Ca, Mg, Na, K and Al). The Modified Quasichemical Model [231, 232] and thermodynamic database [14] were not developed for all oxy-fluoride melts. Thus, the model was modified to reproduce the viscosity of the oxy-fluoride melts with following features;

- MF_x (M = Ca, Mg, Na, K and Al) would behave as network modifiers in silicate or borate melts as modeled for corresponding basic oxides in Chapters 3 and 4.
- The "equilibrated composition" or "formal composition" of the oxy-fluoride melts are calculated from Gibbs free energies of pure liquid oxides and fluorides. Then the calculated X for each liquid oxide and fluoride is given to the model equations developed in Chapters 3 and 4. Note that the formation of SiF_4 and BF_3 in the melts is not considered. We assume all Si and B atoms are bonded only to oxygens because the formation of $SiF_4(l)$ and $BF_3(l)$ in liquid solution is very unstable [15].
- MF_x (M = Ca, Mg, Na, K and Al) would have the same breaking effects on silicate or borate networks as basic oxides containing the same cation. (Note: Each fluoride and oxide should contain same cation) Therefore, all fluorides are regarded as oxides containing the same cation only to calculate all possible second-nearest-neighbor pairs of the system and *p* which is the probability that a particular pair emanating from a given Si or B atom using the present thermodynamic database [15].
- No Charge compensation effect for M^+ and M^{2+} cations with fluorine ions. (No available data and the observed trend implied no charge compensation effect)
- Viscosities of the binary MF_x-SiO_2 and MF_x-B_2O_3 systems were modeled with the same kinds of unary and binary parameters used in the model of Chapters 3 and 4.
- In the alkali-borate system NF-B_2O_3 (N=Na and K), the formation of solid-like clusters such

as 5(NaB_4FO_6) and 5(KB_4FO_6) was modeled using the same model equations developed in Chapter 3.

Using available viscosity data containing MF_x (M = Ca, Mg, Na, K and Al), all unary and binary parameters A_{MF_x} , E_{MF_x} , $E^{1,1}_{MF_x\text{-}Si}$, $E^{Ring}_{MF_x\text{-}Si}$, $E^{R}_{MF_x\text{-}Si}$, $A^{*}_{B(MF_x)}$ and $E^{*}_{B(MF_x)}$ were optimized simultaneously using the modified viscosity model with the overall "equilibrated composition" to fit available viscosity data within experimental error limits.

In Chapters 9 and 10, the viscosities of oxy-fluoride melts containing MF_x (M = Ca, Mg, Na, K and Al) were critically reviewed. The viscosities in all sub-systems of MF_x–SiO_2–B_2O_3–Al_2O_3–CaO–MgO–Na_2O–K_2O–MnO–TiO_y (M = Ca, Mg, Na, K and Al) have been predicted by the model solely from the unary, binary and ternary model parameters. The deviation from the available experimental data does not exceed the scatter of the experimental measurements and experimental error limits.

The predictive ability of the model has been further tested on several industrial mold flux melts and is believed to be in good agreement with the viscosity data within experimental error limits. Overall, the present model provides a very good prediction of the variation of the viscosity with composition.

The very good predictive ability of the present model makes it relatively easy to add a new component MF_x to the chemical system described by the model. The viscosity of multicomponent melts containing this new component can be evaluated without the need to measure and fit the viscosity of multicomponent melts around specific compositions of interest. All necessary model parameters can be obtained from the experimental data on MF_x–SiO_2 and MF_x–B_2O_3, as well as from the viscosity of pure MF_x liquid if such data exist.

Table 10.1 Optimized Model parameters for the viscosity expressed in Pa·s

System	Model parameter	Model parameters ($J \cdot mol^{-1}$)
MgF_2	$A_{MgF_2} = -8.77$	$E_{MgF_2} = 34578$
NaF	$A_{NaF} = -9.59$	$E_{NaF} = 32641$
KF	$A_{KF} = -9.176$	$E_{KF} = 23990$
AlF_3	$A_{AlF_3} = -9.377$	$E_{AlF_3} = 25000$
MgF_2–SiO_2		$E_{MgF_2\text{-}Si} = -86250$ $E^{R}_{MgF_2\text{-}Si} = 72600$ $E^{Ring}_{MgF_2\text{-}Si} = 0$
NaF–SiO_2		$E_{NaF\text{-}Si} = -90000$ $E^{R}_{NaF\text{-}Si} = 10200$ $E^{Ring}_{NaF\text{-}Si} = 20444358$
KF–SiO2		$E_{KF\text{-}Si} = -38200$ $E^{R}_{KF\text{-}Si} = 39000$ $E^{Ring}_{KF\text{-}Si} = 42390018$
AlF_3–SiO2	$A^{R}_{AlF_3\text{-}Si} = -12.3$	$E_{AlF_3\text{-}Si} = -75000$ $E^{R}_{AlF_3\text{-}Si} = 303500$ $E^{Ring}_{AlF_3\text{-}Si} = 0$
MgF_2–B_2O_3	$A^{*}_{B(MgF_2)} = -8.77$	$E^{*}_{B(MgF_2)} = 34578$
NaF–B_2O_3	$A^{*}_{B(NaF)} = -9.59$	$E^{*}_{B(NaF)} = 32641$
KF–B_2O_3	$A^{*}_{B(KF)} = -9.176$	$E^{*}_{B(KF)} = 23990$
AlF_3–B_2O_3	$A^{*}_{B(AlF_3)} = -9.377$	$E^{*}_{B(AlF_3)} = 25000$

The model parameters for subsystems without MF_x (M = Mg, Na, K and Al) that are used for the viscosity calculations in the present study were optimized and reported elsewhere (see Tables 4.1, 4.2, 5.1, 6.1, 7.1 and 8.1 and 9.1)

Table 10.2 Optimized parameters for the boron containing systems

Cluster (MB_4FO_6)	$\Delta G_{m(MB_4FO_6)}$ (J/mol)	$\ln \eta_{m(MB_4FO_6)} = A_{m(MB_4FO_6)} + \frac{E_{m(MB_4FO_6)}}{RT}$ (in $Pa \cdot s$) $E_{m(MB_4FO_6)} = \alpha + \beta T$ (J/mol)	m (Cluster Size)
NaB_4FO_6	−35690	$A_{m(MB_4FO_6)} = -9.59$ $E_{m(MB_4FO_6)} = 216206\text{-}42.857T$	5
KB_4FO_6	−25230	$A_{m(MB_4FO_6)} = -9.176$ $E_{m(MB_4FO_6)} = 204306\text{-}41.214T$	5

CHAPTER 11 EXTENSION OF THE MODEL TO THE GLASS REGION OF SILICATES

11.1 Introduction

It is well-known that any silicate liquid forms a glass when supercooled rapidly enough to avoid crystallization [6, 7, 47, 49]. The supercooled silicate melts are known as glasses. The viscosity of glasses is very high and crystallization from such high-viscosity liquid proceeds with great difficulty. The viscosity of the glass melt is important for the melting and refining conditions in glass furnaces. In the glassmaking process, there are several critical points which are mainly influenced by the viscosity of glass. The value of viscosity is 4 in the logarithm poise scale at the working point. Once glass is formed, the glass should be supported until the viscosity reaches a value sufficiently high to prevent deformation under its own weight which stops at the viscosity of 7.6 in the logarithm poise scale. The temperature range between these two points is the working range. Also, the prediction of temperatures corresponding to the high viscosity range such as 12 and 13 in the logarithm poise scale is important for releasing the internal stress of the glass during the annealing. Therefore, the prediction of viscosity for the glass region is of much importance.

Many glass scientists have tried to develop models to predict the viscosity of glasses. Several models for the viscosity of glasses have been discussed in Chapter 2.

In the melt region, as discussed in Chapters 3 to 10, the viscosity data could be reproduced with an Arrhenian temperature dependence ($\ln\eta \propto 1/T$) at all compositions except for pure B_2O_3. However, the model does not reproduce the high viscosities measured in the glass region because the temperature dependence in the glass region is non-Arrhenian. The model proposed in Chapters 3 to 10 is further developed in the present chapter to predict the viscosity of glasses for all available subsystems of the CaO-MgO-Na_2O-K_2O-ZnO-PbO-Al_2O_3-SiO_2 system from the glass to the melt region within the experimental error limits by the addition of a few non-Arrhenian model parameters.

11.2 Viscosity Model

11.2.1 Structure of Silicate Glasses

The structure of silicate glasses should be similar to that of silicate melts from which the glass is formed by quenching without crystallization. This contention is supported in the case of silicate glasses by in-situ measurements by X-ray, infrared spectrometry and Raman scattering [113, 290]. Kalampounias et al. [113] melted the sample of $MgO\text{-}SiO_2$ system using the container-less levitation techniques and CO_2 laser heating system under Ar gas atmosphere and quenched the sample by a sudden shut down of the laser. Then, they measured the concentration of non-bridging oxygens per Si atom corresponding to M-Si second-nearest-neighbor pairs using Raman spectroscopy. Fig. 11.1 compares the non-bridging oxygens per Si atom in the $MgO\text{-}SiO_2$ system calculated by FactSage [14] from the Modified Quasichemical Model with the experimental results determined by Raman spectroscopy [113]. It can be seen that there is good agreement between the calculated curve and experimental data. A possible source of error in the calculation is the assumption of randomly distributed bonds. On the other hand, the experimental fractions of non-bridging oxygens are derived from the relative intensities of spectral lines and can have substantial uncertainties.

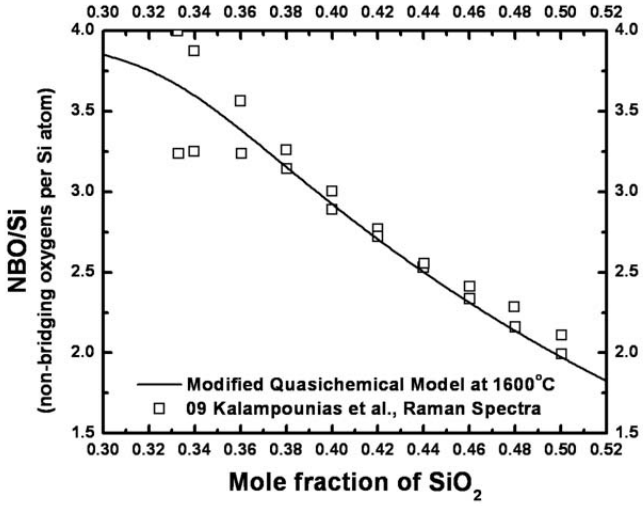

Fig. 11.1 Calculated and experimental [113] non-bridging oxygens (NBO/Si) for the $MgO\text{-}SiO_2$ system at 1600°C.

The structural changes taking place upon formation of the SiO_2 network can be characterized by the amounts of so-called Q^i-species [199] which are defined as Si atoms linked to i bridging oxygens and $(4 - i)$ non-bridging oxygens. In pure SiO_2, all four oxygens surrounding each Si are bridging oxygens and the fraction of Q^4-species is 1. An isolated SiO_4^{4-} ion is a Q^0-species. The calculation of Q^i-species of silicate systems has been discussed in Chapter 3 and can be carried out using the Modified Quasichemical Model [231, 232] and thermodynamic database [14].

11.2.2 Extended Viscosity Model with Non-Arrhenian Temperature Dependence

The viscosity data for silicate glasses and melts can often be fitted, at least over limited temperature ranges, by an Arrhenian temperature dependence expression of the form of Eq.(11.1) with different parameters A and E for each limited temperature range. For example, as shown in Fig. 11.8, viscosity data of the CaO-SiO_2 system measured in different temperature ranges show different linear temperature dependences. However, as will be shown in Figs 11.4 and 11.5, the viscosity data over a wide temperature range obviously show non-Arrhenian temperature dependence as a function temperature. There is no universal agreement about the origin of the non-Arrhenius behavior of viscous liquids.

$$\log \eta = A + \frac{E}{RT} \tag{11.1}$$

In the previous study [82], we considered all available data for pure SiO_2 and the data at all temperatures showed Arrhenian temperature dependence. On the other hand, as shown in Fig. 12.1 of Chapter 12, the viscosities of B_2O_3 show obviously non-Arrhenian temperature dependence. We applied (see Eq.(3.12)) a non-Arrhenian temperature dependence to the model with two adjustable parameters, T_B and n_B, to take into account the viscosity of pure B_2O_3 in the glass region as shown in Eq.(11.2).

$$\log \eta_B = A_B + \frac{E_B}{RT} \cdot \left[1 + \left(\frac{T_B}{T} \right)^{n_B} \right] \tag{11.2}$$

where η is the viscosity in poise, R is the gas constant, T is temperature in kelvins. In previous chapter, shown in Chapters 3 to 10, we have used the unit of Pa·s but many glassmaking engineers working in the industry field are more familiar with the unit of poise. In the present chapter, we will indicate all viscosities with the unit of poise.

Figs 11.2, 11.4 and 11.6 show the viscosities of the $NaO_{0.5}$-SiO_2, $KO_{0.5}$-SiO_2 and PbO-SiO_2 systems. At all temperatures, these systems show similar composition dependence. Therefore, as we did in the unary system in Eq.(11.2), we added two system-dependent non-Arrhenian binary parameters $T_{MO_x\text{-Si}}$ and $n_{MO_x\text{-Si}}$ into the model (Chapters 3 to 10) as shown in Eq.(11.4) to account for the non-Arrhenian temperature dependence of the binary viscosity data. The effects of these terms $T_{MO_x\text{-Si}}$ and $n_{MO_x\text{-Si}}$ on the viscosity calculations are weaker at higher temperatures and stronger at lower temperatures at constant composition.

Then the activation energy E for silicate systems (no borates) is calculated as

$$\log\eta = A + \frac{E}{RT} \tag{11.3}$$

$$E = \left[\sum_{M}(X_{MO_x}E_M)\left[1+X_{MO_x}^{m_{MO_x\text{-Si}}}\left(\frac{T_{MO_x}}{T}\right)^{n_{MO_x}}\right] + \sum_{M}\sum_{i,j}\left(X_{MO_x}^{i}X_{Si}^{j}E_{MO_x\text{-Si}}^{i,j}\right) + X_{Si}\left\{ \begin{array}{l} \left[E_{Si}^{*}+\left(p_{Si}^{B,Si}\right)^4\left(p_{B,Si}^{B,Si}\right)^{36}E_{Si}^{E}\right] \\ +\left(p_{Si}^{B,Si}\right)^4\left[1-\left(p_{B,Si}^{B,Si}\right)^{36}\right]\dfrac{\sum_{M}(X_{MO_x}E_{MO_x\text{-Si}}^{R})}{\sum_{M}X_{MO_x}} \\ +\left(p_{Si}^{Si}\right)^7\left(1-p_{Si}^{Si}\right)^3\dfrac{\sum_{M=Alkali}(X_{MO_x}E_{MO_x\text{-Si}}^{Ring})}{\sum_{M}X_{MO_x}} \end{array} \right\} \right] \left[1+\sum_{M}\left(\left(\frac{T_{MO_x\text{-Si}}}{T}\right)^{n_{MO_x\text{-Si}}}\cdot X_{MO_x}\cdot X_{Si}\right)\right] \tag{11.4}$$

where the values of $p_{Si}^{B,Si}$, $p_{B}^{B,Si}$ and $p_{B,Si}^{B,Si}$ are same as p_{Si}^{Si} in the absence of boron oxide. These values take into account the probability of the network pairs emanating from a given B or Si atom. For a more detailed description for $p_{Si}^{B,Si}$, $p_{B}^{B,Si}$ and $p_{B,Si}^{B,Si}$, see Chapter 3.

We also extended the model to the glass region of the systems containing boron. The systems containing boron required special treatment to reproduce the viscosity data in the glass

region. The extension of the viscosity model to boron-containing systems will be described in detail in Chapter 12.

An equation similar to Eq. (11.4) is used for *A* except that it does not have any non-Arrhenian terms. If needed, the unary parameters T_{MO_x} and n_{MO_x} are added to enable better fitting of viscosity data of binary MO_x-SiO_2(M = basic oxide) systems by the model with binary parameters $T_{MO_x\text{-}Si}$ and $n_{MO_x\text{-}Si}$. In some binary systems, the cross-over point of viscosity of binary MO_x-SiO_2(M = basic oxide) systems was reproduced as will be shown in Figs. 11.8 and 11.9 due to the contribution of these T_{MO_x} and n_{MO_x} parameters. The detailed explanation for the roles of these parameters will be shown in section 11.3.3. The binary parameter $m_{MO_x\text{-}Si}$ was also added to better reproduce the non-linearity of viscosity data as a function of molar ratio of basic oxides at constant SiO_2 contents as will be shown in the ternary CaO-Na_2O-SiO_2, MgO-Na_2O-SiO_2 and CaO-MgO-SiO_2 systems. In the present study, the unary parameters T_{MO_x} and n_{MO_x} are added to the unary CaO, MgO and PbO systems and the binary parameters $m_{MO_x\text{-}Si}$ are added only to the binary CaO-SiO_2 and MgO-SiO_2 systems.

In order to reproduce the maximum in the viscosity of the melt region for the systems containing Al_2O_3, we applied the Gibbs energies for the formation of the associates as discussed in Chapter 3. In the melt region, these Gibbs energies were not dependent on temperature, but were found to vary linearly as a function of SiO_2 content, becoming more negative at higher SiO_2 concentrations. However, these Gibbs energies required a temperature dependence in the glass region because the formation of the associates would be more significant with decreasing temperature. Hence, two more parameters are added to model the Charge Compensation Effect in each ternary glass system MO_x–Al_2O_3–SiO_2 (including the limiting MO_x–Al_2O_3 binary systems) as shown in Eq.(11.5):

$$\Delta G_{MAl_xO_y} = (A+BT)+(C+DT)X(SiO_2)\ [J/mol] \tag{11.5}$$

11.3 Review of the available viscosity data and calibration of the model

In the present study, viscosity data measured from the melt to the glass region are reviewed for all subsystems of the CaO–MgO–Na_2O–K_2O–ZnO–PbO–SiO_2–Al_2O_3 system. The data judged to be most reliable are shown in the figures below. To improve the legibility of the figures, the results of a few studies which substantially deviate from those of other authors are not shown. For multicomponent subsystems, preference was given to extensive systematic studies. If the viscosity is reported for just a few compositions in a multicomponent system and the description of the experiments is insufficient, it is very difficult to evaluate the real accuracy of the data unless similar compositions were also studied by other authors.

The extended model is intended for the single phase regions of the melts and the glasses. The data measured in the two phase regions were not considered. Therefore, the viscosity data were collected mostly for the single phase region at all available temperature ranges. If an abnormally high viscosity value was reported when comparing with other data, this is most likely the result of the effect of crystallization. In most cases such data were discarded, but sometimes these points are still shown in the figures to take into account systematic errors.

11.3.1 The Accuracy and Reliability of Viscosity Measurements

Most experiments to measure viscosity of glasses were carried out with several careful treatments. First, the sample having the targeted composition was melted and stirred to make homogeneous melts without the formation of bubbles. Secondly, the sample was quenched quickly to avoid crystallization. After quenching, some authors attempted to distinguish the presence of glasses without any crystallization by microscopic observation.

Some systems are known to be very difficult to quench to retain the glassy state, such as CaO-SiO_2 and MgO-SiO_2, while other systems such as Na_2O-SiO_2 are known to be easier to quench to retain the glassy state [28, 164, 176, 184, 213]. The viscosity data were collected mainly for melts and glasses where crystallization did not occur. Since the viscosity of silicates in the range from melts to glasses can span more than 15 orders of magnitude (0 to 10^{15} poise) the experimental measurements must differ according to the viscosity range. The measurements of the melt were mostly made with rotational and vibrational viscometers and the measurements in

the glass region were mostly made with the fiber-elongation, ball penetration and micro-penetration methods. The experimental method and the difficulties associated with measurements of the viscosity of glasses and melts over a wide temperature range has been discussed in detail in Chapter 2.

For calibration and testing of the proposed viscosity model, experimental viscosity data were collected for the all subsystems of Al_2O_3–B_2O_3–CaO–MgO–FeO–Fe_2O_3–MnO–NiO–PbO–ZnO–Na_2O–K_2O–TiO_2–Ti_2O_3–SiO_2–F for the melts and all subsystems of Al_2O_3–B_2O_3–CaO–MgO–ZnO–PbO–Na_2O–K_2O–SiO_2 for the glasses. Based on the critical evaluation and analysis for available data collected from the investigated literature data including the Sci-Glass database [274], it can be concluded that most reliable data measured by different best laboratories show the average absolute uncertainty of viscosity measurements within 0.25 to 0.5 for the melts and within 1 to 2 in the logarithm poise scale for the glasses.

11.3.2 Viscosity of the unary systems

The unary SiO_2 system was studied by many researchers due to its technological importance from the melt to glass region and was optimized in the previous study [82] (see Fig. 3.6). Viscosity data of this system were well reproduced by the model with Arrhenian temperature dependence over the entire temperature range of 1000 to 2500ºC [82]. Due to the extremely strong tendency to crystallization and high melting temperatures of CaO and MgO and the reactivity and volatility of Na_2O and K_2O, no viscosity measurements are available for lower temperatures. Data for PbO and Al_2O_3 in the melt are available [82, 128] but data at lower temperatures are not available due to the strong tendency for crystallization. It can be assumed that basic oxides would be formed as a glass when cooled rapidly enough to avoid crystallization. We assumed that the basic oxide is characterized hypothetically as a glass in the silicate systems and the viscosity of the basic oxide has Arrhenian dependence as a function of temperature if the binary data can be reproduced with only binary parameters. But if unary non-Arrhenian parameters were needed to reproduce the binary viscosity data we introduced non-Arrhenian unary parameters into the model. In the present study, the non-Arrhenian unary parameters T_{MO_x} and n_{MO_x} were applied only to CaO, MgO and PbO, and optimized simultaneously with the model parameters A_{MO_x} and E_{MO_x}. Fig. 11.2 shows the viscosities of pure PbO calculated by the

previous model and the extended model. As can be seen in Fig. 11.2, the extended model reproduces non-Arrhenian trend with decreasing temperature and shows a good agreement with the experimental data.

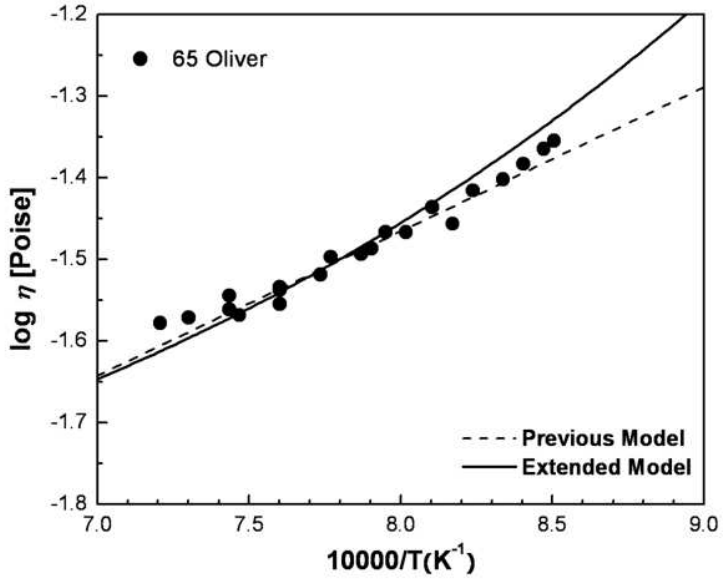

Fig. 11.2 Calculated viscosity in PbO system compared to experimental data [219] as a function of temperature

11.3.3 Viscosity of the binary systems

All optimized model parameters are listed in Tables 11.1 to 11.3. The viscosity parameters A^{*}_{Si}, A^{E}_{Si}, E^{*}_{Si} and E^{E}_{Si} for pure SiO_2 and three parameters for each MO_x–SiO_2 binary system except for MO_x = CaO, MgO, PbO, ZnO and Al_2O_3, $E^{i.j}_{\mathrm{MO_x\text{-}Si}}$, $E^{R}_{\mathrm{MO_x\text{-}Si}}$ and $E^{Ring}_{\mathrm{MO_x\text{-}Si}}$ are taken from Tables 4.1 and 6.1. With the addition of unary and binary non-Arrhenian parameters for each MO_x–SiO_2 binary system (M = Ca, Mg, Pb, Zn and Al), the values of the model parameters $A_{\mathrm{MO_x}}$, $E_{\mathrm{MO_x}}$, $E^{R}_{\mathrm{MO_x-Si}}$ and $E^{i.j}_{\mathrm{MO_x\text{-}Si}}$ were re-optimized simultaneously with the non-Arrhenian unary and binary parameters $T_{\mathrm{MO_x}}$, $n_{\mathrm{MO_x}}$, $m_{\mathrm{MO_x\text{-}Si}}$, $T_{\mathrm{MO_x\text{-}Si}}$ and $n_{\mathrm{MO_x\text{-}Si}}$. The model parameters $A^{i.j}_{\mathrm{MO_x\text{-}Si}}$, $A^{R}_{\mathrm{MO_x\text{-}Si}}$ and $A^{Ring}_{\mathrm{MO_x\text{-}Si}}$ were not required except for the value $A^{R}_{\mathrm{AlO_{1.5}\text{-}Si}}$ and were set equal to zero.

The unary and binary non-Arrhenian parameters T_{MO_x}, n_{MO_x}, $m_{MO_x\text{-}Si}$, $T_{MO_x\text{-}Si}$ and $n_{MO_x\text{-}Si}$ were optimized using all the selected binary and ternary subsystem data simultaneously. For the binary systems CaO-SiO_2, MgO-SiO_2 and PbO-SiO_2 we applied the unary and binary non-Arrhenian parameters simultaneously. On the other hand, no unary non-Arrhenian parameters were applied to the other systems such as ZnO-SiO_2, $NaO_{0.5}$-SiO_2, $KO_{0.5}$-SiO_2 and $AlO_{1.5}$-SiO_2 because only binary non-Arrhenian parameters were enough to reproduce the data for the binary and ternary subsystems containing these basic oxides.

The $NaO_{0.5}$-SiO_2 system is the best–investigated from the melt to glass regions. Figs 11.3 and 11.4 show available viscosity data as a function of $\log\eta$ vs composition and $\log\eta$ vs 10^4/T (Kelvin^{-1}), respectively. In the melt region, most viscosity data were measured using the rotating viscometer [23, 52, 134, 166, 167, 212, 246, 299, 312, 333, 349] and counter balanced sphere methods [88, 223, 267, 283, 294]. In the glass region, the data were measured with the uniaxial compression method [212, 294, 298], the beam bending method [52, 223, 267], the ball penetration method [208, 223], the parallel plate method [290], the micro-penetration method [134] and the fiber-elongation method [238]. Notably, in the different experimental methods, the viscosity data at lower temperatures show a consistent relationship with each other as a function of composition. In Chapter 4, we modified the model to take into account the sharp drop of viscosity in alkali-rich regions of binary silicates [127]. As shown in Fig. 11.3, a sharp decrease of the viscosity below a mole fraction of SiO_2 equal to 0.5 is also shown at lower temperatures. As can be seen in Figure 11.4, the data show obvious non-Arrhenian temperature dependence with decreasing temperature. Examination of the literature reveals that most viscosity data are reported in either the glass region (10^9 to 10^{13} poise) or the melt region (< 10^6 poise), and relatively little can be found for viscosities between these regions (10^6 to 10^9 poise). The paucity of the data within the softening region (10^6 to 10^9 poise) of viscosity versus temperature curve is primarily due to the strong tendency to crystallization within this viscosity range [284]. In the system $NaO_{0.5}$-SiO_2, the data in this middle viscosity range were measured by Ota et al. [223] and Ehrt et al. [51]. This system has good glass-forming ability [28] and thus, the glass can be formed easily by rapid cooling in this system. As mentioned in Section 11.2.2, the effects of the non-Arrhenian binary parameters $T_{NaO_{0.5}\text{-}Si}$ and $n_{NaO_{0.5}\text{-}Si}$ on the viscosity calculation are weaker at higher temperatures and stronger at lower temperatures at constant composition. Thus, the

calculation with the extended model with addition of the parameters $T_{NaO_{0.5}\text{-}Si}$ and $n_{NaO_{0.5}\text{-}Si}$ for the $NaO_{0.5}$-SiO_2 system was almost the same as the calculation with the previous model developed to reproduce the viscosity data measured in the melt region.

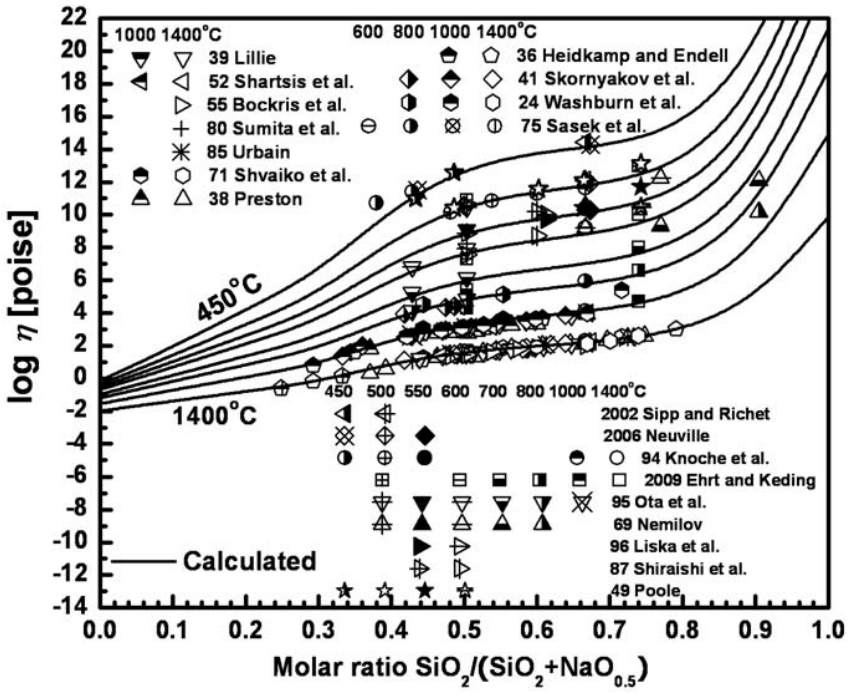

Fig. 11.3 Calculated viscosity in $NaO_{0.5}$-SiO_2 system compared to experimental data [23, 51, 88, 134, 166, 167, 208, 212, 223, 238, 246, 267, 283, 290, 294, 298, 299, 312, 333, 349] as a function of composition

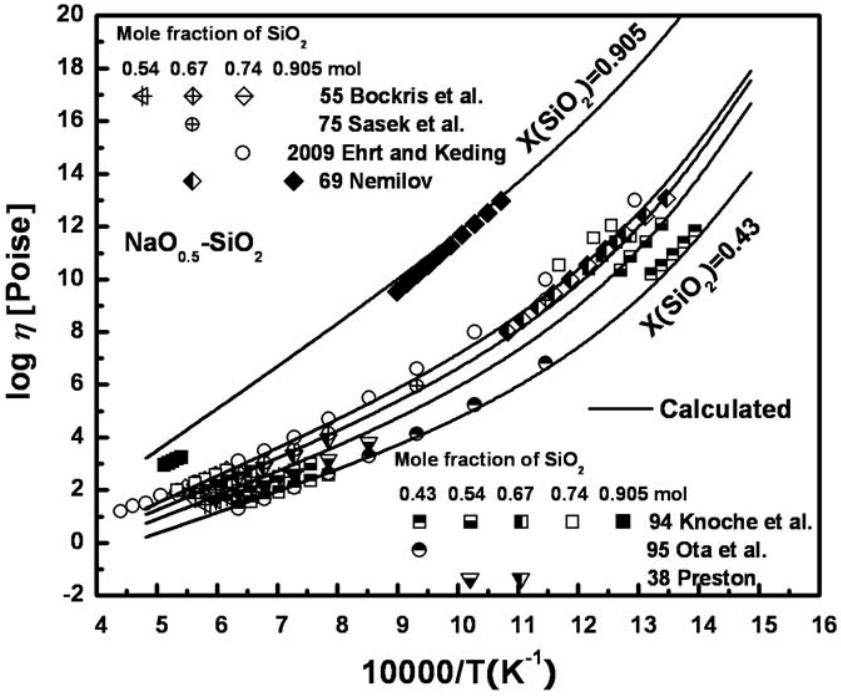

Fig. 11.4 Calculated viscosity in the $NaO_{0.5}$-SiO_2 system compared to experimental data [23, 51, 134, 208, 223, 246, 267] as a function of temperature

The $KO_{0.5}$-SiO_2 system is also one of the best–investigated systems from the melt to the glass region. Figs. 11.5 and 11.6 show available viscosity data plotted as a function of $\log\eta$ vs composition and $\log\eta$ vs 10^4/T (Kelvin^{-1}), respectively. As can be seen in Figs 11.5 and 11.6, the extended model describes very well most viscosity data of the $KO_{0.5}$–SiO_2 system. Two points by Bockris et al. [23] at 1600ºC show systematically lower viscosities than calculated. It should be noted that the viscosity of pure SiO_2 reported in the same paper of Bockris et al. [23] is substantially lower than that reported by other authors as shown in Fig. 3.6 [82]. The reason for this disagreement is not clear. One possible cause may be a reaction of the melt with the molybdenum crucible and cylinder at high temperature since Bockris et al. [23] reported that molybdenum reacted violently with silica at 1900°C. The viscosity data of Nemilov [208] and Poole [238] show a much sharper decreasing trend with increasing $KO_{0.5}$ contents and they show systematically lower viscosities than other data. The reason for this discrepancy may be that

intrinsic experimental difficulties are encountered in the measurements of the viscosity of glasses containing high alkali metal contents due to contamination of samples because of extremely high hygroscopicity. In addition, three points at $X(SiO_2) = 0.9$ by Nemilov [208] in the temperature range of 600 to 800ºC show systematically lower viscosities than calculated. Nemilov [208] did not measure viscosity of pure SiO_2 but the extrapolated value would be systematically lower at pure SiO_2. At lower temperatures, the presence of small amounts of impurities can lead to a large decrease in viscosity. In particular, the presence of water, introduced into the silica-rich region in varying small amounts depending on the method of synthesis, leads to large differences in the measured viscosity. This effect was systematically investigated by Hetherington et al. [92] who observed a decreasing effect with increasing water content in pure SiO_2.

The recent statistical model of Fluegel [67] which fits a very large amount of experimental information on glass melts, is summarized in the SciGlass database [37] and provides a rigorous estimation of errors and validity limits. The calculated lines by Fluegel [67] are shown in Fig. 11.5 for a comparison at 500, 600 and 1600ºC, and the calculations show systematically different trends of viscosity comparing most data at high silica content regions. Their results seem to be more in agreement with the data of Nemilov [208] and Poole [238] at low temperatures. Furthermore, the calculated line at 1600ºC is more consistent with the data of Bockris et al. [23] which show systematically lower viscosities. Thus, it can be concluded that the statistical model of Fluegel [67] gives systematically wrong results in the binary $KO_{0.5}$-SiO_2 system. One point measured at 400°C by Saringyulyan and Kostanyan [263] shows a very similar value to other data [208, 223] measured at 500°C. Their data show a good agreement at higher temperatures as shown in Fig. 11.5. This inconsistency of the data measured at such a low temperature, 400°C, occurred perhaps due to temperature differences between the sample and the furnace. In their study [263], the temperature measurement was indirectly carried out by measuring the atmospheric temperature in the furnace. At low temperatures, temperature equilibration between furnace and sample is much more difficult to attain due to poor heat conduction and high viscosity of the glass sample. As mentioned in Section 11.2.2, the effects of the non-Arrhenian binary parameters $T_{KO_{0.5}\text{-Si}}$ and $n_{KO_{0.5}\text{-Si}}$ on the viscosity calculations are weaker at higher temperatures and stronger at lower temperatures at constant composition. Thus, the calculation of the extended model with addition of the parameters $T_{KO_{0.5}\text{-Si}}$ and $n_{KO_{0.5}\text{-Si}}$ for the

$KO_{0.5}$-SiO_2 system was almost the same as the calculation of the previous model developed to reproduce the viscosity data measured in the melt region.

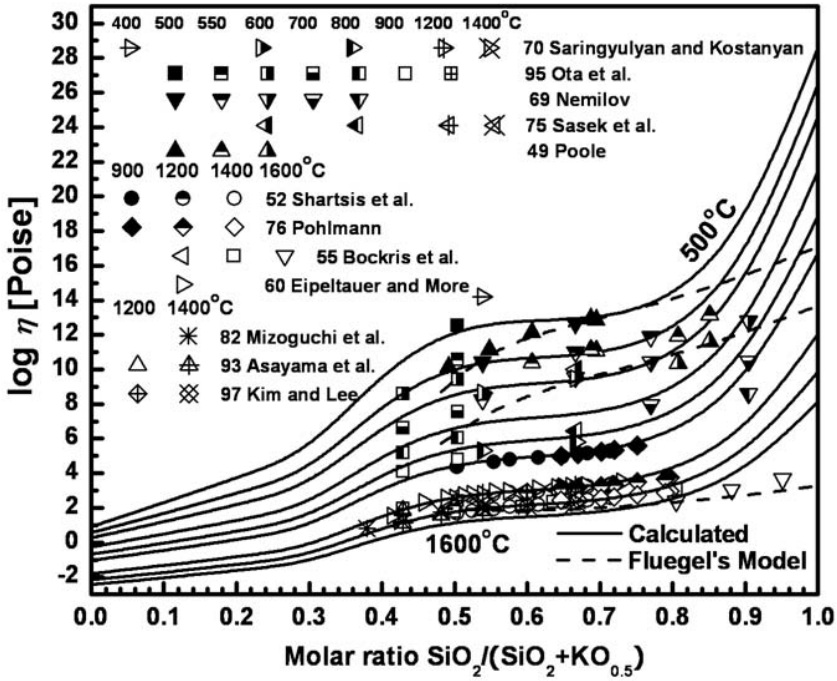

Fig. 11.5 Calculated viscosity in $KO_{0.5}$-SiO_2 system compared to experimental data [23, 208, 223, 237, 263, 267, 283] and the model by Fluegel [67] as a function of composition

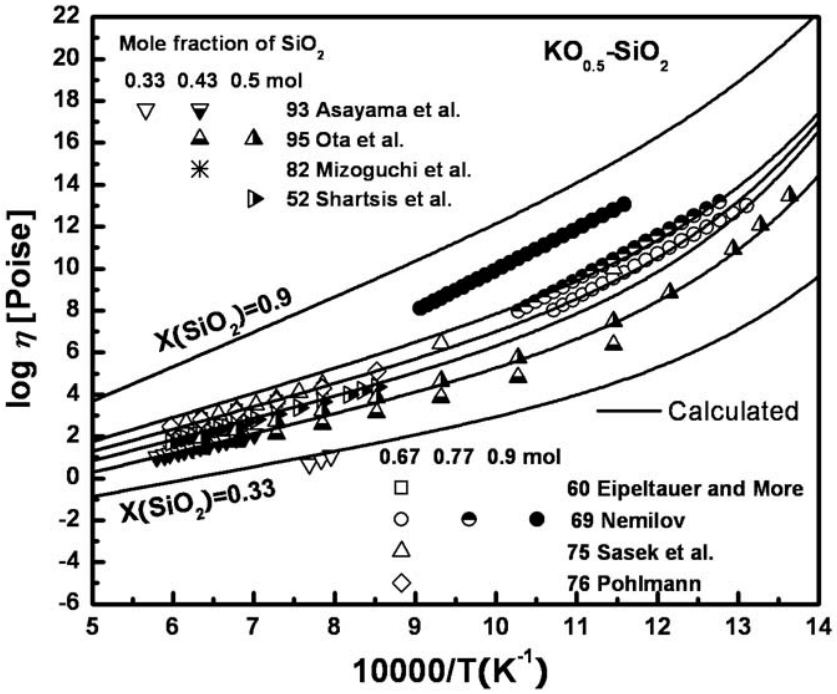

Fig. 11.6 Calculated viscosity in $KO_{0.5}$-SiO_2 system compared to experimental data[11, 193, 223, 283] as a function of temperature

The viscosity of the PbO-SiO_2 system is well investigated from the melt to glass region because of the low-melting temperature in a wide composition range. Fig. 11.7 shows available viscosity data plotted as a function of $\log\eta$ vs composition. High temperature viscosities were measured using the rotating viscometer [69, 85, 137, 207, 209, 302, 332] and the counter balanced sphere method [55, 63, 140, 263]. The viscosity measurements in the glass region were made by the penetration [207, 209, 263], the beam bending [80] and the fiber-elongation methods [63, 74, 137, 243]. As shown in Fig. 11.7-(a), most available data show good agreement with the calculated lines at all temperatures except for two points measured at 400^{o}C by Saringyulyan and Kostanyan [263]. Their measurements were carried out over a wide temperature range from 400 to 1200^{o}C at high silica contents $X(SiO_2)$ = 0.6 and 0.7. During the experiments, the temperature measurement was carried out indirectly by measuring the temperature of the furnace atmosphere. Again, there would be a large error in the temperature measurement due to the difficulty of

achieving temperature homogeneity between the sample and the furnace, due to poor heat conduction and the extremely high viscosity of the sample. As can be seen from Fig. 11.7-(b), the scatter of experimental data can be as high as 1.0 and 0.5 in the log scale for the glass and for the melt respectively, and the extended model describes the measurements within experimental error limits. As mentioned earlier, the model parameters A_{PbO}, E_{PbO}, $E^{R}_{\mathrm{PbO-Si}}$ and $E^{i.j}_{\mathrm{PbO\text{-}Si}}$ were re-optimized simultaneously with the non-Arrhenian unary and binary parameters T_{PbO}, n_{PbO}, $m_{\mathrm{PbO\text{-}Si}}$, $T_{\mathrm{PbO\text{-}Si}}$ and $n_{\mathrm{PbO\text{-}Si}}$. Fig. 11.7-(b) compares the calculations of the extended model using re-optimized parameters with that of the previous model using the previous parameters in Table 5.1 at 800 and 1200ºC. As shown in Fig. 11.7-(b), the reproducibility of the extended model is comparable with the previous model developed to reproduce viscosity data measured in the melt region.

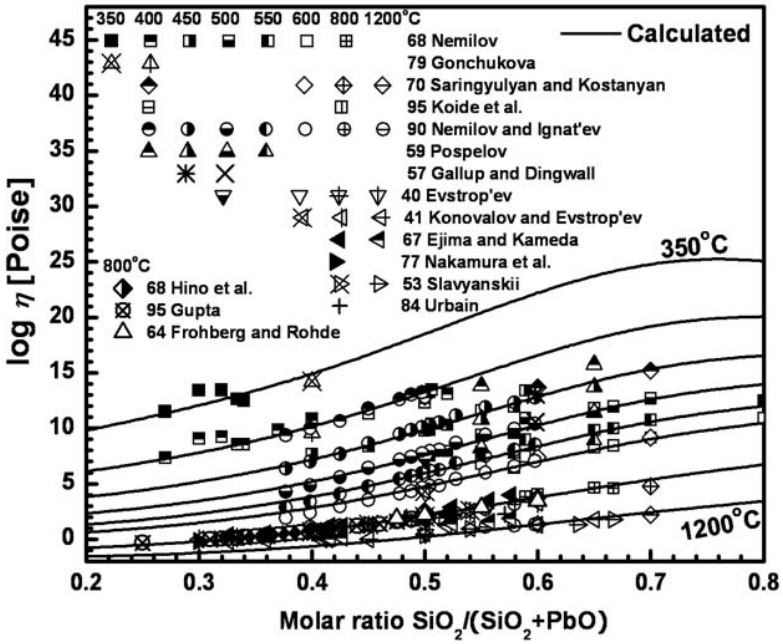

(a)

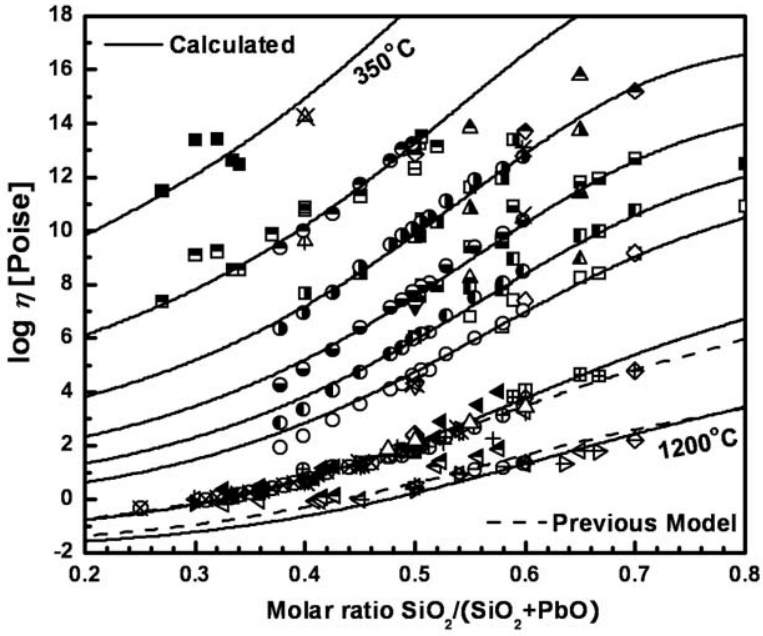

(b)

Fig. 11.7 (a) Calculated viscosity in $PbO\text{-}SiO_2$ system compared to experimental data [55, 63, 69, 74, 80, 85, 137, 140, 202, 207, 209, 243, 263, 302, 332] (b) Compares experimental data with the extended model and the previous model with an expanded scale

The viscosity of the $CaO\text{-}SiO_2$ system at low temperatures was studied by a research group [212, 213] using the uniaxial compression method. No viscosity measurements in the middle viscosity range from 10^3 to 10^8 poise were possible because of the very rapid rate of crystallization in this viscosity-temperature range [176, 184]. As shown in Fig. 11.8, the viscosity data measured at $X(SiO_2) = 0.5$ and 0.6 in the glass region show a decrease with increasing SiO_2 contents at constant temperature while the viscosity data increase in the melt region when SiO_2 is added at constant temperature. Thus, the viscosities of the $CaO\text{-}SiO_2$ system would have a cross-over point as a function of temperature as shown in Fig. 11.8. This trend of viscosities is also supported from ternary measurements of the $CaO\text{-}Na_2O\text{-}SiO_2$ and $MgO\text{-}Na_2O\text{-}SiO_2$ systems. Fig. 11.9 shows the calculated viscosities of the $CaO\text{-}SiO_2$ and $MgO\text{-}SiO_2$ systems at constant temperature obtained from the extrapolation of ternary measurements of the $CaO\text{-}Na_2O\text{-}SiO_2$ and $MgO\text{-}Na_2O\text{-}SiO_2$ systems as will be shown in Figs 11.10-11.25. No viscosity data for $MgO\text{-}SiO_2$

in the glass region are available, but the ternary measurements in MgO-Na_2O-SiO_2 strongly imply viscosity behavior having a cross-over point at a certain temperature as shown in Fig. 11.9. Without the unary and binary parameters T_{MO_x}, n_{MO_x} and $m_{MO_x\text{-}Si}$, the extended viscosity model was not able to reproduce properly the binary, ternary and high-order silicate systems containing CaO and MgO.

The physical reason for such behavior is unclear. As shown in Fig. 3.6, viscosity data of pure SiO_2 show Arrhenius temperature dependence. If these basic oxides such as CaO and MgO would have non-Arrhenian temperature dependences and this would create a cross-over point with changing temperature in the binary MO_x-SiO_2 systems (M = Ca and Mg). Thus, the non-Arrhenian unary and binary parameters T_{MO_x}, n_{MO_x}, $m_{MO_x\text{-}Si}$, $T_{MO_x\text{-}Si}$ and $n_{MO_x\text{-}Si}$ were applied to reproduce the cross-over point as a function of temperature in the binary MO_x-SiO_2 systems (M = Ca and Mg) and were optimized from the available experimental data for the CaO-SiO_2, MgO-SiO_2, CaO-Na_2O-SiO_2, MgO-Na_2O-SiO_2 and CaO-MgO-SiO_2 systems. The calculated lines in Fig. 11.8 show good agreement with all experimental data within the experimental error limits over all available temperature ranges.

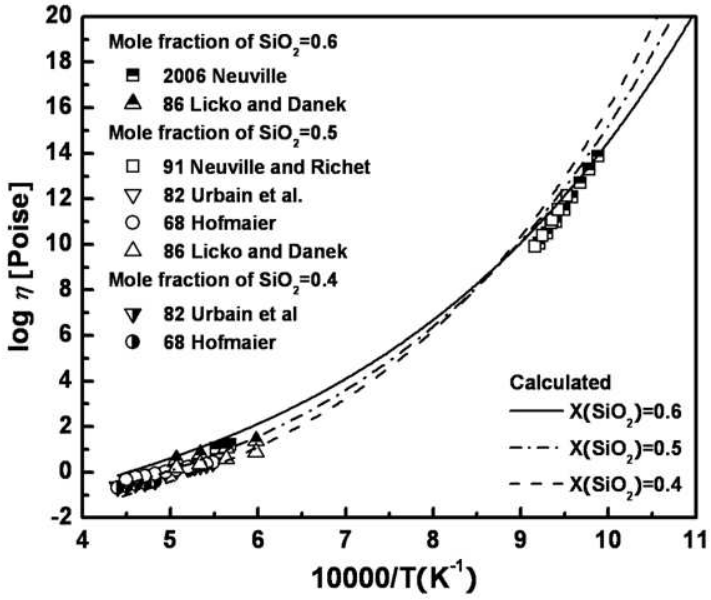

Fig. 11.8 Calculated viscosity in the CaO-SiO_2 system compared to experimental data [96, 164, 212, 213, 335]

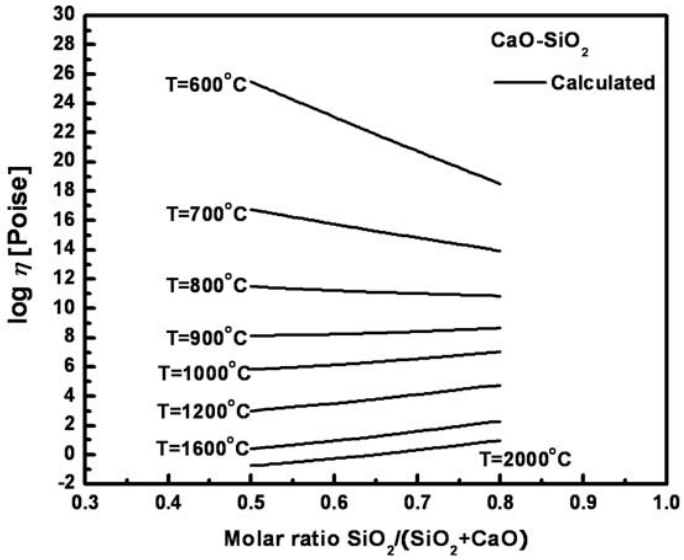

(a)

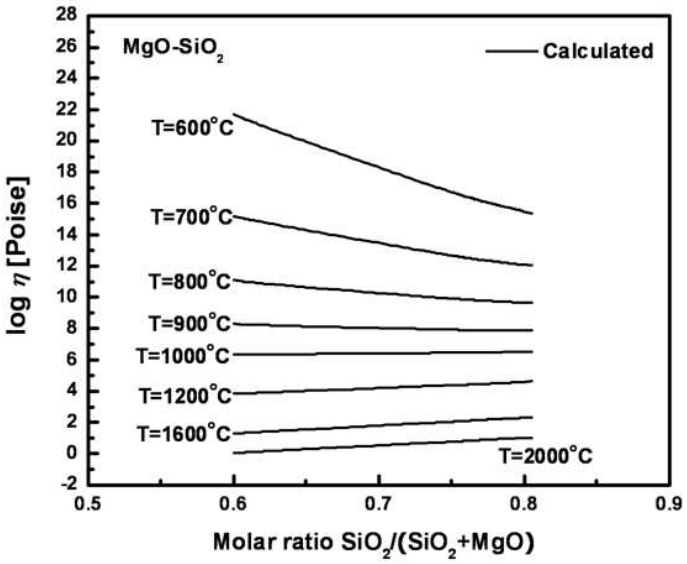

(b)

Fig. 11.9 Calculated viscosities in binary (a) $CaO\text{-}SiO_2$ and (b) $MgO\text{-}SiO_2$ systems at different temperatures

The viscosity of the binary MgO-SiO_2, ZnO-SiO_2 and $AlO_{1.5}$-SiO_2 systems are not available at lower temperatures because of the strong tendency to crystallization. The binary non-Arrhenian parameters, $T_{\text{ZnO-Si}}$ and $n_{\text{ZnO-Si}}$, were optimized using the experimental data of the ZnO-Na_2O-SiO_2 system. For the system $AlO_{1.5}$-SiO_2 the parameters, $T_{\text{AlO}_{1.5}\text{-Si}}$ and $n_{\text{AlO}_{1.5}\text{-Si}}$, were optimized using the available ternary measurements containing $AlO_{1.5}$ as shown in section 11.3.5.

11.3.4 Viscosity of the ternary systems without $AlO_{1.5}$

The viscosities of ternary systems without alumina are predicted by the extended model using the model parameters describing the viscosity of pure oxides and the binary parameters for MO_x–SiO_2 melts with unary and binary non-Arrhenian parameters in Tables 11.1 and 11.2. No additional ternary parameters are used. Hence, the agreement of experimental data and calculated lines in the figures from this section is not the result of fitting, but rather an indication how well the model can predict the viscosity of ternary systems.

The system of CaO–Na_2O–SiO_2 is one of best–investigated systems by many researchers from the glass to melt regions. This system is technologically important since it represents nearly 80% of commercial glasses and in particular, soda-lime-silica glasses are the basis of conventional window and container glasses, as well as bioactive glasses [212]. The predicted viscosities for the CaO–Na_2O–SiO_2 system are compared to the experimental data [30, 48, 68, 105, 165, 179, 212, 239, 262, 266, 294, 349] in Figs 11.11 to 11.16. The viscosity measurements were carried out using the rotating viscometer and counter-balanced method for the melt [68, 105, 165, 212, 262, 266, 294, 349] and using uniaxial compression [212, 294], penetration [48, 68, 105, 262], fiber-elongation [30, 165, 179, 239] and beam-bending methods [266] for the glasses. The experimental data at lower temperatures show a curvature as a function of composition at constant X(SiO_2) while an almost linear relation of viscosity is described at higher temperatures. There is no clear physical reason for this behavior. In the extended model, the curvature can be reproduced by the binary terms $X_{\text{MO}_x}^{m_{\text{MO}_x\text{-Si}}}$ and $\left(\frac{T_{\text{MO}_x\text{-Si}}}{T}\right)^{n_{\text{MO}_x\text{-Si}}} \cdot X_{\text{MO}_x} \cdot X_{\text{Si}}$ in Eq.(11.4). As the effect of these terms on the viscosity calculation becomes larger, the curvature of the calculated viscosity curves at constant SiO_2 contents becomes more significant. As can be seen from Figs.

11.11 to 11.16, the observed trend of the viscosity data at different temperatures is well predicted by the extended model using only unary and binary model parameters.

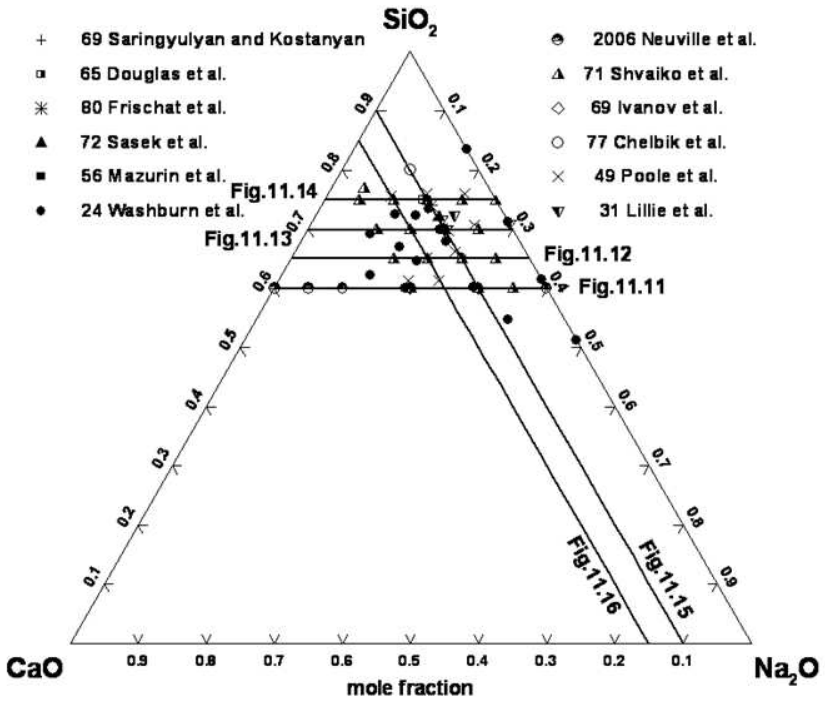

Fig. 11.10 Compositions in the $CaO–Na_2O–SiO_2$ system at which the viscosity was measured and experimental data [30, 48, 68, 105, 165, 179, 212, 239, 262, 266, 294, 349]

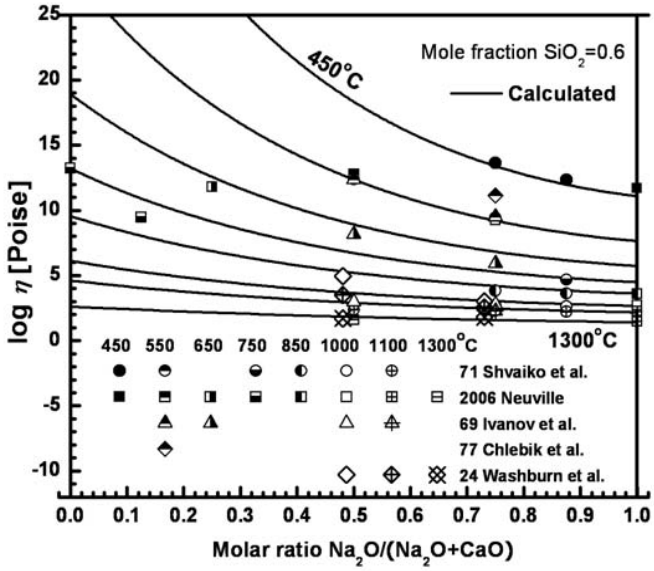

Fig. 11.11 Viscosity of $CaO–Na_2O–SiO_2$ melts at 60 mol% SiO_2: experimental points [30, 105, 212, 294, 349] and calculated lines

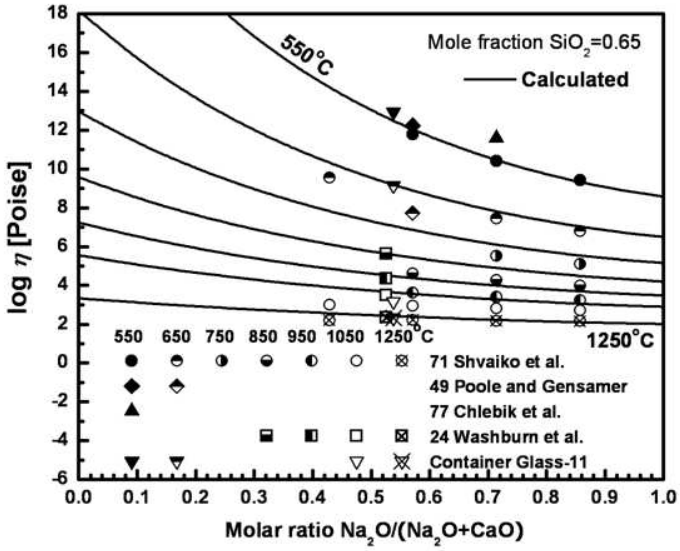

Fig. 11.12 Viscosity of $CaO–Na_2O–SiO_2$ melts at 65 mol% SiO_2: experimental points [30, 239, 279, 294, 349] and calculated lines

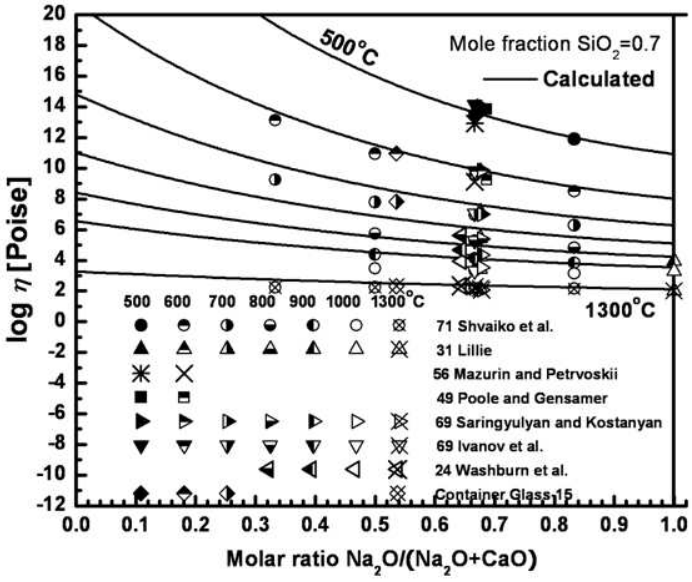

Fig. 11.13 Viscosity of $CaO–Na_2O–SiO_2$ melts at 70 mol% SiO_2: experimental points [105, 165, 179, 239, 262, 279, 294, 349] and calculated lines

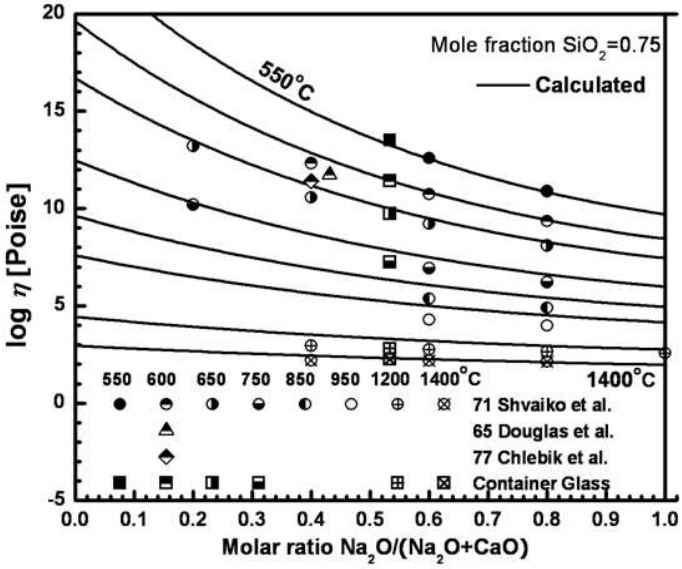

Fig. 11.14 Viscosity of $CaO–Na_2O–SiO_2$ melts at 75 mol% SiO_2: experimental points [30, 48, 279, 294] and calculated lines

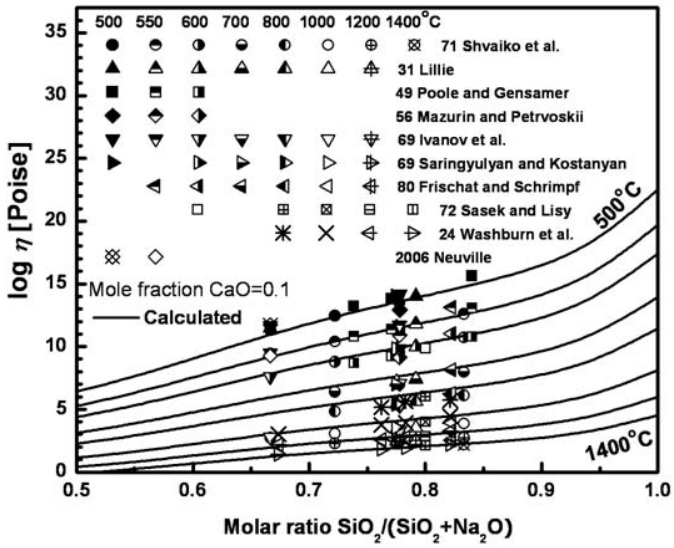

Fig. 11.15 Viscosity of $CaO–Na_2O–SiO_2$ melts at 10 mol% CaO: experimental points [68, 105, 165, 179, 212, 239, 262, 266, 294, 349] and calculated lines

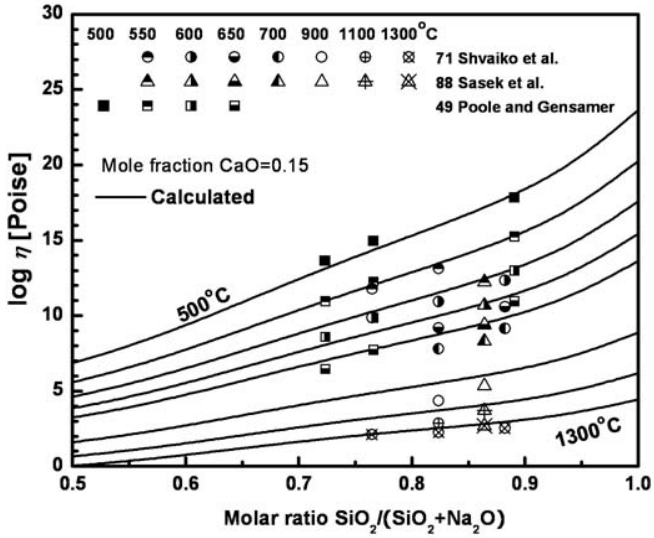

Fig. 11.16 Viscosity of $CaO–Na_2O–SiO_2$ melts at 15 mol% CaO: experimental points [239, 268, 294] and calculated lines

The $MgO–Na_2O–SiO_2$ system has been well-investigated by several researchers from the glass to melt regions. The predicted viscosities for the $MgO–Na_2O–SiO_2$ system are compared to the experimental data [59, 75, 95, 105, 119, 122, 179, 239, 242, 260] in Figs 11.18 to 11.25. The viscosity measurements were carried out using the rotating viscometer method for the melt [59, 75, 105, 119, 122] and the fiber-elongation method [59, 75, 95, 122, 179, 239, 242], the penetration [105] and the beam-bending methods [260] for the glasses. As can be seen from Figs. 11.18 to 11.25, the extended model reproduces most of the viscosity data very well as a function of composition and temperature within experimental error limits. As shown for the $CaO–Na_2O–SiO_2$ system, the viscosity data of $MgO–Na_2O–SiO_2$ system also show the curvature as a function of composition at constant SiO_2 contents while a linear relation of viscosity is described at higher temperatures. Again, the curvature can be reproduced by the binary terms $X_{\mathrm{MO}_x}^{m_{\mathrm{MO}_x\text{-Si}}}$ and $\left(\frac{T_{\mathrm{MO}_x\text{-Si}}}{T}\right)^{n_{\mathrm{MO}_x\text{-Si}}} \cdot X_{\mathrm{MO}_x} \cdot X_{\mathrm{Si}}$ in Eq.(11.4) and the observed trends of the viscosity data at different temperatures are well predicted by the extended model using only unary and binary model parameters.

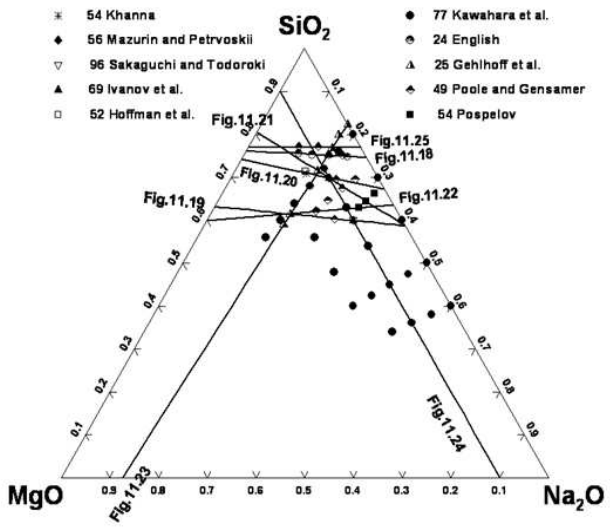

Fig. 11.17 Compositions in the $MgO–Na_2O–SiO_2$ system at which the viscosity was measured and experimental data [59, 75, 95, 105, 119, 122, 179, 239, 242, 260]

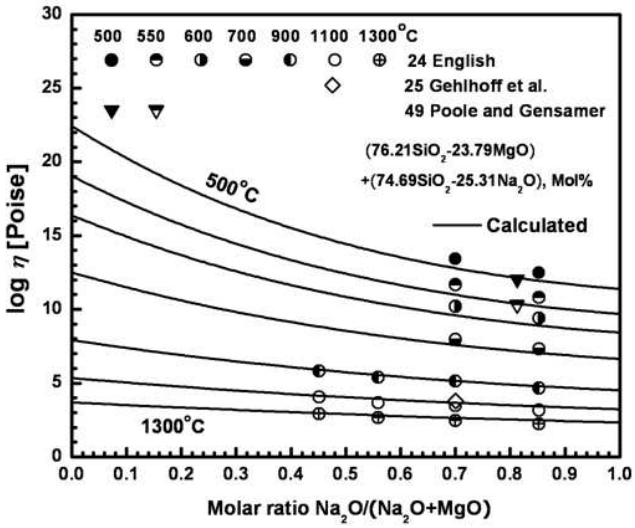

Fig. 11.18 Viscosity of $MgO–Na_2O–SiO_2$ melts for a pseudo-binary section between the compositions (74.69 mol% SiO_2, 25.31 mol% Na_2O) and (76.21 mol% SiO_2, 23.79 mol% MgO): experimental points [59, 75, 239] and calculated lines

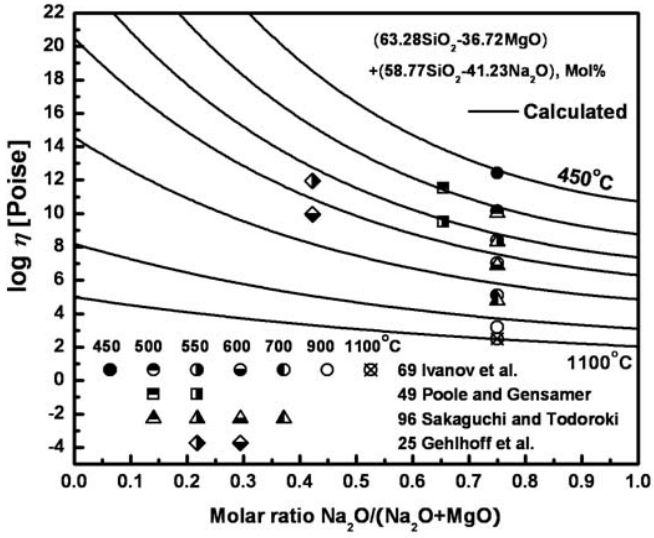

Fig. 11.19 Viscosity of $MgO–Na_2O–SiO_2$ melts for a pseudo-binary section between the compositions (63.28 mol% SiO_2, 36.72 mol% MgO) and (58.77 mol% SiO_2, 41.23 mol% Na_2O): experimental points [75, 105, 239, 260] and calculated lines

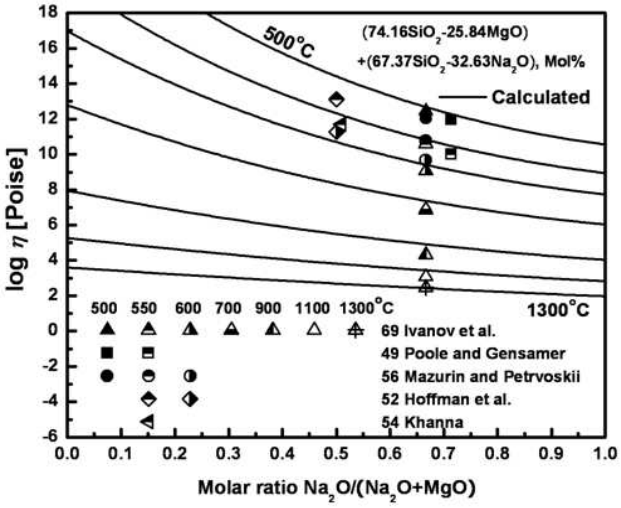

Fig. 11.20 Viscosity of $MgO–Na_2O–SiO_2$ melts for a pseudo-binary section between the compositions (74.16 mol% SiO_2, 25.84 mol% MgO) and (67.37 mol% SiO_2, 32.63 mol% Na_2O): experimental points [95, 105, 122, 179, 239]and calculated lines

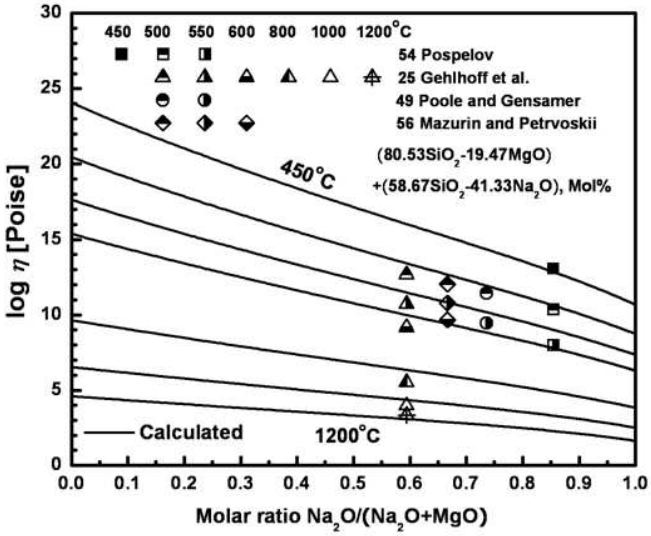

Fig. 11.21 Viscosity of $MgO–Na_2O–SiO_2$ melts for a pseudo-binary section between the compositions (80.53 mol% SiO_2, 19.47 mol% MgO) and (58.67 mol% SiO_2, 41.33 mol% Na_2O): experimental points [75, 179, 239, 242] and calculated lines

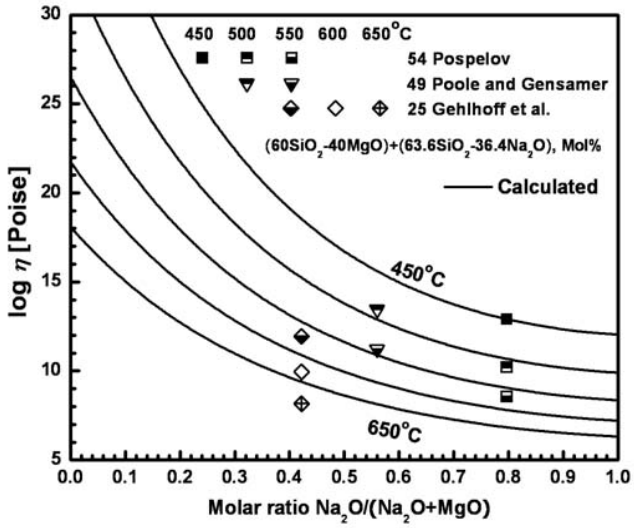

Fig. 11.22 Viscosity of $MgO–Na_2O–SiO_2$ melts for a pseudo-binary section between the compositions (60 mol% SiO_2, 40 mol% MgO) and (63.6 mol% SiO_2, 36.4 mol% Na_2O): experimental points [75, 239, 242] and calculated lines

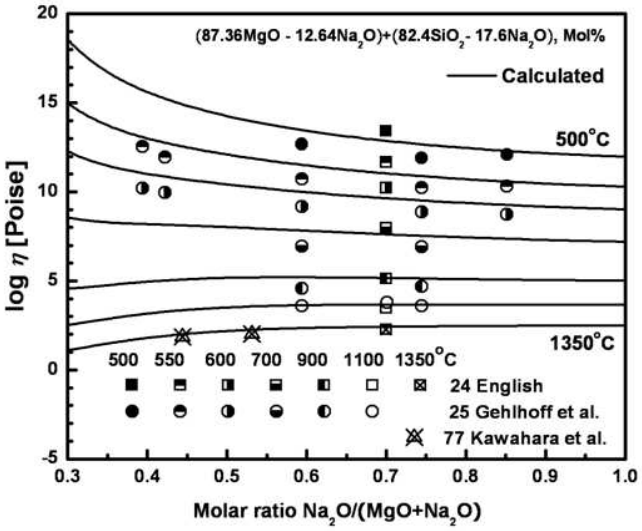

Fig. 11.23 Viscosity of $MgO–Na_2O–SiO_2$ melts for a pseudo-binary section between the compositions (87.36 mol% MgO, 12.64 mol% Na_2O) and (82.4 mol% SiO_2, 17.6 mol% Na_2O): experimental points [59, 75, 119] and calculated lines

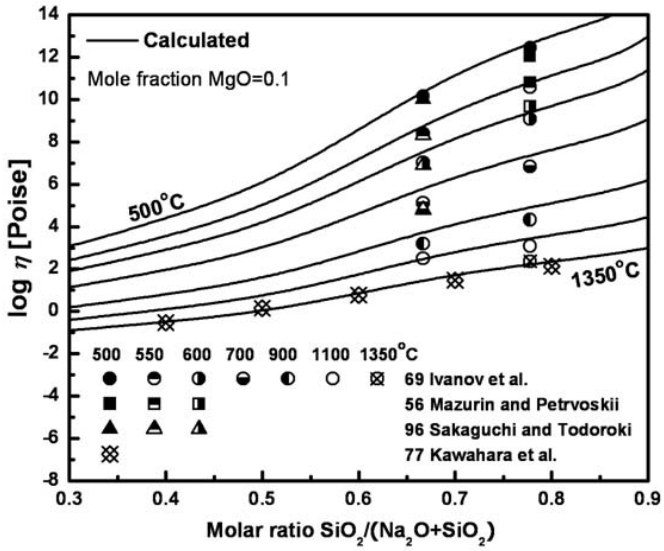

Fig. 11.24 Viscosity of $MgO–Na_2O–SiO_2$ melts at 10 mol% MgO: experimental points [105, 119, 179, 260] and calculated lines

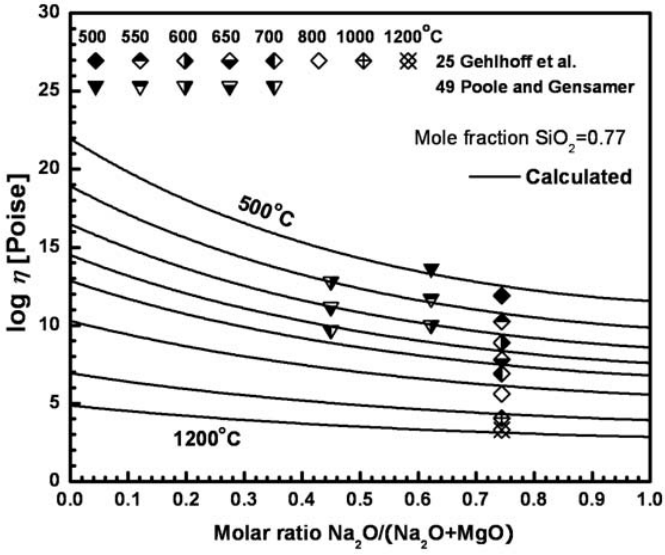

Fig. 11.25 Viscosity of $MgO–Na_2O–SiO_2$ melts at 77 mol% SiO_2: experimental points [75, 239] and calculated lines

The predicted viscosities for the CaO–MgO–SiO_2 system are compared to the experimental data [83, 164, 213, 297, 314, 318, 320] in Figs 11.26 to 11.27. The data of this system are limited because of the strong tendency to crystallization during the experiments [164, 314]. The viscosity measurements were carried out by several investigators using the rotating viscometer [144, 164, 314], the uniaxial compression [213, 297], micro-penetration [320] and fiber-elongation methods [318]. The extended model is in good agreement with most of the data except for the data at the diopside composition ($CaMgSi_2O_6$) in the temperature range from 740 to 780ºC as shown in Figs. 11.26 and 11.27. The temperature dependences of the extended model and the experimental data are not consistent. However, allowing for partial crystallization during the experiment, it may be concluded that the extended model can reproduce most experimental data within the experimental error limits at all temperatures. Neuville and Richet [213] measured the viscosities with the replacement of CaO by MgO at constant X(SiO_2) = 0.5 and observed minima in the viscosity at the diopside composition as shown in Fig. 11.26. The physical reason for such behavior is unclear. In the extended model, the curvature of the viscosity data can be reproduced by the terms of $X_{MO_x}^{m_{MO_x\text{-Si}}}$ and $\left(\frac{T_{MO_x\text{-Si}}}{T}\right)^{n_{MO_x\text{-Si}}} \cdot X_{MO_x} \cdot X_{Si}$ in Eq. (11.4). As the effect of these terms on the viscosity calculation becomes larger, the curvature at constant SiO_2 contents becomes more significant. As can be seen from Fig. 11.26, the observed trends of the viscosity data at different temperatures are well predicted by the extended model using only unary and binary model parameters.

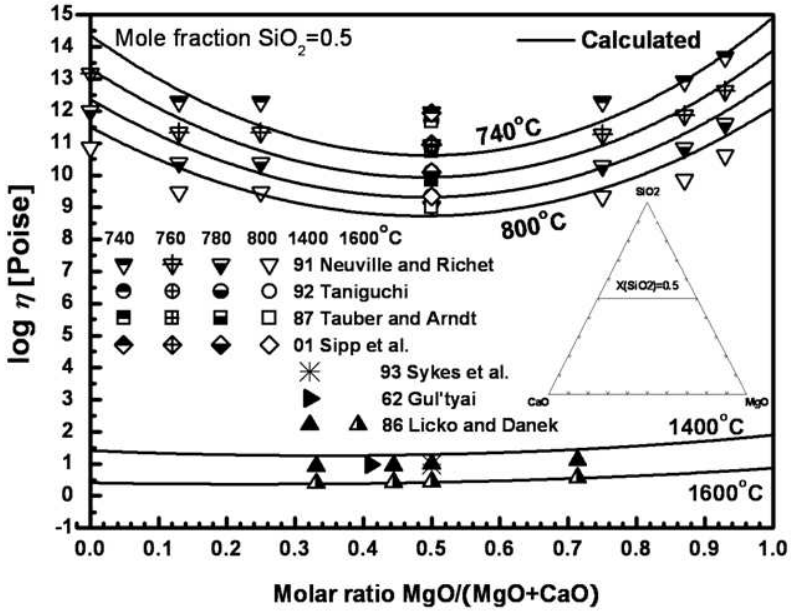

Fig. 11.26 Viscosity of CaO–MgO–SiO_2 melts at 50 mol% SiO_2: experimental points [83, 164, 213, 297, 314, 318, 320] and calculated lines

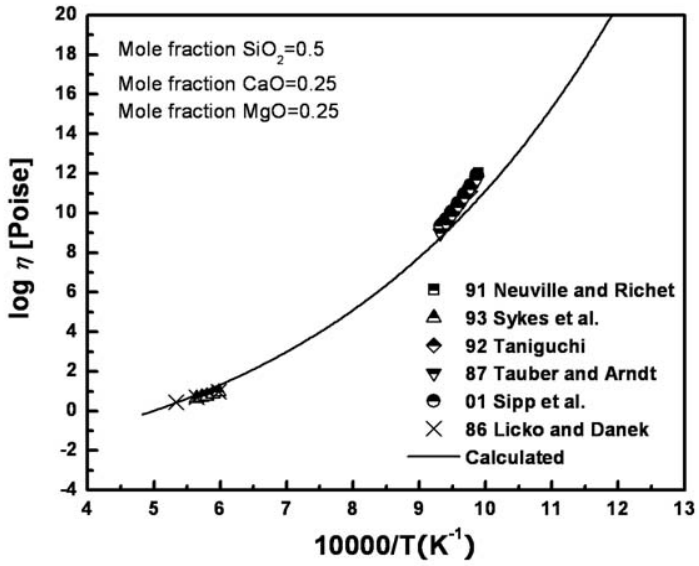

Fig. 11.27 Viscosity of diopside melts as a function of temperature: experimental points [164, 213, 297, 314, 318, 320] and calculated lines

The predicted viscosities for the $Na_2O–K_2O–SiO_2$ system are compared to the experimental data [208, 238] in Figs 11.28 to 11.30. Nemilov [208] and Poole [238] measured the viscosities using the penetration method and the fiber-elongation method in the glass region, respectively. The data of Nemilov [208] at $X(SiO_2)$ = 0.87 of the Na_2O-SiO_2 system are systematically higher than the other data as shown in Fig. 11.2 ($X(SiO_2)$ = 0.77 in $NaO_{0.5}$-SiO_2). On the other hand, the binary data at $X(SiO_2)$ = 0.95 of the K_2O-SiO_2 system show lower values due to the contamination of the sample by extremely high hygroscopicity as shown in Fig. 11.4 ($X(SiO_2)$ = 0.9 in $KO_{0.5}$-SiO_2). On the other hand, the data of Poole [238] in the Na_2O-SiO_2 system show good agreement with most data at all temperatures. However, the data for the K_2O-SiO_2 system at high alkali contents showed systematically lower trends as shown in Figs 11.5 and 11.30. The mixed alkali effect on viscosity of the $Na_2O–K_2O–SiO_2$ system has been discussed by several authors [67, 159, 208]. The mixed alkali effect on viscosity signifies that if a glass contains more than one alkali oxide, the viscosity of alkali–containing glasses at low temperatures is significantly lower than the viscosities of each binary alkali–containing glasses at low total alkali concentrations. With increasing temperature, this effect becomes weaker. However, controversy still exists about the mixed alkali effect. Leko [159] observed a deep minimum of the viscosity in the ternary mixed alkali glasses containing 5 mol% Na_2O+K_2O total while Nemilov [208] as shown in Figs. 11.28 and 11.29 did not observe the mixed alkali effect in the ternary Na_2O-K_2O-SiO_2 system. However, the data of Nemilov[208] have systematic errors in the binary K_2O-SiO_2 and Na_2O-SiO_2 systems, and thus it is difficult to conclude the existence of the mixed alkali effect. In addition, Fluegel [67] attempted to reproduce the mixed alkali effect with the data of Poole [238] as shown in Fig. 11.30. However, as shown in Fig.11.5, his model does not reproduce properly the system K_2O-SiO_2, and thus it appears that Fluegel's model [67] shows systematically wrong results in the ternary Na_2O-K_2O-SiO_2 system. Because of lack of reliable experimental data, more accurate viscosity measurements at low temperatures need to be carried out to take into account the mixed alkali effect in the ternary Na_2O-K_2O-SiO_2 system. On the other hand, as shown in Fig. 11.26, these viscosity minima at low temperatures are also observed in the system CaO-MgO-SiO_2. That is, the viscosity minima are not unique to mixed alkali systems. The extended model reproduces these viscosity minima through the binary terms

$X_{\mathrm{MO}_x}^{m_{\mathrm{MO}_x\text{-Si}}}$ and $\left(\frac{T_{\mathrm{MO}_x\text{-Si}}}{T}\right)^{n_{\mathrm{MO}_x\text{-Si}}} \cdot X_{\mathrm{MO}_x} \cdot X_{\mathrm{Si}}$ in Eq.(11.4). No ternary interaction terms need be invoked.

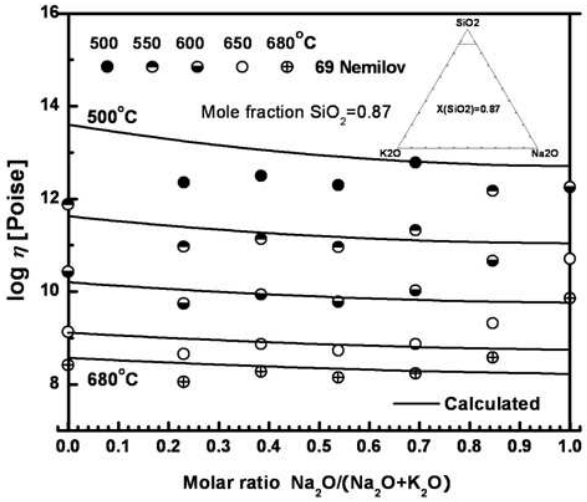

Fig. 11.28 Viscosity of Na_2O–K_2O–SiO_2 melts at 87 mol% SiO_2: experimental points [208] and calculated lines

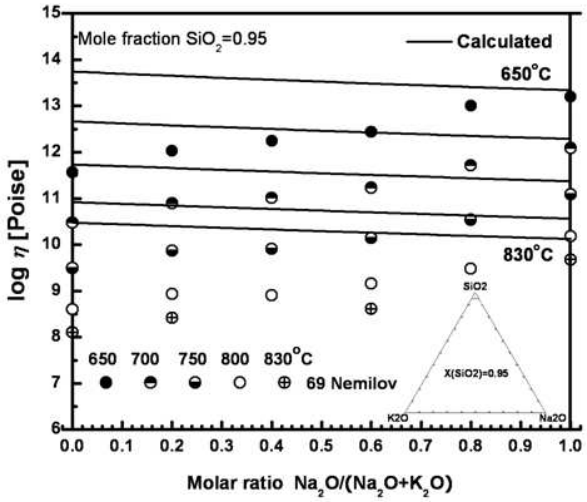

Fig. 11.29 Viscosity of Na_2O–K_2O–SiO_2 melts at 95 mol% SiO_2: experimental points [208] and calculated lines

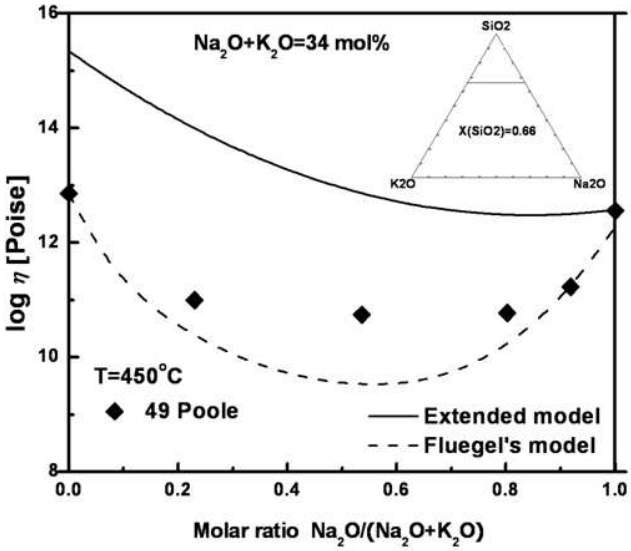

Fig. 11.30 Viscosity of $Na_2O–K_2O–SiO_2$ melts at 34 mol% Na_2O+K_2O total: experimental points [238] and calculated lines

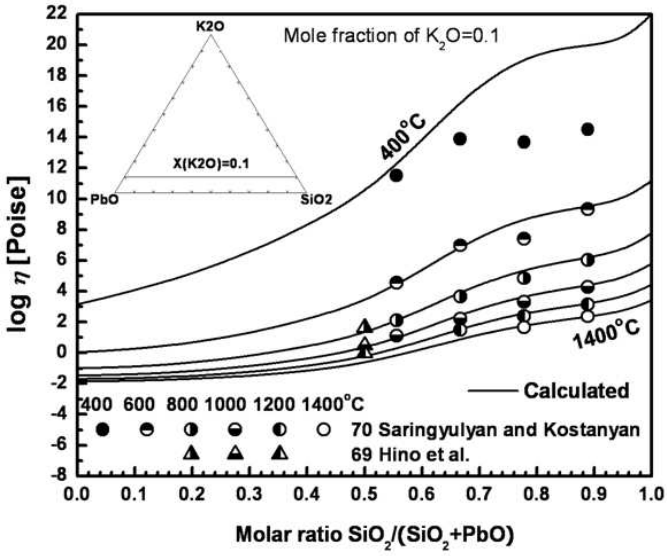

Fig. 11.31 Viscosity of $PbO–K_2O–SiO_2$ melts at 10 mol% K_2O: experimental points [94, 263] and calculated lines

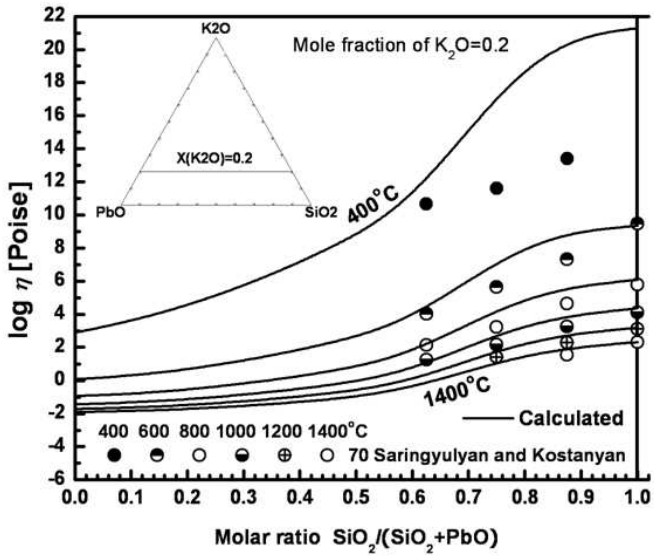

Fig. 11.32 Viscosity of PbO–K_2O–SiO_2 melts at 20 mol% K_2O: experimental points [263] and calculated lines

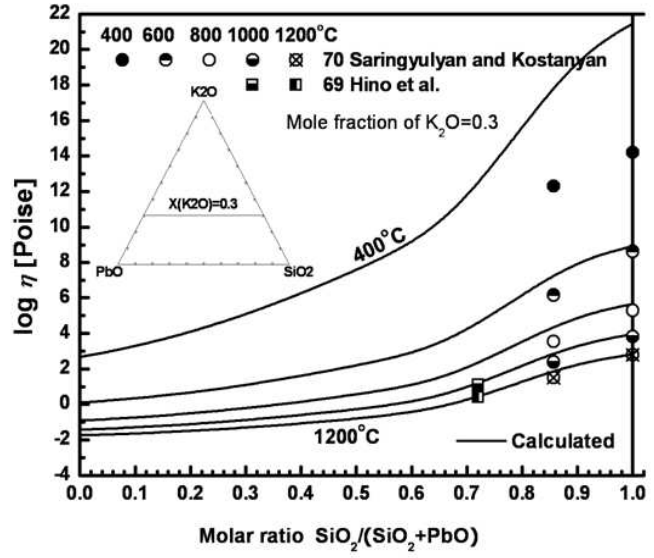

Fig. 11.33 Viscosity of PbO–K_2O–SiO_2 melts at 30 mol% K_2O: experimental points [94, 263] and calculated lines

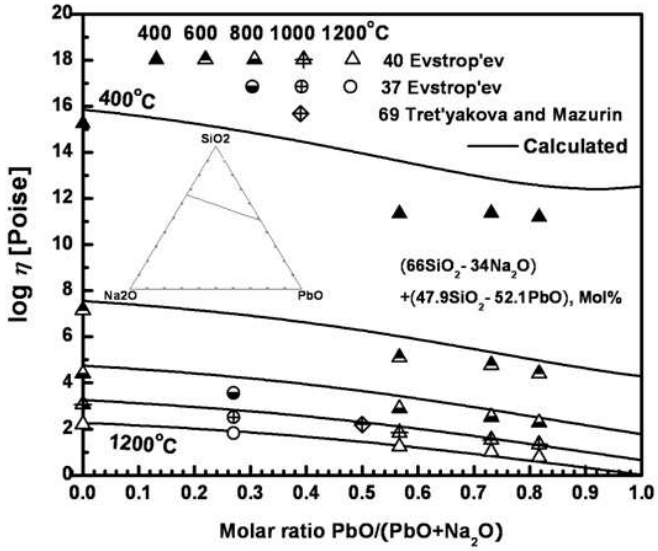

Fig. 11.34 Viscosity of $PbO–Na_2O–SiO_2$ melts for a pseudo-binary section between the compositions (66 mol% SiO_2, 34 mol% Na_2O) and (47.9 mol% SiO_2, 52.1 mol% PbO): experimental points [63, 62, 327] and calculated lines

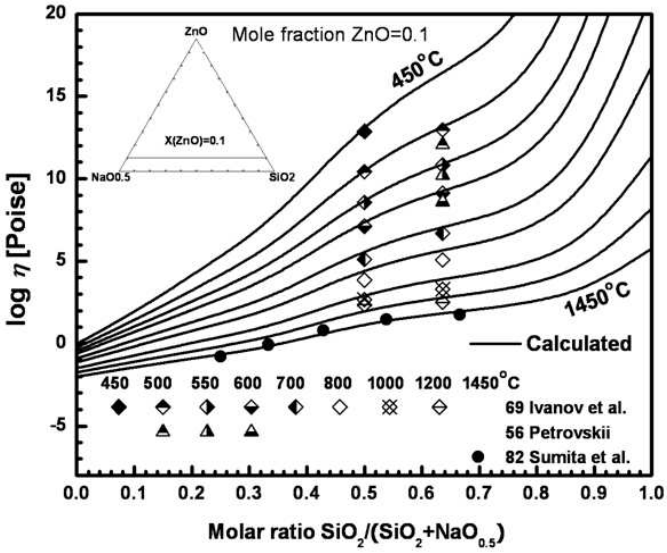

Fig. 11.35 Viscosity of $ZnO–Na_2O–SiO_2$ melts at 10 mol% ZnO: experimental points [105, 235, 313] and calculated lines

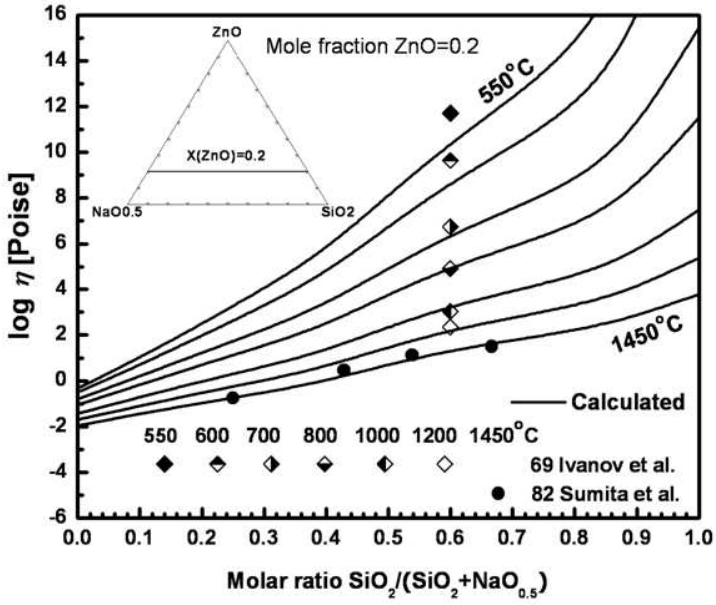

Fig. 11.36 Viscosity of $ZnO–Na_2O–SiO_2$ melts at 20 mol% ZnO: experimental points [105, 313] and calculated lines

The predicted viscosities for the $PbO–K_2O–SiO_2$ system are compared to the experimental data [94, 263] in Figs 11.31 to 11.33. As can be seen from these figures, the model shows excellent reproducibility for most data except for the data measured at 400°C. As shown in Fig. 11.4, the data measured at 400°C by Saringyulyan and Kostanyan [263] show values almost similar to the other data measured at 500°C. Again, this inconsistency of the data measured at such a low temperature, 400°C, could occur due to temperature inhomogeneity between the sample having extremely high viscosity and the furnace. It should be noted that the homogeneity of temperature between furnace and sample at low temperature is much more difficult to achieve due to the poor heat conduction and high viscosity of the glass sample.

The predicted viscosities for the $PbO–Na_2O–SiO_2$ system are compared to the experimental data [63, 62, 327] in Fig. 11.34. The viscosity data measured in the glass region are limited as shown in Fig. 11.34. Evstropiev [63] measured only the viscosity in the glass region using the fiber-elongation method. They also measured the binary Na_2O-SiO_2 system and it shows data slightly lower than those of the other work. Considering the experimental difficulties

and the experimental error limits in viscosity measurement, it is concluded that the model reproduces fairly well the viscosity data as shown in Fig. 11.34.

The predicted viscosities for the $ZnO–Na_2O–SiO_2$ system are compared to the experimental data [105, 235, 313] in Figs. 11.35 and 11.36. The viscosities of the melt were measured by a rotational viscometer [105, 313] and the viscosities of the glasses were measured by the penetration method [105, 235]. As can be seen from Figs. 11.35 and 11.36, the model shows excellent reproducibility for most of the data at all temperatures. The agreement is well within experimental error limits.

11.3.5 Viscosity of the ternary systems with $AlO_{1.5}$

As discussed earlier in Chapter 3, Al cations can assume tetrahedral coordination and replace Si in the network when the missing charge is compensated by a basic cation M. This results in a maximum in the viscosity when the molar ratio of Al_2O_3 to MO or M_2O is unity. We applied two model parameters without temperature dependence to describe the viscosity maximum in the melt region [81]. In the present study, this effect is also extended as described in Eq.(11.10) by adding temperature dependence with only two more parameters for each ternary system $MO_x–Al_2O_3–SiO_2$ which describe the Gibbs energy of reaction (3.40) or (3.41) as a function of composition. Optimized model parameters for the systems $MO_x–Al_2O_3–SiO_2$ (M = Ca, Mg, Na, K, Zn and Pb) are summarized in Table 11.3.

The predicted viscosities for the $Na_2O–Al_2O_3–SiO_2$ system are compared to the experimental data [98, 125, 214, 252, 269, 297, 307, 321, 324, 335] in Figs. 11.37 to 11.41. Because of the strong tendency of crystallization within the viscosity range from 10^6 to 10^9 poise, viscosity data measured within this range is rare [284]. Except for the data of Neuville and Richet [214], which show a different temperature dependence compared with other data at the same composition (Figs 11.38 and 11.41) as shown in Eq.(11.5), this extension resulted in a good description of the experimental data for the $Na_2O–Al_2O_3–SiO_2$ system as shown in Figs. 11.38 to 11.42. Not only the magnitude, but also the shape of the viscosity maxima are well reproduced. Figs. 11.38-11.40 compare the calculations of the extended model using the re-optimized parameters from Tables 11.1 and 11.2 with those of the previous model using the previous parameters in Table 4.1 at 1200, 1400 and 1600ºC. As shown in Figs. 11.38-11.40, the reproducibility of the extended model is comparable to that of the previous model which was

developed to reproduce viscosity data measured only in the melt region. Thus, the extended model is believed to reproduce the viscosity data of the Na_2O–Al_2O_3–SiO_2 system measured over the wide composition and temperature ranges within experimental error limits.

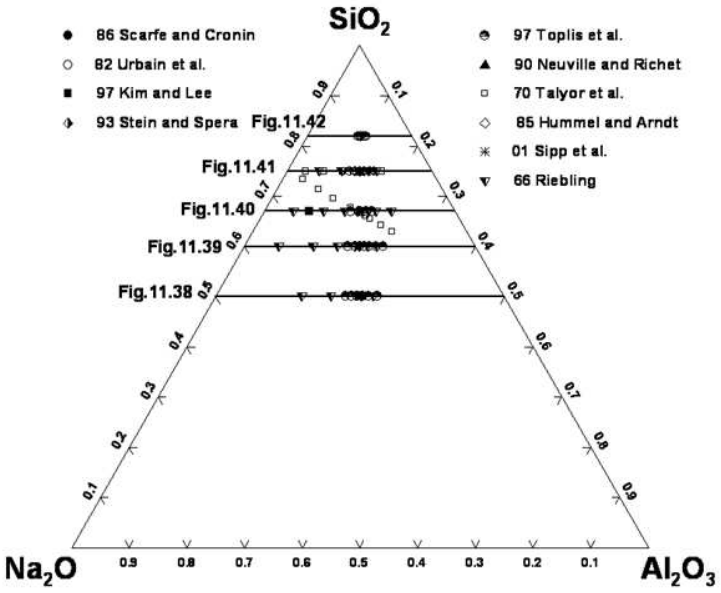

Fig. 11.37 Compositions in the Na_2O–Al_2O_3–SiO_2 system at which the viscosity was measured and experimental data [98, 125, 214, 252, 269, 297, 307, 321, 324, 335]

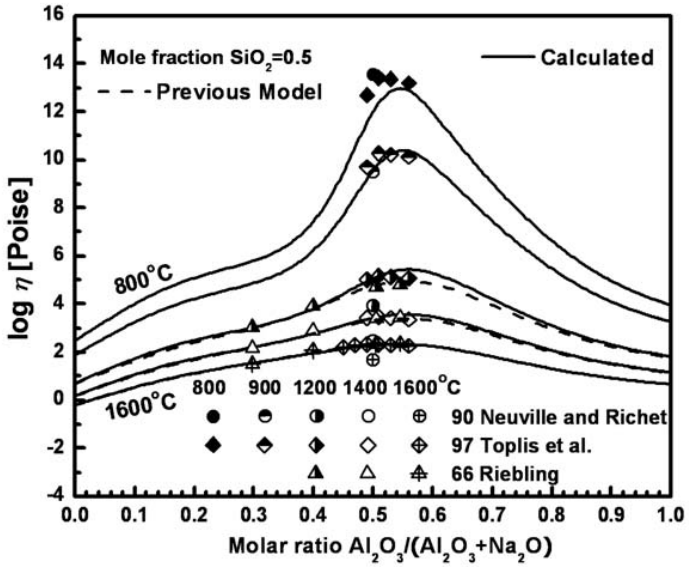

Fig. 11.38 Viscosity of Na_2O–Al_2O_3–SiO_2 melts at 50 mol% SiO_2: experimental points [214, 252, 324] and calculated lines by the extended model and previous model

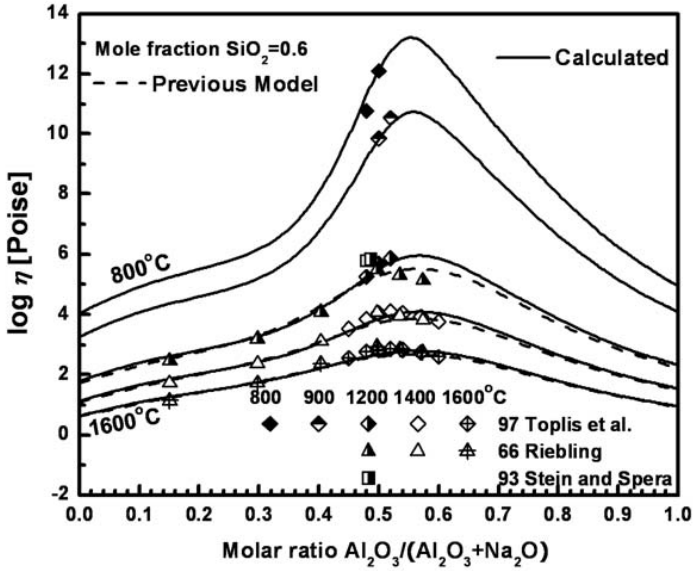

Fig. 11.39 Viscosity of Na_2O–Al_2O_3–SiO_2 melts at 60 mol% SiO_2: experimental points [252, 307, 324] and calculated lines by the extended model and previous model

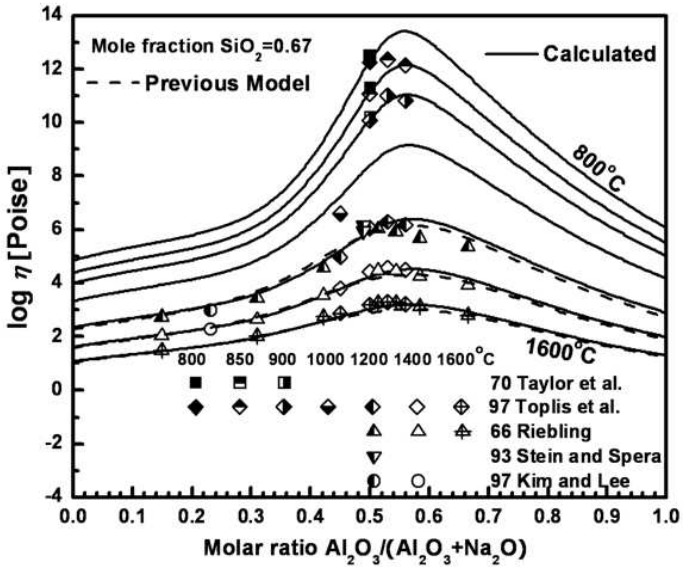

Fig. 11.40 Viscosity of Na_2O–Al_2O_3–SiO_2 melts at 67 mol% SiO_2: experimental points [125, 252, 307, 321, 324] and calculated lines by the extended model and previous model

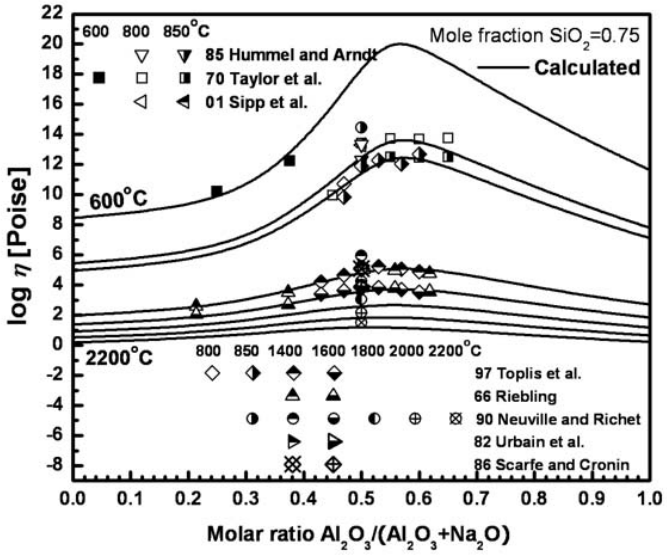

Fig. 11.41 Viscosity of Na_2O–Al_2O_3–SiO_2 melts at 75 mol% SiO_2: experimental points [98, 214, 252, 269, 297, 321, 324, 335] and calculated lines

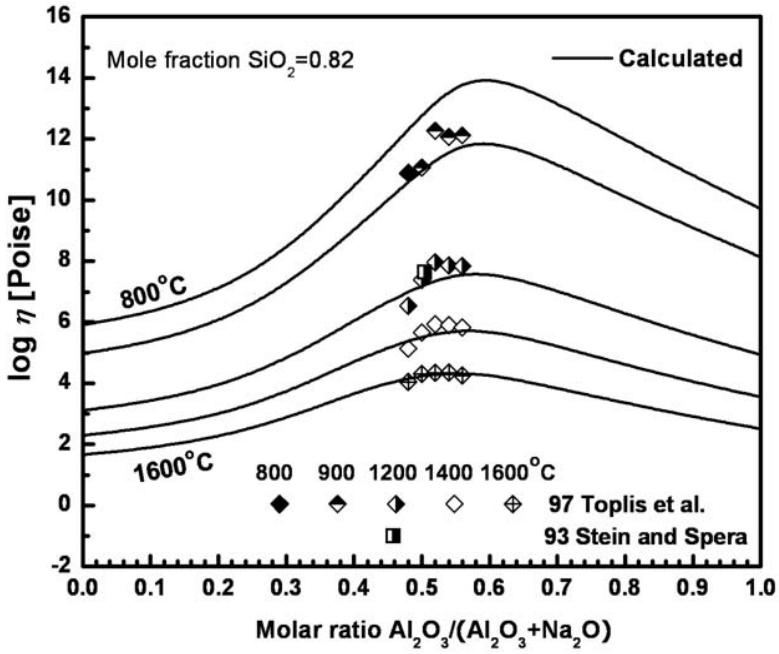

Fig. 11.42 Viscosity of Na_2O–Al_2O_3–SiO_2 melts at 82 mol% SiO_2: experimental points [307, 324] and calculated lines

The predicted viscosities for the CaO–Al_2O_3–SiO_2 system are compared to the experimental data [58, 83, 98, 109, 145, 172, 256, 270, 297, 303, 318, 320, 323, 330, 335] in Figs. 11.44 to 11.47. Again, because of the strong tendency to crystallization within the viscosity range from 10^6 to 10^9 poise, viscosity measurements in this region are very rare [284]. As shown in Figs. 11.44 to 11.47, the model describes well most available data at all temperatures within experimental error limits, except for the one data of Sipp et al. [297]in Fig. 11.47 measured at $X(SiO_2)$ = 0.12 at 800°C. The data of Sipp et al. [297] show a slight increase in viscosity with decreasing SiO_2 at 800°C and this could be caused by a strong tendency to crystallization due to high contents of CaO and Al_2O_3 as pointed out by Shelby [285].

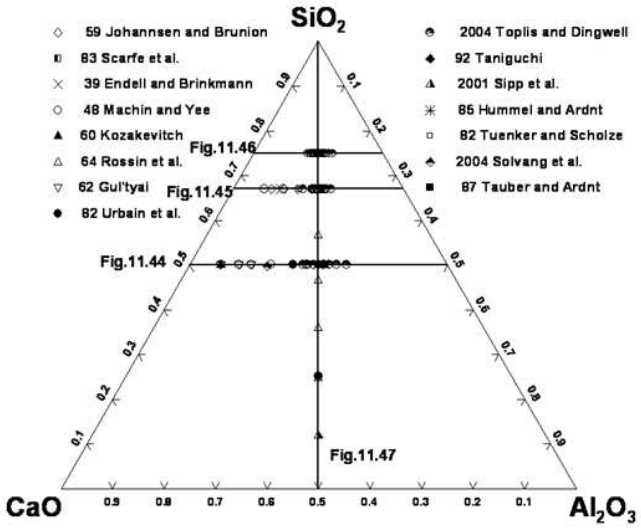

Fig. 11.43 Compositions in the $CaO–Al_2O_3–SiO_2$ system at which the viscosity was measured and experimental data [58, 83, 98, 109, 145, 172, 256, 270, 297, 303, 318, 320, 323, 330, 335]

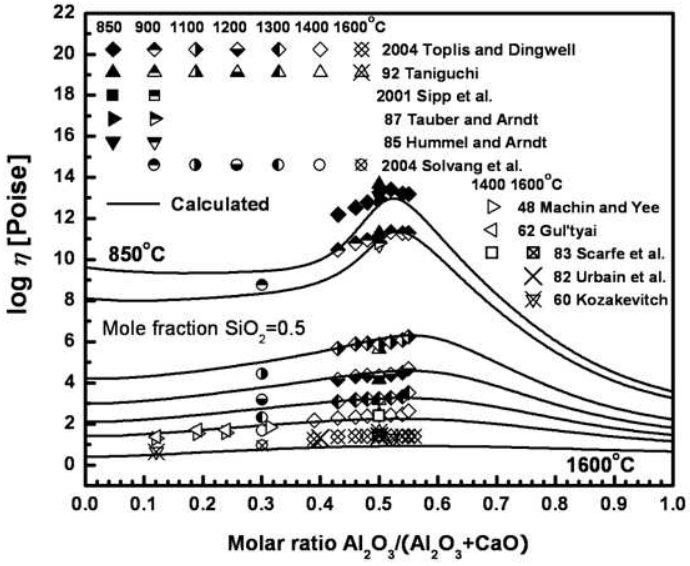

Fig. 11.44 Viscosity of $CaO–Al_2O_3–SiO_2$ melts at 50 mol% SiO_2: experimental points [83, 98, 145, 172, 270, 297, 303, 318, 320, 323, 335] and calculated lines

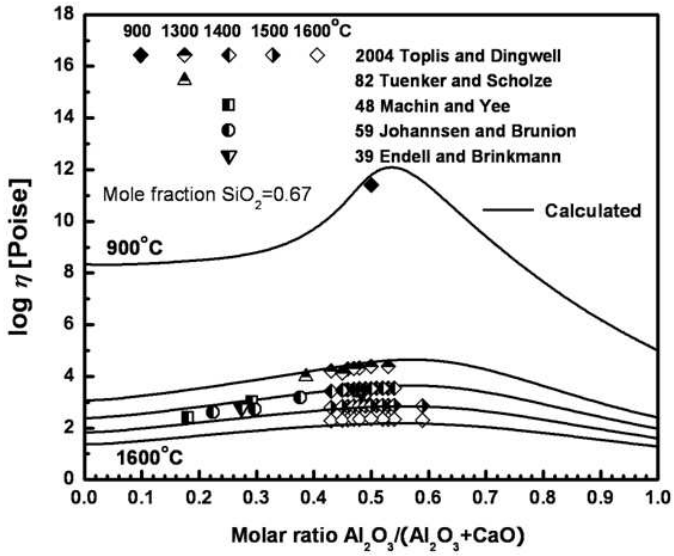

Fig. 11.45 Viscosity of $CaO–Al_2O_3–SiO_2$ melts at 67 mol% SiO_2: experimental points [58, 109, 172, 323, 330] and calculated lines

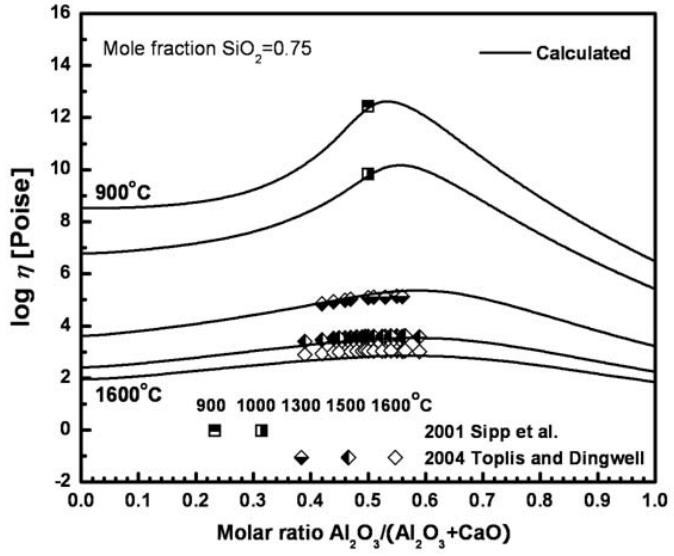

Fig. 11.46 Viscosity of $CaO–Al_2O_3–SiO_2$ melts at 75 mol% SiO_2: experimental points [297, 323] and calculated lines

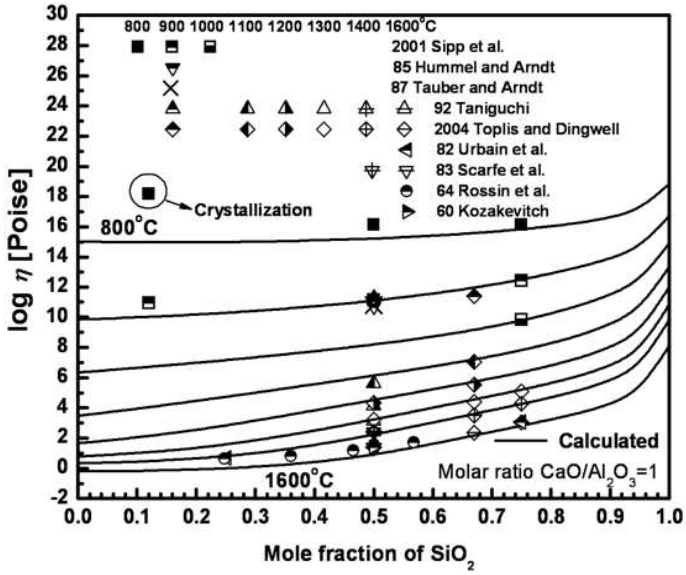

Fig. 11.47 Viscosity of $CaO–Al_2O_3–SiO_2$ melts at constant molar ratios of CaO/Al_2O_3 = 1: experimental points [98, 145, 256, 270, 297, 318, 320, 323, 335] and calculated lines

The only available viscosity data in the glass region for the system $MgO–Al_2O_3–SiO_2$ were measured at $X(SiO_2)$ = 0.5 by several researchers [168, 251, 318, 323, 335, 363]. As can be seen in Fig. 11.48, all experimental data show an excellent agreement with the calculated lines at all temperatures.

No viscosity data for the $K_2O–Al_2O_3–SiO_2$ system at low temperatures are available. The temperature dependence was applied to reproduce the available viscosity data measured in the melt region [126, 193, 200, 335] for the $K_2O–Al_2O_3–SiO_2$ system.

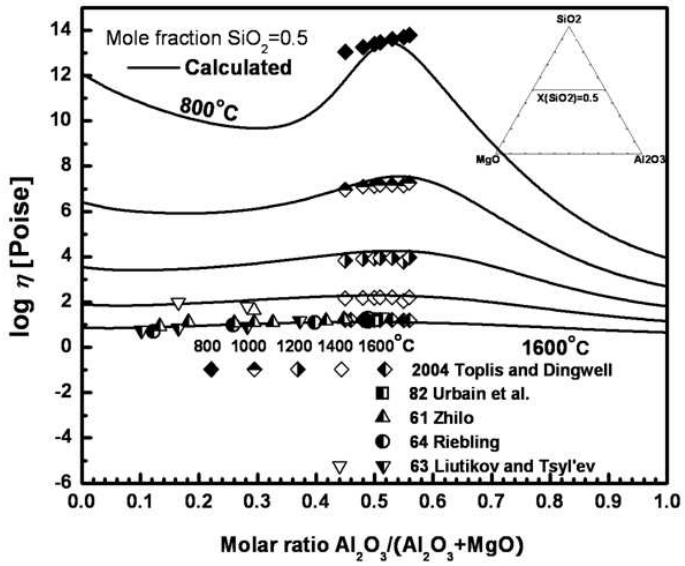

Fig. 11.48 Viscosity of $MgO–Al_2O_3–SiO_2$ melts at 50 mol% SiO_2: experimental points [168, 251, 323, 335, 363] and calculated lines

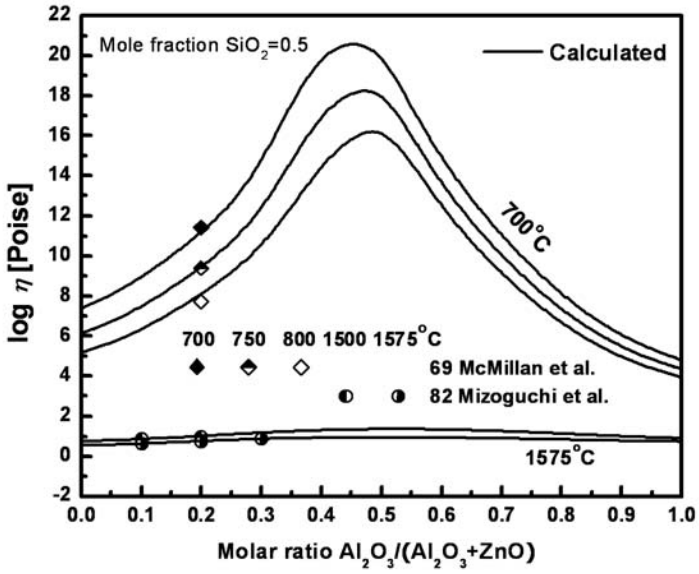

Fig. 11.49 Viscosity of $ZnO–Al_2O_3–SiO_2$ melts at 50 mol% SiO_2: experimental points [183, 193] and calculated lines

The predicted viscosities for the $ZnO–Al_2O_3–SiO_2$ system are compared to the experimental data [183, 193] in Fig. 11.49. McMillan et al. [183] measured only high viscosities in the temperature range of 700 to 800°C using the fiber-elongation method. Mizoguchi et al.[193] measured the viscosities in the melt using a rotational [193] viscometer. As can be seen from Fig. 11.49, the model shows a good agreement with all data points at all temperatures.

There were no available data measured in the glass region for the system $PbO–Al_2O_3–SiO_2$ and thus, the optimized parameters were taken from Table 5.1.

11.3.6 Magmas, Lavas and Multi-component Glasses

The $Al_2O_3–CaO–MgO–Na_2O–K_2O–SiO_2$ system contains sub-systems of importance for petrology. In particular, a knowledge of the viscosity of silicates formed by albite–orthoclase–anorthite feldspars, diopside and nepheline is important for the understanding of the generation, transport and emplacement of igneous rocks. The viscosity of these silicates from the glass to the melt regions was studied by Tauber and Arndt [320], Taniguchi [318], Hummel and Arndt [98], Cranmer and Uhlmann [36], Scarfe et al. [270], N'Dala et al. [200] and Sykes et al. [314].

The viscosities along the diopside–anorthite, nepheline–diopside and anorthite–albite sections predicted by the model are compared with the experimental data in Figs. 11.50 to 11.52. The calculated lines in Fig. 11.50 are in good agreement with the experimental points in the temperature range from 850 to 1600ºC except for the data measured at 750 and 800ºC. It appears that the extrapolation of the data measured in the anorthite section would be much higher than the predicted. At those temperatures, no viscosity data are available at the composition of anorthite because of the strong tendency to crystallization. Again, Shelby [285] observed in the system $CaO-Al_2O_3-SiO_2$ that the glass transition temperature (T_g) increases with increasing molar ratio of Al_2O_3/CaO at constant SiO_2. Shelby [285] presented the glass transition temperature at the composition of anorthite around 800ºC. Below T_g, the glass (supercooled liquid) behaves as a solid which would cause an abrupt increase of the viscosity. This implies that the data measured below 800ºC at the anorthite-rich side in Fig. 11.50 would have large systematic errors because of partial crystallization of the sample. In Fig. 11.51, the data of Sykes et al. [314] are slightly lower than the calculated lines in the temperature range of 1300 to 1500ºC. On the other hand, the viscosity measured in the temperature range from 680 to 720°C shows good agreement with the predicted viscosities within the experimental error limits except for one datum measured at the

nepheline($NaAlSiO_4$)-rich side. The extrapolated viscosity of the data of Sykes et al. [314] to pure nepheline ($NaAlSiO_4$) would show a systematically lower values than the other data measured at the composition of nepheline as shown in Fig. 11.38. As shown in Fig. 11.52, the calculated lines show good agreement with the data measured in the temperature range from 1300 to 1600ºC. On the other hand, the data are reproduced less satisfactorily by the calculated lines in the temperature range from 800 to 950ºC. The data measured by Hummel and Arndt [98] and Cranmer and Uhlmann [36] show U-shaped trends of viscosities in the temperature range from 800 to 950ºC. The extended model predicts the viscosity of anorthite–albite by linearly extrapolating ΔG_{NaAlO_2} and $\Delta G_{CaAl_2O_4}$ and the extended model shows excellent agreement with all available data for the ternary Na_2O-Al_2O_3-SiO_2 and CaO-Al_2O_3-SiO_2 systems as shown in Figs.11.37-11.48. There is no obvious physical reason for such behavior. However, considering the experimental difficulties of viscosity measurement at low temperatures, it appears that the predicted viscosities are in a good agreement within the experimental error limits. Figs. 11.50-11.52 also compare the calculation of the extended model using re-optimized parameters with that of the previous model using the model parameters of Table 4.1 in the temperature range from 1200 to 1600ºC. The lines calculated by the extended model at 1200ºC of Fig. 11.50 and 1300ºC of Fig. 11.51 are somewhat higher than those of the previous model, although the differences are fairly small. The experimental data measured at 1200ºC are plotted in Fig. 11.50 and the difference is believed to be within experimental error limits. As can be seen from Figs 11.50-11.52, the reproducibility of the extended model is comparable with the previous model developed to reproduce viscosity data measured in the melt region. The extended model is believed to reproduce the viscosity data of multicomponent silicate systems measured in the wide composition and temperature ranges within experimental error limits.

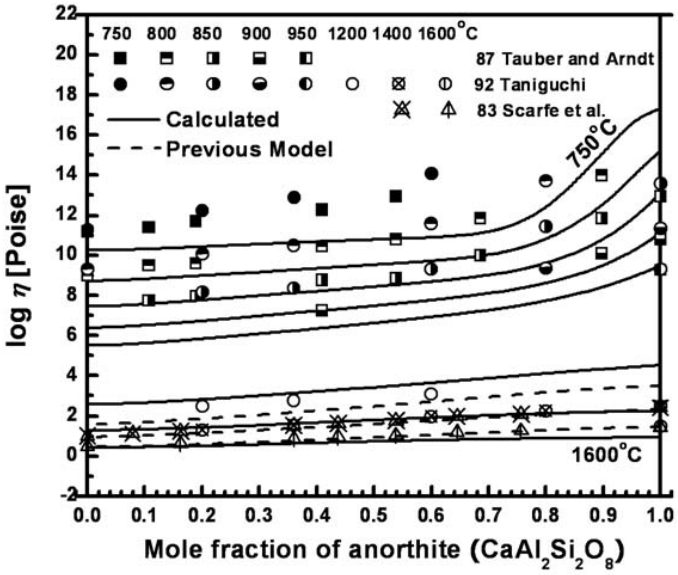

Fig. 11.50 Viscosity of diopside–anorthite ($CaMgSi_2O_6$–$CaAl_2Si_2O_8$) melts: experimental points [270, 318, 320]and lines calculated by the extended model and the previous model

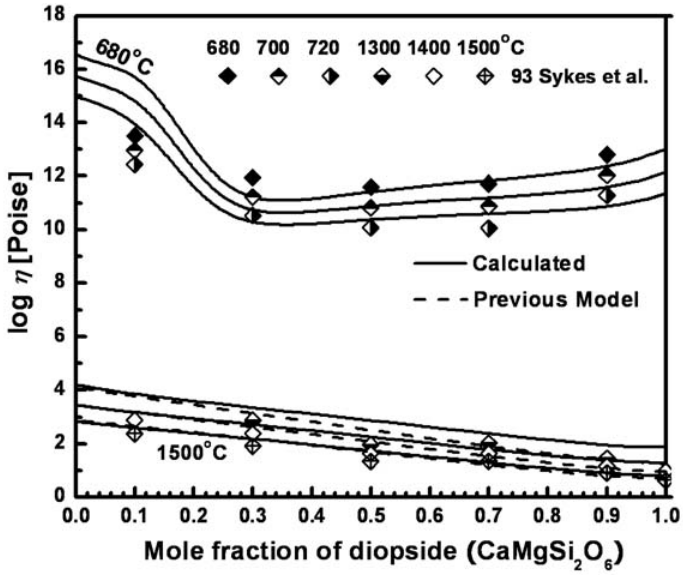

Fig. 11.51 Viscosity of nepheline–diopside ($NaAlSiO_4$–$CaMgSi_2O_6$) melts: experimental points [314] and lines calculated by the extended model and the previous model

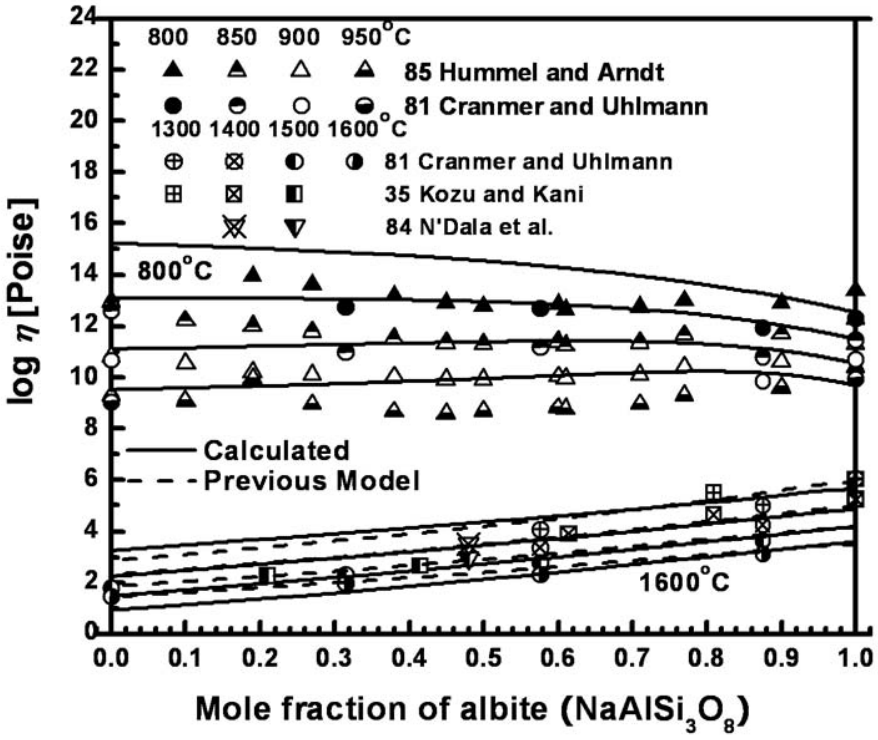

Fig. 11.52 Viscosity of anorthite–albite ($CaAl_2Si_2O_8$–$NaAlSi_3O_8$) melts: experimental points [36, 98, 146, 200]and lines calculated by the extended model and the previous model

The viscosities for all available subsystems of the Al_2O_3–CaO–MgO–ZnO–PbO–Na_2O–K_2O–SiO_2 system are also predicted as shown in Figs. 11.53 to 11.61. The viscosity of multicomponent systems is predicted by the extended model from the unary, binary and ternary parameters given in Tables 11.1 to 11.3 with no additional parameters. In Figs 11.53 and 11.54, the predicted viscosity of the CaO-MgO-Na_2O-SiO_2 system are compared with the data measured by Kim and Vyazkost [124] and Khanna [122]; the extended model is in good agreement with most experimental data at all temperatures. The data of Khanna [122] show slightly lower viscosities in the system MgO-Na_2O-SiO_2 in Fig. 11.20 and represent systematically lower viscosities than the predicted as shown in Fig. 11.54, but the model is still in reasonable agreement within the experimental error limits.

As can be seen from Figs. 11.55 to 11.57, the predicted viscosities for the system CaO–MgO–Na_2O–Al_2O_3–SiO_2 show fairly good agreement with most data at all temperatures within

the experimental error limits. In Fig. 11.55, the data of Okhotin and Andryukhina [218] show systematically higher viscosities than the calculated lines with decreasing temperatures on the section of system CaO–MgO–Al_2O_3–SiO_2. Again, with high contents of CaO, Al_2O_3 and MgO, the viscosity data at lower temperatures would be expected to have large errors because of the tendency for crystallization of the sample during the experiment.

Fig. 11.58 shows the predicted viscosities for the system CaO–Na_2O–K_2O–Al_2O_3–SiO_2 along with the experimental data measured by Startsev et al. [305] using the beam-bending method. The viscosity data with decreasing Na_2O show an abrupt increase in viscosity at 750 and 800°C. Since there is no obvious physical reason for such behavior, it is most likely an effect caused by crystallization. Except for these points, the extended model describes well the viscosity data at all temperatures within the experimental error limits.

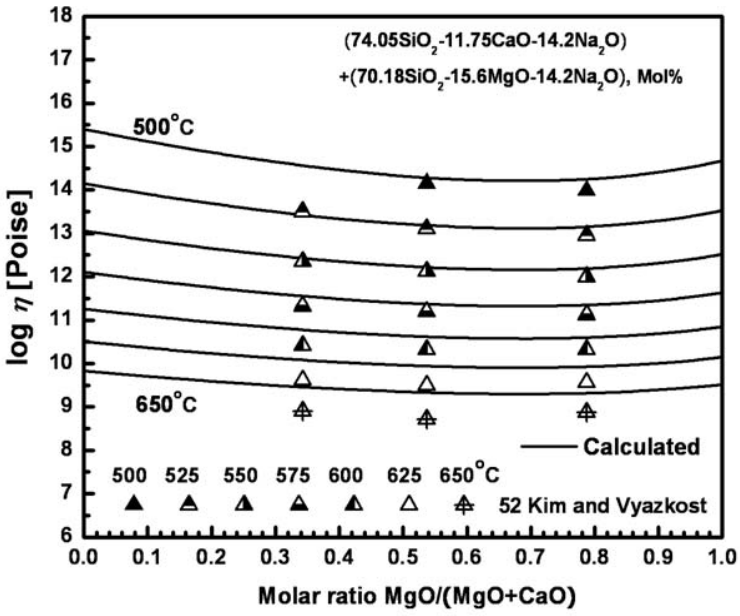

Fig. 11.53 Viscosity of CaO-MgO–Na_2O–SiO_2 for a pseudo-ternary section between the compositions (74.05 mol% SiO_2, 11.75 mol% CaO, 14.2 mol% Na_2O) and (70.18 mol% SiO_2, 15.6 mol% MgO, 14.2 mol% Na_2O): experimental points [124] and calculated lines

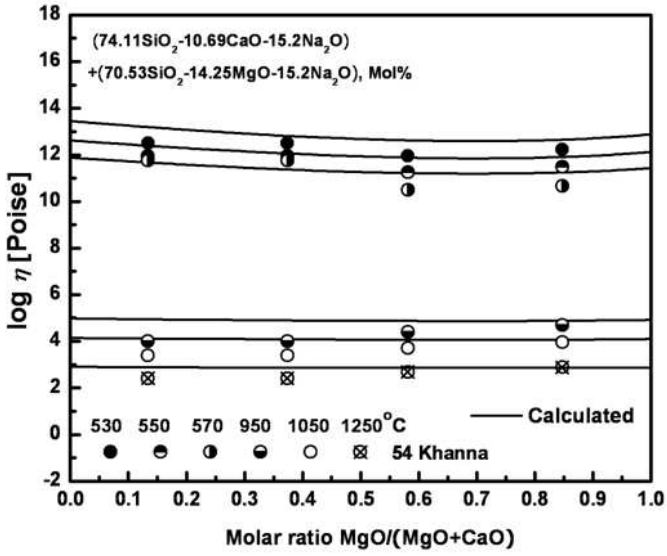

Fig. 11.54 Viscosity of CaO-MgO–Na_2O–SiO_2 for a pseudo-ternary section between the compositions (74.11 mol% SiO_2, 10.69 mol% CaO, 15.2 mol% Na_2O) and (70.53 mol% SiO_2, 14.25 mol% MgO, 15.2 mol% Na_2O): experimental points [122] and calculated lines

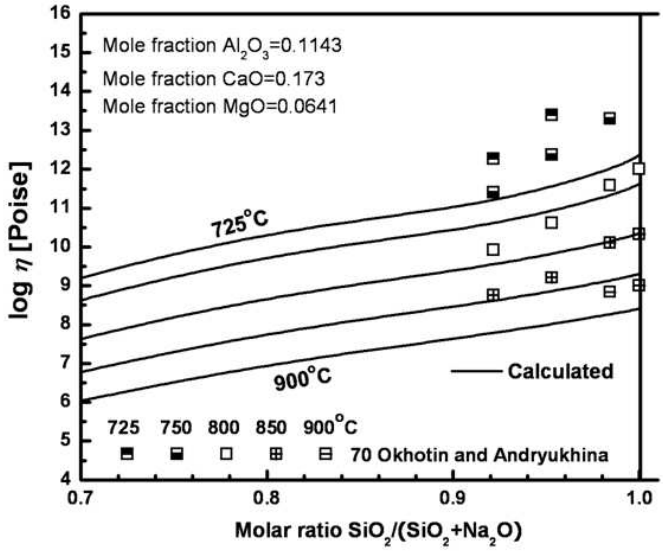

Fig. 11.55 Viscosity of CaO-MgO–Na_2O–Al_2O_3–SiO_2 at 17.3 mol% CaO, 6.41 mol% MgO and 11.43 mol% Al_2O_3: experimental points [218] and calculated lines

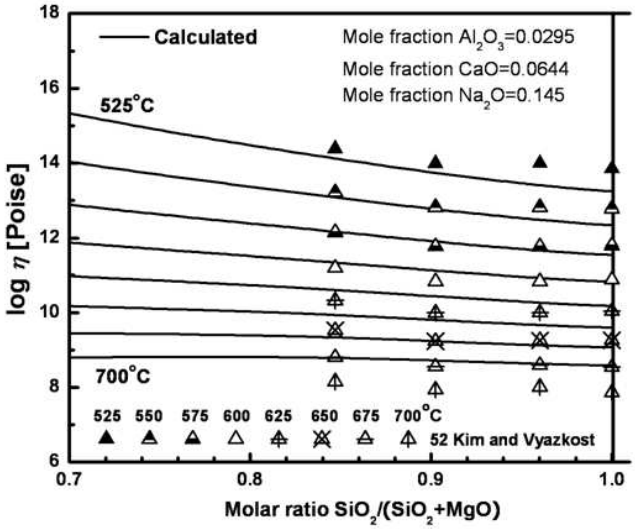

Fig. 11.56 Viscosity of CaO-MgO–Na_2O–Al_2O_3–SiO_2 at 14.5 mol% Na_2O, 6.44 mol% CaO and 2.95 mol% Al_2O_3: experimental points [124] and calculated lines

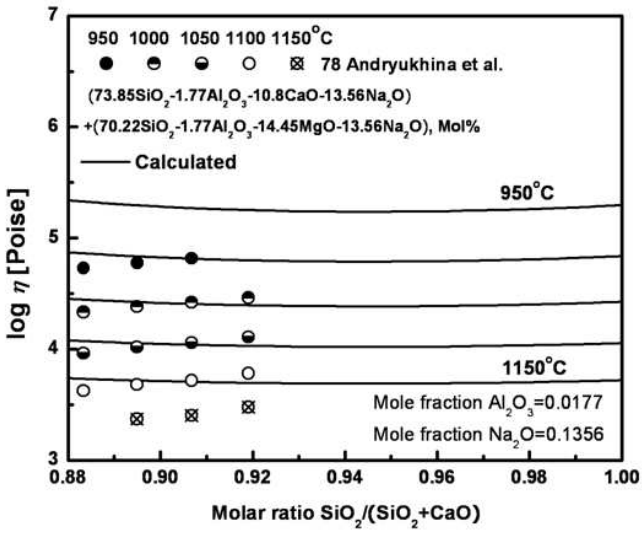

Fig. 11.57 Viscosity of CaO-MgO–Na_2O–Al_2O_3–SiO_2 for a pseudo-ternary section between the compositions (73.85 mol% SiO_2, 1.77 mol % Al_2O_3, 10.8 mol% CaO, 13.56 mol% Na_2O) and (70.22 mol% SiO_2, 1.77 mol % Al_2O_3, 14.45 mol% MgO, 13.56 mol% Na_2O): experimental points [4] and calculated lines

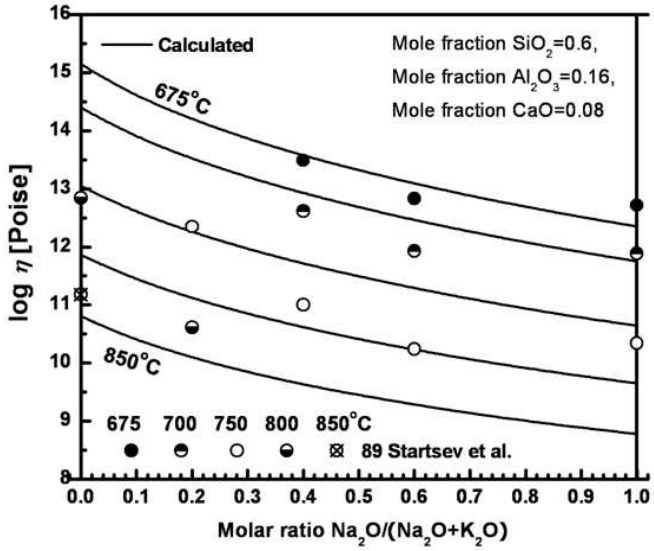

Fig. 11.58 Viscosity of $CaO–Na_2O–K_2O–Al_2O_3–SiO_2$ at 60 mol% SiO_2, 8 mol% CaO and 16 mol% Al_2O_3: experimental points [305] and calculated lines

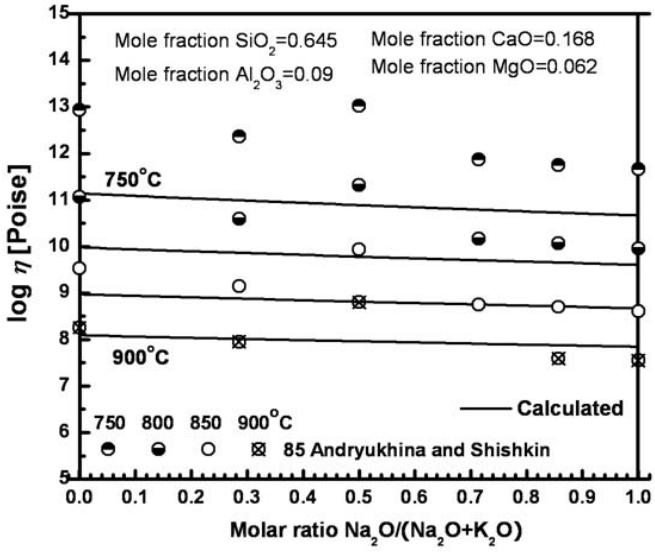

Fig. 11.59 Viscosity of CaO-MgO–$Na_2O–K_2O–Al_2O_3–SiO_2$ at 64.5 mol% SiO_2, 16.8 mol% CaO, 9 mol% Al_2O_3 and 6.2 mol% MgO: experimental points [5] and calculated lines

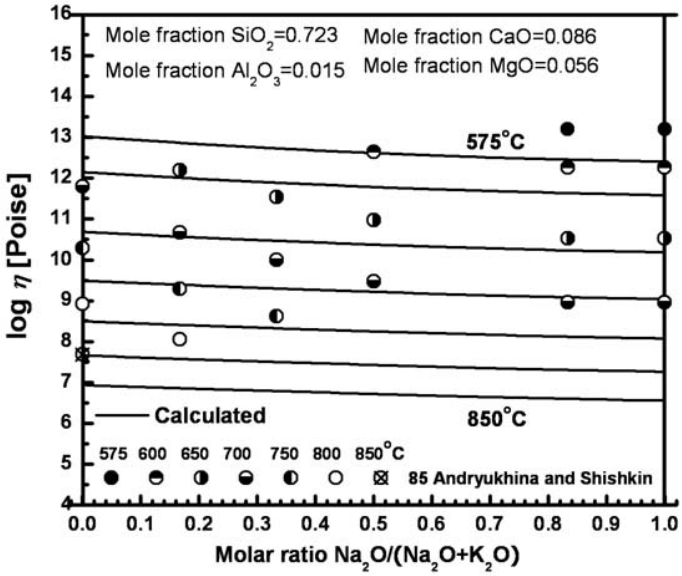

Fig. 11.60 Viscosity of CaO-MgO–Na_2O–K_2O–Al_2O_3–SiO_2 at 72.3 mol% SiO_2, 8.6 mol% CaO, 1.5 mol% Al_2O_3 and 5.6 mol% MgO: experimental points [5] and calculated lines

In Figs. 11.59 and 11.60, the viscosity data for the system CaO–MgO–Na_2O–K_2O–Al_2O_3–SiO_2 are compared with the predicted viscosities. In Fig. 11.59, the total alkali content (Na_2O+K_2O) is 3.5 mol%. Therefore this system is virtually the CaO-MgO–Al_2O_3–SiO_2 system and the viscosity data below 800ºC show systematically higher values than the predicted. This systematic difference could be caused by partial crystallization of the sample containing high contents of CaO, Al_2O_3 and MgO during the experiments. On the other hand, as shown in Fig. 11.60, the viscosity data could be measured up to 575ºC because of the high contents of SiO_2 in the system. However, the experimental data in Fig. 11.60 also show an abrupt increase in viscosity with decreasing Na_2O while the viscosity data show a linear relation as a function of mole fraction of basic oxides in Fig. 11.59. Again, since there is no obvious physical reason for this abrupt increase in viscosity, it is most likely an effect caused by crystallization.

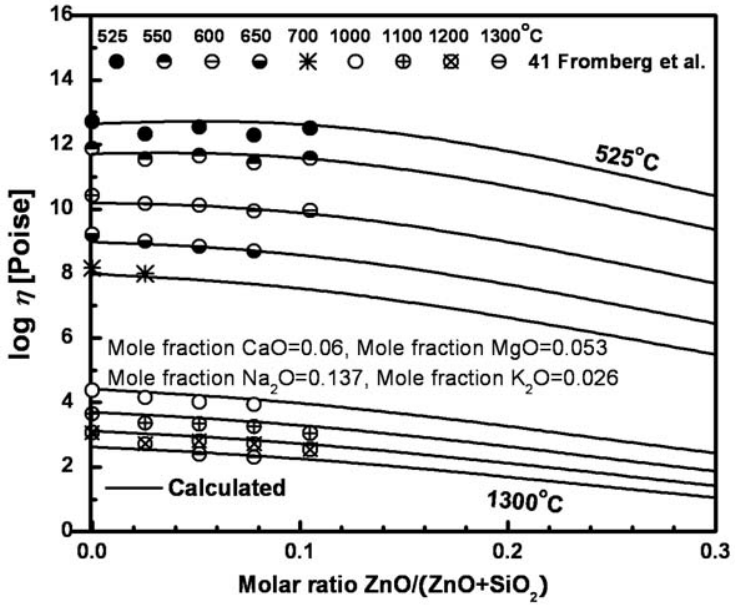

Fig. 11.61 Viscosity of ZnO-CaO-MgO-Na_2O-K_2O-SiO_2 at 6 mol% CaO, 5.3 mol% MgO, 13.7 mol% Na_2O and 2.6 mol% K_2O: experimental points [70] and calculated lines

Fig. 11.61 shows the predicted viscosities for the system ZnO-CaO-MgO-Na_2O-K_2O-SiO_2 with the experimental data measured by Fromberg et al. [70] using the rotational viscometer method for the melt and the fiber-elongation method for the glasses. As can be seen from Fig. 11.61, the experimental data show an excellent agreement with all experimental data at all temperatures within the experimental error limits.

11.3.7 Viscosity of Commercial Glasses

A large number of viscosity measurements are available for glass-forming melts in the Al_2O_3–B_2O_3–CaO–MgO–ZnO–PbO–Na_2O–K_2O–SiO_2 system around some technologically significant compositions. In particular, the compositions of typical soda-lime-silica glass melts for production of container glasses and float glasses, E-glasses, wool glasses, low-expansion borosilicate glasses and lead crystal glasses are within this nine-component system. The concentrations of additional minor components such as Fe, Cr, or Li are normally less than 1 wt %.

Some glass research groups [279] carried out extensive viscosity measurements in a very well–controlled manner using the rotating spindle, parallel plate and beam bending methods with well-characterized samples over a narrow composition range corresponding to a particular type of glass. Commercial glass melts may also be easier to work with since they are specifically designed to avoid crystallization. This minimized the scatter of experimental data and allowed fitting experimental points very accurately using fairly simple regression equations. The equations obtained can be used for reliable interpolations within the limited composition range covered by the net of the experimental points, but extrapolations outside this range are not possible.

A few regression equations for glasses were obtained based on the viscosity measurements by several investigators. In particular, the recent statistical model of Fluegel [67] fits a very large amount of experimental information on glass melts, which is summarized in the SciGlass database [37], and provides a rigorous estimation of errors and validity limits. This model [67] is based on multiple regression using polynomial functions. Fluegel claims that his analysis of systematic differences between laboratories improves the overall accuracy of interpolation [67]. Fluegel's model is most accurate in the vicinity of the commercial glass compositions since it is calibrated based on numerous experimental data for these regions.

The extended model developed in the present study, on the other hand, is designed particularly for wide-range extrapolations of composition and temperature. The experimental data for multicomponent glass melts have not been used for the calibration of our model which is applicable at any composition contrary to the regression equations mentioned above which cannot be extrapolated outside their validity limits. It is interesting to examine how the present model compares with existing regression equations over their ranges of validity.

Float glasses and container glasses are virtually the CaO-MgO-Na_2O-SiO_2 system. Some commercial viscosity data were comparable with the CaO-Na_2O-SiO_2 system as shown in Figs 11.12 to 11.14. All viscosity data for the Container Glass series as shown in Figs 11.12 to 11.14 show good agreement with the calculated results of the extended model. In Fig. 11.62, the viscosity of float glasses and container glasses are compared with the lines calculated by the extended model and the model of Fluegel [67] as an inverse function of temperature and all data show better relations with the model proposed by Fluegel [67]. As mentioned earlier, Fluegel's

model was calibrated based on numerous experimental data for these compositional regions while the extended model developed in the present study was designed particularly for wide-range extrapolations of composition and temperature of the Al_2O_3–B_2O_3–CaO–MgO–ZnO–PbO–Na_2O–K_2O–SiO_2 system. However, it is apparent that the extended model is able to reproduce the commercial glass viscosity data within the experimental error limits and is comparable with Fluegel's model.

In Figs 11.63 and 11.64, the viscosity of float and container glass series are plotted with the experimental data of other authors [122, 124, 181, 268] and the lines calculated by the extended model are also compared with the model by Fluegel [67]. As shown in Figs 11.63 and 11.64, the extended model reproduces well all experimental data including the commercial glasses as a function of composition and temperature, and the extended model is also comparable with the model by Fluegel [67].

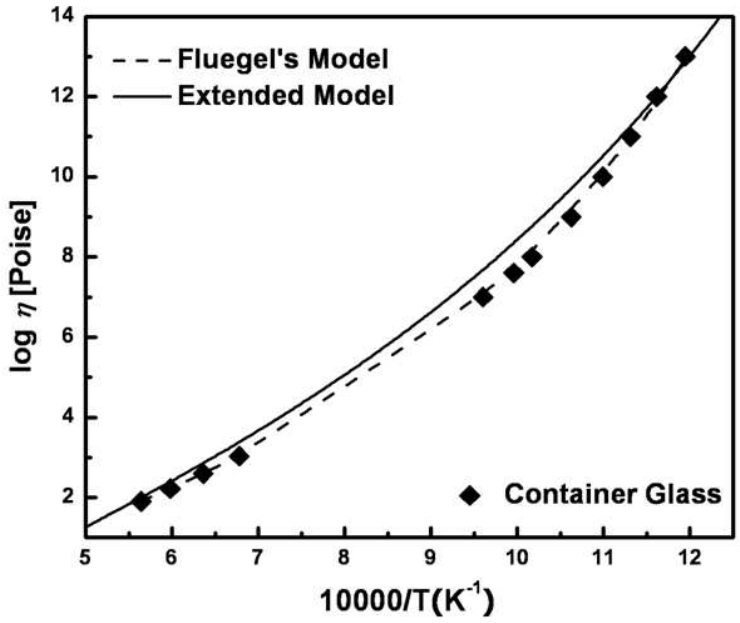

(a)

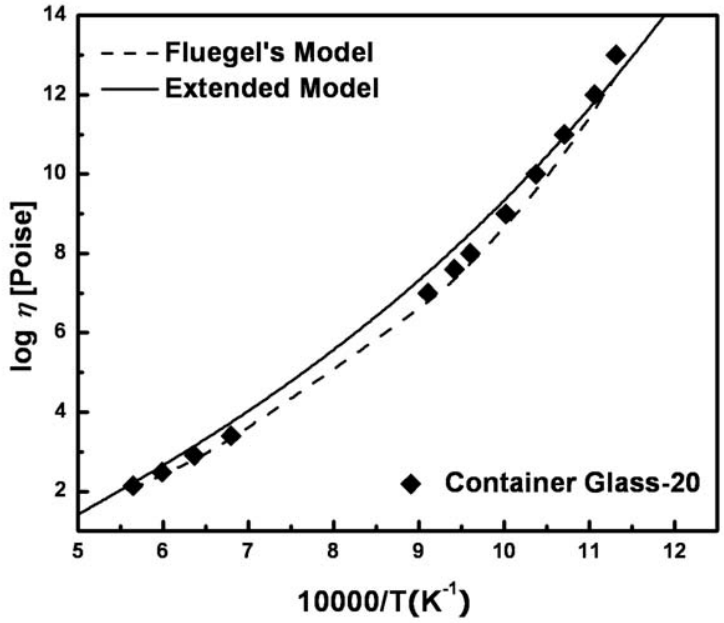
Fluegel's Model
Extended Model
Container Glass-20
log η [Poise]
10000/T(K-1)

(b)

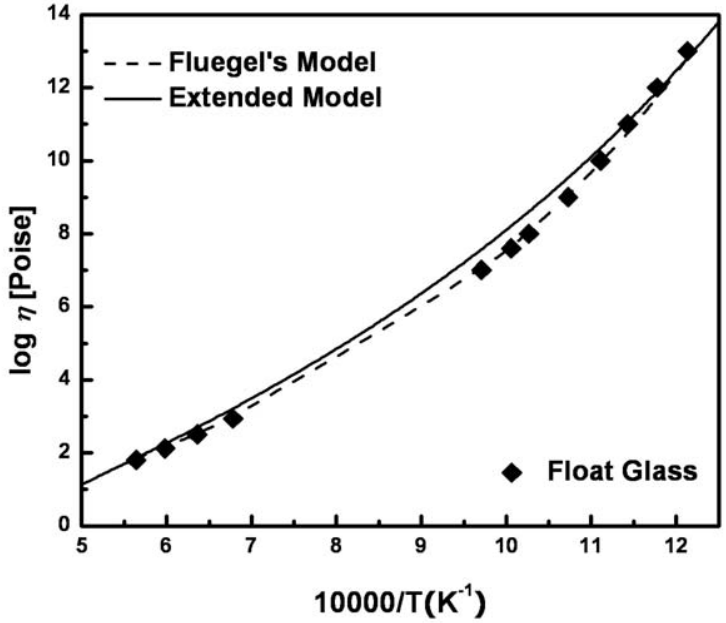
Fluegel's Model
Extended Model
Float Glass
log η [Poise]
10000/T(K-1)

(c)

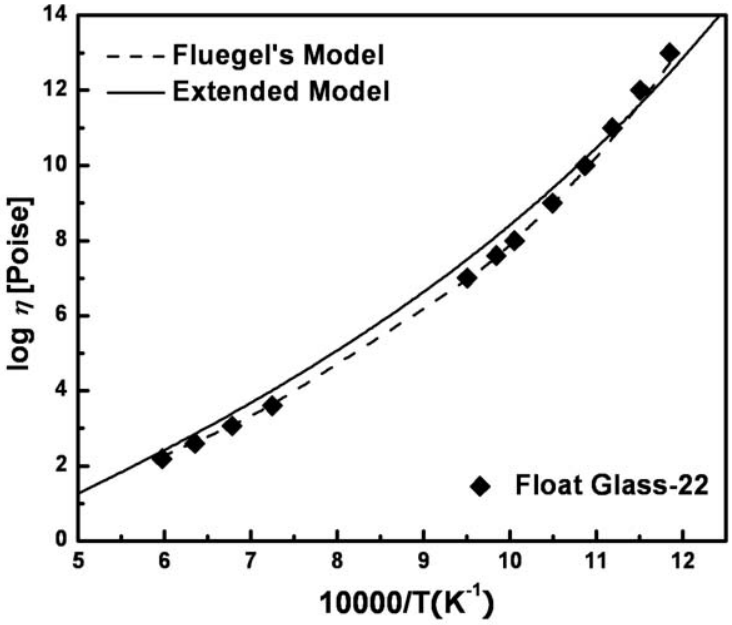

(d)

Fig. 11.62 Viscosity of Container and Float Glasses: Experimental points [279] and calculated lines. Figures (a) to (d) compares the viscosity model proposed in the present study (solid lines) with the model by Fluegel [67] (dashed lines)

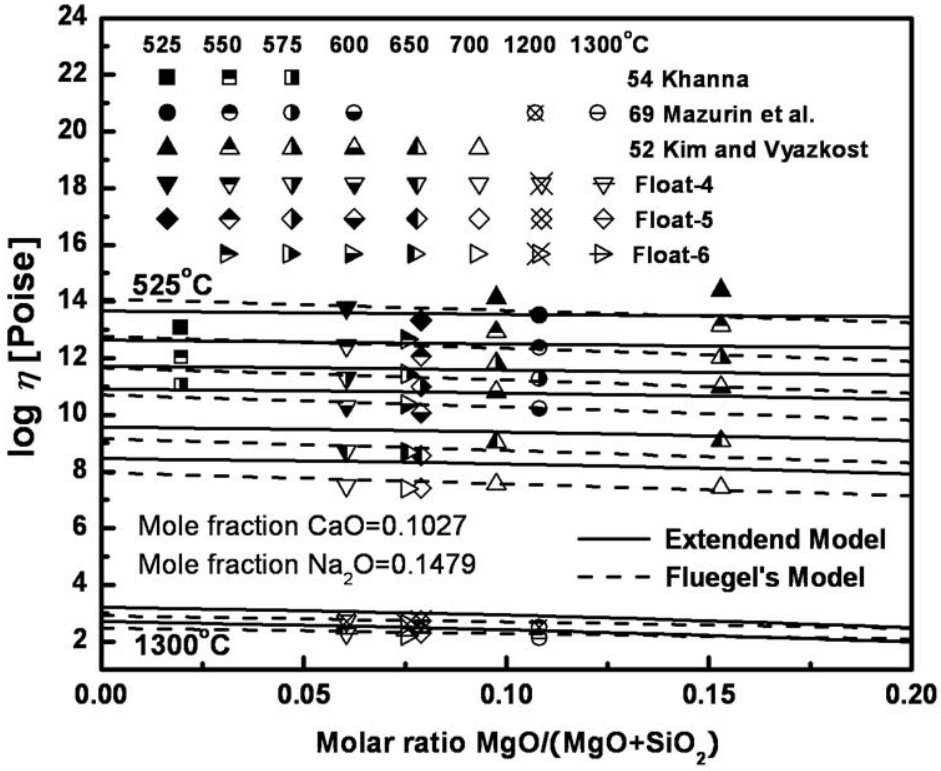

Fig. 11.63 Viscosity of CaO-MgO–Na_2O–SiO_2 at 10.27 mol% CaO and 14.79 mol% Na_2O: experimental points [122, 124, 181, 279] and calculated lines (solid lines) compared with the model proposed by Fluegel [67] (dashed lines)

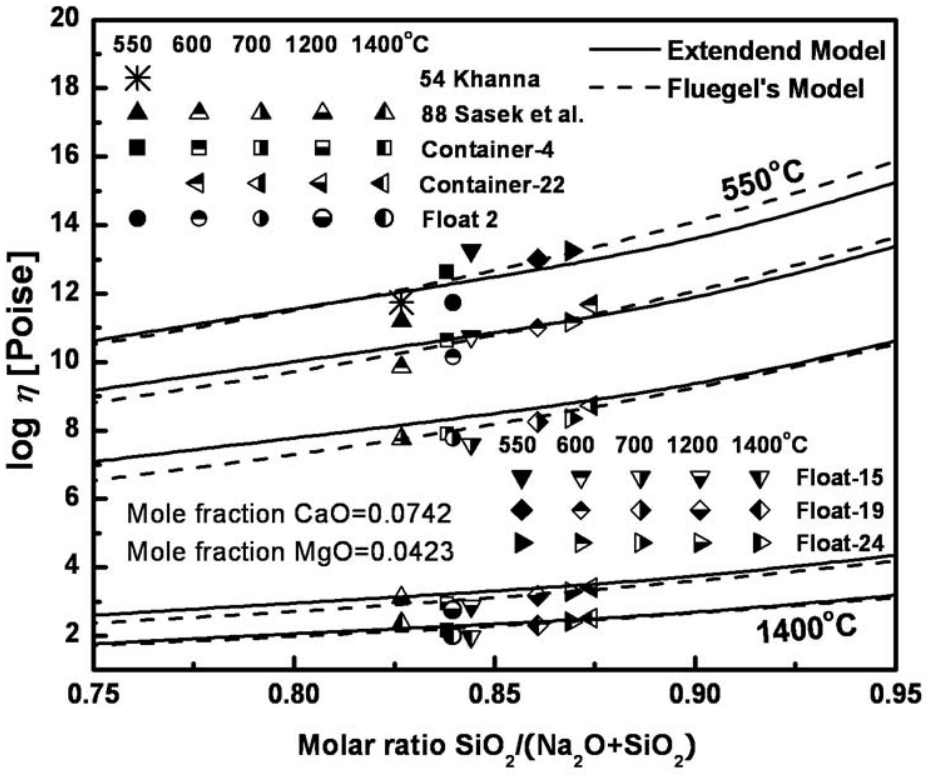

Fig. 11.64 Viscosity of CaO-MgO–Na_2O–SiO_2 at 7.42 mol% CaO and 4.23 mol% MgO: experimental points [122, 268, 279] and calculated (solid lines) compared with the model proposed by Fluegel [67] (dashed lines)

11.4 Conclusions

A model for the viscosity of oxide melts is extended to predict the viscosity of glasses for all available sub-systems of the CaO-MgO-Na_2O-K_2O-ZnO-PbO-Al_2O_3-SiO_2 system from the glass to the melt regions within the experimental error limits.

The structure of silicate glasses quenched from the molten state is similar to the structure of silicate melts, and thus the structure of silicate glasses can be taken into account by the Modified Quasichemical Model [231, 232].

Using all available sub-systems of the CaO-MgO-Na_2O-K_2O-ZnO-PbO-Al_2O_3-SiO_2 system, the values of model parameters A_{MO_x}, E_{MO_x}, $E^R_{MO_x-Si}$ and $E^{i.j}_{MO_x-Si}$ were re-optimized simultaneously with the non-Arrhenian unary and binary parameters T_{MO_x}, n_{MO_x}, m_{MO_x-Si}, T_{MO_x-Si} and n_{MO_x-Si} (M = Ca, Mg, Pb, Zn and Al). The model parameters $A^{i.j}_{MO_x-Si}$, $A^R_{MO_x-Si}$ and $A^{Ring}_{MO_x-Si}$ were not required except for the value $A^R_{AlO_{1.5}-Si}$ and were set equal to zero.

In the binary systems CaO-SiO_2 and MgO-SiO_2, the viscosity data have a cross-over point as a function of temperature and this trend of viscosities is also supported by the ternary measurements in the CaO-Na_2O-SiO_2 and MgO-Na_2O-SiO_2 systems. This cross-over point in the binary MO_x-SiO_2 (M = basic oxide) systems can be taken into account by the terms of T_{MO_x}, n_{MO_x}, m_{MO_x-Si}, T_{MO_x-Si} and n_{MO_x-Si}.

In order to take into account the Charge Compensation Effect for glasses containing Al_2O_3, we added two more parameters into the function of $\Delta G_{MAl_xO_y}$ for the formation of Charge Compensated Species such as $CaAl_2O_4$ or $NaAlO_2$. This simple modification of the model results in good agreement with most viscosity data for ternary and high-order systems containing Al_2O_3 within experimental error limits.

When comparing the reproducibility between the previous model and the extended model, the extended model is able to reproduce the viscosity data not only in the melt region but also the glass region within experimental error limits, and the reproducibility of the extended model in the melt region is comparable with the results of the previous model.

The available viscosity data for the sub-systems of CaO-MgO-Na_2O-K_2O-ZnO-PbO-Al_2O_3-SiO_2 have been reviewed. It is demonstrated that the extended model reproduces the experimental data for the binary and ternary glasses and predicts the viscosities of multicomponent glasses within experimental error limits over wide temperature and composition ranges. In particular, the extended model can be used to provide good estimates of the viscosities of multicomponent glasses, magmas, lavas and commercial glasses. Most importantly, the extended model is believed to reproduce not only the temperature dependence but also composition dependence of available viscosity data within experimental error limits.

Table 11.1 Optimized Model parameters for the viscosity expressed in Pa·s

System	Model parameter	Model parameters (J·mol^{-1})
SiO_2	$A_{Si}^{*} = -10.56$ $A_{Si}^{E} = -6.13$	$E_{Si}^{*} = 217200$ $E_{Si}^{E} = 298520$
$AlO_{1.5}$	$A_{AlO_{1.5}} = -9.11$	$E_{AlO_{1.5}} = 118500$
CaO	$A_{CaO} = -11.25$	$E_{CaO} = 58560$
MgO	$A_{MgO} = -10.20$	$E_{MgO} = 59434$
$NaO_{0.5}$	$A_{NaO_{0.5}} = -10.15$	$E_{NaO_{0.5}} = 45500$
$KO_{0.5}$	$A_{KO_{0.5}} = -13.35$	$E_{KO_{0.5}} = 84500$
ZnO	$A_{ZnO} = -11$	$E_{ZnO} = 80000$
PbO	$A_{PbO} = -6.92$	$E_{PbO} = 3373$
$AlO_{1.5}$–SiO_2	$A_{AlO_{1.5}\text{-}Si}^{R} = -12.78$	$E_{AlO_{1.5}\text{-}Si}^{1,1} = -99699$ $E_{AlO_{1.5}\text{-}Si}^{R} = 303400$
CaO–SiO_2		$E_{CaO\text{-}Si}^{1,1} = -172232$ $E_{CaO\text{-}Si}^{R} = 39893$
MgO–SiO_2		$E_{MgO\text{-}Si}^{1,1} = -209506$ $E_{MgO\text{-}Si}^{R} = 5742$
$NaO_{0.5}$–SiO_2		$E_{NaO_{0.5}\text{-}Si}^{1,1} = 32500$ $E_{NaO_{0.5}\text{-}Si}^{R} = 10200$ $E_{NaO_{0.5}\text{-}Si}^{Ring} = 20444358$

$KO_{0.5}$–SiO_2		$E^{1,1}_{KO_{0.5}\text{-Si}} = -38200$ $E^{R}_{KO_{0.5}\text{-Si}} = 39000$ $E^{Ring}_{KO_{0.5}\text{-Si}} = 42390018$
ZnO–SiO_2		$E^{1,1}_{ZnO\text{-Si}} = -30000$ $E^{R}_{ZnO\text{-Si}} = 95000$
PbO–SiO_2		$E^{1,1}_{PbO\text{-Si}} = -191759$ $E^{2.5}_{PbO\text{-Si}} = 1748612$ $E^{R}_{PbO\text{-Si}} = 26518$

Table 11.2 Optimized non-Arrhenian parameters for the extended viscosity model

System	T (Kelvin), n
CaO	$T_{CaO} = 1873.15$ $n_{CaO} = 2.34$
MgO	$T_{MgO} = 1872.71$ $n_{MgO} = 2.72$
PbO	$T_{PbO} = 1760$ $n_{PbO} = 3.114$
ZnO	–
$NaO_{0.5}$	–
$KO_{0.5}$	–
$AlO_{1.5}$	–
CaO–SiO_2	$T_{CaO\text{-Si}} = 1909.89$ $n_{CaO\text{-Si}} = 1.95$ $m_{CaO\text{-Si}} = 0.416$

$MgO–SiO_2$	$T_{MgO\text{-}Si} = 3665.52$ $n_{MgO\text{-}Si} = 1$ $m_{MgO\text{-}Si} = 0.642$
$PbO–SiO_2$	$T_{PbO\text{-}Si} = 982.18$ $n_{PbO\text{-}Si} = 3.3$ $m_{PbO\text{-}Si} = 0$
$ZnO–SiO_2$	$T_{ZnO\text{-}Si} = 1075$ $n_{ZnO\text{-}Si} = 5.23$
$NaO_{0.5}–SiO_2$	$T_{NaO_{0.5}\text{-}Si} = 785.61$ $n_{NaO_{0.5}\text{-}Si} = 5.08$
$KO_{0.5}–SiO_2$	$T_{KO_{0.5}\text{-}Si} = 780.1$ $n_{KO_{0.5}\text{-}Si} = 6.86$
$AlO_{1.5}–SiO_2$	$T_{AlO_{1.5}\text{-}Si} = 370.36$ $n_{AlO_{1.5}\text{-}Si} = 1$

Table 11.3 Optimized parameters for the ternary systems containing alumina (J mol^{-1})

System	
$KO_{0.5}–AlO_{1.5}–SiO_2$	$\Delta G_{KAlO_2} = (-172290+38.69T)+(153922-59.60T)X(SiO_2)$
$NaO_{0.5}–AlO_{1.5}–SiO_2$	$\Delta G_{NaAlO_2} = (-115182+52.87T)+(153888-123.49T)X(SiO_2)$
$CaO–AlO_{1.5}–SiO_2$	$\Delta G_{CaAl_2O_4} = (-207945+130.8T)+(178900-170.24T)X(SiO_2)$
$MgO–AlO_{1.5}–SiO_2$	$\Delta G_{MgAl_2O_4} = (-182734+109.36T)+(228839-180.42T)X(SiO_2)$
$PbO–AlO_{1.5}–SiO_2$	$\Delta G_{PbAl_2O_4} = -14226-48953X(SiO_2)$
$ZnO–AlO_{1.5}–SiO_2$	$\Delta G_{ZnAl_2O_4} = (-625073+360.94T)+(1085539-653.92T)X(SiO_2)$

CHAPTER 12 EXTENSION OF THE MODEL TO THE GLASS REGION OF BORON–CONTAINING SYSTEMS

12.1 Introduction

Boron oxide is one of the best glass-forming oxides. It plays an essential role in the industrial production of glass due to its high solubility in silicate melts and to the low melting temperatures of boron-containing glasses. Boron is also widely used in ceramics, metallurgy, production of fibers, growing of single-crystal semiconductors from melts, etc. The viscosity of B_2O_3-containing melts is of primary importance for most of these applications.

As shown in Chapter 3, we have developed a model to reproduce the viscosity of oxide melts containing boron. In this model the viscosity is related to the structure of the melt, which in turn is calculated from the thermodynamic description of the melt using the Modified Quasichemical Model [231, 232]. Most importantly, the model takes into account the formation of the borosilicate network which has a profound effect on the viscosity. The model predicts within experimental error limits the viscosity of multicomponent borosilicates from just a few model parameters fitted to the viscosities of the binary and some ternary subsystems.

In Chapter 11, we extended the model to the glass region of silicates by addition of a few non-Arrhenian parameters. The model reproduced most available experimental data for the system CaO-MgO-Na_2O-K_2O-PbO-ZnO-Al_2O_3-SiO_2 within experimental error limits. No other model exists for the viscosity in the glass region of boron-containing systems over wide composition and temperature ranges.

The addition of basic oxides including alkali metals to B_2O_3 has a complex effect on viscosity, known as the "*Boron-Alkali Anomaly*" or "*Borate Anomaly*" [284]. With decreasing the temperature, adding alkali oxides to B_2O_3 melts and glasses causes the viscosity to rise to different maximum values at around 20 and 33 mol% of R_2O, respectively (where R is an alkali metal as Na, K and Li). In addition, additions of other basic oxides such as CaO, MgO and PbO also yield maximum values in viscosity around the metaborate MB_2O_4 (M = Ca, Mg) or diborate compositions MB_4O_7 (M = Pb, Zn) in the glass region. Beyond this maximum, the viscosity decreases monotonically with increasing concentration of these basic oxides. Other properties

such as density and thermal expansion change in a roughly similar fashion [284]. For example, there is a minimum in the thermal expansivity of borate glasses at roughly the same compositions as the viscosity maximum of borate melts [331]. The current understanding of the borate anomaly connects the variation of the various properties to the population of various structural groups in the melt.

In order to take into account the "*Borate Anomaly*" in the melts, we employed the formation of solid-like clusters at the composition of alkali tetraborates MB_4 (M = Na, K) as shown in section 3.4.3 to reproduce the viscosity data measured in the melt region. In the present chapter, we extend the model further to reproduce the abnormal behavior of the viscosity for each B_2O_3–MO_x system from the glass to the melt regions, where M is a basic oxide, by introducing the formation of solid-like clusters also at the diborate composition and we predict the viscosity of multicomponent systems containing boron oxides not only in the melt but also in the glass region within experimental error limits.

12.2 Extended Viscosity Model for Boron-containing Systems

In Chapter 11, Eq. (11.4), we employed the non-Arrhenian unary and binary parameters $T_{\mathrm{MO_x}}$, $n_{\mathrm{MO_x}}$, $m_{\mathrm{MO_x\text{-}Si}}$, $T_{\mathrm{MO_x\text{-}Si}}$ and $n_{\mathrm{MO_x\text{-}Si}}$ to reproduce the viscosity data measured from the glass to the melt regions. We now employ the additional non-Arrhenian binary parameters $T_{\mathrm{MO}_x\text{-B}}$ and $n_{\mathrm{MO}_x\text{-B}}$ to reproduce the viscosity data for boron-containing systems from the glass to the melt regions as shown in Eq. (12.1).

$$
\begin{aligned}
E = & \left[\sum_{\mathrm{M}} (X_{\mathrm{MO_x}} E_{\mathrm{M}}) \left[1 + X_{\mathrm{MO_x}}^{m_{\mathrm{MO_x\text{-}Si}}} \left(\frac{T_{\mathrm{MO_x}}}{T} \right)^{n_{\mathrm{MO_x}}} \right] + \sum_{\mathrm{M}} \sum_{i,j} \left(X_{\mathrm{MO_x}}^{i} X_{\mathrm{Si}}^{j} E_{\mathrm{MO_x\text{-}Si}}^{i,j} \right) \right] \\
& + X_{\mathrm{Si}} \left\{ \begin{array}{l} \left[E_{\mathrm{Si}}^{*} + \left(p_{\mathrm{Si}}^{\mathrm{B,Si}} \right)^{4} \left(p_{\mathrm{B,Si}}^{\mathrm{B,Si}} \right)^{36} E_{\mathrm{Si}}^{E} \right] \\ + \left(p_{\mathrm{Si}}^{\mathrm{B,Si}} \right)^{4} \left[1 - \left(p_{\mathrm{B,Si}}^{\mathrm{B,Si}} \right)^{36} \right] \dfrac{\sum_{\mathrm{M}} (X_{\mathrm{MO_x}} E_{\mathrm{MO_x\text{-}Si}}^{R})}{\sum_{\mathrm{M}} X_{\mathrm{MO_x}}} \\ + \left(p_{\mathrm{Si}}^{\mathrm{Si}} \right)^{7} \left(1 - p_{\mathrm{Si}}^{\mathrm{Si}} \right)^{3} \dfrac{\sum_{\mathrm{M=Alkali}} (X_{\mathrm{MO_x}} E_{\mathrm{MO_x\text{-}Si}}^{Ring})}{\sum_{\mathrm{M}} X_{\mathrm{MO_x}}} \end{array} \right\} \left[1 + \sum_{\mathrm{M}} \left(\left(\frac{T_{\mathrm{MO_x\text{-}Si}}}{T} \right)^{n_{\mathrm{MO_x\text{-}Si}}} \cdot X_{\mathrm{MO_x}} \cdot X_{\mathrm{Si}} \right) \right] \\
& + \left\{ E_{\mathrm{B}}^{*} + \left(p_{\mathrm{B}}^{\mathrm{B,Si}} \right)^{3} \left(p_{\mathrm{B,Si}}^{\mathrm{B,Si}} \right)^{37} \left(E_{\mathrm{B}} \left[1 + \left(\frac{T_{\mathrm{B}}}{T} \right)^{n_{\mathrm{B}}} \right] - E_{\mathrm{B}}^{*} \right) \right\} \left(X_{\mathrm{B}} + \sum_{\mathrm{M}} \left(\frac{T_{\mathrm{MO_x\text{-B}}}}{T} \right)^{n_{\mathrm{MO_x\text{-B}}}} \cdot X_{\mathrm{MO_x}} \cdot X_{\mathrm{B}} \right)
\end{aligned}
\tag{12.1}
$$

The effects of these terms $T_{MO_x\text{-}B}$ and $n_{MO_x\text{-}B}$ on the viscosity calculations are weaker at higher temperatures and stronger at lower temperatures at constant composition. However, no non-Arrhenian binary parameters, $T_{MO_x\text{-}B}$ and $n_{MO_x\text{-}B}$, were required in the model except for the system Al_2O_3-B_2O_3. No formation for the solid-like clusters was applied in the binary Al_2O_3-B_2O_3 system. The solid-like clusters containing Al_2O_3 and B_2O_3 at tetraborate and diborate compositions seem to be much less favorably formed due to the same charge of each cation Al^{3+} and B^{3+}.

As shown in Figs 12.2 to 12.8, viscosity data for the binary B_2O_3–MO_x (M = basic oxides) systems show viscosity maxima at the diborate (MB_2) and tetraborate compositions (MB_4) at lower temperatures. In order to take into account the "*Borate Anomaly*" in the melts, we employed the formation of solid-like clusters at the composition of alkali tetraborates MB_4 (M = Na, K) as shown in section 3.4.3 to reproduce the viscosity data measured in the melt region. However, these viscosity maxima are also seen in the other binary systems CaO-B_2O_3, PbO-B_2O_3 and ZnO-B_2O_3. Thus, we extended the model further to reproduce the abnormal behavior of viscosity for each B_2O_3–MO_x system from the glass to the melt regions, where M is a basic oxide.

Modeling of the solid-like clusters formed at the tetraborate composition was shown in section 3.4.3. We now apply a similar approach to model the formation of solid-like clusters at the diborate composition as well.

The reaction for the formation of the solid-like clusters $m(MB_2O_{x+3})$ at the diborate composition is shown in Eq. (12.2).

$$m \cdot MO_x + 2m \cdot BO_{1.5} \rightleftarrows m(MB_2O_{x+3}) \tag{12.2}$$

We used similar model equations as in section 3.4.3 and optimized model parameters $A^*_{B(MO_x)}$, $E^*_{B(MO_x)}$, m, $\Delta G_{m(MB_2O_{x+3})}$ and $E_{m(MB_2O_{x+3})}$ for the binary MO_x-B_2O_3 systems. The model parameters in section 3.4.3 are simply the Gibbs energy for the formation of solid-like clusters $\Delta G_{m(MB_2O_{x+3})}$ and the activation energy $E_{m(MB_2O_{x+3})}$ which, as a first approximation, are assumed to be independent of temperature. In order to reproduce the viscosity data for the boron-containing systems over a wide temperature range, we added temperature dependences to the Gibbs energy and the activation energy parameters as shown in Eqs (12.3) and (12.4).

$$\Delta G_{m(\mathrm{MB_4O_{x+6}})} = \mathrm{a} + \mathrm{b}T \tag{12.3}$$

$$E_{m(\mathrm{MB_xO_y})} = \alpha + \beta T \tag{12.4}$$

12.3 Review of the available viscosity data and calibration of the model

In the present study, viscosity data measured from the melt to the glass regions are reviewed for all subsystems of the B_2O_3-CaO–MgO–Na_2O–K_2O–PbO–ZnO–SiO_2–Al_2O_3 system. The data judged to be most reliable are shown in the figures below. To improve the legibility of the figures, the results of a few studies which substantially deviate from those of other authors are not shown. For multicomponent subsystems, preference was given to extensive systematic studies. If the viscosity is reported for just a few compositions in a multicomponent system and the description of the experiments is insufficient, it is very difficult to evaluate the real accuracy of the data unless similar compositions were also studied by other authors.

The extended model is intended for the single phase region of the melts and the glasses. The data measured in the two-phase regions were not considered. Therefore, the viscosity data were collected mostly for the single phase region at all available temperature ranges. If an abnormally high viscosity value was reported when compared with other data, this is most likely the result of crystallization. In most cases such data were discarded, but sometimes these points are still shown in the figures to take into account systematic errors.

12.3.1 Viscosity of the unary B_2O_3 system

All optimized model parameters are listed in Table 12.1. The viscosity parameters A_{B}, E_{B}, T_{B} and n_{B} for pure B_2O_3 were taken from the previous study [27, 26]. Two parameters for each MO_x–$BO_{1.5}$ binary system, $A^*_{\mathrm{B(MO_x)}}$ and $E^*_{\mathrm{B(MO_x)}}$ are taken from the previous publication [27, 26]. In order to predict the viscosity in borosilicate glasses, the unary parameters A^*_{Si}, E^*_{Si}, A^E_{Si}, E^E_{Si}, $A_{\mathrm{MO_x}}$, $E_{\mathrm{MO_x}}$, $m_{\mathrm{MO_x\text{-}Si}}$, $n_{\mathrm{MO_x}}$ and $T_{\mathrm{MO_x}}$ for pure silica and basic oxides, and binary parameters $A^{i,j}_{\mathrm{MO_x\text{-}Si}}$, $A^{R}_{\mathrm{MO_x\text{-}Si}}$, $A^{Ring}_{\mathrm{MO_x\text{-}Si}}$, $E^{i,j}_{\mathrm{MO_x\text{-}Si}}$, $E^{R}_{\mathrm{MO_x\text{-}Si}}$, $E^{Ring}_{\mathrm{MO_x\text{-}Si}}$, $T_{\mathrm{MO_x\text{-}Si}}$ and $n_{\mathrm{MO_x\text{-}Si}}$ for MO_x–SiO_2 are taken from Tables 11.1 and 11.2. To take into account the charge compensated effect of

the systems containing $AlO_{1.5}$, the model parameters for the Al_2O_3–CaO–MgO–Na_2O–K_2O–PbO–ZnO–SiO_2 system are taken from Table 11.3.

The low–melting unary B_2O_3 system was studied by many researchers due to its technological importance from the melt to glass region. As shown in Fig. 12.1, all available experimental data are collected and the reliable data are plotted. Some of the data are not shown, even though these data show a good agreement with the extended model, in order to improve the legibility of the figures. Some of the data are shown in the figures for the binary systems. In the melt region, most of the viscosity data were measured using the rotating viscometer [60, 106, 148, 162, 204, 220, 228, 258, 265, 291, 301], counter-balanced [35, 173, 178, 281, 326], ball pulling-up [355], oscillation viscometer [100] and vibration viscometer methods [197]. For the high viscosity measurement in the glass region, the beam-bending [131, 236], the penetration [178, 345, 355] and the fiber-elongation methods [220, 247] were used. In Fig. 12.1-b), the data of Napolitano et al.[204] and Shiraishi et al. [291] show a more sharply increasing behavior of viscosity with decreasing temperature than the other data. Napolitano et al. [204] and Shiraishi et al. [291] measured viscosities from high to low temperatures with the rotating viscometer method. As mentioned in Section 11.3.1, a rotational viscometer is most suitable for measurements of viscosity in the melt and the optimum range for a rotational viscometer is from -1 to 5 in the logarithm poise scale. Viscosity measurements outside the optimum range for each viscometer method would cause large errors and the real accuracy can be much lower. As can be seen from Figs 12.1-b) and c), the model describes well most viscosity data within the experimental error limits and the scatter of experimental data can be as high as 0.5 in Fig.12.1-b) and 1 in Fig. 12.1-c) in the logarithm poise scale.

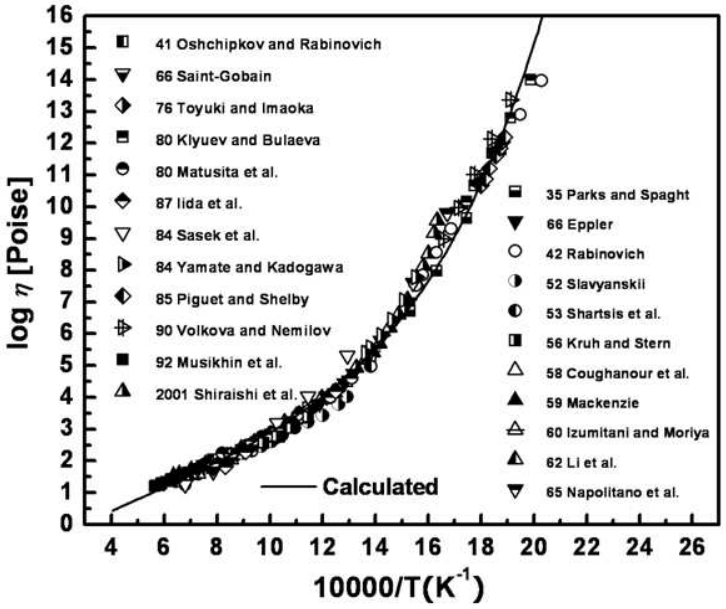
log η [Poise]
10000/T(K-1)
41 Oshchipkov and Rabinovich
66 Saint-Gobain
76 Toyuki and Imaoka
80 Klyuev and Bulaeva
80 Matusita et al.
87 Iida et al.
84 Sasek et al.
84 Yamate and Kadogawa
85 Piguet and Shelby
90 Volkova and Nemilov
92 Musikhin et al.
2001 Shiraishi et al.
35 Parks and Spaght
66 Eppler
42 Rabinovich
52 Slavyanskii
53 Shartsis et al.
56 Kruh and Stern
58 Coughanour et al.
59 Mackenzie
60 Izumitani and Moriya
62 Li et al.
65 Napolitano et al.
Calculated

a)

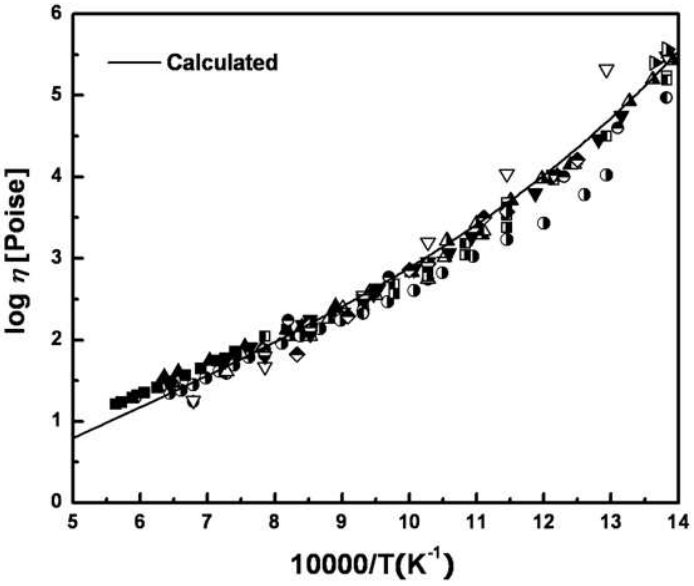
log η [Poise]
10000/T(K-1)
Calculated

b)

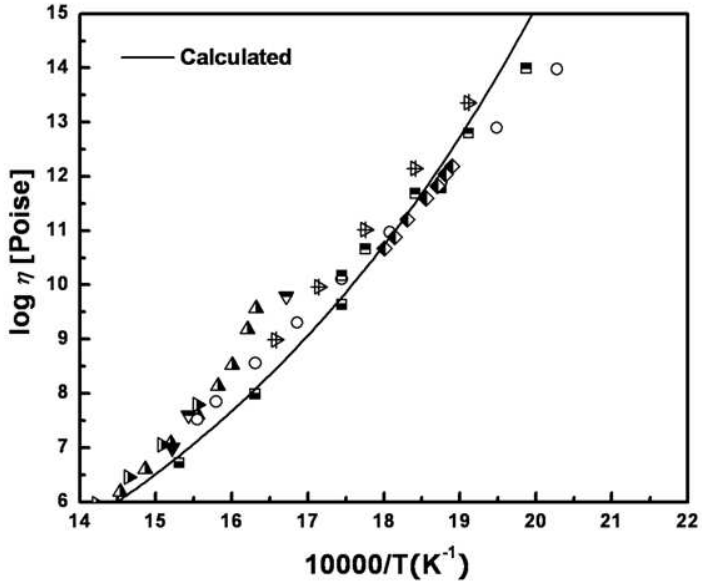

c)

Fig. 12.1 a) Calculated viscosity in B_2O_3 compared to experimental data [35, 60, 100, 106, 131, 148, 162, 173, 178, 197, 204, 220, 228, 236, 247, 258, 265, 281, 291, 301, 326, 345, 355] b) Comparison of experimental data with the extended model prediction with expanded scale in the melt c) Comparison of experimental data with the extended model with expanded scale in the glass

12.3.2 Viscosity of the Na_2O-B_2O_3 system

The system Na_2O-B_2O_3 is the best–investigated system for the study of the "*Boron-Alkali Anomaly*". Thus, many researchers measured the viscosity using the rotating viscometer [112, 157, 265], vibration viscometer [71], counter-balanced [281] and ball pulling-up [355] methods for low viscosity measurement and the penetration [206, 261, 355], beam-bending [306] and Pochettino viscometer methods [343] for high viscosities. As can be seen from Figs. 12.2-a) and b), two maxima in viscosity are observed in the viscosity data measured from melt to glass regions. As mentioned earlier, it is well-known that stable clusters at the tetraborate composition, Na:B = 1:4, and diborate composition, Na:B = 1:2, were proposed based on studies by Raman and Infrared spectroscopy, ^{11}B NMR, X-ray and neutron diffraction [45]. The glass-transition

temperature is defined as the temperature corresponding to a viscosity of 10^{13} poise. Chryssikos et al. [32, 33, 358] systematically investigated the structure of alkali(A = Li, K, Na, Rb, Cs) and alkaline earth(B = Mg, Ca, Sr, Ba) borates by measuring the glass-transition temperature and they observed a maximum in viscosity around the composition of X(A) = 0.33 for alkali borate and X(B) = 0.45 to 0.5 for alkaline earth borates. No temperature dependence in Eqs. (12.3) and (12.4) was applied in the previous model of Section 3.4.3 for the melt region. As shown in Fig. 3.3 of Section 3.4.3, the viscosities measured above 700°C were reproduced by considering only the tetraborate clusters MB_4. At 600°C in Fig. 12.2-b), the maximum has been shifted from the tetraborate to the diborate composition. It appears that the relative tendencies for the formation of the stable tetraborate (NaB_4) and diborate (NaB_2) clusters shift with temperature. Therefore, we considered the formation of two clusters, tetraborate (NaB_4) and diborate (NaB_2), by assigning Gibbs energy parameters for the formation of these clusters along with the activation energies given with temperature dependence as shown in Eqs. (12.3) and (12.4). In Figs. 12.2-a) and b), most of the data show an excellent agreement with the calculated lines at all temperatures except for the data of Visser and Stevels [343] at 350 and 450°C. Their data show higher values than the other data measured at the same temperatures. Visser and Stevels [343] measured the viscosity using the Pochettino viscometer, used mostly for polymer melts having low viscosity. The viscosity measurement outside the optimum range for each viscometer method would cause a large error. Sasek et al. [265] measured the viscosity using the rotating viscometer method in the temperature range from 500 to 1200°C. As shown in Fig. 12.2-a), their data measured in the temperature range from 600 to 1200°C show good agreement with the predicted viscosities and the other data within the experimental error limits. The data measured at 500°C show good agreement with the data of Nemilov [206] up to $X(Na_2O)$ = 0.3, while the data measured at $X(Na_2O)$ = 0.33 are much lower than the predicted viscosities. In addition the data of Sasek et al. [265] shows an inconsistency for the maximum viscosity at $X(Na_2O)$ = 0.33. As mentioned earlier, the optimum measurement range for the rotating viscometer method is in the viscosity range of -1 to 5 in the logarithm poise scale. Again, viscosity measurements outside the optimum range for each viscometer method would result in large errors.

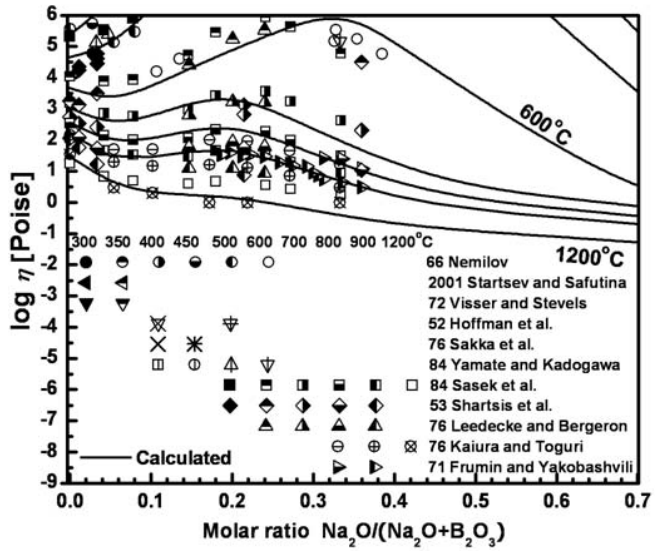

a)

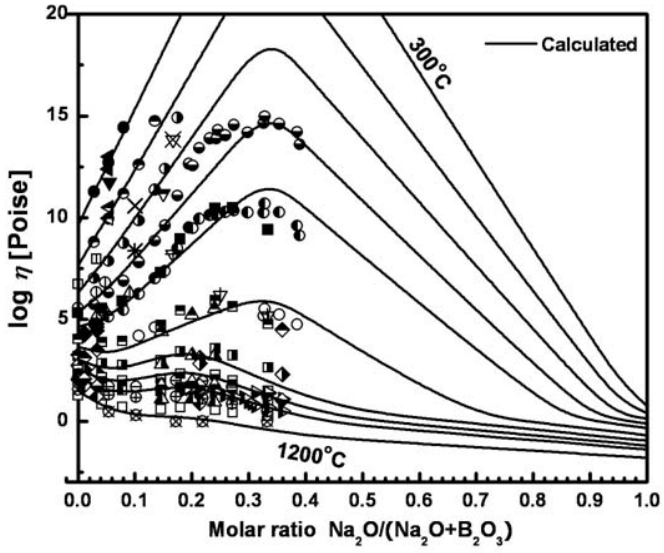

b)

Fig. 12.2 a) Calculated viscosity in Na_2O-B_2O_3 system compared to experimental data [71, 95, 112, 157, 206, 261, 265, 281, 306, 343, 355] with expanded scale b) Compares experimental data with the extended model

12.3.3 Viscosity of the K_2O-B_2O_3 system

The system K_2O-B_2O_3 has also been investigated by many researchers using the rotating viscometer [148, 157, 258], counter-balanced [35, 281, 326] and ball pulling-up methods [355] for low viscosity measurement and the penetration method [112, 355] for high viscosity measurements. Unfortunately, viscosity data measured at the composition of $X(K_2O) = 0.33$ in the temperature range from 350 to 600°C are not available, but we can see that the viscosity data show a maximum near the composition $X(K_2O) = 0.2$ in the temperature range from 700 to 1000°C. As shown in Fig. 2 of the previous paper [26], the viscosities measured above 700°C were reproduced by considering only the tetraborate clusters MB_4. Viscosities calculated at 600°C using the previous model of Sections 3.4.2 and 3.4.3 are shown in Fig. 12.3-a). It can be seen that the previous model is not able to reproduce the data of Yamate and Kadogawa [355] measured at 600°C. It seems that, similarly to the Na_2O-B_2O_3 system, the viscosity maximum shifts with decreasing temperature from the tetraborate towards the diborate composition. Accordingly, we included parameters for diborate formation in the model as in the case of the Na_2O-B_2O_3 system. The predicted viscosities reproduce well most of the viscosity data at all temperatures within the experimental error limits.

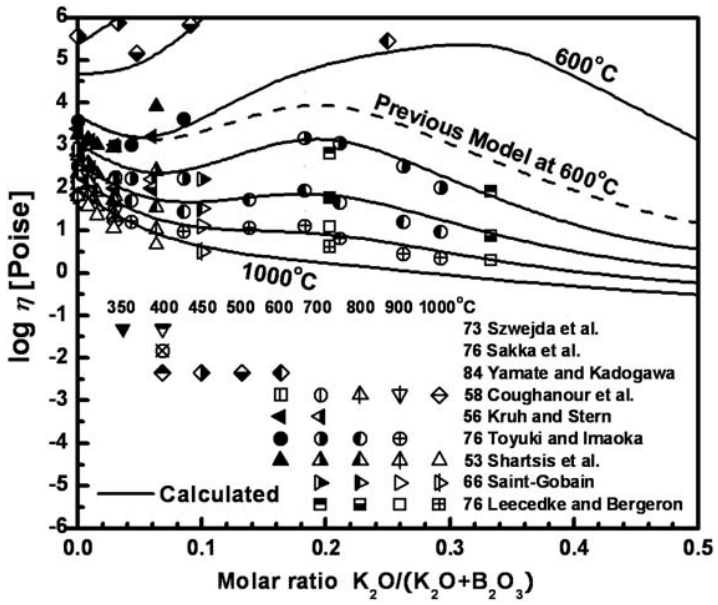

a)

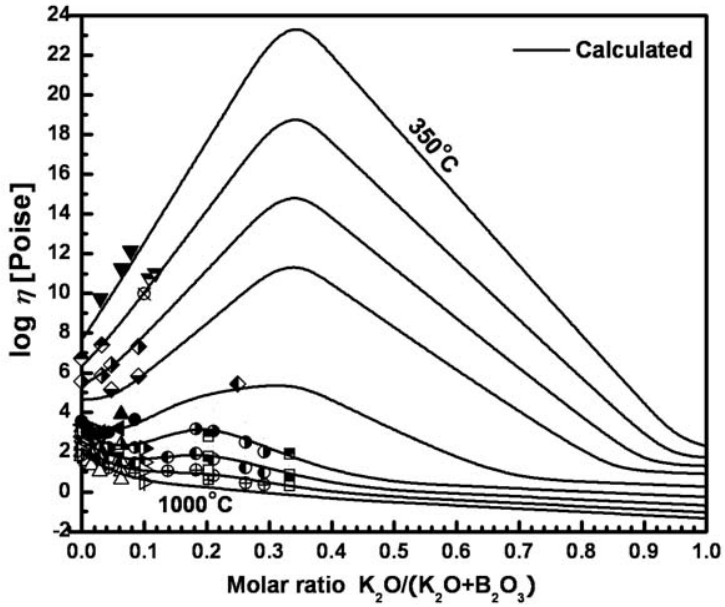

b)

Fig. 12.3 a) Calculated viscosity in K_2O-B_2O_3 system compared to experimental data [35, 112, 148, 157, 258, 281, 315, 326, 355] with expanded scale and to the lines calculated (dashed line) using the previous model of Sections 3.4.2 and 3.4.3 at 600ºC, b) Comparison of experimental data with the extended model

12.3.4 Viscosity of the CaO-B_2O_3 system

The viscosity of the system CaO-B_2O_3 in the glass region was directly measured only by Nemilov [205] using the penetration method. Klyuev and Pevzner [133] determined the glass transition temperature of the CaO-B_2O_3 system using dilatometry curves. It is well-known that the viscosity of glasses at the glass transition temperature is appromimately 10^{13} poise. As mentioned earlier, we optimized the Gibbs energy for the formation of CaB_2O_4 as a solid-like cluster and the extended model including this cluster shows good agreement with experimental data at low temperatures. In the previous model of Sections 3.4.2 and 3.4.3, we did not apply the formation of solid-like clusters for the CaO-B_2O_3 binary system. In Fig. 12.4, we show calculated viscosities at 700 and 1200ºC using the previous model with the model parameters taken from the previous studies [27, 26], and compare to calculations of the extended model. The previous

model could not reproduce the viscosity data measured at low temperatures such as 700ºC, while the calculated line of the previous model [27, 26] at 1200ºC is comparable with that of the extended model as shown in Fig. 12.4. Istomin et al. [101] measured viscosities using the vibration viscometer method and their data are lower than the calculated lines. Their reported lower viscosity may have been caused by incomplete dehydration of the melts. A significant reduction of the viscosity of pure B_2O_3 by the effect of residual water in the sample was reported by Istomin et al. [101].

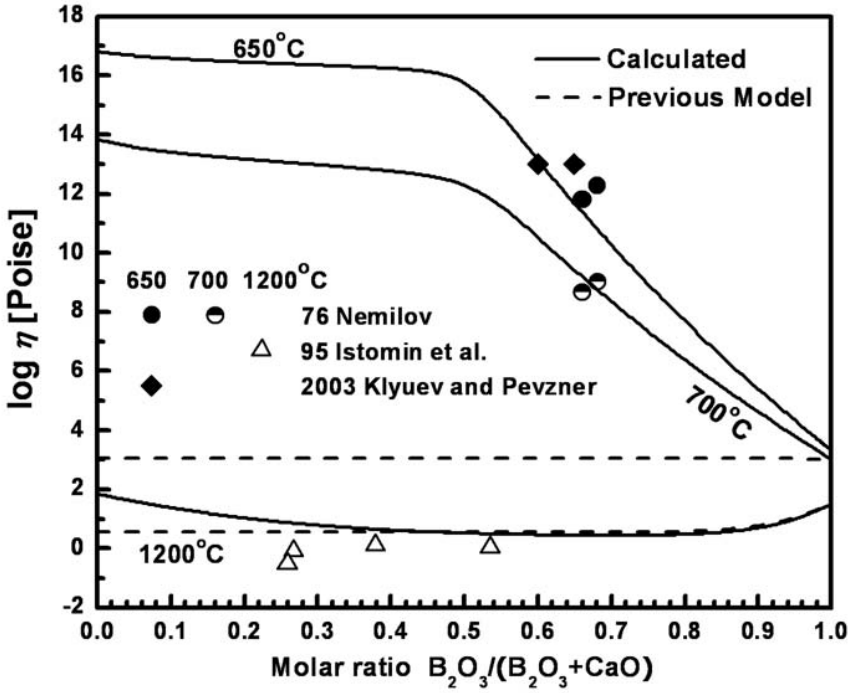

Fig. 12.4 Calculated viscosity in $CaO\text{-}B_2O_3$ system compared to experimental data [101, 133, 205] and to the line calculated (dashed line) using the previous model of the Sections 3.4.2 and 3.4.3 at 700 and 1200ºC

12.3.5 Viscosity of the $PbO\text{-}B_2O_3$ system

The viscosity of the system $PbO\text{-}B_2O_3$ was measured by many researchers using the rotating viscometer [55, 210], vibration viscometer [300] and counter-balanced methods [55] for low viscosity measurement and the fiber-elongation [74, 241], compression [86], beam-bending

[131] and penetration methods [210] for high viscosities. From phase diagram data, Geller and Bunting[76] reported $PbO{\bullet}2B_2O_3$ as a congruently melting composition. In addition, De Luca et al. [39] measured viscosity and observed the growth of the phase $PbO{\bullet}2B_2O_3$ using a micro-photographic method. Another investigator, Habeck et al. [86] also reported that the glass melt with concentrations smaller than 10 mol% PbO in the temperature range of 256 to 335°C is a micro-heterogeneous melt including liquid and solid-like particles. This micro-heterogeneity contributed to an increase of the viscosity with increasing PbO contents. We compared the lines calculated at 600ºC by the extended model and the previous model of Sections 3.4.2 and 3.4.3 in Fig. 12.5. As can be seen from this figure, the previous model is not able to reproduce the viscosity because no formation of solid-like clusters was considered. On the other hand, the extended model applied with Gibbs energies for the formation of PbB_4O_7 clusters reproduces well most of the available data at all temperatures within the experimental error limits, except for the data measured at 450°C by Habeck et al. [86] and Klyuev and Bulaeva [131]. Both authors' data show higher values than the calculated viscosities. The data of Habeck et al. [86] at 450°C show almost similar viscosities to their data [86] measured at 300°C even though the data have a similar composition (X(PbO) = 0.1 at 450°C and X(PbO) = 0.07 at 300°C). Habeck et al. [86] reported that the region of the glass melt with PbO contents equal to and larger than 10 mol% in the temperature range of 420 to 496°C was a two–liquid region. The viscosity of a two–liquid region can be significantly changed according to the amounts of each phase depending on composition. Thus, this difference could be caused by measurement in a two–liquid region. It should be noted that the extended model is intended for a single-phase melt or glass.

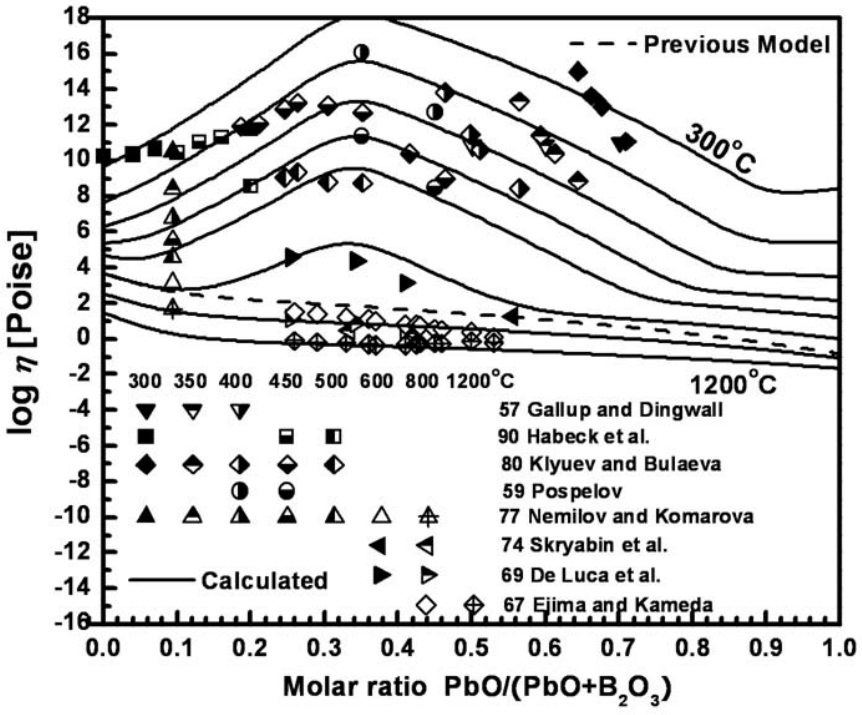

Fig. 12.5 Calculated viscosity in PbO-B_2O_3 system compared to experimental data [39, 55, 74, 86, 131, 210, 241, 300] and to the line calculated (dashed line) using the previous model of the Sections 3.4.2 and 3.4.3 at 600ºC

12.3.6 Viscosity of the Al_2O_3-B_2O_3 system

The viscosity of the system Al_2O_3-B_2O_3 was measured only by Musikhin et al. [197] using the vibration viscometer method in the temperature range from 1200 to 1500°C. Neither structural data nor viscosity data exist in the glass region. No reliable phase diagram information which can support the existence of solid-like clusters is available. However, ternary data such as for the systems B_2O_3-Al_2O_3-CaO and B_2O_3-Al_2O_3-PbO required binary non-Arrehnian parameters, $T_{AlO_{1.5}\text{-}B}$ and $n_{AlO_{1.5}\text{-}B}$, to be reproduced by the extended model in the glass region. In addition, Klyuev and Pevzner [130, 132] measured the glass-transition temperature corresponding to the viscosity 10^{13} poise in the system B_2O_3-Al_2O_3-Na_2O. They reported that the glass-transition temperature at constant Na_2O = 0.085, 0.15 and 0.22 shows maximum values in

the composition range from $X(Al_2O_3)$ = 0.4 to 0.5 as shown in Fig. 12.6. This implies that the viscosity of the B_2O_3-Al_2O_3 system on the isothermal section will increase with addition of Al_2O_3 and show a maximum in viscosity around $X(Al_2O_3)$ = 0.4 to 0.5. Thus, the binary non-Arrhenian parameters, $T_{AlO_{1.5}\text{-}B}$ and $n_{AlO_{1.5}\text{-}B}$ were applied to take into account the high viscosity of the system containing B_2O_3 and Al_2O_3 at low temperatures as shown in Eq.(12.9). With the addition of these parameters, the extended model shows an excellent agreement with the viscosity data as shown in Fig. 12.7.

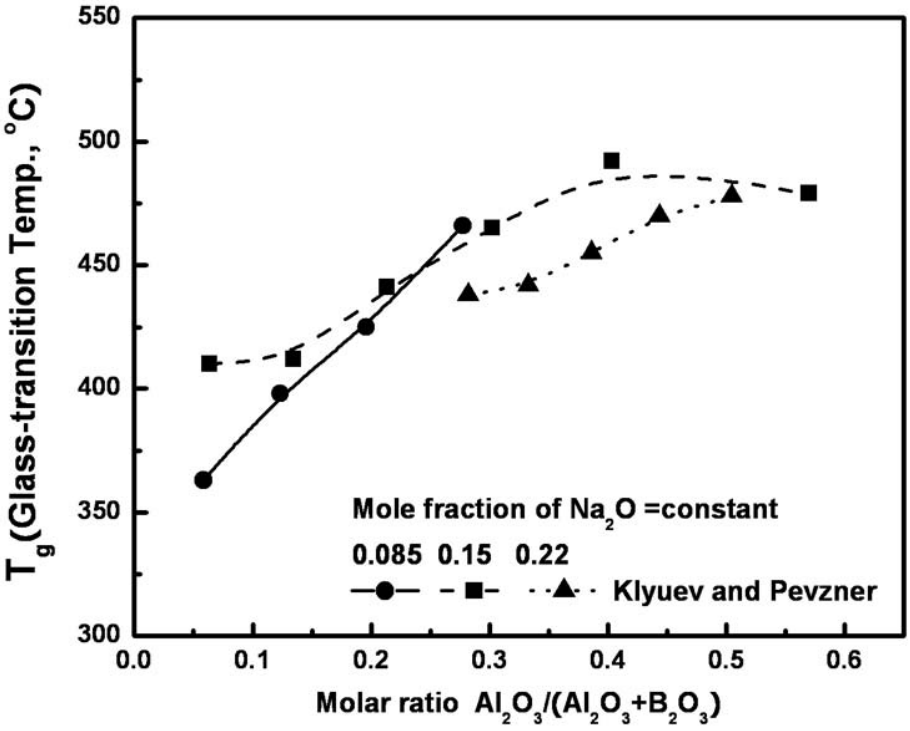

Fig. 12.6 T_g (Glass-transition Temp.) data at 8.5 mol%, 15 mol% and 22 mol% Na_2O in the system B_2O_3-Al_2O_3-Na_2O [130, 132]

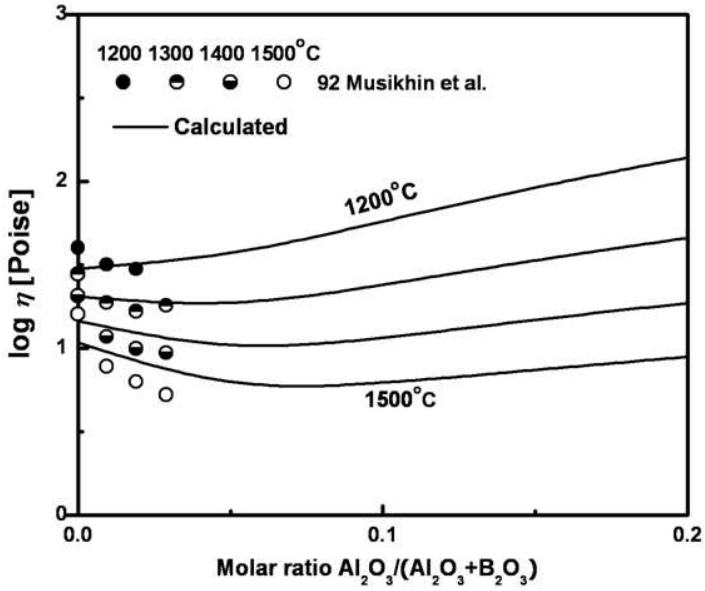

Fig. 12.7 Calculated viscosity in the Al_2O_3-B_2O_3 system compared to experimental data [197]

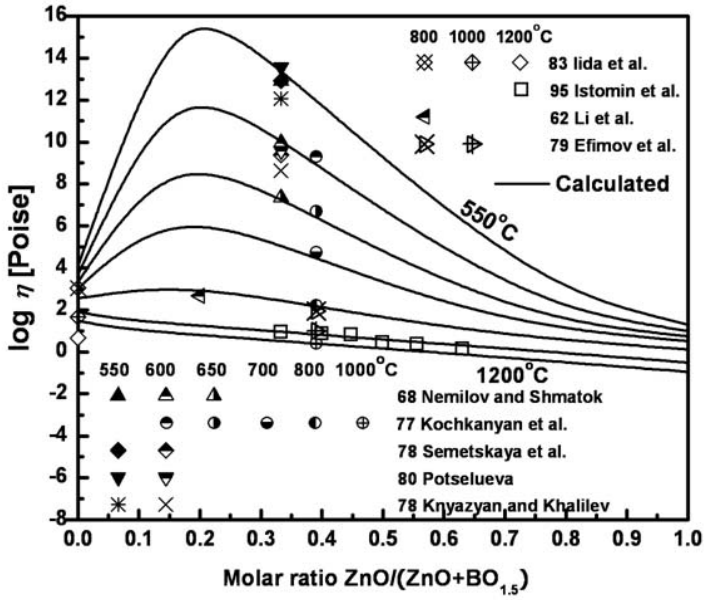

Fig. 12.8 Calculated viscosity in the ZnO-$BO_{1.5}$ system compared to experimental data [50, 100, 101, 135, 136, 162, 211, 244, 276]

12.3.7 Viscosity of the ZnO-B_2O_3 system

The viscosity of the system ZnO-B_2O_3 was measured by many researchers using the rotating viscometer [162], vibration viscometer [50, 101] and oscillating viscometer methods [100] for low viscosity measurement and the fiber-elongation [244], beam-bending [244] and penetration methods [135, 136, 211, 276] for high viscosities. No reliable phase diagram is available for ZnO-B_2O_3. As can be seen from Fig. 12.8, there are only two compositions with experimental data at low temperatures. The viscosities of the ternary ZnO-PbO-B_2O_3 system measured by Kochkanyan et al. [136] as shown in Figs. 12.24 to 12.26 were also considered for modeling the Gibbs energy of formation of the solid-like clusters. The ternary data suggested the formation of ZnB_4O_7 at low temperatures even though the data show systematic experimental errors. The extended model applied with Gibbs energies for the formation of ZnB_4O_7 show good agreement with most available data at all temperatures within the experimental error limits.

12.3.8 Viscosity of the MgO-B_2O_3 system

For the system of MgO-B_2O_3, no viscosity data exist. As mentioned earlier, Chryssikos et al. [32, 33, 358] systematically investigated the structure of alkaline earth (M = Mg, Ca, Sr, Ba) borates by measuring the glass-transition temperature and they observed a maximum in viscosity around the composition X(M) = 0.45 to 0.5 for alkaline earth borates. Therefore, we assumed that the MgO-B_2O_3 system would form similar solid-like clusters as the CaO-B_2O_3 system and so we estimated that the Gibbs energies for the formation of MgB_2O_4 for the extended model are the same as for CaB_2O_4 clusters.

12.3.9 Viscosity of the Borosilicates (B_2O_3-SiO_2)

The viscosities of the B_2O_3-SiO_2 system were measured by several investigators using the vibration viscometer [197], oscillating viscometer [100], and rotating viscometer methods [8, 337] for low viscosities and the compression [180] and fiber-elongation methods [225] for high viscosities in the temperature range from 300 to 1800°C as shown in Fig. 12.9. Without additional binary parameters, the calculated viscosities of the extended model show excellent agreement with all experimental data at all temperatures within the experimental error limits. It should be noted that, most importantly, the model takes into account the formation of the borosilicate network which has a profound effect on the viscosity as shown in Eqs. (3.7) to (3.9).

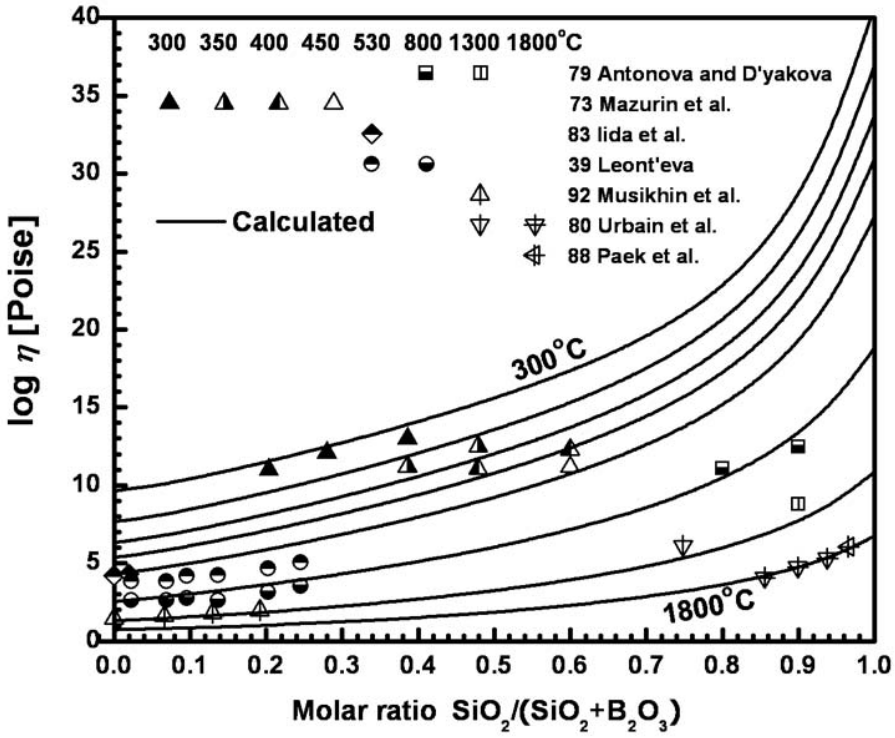

Fig. 12.9 Calculated viscosity in the B_2O_3-SiO_2 system compared to experimental data [8, 100, 161, 180, 197, 225, 337]

12.3.10 Viscosities of ternary systems

The viscosities of ternary systems containing B_2O_3 are predicted by the extended model using the model parameters describing the viscosities of pure oxides and the binary parameters for MO_x–$BO_{1.5}$ and MO_x–SiO_2 melts taken from the previous studies [27], Tables 11.1-11.3 and 12.1. No additional ternary parameters are used. Hence, the agreement of experimental data and calculated lines in the figures from this section is not the result of fitting, but rather an indication of how well the model can predict the viscosity of ternary systems.

The predicted viscosities for the Na_2O–K_2O–B_2O_3 system are compared to the experimental data [95, 150, 178, 261, 343] in Figs. 12.11 to 12.13. The viscosity measurements were carried out using the counter-balanced [178], beam-bending [150], Pochettino viscometer [343], fiber-elongation [95] and penetration methods [261]. As can be seen from Fig. 12.11, the

extended model reproduces the maxima at $X(B_2O_3)$ = 0.67 and 0.8 and it shows the maximum in viscosity at 600°C as shifted from $X(B_2O_3)$ = 0.8 to 0.67. In Fig. 12.11, the predicted viscosities show a good agreement with all available data at all temperatures within the experimental error limits except the data of Matusita et al. [178] at 500°C and the data of Visser and Stevels [343] at 450°C, which show much lower values than the predicted. The data of Matusita et al. [178] were measured by the counter-balanced method which is the most suitable in the viscosity range of -1 to 5 in the logarithm poise scale and the data of Visser and Stevels [343] were measured by the Pochettino viscometer method which is most suitable for measurement of low viscosity fluids. The errors of the viscosity measurements could correspond to those of measurements outside the optimum range of each method. In Figs. 12.12 and 12.13, the viscosity data of Hoffman et al. [95] and Sakka et al. [261] represent a linear relation as a function of mole fraction of alkali oxides and show an excellent agreement with the predicted viscosities, considering the scatter of the experimental data which is within 2 in the logarithmic poise scale.

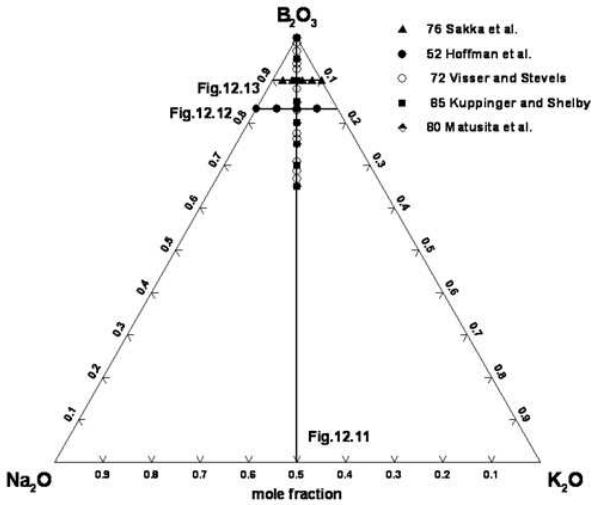

Fig. 12.10 Compositions in the $Na_2O–K_2O–B_2O_3$ system at which the viscosity was measured [95, 150, 178, 261, 343]

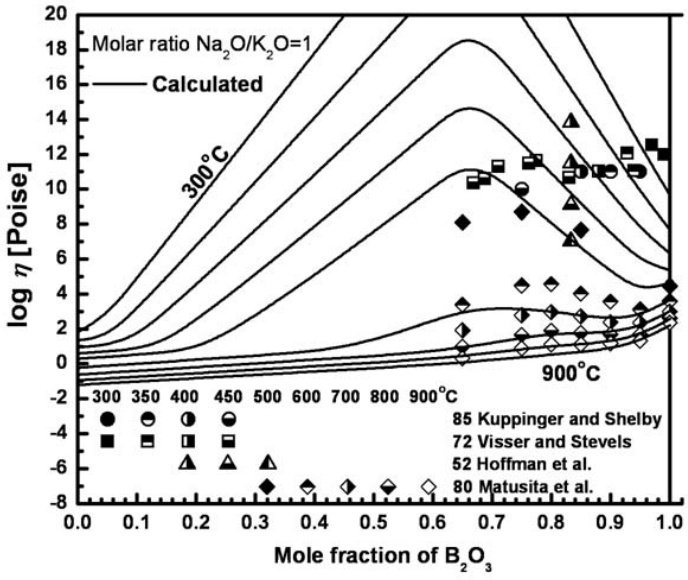

Fig. 12.11 Viscosity of the $Na_2O–K_2O–B_2O_3$ system at constant molar ratios of Na_2O/K_2O = 1: experimental points [95, 150, 178, 343] and calculated lines

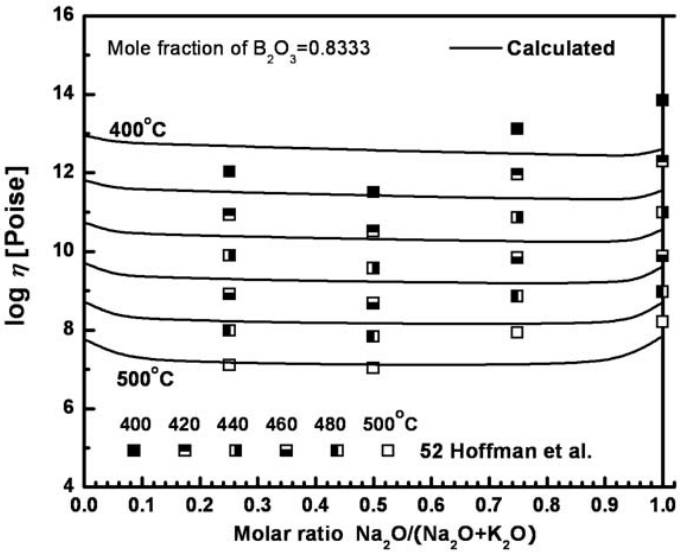

Fig. 12.12 Viscosity of $Na_2O–K_2O–B_2O_3$ system at 83.33 mol% B_2O_3: experimental points [95] and calculated lines

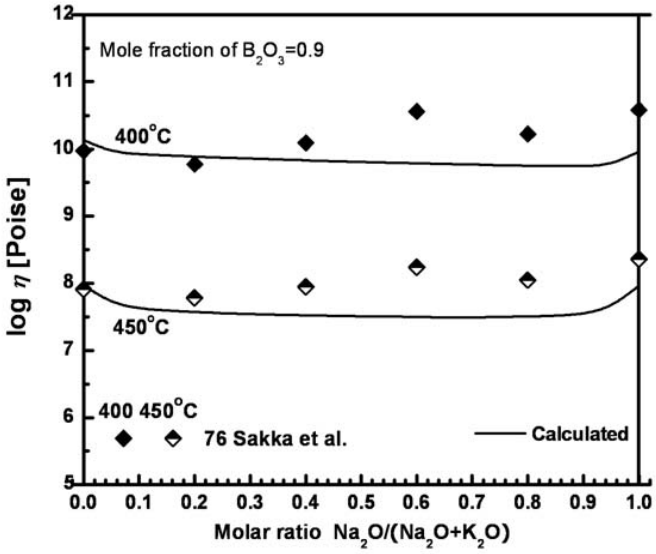

Fig. 12.13 Viscosity of the $Na_2O–K_2O–B_2O_3$ system at 90 mol% B_2O_3: experimental points [261] and calculated lines

The predicted viscosities for the $Na_2O–B_2O_3–SiO_2$ system are compared to the experimental data [51, 203, 229, 290, 316] in Figs. 12.15 to 12.16. As can be seen from these figures, the viscosity data measured in the melt region show good agreement with the predicted viscosities, while the measured viscosity data in the temperature range of 450 to 600°C are much higher than the predicted viscosities. Discussion of viscosity for alkali borosilicate glasses must begin with a consideration of the composition regions of two–phase glasses or homogeneous single–phase glasses. It is well-known that alkali borosilicate systems (alkali = Li, Na, K) have a strong tendency to phase separation below liquidus temperatures [284]. Fluegel [67] also observed systematic difference in the viscosity in the $Na_2O–B_2O_3–SiO_2$ system. He mentioned that the viscosities calculated by his model were systematically lower than the measured data in the glass-softening range [67]. The phase separation below the liquidus temperature would significantly influence the viscosity. Especially, when cooling the alkali borosilicates below the liquidus temperature, the glass formed at the borosilicate-rich side separates into silica-rich and borate-rich phases. The phase separation can be affected by the heat treatment temperature, composition and elapsed experimental time. Ehrt and Keding [51] and Pascual et al. [229] indeed measured the viscosities of phase–separated phases in the glass region. They also confirmed the existence of phase separation of silica-rich and borate-rich phase under heat treatment using a micrographic method [51, 229]. Shiraishi et al. [290] did not mention phase separation, and it is most likely that phase separation would cause systematic errors in the measurements. It should be noted that the extended model takes into account only the viscosity of single–phase glasses and melts.

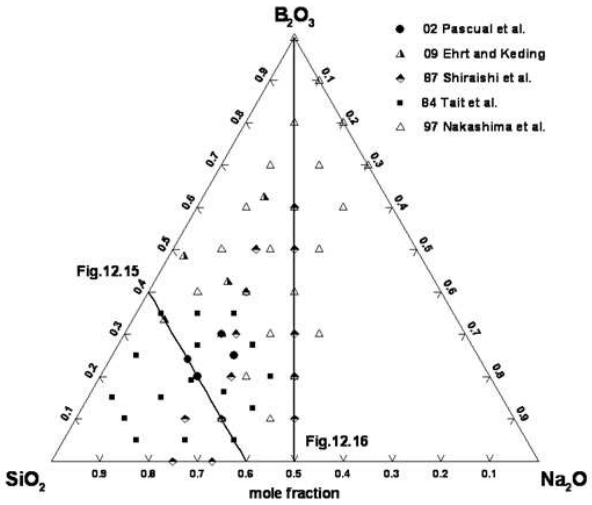

Fig. 12.14 Compositions in the Na_2O–B_2O_3–SiO_2 system at which the viscosity was measured [51, 203, 229, 290, 316]

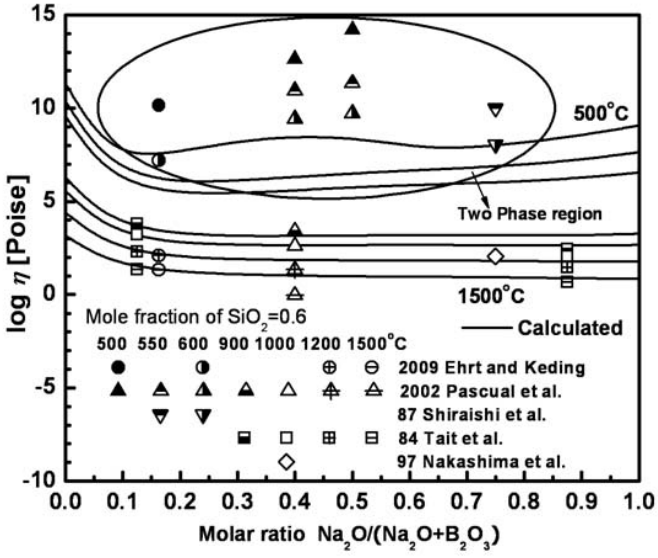

Fig. 12.15 Viscosity of the Na_2O– B_2O_3–SiO_2 system at 60 mol% SiO_2: experimental points [51, 203, 229, 290, 316] and calculated lines

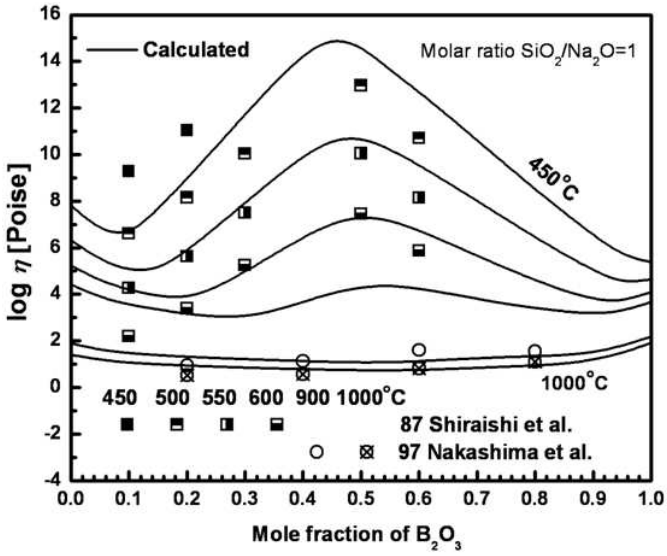

Fig. 12.16 Viscosity of the Na_2O– B_2O_3–SiO_2 system at constant molar ratios of SiO_2/Na_2O = 1: experimental points [203, 290] and calculated lines

The predicted viscosities of the B_2O_3–PbO–Al_2O_3 system are compared to the experimental data [194, 210] in Figs. 12.18 to 12.20. The viscosity measurements were carried out using the rotating viscometer [210], penetration [210] and fiber-elongation methods [194]. As can be seen from Fig. 12.18, the predicted lines of the extended model show a good agreement with all available data at all temperatures within the experimental error limits except for the data measured at Al_2O_3:PbO ratios higher than 0.162 at 450 and 500°C. The data measured at 450 and 500°C show a slightly increasing trend with the addition of Al_2O_3 and the viscosities reported at $Al_2O_3/(Al_2O_3+PbO)$ = 0.162 sharply increase and then show a slightly increasing trend with the addition of Al_2O_3. It is most likely that this abnormal increase in viscosity would be caused by crystallization of the sample during the experiment. In Figs. 12.19 and 12.20, the predicted viscosities show an excellent agreement with the viscosity data at 475°C. The extended model describes the sharp increase and decrease in viscosity with decreasing B_2O_3 and reproduces very well the viscosity data at the abrupt viscosity change of 5 to 8 orders of magnitude in the logarithm poise scale in the very narrow composition range.

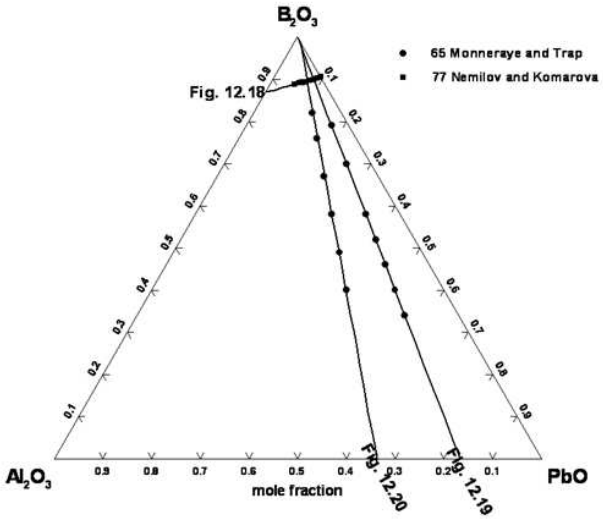

Fig. 12.17 Compositions in the B_2O_3–PbO–Al_2O_3 system at which the viscosity was measured [194, 210]

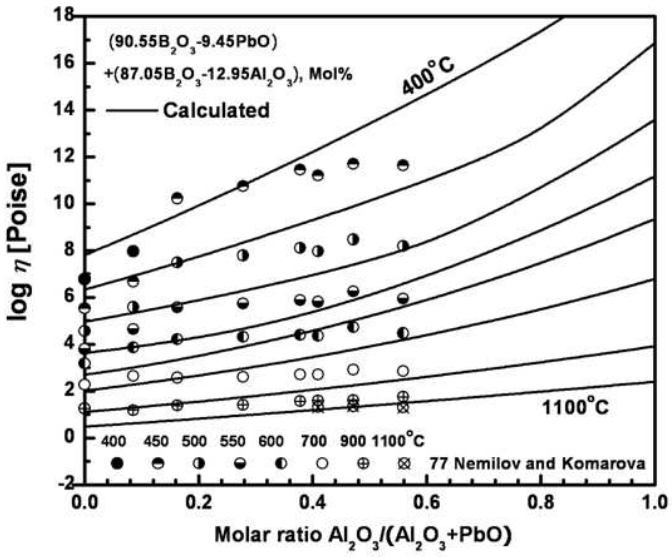

Fig. 12.18 Viscosity of the B_2O_3–PbO–Al_2O_3 system for a pseudo-binary section between the compositions (90.55 mol% B_2O_3, 9.45 mol% PbO) and (87.05 mol% B_2O_3, 12.95 mol% Al_2O_3):: experimental points [210] and calculated lines

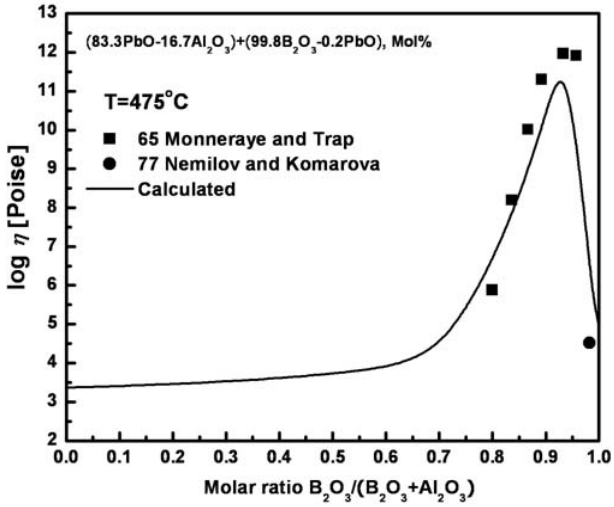

Fig. 12.19 Viscosity of the B_2O_3–PbO–Al_2O_3 system for a pseudo-binary section between the compositions (83.3 mol% PbO, 16.7 mol% Al_2O_3) and (99.8 mol% B_2O_3, 0.2 mol% PbO): experimental points [194, 210] and calculated lines

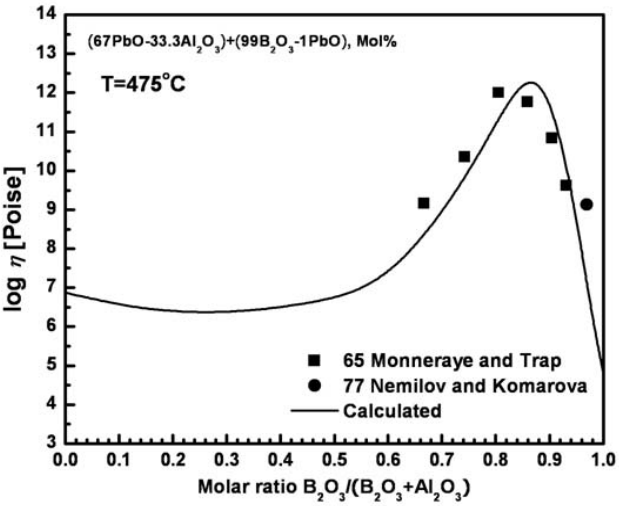

Fig. 12.20 Viscosity of the B_2O_3–PbO–Al_2O_3 system for a pseudo-binary section between the compositions (67 mol% PbO, 33.3 mol% Al_2O_3) and (99 mol% B_2O_3, 1 mol% PbO): experimental points [194, 210] and calculated lines

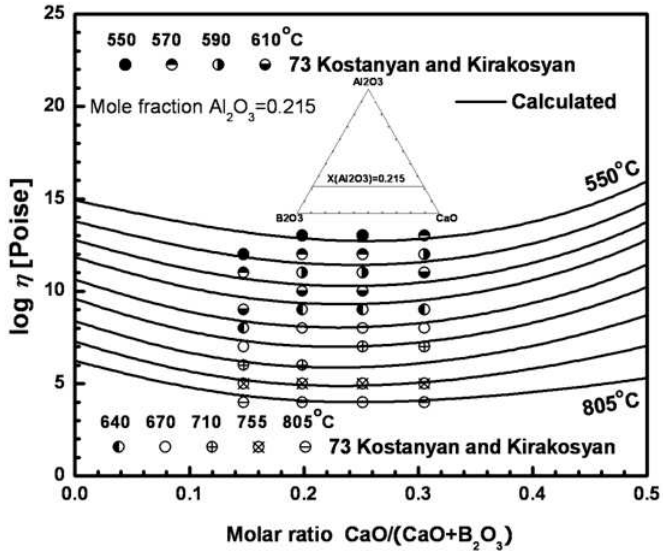

Fig. 12.21 Viscosity of the B_2O_3–CaO–Al_2O_3 system at 21.5 mol% Al_2O_3: experimental points [142] and calculated lines

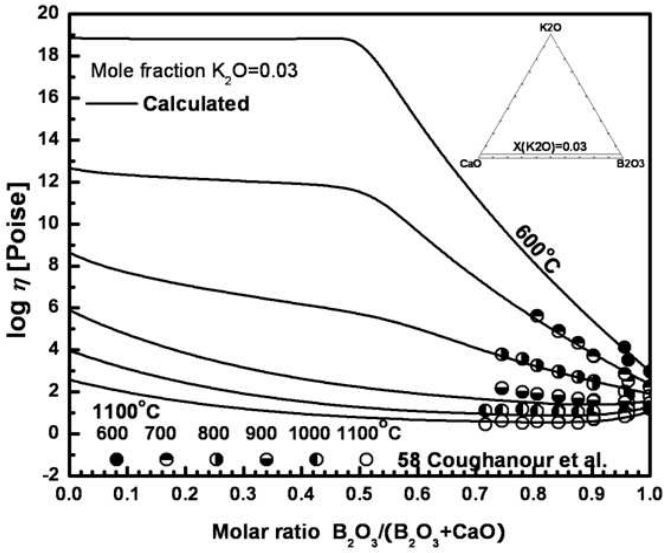

Fig. 12.22 Viscosity of the B_2O_3–CaO–K_2O system at 3 mol% K_2O: experimental points [35] and calculated lines

The viscosity of the B_2O_3–CaO–Al_2O_3 system was measured by Kostanyan and Kirakosyan [142] using the counter balanced (1 to 4 in log poise) and penetration methods (5 to 13 in log poise). The viscosity of the B_2O_3–CaO–K_2O system was measured by Coughanour et al.[35], who also measured the binary B_2O_3–K_2O system using the counter-balanced method. As can be seen from Figs. 12.21 and 12.22, the extended model reproduces the viscosity data very well from the glass to melt regions within the experimental error limits.

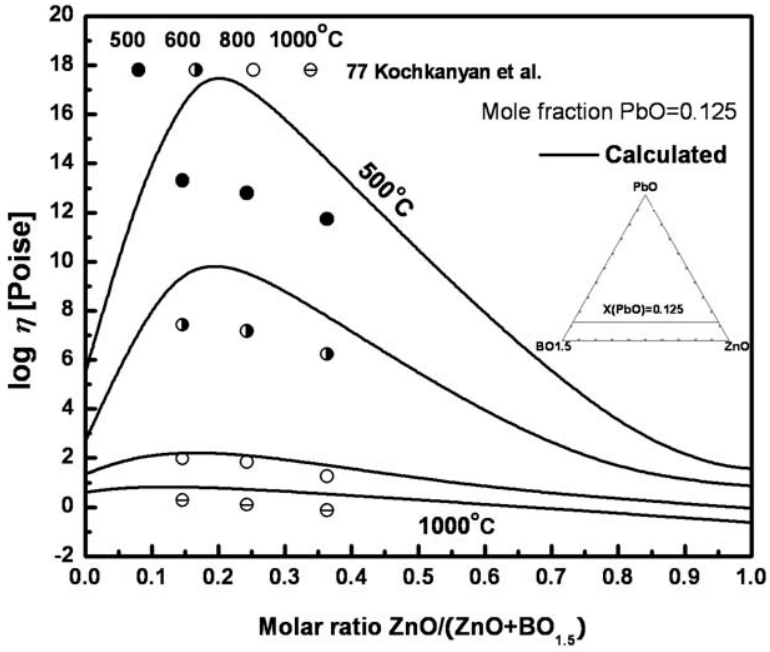

Fig. 12.23 Viscosity of ZnO-PbO-B_2O_3 system at 12.5 mol% PbO: experimental points [136] and calculated lines

The viscosity of the system ZnO-PbO-B_2O_3 was measured only by Kochkanyan et al.[136] using the rotational viscometer for the melt and the penetration method for the glasses in the temperature range of 500 to 1000°C. The Gibbs energy for the formation of solid-like clusters ZnB_4O_7 was modeled in consideration of the composition dependence of viscosities in Figs 12.8 and 12.23. As can be seen from Fig 12.23, the data measured at low temperatures are systematically lower than the predicted viscosities. Kochkanyan et al. [136] are in the same reasearch group with Saringyulyan and Kostanyan [263] and they also measured the viscosity of

the K_2O-SiO_2, PbO-SiO_2 and PbO-K_2O-SiO_2 systems and all data measured in the temperature range of 400 to 600°C were considerably lower than the other data of each system as shown in Chapter 11. They carried out temperature measurements indirectly by measuring the atmospheric temperature over the wide temperature range from 500 to 1000°C. Thus, the experimental data of Saringyulyan's group would most probably have a large systematic error source for temperature measurement due to possible differences in temperature between the sample and the furnace because of the extremely high viscosity and poor heat conduction of the sample.

12.3.11 Viscosity of Multicomponent Glasses

For multicomponent subsystems, the available experimental data in the glass industry are numerous. However, most of the data were measured within a narrow composition range because the industry mainly needs the viscosity at specific compositions in which they are interested. In the present study preference was given to extensive systematic studies. Using the unary, binary and ternary parameters taken from the previous studies [27], Tables 11.1-11.3 and 12.1, the viscosity of multicomponent systems is predicted by the extended model without any additional parameters. In the case of multicomponent systems containing B_2O_3, it was difficult to find systematic studies and thus we attempted to show how the extended model reproduces the viscosity data measured in each different system as shown in Fig. 12.25.

As shown in Fig. 12.24, a systematic study for the B_2O_3–CaO–Al_2O_3–K_2O–Na_2O system was carried out by Oshchipkov et al. [220] using the rotating viscometer and the fiber-elongation method. The extended model shows excellent agreement with all viscosity data at all temperatures within the experimental error limits. Fig. 12.25 compares the predicted viscosities with all available experimental data of subsystems of the B_2O_3–SiO_2–CaO–MgO–Al_2O_3–K_2O–Na_2O system from the glass to the melt region and the extended model predicts very well the viscosity data of multicomponent systems at all temperatures within the experimental error limits.

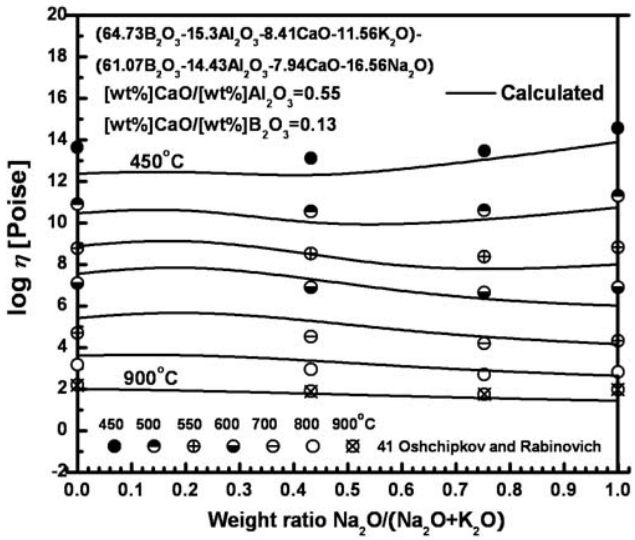

Fig. 12.24 Viscosity of B_2O_3–CaO–Al_2O_3–K_2O–Na_2O system for a pseudo-binary section between the compositions (64.73 mol% B_2O_3, 15.3 mol% Al_2O_3, 8.41 mol% CaO, 1.56 mol% K_2O) and (61.07 mol% B_2O_3, 14.43 mol% Al_2O_3, 7.94 mol% CaO, 16.56 mol% Na_2O): experimental points [220] and calculated lines

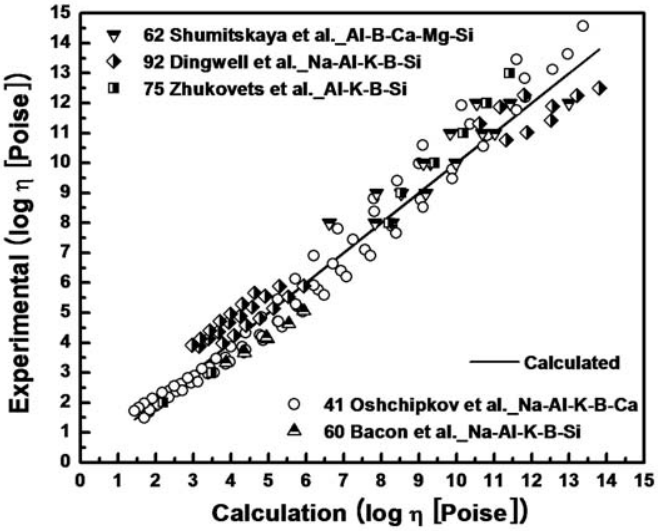

Fig. 12.25 Viscosity of subsystems of B_2O_3–SiO_2–CaO–MgO–Al_2O_3–K_2O–Na_2O system: comparison of experimental points [13, 43, 220, 293, 369] with calculation

12.3.12 Viscosity of Commercial Glasses

A large number of viscosity measurements is available for glass-forming melts in the Al_2O_3–B_2O_3–CaO–MgO–ZnO–PbO–Na_2O–K_2O–SiO_2 system around some technologically significant compositions. In particular, the compositions of typical soda-lime-silica glass melts for production of container glasses and float glasses, E-glasses, wool glasses, low-expansion borosilicate glasses and lead crystal glasses are within this nine-component system. The concentrations of additional minor components such as Fe_tO, CrO_x, or $LiO_{0.5}$ are normally less than 1 wt %. The calculation of viscosity of commercial glasses was carried out by the extended model with ignorance of the amount of these minor components.

As mentioned in Chapter 4, the commercial viscosity data were measured in a very well controlled manner using the rotating spindle, the parallel plate and the beam bending methods with well-characterized samples over very narrow composition ranges corresponding to particular types of glass. Using these viscosity data and large numbers of experimental data from the SciGlass database [37], the statistical model of Fluegel [67] was optimized and provides a rigorous estimation of error and validity limits. This model is based on multiple regression using polynomial functions and is most accurate model for the commercial glass compositions since it is calibrated based on numerous experimental data of these compositions and temperature regions.

The extended model developed in the present study, on the other hand, is designed particularly for wide-range extrapolations of composition and temperature. The experimental data for multicomponent glass melts have not been used for the calibration of our model. It is applicable at any composition contrary to the regression equations mentioned above which cannot be extrapolated outside their validity limits. It is interesting to examine how the present model compares with existing regression equations in their own ranges of validity.

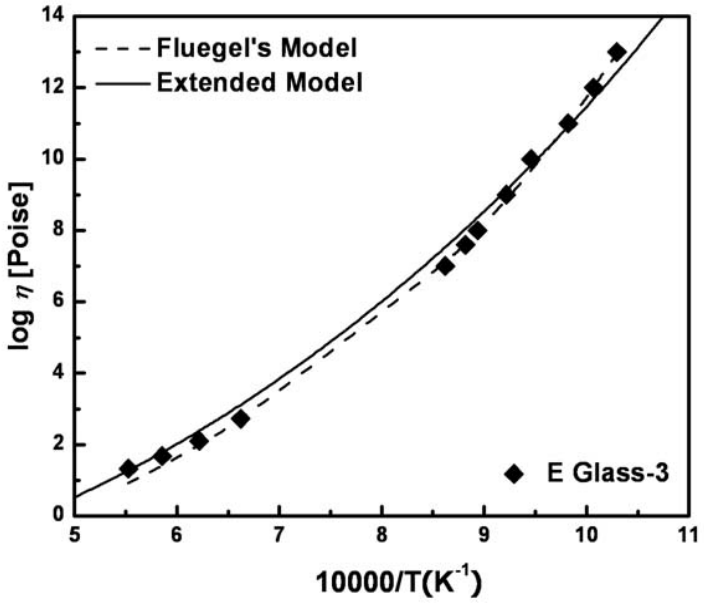
Fluegel's Model
Extended Model
E Glass-3
log η [Poise]
10000/T(K-1)

(a)

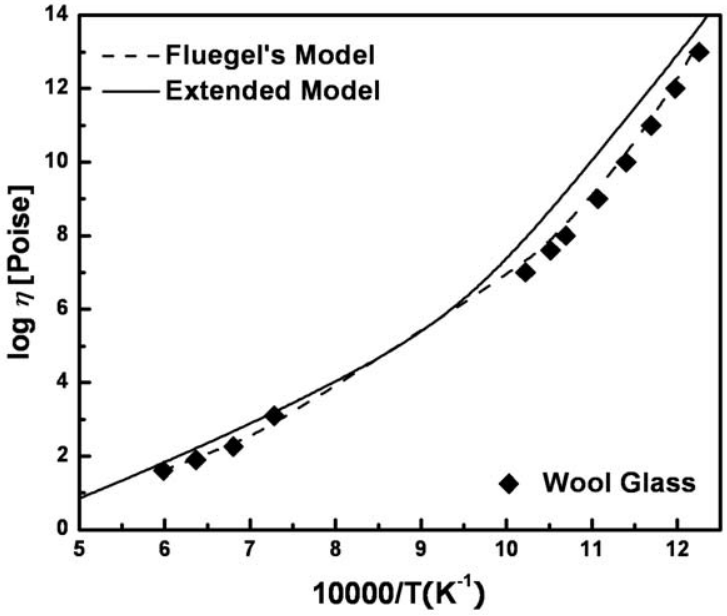
Fluegel's Model
Extended Model
Wool Glass
log η [Poise]
10000/T(K-1)

(b)

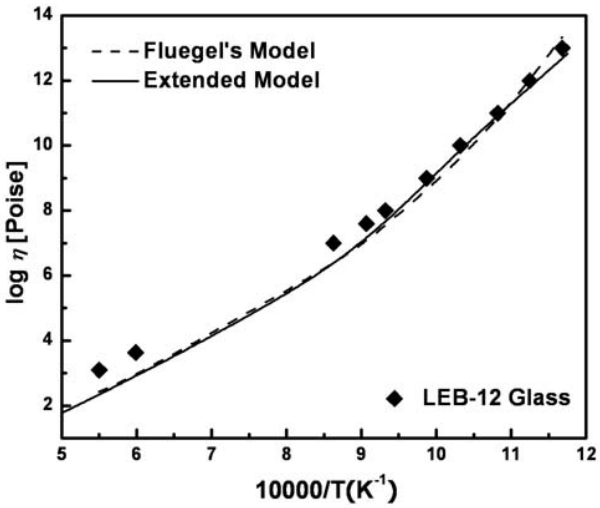

(c)

Fig. 12.26 Viscosity of E glass-3, Wool glass and Low expansion borosilicate(LEB)-12 glass: Experimental points [279] and calculated lines. Figures (a) to (c) compares the viscosity model proposed in the present study (solid lines) with the model by Fluegel [67] (dashed lines)

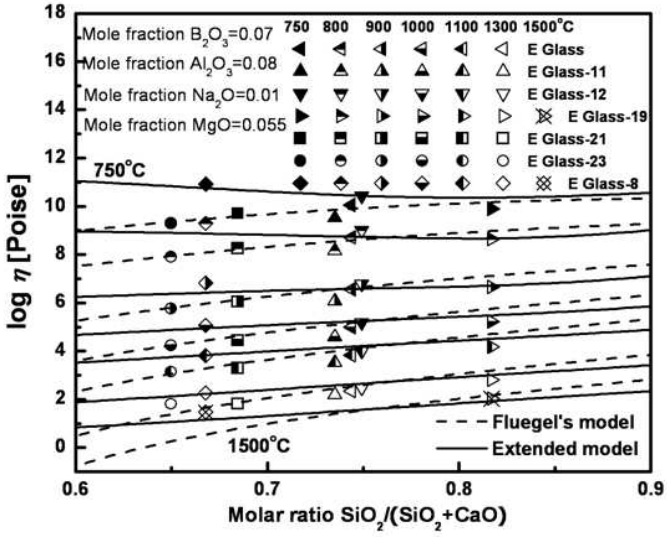

Fig. 12.27 Viscosity of E glass series: Experimental points [279] and calculated lines by the extended model(solid lines) and by Fluegel [67] (dashed lines)

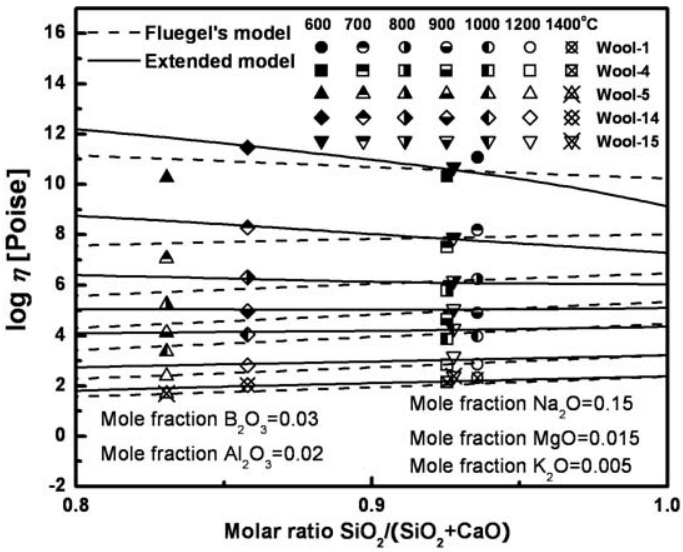

Fig. 12.28 Viscosity of wool glass series: Experimental points [279] and calculated lines by the extended model(solid lines) and by Fluegel [67] (dashed lines)

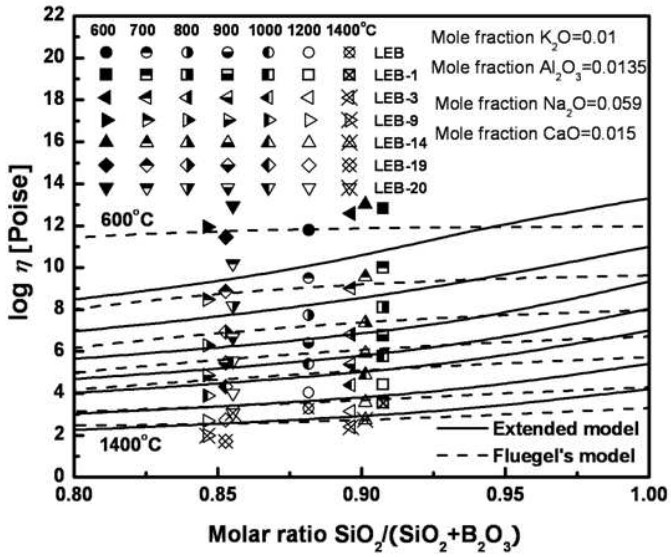

Fig. 12.29 Viscosity of low expansion borosilicate(LEB) glass series: Experimental points [279] and calculated lines by the extended model(solid lines) and by Fluegel [67] (dashed lines)

We compared the viscosity data of container and float glasses with the extended model in Chapter 11 and the extended model was in good agreement with not only the temperature but also the composition dependence. E-glass, wool glass and low-expansion borosilicate series contain up to 14 mol% boron. These predicted viscosity data were also compared with the commercial viscosity data of E-glass, wool glass and low-expansion series. As shown in Fig. 12.26, the viscosity of E glass-3, wool glass and low expansion borosilicate-12 glass were compared with the calculated lines by the extended model and the model of Fluegel [67] as an inverse function of temperature and all data show better agreement with the model proposed by Fluegel [67]. As mentioned earlier, Fluegel's model was calibrated based on numerous experimental data for these composition regions while the extended model developed in the present study was designed particularly for wide-range extrapolations of composition and temperature of the Al_2O_3–B_2O_3–CaO–MgO–ZnO–PbO–Na_2O–K_2O–SiO_2 system. However, it is seen that the extended model is able to reproduce the commercial glass viscosity data within the experimental error limits and is comparable with Fluegel's model.

E-glass series are subsystems of the Al_2O_3–B_2O_3–CaO–MgO–Na_2O–SiO_2 system as shown in Fig. 12.27 and it is seen that the viscosity data measured by one research group [279] show an experimental scatter of 1 to 1.5 in the temperature range of 750 to 900ºC and 0.5 to 1 in the logarithmic poise scale at higher temperatures. The extended model shows quite good agreement with all experimental data at all temperatures within experimental error limits and experimental scatterings.

In Fig. 12.28, wool glass series were also compared with the extended model and the model by Fluegel [67], and the model also shows a good agreement with most of the data except for the wool-5 glass. These data are systematically lower than the values predicted by both the extended model and the model of Fluegel [67]. However, allowing for the intrinsic difficulties of the viscosity measurements, the predictions of the two models show a reasonable reproducibility within the experimental error limits.

Many series of low-expansion borosilicate glasses were plotted in the present work with two models for comparison. The viscosity data are in a good agreement with the extended model predictions above 800ºC while the extended model shows systematically lower predictions than the measured data [279] in the temperature range from 600 to 700ºC. These systematic

differences could arise from phase separation because the main composition ranges of low expansion borosilicate glasses are covered by the system Na_2O–B_2O_3–SiO_2. As pointed out by Fluegel [67], phase separation can be present in the glass softening range at borosilicate-rich compositions and the model of Fluegel [67] also shows slightly lower values in the same temperature range.

12.4 Conclusions

The extended model for the viscosity of molten slags and glasses is further developed to reproduce the viscosity of glasses containing boron oxides in the CaO-MgO-Na_2O-K_2O-ZnO-PbO-Al_2O_3-SiO_2 system from the glass to the melt region within the experimental error limits.

Boron oxide is one of the best glass-forming oxides. From available viscosity data and micro-graphing studies, meta-stable solid-like clusters are seen to form preferentially in the binary MO_x-B_2O_3 glasses(M = Basic Oxides). In order to model the formation of these solid-like clusters in the glass region, we employed parameters for the Gibbs energies $\Delta G_{m(\mathrm{MB_xO_y})}$ for the formation of clusters. A total of five binary parameters are used to reproduce the viscosity data in each basic oxide-boron oxide binary system: $A^*_{\mathrm{B(MO_x)}}$, $E^*_{\mathrm{B(MO_x)}}$, m, $\Delta G_{m(\mathrm{MB_xO_y})}$ and $E_{m(\mathrm{MB_xO_y})}$. The average size of the cluster, m, was optimized differently according to the binary MO_x-B_2O_3 glass.

Only the model parameters A_{B}, E_{B}, T_{B} and n_{B} for pure B_2O_3 ,and $T_{\mathrm{AlO_{1.5}\text{-}B}}$ and $n_{\mathrm{AlO_{1.5}\text{-}B}}$ for the binary Al_2O_3-B_2O_3 system were applied to the extended model to reproduce the non-Arrhenian viscosity behavior of the systems containing B_2O_3.

The extended model is able to reproduce viscosity data not only in the melt region but also in the glass region within experimental error limits, and is comparable with the previous model in the melt region.

The available viscosity data for the sub-systems of the B_2O_3-CaO-MgO-Na_2O-K_2O-ZnO-PbO-Al_2O_3-SiO_2 system have been reviewed. It is demonstrated that the extended model reproduces the experimental data for the binary and ternary glasses and predicts the viscosities of multicomponent glasses within experimental error limits. In particular, the extended model can be used to provide good estimates of the viscosities of multicomponent glasses and commercial glasses. Most importantly, the extended model is believed to reproduce not only the temperature

dependence but also the composition dependence of available viscosity data within experimental error limits.

Table 12.1 Optimized parameters for the boron containing systems

Additional parameters for pure B_2O_3: $T_B = 520K$, $n_B = 4$, $A_B = -4.7$, $E_B = 70000\,\mathrm{J\cdot mol^{-1}}$.

Cluster (MB_x) or System	$\Delta G_{m(MB_xO_y)} = a + bT$ (J/mol)	$\log \eta_{m(MB_xO_y)} = A_{m(MB_xO_y)} + \frac{E_{m(MB_xO_y)}}{RT}$ (in poise) $E_{m(MB_xO_y)} = \alpha + \beta T$ (J/mol)	m (Cluster Size)	T (Kelvin), n
$NaB_4O_{6.5}$	$-9047.15 - 8.368T$	$A_{m(NaB_4O_{6.5})} = -3.703$ $E_{m(NaB_4O_{6.5})} = 84992\text{-}14.15T$	5	–
$KB_4O_{6.5}$	$-8210.35 - 8.368T$	$A_{m(KB_4O_{6.5})} = -3.026$ $E_{m(KB_4O_{6.5})} = 171862\text{-}104.03T$	5	–
$NaB_2O_{3.5}$	$-66651 + 57.9T$	$A_{m(NaB_2O_{3.5})} = -3.656$ $E_{m(NaB_2O_{3.5})} = 302777\text{-}258.77T$	10	–
$KB_2O_{3.5}$	$-69413 + 62T$	$A_{m(KB_2O_{3.5})} = -3.321$ $E_{m(KB_2O_{3.5})} = 326204\text{-}292.56T$	10	–
PbB_4O_7	$-57614 + 46.82T$	$A_{m(PbB_4O_7)} = -3.421$ $E_{m(PbB_4O_7)} = 152004\text{-}80.8T$	10	–
CaB_2O_4	$-271960 + 230.12T$	$A_{m(CaB_2O_4)} = -4.181$ $E_{m(CaB_2O_4)} = 492926\text{-}362.5T$	1	–
MgB_2O_4	$-108784 + 83.68T$	$A_{m(MgB_2O_4)} = -3.538$ $E_{m(MgB_2O_4)} = 427782\text{-}293.26T$	1	–
ZnB_4O_7	$-108789 + 104.605T$	$A_{m(ZnB_4O_7)} = -1.692$ $E_{m(ZnB_4O_7)} = 395231\text{-}283.85T$	1	–
$AlO_{1.5}$–$BO_{1.5}$	–	–	–	$T_{AlO_{1.5}\text{-}B} = 1600$ $n_{AlO_{1.5}\text{-}B} = 3.2$

CHAPTER 13 CONCLUSIONS

Recently, a new viscosity model for the viscosity of single-phase oxide melts was developed in this laboratory and calibrated using available viscosity data for the system CaO-MgO-K_2O-Na_2O-Al_2O_3-SiO_2-B_2O_3 [27, 81, 82]. In this model, the viscosity is related to the structure of the melt characterized by the amounts and connectivity of Q^i-species. The structure in turn is calculated from the thermodynamic description of the melt using the Modified Quasichemical Model [231, 232] and the FactSage thermodynamic database [14]. Most importantly, the model takes into account the formation of the silicate or borate network which has a profound effect on the viscosity. For each Al_2O_3-containing ternary system MO_x–Al_2O_3–SiO_2 exhibiting the Charge Compensation Effect (where Al^{3+} assumes a tetrahedral coordination and enters the silica network with a basic cation M staying close to Al^{3+} to compensate the missing charge) the model incorporates two additional ternary parameters. The viscosity of multi-component melts CaO-MgO-K_2O-Na_2O-Al_2O_3-SiO_2-B_2O_3 [27, 81, 82] is then predicted by the model without any additional adjustable model parameters and in good agreement with the model within experimental error limits except for systems containing alkali oxides.

In the present work, the model is modified to reproduce the complex behavior of the viscosity on the alkali-rich side of the alkali-silica systems. This behavior is attributed to ring clusters formed by Q^2- and Q^3-species. An excess contribution to the viscosity due to polymerization of Q^2- and Q^3-species into large rings is taken into account by the introduction of one additional binary parameter for each alkali-silica system. The viscosity of binary, ternary and higher-order oxide melts containing alkali oxides is calculated by the model without any additional adjustable model parameters and is in good agreement within experimental error limits.

Also, in the present work, with the modified model, the viscosity of oxide melts containing PbO, ZnO, MnO and TiO_x have been reviewed. Only 6 model parameters related to each MO_x (M = Pb, Zn, Mn) are required. Available experimental viscosity data of all sub-systems of the SiO_2–Al_2O_3–CaO–MgO–Na_2O–K_2O–PbO–ZnO–MnO–TiO_x system were collected and used to calibrate the model. The deviation of the available experimental data from the viscosities predicted by the model does not exceed the scatter of experimental points among different authors. In particular, the model predicts the viscosity of multicomponent silicate melts

and commercial glass melts with an accuracy similar to the accuracy of regression equations which have been fitted by Flugel [67] to the experimental data over narrow composition ranges.

The model has also been extended in the present work to describe and predict the viscosities of oxy-fluoride melts containing MF_x (M = Ca, Mg, Na, K and Al). Structural roles of MF_x (M = Ca, Mg, Na, K and Al) are reviewed and regarded as network modifiers in silicate and borate melts and simply approximated to have the same breaking effects on the silicate or borate networks as basic oxides containing the same cations. For the systems MF_x, MF_x-SiO_2 and MF_x-B_2O_3 (M = Ca, Mg, Na, K and Al), the same kinds of unary and binary parameters developed in the oxide model were applied. No charge compensation effect between MF_x and Al_2O_3 is observed, and thus the model reproduces the experimental data for binary and ternary melts without applying any charge compensation effect between MF_x and Al_2O_3. In order to take into account the *"Borate Anomaly"* for each MF_x-B_2O_3 melt, where MF_x is an alkali fluoride, the formation of solid-like clusters at the tetraborate composition was employed in the model. The available viscosity data for all sub-systems of MF_x–SiO_2–B_2O_3–Al_2O_3–CaO–MgO–Na_2O–K_2O–PbO–MnO–TiO_y melts (M = Ca, Mg, Na, K and Al) are critically reviewed and in good agreement within experimental error limits.

The modified model with Arrhenian temperature dependence for the viscosity of oxy-fluoride melts is further extended in the present work to take into account non-Arrhenian temperature dependence of the viscosity data measured from the glass to the melt regions. A few unary and binary non-Arrhenian model parameters were added in the model to reproduce the viscosity data of all available sub-systems of the CaO-MgO-Na_2O-K_2O-ZnO-PbO-Al_2O_3-B_2O_3-SiO_2 system within experimental error limits. In order to take into account the Charge Compensation Effect for Glasses containing Al_2O_3, two more parameters were added to the Gibbs energy function for the formation of Charge Compensated species such as $CaAl_2O_4$ or $NaAlO_2$. In order to model the formation of solid-like clusters in the binary MO_x-B_2O_3 glasses (M = Basic Oxides), Gibbs energy parameters were introduced for the formation of solid-like clusters. From a critical review of available viscosity data for the sub-systems of the CaO-MgO-Na_2O-K_2O-ZnO-PbO-Al_2O_3-B_2O_3-SiO_2 system, the extended model is believed to reproduce not only the temperature dependence but also the composition dependence of the available viscosity

data of the system CaO-MgO-Na_2O-K_2O-ZnO-PbO-Al_2O_3-B_2O_3-SiO_2 within experimental error limits.

In summary, the extended model applies over the entire temperature range from the glass region to the melt region. The viscosity model now reproduces all available viscosity data for melts and glasses for the system MF_x–SiO_2–B_2O_3–Al_2O_3–CaO–MgO–Na_2O–K_2O–PbO–ZnO–MnO–TiO_y (M = Ca, Mg, Na, K and Al) within experimental error limits at all compositions and over the temperature range from 300 to 2000ºC.

The viscosity model and databases have been programmed and included in the FactSage thermodynamic software and database [14].

REFERENCES

1. Abramov, V.N., *Theoretical principles of the Electrometallurgy of Aluminum*. 1953: Metallurgizdat, Moscow.
2. Adam, G. and J.H. Gibbs," The temperature dependence of cooperative relaxation properties in glass-forming liquids", *J. Chem. Phys.*, vol. 43, pp. 139-46, 1965
3. Ali Bouhifd, M., A. Sipp, and P. Richet," Heat capacity, viscosity, and configurational entropy of alkali titanosilicate melts", *Geochim. Cosmochim. Acta*, vol. 63, pp. 2429-2437, 1999
4. Andryukhina, T.D., et al.," Optimum content and proportion of alkaline earth oxides in glasses", *Steklo Keram.*, vol. pp. 4-5, 1978
5. Andryukhina, T.D. and G.K. Shishkin," Effect of alkali metal oxides on glass viscosity", *Steklo i Keramika*, vol. 9, pp. 11-12, 1985
6. Angell, C.A.," Relaxation in liquids, polymers and plastic crystals - strong/fragile patterns and problems", *J. Non-Cryst. Solids*, vol. 131-133, pp. 13-31, 1991
7. Angell, C.A., et al.," Relaxation in glassforming liquids and amorphous solids", *J. Appl. Phys.*, vol. 88, pp. 3113-3157, 2000
8. Antonova, S.L. and V.V. D'yakova," Study of the glass formation of two-component high-silicon borosilicate glasses synthesized by the "sol-gel" method", *Fiz. Khim. Stekla*, vol. 5, pp. 671-4, 1979
9. Artamonov, V.L., et al.," Viscosity of fluxes of the calcium fluoride-calcium oxide-magnesium oxide-aluminum oxide-silicon dioxide system", *Problemy Spetsial'noi Elektrometallurgii (1975-1984)*, vol. 5, pp. 20-1, 1976
10. Artem'ev, V.I. and A.A. Appen," Reaction of iron with three-component silicate melts", *Zh. Prikl. Khim. (S.-Peterburg, Russ. Fed.)*, vol. 38, pp. 409-11, 1965
11. Asayama, E., H. Takebe, and K. Morinaga," Critical Cooling Rates for the Formation of Glass for Silicate Melts", *ISIJ Int.*, vol. 33, pp. 233-238, 1993
12. Baak, T. *The action of calcium fluoride in slags*. 1956.
13. Bacon, J.F., et al.," Viscosity and Density of Molten Silica and High Silica Content Glasses", *Phys. Chem. Glasses*, vol. 1, pp. 90-98, 1960
14. Bale, C.W., et al.," FactSage thermochemical software and databases - recent developments", *Calphad*, vol. 33, pp. 295-311, 2009
15. Bale, C.W., et al.," FactSage Thermochemical Software and Databases", *Calphad*, vol. 26, pp. 189-228, 2002
16. Basov, A.V., et al.," Density and surface tension of calcium oxide-aluminum oxide-calcium fluoride-sodium oxide melts", *Rasplavy*, vol. pp. 52-7, 1989
17. Battle, T.P. and J.P. Hager," Viscosities and Activities in Lead-Smelting Slags", *Metall. Trans. B.*, vol. 21B, pp. 501-510, 1990

18. Benesch, R., et al.," Physicochemical properties of the blast furnace slags with TiO2 addition", *Archives of Metallurgy*, vol. 40, pp. 461-74, 1995

19. Bills, P.M.," Viscosities in Silicate Slag Systems", *J. Iron Steel Inst.*, vol. 201, pp. 133-140, 1963

20. Birch, F. and E.B. Dane, *Viscosity*, in *Handbook of Physical Constants: Geological Society of America Special*. 1942. p. 131-137.

21. Bobylev, I.B., et al.," Viscosity of silicate and silicate-salt melts", *Fiz. Khim. Stekla*, vol. 6, pp. 401-407, 1980

22. Bockris, J.O.M. and D.C. Lowe," Viscosity and the Structure of Molten Silicates", *Proc. Roy. Soc. London, Ser. A*, vol. A226, pp. 423-435, 1954

23. Bockris, J.O.M., J.D. Mackenzie, and K.J. A.," Viscous Flow in Silica and Binary Liquid Silicates", *Trans. Faraday Soc.*, vol. 51, pp. 1734-1748, 1955

24. Bowen, N.L. and J.W. Greig," The System: Al2O3.SiO2", *J. Am. Ceram. Soc.*, vol. 7, pp. 238-254, 1924

25. Brockner, W., K. Toerklep, and H.A. Oeye," Viscosity of sodium fluoride-aluminum fluoride melt mixtures", *Ber. Bunsenges. Phys. Chem.*, vol. 83, pp. 12-19, 1979

26. Brosh, E., A.D. Pelton, and S.A. Decterov," A Model to Calculate the Viscosity of Silicate Melts. Part V: Borosilicate melts containing alkali oxides", *Int. J. Mat. Res., submitted*, vol. 2011

27. Brosh, E., A.D. Pelton, and S.A. Decterov," A Model to Calculate the Viscosity of Silicate Melts. Part IV: Borosilicate melts", *Int. J. Mat. Res., submitted*, vol. 2011

28. Cabral, A.A., A.A.D. Cardoso, and E.D. Zanotto," Glass-Forming Ability Versus Stability of Silicate Glasses. I. Experimental Test", *J. Non-Cryst. Solids*, vol. 320, pp. 1-8, 2003

29. Chervinskii, Y.F., S.P. Raspopin, and A.I. Nechaev," Interaction in molten mixtures of sodium and uranium fluorides", *Radiokhimiya*, vol. 27, pp. 674-6, 1985

30. Chlebik, A., R. Adams, and P.W. McMillan," The influence of composition on Hertzian fracture characteristics of soda-lime-silica glass", *Phys. Chem. Glasses*, vol. 18, pp. 59-64, 1977

31. Choi, S.-Y., et al.," Properties of F-free Glass System as a Mold Flux: Viscosity, Thermal Conductivity and Crystallization Behavior", *J. Non-Cryst. Solids*, vol. 345&346, pp. 157-160, 2004

32. Chryssikos, G.D., E.I. Kamitsos, and M.A. Karakassides," Structure of Borate Glasses. Part 2. Alkali Induced Network Modifications in Terms of Structure and Properties", *Phys. Chem. Glasses*, vol. 31, pp. 109-116, 1990

33. Chryssikos, G.D., E.I. Kamitsos, and Y.D. Yiannopoulos," Towards a structural interpretation of fragility and decoupling trends in borate systems", *J. Non-Cryst. Solids*, vol. 196, pp. 244-248, 1996

34. Chubinidze, T.A. and M.A. Kekelidze," Viscosity and electrical conductivity of melts in the manganous oxide calcium oxide-silica system at 10% alumina", *Soobshcheniya Akademii Nauk Gruzinskoi SSR*, vol. 43, pp. 667-74, 1966

35. Coughanour, L.W., L. Shartis, and H.F. Shermer," Viscosity, density, and electrical resistivity of molten alkaline earth borate glasses with 3 mole % of potassium oxide", *J. Am. Ceram. Soc.*, vol. 41, pp. 324-9, 1958

36. Cranmer, D. and D.R. Uhlmann," Viscosities in the system albite-anorthite", *J. Geophys. Res.*, vol. 86, pp. 7951-7956, 1981

37. Database, S. and I. System," vol. 2005

38. Davies, M.W. and F.A. Wright," Viscosity of calcium fluoride-based slags", *Chemistry , Industry (London, United Kingdom)*, vol. 11, pp. 359-63, 1970

39. De Luca, J.P., R.J. Eagan, and C.G. Bergeron," Crystallization of PbO2B2O3 from its supercooled melt", *J. Amer. Ceram. Soc.*, vol. 52, pp. 322-6, 1969

40. Desyatnik, V.N.," vol. 54, pp. 2035-2037, 1982

41. Dienes, G.J. and H.F. Klemm," Theory and application of the parallel plate plastometer", *J. Appl. Phys.*, vol. 17, pp. 458-71, 1946

42. Dingwell, D.B.," Shear viscosity of alkali and alkaline earth titanium silicate liquids", *Am. Mineral.*, vol. 77, pp. 270-274, 1992

43. Dingwell, D.B., et al.," The Effects of Boron Oxide on the Viscosity of Haplogranitic Liquids", *Am. Mineral.*, vol. 77, pp. 457-461, 1992

44. Dingwell, D.B., M. Pichavant, and F. Holtz, *Structural Role of Boron in Melts*, in *Reviews in Mineralogy*. 1996, Mineralogical Society of America. p. 333-341.

45. Dingwell, D.B., M. Pichavant, and F. Holtz, *Experimental studies of boron in granitic melts*, in *Reviews in Mineralogy (Boron: Mineralogy, Petrology and Geochemistry)*. 1996, Mineralogical Society of America. p. 331-385.

46. Dingwell, D.B., C. Romano, and K.-U. Hess," The effect of water on the viscosity of a haplogranitic melt under P-T-X conditions relevant to silicic volcanism", *Contrib. Mineral. Petrol.*, vol. 124, pp. 19-28, 1996

47. Donth, E., *The Glass Transition: Relaxation Dynamics in Liquids and Disordered Materials*. 2001: Springer-Verlag, Berlin, Germany. 418 pp.

48. Douglas, R.W., et al.," A penetration viscometer", *Glass Technol.*, vol. 6, pp. 52-5, 1965

49. Dyre, J.C.," Colloquium: the glass transition and elastic models of glass-forming liquids", *Rev. Mod. Phys.*, vol. 78, pp. 953-972, 2006

50. Efimov, V.N., S.A. Lyamkin, and A.M. Pogodaev. *Viscosity and density of molten borates containing zinc oxide*. 1979: Akad. Nauk SSSR, Ural. Nauchn. Tsentr, Sverdlovsk, USSR.

51. Ehrt, D. and R. Keding," Electrical conductivity and viscosity of borosilicate glasses and melts", *Phys. Chem. Glasses: Eur. J. Glass Sci. Technol., Part B*, vol. 50, pp. 165-171, 2009

52. Ehrt, D., M. Leister, and A. Matthai," Polyvalent elements iron, tin and titanium in silicate, phosphate and fluoride glasses and melts", *Phys. Chem. Glasses*, vol. 42, pp. 231-239, 2001

53. Eipeltauer, E. and A. More," Viscosity of Binary Potassium Silicate Glasses", *Radex Rundsch.*, vol. 4, pp. 230-8, 1960

54. Ejima, T., M. Hino, and M. Kameda," Surface Tension, Density and Viscosity of PbO-SiO2-LiO2 Ternary Melts", *Nippon Kinzoku Gakkaishi*, vol. 34, pp. 546-550, 1970

55. Ejima, T. and M. Kameda," Viscosity of Liquid Lead Silicate and Lead Borate", *Nippon Kinzoku Gakkaishi*, vol. 31, pp. 120-125, 1967

56. Ejima, T., et al.," Viscosity of molten alkali fluorides", *Nippon Kinzoku Gakkaishi*, vol. 51, pp. 328-37, 1987

57. Endell, K. and W. Strasmann," Effect of oxides, fluorides, chlorides, and sulfides on the temperature-viscosity relation of sodium disilicate melts", *Glastech. Ber.*, vol. 19, pp. 281-287, 1941

58. Endell, V.K. and G. Brinkmann," Influence of SiO2, TiO2 and Al2O3 on the Viscosity of a Synthetic Slags and the Calculation of the Viscosity of Acid and Basic Blast-Furnace Slags from their Chemical Composition", *Stahl und Eisen*, vol. 59, pp. 1319-1321, 1939

59. English, S.," The Effect of Composition on the Viscosity of Glass. Part II", *J. Soc. Glass Technol.*, vol. 8, pp. 205-48, 1924

60. Eppler, R.A.," Viscosity of Molten Boron Oxide", *J. Am. Ceram. Soc.*, vol. 49, pp. 679-80, 1966

61. Evseev, P.P.," Physical properties of industrial slags of a calcium oxide-aluminum oxide-calcium fluoride system", *Avtomaticheskaya Svarka*, vol. 20, pp. 42-5, 1967

62. Evstrop'ev, K.S.," Viscosity and electric conductivity of fused salts and glasses", *Bull. acad. sci. U. R. S. S., Classe sci. math. nat., Ser. phys.*, vol. 3, pp. 359-374, 1937

63. Evstrop'ev, K.S.," The structure of glass-like and salt-like liquid binary mixtures according to the data of their viscosity and the electric conductivity", *Izv. Akad. Nauk SSSR, Ser. Fiz.*, vol. 4, pp. 616-626, 1940

64. Evstrop'ev, K.S., L.L. Gutorova, and G.M. Komleva," Viscosity of titanium enamels", *Steklo i Keramika*, vol. 25, pp. 16-18, 1968

65. Fayon, F., et al.," 29Si and 207Pb NMR Study of Local Order in Lead Silicate Glasses", *J. Non-Cryst. Solids*, vol. 232-234, pp. 403-408, 1998

66. Fincham, C.J.B. and F.D. Richardson," The Behaviour of Sulphur in Silicate and Aluminate Melts", *Proc. Roy. Soc. (London)*, vol. 223, pp. 40-62, 1954

67. Fluegel, A.," Glass viscosity calculation based on a global statistical modelling approach", *Glass Technol.: Eur. J. Glass Sci. Technol., Part A*, vol. 48, pp. 13-30, 2007

68. Frischat, G.H. and C. Schrimpf," Preparation of nitrogen-containing sodium oxide-calcium oxide-silicon dioxide", *J. Am. Ceram. Soc.*, vol. 63, pp. 714-15, 1980

69. Frohberg, M.G. and W. Rohde," The Viscosity of Liquids of the System PbO-K2O-SiO2", *Glastech. Ber.*, vol. 37, pp. 453-459, 1964

70. Fromberg, B.M., Z.N. Tsyplenkova, and B.V. Rabinovich. *Viscosity of electric bulb glass of various compositions*. 1941.

71. Frumin, E.I. and S.B. Yakobashvili. *Surface tension, density, and viscosity of molten borates*. 1971: "Naukova Dumka", Kiev, USSR.

72. Fujimura, H., et al.," Effect of oxide composition on solidification structure of Ti added ferritic stainless steel", *Tetsu to Hagane*, vol. 87, pp. 707-712, 2001

73. Fulcher, G.S.," Analysis of recent measurements of the viscosity of glasses", *J. Am. Ceram. Soc.*, vol. 8, pp. 339-355, 1925

74. Gallup, J. and A.G.F. Dingwall," Properties of low-temperature solder glasses", *Am. Ceram. Soc. Bull.*, vol. 36, pp. 47-51, 1957

75. Gehlhoff, G. and M. Thomas," The physical properties of glass in relation to its composition I The electrical conductivity of glasses", *Z. Tech. Phys.*, vol. 6, pp. 544-54, 1925

76. Geller, R.F. and E.N. Bunting," System PbO-B2O3", *J. Res. Natl. Bur. Stand. (U. S.)*, vol. 18, pp. 585-93 (Research Paper No. 995), 1937

77. Giordano, D., J.K. Russell, and D.B. Dingwell," Viscosity of magmatic liquids: A model", *Earth Planet. Sci. Lett.*, vol. 271, pp. 123-134, 2008

78. Gladkii, V.N., E.A. Kapustin, and N.T. Shevelev," Viscosity of calcium fluoride melt", *Izvestiya Akademii Nauk SSSR, Metally*, vol. 5, pp. 52-5, 1985

79. Goncharov, A.E., A.I. Manakov, and P.K. Kovalev," Surface tension, density, viscosity, and electrical conductivity of calcium fluoride-based fluxes", *Tr. Inst. Metall., Akad. nauk SSSR, Ural'skii Nauchn. Tsentr*, vol. 27, pp. 159-166, 1972

80. Gonchukova, N.O.," Calculation of the relaxation part of the heat capacity of lead monoxide-silicon dioxide glass (06PbO04SiO2) according to equations of the model of structural relaxation", *Fiz. Khim. Stekla*, vol. 5, pp. 410-15, 1979

81. Grundy, A.N., et al.," A Model to Calculate the Viscosity of Silicate Melts. Part II.: Viscosity of the Multicomponent NaO0.5-MgO-CaO-AlO1.5-SiO2 System", *Int. J. Mat. Res.*, vol. 99, pp. 1195-1209, 2008

82. Grundy, A.N., et al.," A Model to Calculate the Viscosity of Silicate Melts. Part I.: Viscosity of Binary SiO2-MeOx Systems (Me = Na, K, Ca, Mg, Al)", *Int. J. Mat. Res.*, vol. 99, pp. 1185-1194, 2008

83. Gul'tyai, I.I.," Effect of Al2O3 on the Viscosity of Slags of the System CaO-MgO-SiO2", *Izv. Akad. Nauk SSSR, Otd. Tekhn. Nauk, Metall. Toplivo*, vol. 5, pp. 52-65, 1962

84. Gul'tyai, I.I., et al.," The Effect of Potassium Oxide on the Viscosity of the Lime-Alumina-Silica System, in the Region Corresponding to the Composition of the Original Blast-Furnace Slag", *Izvest. Akad. Nauk S.S.S.R., Otdel. Tekh. Nauk, Metallurgiya i Toplivo*, vol. 2, pp. 3-7, 1959

85. Gupta, S.K.," Viscosity of PbO-SiO2 Melts", *Metall. Mater. Trans. B*, vol. 26B, pp. 281-287, 1995

86. Habeck, A., H. Hessenkemper, and R. Brueckner," Influence of microheterogeneities on the mechanical properties of high-viscous melts", *Glastech. Ber.*, vol. 63, pp. 111-17, 1990

87. Handfield, G., G.G. Charette, and H.Y. Lee," Titanium Bearing Ore and Blast Furnace Slag Viscosity", *JOM*, vol. 24, pp. 37-40, 1972

88. Heidtkamp, G. and K. Endell," The Dependence of Density and Viscosity on Temperature in the System Soda-Silica", *Glastech. Ber.*, vol. 14, pp. 89-103, 1936

89. Herty, C.H.J., et al., *Temperature-viscosity measurement in the systems CaO-SiO2 and CaO-SiO2-CaF2*, in *3232*. 1934: Bureau of Mines Report of Investigations. p. 31 pp.

90. Herty, C.H.J., F.A. Hartgen, and G.T. Jones," Temperature-viscosity relations in the system: CaO-SiO2-CaF2", *Mining and Met. Investigations, U. S. Bureau of Mines, Carnegie Inst. Tech. and Mining and Met. Advisory Boards Coop. Bull.*, vol. 56, pp. 1-31, 1931

91. Hess, K.-U., D.B. Dingwell, and S.L. Webb," The Influence of Excess Alkalis on the Viscosity of a Haplogranitic Melt", *Am. Mineral.*, vol. 80, pp. 297-304, 1995

92. Hetherington, G., K.H. Jack, and J.C. Kennedy," Viscosity of vitreous SiO2", *Phys. Chem. Glasses*, vol. 5, pp. 130-6, 1964

93. Hino, M., T. Ejima, and M. Kameda," Measurements on Physical Properties of Molten Lead Silicate. III. Surface Tension, Density, and Viscosity of Lead Oxide-Sodium Oxide-Silicon Dioxide Ternary Melt", *Nippon Kinzoku Gakkaishi*, vol. 32, pp. 809-814, 1968

94. Hino, M., T. Ejima, and M. Kameda," Surface Tension, Density, and Viscosity of Lead Monoxide-Potassium Oxide-Silicon Dioxide Ternary Melts", *Nippon Kinzoku Gakkaishi*, vol. 33, pp. 617-622, 1969

95. Hoffman, L.C., et al.," The Low-temperature Viscosity of Glass", *J. Soc. Glass Technol.*, vol. 36, pp. 196-216, 1952

96. Hofmaier, G.," Viscosity and Structure of Liquid Silicates", *Berg- und Huettenmaennische Monatshefte*, vol. 113, pp. 270-81, 1968

97. Hoshino, Y., et al.," Precise measurement of the viscosity of molten alkaline earth fluoride", *Nippon Netsubussei Shinpojumu Koen Ronbunshu, 27th*, vol. pp. 203-205, 2006

98. Hummel, W. and J. Arndt," Variation of viscosity with temperature and composition in the plagioclase system", *Contrib. Mineral. Petrol.*, vol. 90, pp. 83-92, 1985

99. Iguchi, Y., et al. *Raman Spectroscopic Study on Structure of Binary Silicates and Ternary Oxide Melts with and without Fluoride*. 1984.

100. Iida, T., et al.," Viscosities of Borate-base Binary Molten Oxides and Characteristic Features of the Viscosity of Molten Salts", *Tetsu to Hagane*, vol. 73, pp. 469-475, 1987

101. Istomin, S.A., et al.," Viscosity and Electrical Conductivity of B2O3-CaO and B2O3-ZnO Melts", *Rasplavy*, vol. 5, pp. 36-43, 1995

102. Istomin, S.A., et al.," Physicochemical properties of calcium fluoride-magnesium oxide-silicon dioxide system melts", *Izvestiya Akademii Nauk SSSR, Metally*, vol. 3, pp. 74-7, 1980

103. Ito, H. and Y. Tsutomu," Lead silicate melts", *Trans. Japan Inst. Metals*, vol. 1, pp. 115-20, 1960

104. Ito, H., T. Yanagase, and Y. Suginohara," The effects of an additional oxide on the viscosity of lead silicate melts", *Nippon Kinzoku Gakkaishi*, vol. 27, pp. 182-6, 1963

105. Ivanov, O.G., N.I. Tret'yakova, and O.V. Mazurin," Modernized indenter-type viscometer and a study of the viscosity of K2O-RO-SiO2 system glasses", *Steklo i Keramika*, vol. 26, pp. 42-5, 1969

106. Izumitani, T. and Y. Moriya," vol. 11, pp. 274, 1960

107. Jak, E. *Viscosity model for slags in the Al2O3-CaO-'FeO'-K2O-Na2O-MgO-SiO2 system*. 2009: Santiago, Chile.

108. Jak, E. and P. Hayes," Phase equilibria and thermodynamics of zinc fuming slags", *Can. Metall. Q.*, vol. 41, pp. 163-174, 2002

109. Johannsen, V.F. and H. Brunion," Viscosity of Direct Process Slags", *Erzmetall*, vol. 12, pp. 272-279, 1959

110. Jung, S.-M.," Quantitative chemical analysis of fluorine in the slags produced in stainless argon-oxygen decarburization process by x-ray fluorescence spectrometry", *ISIJ Int.*, vol. 47, pp. 1141-1148, 2007

111. Kadogawa, Y. and T. Yamate," Viscosity of molten glass of mixed alkali lead silicates", *Zairyo*, vol. 21, pp. 646-51, 1972

112. Kaiura, G.H. and J.M. Toguri," The viscosity and structure of sodium borate melts", *Phys. Chem. Glasses*, vol. 17, pp. 62-9, 1976

113. Kalampounias, A.G., N.K. Nasikas, and G.N. Papatheodorou," Levitation / CO2 laser melting and glass formation in MgO rich mixtures with SiO2: Raman spectra and structure", *ECS Trans.*, vol. 16, pp. 343-355, 2009

114. Kalyadina, S.A., *Issledovanie Vyazkosti i Udel'noi Elektroprovodnosti Fosfatno-Kremnistykh Rasplavov*. 1977: Leningrad.

115. Kapoor, M.L. and Frohberg," Theoretical treatment of activities in silicate melts", *Proceedings of the International Symposium Chemical Metallurgy of Iron and Steel, Sheffield, England, The Institute of Metals, London*, vol. pp. 17-22, 1971

116. Karyazin, I.A., A.A. Morozov, and V.A. Reznichenko," Viscosity and Fusibility of High-Titanium Slag Melts Based on a Titanium Dioxide-Titanium Sesquioxide-Ferrous Oxide System", *Izv. Akadem. Nauk SSSR, Metally*, vol. 5, pp. 28-34, 1969

117. Kato, M. and S. Minowa," Properties of Slag at Elevated Temperature. I. Viscosity Measurements of Molten Slag", *Trans. Iron Steel Inst. Jpn.*, vol. 9, pp. 31-38, 1969

118. Kawahara, M., K. Mizoguchi, and Y. Suginohara," Viscosity and Infrared Spectra of Calcium Oxide-Silicon Dioxide-Manganese Oxide and Manganese Oxide-Silicon Dioxide-Aluminum Oxide Melts", *Kyushu Kogyo Daigaku Kenkyu Hokoku, Kogaku*, vol. 43, pp. 53-59, 1981

119. Kawahara, M., K. Morinaga, and T. Yanagase," Measurements of the Viscosity and the Infrared Spectrum of the Sodium Oxide-Silicon Dioxide-Magnesium Oxide Ternary System", *J. Jpn. Inst. Metals*, vol. 41, pp. 1047-1052, 1977

120. Kawahara, M., K. Morinaga, and T. Yanagase," The Behavior of Magnesium Oxide and Nickel(II) Oxide in Molten Lead Oxide-Silicon Dioxide System", *Nippon Kinzoku Gakkaishi*, vol. 43, pp. 309-345, 1979

121. Kawamoto, T., *Corrosion-resistant glass fiber without containing fluorine and boron*, in *JP Patent No. 10231143*. 1998.

122. Khanna, S.R.," Viscosity variations of soda-lime glass within the working temperature due to substitution of lime by magnesia", *Trans. Indian Ceram. Soc.*, vol. 13, pp. 154-9, 1954

123. Kim, D.S., et al.," Deoxidation and denitrogenation of 18% Cr-8% Ni stainless steel by Ti addition", *Taehan Kumsok Hakhoechi*, vol. 32, pp. 1210-1218, 1994

124. Kim, I.S., *Viscosity of Na2O-CaO-MgO-Al2O3-SiO2 glasses in the annealing temperature range*. 1952: Leningrad.

125. Kim, K.-D. and S.-H. Lee," Viscosity behavior and mixed alkali effect of alkali aluminosilicate glass melts", *J. Ceram. Soc. Jpn.*, vol. 105, pp. 827-832, 1997

126. Kim, K.-D. and S.-H. Lee," Prediction of viscosity in the two-phase range of a ternary glass-forming system", *J. Mater. Sci.*, vol. 32, pp. 6561-6565, 1997

127. Kim, W.-Y., A.D. Pelton, and S.A. Decterov," A Model to Calculate the Viscosity of Silicate Melts. Part III: Modification of the model for melts containing alkali metals", *Int. J. Mat. Res., submitted*, vol. 2011

128. Kim, W.-Y., A.D. Pelton, and S.A. Decterov," Modeling Viscosity of Silicate Melts Containing Lead Oxide", *Metall. Mater. Trans., submitted*, vol. 2011

129. Kimura, T.," Accuracy of beam-bending method for viscosity measurement of glass", *Jap. J. Appl. Phys.*, vol. 10, pp. 1261-5, 1971

130. Klyuev, V.P.," Dependence of the dilatometric properties of glasses on their structure: I Borate, aluminoborate, and lead-containing glasses", *Glass Phys. Chem.*, vol. 31, pp. 749-759, 2005

131. Klyuev, V.P. and A.V. Bulaeva," Viscosity and thermal expansion of lead borate glasses in the glass transition region", *Fizika i Khimiya Stekla*, vol. 6, pp. 674-678, 1980

132. Klyuev, V.P. and B.Z. Pevzner," The influence of aluminum oxide on the thermal expansion, glass transition temperature, and viscosity of lithium and sodium aluminoborate glasses", *Glass Phys. Chem.*, vol. 28, pp. 207-220, 2002

133. Klyuev, V.P. and B.Z. Pevzner," Thermal Expansion and Glass Transition Temperature of Calcium Borate and Calcium Aluminoborate Glasses", *Glass Phys. Chem.*, vol. 29, pp. 127-136, 2003

134. Knoche, R., et al.," Non-linear Properties of Supercooled Liquids in the System Na2O-SiO2", *Chem. Geol.*, vol. 116, pp. 1-16, 1994

135. Knyazyan, N.B. and V.D. Khalilev," Some physicochemical properties of glasses of the ZnB2O4-RF2 system (R = magnesium, calcium, strontium, barium)", *Fiz. Khim. Stekla*, vol. 4, pp. 625-7, 1978

136. Kochkanyan, R.M., R.S. Saringyulyan, and S.B. Gukasyan. *Electrical conductivity and viscosity of glasses of the system lead monoxide-boron oxide-zinc oxide over a wide interval of temperatures*. 1977: Akad. Nauk Armyanskoi SSR, Yerevan, USSR.

137. Koide, M., et al.," Viscosity of lead silicate glasses below glass transition temperature by the fiber bending method", *Phys. Chem. Glasses*, vol. 36, pp. 172-5, 1995

138. Komel'kov, V.K., et al.," Viscosity of lime-alumina slags containing silica, magnesia, and calcium fluoride", *Sbornik Trudov Tsentral'nogo Nauchno-Issledovatel'skogo Instituta Chernoi Metallurgii*, vol. 61, pp. 16-19, 1968

139. Kondratiev, A. and E. Jak," A Quasi-Chemical Viscosity Model for Fully Liquid Slags in the Al2O3-CaO-'FeO'-SiO2 System", *Metall. Trans. B*, vol. 36B, pp. 623-638, 2005

140. Konovalov, A.S. and K.S. Evstrop'ev," Viscosity in the silica-lead monoxide system", *J. Phys. Chem. (U. S. S. R.)*, vol. 15, pp. 109-15, 1941

141. Koo, C.H. and H.S. Koo," A viscosity study of the calcium fluoride-calcium oxide-aluminum oxide system at 1400-1700°", *Cailiao Kexue*, vol. 20, pp. 51-7, 1988

142. Kostanyan, K.A. and S.S. Kirakosyan," Viscosity of aluminum calcium borate glasses in a large temperature range", *Armyanskii Khimicheskii Zhurnal*, vol. 26, pp. 555-62, 1973

143. Kou, T., K. Mizoguchi, and Y. Suginohara," The Effect of Al2O3 on the Viscosity of Silicate Melts", *Nippon Kinzoku Gakkaishi*, vol. 42, pp. 775-781, 1978

144. Kozakevitch, P.," Tension Superficielle et Viscosité des Scories Synthétiques", *Rev. Métall.*, vol. 46, pp. 505-516; 572-582, 1949

145. Kozakevitch, P.," Viscosité et Éléments Structuraux des Aluminosilicates Fondus: Laitiers CaO-Al2O3-SiO2 entre 1600 et 2100 °C", *Rev. Métall.*, vol. 57, pp. 149-160, 1960

146. Kozu, S. and K. Kani. *Viscosity measurements of the ternary system diopsidealbite-anorthite at high temperatures*. 1935.

147. Kracek, F.C., N.L. Bowen, and G.W. Morey," The System Potassium Metasilicate-Silica", *J. Phys. Chem.*, vol. 33, pp. 1857-1879, 1929

148. Kruh, R. and K.H. Stern," The effect of solutes on the properties and structure of liquid boric oxide", *J. Am. Chem. Soc.*, vol. 78, pp. 278-81, 1956

149. Kulifeev, V.K., V.I. Panchishnyi, and G.P. Stanolevich," The density and viscosity of calcium, magnesium, and barium fluorides", *Izv. Vyssh. Ucheb. Zaved., Tsvet. Met.*, vol. 11, pp. 116-19, 1968

150. Kuppinger, C.M. and J.E. Shelby," Viscosity and thermal expansion of mixed-alkali sodium-potassium borate glasses", *J. Am. Ceram. Soc.*, vol. 68, pp. 463-7, 1985

151. Lakatos, T.," Viscosity-temperature relations in glasses composed of silicon dioxide-aluminum oxide-sodium oxide-potassium oxide-lithium oxide-calcium oxide-magnesium oxide-barium oxide-zinc oxide-lead(II) oxide-boron oxide", *Glasteknisk Tidskrift*, vol. 31, pp. 51-54, 1976

152. Lakatos, T., L.G. Johansson, and B. Simmingskoeld," Viscosity-temperature relations in glasses composed of silica-alumina-sodium oxide-lead monoxide-boron oxide-calcium

oxide-zinc oxide-lithium oxide in the compositional range of "crystalline" glasses", *Glasteknisk Tidskrift*, vol. 34, pp. 61-65, 1979

153. Lakatos, T., L.G. Johansson, and B. Simmingskoeld," Viscosity and liquidus temperature relations in the mineral-wool part of the silicon dioxide-aluminum oxide-calcium oxide-magnesium oxide-alkali-iron(II) oxide-iron(III) oxide system", *Glasteknisk Tidskrift*, vol. 36, pp. 51-55, 1981

154. Lakatos, T., L.G. Johansson, and B. Simmingskold," Effect of Some Glass Components of the Viscosity of Glass", *Glasteknisk Tidskrift*, vol. 27, pp. 25-28, 1972

155. Lakatos, T., L.G. Johansson, and B. Simmingskold," Investigations on viscosity-temperature relations in the lead crystal system containing 24-30% lead(II) oxide. Part II", *Glasteknisk Tidskrift*, vol. 33, pp. 55-59, 1978

156. Lanyi, M.D. and C.J. Rosa," Viscosity of casting fluxes used during continuous casting of steel", *Metall. Trans., B*, vol. 12B, pp. 287-98, 1981

157. Leedecke, C.J. and C.G. Bergeron," The growth of potassium borate (K2B8O13) in its stoichiometric melt", *J. Cryst. Growth*, vol. 32, pp. 327-31, 1976

158. Leedecke, C.J. and C.G. Bergeron," Viscous flow in binary borate melts", *Mater. Sci. Res.*, vol. 12 (Borate Glasses), pp. 413-426, 1978

159. Leko, V.K.," Structure and properties of alkali metal silicate glasses containing two different alkali metal oxides", *Izv. Akad. Nauk SSSR, Neorg. Mater.*, vol. 3, pp. 1888-91, 1967

160. Leko, V.K., et al.," Viscosity of titanosilicate glass", *Fizika i Khimiya Stekla*, vol. 1, pp. 174-6, 1975

161. Leont'eva, A.," Measurements of the Viscosity of the System Boron Oxide-Silica and the Calculation of the Energy of Activation for Vitreous Systems", *Zh. Fiz. Khim.*, vol. 13, pp. 1020-1023, 1939

162. Li, P.-C., A.C. Ghose, and K.-J. Su," Viscosity determination of boron oxide and binary borates", *J. Am. Ceram. Soc.*, vol. 45, pp. 83-8, 1962

163. Li, T.-C. and L.M. Tsylev," Viscosity of synthetic slags of the system calcium fluoride-calcium oxide-silica at 5% alumina", *Izvestiya Akademii Nauk SSSR, Otdelenie Tekhnicheskikh Nauk, Metallurgiya i Toplivo*, vol. 1, pp. 21-9, 1960

164. Licko, T. and V. Danek," Viscosity and Structure of Melts in the System CaO-MgO-SiO2", *Phys. Chem. Glasses*, vol. 27, pp. 22-26, 1986

165. Lillie, H.R.," Viscosity of glass between the strain point and melting temperature", *J. Am. Ceram. Soc.*, vol. 14, pp. 502-11, 1931

166. Lillie, H.R.," High-Temperature Viscosities of Soda-Silica Glasses", *J. Am. Ceram. Soc.*, vol. 22, pp. 367-74, 1939

167. Liska, M., et al.," Viscosity of Titania-Bearing Sodium Silicate Melts", *Chem. Geol.*, vol. 128, pp. 199-206, 1996

168. Liutikov, R.A. and L.M. Tsyl'ev," Viscosity and Electrical Conductivity of Melts of the Magnesia-Silica-Alumina System", *Translation of Izv. Akad. Nauk SSSR, Otd. Tekhn. Nauk, Met. i Gorn. Delo 1 (1963) 41-52*, vol. 1, pp. 12-19, 1963

169. Lobzhanidze, R.B., A.F. Filippov, and P.P. Evseev," Physicochemical properties of slags of the CaF2-MxOy-Cr2O3 system", *Izv. Vyssh. Ucheb. Zaved., Chern. Metall.*, vol. 13, pp. 57-60, 1970

170. Luth, R.W.," Raman spectroscopic study of the solubility mechanisms of fluorine in glasses in the system calcium oxide-calcium fluoride-silica", *Am. Mineral.*, vol. 73, pp. 297-305, 1988

171. Lyamkin, S.A., et al. 1978: Sverdlovsk.

172. Machin, J.S. and T.B. Yee," Viscosity Studies of System CaO-MgO-Al2O3-SiO2: II, CaO-Al2O3-SiO2", *J. Am. Ceram. Soc.*, vol. 31, pp. 200-204, 1948

173. Mackenzie, J.D.," Structure of Liquid Boron Trioxide", *J. Phys. Chem.*, vol. 63, pp. 1875-1878, 1959

174. Mal'kov, N.V., V.E. Roshchin, and A.A. Gainullin," Viscosity of slag melts of the fluorite-silica-rare earth oxide system", *Izvestiya Vysshikh Uchebnykh Zavedenii, Chernaya Metallurgiya*, vol. 4, pp. 31-34, 1986

175. Malfait, W.J., et al.," Structural control on bulk melt properties: Single and double quantum 29Si NMR spectroscopy on alkali-silicate glasses", *Geochim. Cosmochim. Acta*, vol. 71, pp. 6002-6018, 2007

176. Mastelaro, V.R., et al.," Relationship between short-range order and ease of nucleation in Na2Ca2Si3O9, CaSiO3 and PbSiO3 glasses", *J. Non-Cryst. Solids*, vol. 262, pp. 191-199, 2000

177. Matson, D.W., S.K. Sharma, and J.A. Philpotts," The structure of high-silica alkali-silicate glasses. A Raman spectroscopic investigation", *J. Non-Cryst. Solids*, vol. 58, pp. 323-352, 1983

178. Matusita, K., et al.," Viscosities of single and mixed alkali borate glasses", *Phys. Chem. Glasses*, vol. 21, pp. 78-84, 1980

179. Mazurin, O.V. and G.T. Petrvoskii," The Influence of manganese Oxides on the Electrical Conductivity of Glasses", *Tr. Leningr. Tekhnol. Inst. im. Lensoveta*, vol. pp. 30-51, 1956

180. Mazurin, O.V., M.V. Strel'tsina, and T.N. Shvaiko-Shvaikovskaya, *Glassy Silica and Two-Component Silicate Systems*, in *Properties of Glasses and Glass-Forming Melts*. 1973, Nauka, Leningrad. Otd., Leningrad, USSR. p. 386-.

181. Mazurin, O.V., N.I. Tretjakova, and T.P. Shvaiko-Shvaikovskaya," Method for calculating the viscosity of silicate glasses", *Deposited in VINITI, Moscow, No.1091-69 Dep.*, vol. 1969

182. McCauley, W.L. and D. Apelian," Viscosity of fluxes for the continuous casting of steel", *ACS Symposium Series*, vol. 301, pp. 215-22, 1986

183. McMillan, P.W., G. Partridge, and J.G. Darrant," Crystal growth studies in zinc oxide-alumina-silica glasses", *Phys. Chem. Glasses*, vol. 10, pp. 153-8, 1969

184. Meiling, G.S. and D.R. Uhlmann," Crystallization and melting kinetics of sodium disilicate", *Phys. Chem. Glasses*, vol. 8, pp. 62-8, 1967

185. Michel, J.R. and A. Mitchell," Rheological behavior of some slags in the system calcium oxide-silicon dioxide-aluminum oxide-calcium fluoride", *Can. Metall. Q.*, vol. 14, pp. 153-159, 1975

186. Mikiashvili, S.M., A.Y. Arsenishvili, and A.G. Bukhrashvili," Viscosity of melts in the system CaO-MnO-SiO2", *Soobshcheniya Akademii Nauk Gruzinskoi SSR*, vol. 27, pp. 313-20, 1961

187. Mikiashvili, S.M., L.M. Tsylev, and A.M. Samarin. *Properties of the molten MnO-SiO2-Al2O3 system*. 1957.

188. Miller, V.Y. and N.M. Babushkin," Physical and chemical properties of titania-magnesia slags with a high alumina content", *Stal'*, vol. 21, pp. 391-7, 1961

189. Mills, K.C., *Viscosities of molten slags*, in *NPL Rep. DMM(A) (U. K., Natl. Phys. Lab., Div. Mater. Metrol.)*. 1992: U. K., Natl. Phys. Lab., Div. Mater. Metrol. p. 116 pp.

190. Mills, K.C., et al.," 'Round Robin' Project on the Estimation of Slag Viscosities", *Scand. J. Metall.*, vol. 30, pp. 396-403, 2001

191. Mitin, B.S. and Y.A. Nagibin," Properties of molten titanium dioxide", *Izvestiya Akademii Nauk SSSR, Neorganicheskie Materialy*, vol. 7, pp. 814-16, 1971

192. Mizani, S., *Modeling the viscosity of liquid solutions used in aluminum alloys production*. 2008, École Polytechnique de Montréal: Montréal, Québec.

193. Mizoguchi, K., K. Okamoto, and Y. Suginohara," Oxygen Coordination of Al3+ Ion in Several Silicate Melts Studied by Viscosity Measurements", *Nippon Kinzoku Gakkaishi*, vol. 46, pp. 1055-1060, 1982

194. Monneraye, M. and H.J.L. Trap. *Effets de l'addition de TiO2 sur les propriete dielectriques des verres et des produits vitrocristallins du type Cabal*. 1965: Bruxelles.

195. Morozov, A.A., et al.," Thermophysical Properties and Phase Composition of Slags from the Electric Melting of Titanomagnetite Concentrates of the Malo-Tagul'skoe Deposit", *Izv. Akadem. Nauk SSSR, Metally*, vol. 5, pp. 43-47, 1982

196. Muratov, A.M.," Viscosity of electroslag remelting fluxes", *Izv. Akad. Nauk SSSR, Metal.*, vol. pp. 63-65, 1972

197. Musikhin, V.I., et al.," Viscosity of melts in boron oxide-based systems", *Rasplavy*, vol. pp. 40-5, 1992

198. Musorin, G.V.," Viscosity of synthetic slags in the reduction period of electric steelmaking", *Trudy Ural'skogo Politekhnicheskogo Instituta im. S. M. Kirova*, vol. 75, pp. 142-56, 1959

199. Mysen, B.," Physics and Chemistry of Silicate Glasses and Melts", *Eur. J. Mineral.*, vol. 15, pp. 781-802, 2003

200. N'Dala, I., et al.," Viscosity of Liquid Feldspars. Part I: Viscosity Measurements", *Br. Ceram. Trans. J.*, vol. 83, pp. 105-107, 1984

201. Nakamoto, M., J. Lee, and T. Tanaka," A Model for Estimation of Viscosity of Molten Silicate Slag", *ISIJ Int.*, vol. 45, pp. 651-656, 2005

202. Nakamura, T., K. Morinaga, and T. Yanagase," The Viscosity of the Molten Silicate Containing TiO2", *Nippon Konzoku Gakkaishi*, vol. 41, pp. 1300-1304, 1977

203. Nakashima, K., et al. *Viscosity of binary borate and ternary borosilicate melts*. 1997: Iron and Steel Society, Warrendale, Pa.

204. Napolitano, A., P.B. Macedo, and E.G. Hawkins," Viscosity and Density of Boron Trioxide", *J. Am. Ceram. Soc.*, vol. 48, pp. 613-616, 1965

205. Nemilov, S.V.," Relation between the values of the configurational entropy and the entropy of activation of the viscous flow of supercooled glass-forming liquids", *Fizika i Khimiya Stekla*, vol. 2, pp. 193-203, 1976

206. Nemilov, S.V.," Studies on the structure of glasses in B2O3-Na2O system by the viscosimetric method", *Izvestiya Akademii Nauk SSSR, Neorganicheskie Materialy*, vol. 2, pp. 349-56, 1966

207. Nemilov, S.V.," Viscosity and Structure of Lead Oxide-Silicon Dioxide System Glasses", *Neorg. Mater.*, vol. 4, pp. 835-839, 1968

208. Nemilov, S.V.," Viscosity of glasses of sodium oxide-potassium oxide-silicon dioxide and lithium oxide-potassium oxide-silicon dioxide systems in softening point regions", *Zhurnal Prikladnoi Khimii (Sankt-Peterburg, Russian Federation)*, vol. 42, pp. 55-62, 1969

209. Nemilov, S.V. and A.I. Ignat'ev," Viscosity of PbO-SiO2 Melts in the Region of Softened and Liquid States", *Fiz. Khim. Stekla*, vol. 16, pp. 85-93, 1990

210. Nemilov, S.V. and N.V. Komarova," Effect of supercritical fluctuations and phase separation on the viscosity of melts and glasses of the lead(II) oxide-boron oxide-aluminum oxide system", *Fizika i Khimiya Stekla*, vol. 3, pp. 568-75, 1977

211. Nemilov, S.V. and L.K. Shmatok," Viscosity and structure of zinc oxide-lanthanum oxide-boron oxide system glasses", *Izv. Akad. Nauk SSSR, Neorg. Mater.*, vol. 4, pp. 2166-70, 1968

212. Neuville, D.R.," Viscosity, Structure, and Mixing in (Ca, Na) Silicate Melts", *Chem. Geol.*, vol. 229, pp. 28-41, 2006

213. Neuville, D.R. and P. Richet," Viscosity and mixing in molten (calcium, magnesium) pyroxenes and garnets", *Geochim. Cosmochim. Acta*, vol. 55, pp. 1011-1019, 1991

214. Neuville, D.R. and P. Richet," Viscosity and entropy of molten silicates", *Rivista della Stazione Sperimentale del Vetro (Murano, Italy)*, vol. 20, pp. 213-20, 1990

215. Nikitin, Y.P., et al.," Temperature Dependence of the Viscosity of Liquid Borosilicates", *Izv. Vyssh. Uch. Zaved., Chernaya metall.*, vol. 10, pp. 5-7, 1972

216. Ogino, K., J. Nishiwaki, and H. Onishi," vol. pp. 73, 1979

217. Ohta, T., *Thesis No 25*. 1974, Trondheim.

218. Okhotin, M.V. and T.D. Andryukhina," Calculation of the viscosity of low-alkaline and alkaline free glasses", *Steklo Keram.*, vol. 27, pp. 12-13, 1970

219. Oliver, C.B.," Viscosity of Some Molten Lead Compounds", *J. Electrochem. Soc.*, vol. 112, pp. 629-631, 1965

220. Oshchipkov, F.P. and B.V. Rabinovich," Viscosity of nonsilicate glasses", *Akad. Nauk S.S.S.R., Otdel. Tekh. Nauk, Inst. Mashinovedeniya, Soveshchanie Vyazkosti Zhidkostei i Kolloid. Rastvorov (Conf. on Viscosity of Liquids and Colloidal Solns.)*, vol. 1, pp. 353-7, 1941

221. Ota, R., W. Kotani, and J. Fukunaga," Crystallization Behavior in Oxyfluorodiborate Glass", *J. Ceram. Soc. Jpn.*, vol. 98, pp. 1125-1131, 1990

222. Ota, R., et al.," Structure and some physical properties of silica-alumina-calcium oxide-zinc oxide", *Zairyo*, vol. 42, pp. 467-72, 1993

223. Ota, R., et al.," Glass Formation and Crystallization in Li2O-Na2O-K2O-SiO2", *J. Non-Cryst. Solids*, vol. 188, pp. 136-146, 1995

224. Ouchi, Y. and E. Kato," The Effects of Alkaline Earth Metal Oxides, Nickel Oxide, and Cobalt Oxide on the Viscosity of Lead-Metasilicate Melts", *Nippon Kinzoku Gakkaishi*, vol. 43, pp. 625-633, 1979

225. Paek, U.C., C.M. Schroeder, and C.R. Kurkjian," Determination of the viscosity of high silica glasses during fiber drawing", *Glass Technol.*, vol. 29, pp. 263-6, 1988

226. Park, H.S., H. Kim, and I. Sohn," Influence of CaF2 and Li2O on the Viscous Behavior of Calcium Silicate Melts Containing 12 wt pct Na2O", *Metall. Mater. Trans. B*, vol. 42, pp. 324-330, 2011

227. Park, J.H., D.J. Min, and H.S. Song," FT-IR spectroscopic study on structure of CaO-SiO2 and CaO-SiO2-CaF2 slags", *ISIJ Int.*, vol. 42, pp. 344-351, 2002

228. Parks, G.S. and M.E. Spaght," Viscosity data for boron trioxide", *Physica (The Hague)*, vol. 6, pp. 69-71, 1935

229. Pascual, M.J., A. Duran, and L. Pascual," Sintering process of glasses in the system Na2O-B2O3-SiO2", *J. Non-Cryst. Solids*, vol. 306, pp. 58-69, 2002

230. Pelton, A.D. and M. Blander," Thermodynamic Analysis of Ordered Liquid Solutions by a Modified Quasi-Chemical Approach. Application to Silicate Slags", *Metall. Trans. B*, vol. 17B, pp. 805-815, 1986

231. Pelton, A.D. and P. Chartrand," The Modified Quasichemical Model. II - Multicomponent Solutions", *Metall. Mater. Trans. A*, vol. 32A, pp. 1355-1360, 2001

232. Pelton, A.D., et al.," The Modified Quasichemical Model. I - Binary Solutions", *Metall. Mater. Trans. B*, vol. 31B, pp. 651-659, 2000

233. Persson, M., M. Goernerup, and S. Seetharaman," Viscosity measurements of some mould flux slags", *ISIJ Int.*, vol. 47, pp. 1533-1540, 2007

234. Persson, M., S. Seetharaman, and S. Seetharaman," Kinetic studies of fluoride evaporation from slags", *ISIJ Int.*, vol. 47, pp. 1711-1717, 2007

235. Petrovskii, G.T.," Study of viscosity and conductivity of softened glass by the radius of the ions within the glass", *Collection of Students Work, Trans. LTI im. Lensovet*, vol. pp. 37, 1956

236. Piguet, J.L. and J.E. Shelby," Preparation and properties of silver borate glasses", *J. Am. Ceram. Soc.*, vol. 68, pp. 450-5, 1985

237. Pohlmann, H.J.," Investigation of viscosity of glasses in the silica-rich part of the system potassium oxide-lead(II) oxide-silicon dioxide", *Glastech. Ber.*, vol. 49, pp. 177-82, 1976

238. Poole, J.P.," Low-temperature viscosity of alkali silicate glasses", *J. Am. Ceram. Soc.*, vol. 32, pp. 230-3, 1949

239. Poole, J.P. and M. Gensamer," Systematic study of effect of oxide constituents on viscosity of silicate glasses at annealing temperatures", *J. Am. Ceram. Soc.*, vol. 32, pp. 220-9, 1949

240. Popescu, A.M.," The viscosity of molten alkali fluorides", *Rev. Roum. Chim.*, vol. 44, pp. 765-770, 2000

241. Pospelov, B.A.," The Viscosity of the Binary Lead Silicate, Lead Borate, and Lead Phosphate Glasses in the Temperature Interval between Softening and Annealing", *Zh. Fiz. Khim.*, vol. 33, pp. 543-546, 1959

242. Pospelov, B.A.," Viscosity of several glasses in the temperature interval between softening and annealing. I", *Zhurnal Fizicheskoi Khimii*, vol. 28, pp. 2178-84, 1954

243. Pospelov, B.A.," Viscosity of some glasses in the temperature interval of softening-annealing. III. Relation between glass viscosity and composition", *Zhurnal Fizicheskoi Khimii*, vol. 33, pp. 547-9, 1959

244. Potselueva, L.N.," Study of the temperature dependence of the equilibrium viscosity of some alkali-free borate glasses in the 1010-1015 P range", *Fiz. Khim. Stekla*, vol. 6, pp. 415-18, 1980

245. Povolotskii, D.Y., et al.," Physicochemical properties of calcium oxide-aluminum oxide-calcium fluoride system melts", *Izvestiya Vysshikh Uchebnykh Zavedenii, Chernaya Metallurgiya*, vol. 13, pp. 8-12, 1970

246. Preston, E.," The viscosity of the soda-silica glasses at high temperatures and its bearing on their constitution", *J. Soc. Glass Technol.*, vol. 22, pp. 45-82, 1938

247. Rabinovich, B.V.," Viscosity of borax and boric anhydride in the interval of softening", *Zh. Fiz. Khim.*, vol. 16, pp. 23-6, 1942

248. Rait, J.R., Q.C. M'Millan, and R. Hay," Viscosity Determinations of Slag Systems", *J. R. Technol. College*, vol. 4, pp. 449-466, 1939

249. Riboud, P.V., et al.," Improvement of Continuous Casting Powders", *Fachber. Hüttenprax. Metallweiterverarbei.*, vol. 19, pp. 859-869, 1981

250. Richet, P.," Residual and configurational entropy: Quantitative checks through applications of Adam-Gibbs theory to the viscosity of silicate melts", *J. Non-Cryst. Solids*, vol. 355, pp. 628-635, 2009

251. Riebling, E.F.," Structure of Magnesium Aluminosilicate Liquids at 1700° C", *Can. J. Chem.*, vol. 42, pp. 2811-2820, 1964

252. Riebling, E.F.," Structure of Sodium Aluminosilicate Melts Containing at least 50 Mole % SiO2 at 1500°", *J. Chem. Phys.*, vol. 44, pp. 2857-2865, 1966

253. Robelin, C. and P. Chartrand," A viscosity model for the (NaF + AlF3 + CaF2 + Al2O3) electrolyte", *J. Chem. Thermodyn.*, vol. 43, pp. 764-774, 2011

254. Roshchin, V.E., et al. 1983: Sverdlovsk.

255. Rosina, A.," Measurement of the viscosity of metallurgical slags with a vibrational viscometer. I. Viscosity of refining slags for electroslag remelting", *Zelezarski Zbornik*, vol. 15, pp. 19-24, 1981

256. Rossin, R., J. Bersan, and G. Urbain," Viscosity of Liquid Slags Belonging to the Ternary System SiO2-Al2O3-CaO", *Rev. Hautes Temp. Refractaires*, vol. 1, pp. 159-170, 1964

257. Rudneva, A.V., et al.," Viscosity and Mineralogical Composition of Slags of the K2O-CaO-Al2O3-SiO2 System Containing Additions of MnO", *Trudy Inst. Met. im. A. A. Baikova*, vol. 8, pp. 11-29, 1961

258. Saint-Gobain Co., G.P.N.C.C.b., Abridg. Specif., in *No.x-14*. 1966.

259. Saito, N., et al.," Effect of adding alkali oxides on viscosity of CaO-SiO2-Al2O3 slags", *Yoyuen oyobi Koon Kagaku*, vol. 47, pp. 140-146, 2004

260. Sakaguchi, S. and S.-i. Todoroki," Evaluation of critical cooling rate for 30Na2O10MgO60SiO2 glass based on viscosity", *J. Ceram. Soc. Jpn.*, vol. 104, pp. 405-408, 1996

261. Sakka, S., et al.," Viscosity of mixed-alkali borate glasses", *Res. Rep. Fac. Eng. Mie Univ.*, vol. 1, pp. 47-58, 1976

262. Saringyulyan, R.S. and K.A. Kostanyan," Viscosity and electrical conductivity of glasses in a wide temperature range", *Arm. Khim. Zh.*, vol. 22, pp. 1043, 1969

263. Saringyulyan, R.S. and K.A. Kostanyan," Temperature dependence of the electrical conductivity of glasses in a wide range of temperatures", *Arm. Khim. Zh.*, vol. 23, pp. 928-36, 1970

264. Sasaki, Y., M. Iguchi, and M. Hino," The role of Ca and Na ions in the effect of F ion on silicate polymerization in molten silicate system", *ISIJ Int.*, vol. 47, pp. 638-642, 2007

265. Sasek, L., J. Kovandova, and M. Drahonovsky," Viscosity of soda-borate glasses and glass melts", *Sbornik Vysoke Skoly Chemicko-Technologicke v Praze, L: Chemie a Technologie Silikatu*, vol. L12, pp. 47-72, 1984

266. Sasek, L. and A. Lisy," Structure and properties of silicate melts I Effect of the size of ions on glass melt density at high temperatures", *Sb. Vys. Sk. Chem.-Technol. Praze, Chem. Technol. Silikatu*, vol. L2, pp. 165-215, 1972

267. Sasek, L., H. Meissnerova, and J. Prochazka," Structure and properties of silicate melts. 7. Effect of the size of the Me+ and Me++ ions on the viscosity of silicate glass melts", *Sbornik Vysoke Skoly Chemicko-Technologicke v Praze, L: Chemie a Technologie Silikatu*, vol. L6, pp. 95-129, 1975

268. Sasek, L., M. Mika, and M. Rada," Method for graphical processing of the temperature dependence of the viscosity of glass melts on their chemical composition", *Silikaty (Prague)*, vol. 32, pp. 209-26, 1988

269. Scarfe, C.M. and D.J. Cronin," Viscosity-Temperature Relationships of Melts at 1 atm in the System Diopside-Albite", *Am. Mineral.*, vol. 81, pp. 767-771, 1986

270. Scarfe, C.M., et al.," Viscosity-Temperature Relationschips at 1 atm in the System Diopside-Anorthite", *Am. Mineral.*, vol. 68, pp. 1083-1088, 1983

271. Schairer, J.F. and N.L. Bowen," The System K2O-Al2O3-SiO2", *Am. J. Sci.*, vol. 253, pp. 681-746, 1955

272. Schenck, V.H. and M.G. Frohberg," Viscosity Measurements of Liquid Slags of the System CaO-SiO2-TiO2 at 1300-1600°C", *Arch. Eisenhuettenwes.*, vol. 33, pp. 421-425, 1962

273. Schwerin, L.," The effect of fluorspar on the viscosity of basic slags", *Met. Alloys*, vol. 5, pp. 118-23, 1934

274. Sci Glass Version 5.5, M.I.S.I.," vol.

275. Segers, L., A. Fontana, and R. Winand," Viscosité de Mélanges de Silicates Fondus du Systeme CaO-SiO2-MnO", *Electrochim. Acta*, vol. 24, pp. 213-218, 1979

276. Semetskaya, N.M., N.B. Knyazyan, and V.D. Khalilev. 1978: Sverdlovsk.

277. Semik, I.P.," Viscosity, melting, and thickening of Ti slags of the system SiO2-TiO2-CaO at a constant content of Al2O3 17% and MgO 8%", *Izv. Akad. nauk SSSR, Otd. Tekhn. Nauk*, vol. 9, pp. 59-76, 1941

278. Semik, I.P.," Viscosity of Magnitogorsk blast furnace slags", *Sovetskaya Metallurgiya*, vol. 10, pp. 22-34, 1938

279. Seward, T.P.I. and T. Vascott, *High Temperature Glass Melt Property Database for Process Modeling*. 2005: American Ceramic Society, Westerville, Ohio. 291 pp.

280. Shahbazian, F., et al.," Experimental Studies of Viscosities of Some CaO-CaF2-SiO2 Slags", *Ironmaking Steelmaking*, vol. 26, pp. 193-199, 1999

281. Shartsis, L., W. Capps, and S. Spinner," Viscosity and Electrical Resistivity of Molten Alkali Borates", *J. Am. Ceram. Soc.*, vol. 36, pp. 319-326, 1953

282. Shartsis, L. and S. Spinner," Viscosity and density of molten optical glasses", *J. Research Natl. Bur. Standards*, vol. 46, pp. 176-94, 1951

283. Shartsis, L., S. Spinner, and W. Capps," Density, Expansivity, and Viscosity of Molten Alkali Silicates", *J. Am. Ceram. Soc.*, vol. 35, pp. 155-60, 1952

284. Shelby, J.E., *Introduction to Glass Science and Technology, 2d Edition*. 2005: The Royal Society of Chemistry, Thomas Graham House, Science Park, Milton Road, Cambridge CB4 OWF, UK. 291 pp.

285. Shelby, J.E.," Formation and properties of calcium aluminosilicate glasses", *J. Am. Ceram. Soc.*, vol. 68, pp. 155-8, 1985

286. Sheludyakov, L.N., et al.," Viscosity of homogeneous melts of calcium oxide-aluminum oxide-silicon dioxide-ferrous oxide and calcium oxide-aluminum oxide-silicon dioxide-ferrous oxide-magnesium oxide systems", *Kompleksnoe Ispol'zovanie Mineral'nogo Syr'ya*, vol. 4, pp. 62-5, 1983

287. Sheludyakov, L.N., E.T. Sarancha, and A.A. Vakhitov," Viscosity of Aluminosilicate Melts of the MxOy-Alumina-Silica System", *Trudy Inst. Khim. Nauk, Akad. Nauk Kazakh. SSR*, vol. 15, pp. 158-163, 1967

288. Shilo, N.L., G.A. Sokolov, and A.V. Rudneva," Effect of K2O on the Physical Properties of Slags Determined by Calculating the Energy of Activation of Viscous Flow from Results of Measurements", *Bergakademie*, vol. 11, pp. 12-17, 1959

289. Shin, D., R. Arroyave, and Z.-K. Liu," Thermodynamic Modeling of the Hf-Si-O System", *Calphad*, vol. 30, pp. 375-386, 2006

290. Shiraishi, Y., et al.," Viscosity of Glassy Sodium Oxide-Boron Oxide-Silica (Na2O-B2O3-SiO2) System", *J. Non-Cryst. Solids*, vol. 95-96, pp. 1031-8, 1987

291. Shiraishi, Y., S. Nagasaki, and M. Yamashiro," Viscosity of Potassium Boro-Silicate System in Glassy and Liquid States", *J. Non-Cryst. Solids*, vol. 282, pp. 86-97, 2001

292. Shiraishi, Y. and T. Saito," The viscosity of molten slags. I. The viscosity of CaO-Si O2-alkaline earth fluoride systems", *Nippon Kinzoku Gakkaishi*, vol. 29, pp. 614-22, 1965

293. Shumitskaya, L.F., *Development of glass resistant to sodium vapor*, in *Vopr. Radioelektron., Ser. 4: Tekhnol. Proizv. Oborud.* 1962. p. 32-45.

294. Shvaiko-Shvaikovskaya, T.P., N.K. Gusakova, and O.V. Mazurin," Viscosity of sodium oxide-calcium oxide-silicon dioxide system glasses in a wide temperature range", *Izvestiya Akademii Nauk SSSR, Neorganicheskie Materialy*, vol. 7, pp. 620-621, 1971

295. Shvaiko-Shvaikovskaya, T.P., O.V. Mazurin, and Z.S. Bashun," Viscosity of sodium oxide-silicon dioxide system glasses in molten state", *Izvestiya Akademii Nauk SSSR, Neorganicheskie Materialy*, vol. 7, pp. 128-131, 1971

296. Sikora, B. and M. Zielinski," Density surface tension, viscosity, and electric conductivity of fused calcium oxide-alumina-calcium fluoride systems", *Hutnik*, vol. 41, pp. 433-437, 1974

297. Sipp, A., Y. Bottinga, and P. Richet," New High Viscosity Data for 3D Network Liquids and New Correlations between Old Parameters", *J. Non-Cryst. Solids*, vol. 288, pp. 166-174, 2001

298. Sipp, A. and P. Richet," Equivalence of Volume, Enthalpy and Viscosity Relaxation Kinetics in Glass-Forming Silicate Liquids", *J. Non-Cryst. Solids*, vol. 298, pp. 202-212, 2002

299. Skornyakov, M.M., A.Y. Kuznetsov, and K.S. Evstrop'ev," Viscosity of the system Na2SiO3-SiO2 in the molten state", *J. Phys. Chem. (U. S. S. R.)*, vol. 15, pp. 116-23, 1941

300. Skryabin, V.G., et al. *Effect of water vapor on the viscosity of oxide melts*. 1974: "Nauka", Moscow, USSR.

301. Slavyanskii, V.T.," A method of determination of the viscosity of molten glasses", *Zhurnal Fizicheskoi Khimii*, vol. 26, pp. 1721-6, 1952

302. Slavyanskii, V.T.," The temperature dependence of the viscosity of liquids and molten glasses", *Zhurnal Fizicheskoi Khimii*, vol. 27, pp. 1776-83, 1953

303. Solvang, M., et al.," Rheological and thermodynamic behaviors of different calcium aluminosilicate melts with the same non-bridging oxygen content", *J. Non-Cryst. Solids*, vol. 336, pp. 179-188, 2004

304. Sridhar, S., et al.," Viscosity Estimation Models for Ternary Slags", *Steel Res.*, vol. 72, pp. 3-10, 2001

305. Startsev, Y.K., et al. 1989: Leningrad.

306. Startsev, Y.K. and T.V. Safutina," Influence of residual water in a glass on its rheological and relaxation properties (by the example of a 5Na2O95B2O3 glass)", *Glass Phys. Chem.*, vol. 27, pp. 411-417, 2001

307. Stein, D.J. and F.J. Spera," Experimental rheometry of melts and supercooled liquids in the system NaAlSiO4-SiO2: Implications for structure and dynamics", *Am. Mineral.*, vol. 78, pp. 710-723, 1993

308. Stepanov, V.V., R.V. Balyabin, and B.M. Lepinskikh," Viscosity of flux systems containing calcium fluorides", *Tr. Inst. Met., Akad. Nauk SSSR, Ural. Nauch. Tsentr*, vol. No. 25, pp. 78-84, 1971

309. Stepanov, V.V., B.E. Lopaev, and S.V. Shtengelmeier," Viscosity of fluxes and their applicability to electroslag formation, remelting, and heating", *Avtomatich. Svarka*, vol. 18, pp. 28-30, 1965

310. Suk, M.O. and J.H. Park," Corrosion behaviors of zirconia refractory by CaO-SiO2-MgO-CaF2 slag", *J. Am. Ceram. Soc.*, vol. 92, pp. 717-723, 2009

311. Sukenaga, S., et al.," Viscosities of CaO-SiO2-Al2O3-(R2O or RO) melts", *ISIJ Int.*, vol. 46, pp. 352-358, 2006

312. Sumita, S., et al.," Viscosity of Slag Melts Containing Iron(III) Oxide", *Nippon Kinzoku Gakkaishi*, vol. 44, pp. 94-99, 1980

313. Sumita, S., et al.," Viscosity and Electrical Conductivity of Na2O-SiO2-ZnO and CaO-SiO2-ZnO Melts", *J. Jpn. Inst. Met.*, vol. 46, pp. 280-285, 1982

314. Sykes, D., et al.," Viscosity-Temperature Relationships at 1 atm in the System Nepheline-Diopside", *Geochim. Cosmochim. Acta*, vol. 57, pp. 1291-1295, 1993

315. Szwejda, K.A., D.L. Vogel, and J.M. Stevels," Rheological properties of potassium barium borate glasses", *J. Non-Cryst. Solids*, vol. 12, pp. 150-60, 1973

316. Tait, J.C., D.L. Mandolesi, and H.E.C. Rummens," Viscosity of Melts in the Sodium Borosilicate System", *Phys. Chem. Glasses*, vol. 25, pp. 100-104, 1984

317. Tanabe, I., K. Oku, and T. Honda," Effect of manganese oxide and alumina on the viscosity of high-carbon ferromanganese slags", *Denki Kagaku*, vol. 28, pp. 681-6, 1960

318. Taniguchi, H.," Entropy Dependence of Viscosity and the Glass-Transition Temperature of Melts in the System Diopside-Anorthite", *Contrib. Mineral. Petrol.*, vol. 109, pp. 295-303, 1992

319. Taniguchi, S., Y. Tachikawa, and T. Shibata," Influence of oxygen partial pressure on the oxidation behavior of TiAl at 1300 K", *Mater. Sci. Eng., A*, vol. A232, pp. 47-54, 1997

320. Tauber, P. and J. Arndt," The relationship between viscosity and temperature in the system anorthite-diopside", *Chem. Geol.*, vol. 62, pp. 71-81, 1987

321. Taylor, T.D. and G.E. Rindone," Properties of soda aluminosilicate glasses. V. Low-temperature viscosities", *J. Am. Ceram. Soc.*, vol. 53, pp. 692-5, 1970

322. Tkach, G.D., A.G. Kucher, and M.I. Gasik," Effect of alkali metal oxides on the slag viscosity during the smelting of silicomanganese", *Izvestiya Vysshikh Uchebnykh Zavedenii, Chernaya Metallurgiya*, vol. 10, pp. 68-70, 1976

323. Toplis, M.J. and D.B. Dingwell," Shear Viscosities of CaO-Al2O3-SiO2 and MgO-Al2O3-SiO2 Liquids: Implications for the Structural Role of Aluminium and the Degree of Polymerisation of Synthetic and Natural Aluminosilicate Melts", *Geochim. Cosmochim. Acta*, vol. 68, pp. 5169-5188, 2004

324. Toplis, M.J., D.B. Dingwell, and T. Lenci," Peraluminous Viscosity Maxima in Na2O-Al2O3-SiO2 Liquids: the Role of Triclusters in Tectosilicate Melts", *Geochim. Cosmochim. Acta*, vol. 61, pp. 2605-2612, 1997

325. Toropov, N.A. and F. Ya," vol. 2, pp. 245-55, 1953

326. Toyuki, H. and M. Imaoka," Viscous behavior of potassium oxide-boron oxide and potassium fluoride-boron oxide system glasses", *Yogyo Kyokai Shi*, vol. 84, pp. 175-81, 1976

327. Tret'yakova, N.I. and O.V. Mazurin," Effect of divalent metal oxides on the viscosity of simple silicate glasses", *Izvestiya Akademii Nauk SSSR, Neorganicheskie Materialy*, vol. 5, pp. 1856, 1969

328. Tribe, T.S., P.W. Kingston, and W.F. Caley," Rheology and Constitution of the CaO-SiO2-MgO-CaF2 System", *Can. Metall. Q.*, vol. 36, pp. 95-101, 1997

329. Tsunawaki, Y., et al.," Analysis of calcium oxide-silicon dioxide and calcium oxide-silicon dioxide-calcium fluoride glasses by Raman spectroscopy", *J. Non-Cryst. Solids*, vol. 44, pp. 369-78, 1981

330. Tuenker, G. and H. Scholze," Possibilities of replacing boric oxide by alkaline earth or zinc oxides in technical glasses", *Glastech. Ber.*, vol. 55, pp. 61-5, 1982

331. Uhlmann, D.R. and R.R. Shaw," Thermal expansion of alkali borate glasses and the boric oxide anomaly", *J. Non-Cryst. Solids*, vol. 1, pp. 347-59, 1969

332. Urbain, G.," Viscosity of Silicon Dioxide-Lead(II) Oxide Melts", *Rev. Int. Hautes Temp. Refract.*, vol. 21, pp. 107-111, 1984

333. Urbain, G.," Viscosité de Liquides Silice-Alumine-Oxydes Na et K. Mesures et Estimations", *Rev. Int. Hautes Tempér. Réfract., Fr.*, vol. 22, pp. 39-45, 1985

334. Urbain, G.," Viscosity Estimation of Slags", *Steel Res.*, vol. 58, pp. 111-116, 1987

335. Urbain, G., Y. Bottinga, and P. Richet," Viscosity of Liquid Silica, Silicates and Alumo-Silicates", *Geochim. Cosmochim. Acta*, vol. 46, pp. 1061-1072, 1982

336. Urbain, G., et al.," Viscosity of Silicate Melts", *Trans. J. Br. Ceram. Soc.*, vol. 80, pp. 139-141, 1981

337. Urbain, G., F. Millon, and S. Cariset," Viscosities of Some Silica-Rich Liquids in the Silica-Boron Oxide System", *Comptes Rendus des Seances de l'Academie des Sciences, Serie C: Sciences Chimiques*, vol. 290, pp. 137-140, 1980

338. Van Bemst, A. and C. Delaunois," Role of titanium oxide in the system silica-titanium oxide-potassium oxide. I. Viscosity measurements", *Verres et Refractaires*, vol. 20, pp. 435-47, 1966

339. Vargas, S., F.J. Frandsen, and K. Dam-Johansen," Rheological Properties of High-Temperature Melts of Coal Ashes and Other Silicates", *Progress in Energy and Combustion Science*, vol. 27, pp. 237-429, 2001

340. Varshneya, A.K., *Fundamentals of Inorganic Glasses*. 1993: Academic Press, Inc. 570 pp.

341. Vatolin, N.A., et al., *Study of the viscosity of melts of some binary systems*, in *VINITI 4190-77*. 1977. p. 17 pp.

342. Vetyukov, M.M. and V.Y. Nikitin," Viscosity of melts of NaF-MgF2 and Na3AlF6-NaMgF3 binary systems", *Zh. Prikl. Khim. (S.-Peterburg, Russ. Fed.)*, vol. 32, pp. 2793-6, 1959

343. Visser, T.J.M. and J.M. Stevels," Rheological properties of boric oxide and alkali borate glasses", *J. Non-Cryst. Solids*, vol. 7, pp. 376-94, 1972

344. Vogel, H.," The law of the relation between the viscosity of liquids and the temperature", *Phys. Z.*, vol. 22, pp. 645-6, 1921

345. Volkova, N.E. and S.V. Nemilov," Effect of heat treatment on the low-temperature viscosity of lithium oxide-boron oxide-system glasses", *Fiz. Khim. Stekla*, vol. 16, pp. 207-12, 1990

346. Vulchev, I. and K. Todorov," Effect of manganese oxide (MnO) on the viscosity of synthetic blast furnace slag", *Godishnik na Visshiya Khimikotekhnologicheski Institut, Sofiya*, vol. 16, pp. 107-19, 1971

347. Vyatkin, G.P., V.Y. Mischenko, and V.K. Gerasimov," Electroconductivity, viscosity and surface properties of fluoride slags", *Tr. Chelyab. Politekhn. Inst.*, vol. 118, pp. 91, 1973

348. Washburn, E.W.," Measurement of the viscosity and surface tension of viscous liquids at high temperatures", *Recueil des Travaux Chimiques des Pays-Bas et de la Belgique*, vol. 42, pp. 686-96, 1923

349. Washburn, E.W., G.R. Shelton, and E.E. Libman," The viscosities and surface tensions of the soda-lime-silica glasses at high temperatures", *Bull.*, vol. 140, pp. 71 pp., 1924

350. Wright, S., L. Zhang, and S. Jahanshahi. *The Effect of CaO on the Viscosity of PbO-SiO2 Melts*. 1997: Iron and Steel Society, Warrendale, Pa.

351. Wu, P., G. Eriksson, and A.D. Pelton," Optimization of the Thermodynamic Properties and Phase Diagrams of the Na2O-SiO2 and K2O-SiO2", *J. Am. Ceram. Soc.*, vol. 76, pp. 2059-64, 1993

352. Wu, P., et al.," Prediction of the Thermodynamic Properties and Phase Diagrams of Silicate Systems - Evaluation of the FeO-MgO-SiO2 System", *ISIJ Int.*, vol. 33, pp. 26-35, 1993

353. Yagi, S., K. Mizoguchi, and Y. Suginohara," Viscosity of the Molten Manganese Oxide (MnO)-Titanium Dioxide-Silicon Dioxide System and Infrared Absorption Spectra of Its Glasses", *Kyushu Kogyo Daigaku Kenkyu Hokoku, Kogaku*, vol. 40, pp. 33-38, 1980

354. Yakobashvili, S.B. 1963, Akad. Nauk Ukr. SSR: Kiev.

355. Yamate, T. and Y. Kadogawa," Effect of glass composition on its viscosity. Viscosity of binary alkali borate glasses", *Kenkyu Hokoku - Asahi Garasu Kogyo Gijutsu Shoreikai*, vol. 44, pp. 15-24, 1984

356. Yanagase, T., et al. *Physical properties of calcium oxide-aluminum oxide-calcium fluoride melts*. 1984: Metall. Soc. AIME, Warrendale, Pa.

357. Yasukouchi, T., K. Nakashima, and K. Mori," Viscosity of Ternary CaO-SiO2-Mx(F, O)y and CaO-Al2O3-Fe2O3 Melts", *Tetsu to Hagane*, vol. 85, pp. 571-577, 1999

358. Yiannopoulos, Y.D., G.D. Chryssikos, and E.I. Kamitsos," Structure and properties of alkaline earth borate glasses", *Phys. Chem. Glasses*, vol. 42, pp. 164-172, 2001

359. Zhang, L. and S. Jahanshahi," Review and Modeling of Viscosity of Silicate Melts: Part I. Viscosity of Binary and Ternary Silicates Containing CaO, MgO, and MnO", *Metall. Mater. Trans. B*, vol. 29B, pp. 177-186, 1998

360. Zhang, L. and S. Jahanshahi," Review and Modeling of Viscosity of Silicate Melts: Part II. Viscosity of Melts Containing Iron Oxide in the CaO-MgO-MnO-FeO-Fe2O3-SiO2 System", *Metall. Mater. Trans. B*, vol. 29B, pp. 187-195, 1998

361. Zhang, P. and Z. Sui," Effect of Factors on the Extraction of Boron from Slags", *Metall. Mater. Trans. B*, vol. 26B, pp. 345-351, 1995

362. Zhang, Z. and R.G. Reddy. *Viscosity Measurement and modeling of Borate and borosilicate Melts*. 1999: Minerals, Metals & Materials Society, Warrendale, Pa.

363. Zhilo, N.L.," Effect of calcium oxide and fluoride on the viscosity of slag of the system MgO-SiO2-Al2O3", *Sb. Nauchn.-Tekhn. Tr., Nauchn.-Issled. Inst. Met. Chelyab. Sovnarkhoza*, vol. 4, pp. 101-14, 1961

364. Zhilo, N.L., et al.," Physical Properties and Mineralogical Composition of Titanium Blast-Furnace Slags", *Izv. Akadem. Nauk SSSR, Metally*, vol. 6, pp. 3-8, 1969

365. Zhmoidin, G.I.," Fusibility of fluorine-containing slags", *Izv. Akad. Nauk, Metally*, vol. 6, pp. 9-16, 1969

366. Zhmoidin, G.I.," Structural anomalies in the viscosities of fluorite-based melts", *Zhurnal Fizicheskoi Khimii*, vol. 59, pp. 1620-3, 1985

367. Zhmoidin, G.I. and O.D. Moldavskii," Viscosity of Fluorine-Containing Melts", *Izv. Akad. Nauk SSSR, Metally*, vol. 1, pp. 70-73, 1970

368. Zhukova, T.S. and L.N. Sheludyakov," On the possibility of estimating the viscosity of fluorine-containing multicomponent aluminosilicate melts according to their composition", *Trudy Instituta Khimicheskikh Nauk, Akademiya Nauk Kazakhskoi SSR*, vol. 40, pp. 72-7, 1975

369. Zhukovets, Z.G.," Effect of fluorine on the properties of glasses from systems composed of silicon dioxide, boron oxide, aluminum oxide, and potassium oxide", *Fizika i Khimiya Stekla*, vol. 1, pp. 285-7, 1975